

OPEN PIT MINING SLOPES: SPECIAL STABILITY CONSIDERATIONS

A Dissertation

by

ANNA TIMCHENKO

Submitted to the Graduate and Professional School of
Texas A&M University
in partial fulfillment of the requirements for the degree of

DOCTOR OF PHILOSOPHY

Chair of Committee,
Committee Members,

Head of Department,

Jean-Louis Briaud
Charles P. Aubeny
Ivan Damnjanovic
John R. Giardino
Zachary Grasley

December 2021

Major Subject: Civil Engineering

Copyright 2021 Anna Timchenko

ABSTRACT

Slope stability analysis and design are important in mining geotechnical engineering, as open-pits have slopes cut as steep as possible to ensure efficient mining. We must mine the ore while keeping the total waste to a minimum, aiming for a reasonable factor of safety (FS) and tolerable probability of failure (PoF). Therefore the safety issues along with economic issues should be taken into consideration during the mine slope design.

In order to tackle this problem, the researcher focused on the following three objectives: (a) to develop solutions to predict the debris travel distance for improved management and repairs, the setback distance for equipment at the top of the slope, and a stability chart for preliminary selection of the slope angle, based on a large open-pit slope failures collection; (b) to compare the two-dimensional (2-D) and three-dimensional (3-D) slope stability methods to obtain the FS; (c) to compare the slope behavior at corners and in plane strain.

The first objective was accomplished based on published evidence. The researcher created the TAMU-MineSlope Spreadsheet including 134 open pit slope failures that occurred at 60 mines worldwide. Analysis by an energy principle approach along with the TAMU-MineSlope data analysis allowed us to come up with the best prediction equation for the debris travel distance L_{TRAV} : $L_{TRAV}(m) = 1.75 \cdot \frac{H_{FALL}(m)}{\tan \phi}$ where H_{FALL} is the vertical distance from the crest of the failure to the end of the debris flow tongue. Also based on the case histories analysis, the best setback distance equation was found to be: $L_{SB}(m) = H_{FAIL}^{0.82}(m)$, where H_{FAIL} is the vertical distance from the crest of the failure to the toe of the slip surface. The researcher reviewed and evaluated the existing stability charts (Taylor's, Hoek&Bray's) and proposed a new one as part of this research. The proposed chart can be used for the preliminary design of open-pit slopes. Finally, the researcher updated the f-n chart presented by Whitman in 1981 and advocate that risk values

of 0.001 fatalities/year and \$10,000/year are reasonably tolerable as they are consistent with other daily human activities tolerated by the general public.

To address the second objective, the researcher compared the FS obtained by the 2-D and 3-D slope stability methods. The numerical simulation results showed that the 3-D analysis must be performed for slopes with $W/H < 4$ where W is the width of the failed soil mass and H is the height of the slope. It was shown that the minimum 3-D FS is greater than the minimum 2-D FS for all conditions considered herein. It was shown that the parameters that have the greatest significant influence on the FS are the slope geometry and the cohesion rather than the friction angle. The FS and PoF acceptance criteria in open-pit mining design were also discussed. Acceptable values were found to be $FS = 1.3$ and $PoF < 0.05 - 0.3$ for mining slopes; these values are much higher than the values commonly employed in civil engineering ($PoF < 0.001$).

To address the third objective of the study, the researcher studied the factor of safety for complicated open-pit wall geometries (concave- or convex-shaped corners). The researcher simulated numerically the behavior of 3-D slopes using the RS3 software (Rocscience Inc.). The results show that the displacement-based approach is more effective in determining the corner stability than the traditional FS approach. The researcher showed that the displacement is inversely proportional to the FS. Furthermore, the sharp convex corner FS is up to 40% lower than the plane strain case, while the sharp concave corner is up to 3 times greater than the plane strain FS. Lastly, with the increase of the radius of curvature, the difference between the corner stability and plane strain case is decreasing with an increase in the plan view radius of curvature. The researcher reviewed the influence of benching for slope stability and showed that for materials with low cohesion, the use of benching is not useful. As for the effect of water level fluctuation, our research findings show that the lowest factor of safety is reached when the water level is at 40% of the slope height.

DEDICATION

To my parents.

I cannot thank them enough for their love and support throughout my studies.

ACKNOWLEDGEMENTS

The three years of my PhD program at Texas A&M University were full of great life lessons. I take this opportunity to thank all the people that made this great journey meaningful and unforgettable.

It is difficult to overstate my gratitude to my advisor, Professor Jean-Louis Briaud for his generous support and all the great ideas that he shared with me throughout this time. The joy and enthusiasm he has for his research was contagious and motivational, even during tough times of my Ph.D. pursuit. I am also thankful for the excellent example he has provided for me as a successful geotechnical professional and professor. It has been a great honor to be his Ph.D. student.

I would also like to thank Professors Charles Aubeny, Ivan Damnjanovic, and John R. Giardino for agreeing to serve as members of my committee and for their contributions and guidance throughout the course of this research.

I would like to thank my family and friends for all their love and constant encouragement during my studies.

Lastly, I offer my regards to all of those who supported me in any aspect of my courses and research.

CONTRIBUTORS AND FUNDING SOURCES

Contributors

This research was supported by a dissertation committee consisting of the student academic advisor and committee chair Professors Jean-Louis Briaud, and Professors Charles Aubeny, and Ivan Damnjanovic of the Department of Civil Engineering and Professor John R. Giardino of the Department of Geology and Geophysics.

Funding Sources

The research was funded by the Spencer J. Buchanan chair at Texas A&M University.

TABLE OF CONTENTS

	Page
ABSTRACT.....	ii
DEDICATION.....	iv
ACKNOWLEDGEMENTS.....	v
CONTRIBUTORS AND FUNDING SOURCES	vi
TABLE OF CONTENTS.....	vii
LIST OF FIGURES	x
LIST OF TABLES.....	xxii
LIST OF ABBREVIATIONS.....	xxv
1. INTRODUCTION.....	1
1.1 State of the problem	1
1.2 Research objectives.....	6
1.3 Scope and Outline of Current Study.....	7
2. OVERVIEW OF OPEN-PIT MINING.....	10
2.1 Open-pit mining issues.....	10
2.2 Slope failures in open pit mining	14
2.2.1 Definition of an open pit slope failure	16
2.2.2 Types of open pit failures	17
2.2.3 Trigger factors for open pit slope failures.....	25
2.3 Available slope stability software	33
2.4 Overview on slope monitoring systems	38
2.4.1 Methods of monitoring systems for open-pit mining	42
2.4.2 Conventional monitoring	48
2.4.3 Surface measurements	51
2.4.4 Subsurface measurements.....	62
2.4.5 Summary of various slope monitoring techniques.....	71
3. ANALYSIS OF CASE HISTORIES OF OPEN PIT MINING SLOPE FAILURES INCLUDING RISK	77
3.1 Existing slope failure databases	77
3.2 Development and Organization of the TAMU-MineSlope Spreadsheet.....	85
3.2.1 Part 1: Record information.....	87

3.2.2	Part 2: Open Pit Parameters	88
3.2.3	Part 3: Geological and Geotechnical Characteristics	90
3.2.4	Part 4: Slope Failure Parameters.....	93
3.2.5	Part 5: Slope Failure Plan and Scheme	103
3.2.6	Part 6: General Information	103
3.3	Analysis of the data	105
3.3.1	Travel distance prediction.....	105
3.3.2	Setback distance prediction.....	137
3.4	Stability Charts Evaluation.....	152
3.4.1	Background information	152
3.4.2	Taylor chart evaluation	158
3.4.3	Hoek &Bray’s chart evaluation	163
3.4.4	A new stability chart development	168
3.5	Risk associated with open pit mining slopes.....	178
3.5.1	Existing knowledge on ‘bubble chart’ development	179
3.5.2	Procedure	182
3.5.3	Application to various activities	184
3.5.4	Fatalities and cost risk charts	192
4.	COMPARISON OF SLOPE FACTOR OF SAFETY BY VARIOUS METHODS.....	200
4.1	Definition of the FS	200
4.2	2-D slope stability by the limit equilibrium method	202
4.3	3-D slope stability by the limit equilibrium method	205
4.4	2-D and 3-D slope stability by the finite element method	206
4.4.1	Advantages of Finite Element Method	209
4.4.2	Limitations of Finite Element Method.....	210
4.5	Comparison between analysis methods.....	211
4.6	Probabilistic analysis.....	224
4.6.1	Coefficient of variation	227
4.6.2	Spatial variability and correlation length.....	228
4.6.3	Number of layers of the slope and Probability of failure.....	230
4.7	Target FS and PoF.....	241
4.7.1	Target FS in open pit mining slope stability.....	241
4.7.2	FS and PoF acceptance criteria for open-pit slopes design.....	244
4.7.3	Target PoF in open pit mining slope stability	248
4.7.4	Observation on FS obtained by strength reduction and load increase techniques	250
5.	STABILITY OF SLOPE CORNERS AND OTHER UNUSUAL SLOPE CASES.....	256
5.1	Corner slopes.....	256
5.1.1	Existing knowledge on slope corner stability	256
5.1.2	Parameters for various corner configurations	264
5.1.3	Mesh and boundary conditions	267
5.1.4	Role of convergence criteria and parameters.....	271
5.1.5	Soil model	273

5.1.6	Displacement based approach to corner stability.....	279
5.1.7	Effect of 3-D complex geometry for corner stability.....	287
5.2	Stability of benched slopes.....	297
5.2.1	Bench configuration.....	297
5.2.2	Influence of benching on the open pit slope stability	300
5.2.3	A risk-based approach to the stability of benches	305
5.3	Impact of the water-level variations on slope stability.....	311
6.	CONCLUSIONS AND RECOMMENDATIONS.....	317
6.1	Summary	317
6.2	Conclusions and recommendations	317
6.2.1	Chapter 1 – Introduction	317
6.2.2	Chapter 2 – Overview of open-pit mining	317
6.2.3	Chapter 3 – Analysis of case histories of open pit mining slope failures including risk	319
6.2.4	Chapter 4 – Comparison of FS by various methods	328
6.2.5	Chapter 5 – Stability of slope corners and other unusual slope cases	332
6.3	Summary contribution to new knowledge.....	339
6.4	Future research directions	340
	REFERENCES	341
	APPENDIX A. TAMU-MINESLOPE DATABASE.....	368
	APPENDIX B. BIBLIOGRAPHY FOR TAMU-MINESLOPE.....	383

LIST OF FIGURES

	Page
Figure 1.1 Slope failures in open pit mining (reprinted from Crouse and Wright 2015; Petley 2020; Wessels 2009; Cremeens et al. 2000, Rose and Sharon 2000, Pankow et al. 2014).....	2
Figure 1.2 Slope failure occurred at Gamsberg mine (South Africa) on 17 November 2020 (photo from public source www.reddit.com)	3
Figure 1.3 Slope failure occurred at Carmen Copper mine (Philippines) on 21 December 2020 (Image tweeted by News5).....	3
Figure 1.4 Potential impacts of slope steepening (reprinted from Read and Stacey 2009).....	6
Figure 2.1 Open pit wall terminology (adapted from Martin and Stacey 2018, Wyllie and Mah 2005)	11
Figure 2.2 Typical open pit mine (reprinted from Harraz 2016)	12
Figure 2.3 Catch bench terminology (adapted from Hustrulid et al. 2013).....	13
Figure 2.4 Slope failure in the open pit mine (photo by FOX 13).....	16
Figure 2.5 Examples of the main types of slide mechanisms (adapted from Wyllie and Mah 2004, Høeg 2013).....	18
Figure 2.6 Four types of failure mechanisms important for slopes in rock (reprinted from Hoek 1972).....	19
Figure 2.7 Three principal types of slope failures in open-pit mines (reprinted from Borreto dos Santos et al. 2019).....	19
Figure 2.8 Classification of progressive and regressive failures (reprinted from Call et al. 2000)	24
Figure 2.9 Cumulative deformation, deformation rate, and inverse velocity vs. time plots (reprinted from Dick et al. 2015)	25
Figure 2.10 The selected categories and principal parameters for the system (modified from Naghadehi et al. 2013)	27
Figure 2.11 Relationship between the FS and jointed rock mass saturation (c =cohesion (kPa), J_p = joint angle ($^\circ$), H = slope height, H_w = height of the water table in the slope) Note: the term saturation 100% saturation indicates the water table location at the surface. Input parameters: $\gamma=29$ kN/m ³ , $\gamma_w=10$ kN/m ³ , $\phi=32^\circ$, $H=30$ m, $\beta=69^\circ$, no tension crack (reprinted from Bye and Bell, 2001).....	30

Figure 2.12 Loading of a mining slope (reprinted from Singh and Ghose 2006).....	33
Figure 2.13 Pit slope design flow diagram (reprinted from Lelono et al. 2016)	42
Figure 2.14 Alarm levels as function of displacement velocities (reprinted from Nadim and Lacasse 2008).....	46
Figure 2.15 Methods of monitoring systems for open-pit mining (modified from Sjoberg 1996, Girard 2001, Lacasse and Nadim 2009, Osasan 2012, Nunoo et al. 2016).....	48
Figure 2.16 Scheme of typical Wireline Extensometer (reprinted from Girard 2001).....	52
Figure 2.17 Wireline extensometer (photo from a public source https://www.cnitucson.com/). 52	
Figure 2.18 Concept of digital photogrammetry (reprinted from Ohnishi et al. 2006)	53
Figure 2.19 Scheme of Digital photogrammetry (reprinted from Vinoth et al. 2016).....	54
Figure 2.20 Survey network for open pit slope monitoring (modified from Sjoberg 1996)	56
Figure 2.21 Network of Prisms and Automatic Total Station (reprinted from Vinoth et al. 2016)	56
Figure 2.22 Elements of the GPS monitoring system (reprinted from Ma et al. 2001).....	57
Figure 2.23 Example of locations of the GPS elements in the large open pit mine (reprinted after Bond et al. 2005).....	58
Figure 2.24 Principals of laser scanner data acquisition (reprinted from Jaboyedoff et al. 2012)	59
Figure 2.25 Slope Stability Radar (modified from https://www.groundprobe.com/).....	60
Figure 2.26 Typical slope failure measurements obtained by a Ground Probe SSR (reprinted from Dick et al. 2015)	62
Figure 2.27 Sketch of the borehole extensometer device (reprinted from Corominas et al. 2000)	63
Figure 2.28 In-place inclinometer: a) example of the equipment parts, b) inclinometer probe (reprinted from Abzar 2019)	64
Figure 2.29 Outline of piezometer (modified from Rapinski et al. 2014).....	66
Figure 2.30 TDR technology: a) deformed cable resulting in signature “spike” on cable tester screen, b) TDR cable signatures showing deformation which activated alarm circuit (reprinted from Kane and Beck 1998).....	67

Figure 2.31 Microseismic monitoring in opencast mine (modified from Institute of Mine Seismology 2015).....	69
Figure 2.32 Main parts of the microseismic monitoring system. (a) microseismic sensor, (b) NetADC, (c) NetSP, (d) microseismic data collecting and processing system (reprinted after Li et al. 2016)	70
Figure 3.1 Case histories map.....	83
Figure 3.2 Parameters of the slope.....	86
Figure 3.3 General view of the TAMU-MineSlope Spreadsheet	89
Figure 3.4 Strength grade distribution (total number of cases = 134)	91
Figure 3.5 Distribution of rock mass rating (total number of cases = 134).....	92
Figure 3.6 Distribution of the friction angle ϕ ($^{\circ}$) (total number of cases = 106)	93
Figure 3.7 Distribution of the cases with different failure mechanisms (total number of cases = 134).....	94
Figure 3.8 Distribution of reported triggering events (total number of cases = 134).....	95
Figure 3.9 Distribution of the slope failure volume (total number of cases = 134).....	96
Figure 3.10 Distribution of the slope failure mass (total number of cases = 134).....	97
Figure 3.11 Distribution of the slope angle β_{FAIL} ($^{\circ}$) (total number of cases = 134)	98
Figure 3.12 Distribution of the fall height H_{FAIL} (m) (total number of cases = 134).....	99
Figure 3.13 Distribution of the travel distance L_{TRAV} (m) (total number of cases = 134).....	100
Figure 3.14 Distribution of the average width, W_{FAIL} (m) (total number of cases = 104)	101
Figure 3.15 Distribution of the setback distance, L_{SB} (m) (total number of cases = 112).....	102
Figure 3.16 Distribution of the height of the failure, H_{FAIL} (m) (total number of cases =116).....	103
Figure 3.17 Sunburst with hierarchical data corresponding to the countries where the data were obtained	104
Figure 3.18 Available material travel distance analysis methods (reprinted from McDougall, 2016)	105
Figure 3.19 Schematic definition of the travel distance (adapted from Whittall 2017 and Crouse and Wright 2015).	107

Figure 3.20 Comparison of apparent friction coefficient (Fahrböschung) with real friction coefficient (reprinted from Shea and Vries 2008).....	108
Figure 3.21 East wall failures at Cowal gold mine, Australia (reprinted from Crouse and Wright 2015)	109
Figure 3.22 Cross section of the east wall failures at Cowal gold mine, Australia (adapted from Crouse and Wright 2015)	110
Figure 3.23 Diagram of stricture genesis in laboratory scale rockslide avalanches during flow (reprinted from Shear and Vrise 2008)	111
Figure 3.24 Basic geometrical parameters used for the travel distance prediction	113
Figure 3.25 Relationship between Failure Height and Travel Distance of the failure mass based on the TAMU-MineSlope Spreadsheet	114
Figure 3.26 Predicted vs. measured travel distance records based on TAMU-MineSlope	119
Figure 3.27 Probability of higher than predicted travel distance occurrence for all data in TAMU-MineSlope (referred equation is $L_{TRAV}=3.06 \cdot H_{FALL}$).....	120
Figure 3.28 Predicted versus measured travel distance records for TAMU-MineSlope (red line represents regression line with a 90% probability to be safe, failure height is the reference value).....	121
Figure 3.29 Variation of the $\ln(L_{TRAV})$ with respect to $\ln(H_{FALL})$	123
Figure 3.30 Design chart for $\ln(L_{TRAV})$ vs. $\ln(H_{FALL})$ with 80% prediction interval plotted on the same graph. The upper level corresponds to a 90% exceedance probability, the lower level - to a 10% exceedance probability.....	124
Figure 3.31 Comparison of the probability approach and prediction interval approach	125
Figure 3.32 Relationship between Fall Height and Travel Distance of the failure mass (total number of points = 125)	126
Figure 3.33 Probability of higher than predicted travel distance occurrence for all data in the TAMU-MineSlope Spreadsheet (the referred equation is $L_{TRAV}=2.42 \cdot H_{FALL}$)	127
Figure 3.34 Predicted versus measured travel distance records for open pit failure database (red line represents regression line with a 90% probability to be safe; fall height is the reference value).....	128
Figure 3.35 Design chart for $\ln(L_{TRAV})$ vs. $\ln(H_{FALL})$ with an 80% prediction interval plotted on the same graph. The upper level corresponds to a 90% exceedance probability: the lower level corresponds to a 10% exceedance probability.	129
Figure 3.36 Cut slope failure geometry	130

Figure 3.37 Free body diagram	131
Figure 3.38 Relationship between travel distance and fall height normalized by $\tan\phi$ (total number of points =80)	133
Figure 3.39 Probability of higher than predicted travel distance occurrence for all data in the TAMU-MineSlope Spreadsheet (referred equation is $L_{TRAV}=0.98 \cdot (H_{FALL}/\tan\phi)$).....	134
Figure 3.40 Predicted versus measured travel distance records for TAMU-MineSlope (red line represents regression line with the 90% to be safe; $(H_{FALL}/\tan\phi)$ is the reference value).....	135
Figure 3.41 Design chart for $\ln(L_{TRAV})$ vs. $\ln(H_{FALL}/\tan\phi)$ with an 80% prediction interval plotted on the same graph. The upper level corresponds to a 90% exceedance probability: the lower level corresponds to a 10% exceedance probability.....	136
Figure 3.42 Setback distance in open pit mining	138
Figure 3.43 Design chart for estimating the crest zone of influence in a transition from open pit to underground mining by block/panel caving for rock masses of different geotechnical quality and undercut level (crater depths in the range from 0 to 1700 m) (reprinted from de Graaf et al. 2019)	139
Figure 3.44 Evaluation of a zone of potential instability (reprinted from Department of Industry and Resources 1997, Safety Bund Walls Around Abandoned Open Pit Mines Guideline, Government of Western Australia).....	140
Figure 3.45 Location of the tension crack behind the slope crest (modified from Hoek and Bray 1974).....	140
Figure 3.46 Critical tension crack location for a dry slope (reprinted from Hoek and Bray 1974).....	141
Figure 3.47 Location of critical sliding surface and critical tension crack for slopes with ground water present (reprinted from Hoek and Bray1981, Wyllie and Mah 2005)	141
Figure 3.48 Method for a setback distance evaluation proposed by Huang (1982)	142
Figure 3.49 Slope parameters used in the VNIMI's equation	142
Figure 3.50 Relationship between setback distance L_{SB} and failure height H_{FAIL}	144
Figure 3.51 Probability of higher than predicted setback distance occurrence for all data in TAMU-MineSlope (referred equation is $L_{SB}=0.42 \cdot (H_{FAIL})^{0.82}$).....	144
Figure 3.52 Predicted versus measured setback distance records for open pit failure database (red line represents regression line with the 90% to be safe; H_{FAIL} is the reference value).....	145

Figure 3.53 Design chart for $\ln(L_{SB})$ vs. $\ln(H_{FAIL})$ with an 80% prediction interval plotted on the same graph. The upper level corresponds to a 90% exceedance probability: the lower level corresponds to a 10% exceedance probability.	146
Figure 3.54 Parameters of CAT 793F (reprinted from https://www.cat.com/)	148
Figure 3.55 A typical slope stability model as analyzed by Slide2 (Rocscience Inc.), showing the critical failure surface and the corresponding FS	149
Figure 3.56 Distance ratio (SDR) vs. Distance from the crest to the mining truck (m) for different slope inclinations. Note that the parameters of the slope were picked such that the analyzed slope without loading is at failure (FS=1).....	150
Figure 3.57 Variation of the critical distance from the crest of the slope to mining truck (m) with respect to the value of $(c+\gamma H \tan\phi)$	151
Figure 3.58 Taylor chart for $\phi' > 0, c' > 0$, no water in soils (reprinted from Briaud, 2013)	153
Figure 3.59 Spencer chart for $\phi' > 0, c' > 0$, and $ru=0.25$ (reprinted from Briaud 2013)	154
Figure 3.60 Circular failure chart with the ground water flow model #3 (reprinted from Hoek and Bray 1981).....	155
Figure 3.61 Morgenstern charts for rapid drawdown for stability number $c'/\gamma H=0.0125$ and slope angles $\beta=27^\circ$ and $\beta=18^\circ$ (reprinted from Briaud 2013).....	156
Figure 3.62 Michalowski stability charts for uniform slopes: a) for $N^* \leq 3, F/\tan\phi \leq 14$ and $ru=0$ and b) for $N^* \leq 0.5, F/\tan\phi \leq 5$, and $ru=0.25$ (reprinted from Michalowski 2002)	157
Figure 3.63 Verification of Taylor's chart with the open pit slope failure case histories (1 – 'unsafe' point, 2 – 'safe' point).....	160
Figure 3.64 Comparison between slope angle ($\beta, ^\circ$) from the case history database and Taylor's chart for the domain: a) $0^\circ \leq \phi \leq 5^\circ$, b) $5^\circ \leq \phi \leq 10^\circ$, c) $10^\circ \leq \phi \leq 15^\circ$, d) $15^\circ \leq \phi \leq 20^\circ$, e) $20^\circ \leq \phi \leq 25^\circ$, f) $25^\circ \leq \phi \leq 30^\circ$, and g) $30^\circ \leq \phi \leq 35^\circ$	162
Figure 3.65 Verification of Hoek&Bray's chart with the open pit slope failure case histories (1 – 'unsafe' point, 2 – 'safe' point).....	163
Figure 3.66 Comparison between friction angle ($\phi, ^\circ$) from the case history database and Hoek and Bray's chart for the domain a) $10^\circ \leq \beta \leq 20^\circ$, b) $20^\circ \leq \beta \leq 30^\circ$, c) $30^\circ \leq \beta \leq 40^\circ$, d) $40^\circ \leq \beta \leq 50^\circ$, e) $50^\circ \leq \beta \leq 60^\circ$, and f) $60^\circ \leq \beta \leq 70^\circ$	167
Figure 3.67 Stability chart development based on the collected open pit slope failure case histories (FS=1).....	169
Figure 3.68 Correction factor needed to meet a given probability that the prediction will be greater than the observed value	170

Figure 3.69 Proposed stability chart based on the 134 open pit slope failure case histories, H is the designed height of the slope in meters	171
Figure 3.70 An example of an open pit slope consists of several strata	172
Figure 3.71 Comparison between friction angle (ϕ , °) from the case history database and new developed stability chart for the domain a) $\beta \leq 15^\circ$, b) $15^\circ \leq \beta \leq 20^\circ$, c) $20^\circ \leq \beta \leq 25^\circ$, d) $25^\circ \leq \beta \leq 30^\circ$, e) $30^\circ \leq \beta \leq 35^\circ$, f) $35^\circ \leq \beta \leq 40^\circ$, g) $40^\circ \leq \beta \leq 45^\circ$, and h) $45^\circ \leq \beta \leq 50^\circ$	177
Figure 3.72 Risks for selected engineering projects (reprinted from Whitman 1984)	180
Figure 3.73 F-N chart showing average annual risks posed by a variety of traditional civil facilities and other large structures or projects (reprinted from Baecher and Christian 2003).....	180
Figure 3.74 Comparison of risk acceptable criteria with statistics (reprinted from Steffen et al. 2008)	180
Figure 3.75 Risk f-N chart for human activities (reprinted from Briaud et al. 2012).....	181
Figure 3.76 Number of fatalities in open pit mining industry by year, 1983 – 2019 (reprinted from NIOSH 2020).....	182
Figure 3.77 Example of the risk chart; the location of the activity has coordinates of Pa and C.	193
Figure 3.78 Annual PoF vs. annual number of fatalities due to the failure	195
Figure 3.79 Annual PoF vs. annual economic loss corresponding to the failure.....	195
Figure 3.80 Comparison of the open pit slope risk ellipse's location (a) in term of fatalities, and (b) in terms of dollars lost (adapted from Whitman 1984).....	196
Figure 4.1 FS for the circular failure surface (reprinted from Briaud, 2013)	201
Figure 4.2 Example of the simple slope stability problem (reprinted from Briaud 2013).....	201
Figure 4.3 2-D finite element model of a slope	209
Figure 4.4 The geometry and boundary conditions of the three-dimensional slope.....	214
Figure 4.5 Geometry of the three-dimensional slope with W/H=0.5, 1, 2, 3, 4, 5, 7 and 10.....	215
Figure 4.6 FS _{3D LEM} /FS _{2-D LEM} versus W/H	216
Figure 4.7 FS _{3D FEM} /FS _{2-D LEM} versus W/H	216

Figure 4.8 The bar chart for W/H ratio based on the open pit slope failure case history collection	217
Figure 4.9 Variation of normalized total displacement with respect to the normalized FS _{3D FEM} (W/H=0.5, 1, 2, 3, 4, 5, 7 and 10)	218
Figure 4.10 Variation of the normalized FS with respect to tan ϕ	222
Figure 4.11 Variation of the normalized FS with respect to c, (kPa)	222
Figure 4.12 Variation of the normalized FS with respect to tan β	223
Figure 4.13 Variation of the normalized FS with respect to W/H.....	223
Figure 4.14 Exponential correlation coefficient functions for different isotropic separation distance τ (θ is the scale of fluctuation) (modified from Kim and Salgado 2009).....	230
Figure 4.15 Results of the simulations for homogeneous slope divided into n-layers (n = number of layers with identical material properties intersected by the critical slip surface). Note: results are presenter for case with coefficient of correlation $\theta=0$	233
Figure 4.16 PoF vs. number of layers with identical material properties intersected by the critical slip surface (n).....	235
Figure 4.17 A slope formed with no layered homogeneous material (modified from Briaud 2013).....	236
Figure 4.18 A slope formed of two layers A and B (modified from Briaud 2013)	237
Figure 4.19 Variation of PoF (%) with correlation length θ (m) for the homogeneous slope...	239
Figure 4.20 The influence of the number of identical layers intersected by the critical slip surface (n) on the PoF (%) for different spatial variability of soil and slope with no spatial variability	240
Figure 4.21 Examples of acceptable FS values for different civil engineering projects and open pit mining (modified from Read and Stacey 2009).....	242
Figure 4.22 Footing problem used to illustrate differences between factors of safety applied to load and to soil shear strength ($\phi'=30^\circ$, $c'=16$ kPa, $\gamma=18$ kN/m ³ , B=4 m, and q=18 kPa)	251
Figure 4.23 Variation of the PoF with respect to the FS, assuming a log normal distribution of FS, CoV of shear strength = 0.3, and CoV of shear stress = 0 (modified from Briaud and Gardoni 2009).....	255
Figure 5.1 Convex shape of the pit wall. This “nose” shape is less stable than plane strain wall (reprinted from McQuillan et al. 2018).....	257

Figure 5.2 Slip surface of a vertical cut with two unconstrained vertical planes. The slip surface is found to be composed of two 2D failure modes (reprinted from Wei et al. 2009)	260
Figure 5.3 Shear strain contours of different turning corners with FS (reprinted from Zhang et al. 2013).....	261
Figure 5.4 The failure mechanism of convex- and concave-shaped slopes with different corner angles and FS (reprinted from Zhou et al. 2020)	262
Figure 5.5 Examples of concave and convex shapes in open pit mining	263
Figure 5.6 Typical shapes and parameters of convex and concave 3-D models	264
Figure 5.7 Variation of the normalized 3-D FS with respect to W/H ratio. Homogenous slope, $\gamma=20$ kN/m ³ , $c=10$ (kPa), $\phi=30^\circ$, $\psi=0^\circ$, $E=30$ MPa, $\nu=0.28$	266
Figure 5.8 Variation of the FS with respect to distance from crest to the back side of the model, L (m). Homogenous slope, $\gamma=20$ kN/m ³ , $c=10$ (kPa), $\phi=30^\circ$, $\psi=0^\circ$, $\nu=0.28$	266
Figure 5.9 Influence of mesh size on FS.....	268
Figure 5.10 Effect of element size on the critical slip surface: a) element size – 1.0m, b) element size – 0.5m , c) element size – 0.25 m (reprinted from Cheng et al. 2018)	268
Figure 5.11 The failure shape variation due to the size of the mesh element.....	269
Figure 5.12 Boundary conditions: (a) general model, (b) plane strain case, (c) concave-shaped corner, (d) convex-shaped corner.....	270
Figure 5.13 The iterative finite element procedure for determining the spring's behavior under applied loads (reprinted from Rocscience 2021a).....	272
Figure 5.14 Location of the reference point for data collection	275
Figure 5.15 The impact of the dilation angle on the slope stability result for a homogeneous slope with $E=30$ MPa and $\nu=0.28$. Normalized FS vs. Dilation angle.....	276
Figure 5.16 The impact of the dilation angle on the slope stability result for a homogeneous slope with $E=30$ MPa and $\nu=0.28$. Normalized total displacement vs. Dilation angle ($^\circ$).....	276
Figure 5.17 Elastic-perfectly plastic assumption for Mohr-Coulomb model	277
Figure 5.18 A Mohr-Coulomb criterion drawn in shear-normal stress space, and the resulting curve when the envelope is reduced by a shear strength reduction factor (reprinted from Yacoub 2016)	278

Figure 5.19 The shear stress reduction solution using FE method (Software: RS3) (reprinted from Rocscience 2021b).....	279
Figure 5.20 Normalized total displacement vs. normalized FS for the performed corner stability simulation	280
Figure 5.21 3D slope conceptual model: (a) 3D slope sketch; (b) side view (x-z plane).....	281
Figure 5.22 Variation of the total displacement with respect to the FS (E=50,000 kPa)	282
Figure 5.23 Variation of the total displacement with respect to the FS (E=30,000 kPa)	283
Figure 5.24 Variation of the total displacement with respect to the FS (E=10,000 kPa)	283
Figure 5.25 Variation of the total displacement with respect to the FS: (a) W/H=0.5; (b) W/H=1; (c) W/H=2; (d) W/H= 3.....	286
Figure 5.26 Variation of the K-value with respect to Young's modulus, E (kPa). Homogenous slope, $\gamma=20 \text{ kN/m}^3$, $c=10 \text{ (kPa)}$, $\phi=30^\circ$, $\psi=0^\circ$, $\nu=0.28$	287
Figure 5.27 The difference in the normalized total displacement with respect to the normalized plane view angle for different slope angles: (a) $r/H=0.07$, (b) $r/H=0.33$, (c) $r/H=0.67$, and (d) $r/H=1$	290
Figure 5.28 Variation of the normalized total displacement with respect to the normalized plane view angle (for $r/H=0.07$).....	291
Figure 5.29 Variation of the normalized total displacement with respect to the normalized plane view angle (for $r/H=0.33$).....	292
Figure 5.30 Variation of the normalized total displacement with respect to the normalized plane view angle (for $r/H=0.67$).....	293
Figure 5.31 Variation of the normalized total displacement with respect to the normalized plane view angle (for $r/H=1$).....	294
Figure 5.32 Components of bench geometry.....	298
Figure 5.33 Example of the FS calculation results (for the slope formed by material with $c=10 \text{ kPa}$, $\phi=30^\circ$ and $\gamma=20\text{kN/m}^3$): a) no benches, b) two benches, c) four benches, d) eight benches, and e) sixteen benches.....	302
Figure 5.34 Relationship between normalized bench FS and $W_{\text{bench}}/H_{\text{bench}}$	303
Figure 5.35 Relationship between normalized bench FS and the number of benches forming the slope.....	304
Figure 5.36 Relationship between normalized benched slope FS and the number of benches forming the slope.....	304

Figure 5.37 Relationship between normalized benched slope FS and $W_{\text{bench}}/H_{\text{bench}}$	305
Figure 5.38 Constant risk approach in terms of dollars loss (dotted red line indicates risk based on Read and Stacey 2009 and Steffen et al. 2008)	309
Figure 5.39 Constant risk approach in term of volume of the failure (m^3) (reprinted from Fergusson et al. 2001)	310
Figure 5.40 Basic modes of water level change; water level drawdown (A), raised water level (B), and fluctuating water level (C). Water loads (U_w), positions of the ground-water table (GWT), and the external water level (EWL), are shown (reprinted from Johansson 2014)	311
Figure 5.41 Typical scheme of the slope	312
Figure 5.42 Normalized FS vs. the normalized height of the water table	313
Figure 5.43 Case with the no water slope	314
Figure 5.44 Case with the a little bit of water at the bottom.....	314
Figure 5.45 Case with the a water level at 2/3 of the height of the slope	315
Figure 5.46 FS in a “slow” drawdown problem for different values of the drawdown ratio L/H. Homogeneous slope 2H:1V with a horizontal free surface, $\phi'=20^\circ$, $c'/\gamma H=0.05$ (adapted from Griffiths 2001)	316
Figure 6.1 (REPEATED) Three principal levels of slope failures in open-pit mining.....	318
Figure 6.2 (REPEATED) Cut slope failure geometry	320
Figure 6.3 (REPEATED) Distance ratio (SDR) vs. Distance from the crest to the mining truck (m) for different slope inclinations. Note that the parameters of the slope were picked such that the analyzed slope without loading is at failure (FS=1)	322
Figure 6.4 (REPEATED) Variation of the critical distance from the crest of the slope to mining truck, b (m), with respect to the value of $(c+\gamma H \tan\phi)$	323
Figure 6.5 (REPEATED) Proposed stability chart based on the 134 open pit slope failure case histories, H is the designed height of the slope in meters	324
Figure 6.6 (REPEATED) Annual PoF vs. annual number of fatalities due to the failure	326
Figure 6.7 (REPEATED) Annual PoF vs. annual economic loss corresponding to the failure .	326
Figure 6.8 (REPEATED) FS $_{3D \text{ FEM}}/FS_{2-D \text{ LEM}}$ versus W/H	329
Figure 6.9 (REPEATED) PoF vs. number of layers with identical material properties intersected by the critical slip surface (n)	331

Figure 6.10 (REPEATED) Variation of the K-value with respect to Young's modulus, E (kPa). Homogenous slope, $\gamma=20$ kN/m ³ , $c=10$ (kPa), $\phi=30^\circ$, $\psi=0^\circ$, $\nu=0.28$	334
Figure 6.11 The difference in the normalized total displacement with respect to the normalized plan view angle for different slope angles (for $r/H=0.07$).....	335
Figure 6.12 The difference in the normalized total displacement with respect to the normalized plan view angle for different slope angles (for $r/H=0.33$).....	335
Figure 6.13 The difference in the normalized total displacement with respect to the normalized plan view angle for different slope angles (for $r/H=0.67$).....	336
Figure 6.14 The difference in the normalized total displacement with respect to the normalized plan view angle for different slope angles (for $r/H=1$).....	336
Figure 6.15 (REPEATED) Normalized FS vs. the normalized height of the water table	338

LIST OF TABLES

	Page
Table 2.1 The most common open pit slope failure modes (modified from Hoek and Bray 1977, Cruden and Varnes 1996, Hoek 2013)	20
Table 2.2 Types of failure and their possible consequences (modified from Priest and Brown 1983, Swan and Sepulveda 2000, Read and Stacy 2009, Borreto dos Santos et al. 2019).....	22
Table 2.3 Failure velocity scale (reprinted from Hungr et al. 2014)	23
Table 2.4 Typical bench slopes produced by excavating equipment in open pit mining (reprinted from Singh and Ghose, 2006).....	31
Table 2.5 Summary of commercial slope stability software available for open pit mining design (adapted from Stead and Wolter 2015)	36
Table 2.6 Example of the open pit movement thresholds (reprinted from Nanoo et al. 2016) ...	46
Table 2.7 Alarm levels and actions for the warning system (modified from Nadim and Lacasse 2008).....	47
Table 2.8 Open-pit mine sites referred to in literature where microseismic monitoring has been performed (adapted from Sjoberg 2006, Lynch et al. 2005, Wesseloo et al. 2009).....	68
Table 2.9 Different types of the monitoring systems: strength and limitations (reprinted from Osasan 2012)	74
Table 3.1 Summary of the existing slope failure datasets	78
Table 3.2 List of entries in the TAMU-MineSlope Spreadsheet	87
Table 3.3 Strength grade classification (reprinted from ISRM 1978)	90
Table 3.4 RMR calibrated against rock mass quality (reprinted from Read and Stacey 2009)....	91
Table 3.5 Summary of the available mobility relationships (modified from Whittall et al. 2017)	112
Table 3.6 Correction factor $\alpha(\text{PoE})$ and corresponding PoE (%) to predict travel distance based on the failure height.....	116
Table 3.7 Parameters of the models used in calculation of the loaded slope.....	149
Table 3.8 Comparative study of the results obtained using Taylor’s chart, Hoek&Bray’s chart and proposed stability chart.....	175

Table 3.9 Risk Levels for the United States	194
Table 3.10 Summary of the calculations for the risks associated with the different public and civil engineering activities	197
Table 4.1 Methods and Limitations for Limit Equilibrium Method (adapted from Duncan and Wright 1980, Briaud 2013)	203
Table 4.2 Comparison of slope stability analysis methods (adapted Coggan et al. 1998, Stead et al. 2005).....	213
Table 4.3 A reference set of average soil and model parameters	220
Table 4.4 Comparison between deterministic and probabilistic approaches (reprinted from Assis 2020).....	226
Table 4.5 Typical values of CoV for some geotechnical properties used in slope stability analysis	228
Table 4.6 Statistical input parameters.....	231
Table 4.7 Limit equilibrium results for lowest FS and automatically calculated probability of failures of the layered homogenous slope	234
Table 4.8 Acceptable FS values in slope mining engineering.....	243
Table 4.9 Typical FS and PoF acceptance criteria for open-pit mining slope design (modified from Read and Stacey 2009).....	244
Table 4.10 Typical FS and PoF acceptance criteria for open-pit mining slopes based on the failure's tonnage (modified from Schellman et al. 2006)	245
Table 4.11 Typical FS and PoF acceptance criteria for open-pit mining slope design based on its lifetime and volume of the failed material (reprinted from Swan and Sepulveda 2000).....	246
Table 4.12 Acceptable PoF in slope mining engineering	249
Table 5.1 Summary of significant studies on the FS for homogeneous slopes with turning corners	258
Table 5.2 Studied cases.....	265
Table 5.3 Material properties.....	282
Table 5.4 A number of studied cases and results illustrating the influence of benching in open pit mining	301

Table 5.5 Constant risk design approach for the different categories of the open-pit slope failures	308
Table 5.6 Summary of the simulation results for the water level rise	313
Table 6.1 (REPEAED) Comparative study of the results obtained using Taylor’s chart, Hoek&Bray’s chart and proposed stability chart	325
Table 6.2 (REPEATED) Risk Levels for the United States	327
Table 6.3 (REPEATED) Typical values of CoV for some geotechnical properties used in slope stability analysis	330
Table 6.4 (REPEATED) Typical FS and PoF acceptance criteria for open-pit mining slopes .	331

LIST OF ABBREVIATIONS

2-D	Two-Dimensional
3-D	Three-Dimensional
FS	Factor of Safety
FS _{2-D}	Two-dimensional factor of safety
FS _{3-D}	Three-dimensional factor of safety
PoF	Probability of Failure
FE	Finite Element
LE	Limit Equilibrium
m	Meter
mm	Millimeter
SRM	Strength Reduction Method
SRF	Shear Strength Reduction Factor
γ	Unit Weight (kN/m ³)
c	Cohesion (total stress) (kPa)
c'	Cohesion (effective stress) (kPa)
ϕ	Friction Angle (total stress) (°)
ϕ'	Friction Angle (effective stress) (°)
ψ	Dilation angle (°)
E	Young's modulus (kPa)
ν	Poisson's ratio
u_t	Total displacement (m)
u_x	Displacement in x-direction (m)
u_y	Displacement in y-direction (m)
u_z	Displacement in z-direction (m)

1. INTRODUCTION

1.1 State of the problem

Slope design is one of the main challenges in open pit mining at every stage of planning and operation. The cut slope stability has the most prominent influence in the mine lifetime and production, collapse of which can lead to enormous damages to people and equipment. It is always considered as an economic burden to mine production and requires special knowledge of the complex geological, geotechnical, and hydrogeological conditions. Furthermore, the materials forming the open pit walls are highly variable. Slope stability analysis also requires an understanding of the practical aspects of design implementation.

The aim of any open pit mine design is to provide an optimal excavation configuration in the context of safety, complexity, ore excavation and recovery, and financial return. The slope stability issues in the open pit mining industry have come to the forefront in the mining operations due to increasing open pit depth and steepening of the pit walls. With the recent developments in data acquisition techniques, slope monitoring, and numerical simulation, our understanding of the behavior of open pit slopes has improved significantly over the last three decades. Notwithstanding, challenges still remain in the application of these methods, and open pit slope failures still impose significant economic, social, and environmental threats to the industry and society in general.

Figure 1.1 presents some examples of slope failures that happened in the surface mining industry.



Cowal mine (Australia) 2007



Gamsberg mine (South Africa) 2020



Carmen Copper mine (Philippines) 2020



Nchanga mine (Zambia) 2004



Homestake Pitch mine (USA) 1983

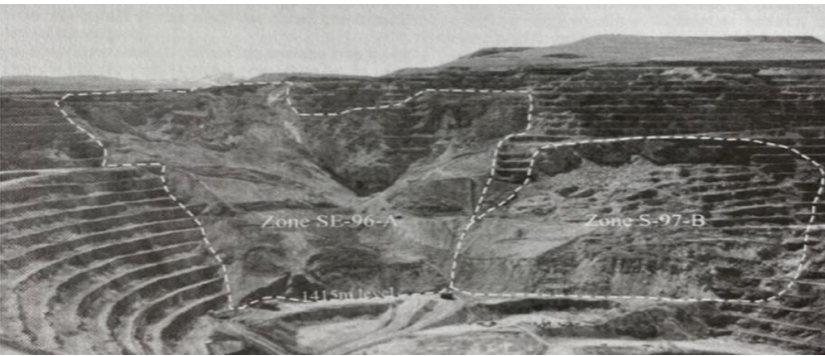
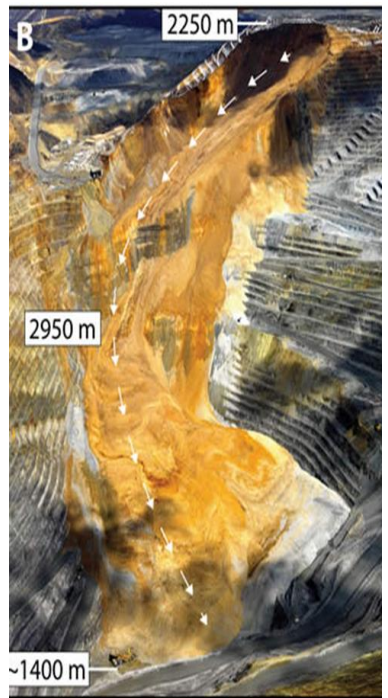
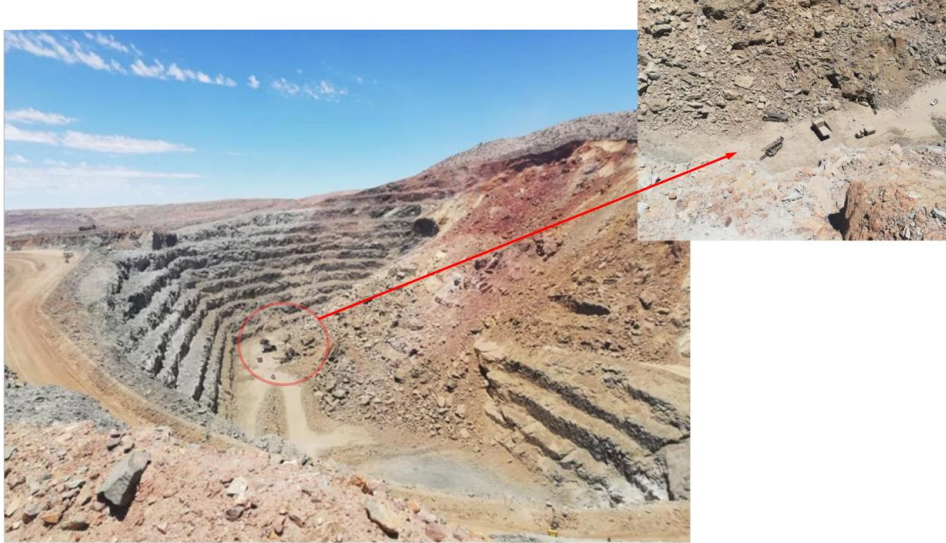


Figure 1.1 Slope failures in open pit mining (reprinted from Crouse and Wright 2015; Petley 2020; Wessels 2009; Cremeens et al. 2000; Rose and Sharon 2000; Pankow et al. 2014).

The failures in opencast mining occur every year. For example, at the end of 2020 there were two disasters in the industry. One failure occurred at Gamsberg Zinc mine, South Africa (Figure 1.2). This failure took one person, and 8 were injured. Another thing that should be mentioned is that after the failure, the world zinc prices rose by 30%.



*Note several pieces of equipment buried in slide debris, 1 person died, 8 miners were rescued

Figure 1.2 Slope failure occurred at Gamsberg mine (South Africa) on 17 November 2020 (photo from public source www.reddit.com)

Another failure happened at Carmen Copper mine, Philippines (Figure 1.3), which took 4 people and 6 were injured, let alone a lot of equipment was buried under the debris flow.



* Note 4 people died, 6 miners were rescued

Figure 1.3 Slope failure occurred at Carmen Copper mine (Philippines) on 21 December 2020 (Image tweeted by News5)

It is essential that a degree of stability is ensured for the slope open pit mining industry to minimize the risks related to the safety of operating personnel and equipment and economic risks to the reserves. At the same time, to address the economic needs of the owners, ore recovery should be maximized, and waste stripping kept to a minimum throughout the mine life. The proposed research aims to link innovative geotechnical engineering research with best current practice by collecting, studying, and analyzing the open-pit mining slope failures that have happened all over the world.

Slope stability prediction for slopes with complicated geometry (e.g., concave or convex corners) is another challenge in mining and geotechnical engineering. A common practice is to treat slopes two-dimensionally, i.e., it is assumed that the section of slope under consideration is part of an infinitely long straight slope. It is also generally assumed that the slope is planar from crest to toe, meaning that the slope face is not curved in section, and a single slope angle can define it.

The vast majority of slopes exhibit a complex geometric configuration and three-dimensional (3D) state, whereas slopes satisfying the assumption of plane strain (infinite length) are seldom encountered. Existing research (Duncan 1996; Griffiths and Lane 1999, Griffiths and Marquez 2007; Michalowski and Drescher 2009; Wei et al. 2009; Zhang et al. 2011, Zhou et al. 2020) mainly emphasizes the 3D dimensions and boundary effect in slope stability analysis, at the same time the effect of complex geometry on 3D slope stability is rarely reported. It also has to be mentioned that the accuracy of the prediction is very important for mitigating the risk of slope instability and enhancing mine safety in preliminary design. However, existing methods such as conventional 2D models utilizing limit equilibrium or 2D and 3D finite element approach are unable to provide accurate results for slope stability estimation due to the complexity and 3D shape

of the actual open pit slopes. Thus, a sophisticated 3D numerical modeling approach has to be utilized to investigate the effect of the complicated geometry of the slopes.

Open pit slope design is often performed based on the limited geological and geotechnical data due to the area and depth of the planned construction. There are three main approaches commonly used to account for the uncertainties in slope design: a factor of safety (FS), probability of failure (PoF), and risk analysis. The oldest approach to slope design is based on the calculation of the FS. The FS can be defined as the ratio between the resisting forces (strength) and the driving forces (loading) along a potential failure surface. FS-method accounts for the uncertainties through the selection of a design FS larger than 1.0. It is a very fast, but conservative method. In recent years, probabilistic methods have been increasingly used in slope design. These methods are based on the calculation of the PF of the slope. The PoF-method presented by the probability distributions to assess the probability of having a FS less than a critical value representing the failure of the slope. A major drawback of PoF methodology is the difficulty to define an adequate acceptability criterion (Sullivan 2006; Steffen et al. 2008; Golestanifar et al. 2018). With the risk analysis approach, the appropriate acceptance criteria have to be defined. In slope design, risk can be defined as the PoF of the slope combined with the consequence or potential loss associated with the failure of the slope. In the case of slope failure, the consequences can be twofold: personnel impact and economic impact. Based on the risk analysis, the acceptable value of the project risk should be estimated. In any case, the choice of acceptable/tolerable risk is difficult because so many factors enter into the decision.

In broad terms, open-pit mines are excavations created to extract valuable materials (ore) located below the surface. A considerable amount of material usually accompanies ore with little or no value (waste material), which must be extracted before reaching the ore; this process is called

stripping. During the life of the mine, the ore is hauled to processing plants or stockpiles, while waste material is transported to waste dumps surrounding the open pit. Thus, economic issues also have to be taken into consideration for an open-pit design process. In a large open-pit, steepening a wall by only a few degrees can significantly impact the return on the operations through the increased ore recovery and reduced stripping (Figure 1.4). For example, in large open pits (>500 m deep), the steepening of the slope by 1° per 1 km of an open pit shoreline could reduce the volume of stripping work by 600,000 m³ or coarse 1.65M\$ of additional revenue (personal communication and Melnikov et al. 2005). In addition, optimization of slope design can extend the life of mine allows to generate additional revenue. For example, in the case of the largest platinum mine in the world, Sandsloot open pit (South Africa), the steepening a 300 m slope by 7° had extended the life of the open pit by two benches, which allowed to generate over 23.3M\$ (Bye and Bell, 2001).

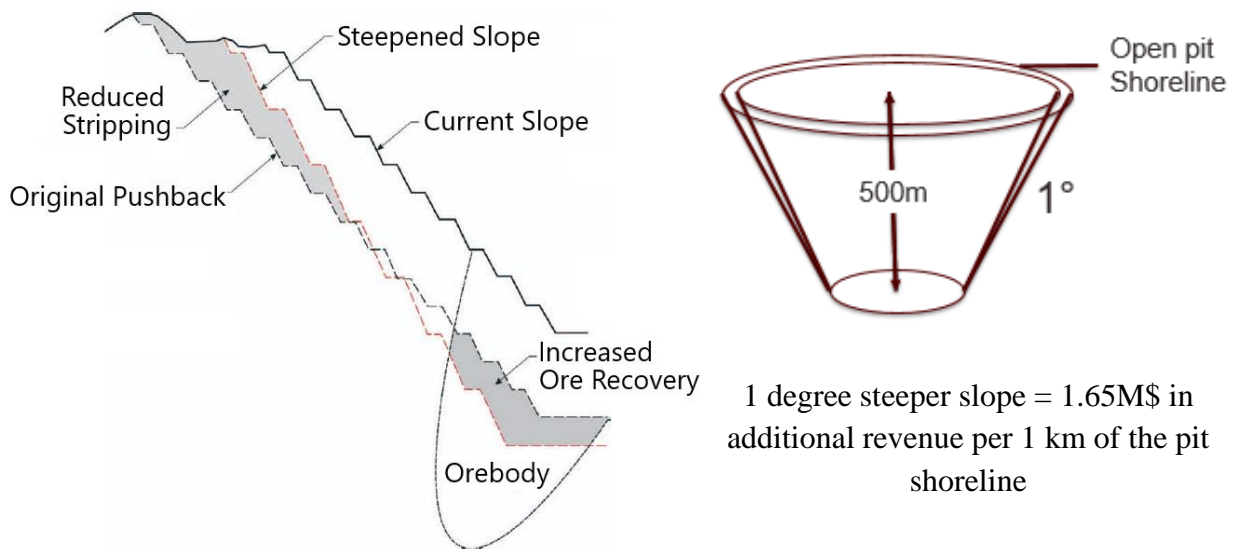


Figure 1.4 Potential impacts of slope steepening (reprinted from Read and Stacey 2009)

1.2 Research objectives

There are three primary objectives of the study.

The first objective is to develop solutions to predict the debris travel distance for improved management and repairs, the setback distance for equipment at the top of the slope, and a stability chart for preliminary selection of the slope angle.

The second objective is to compare the 2-D and 3-D slope stability methods to obtain the FS.

The third objective is to compare the slope behavior at corners and in plane strain.

1.3 Scope and Outline of Current Study

To accomplish the Objective #1 the following main steps were performed.

1. Step 1. Collect and organize a database of open pit slope failures.
2. Step 2. Establish a theoretical solution for the travel distance based on an energy balance.
3. Step 3. Develop an empirical correlation between the debris travel distance and relevant parameters using the database.
4. Step 4. Compare the theoretical solution to the empirical correlation and make recommendations.
5. Step 5. Establish a theoretical solution for the setback distance based on LE analysis.
6. Step 6. Develop an empirical correlation between a setback distance and relevant parameters using the database.
7. Step 7. Compare the theoretical solution to the empirical correlation and make recommendations.
8. Step 8. Develop a stability chart for preliminary selection of the slope angle using the database and compare it to Taylor charts.
9. Step 9. Identify the risk level associated with open pit mining slopes compared to other civil engineering and human activities.

To accomplish the Objective #2 the following main steps were performed.

1. Step 1. Review existing 2-D and 3-D stability methods and accompanying literature.
2. Step 2. Establish a list of fictitious but realistic slope stability cases.
3. Step 3. Obtain the FS for those cases by the 2-D LEM.
4. Step 4. Obtain the FS for those cases by the 3-D LEM.
5. Step 5. Obtain the FS for those cases by the 3-D FEM.
6. Step 6. Compare the results obtained in steps 2, 3 and 4 including a probabilistic analysis.
7. Step 7. Based on the comparison, comment on a target FS found in various codes.

To accomplish the Objective #3 the following main steps were performed.

1. Step 1. Review existing knowledge on corner stability.
2. Step 2. Define the parameters for various corner configurations.
3. Step 3. Select the FEM mesh dimensions and boundary conditions.
4. Step 4. Select a number of cases of corner configurations to be studied (e.g.: plan view angle, slope angle, radius of curvature, slope height).
5. Step 5. Perform the simulations and collect the output.
6. Step 6. Prepare charts giving the difference between the corner behavior and a plane strain case as a function of relevant parameters.

The remainder of this dissertation is organized as follows.

Chapter 2 provides an overview of existing knowledge on slope stability and open pit mining. The summary of open pit mining slope failure case histories is presented in Chapter 3. The comparison of the FS obtained by various methods (2-D LEM, 3-D LEM, 2-D FEM, and 3-D

FEM) are presented in Chapter 4. Chapter 5 provides the results of concave and convex corner stability calculations and all the results are compared with 2-D plane strain case. Chapter 6 summarizes the research contributions and provides directions for future research.

2. OVERVIEW OF OPEN-PIT MINING

2.1 Open-pit mining issues

Any mineral resource can be removed from the ground by open-pit mining, underground mining, or combinations of both methods. The selection of a mining method is a decision that is made based on the results of the deposit exploration, which should provide enough information to the property owner so that a preliminary mining feasibility study of the mineral deposit can begin.

A list of the factors that affect the selection of a mining method are as follows (Morrison and Russell, 1973)

- the spatial characteristics of the deposit (size, shape, attitude and depth);
- the physical (or mechanical) properties of the mineral deposit and surrounding rock;
- ground water and hydraulic conditions;
- economic factors, including grade of the ore, comparative mining costs and desired production rates; and
- environmental factors, such as the preservation of the surface overlying the mine, and the prevention of air and water pollution.

Of these factors, the spatial characteristics of the deposit and the physical (or mechanical) properties of the mineral and surrounding rock are fixed and limit the methods that can be employed in mining it. The last three factors are subject to change and are not as restrictive.

Open-pit (or surface) mining is a generic term describing several methods of mining mineral deposits from the surface, which entails removing the vegetation, top soil, and rock (called overburden materials) above the mineral deposit, removing the deposit, and reclaiming the affected land for post mining land use (Evolutionary and Revolutionary Technologies for Mining, 2002). Many factors contribute to the selection of an open-pit mining method. Probably the most significant are economic and technical:

- (a) the geometric configuration of the orebody;

- (b) the geologic nature of the deposit and surrounding rock and soil;
- (c) economic factors (price of the product, the cost of the production, the quantity of the deposit and the volume of the overburden to be removed per ton of the deposit, and the feasibility of the reclamation); and
- (d) company experience and preference.

In open-pit mining, waste is transported to a disposal site, and the ore is transported to a downstream processing site. This method commonly involves a sequence of benches from the surface to the deposit. As the open pit goes deeper into the ground, all of the benches above are extended outward. In appearance, an open-pit excavation resembles an inverted pyramid with its tip in the Earth. Large open-pit mines (a depth more than 100 m) can produce up to a million tons of waste and ore per day and can be mined at that rate for decades. The standard terminology used to describe the geometric arrangement of the benches and haul road ramps on the pit wall is illustrated in Figure 2.1 and Figure 2.2.

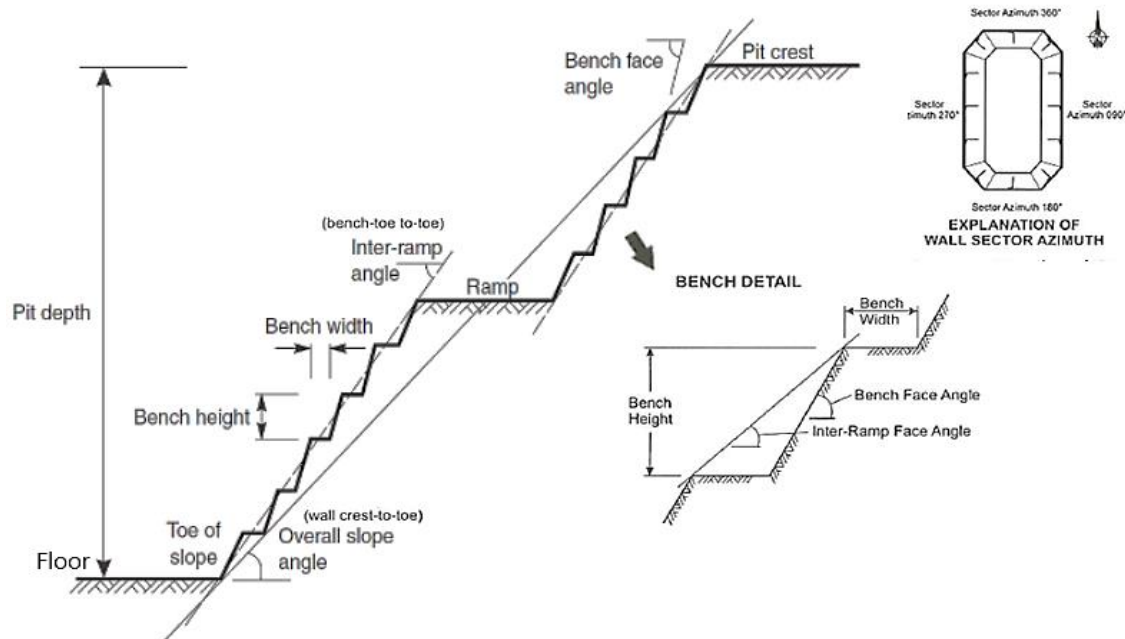


Figure 2.1 Open pit wall terminology (adapted from Martin and Stacey 2018, Wyllie and Mah 2005)

Each open pit has a hanging wall and a foot wall. A pit slope consists of sets of benches. Each open pit wall has three major components: bench configuration, interramp slope, and overall slope. The bench configuration is defined by bench height, bench face angle, and catch bench width (Figure 2.1). A series of benches form the interramp slope, and the overall slope is formed by a series of interramp slopes separated by haul roads (Figure 2.2). The bench height is determined by the geological conditions and size of the chosen mining equipment. The bench face angle is determined by the geologic structure, given that there are good blasting and digging practices.

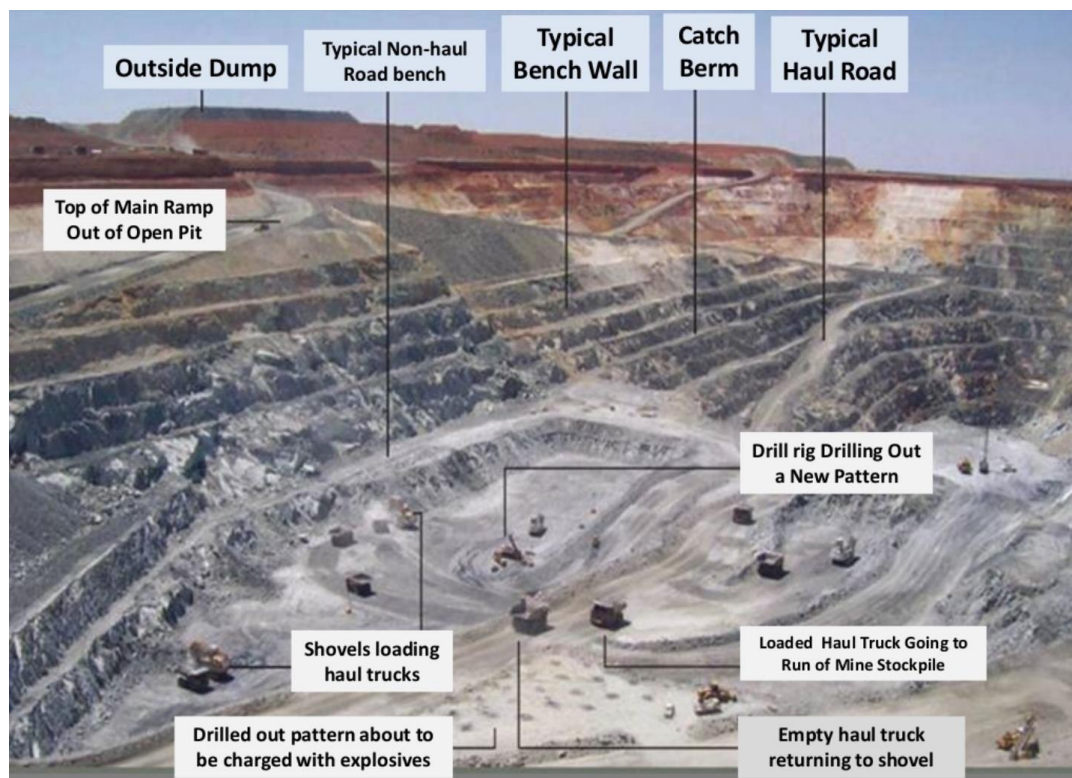


Figure 2.2 Typical open pit mine (reprinted from Harraz 2016)

The safety benches, berms (piles) of broken materials are often constructed along the crest. These serve the function of forming a 'ditch' between the berm and the toe of the slope to catch falling rocks. The typical design catch bench geometry illustrated in the Figure 2.1. The structures controlling the bench face angle are usually the rock fabric because of their high frequency of

occurrence, but the bench face angle can also be controlled by the intermediate and regional structures. Interramp, multiple-bench, slope-stability analysis concerns only those failures that incorporate two or more benches. Structures that affect the interramp stability must therefore be equal to or greater in length than the height of two design benches. The structures that have a minimum cut-off length equal to the height of two design benches are, by definition, the intermediate structures. The intermediate structures are analyzed statistically to determine the probability of structurally controlled multiple bench failures that affect the interramp slope stability (Hustrulid et al. 2013).

A safety berm is also left (Figure 2.3) along the outer edge of a bench to prevent trucks and other machines from backing over. Normally the pile has a height greater than or equal to the tire radius. The berm slope is taken to be about $35\text{-}37^\circ$ (the angle of repose of the crashed material).

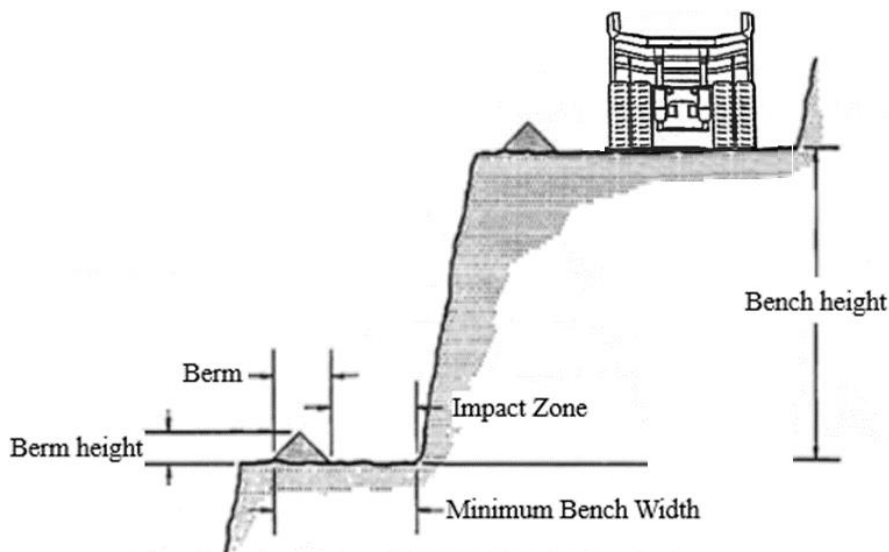


Figure 2.3 Catch bench terminology (adapted from Hustrulid et al. 2013)

The overall slope angle of the open pit is the angle between the horizontal and straight line that joins the toe of the bottom bench and the top edge of the pit. It is clear that the steeper the angle, the less overburden is required to be removed for exposing a certain volume of ore. At the

same time the risk of failure of that slope is increased. Uncontrolled instability of an open pit slope, can have safety/social and economic circumstances including (Read and Stacey, 2009):

Safety/social factors:

- loss of life or injury;
- loss of worker income;
- loss of worker confidence;
- loss of corporate credibility.

Economic factors:

- disruption of operations;
- loss of ore;
- increase of waste;
- loss of equipment;
- increased stripping;
- high insurance premiums.

2.2 Slope failures in open pit mining

Safety and environmental friendliness have attracted great attention in the mining industry, which has led to a comprehensive understanding of the deformation and failure behaviors of the soil and rock masses formed by the open pit walls and the development of methods for smartly controlling them. The in situ material is in a complicated stress state in equilibrium with the surrounding geological environment. Mining-induced perturbations may disturb the equilibrium, resulting in stress redistribution and deformation, which may cause damage and eventual collapse of the soil or rock material. The stress redistribution changes the complicated inner structure of the ore body and surrounding material because the material usually contains several discontinuities

such as pores, cracks, fractures, and joints, which induce distinctly nonlinear and discontinuous displacement or deformation under loading (Peng et al. 2015).

Slope failures are an inevitable aspect of economic pit slope designs in the mining industry. Nowadays many high slopes are being designed with a managed risk approach, in which slope failures can be tolerated as long as miner safety is not compromised. Large open pit guidelines and industry standards accept up to 30% of benches in open pits to collapse provided that they are controlled and that no personnel are at risk (Lynch et al. 2005, Bar et al. 2020). Location of the instability may significantly impact the open pit operation because even relatively small failure in the benches immediately above or below the main ramp can seriously affect open pit production. Understanding the link between the deformation (or failure) behaviors and their inherent governing mechanisms is of great significance to monitoring, predicting, and early detection of potentially disruptive mining-induced disasters.

A slope can be considered to have failed when displacement has reached a level where it is no longer safe to operate, or the intended function cannot be met, e.g., when ramp access across the slope is no longer possible (Figure 2.4). In open-pit mining, the terms ‘failure’ and ‘collapse’ have been used synonymously, particularly when the slope failure occurs rapidly. In the case of a ‘progressive failure’ model, failure of a pit slope occurs when ‘the displacement will continue to accelerate to the point of collapse (or greatly accelerated movement)’ (Read and Stacey 2009, Call et al. 2000).

During and after the slope's failure, the original design configuration is normally eradicated. Continued mining always involves modifying the slope configuration by flattening the walls from the crest or stepping out at the toe. This typically results in increased stripping (removal) of waste and/or loss of ore, with significant financial losses.



Figure 2.4 Slope failure in the open pit mine (photo by FOX 13)

2.2.1 Definition of an open pit slope failure

A landslide is a physical system that develops in time through several stages: pre-failure deformations, failure itself, and post-failure displacements. Many landslides exhibit several movement episodes, separated by long or short periods of relative immobility. The following definition of the term “failure” was given by Hungr et al. (2014): **Failure** is the single most significant movement episode in the known or anticipated history of a landslide, which usually involves the first formation of a fully developed rupture surface as a displacement or strain discontinuity.

According to Hoek et al. (2000), a slope that falls and deposits a pile of rubble on a haulage ramp is called failure.

Sjoberg (1996) defined slope collapse as a situation where the consequences of the developing failure render the slope impossible to mine. He also distinguished between local and

global slope collapses. The first one involves one or a few benches, while the global one involves the entire slope.

Mercer (2006) defined the terms “collapse,” “functional failure,” and “instability” as follows: “Collapse” is defined as the complete overall loss of rock mass integrity and structure. “Functional failure” is when a pit slope cannot perform the function for which it was intended. This implies that it does not necessarily involve overall collapse, although localized sections of the structure may have collapsed. “Instability” is defined as any other deformational movement or behavior that does not involve collapse and/or functional failure.

Wessels (2009) has collected the definitions of the term “failure” from different authors. The distinction was made between a slope that has “failed” and a slope that has “collapsed” (Sullivan 1993; Zavodni 2001, Call et al. 2000, Mercer 2006 and Sullivan 2006). Zavodni (2001) explained that the technical definition of a slope failure is when the driving stress exceeds the resisting stress and yielding movements develop. Call (1992) and Zavodni (2001) distinguish between a theoretical and an operational failure. Theoretical failure is displacement beyond recoverable strain if the rock is considered to be an elastic material. Operational failure is defined when “the rate of displacement is greater than the rate at which the failed material can be mined safely and economically, or the movement produces unacceptable damage to a permanent facility.”

2.2.2 Types of open pit failures

History of the development of the knowledge of failures was summarized by Hungr et al. (2014) in work “The Varnes classification of landslide types, an update”. According to the paper, some of the earliest landslide classification systems originated in the Alpine countries. Baltzer (1875) in Switzerland seems to have been the first to distinguish between the various basic modes

of motion: fall, slide, and flow. This division persists to the present time, supplemented by toppling, spreading and wedge (Figure 2.5).

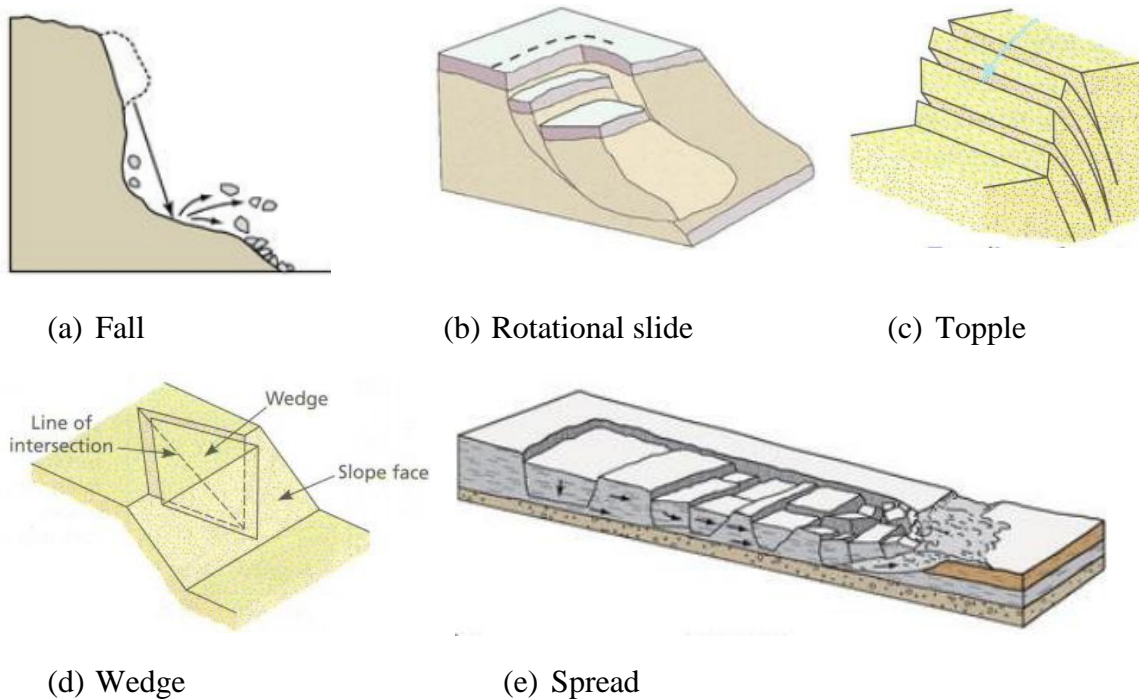


Figure 2.5 Examples of the main types of slide mechanisms (adapted from Wyllie and Mah 2004, Høeg 2013)

Intensive studies of the mining slopes were undertaken from the 1960s. Notable studies during the 1960s for open pit mines were those in the USA (Patton and Deere 1970 and Broadbent 1971), Great Britain (Hoek, 1972) and Canada (Piteau 1970). These were based on studies at mine sites and in laboratories. Hoek (1972) concluded that four types of failure mechanisms were important for slopes in rock (Figure 2.6). According to Hoek (1972), rotational failures occurred principally in soils and granular materials, without a pattern of geologic structures. Plane failure was regarded as uncommon, and then only a special case of a wedge failure. Wedge failure was regarded as the commonest type of open-pit failure. Toppling was regarded as a special case in a specific geological condition, where columns of rock dip into a wall.

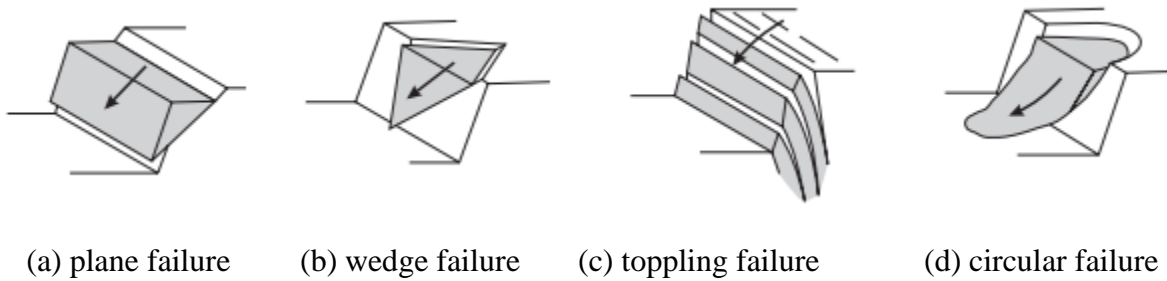


Figure 2.6 Four types of failure mechanisms important for slopes in rock (reprinted from Hoek 1972)

The summary of different models of the failures that occur in open pit mining presented in Table 2.1.

Slope failures that can occur in the open-pit mine excavation can be grouped into three categories directly related to their volume (Patton and Deere 1970; Gayer et al. 1995; Borreto dos Santos et al. 2019): bench failure, inter-ramp failure and overall failure (Figure 2.7).

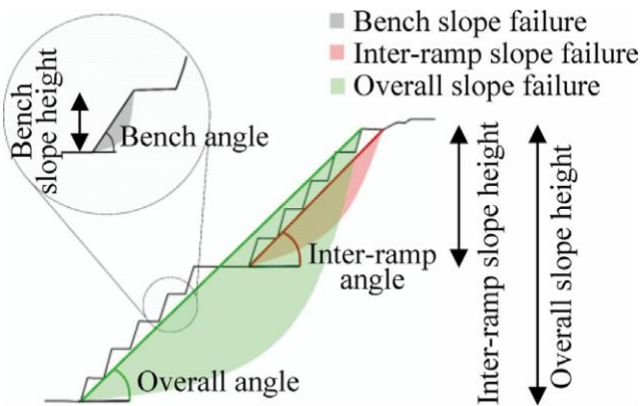


Figure 2.7 Three principal types of slope failures in open-pit mines (reprinted from Borreto dos Santos et al. 2019)

Table 2.1 The most common open pit slope failure modes (modified from Hoek and Bray 1977; Cruden and Varnes 1996; Hoek 2013)

Failure model	Description of the physical process	Critical parameters	Remarks
Fall	Very rapid to the extremely rapid gravitational movement (sliding, rolling, falling and bouncing) of masses and single fragments on steep slopes	<ul style="list-style-type: none"> • Geometry of a slope • Presence of loose boulders at a relatively great distance compared to their original position due to the high kinetic energy. • These rapid movements may be preceded by other types of movement, such as toppling and sliding. 	Presence of structures to arrest falling and bouncing rocks like draped mesh, catch fences, and ditches at the toe of the slope can prevent the severeness of a falling event
Slide (rotational, translational, compound, and complex and composite slides)	Complex failure along a circular (a spoon-shaped) or near circular failure surface through soil or heavily jointed rock masses	<ul style="list-style-type: none"> • Slope geometry (Height and angle of slope face) • Shear strength of materials along the failure surface. • Groundwater distribution in slope, particularly in respect to rainfall or to submergence of slope toe. • Potential surcharge of the slope crest or earthquake loading 	Design of the slope should be based on the minimum allowable FS and PoF (see chapter 4.7.1). Long term monitoring of surface and subsurface displacement in slope is the only practical means of evaluating slope behavior and effectiveness of remedial action
Planar or wedge sliding	Failure on one structural feature or along the line of intersection of two structural features	<ul style="list-style-type: none"> • Geometry of the slope (height and slope angle) • Dip and strike of structural features • Groundwater distribution in slope • Potential earthquake loading • Sequence of excavation and support installation 	Design of the slope should be based on the minimum allowable FS and PoF (see chapter 4.7.1).

Failure model	Description of the physical process	Critical parameters	Remarks
Toppling failure	Parallel or nearly parallel to the slope face overturning movement of the rock columns through rotation or flexure under the forces of gravity, or the forces exerted by adjacent units or fluids within discontinuities.	<ul style="list-style-type: none"> • Geometry of the slope (height and slope angle) • Dip and strike of structural features • Groundwater distribution in slope • Potential earthquake loading 	No generally acceptable criterion for toppling failure is available. Monitoring of slope displacements is the only practical means of evaluating slope behavior and effectiveness of remedial action
Spread	Slope movement characterized by extension of a cohesive soil or rock mass combined with a general subsidence of the fractured mass of cohesive material into softer underlying material	<ul style="list-style-type: none"> • Geological condition (The uppermost materials are more cohesive compare to the underlying one) • Potential surcharge of the slope crest or earthquake loading • Groundwater distribution in slope 	No generally acceptable criterion for toppling failure is available. Monitoring of slope displacements is the only practical means of evaluating slope behavior and effectiveness of remedial action

All three types of the scale of slope failures presented in Figure 2.7 are directly related to the volume of the failed material and, therefore, related to the value of the consequences of these failures. Once the volume of failures is related to the consequences of these failures, the levels of acceptance criteria in probabilistic stability analysis vary according to the severity of the failure (Table 2.2). Generally, the greater the failure consequences, the lower the level of tolerance accepted (Borreto dos Santos et al. 2019).

Table 2.2 Types of failure and their possible consequences (modified from Priest and Brown 1983, Swan and Sepulveda 2000, Read and Stacy 2009, Borreto dos Santos et al. 2019)

Type of failure	Level of severity	Possible consequence	
		Economic loss	Damage to equipment and injuries to personnel
Bench failure	Not serious	Minimum impact on production, mostly related to cleanup costs	Unlikely. Possible only if the failure occurs when the slope is under construction
Inter-ramp failure	Moderately serious to serious	More significant as the production losses and cleanup costs are usually greater than the bench failures. Inter-ramp slopes of 50 to 100 m in height, with haulage roads or close to permanent mine installations may have serious consequences	Likely if the failure occurs in working hours.
Overall slope failure	Very serious	Irreversible impact because failure can lead to ore dilution and can cause a decrease in its economic value. Public and stakeholder relationships may be severely affected and may even lead to the loss of permission to mine	Highly likely if failure occurs in working hours

Slope failures in open pit mining can be divided and classified according to numerous factors, including type and speed of movement, type of material involved, deposit age, state of

activity, genesis, and movement geometry (Varnes 1978, Hutchinson 1988, Hungr et al. 2001 among others). The failure velocity scale is presented in Table 2.3.

Table 2.3 Failure velocity scale (reprinted from Hungr et al. 2014)

Velocity class	Description	Velocity (mm/s)	Typical velocity
7	Extremely rapid	5×10^3	5 m/s
6	Very rapid	5×10^1	3 m/min
5	Rapid	5×10^{-1}	1.8 m/h
4	Moderate	5×10^{-3}	13 m/month
3	Slow	5×10^{-5}	1.6 m/year
2	Very slow	5×10^{-7}	16 mm/year
1	Extremely Slow	$< (5 \times 10^{-7})$	

The advanced stages of slope movement (cracking and dislocation and failure) described by Sullivan (1993) can be related to the “Regressive” and “Progressive” phases of time-dependent movement of slopes, as proposed by Broadbent and Zavodni (1982) and Hustrulid et al. (2001), which are defined as follows (Figure 2.8). A regressive failure shows short-term decelerating displacement cycles if disturbing events external to the rock are removed from the slope environment. On the other hand, a progressive failure will displace at an accelerating rate to the point of collapse unless active and effective control measures are taken.

Figure 2.9 visually defines regressive, progressive, and post-failure stages. The failure point on cumulative deformation, deformation rate, and inverse velocity versus time plots are also presented in the figure. The slope failure is taken at the end of the progressive deformation stage and typically coincides with a major acceleration event in which the integrity of the slope is lost (Dick et al., 2015).

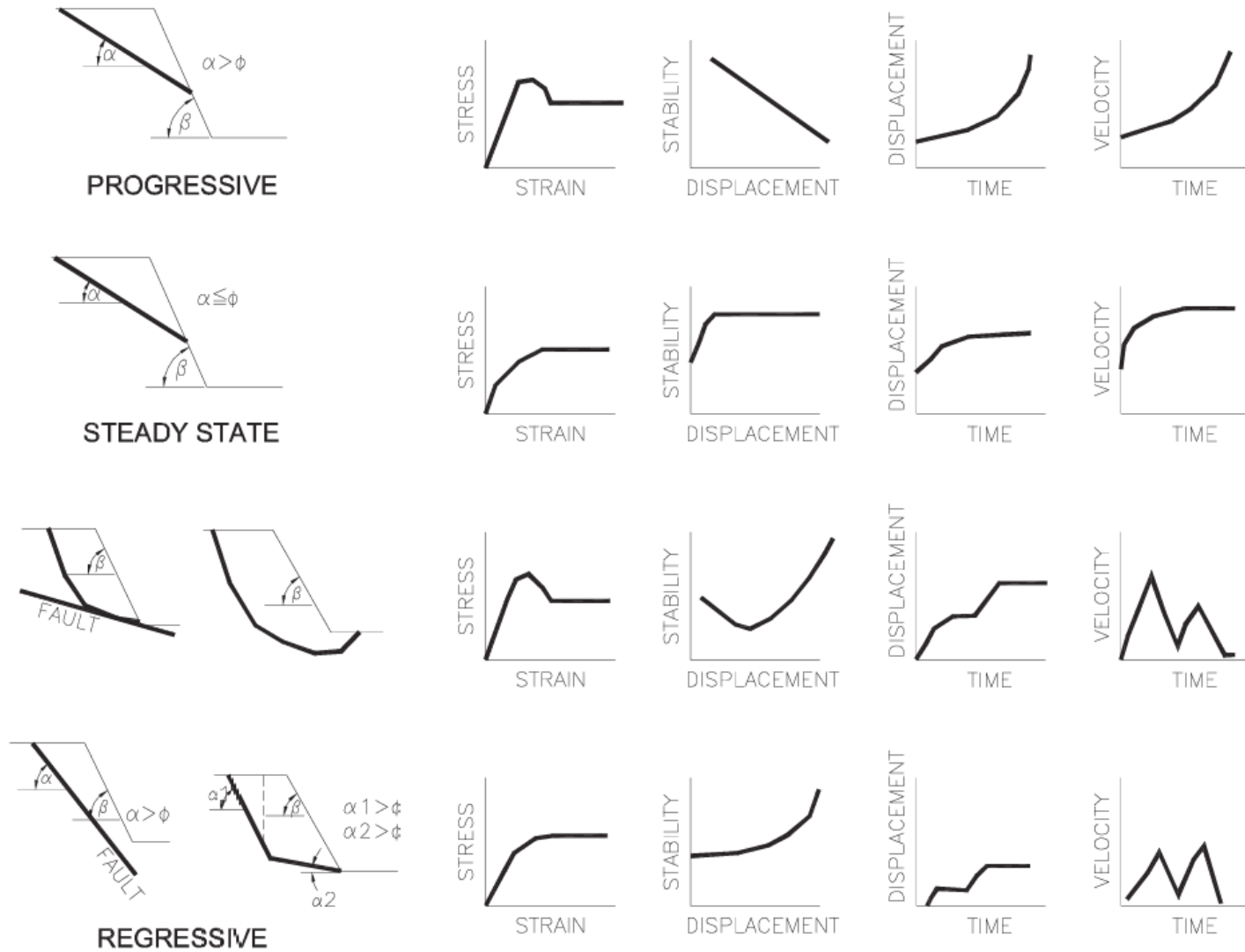


Figure 2.8 Classification of progressive and regressive failures (reprinted from Call et al. 2000)

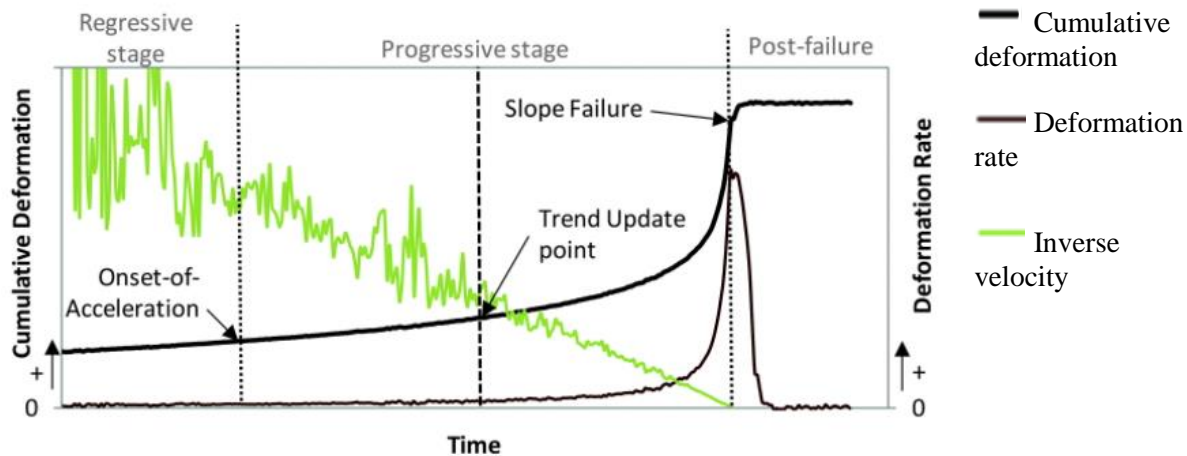


Figure 2.9 Cumulative deformation, deformation rate, and inverse velocity vs. time plots (reprinted from Dick et al. 2015)

2.2.3 Trigger factors for open pit slope failures

Slope stability accidents are one of the leading causes of fatalities at U.S. surface mining operations. The Spokane Research Laboratory of the National Institute for Occupational Safety and Health (NIOSH) is currently conducting research to reduce the fatalities associated with slope failures and other unexpected failures of ground. Unexpected movement of ground causes the potential to endanger lives, demolish equipment, or destroy property.

There are two main reasons why it is important to understand the agents of instability in slopes. First, for purposes of designing and constructing new slopes, it is important to be able to anticipate the changes in the properties of the material within the slope that may occur over time and the various loading and seepage conditions to which the slope will be subjected over the course of its life. Second, for purposes of repairing failed slopes, it is important to understand the essential elements of the situation that led to its failure, so that repetition of the failure can be avoided. Experience is the best teacher – from experiences with failures of slopes come the important lessons regarding what steps are necessary to design, construct, and repair slopes so that they will remain stable and safe (Duncan et al., 2014).

Duncan et al. (2014) summarized possible causes of slope failures and claimed that the fundamental requirement for the stability of slopes is that the shear strength of the soil must be greater than the shear stress required for equilibrium. This condition can be reached in two ways:

1. Through a decrease in the shear strength of the soil:

- (i) Increased pore pressure (reduced effective stress)
- (ii) Cracking
- (iii) Swelling (increase in void ratio)
- (iv) Development of slickensides
- (v) Decomposition of clayey rock fills
- (vi) Creep under sustained loads
- (vii) Leaching
- (viii) Strain softening
- (ix) Weathering
- (x) Cyclic loading

2. Through an increase in the shear stress required for equilibrium:

- (xi) Loads at the top of the slope
- (xii) Water pressure in cracks at the top of the slope
- (xiii) Increase in soil weight due to increased water content
- (xiv) Excavation at the bottom of the slope
- (xv) Drop in water level at the base of a slope
- (xvi) Earthquake shaking

Naghadehi et al. (2013) published another gradation of the failure causes. Eighteen key parameters (divided into 9 main categories) were selected to represent the instability potential of

open-pit walls (see Figure 2.10). The selection of parameters was based on recommendations from the literature and also on the experience gained from the analysis of failures in open-pit mines. It is important that the authors selected parameters that are easily obtainable without having to resort to special site investigation techniques.

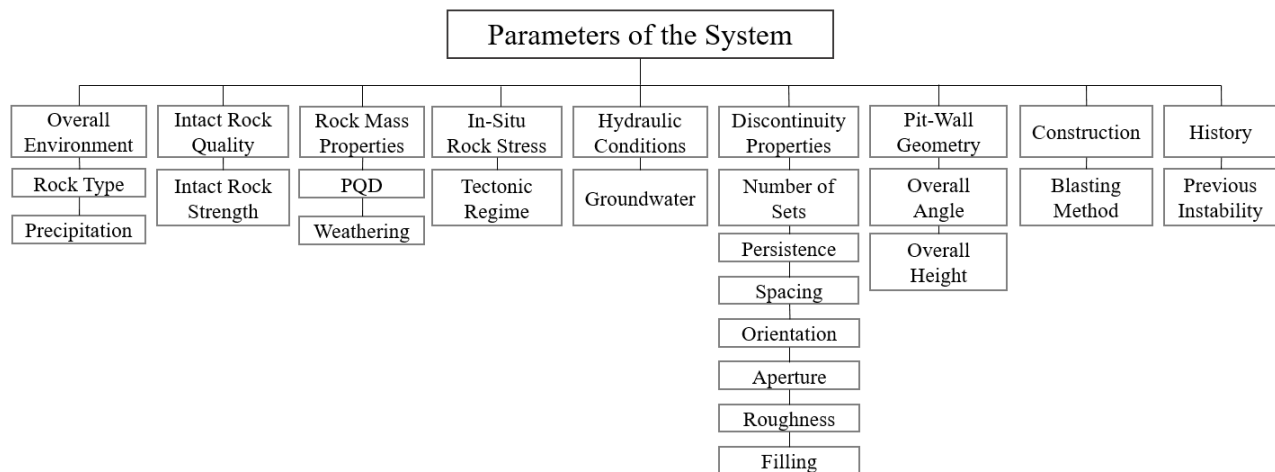


Figure 2.10 The selected categories and principal parameters for the system (modified from Naghadehi et al. 2013)

Some basic factors influencing the stability of open pit walls include:

- the geology of the deposit and the wall material;
- the tectonic regime;
- the shear strength of the wall material and the planes of weakness;
- the influence of groundwater; and
- the method of excavation.

The open-pit design has to be preceded by determining the unique geological, hydrogeological, and geotechnical conditions associated with each deposit and which needed to be determined to an appropriate level of detail. The scope of any geotechnical investigation is a balance between the geological complexity (i.e., tectonic, hydrogeology, different types of soil and rock material) and economic considerations (i.e., cost of investigations). All geotechnical

investigations involve accepting some uncertainty level that must be reflected in the final pit design and later adopting an appropriate slope monitoring program.

2.2.3.1 Geology and weathering

The geology and weathering and/or alteration profile will control the variation in rock strength or competence of the intact rock substance. The level of detail required for the investigation of these factors should vary depending on the complexity of the geological conditions and the scale and duration of the mining operation. Rocks and indurated soils are subject to strength loss due to weathering, which involves various physical disintegrations, chemical decompositions, and biological activity (Mitchell, 1993; Duncan et al., 2014). Physical processes break the strong soil or rock into smaller pieces, and the chemical and biological processes change it into material with fundamentally different properties. Weaker soils are also subject to weathering effects but may become stronger rather than weaker (Mitchell, 1993). Weathering and alteration can result in significant lateral and vertical variability in strength and the presence of material prone to slaking, swelling, or progressive degradation. The weathering effect increases if there are planes of weakness or discontinuities, such as foliation, joints, faults, and shears in both the ore and the wall materials.

2.2.3.2 Type and material properties of soil or rock

Experience suggests that lithology or soil/rock type influences slope failure. For a slope to fail, the shear stress acting on the slope mass must exceed the shear strength of the slope material along the failure plane. The shear strength of the material is usually expressed by the Coulomb equation (Eq.2.1), which is a linear combination of both cohesion and tangent of friction as follows (Singh and Ghose, 2006):

$$\tau = c' + \sigma' \cdot \tan \varphi' \quad \text{Eq. 2.1}$$

where τ is shear strength, c' is the effective stress cohesion intercept, σ' is the effective stress normal to the plane of failure ($\sigma - \alpha u_w$), and φ' is the effective stress friction angle.

Therefore, shear strength parameters of slope material are important properties for stability evaluation of the open pit mining slopes.

2.2.3.3 Groundwater regime

The high groundwater level is the most frequent reason for increased pore pressures and associated decrease in effective stresses within slopes (Eq. 2.1). Weighty rainfall or problems with the dewatering system of the open pit can be a rise in groundwater levels and more adverse seepage. All types of soils and fissured rocks are affected.

Bye and Bell (2001) studied the effect of saturation on the different joined materials. The research proves that the joints showed significant water flow after heavy rainfall, which reduces the slope stability (Figure 2.11). Water tends to flow along such joints after heavy rainfall.

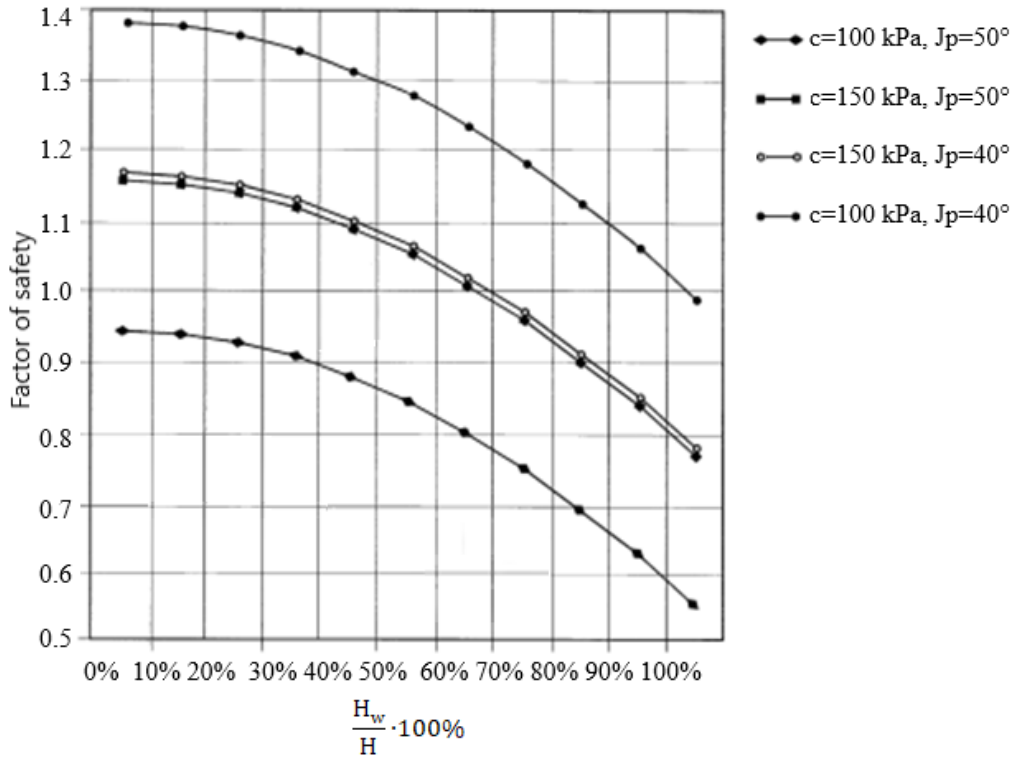


Figure 2.11 Relationship between the FS and jointed rock mass saturation (c=cohesion (kPa), Jp = joint angle (°), H= slope height, H_w = height of the water table in the slope)
Note: the term saturation 100% saturation indicates the water table location at the surface.
Input parameters: $\gamma=29 \text{ kN/m}^3$, $\gamma_w=10 \text{ kN/m}^3$, $\phi=32^\circ$, $H=30 \text{ m}$, $\beta=69^\circ$, no tension crack
 (reprinted from Bye and Bell, 2001)

The length of time required for the pore pressures to change depends on the material's permeability (or hydraulic conductivity). In soils or rocks with high permeability, changes in groundwater conditions can occur rapidly, and in soils/rocks with low permeability, changes are slow.

2.2.3.4 Open pit wall geometry

The typical geometry of an open-pit mine slope is shown in Figure 2.1. Overall slope angle plays an important role in open pit slope stability design. According to the statistics, slope failure would be more frequent on steep slopes in open pit mining. To decrease the overall slope angle

and optimize the highwall geometry, the benching technique is used. The typical slope angles that cut with different excavating equipment are outlined in Table 2.4.

Table 2.4 Typical bench slopes produced by excavating equipment in open pit mining
(reprinted from Singh and Ghose, 2006)

Equipment type and mode of operation	Slope angle	Equipment type and mode of operation	Slope angle
Dragline With key cut Without key cut Forecut Crosschop with key cut Crosschop without key cut	60-80° 70-80° 70° 60-80° 90°	Bucket wheel excavator Dropcut, digging face only Dropcut, highwall Terrace cut, digging face Terrace cut, highwall	90° 45-70° 60° 50-70°
Stripping shovel	70-80°	Loading shovel, standard crowd	60-80°
Hydraulic excavator Shovel Backhoe	45-90° 30-90°	Tractor-scraper Conventional Tandem powered with rip dozer at toe	<30° <40° <40° <90°

Overall slope height also affects slope stability. Rock blocks in higher slopes have more potential energy than rocks in lower slopes; thus they present a greater instability hazard and are more failure prone. In addition, the stress levels are higher around the slopes in deeper pits (Singh and Ghose, 2006).

Excavation that makes a slope higher or steeper will increase the shear stresses in the material within the slope and reduce stability.

2.2.3.5 External factors

The following external factors that control the stability open pit slopes are as follows (Singh and Ghose, 2006):

1. Effect of blasting.

2. Effect of time.
3. Surface mining above underground excavation.
4. Effect of surcharge loading conditions.

Blasting is a common method of ground preparation for hard overburden in open pit mining operations. Blasting includes artificial seismic effects. The short-wavelength high-frequency vibrations are developed due to the propagation of a detonation wave through the surrounding rock. The man-made seismic loads due to blasting may impose dynamic loads on the soil or rock slope and decrease its FS, leading to instability.

Most of the factors affecting the stability of the surface mining slopes are time-dependent. The first phase of open-pit mine development (stripping) advances rapidly, but delays in the deeper excavations generally increase the PoF due to a decrease in peak strength parameters with time. Also, most open pits have a dewatering system, and the rate of change of pore water pressure in the excavated slope has an important role in the stability of the slope. Another time-dependent factor is the development of the weathering on the slope.

Figure 2.12 shows the possible surcharge loading by static and dynamic loading of the surface mining slopes due to traffic of heavy mining machinery. The dynamic load of the moving traffic may decrease the FS of the marginally stable surface mining slope and induce slope failure, especially where the stability condition is aggravated by pore water pressure. In many mine-sites the surface land is so restricted that the boundary of lagoons or ponds may lie in the closeness of the excavated slopes. The weight of the dam and wastewater leaking from the pond onto the mining slope may increase the pore water pressure and decrease the overall stability of the excavated slope (Singh and Ghose, 2006).

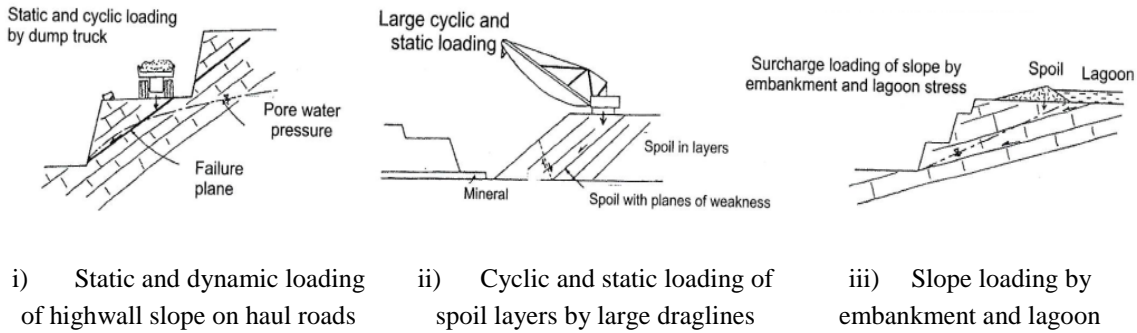


Figure 2.12 Loading of a mining slope (reprinted from Singh and Ghose 2006)

2.3 Available slope stability software

Open pit mining slope stability analysis today can be performed by using various computer based geotechnical software. The computer programs help guide judgment on the solution to any types of slope problem. It is important that engineers understand the limitations of each method and the significance of choosing one method over another, based on the available initial parameters and required final results. Different software can be applied to distinguish between problems of high risk and problems of low risk, consider soil or rock and groundwater conditions, and appreciate the importance of slope geology.

The different software is based on the stability methods that can broadly be classified as the limit equilibrium methods and numerical methods (the finite element method and the finite difference method). Limit equilibrium methods are the most commonly used methods for slope stability analysis. Even though some literatures states that using the finite element method slopes can be analyzed with better accuracy. With the rapid development of computer hardware and numerical software, not only 2D but also 3D slope analysis is now available for different problems.

In order to be effective for practical geotechnical design a computer program for slope stability analysis utilizing the LEM approach should be offered (Oliphant and Horne, 1992).

- The analysis of circular and non-circular slip surfaces for drained and undrained conditions.
- A number of limit equilibrium methods to allow comparison of results.
- Features that allow the checking of input data and make the program easy to use.
- The facilities to model a variety of external loadings, soil stratification, submergence, common boundary conditions, soil and groundwater conditions.
- Good supportive documentation.
- Flexibility of use to allow the engineer to exercise proper engineering judgement.

In recent years, FE and FD methods are becoming increasingly popular and its application is spreading. Since the numerical methods are based on compatibility relationships, and thus can handle the stress-strain behavior of slope material, a more realistic stress situation can be computed (Aryal 2006). The effective FEM and FDM software should offer:

- Should be applicable for soil and rock materials.
- Should be used for a range of engineering projects including excavation design, slope stability, groundwater seepage, probabilistic analysis, consolidation, and dynamic analysis.
- Can effectively analyze both simple and complex problems for a variety of surface shapes, pore-water pressure conditions, soil properties, and loading conditions.
- Support a comprehensive list of failure criteria and material models, including Mohr-Coulomb, undrained, anisotropic strength SHANSEP, spatial Mohr-Coulomb, Drucker-Prager, Generalized Hoek-Brown, and Cam-Clay among others.
- Different options for boundary conditions (displacement and stress boundaries) and meshing (for 2D: 3- and 6-noded triangles, 4- and 8-noded quadrilaterals; for 3D: 4- and 10-noded tetrahedras).

Summary of commercially available slope stability software based on the different approaches is presented in Table 2.5. Software examples presented in the table can be used in civil engineering and open pit mining slope stability assessment.

Nowadays, slope stability computations are the most effective method using in open pit design. Computer analysis can be accomplished quickly when suitable software is available (Duncan 1996). Modern slope stability software can accommodate complex conditions of site geometry, groundwater conditions, and shear strength. Slope stability analysis can be performed using advanced LEM methods that satisfy all equilibrium conditions, and they can be used to perform thorough analyses to locate the critical slip surface. The slope stability calculations can also be performed using different numerical methods (e.g., FEM, FDM), which can model the stress-strain behavior of slope material (Krahn 2003, Aryal 2006).

However, slope stability computations must be checked and verified before the results can be relied upon in the slope design. Analyses can be checked using charts, manual calculations for the critical slip surface, and independent analysis with another slope stability software using independent input (Duncan 1996, Rocscience 2021). Common sense and engineering judgment must always be used to ensure that analysis conditions and results are reasonable.

Table 2.5 Summary of commercial slope stability software available for open pit mining design (adapted from Stead and Wolter 2015)

Modelling Technique	Advantages	Limitations	Examples of the software
Limit-Equilibrium	<ul style="list-style-type: none"> – Utilizes the routinely used method of slices (Bishop (1955), Janbu (1968), Spencer (1967), Sarma (1973), Morgenstern-Price, GLE), which are based on satisfying force and/or moment equilibrium – Some software offers both deterministic and probabilistic approach – The spatial variability option is also can be incorporated into the software – Possible to include influence of groundwater table 	<ul style="list-style-type: none"> – The failure surface has to be pre assumed. – The concept of slices requires assumptions about slice side forces. – Slope modeling mainly contained 2D, and only a few software developers offer a 3D option. 	Slide2, Slide3 SLOPE/W Visual Slope SVSlope TSlope UTexas GEOSTASE
Finite-Element	<ul style="list-style-type: none"> – Utilizes SRM approach – Automatic determination of failure mechanisms with no prior assumptions regarding the type, shape, or location. – Different failure surfaces can occur at the same time – The FE method preserves global equilibrium until ‘failure’ is reached. – Indicates the stress and strain distribution within critically unstable failure zones, element displacement vectors and the plastic state of slopes – Possible to include influence of groundwater 	<ul style="list-style-type: none"> – Requires modelling experience – More soil parameters are required compared to LEM approach – Polygon size may influence kinematics of moment – Long model run times for larger-scale problems, especially for 3D problems, which may not be feasible in some cases 	PLAXIS 3D/2D SIMULIA Abaqus RS2, RS3 SIGMA/W

Modelling Technique	Advantages	Limitations	Examples of the software
Finite-Discrete	<ul style="list-style-type: none"> – Utilizes SRM approach – Automatic determination of failure mechanisms with no prior assumptions regarding the type, shape, or location. – Different failure surfaces can occur at the same time – Simulates intact rock fracture in rock slopes from continuum to discontinuum (Stead and Wolter 2015) – Possible to include influence of groundwater 	<ul style="list-style-type: none"> – Requires modelling experience – More soil parameters are required compared to LEM approach – Long model run times for larger-scale problems, especially for 3D problems, which may not be feasible in some cases 	FLAC, FLAC3D

2.4 Overview on slope monitoring systems

The slope stability monitoring in open pit mining operations is a critical task. Slope monitoring is necessary to ensure that the open pit slopes are safe and movements are within acceptable limits. Effective monitoring of open pit walls is an integral part of ground behavior characterization and risk management. Various instrumentation methods can be employed to measure and monitor ground movement and subsidence at open pit mines. A comprehensive monitoring system is being implemented, and data gathered helps provide a rational basis for evaluating stability conditions. In other words, a record of displacement data can be used to help predict the behavior of a potentially unstable slope.

Monitoring slope movement has proved to be the most reliable method for detecting slope instability. The more accurate the measurements, the earlier the developing problem can be detected. Tools for slope displacement are well developed and used routinely on most large open pit mines. These tools are generally based on observations of numerous targets placed at carefully selected locations on the open pit benches. Global positioning by satellite (GPS) systems is used to monitor these targets' relative positions on a regular basis. High-quality GPS systems can provide an accuracy of less than 1 cm over measuring distances of 1 km or more. This order of measurement accuracy is generally sufficient to warn of most slope-stability problems (Hoek et al. 2005).

In open pit mining, large slope failures are preceded by measurable displacement. Once unusual movements have been observed, almost 35% of all failures occur within three months and 75% within one and a half to two years (Sullivan 1993, Szwedzicki 2001). However, there are some mine slopes that have been in an advanced stage of movement for decades. In regard to rock mass failure in open pits Call et al. (2000) noted that:

- Slope failures do not occur spontaneously. A rock mass does not move unless there is a change in forces acting on it. The common factors that lead to instability in an open pit are removal of support by excavation, increased pore pressure, and earthquakes.
- Analysis of documented case studies of large-scale rock mass failures indicates that collapse doesn't happen without warning. Prior to a major movement, measurable deformation and other observable phenomena occur from hours to years before major displacements.

According to Sjoberg (1996), failure occurs when the loads or stresses acting on the rock material (intact rock or discontinuity) exceed the strength (compressive or tensile) of the rock. Failure could also occur through the distressing of the rock. In the case of an open pit, slope failure can occur when the construction element has exceeded its capacity to carry more of the loads and forces acting upon the slope.

Slope failure is both a safety and business risk to an open pit mine. It can have devastating consequences such as loss of production, damage to equipment, injury to personnel, and most serious of all, loss of life. High insurance premiums, loss of reputation, and legal action are other impacts that could arise out of a serious slope failure. According to Lynch et al. (2005), it is important to carefully monitor especially high and/or steep slopes for indications of impending failure in open pit mining. Nowadays, many high slopes are being designed with a managed risk approach, in which slope failures can be tolerated as long as miner safety is not compromised.

The main aim of the open pit monitoring is to establish a network of points distributed on the surface of the wall, which is monitored regularly to follow critical rates of change in ground motions. With continuous monitoring of creep and acceleration of the rock movement, a warning can be given to evacuating equipment and personnel in advance of a failure. In order to perform such tasks, a dense grid of hundreds of targets to be continuously monitored with accuracies of up

to ± 5 mm with 95% confidence level have been requested (Bond et al. 2005). Another challenge that can be faced is that the slopes of the open pit are moving during the design life. Thus the equipment has to be removable. At the same time, the monitoring points situated in pits can be up to several hundred meters deep and may cause limitations in the observability of the full available equipment (Tsakiri and Stewart 2000, Bond et al. 2005).

Determination of the failure mechanism is one of the most important tasks of open pit slope design. The soil or rock mass of each slope has unique characteristics and the scale of the operation. The following factors can be considered as factors affecting the stability of the slope: the geological and geotechnical conditions, material resistance, groundwater level, and the height of the open mine wall. An important issue after the design phase is continuous measurements of the parameters needed to examine the stability of the open pit slopes. Thus, slope stability is one of the major issues throughout open pit mine life. (Sjoberg 1996, Kayesa 2006, Read and Stacey 2009, Osasan 2012, Abzar 2019).

One of the most important and beneficial slope stability management tools is slope monitoring. Well-performed monitoring of the slopes of surface mines can prevent loss of life, equipment, production, and possibly the loss of the mine (Cawood and Stasey 2006). The main objectives of slope stability monitoring are (Sjoberg 1996, Angeli et al. 2000, Galperin 2003, Eaton 2001, Kayesa 2006, Dunnicliff et al. 2012):

1. To verify mine design. Slope monitoring measurements usually can be used to maintain, steepening or reduce slope angles with the resultant economic and safety benefits. Slope monitoring measurements can also be used as a basis for future mine designs.
2. To give technical assurance to production and management officials on the stability status of the open pit mine.

3. To maintain safe operational practices.
4. To serve as a warning system as to which areas of the pit are unstable. Monitoring provides sufficient warning to clear personnel and equipment from the crest and toe areas if necessary (Bingham Canyon example).
5. To identify the geometry of the moving mass with precision. To quantify the principal kinematic parameters (velocity, acceleration, etc.) and their possible correlation with geotechnical, hydrogeological, and climatic characteristics.
6. To give measurements of movement rates in the unstable zones and correlate them to the critical movements obtained with analytical calculations. A well-documented performance history of slope movements helps change the open pit's excavation and operating status.
7. To serve as a major slope stability risk management tool. Slope failure can have serious economic consequences on an open pit mine. Therefore slope monitoring is an essential basis for making management decisions for the safety of workers and equipment.
8. To determine the groundwater level during the design life of the open pit.
9. To provide additional geotechnical information regarding slope behavior.

Another important issue is to evaluate the experience-based slope and develop a geotechnical database for easy access by anyone on mine site. As part of the ground control management program, evaluation of the historical slope performance is required. The design process that involved the historical slope performance can be seen in Figure 2.13.

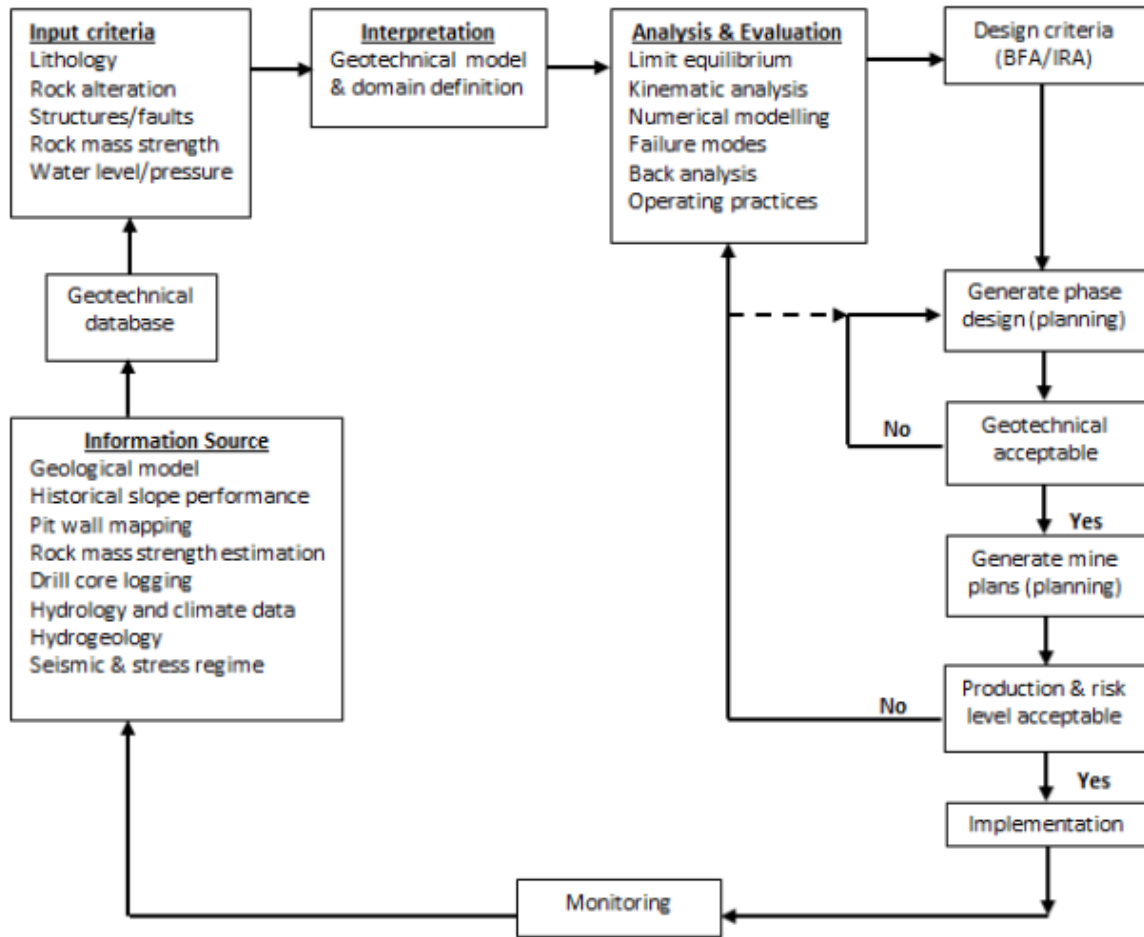


Figure 2.13 Pit slope design flow diagram (reprinted from Lelono et al. 2016)

2.4.1 Methods of monitoring systems for open-pit mining

Sufficient failure management and monitoring is an essential part of both the prediction of new and management of existing open pit slope failures. Unexpected open pit slope failures not only represent a significant hazard to personnel and equipment, particularly when they are located adjacent to current mining activities or main access ways like haul roads but may also have significant economic consequences (e.g., failed material may need to be removed, mining activities may be disrupted, etc.). Monitoring should be based on identifying potential problem areas for

failure before the event and managing active failures to minimize hazards associated with unexpected movements (Chappel 1998).

This chapter presents an overview of available and currently practiced slope monitoring techniques with their advantages and limitations. According to many authors (Sjoberg 1996, Read and Stacey 2009, Wessels 2009) monitoring in an open pit should not only concentrate on surface movement, but systems should also be installed to monitor sub-surface movements. The timely collection and interpretation of the data, followed by distribution of the results, forms the complete slope monitoring system. Displacement measurements are the most common type of monitoring, complemented by monitoring of groundwater pressure and microseismic monitoring (Sjoberg 1996). There are numerous case studies available and various authors that have described monitoring systems for open pits. The details of the monitoring systems described below are a compilation of descriptions by Call and Savely (1990), Sjoberg (1996), Girard (2001), Cawood and Stacey (2006), Little (2006), Wessels (2009), Lacasse and Nadim (2009), Dunningcliff et al. (2012), Osasan (2012), Vinoth et al. (2016).

Until the early 1980s, deformations of engineering structures were carried out by visual inspections and determined using traditional measurement techniques. The development of modern technology and computers have produced more sophisticated monitoring equipment that requires less personnel to perform the observation. In the past few decades new equipment has become available which is ideally suited to slope monitoring in a mining environment and also for critical natural slopes (Cawood and Stacey 2006). Such equipment is seismic monitoring (Stacey et al. 2004), laser monitoring (Lichti et al. 2002, McIntosh and Krupnik 2002), radar monitoring (Groundprobe 2012) and satellite monitoring (Kaab et al. 2002). Usually the type of instruments selected for a slope monitoring program depends on the particular problems to be monitored

(Cawood 2006). Some of the most common monitoring techniques and equipment are profiled below.

Based on Chappel (1998) open pit slope failures monitoring and management involves five major types:

a. Conventional monitoring.

Berms above actively mined areas should be inspected on a weekly basis for signs of movement. When mining activities are situated immediately below a pit slope then these slopes should be inspected on a daily basis. When movement is identified then features should be mapped, photographed and have the appropriate movement monitoring installed. Final berms should also be photographed. Failures and features associated with movement (cracks, scarps, etc.) should be photographed for future reference and comparison. Photos should be catalogued according to location and date of photo, for easy retrieval and future reference.

b. Movement monitoring (crack pins, survey prisms, inclinometers, etc.).

Crack pins provide a relatively crude method for monitoring failure movements but are cheap, and information can be collected rapidly. Survey prisms are much more accurate than crack pins and, while more expensive, have several advantages. Prisms will detect movement that may not be detectable by visual observation or crack pins. Prisms should be installed on failures and areas of the pit slope which are difficult/and or hazardous to access, to monitor movements. Inclinometers should be installed on large deep-seated pit slope failures (failure surface >50 m deep) at an early stage to supplement other data and identify how and which areas of the main failure block are moving. Data from inclinometers will supplement other movement monitoring data so that the most appropriate remedial measures may be undertaken (toe buttressing, dewatering, head unloading, etc.)

c. Hydraulic monitoring.

Precipitation records should be kept to correlate with piezometric records and movement records so relationships between rain and groundwater response and precipitation and movement rates of failures may be established. Piezometers should be monitored to assess groundwater levels in the slope and effectiveness of horizontal drainage as it is installed and correlate with both movement and rainfall records. Horizontal drains should be monitored for flow rates and correlated with piezometric records to assess the effectiveness of slope depressurization.

d. Operational monitoring.

Ground vibrations associated with blasting at the mine may affect failure movements. Records and locations of major blasts should be kept to correlate with movement rates of failures (particularly those situated immediately adjacent to blasts). Excavation records should be kept to correlate between excavation and development of failure.

e. Warning monitoring.

Wire extensometer alarm system (Figure 2.16) should be installed on active failures located above open pit mining activities, which are triggered after a predetermined movement threshold is exceeded so that access is restricted beneath failures until visual inspections can verify the safety of the failure.

An example of the alarm and response system is presented below. Illustration of the alarm levels as function of displacement velocities is presented in Figure 2.14. On the vertical axis the displacement rate in mm/day and on the horizontal axis is the relative time before failure. Example of the open pit movement thresholds is presented in Table 2.6. The displacement limits are usually set based on the experience and early monitoring data and may vary from mine to mine. Each slope has a unique geometry, rock mass conditions and structural setting. Therefore, the threshold

criteria are very site specific, even slope specific. Table 2.7 presents the example of alarm levels and actions for the warning system at the open-pit mine.

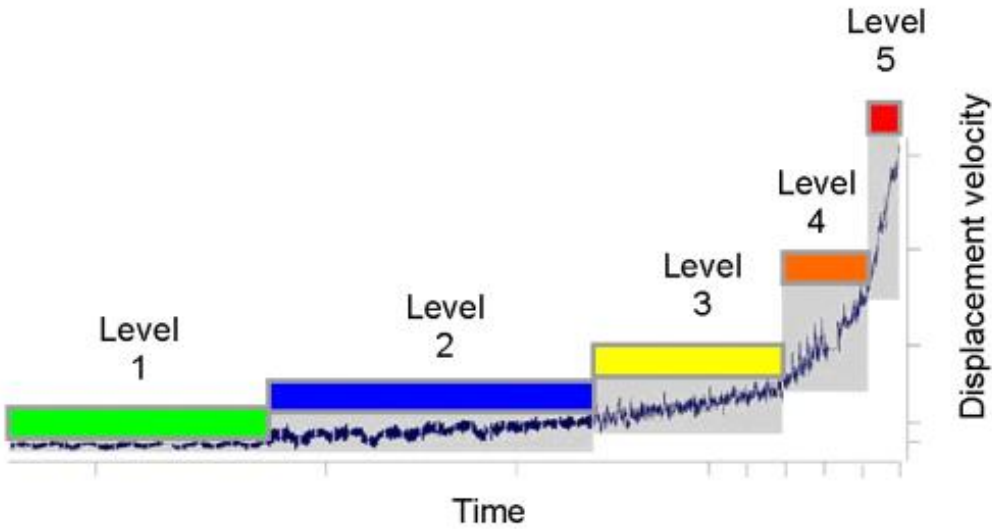


Figure 2.14 Alarm levels as function of displacement velocities (reprinted from Nadim and Lacasse 2008)

Table 2.6 Example of the open pit movement thresholds (reprinted from Nanoo et al. 2016)

Movement rate (mm/day)	Response
0-15	Normal
15-25	Caution
25-50	Alert
>50	Suspend production
<50	Resume mining with restrictions

Table 2.7 Alarm levels and actions for the warning system (modified from Nadim and Lacasse 2008)

Alarm level	Activities and alarms	Response
Level 1 Normal situation	Minor seasonal variations. No alarm	Technical maintenance
Level 2 Awareness	Important seasonal fluctuations for individual and multiple sensors. Values < excess thresholds for Level 2	Increase frequency of data review, compare different seasons
Level 3 Increase awareness	Increase displacement velocity, seen on from several individual sensors Values < excess thresholds for Level 3	Do continuous review, do field surveys.
Level 4 High hazard	Acceleration displacement velocity observed on multiple sensors. Values < excess thresholds for Level 4	Increase preparedness. Continuous data analysis. To start preparing for production suspension.
Level 5 Critical situation	Continues displacement acceleration. Values > excess thresholds for Level 4	Suspend production

The techniques available for slope monitoring can be divided into three main groups: (i) conventional methods, (ii) surface, and (iii) subsurface measurements. In the first category one finds visual inspection and tension crack mapping. Surface measurement method includes surface wire extensometers, digital photogrammetry, survey network, global positioning system, non-reflective LiDAR, slope stability radar. Extensometers, inclinometers, piezometers, failure indicators, time domain reflectometry and microseismic monitoring are the part of subsurface measurements.

Figure 2.15 presents a simplified classification of available slope monitoring techniques modified.

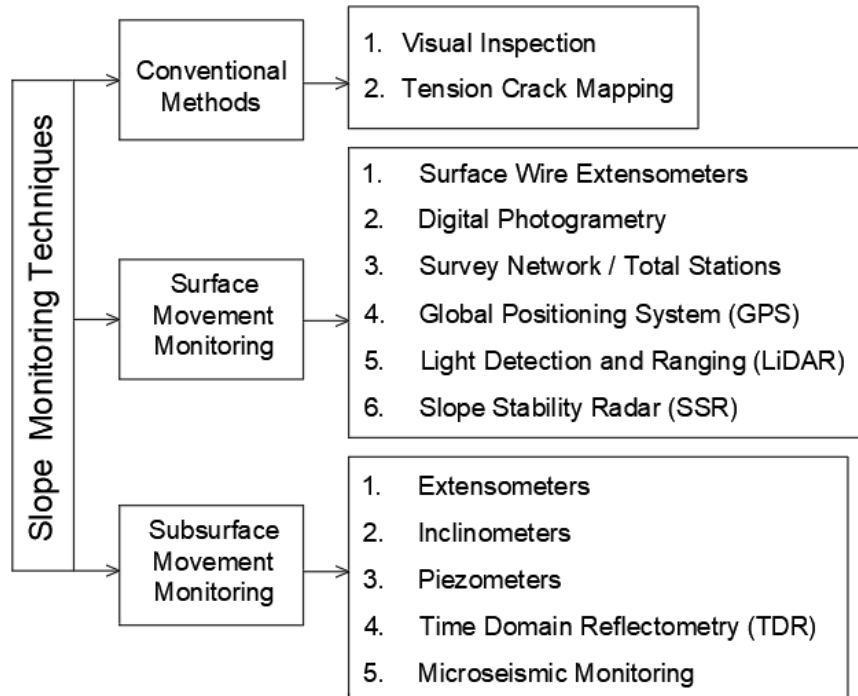


Figure 2.15 Methods of monitoring systems for open-pit mining (modified from Sjoberg 1996, Girard 2001, Lacasse and Nadim 2009, Osasan 2012, Nunoo et al. 2016)

2.4.2 Conventional monitoring

The conventional techniques include manual inspection and mapping of tension crack along the slope face. These methods chiefly utilize manual supervision for slope monitoring. These methods are routinely practiced for the slope stability assessment on a daily basis from early days. Conventional geotechnical instrumentation and survey options will continue to have their place in slope monitoring, in complement with the latest monitoring systems (Cawood and Stacey 2006).

2.4.2.1 Visual inspection

All mines routinely use visual walkover inspections. The Code of Federal Regulations and The Federal Mine Safety and Health Act of 1977 place a requirement upon operating mines that all work shall be carried out without undue risk to the health or safety of any person (see, e.g., 30 C.F.R §§56.1-56.20014). The Mine Safety and Health Administration (MSHA), Title 30 of the

Code of Federal Regulations, Section 56.3130 requirements for open pit slopes demand that adequate benches must be in place to retain rockfall above work or travel area

Section 56.3131 of the Code states that in places where persons work or travel in performing their assigned tasks, loose or unconsolidated material shall be sloped to the angle of repose or stripped back for at least 10 feet from the top of the pit or quarry wall. Other conditions at or near the perimeter of the pit or quarry wall which create a fall-of-material hazard to persons shall be corrected. At a minimum, visual monitoring of the pit walls is implied by this statement. Section 56.3401 of the Code states that highwalls and banks adjoining travel ways shall be examined weekly or more often if changing ground conditions warrant. An initial assessment of open pit slopes requires a visual inspection.

Visual monitoring is an important component of a pit wall monitoring program. Typically, some instrumentation is used in addition to visual monitoring. According to Nunoo et al. (2016), visual monitoring is necessary but not necessarily sufficient to meet the needs of an appropriate pit wall monitoring program. A visual monitoring program should be restricted to low-risk pit walls and have the following attributes:

- written standard procedures including frequency of observations, personnel responsible (experienced in examining and testing for loose ground), areas of concern, visual cues, record keeping, etc.
- written documentation and a photographic record, and
- should be re-evaluated if significant instabilities are observed or anticipated.

Visual inspections focus on identifying features such as tension cracks and revealing of materials from the pit walls. Mine operations personnel working in the pit typically watch for unusual or potentially unsafe pit wall behavior evidence. Geotechnical engineers, mining

engineers, and technicians (in some operations) generally perform formal inspections. However, some of the mines have implemented formal hazard recognition programs so that other mine personnel can assist with visual monitoring to provide more comprehensive monitoring. Photographs are usually taken as part of the visual inspection record. Records of visits and observations of any changes in the rock mass behavior over time are recorded. The occurrence of soil or rock falls or the presence of new instabilities or cracks generally triggers the need for more formal and more frequent visual inspections and often leads to the implementation of other monitoring techniques.

The frequency of the visual inspection depends on the soil or rock mass conditions and the risk associated with the slope instability. Typically, in the US mines conduct a formal visual inspection on a weekly basis (30 C.F.R §§56.3401). However, informal monitoring is performed by all personnel working in the open pit continuously.

2.4.2.2 Tension crack mapping

One early obvious indication of slope instability is the development of tension cracks. By systematically mapping these cracks, the extent of the unstable area can be established (Call and Savely 1990). According to Girard (2001), measurement and monitoring of the changes in crack width and direction of crack propagation are required to establish the extent of the unstable area. Girard (2001) suggested that observed cracks should be painted or flagged for easy detection of new cracks or propagation along existing cracks during routine inspections and to notify mine personnel of the risk in such areas. Crack measuring pins located on both sides of the crack are used for measuring tension cracks. The displacement of the crack is determined by measuring the distance between the pins with a measuring tape or a vernier caliper (Hawley et al. 2009). Commercial crack gages with electrical readout are also available, but often in the case of mine

slope problems, the racks exceed the measurement limits of the instruments (Girard 2001). But no matter what method is selected to measure crack displacement, the devices should be marked with dated installation and show the magnitude and direction of the movement. Tension crack mapping should be taken at regular time intervals.

On the one hand, tension crack mapping is a simple method that provides some information on the degree of instability and its location. On the other hand, this method does not give a quantitative measure of the amount of instability (Sjoberg 1996).

2.4.3 Surface measurements

2.4.3.1 Wireline Extensometers

Another common method for monitoring movement across tension cracks is with a portable wire-line extensometer (Figure 2.16). The most common setup comprises a wire anchored in the unstable portion of the ground, with the monitor and pulley station located on a stable portion of the ground behind the last tension crack. The wire runs over the top of a pulley and is tensioned by a weight suspended from the other end. As the unstable portion of the ground moves away from the pulley stand, the weight will move, and the displacements can be recorded either electronically or manually (Girard 2001, Osasan 2012, Vinoth et al. 2016). Electronic monitoring equipment can be programmed to set off alarms if the displacement reaches certain threshold limits (Figure 2.17). According to Sjoberg (1996), wire extensometers are easy to use and can be moved from one location to other unstable areas but do not provide the long-term monitoring of a survey network. Another flaw of the equipment is the length of the extensometer wire which is limited to approximately 60 m to keep the errors due to line sag at a minimum (Call and Savely 1990; Girard 2001). Long lengths of wire can lead to errors due to sag, so readjustments and corrections are often necessary. Some extensometers are sensitive to movements of 1 mm, so simultaneous

temperature readings should be taken to adjust for the thermal expansion of the wire. Birds and animals can be a source of a large number of false alarms and wildly inaccurate readings. Provisions for keeping the wildlife away from the instrumentation should be made at operations where this may be an issue (Girard 2001).

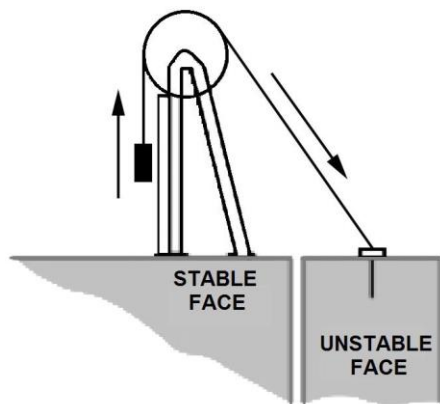


Figure 2.16 Scheme of typical Wireline Extensometer (reprinted from Girard 2001)



Figure 2.17 Wireline extensometer (photo from a public source <https://www.cnitucson.com/>)

2.4.3.2 Digital Photogrammetry

Photogrammetry uses overlapping photographs to create 3-D surfaces over which an image is draped or from which measurements are made (Haneberg 2008). The use of digital photogrammetry is the most common and simple remote sensing technique to identify rock movements. The objective of digital photogrammetry is to identify the wide displacement behavior of a target inferred by the comparison of photographed images using a digital camera (Ohnishi et al. 2006, Vinoth et al. 2016).

Figure 2.18 shows the main principle of digital photogrammetry in graphical. In the figure, the geometrical relations between a measurement point, the camera, and the measurement point's

imagery appearing on the image taken are shown. The image plane is equivalent to a film of the camera. A digital camera uses electric sensing devices in place of the conventional film.

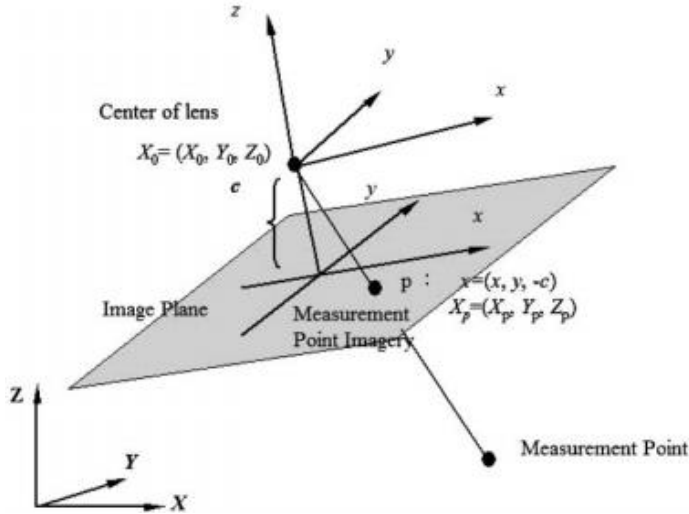


Figure 2.18 Concept of digital photogrammetry (reprinted from Ohnishi et al. 2006)

The object is on the x–y–z ground coordinate system. The light from measurement point P on the object goes through the center of lens X0 and focuses into imagery p. Considering the geometrical relation between these elements, the measurement point, lens, and imagery align with each other. Such a relation is called the central projection. Based on the similarity of triangles, the relation between the measurement point’s coordinate P, namely $X_v=(X_v; Y_v; Z_v)$ and that of imagery p, namely $x=(x; y; -c)$ on the camera coordinate system, can be expressed by Eq. (2.2) below using focal length c:

$$x = -\frac{c}{Z_p} X_p \quad \text{Eq. 2.2}$$

When an object is photographed from two different locations, different lines of sight from each location are obtained. The lines of sight for the object from each location are intersected mathematically to produce a three dimensional image of the object. Using such a technique, it is possible to construct a three dimensional image of the object from different two-dimensional

images (Kumar and Villuri 2015). Thus, digital photographs (Figure 2.19) help to estimate the geometric properties of the objects (Shape and Position), location, progress, extent and cause of slope deformation (Little 2005, Ohnishi et al. 2006, Firpo et al. 2011, Vinoth et al. 2016).

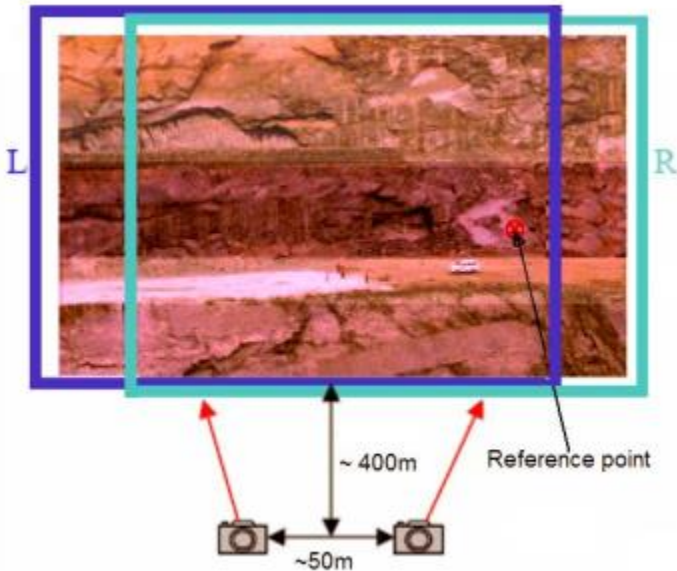


Figure 2.19 Scheme of Digital photogrammetry (reprinted from Vinoth et al. 2016)

Recent developments in the method have provisions for the generation of 3D models from terrestrial photographs (Sturzenegger and Stead 2009, Vinoth et al. 2016). The digital image processing techniques available nowadays offer the possibility of gathering discontinuities and associated information automatically, thereby reducing the chance of human biasing (Vinoth et al. 2016). The method has the ability to survey inaccessible areas. High rock faces in rapid time, providing remote characterization tool for rock slope practitioners, thereby making a permanent record of the status of the slope for future reference (Ohnishi et al. 2006, Haneberg 2008, Sturzenegger and Stead 2009, Kumar and Villuri 2015, Vinoth et al. 2016).

2.4.3.3 Survey network

The use of total station surveying instruments for monitoring structures movement with good results was reported by many authors, such as Teskey and Radovanovic (2001), Hill and Sippel (2002), Kuhlmann and Glaser (2002), Zahariadis and Tsakiri (2006). A survey network consists of target prisms placed on and around areas of anticipated instability on the pit slope and instrument stations from which distance and angles to the target is measured regularly to establish a movement history (Call and Savely 1992, Sjoberg 1996, Girard 2001). The relative movements of the target prism at the monitoring points will help identify the deformation and critical failure zones in advance utilizing the movement of prisms (Figure 2.20 and Figure 2.21). For a survey network to function properly, the base station must be located on completely stable ground, but at the same time close enough to the pit crest so that all prisms can be seen (Sjoberg 1996, Girard, 2001). Up to the beginning of the 21st century, triangulation with theodolite was used (Husrtulit and Boisen 1992). Nowadays, surveying robots are used for the open pit slope monitoring because they relieve personnel from repetitive around-the-clock measurements. According to Afeni and Cawood (2013), the monitoring frequency depends on the nature of the rock type, operations around the slope, and the objectives of the monitoring program in place. For slow-moving slopes, the measurements may be taken every few weeks or even months. An automated system should be set up to take more frequent readings at pre-set intervals for a potentially rapidly moving slope.

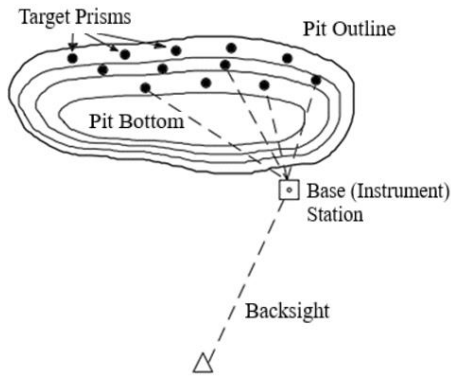


Figure 2.20 Survey network for open pit slope monitoring (modified from Sjöberg 1996)

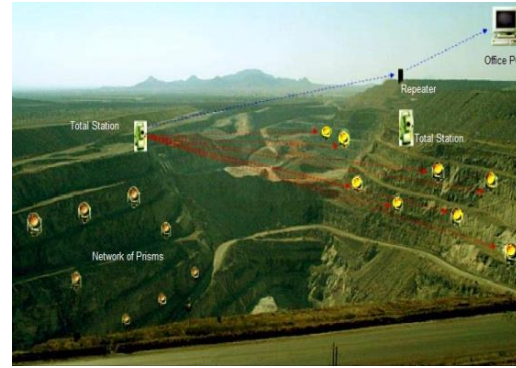


Figure 2.21 Network of Prisms and Automatic Total Station (reprinted from Vinoth et al. 2016)

There are some flaws in using the survey networks, and manufacturers generally publish the accuracy and error limits of the equipment. Dunncliff (1988), Sjöberg (1996), Ding et al. (1998), Girard (2001), and Newcomen et al. (2003) mentioned climatic conditions such as wind, snow, rain, dust, and atmospheric variations as contributing factors to total station survey errors. Although these factors cannot be controlled, their effects on the accuracy of the survey can be reduced. Some problems can be connected to the damage to the prism or displacement of the survey station, which may need to be replaced. More so, some new prisms should be installed as the open pit is being deepened. The installation or relocation of the monitoring prisms could cause monitoring interruption with continued mining and extension of the slope face. Human error and errors introduced by instrument or reflector setup inaccuracies can equally affect measurement accuracy.

On the other hand, one of the major advantages of the method is that survey networks are probably the most cost-effective monitoring method. The other pros for using this method on a routine basis is that monitoring with the help of a survey network is performed continuously. According to Alfeni and Cawood (2013), the use of the total station to monitor mine slope stability is still widely used. The survey network provides a detailed movement history in terms of

displacement directions and rates in unstable areas, and it also defines the extent of the failure areas.

2.4.3.4 Global Positioning System

The Global Positioning System (GPS) is a satellite-based radio navigation, timing, and positioning system that tracks the electromagnetic signals that the GPS satellites transmit round the clock (Collier 1993; Vinoth et al. 2016). Primarily the system is intended for military use. However, civilian access to the broadcast signals is currently unrestricted. GPS is mainly composed of three parts: the space satellites, a ground monitoring network, and user equipment. The GPS can measure ground movements (displacements) over the extensive area in different engineering projects involving landslides and open pit mining high walls and slopes. Slope monitoring with GPS is a system where multiple GPS antennas are connected to a single GPS receiver at the deformation site (Figure 2.22) (Forward et al. 2001; Ma et al. 2001). Deformation rate and the slope movements are estimated by comparing the final and initial positions of the GPS stations.

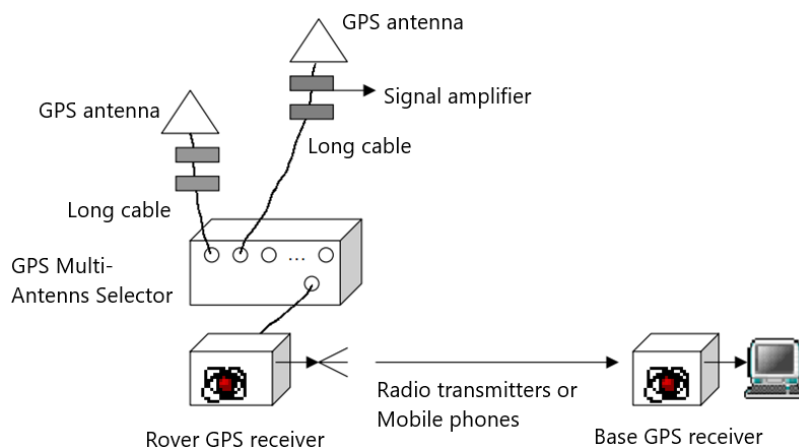


Figure 2.22 Elements of the GPS monitoring system (reprinted from Ma et al. 2001)

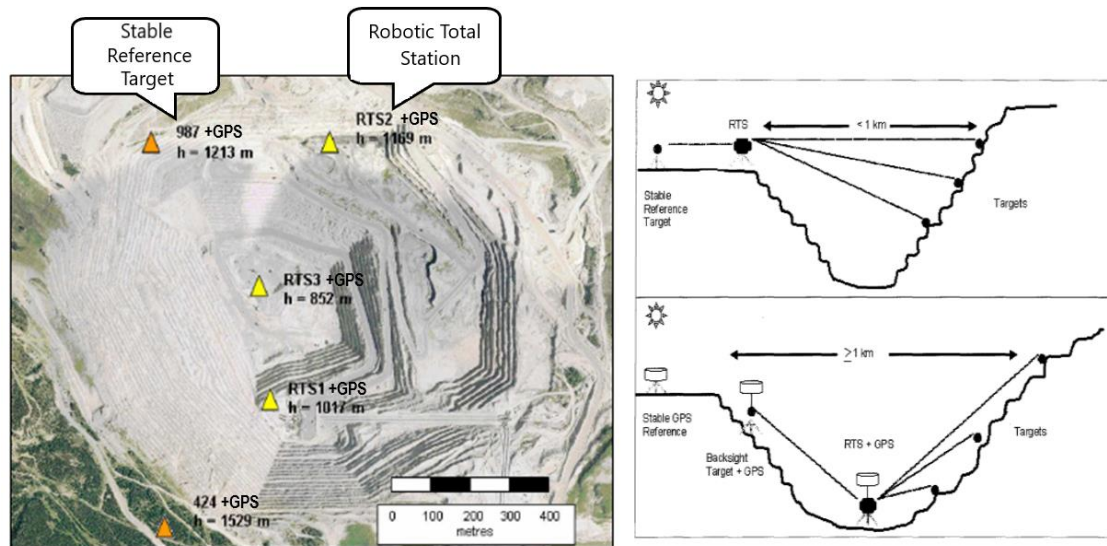


Figure 2.23 Example of locations of the GPS elements in the large open pit mine (reprinted after Bond et al. 2005)

The availability of GPS provides real-time information on the slope's stability status and the deformation rate 24-hours a day. The method has a great advantage when it comes to open sky surface mines with the installation of a series of receivers along monitoring regions. With its high positioning accuracy, light user's equipment, small size, simple and practical system, low-cost applications, the GPS technology has now been greatly used in safety monitoring of open pit mine high/steep slope (Zhou et al. 2008). But, the use of GPS is limited by the environmental characteristics, such as the vegetation and mountains, and in rapid deformation scenarios. Nowadays, GPS equipment is used in combination with photogrammetry, total stations network, and remote sensing images as the control points for monitoring the slope stability of the mines (Vinoth et al. 2016).

2.4.3.5 LiDAR

The Light Detection and Ranging (or LiDAR) technique is based on the principle of triangulation, that light travels in a straight line and at a constant speed. The LiDAR unit emits a

laser pulse, targeted towards the area of monitoring, and determines the distance to a target based on the time required for the laser to reach the target and reflect to the unit. Triangulation implies between the scanner lens, laser, and object being scanned to obtain accurate 3D data as point cloud (Shankar et al. 2013). The distance between the scanner lens and laser (parallax base) is known and to find the time of flight/distance (ρ) between the scanner and the object is by using speed of light (c) and the travel time (Δt):

$$\rho = \frac{c \Delta t}{2} \quad \text{Eq. 2.3}$$

Typical LiDAR machines are able to scan from distance up to 1 km and at rates of 2,000 to 4,000 points per second creating a three-dimensional data set composed of millions of individual points collectively referred to as a point cloud. Typical accuracy within such point clouds is within several millimeters (Levy and Visca 2009). The basic principles of laser scanner data acquisition are presented in Figure 2.25.

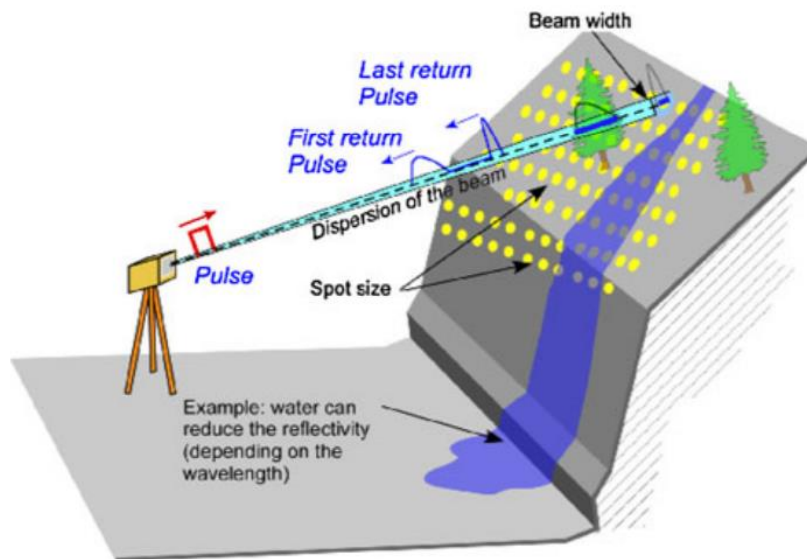


Figure 2.24 Principals of laser scanner data acquisition (reprinted from Jaboyedoff et al. 2012)

LiDAR provides virtual copies of slope in minutes, like photographic images highlighting critical areas. The application of LiDAR on mine surveying is simple, high economic benefit with rapid time saving thus providing successful slope monitoring, however LiDAR can be influenced by atmospheric (fog, rain, dust), which can result in data scatter and limits the effective range.

2.4.3.6 Slope stability Radar (SSR)

Ground-based slope stability radar systems (Figure 2.25) remotely measure the surface deformation of a slope from a stationary platform without the need for reflectors or prisms (Dick et al. 2015). The system uses real aperture 2° beam-width radar to scan a slope in both vertical (height) and horizontal (azimuth) directions. Scanning at a rate of 10°/second over a range of $\pm 60^\circ$ vertically and 340° horizontally, the system continuously monitors the slope face for deformations (Osasan and Afeni 2013). The system can operate at a range of 450 m from the target slope.

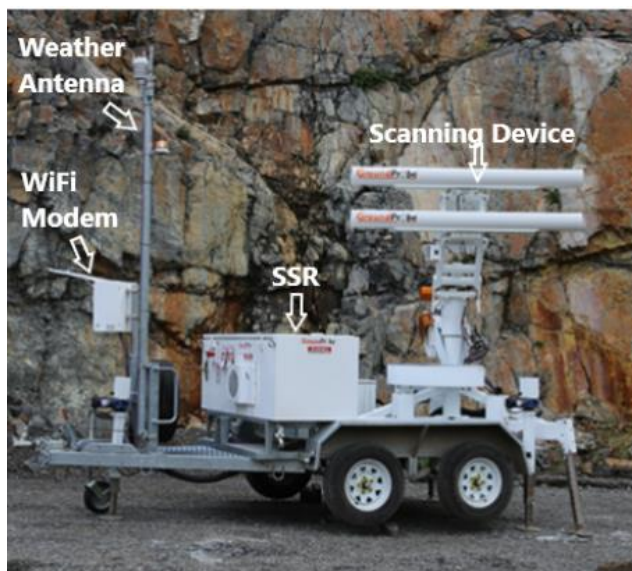


Figure 2.25 Slope Stability Radar (modified from <https://www.groundprobe.com/>)

An SSR system is installed to provide near-continuous displacement monitoring of open-pit walls. SSR scans a region of the slope and divides the area of interest into pixels. The amount of movement is measured for each pixel and compared with the amount of movement from the previous scan. Remote monitoring using ground-based radar allows for active monitoring of a slope with deformation alerts of submillimeter precision, making the data available for interpretation usually within minutes and without adverse effects from rain, fog, dust, or smoke (Dick et al. 2015).

Measurement intervals can be set up at any time rate, but typical scan repeat time is 15 minutes. The results can automatically be analyzed. For example, when a movement rate reached the designated threshold, an alarm would sound, and the mine would broadcast the evacuation order, forcing all personnel to leave the pit immediately.

Figure 2.26 shows a typical photo taken by the radar system of the open pit wall. The image clearly shows the displacement within the slope material. The figure also shows the deformation image for the same area. The images give a sense of the resolution that is possible with these types of slope monitoring systems. SSR can provide the single pixel measurements in the form deformation plot, which provides the cumulative horizontal slope displacement (between the SSR and the slope) with each progressive scan starting from the beginning of deployment. The amplitude, the range, and the coherence plots are also available. The amplitude is the signal strength of the reflection from the slope face. The range is the distance between the SSR dish and the slope. The coherence is a correlation measurement based on the range and amplitude between the current scan and the immediately preceding scan, with values close to 1.0 indicating little difference in range and amplitude between the two scans. The coherence measurement is especially useful for establishing the time of slope collapse (Dick et al. 2015).

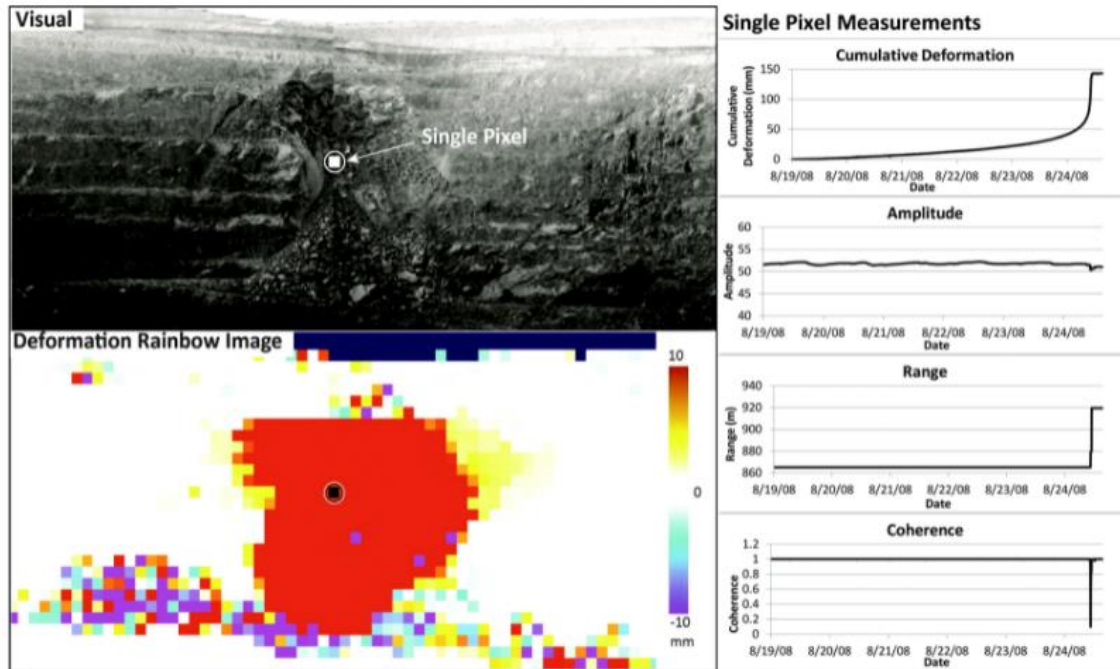


Figure 2.26 Typical slope failure measurements obtained by a Ground Probe SSR
(reprinted from Dick et al. 2015)

Ground-based radar systems are being integrated into the slope monitoring and management programs of most major open-pit mines in the United States, Canada, Australia, South Africa, Chile, and others (Harries et al. 2006, Osasan and Afeni 2010, Ginting et al. 2011, Yang et al. 2011).

2.4.4 Subsurface measurements

2.4.4.1 Extensometers

Borehole extensometer is a geotechnical instrument designed to assist in the estimation of deformation of rock mass and adjacent or surrounding soil (Figure 2.27). The borehole extensometer includes anchors, extension rods and a reference head, it constitutes an integral piece of equipment used to investigate and monitor the slopes in order to study the behavior of the rock around mines. The anchor is connected to the head of the instrument by extension rods typically placed within a protective sleeve. This sleeve ensures that the rods can move freely and translate

all movement of the anchor to the tip of the rod. Movement of the rock or soil mass relative to the head can then be calculated by measuring the displacement of the tip of the extension rod to a reference plate located in the head of the extensometer (RocTest 2021).

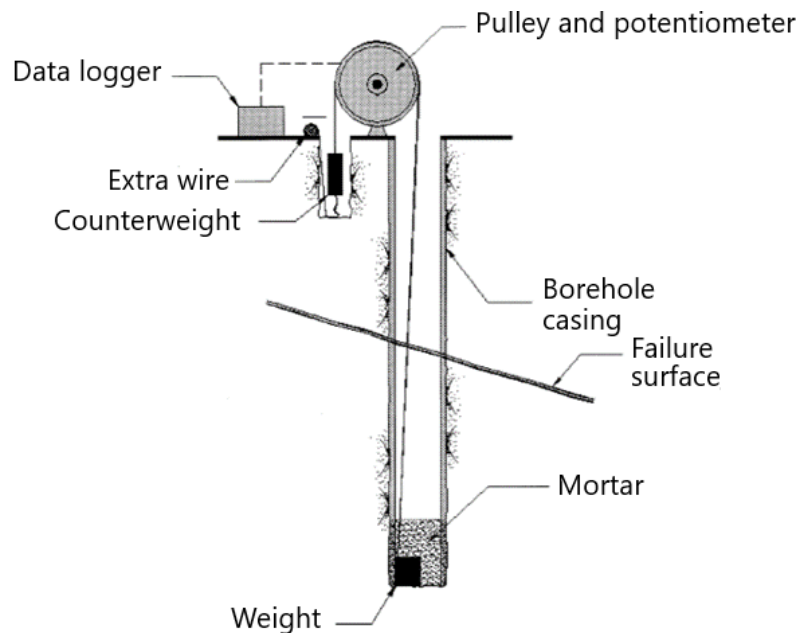


Figure 2.27 Sketch of the borehole extensometer device (reprinted from Corominas et al. 2000)

Borehole extensometer requires a borehole drilled through the slope failure mass up to other stable ground. The device reading cannot be properly interpreted unless the general pattern of the movement is known.

2.4.4.2 Inclinerometers

Inclinerometers are instruments installed in boreholes drilled within the slope. They measure the curvature of initially straight boreholes, thus detecting any change in inclination of the borehole casing (Savvaidis 2003, Read and Stacey 2009).

Inclinerometers are used to determine the location of slip surface or zone of movement, and they reveal the depth of the failure plane. The most common inclinerometers used in open pit slope

monitoring are the probe inclinometers and in-place inclinometers (Figure 2.28). The first type must be inserted in the hole each time a set of readings is required, and the second type can be lowered into the hole to provide real-time changes in the inclination of a drill hole (Read and Stacey 2009). The sensors measure the inclination of the casing in two axes (x ,y). Changes in the inclination readings indicate that the casing has been displaced by ground movement. The amount of displacement is calculated by finding the difference between the current inclination reading and the initial reading and then converting the result to a lateral distance (Abzar 2019).

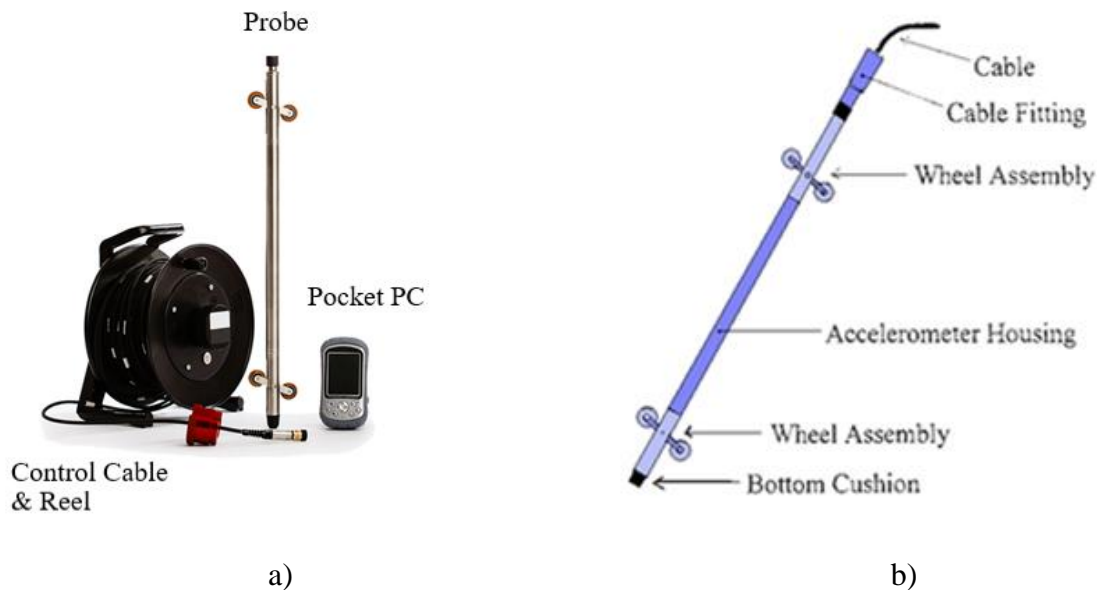


Figure 2.28 In-place inclinometer: a) example of the equipment parts, b) inclinometer probe (reprinted from Abzar 2019)

The precision can be of the order of $\pm 2.00\text{mm}$. Strong wheels make it practical to install and remove these sensors as needed. Assuming that displacements have not closed off the inclinometer casing, the sensors can be recovered and reinstalled at another project site. The main disadvantage of this type of monitoring instrument is that curvature is only observed in one axis (Abzar 2019, Tsakiri and Stewart 2000).

2.4.4.1 Piezometers

Measurement or calculation of water pressure is an important part of site investigation for stability studies. Information on water pressures is essential for designing and maintaining safe slopes. The effect of ground water present within the rock mass surrounding an open pit can be detrimental to the stability of the slope (Hoek and Bray 1981). Groundwater monitoring is typically done using piezometers. The effectiveness of the dewatering system also can be monitored with help of piezometers (Osasan 2012). Piezometers are commonly used for groundwater table monitoring in the slope because they consist of economical components, simple to read and have long-term reliability.

A typical groundwater monitoring well with piezometers consists of gravel-packed slotted casing installed in a drill hole (Figure 2.29). Piezometers provide a direct measurement of pore pressure at specific locations and obtain samples for water quality testing. A water level meter is lowered into the hole to record the static phreatic surface. Transducer can also be installed to provide real-time continuous readings.

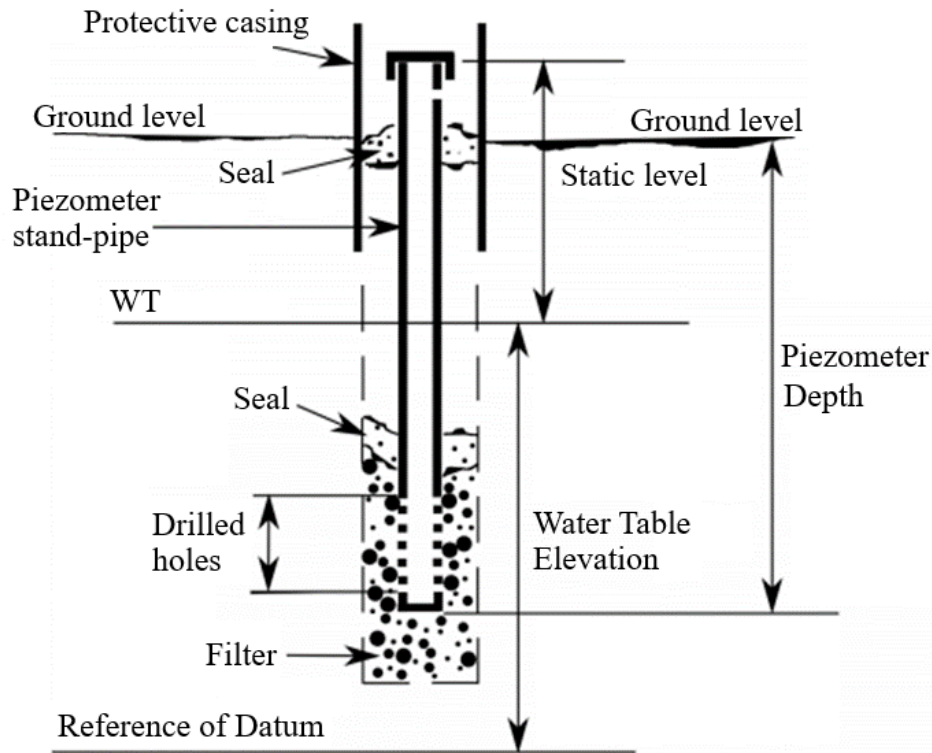


Figure 2.29 Outline of piezometer (modified from Rapinski et al., 2014)

2.4.4.2 Time Domain Reflectometers

With a cable tester, the Time Domain Reflectometers (TDR) sends an electrical pulse down a coaxial cable grouted in a borehole. When the electrical pulse encounters a break or deformation in the cable, it is reflected as a “spike” in the cable signature (Figure 2.30). The relative magnitude, rate of displacement and the location of the region of deformation can be determined immediately and accurately (Kane and Beck 1998).

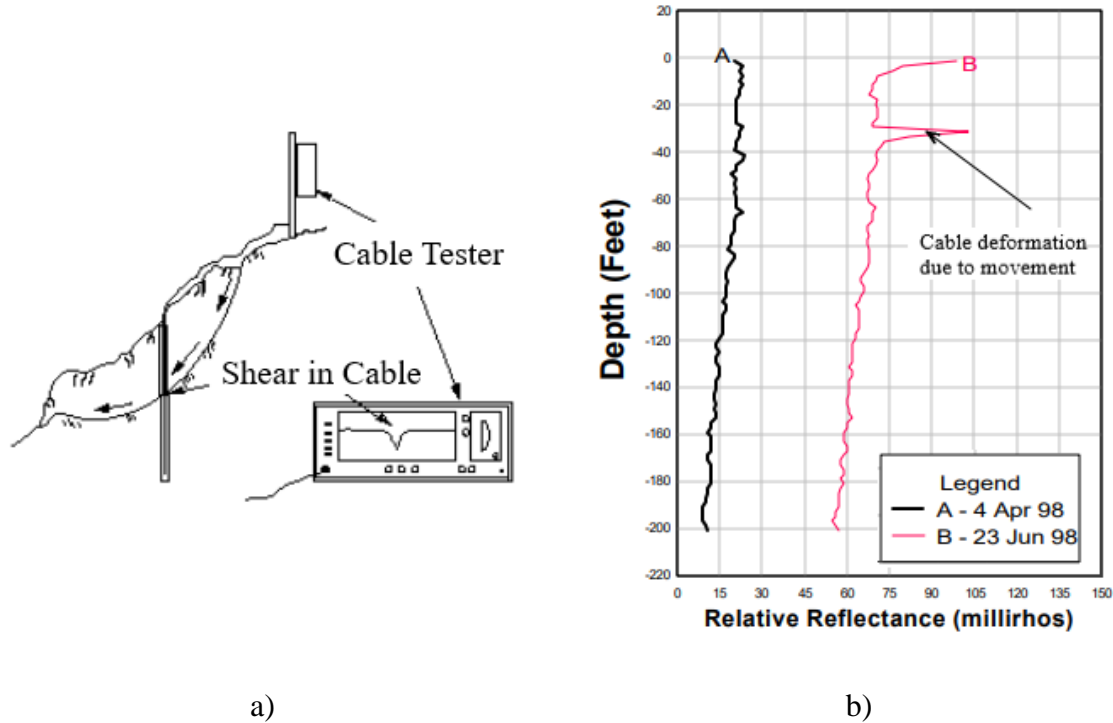


Figure 2.30 TDR technology: a) deformed cable resulting in signature “spike” on cable tester screen, b) TDR cable signatures showing deformation which activated alarm circuit (reprinted from Kane and Beck 1998)

There are some advantages and drawbacks of the TDR technology. The advantages are: a) TDR cables give very valuable and precise information on the locations of deep-seated slide surfaces (Mohammed 2021); b) the hole depth can be deeper compared to one required for inclinometer techniques, because the all TDR monitoring equipment are at the surface; c) locations of any movement are determined immediately using TDR; d) rapid and remote monitoring is possible, because TDR data can be transmitted via telecommunications with scanning and recording intervals programmed remotely to examine zones of interest (Kane and Beck 1998, Osasan 2012). The disadvantages are: a) TDR technique is more expensive than surface monitoring due to the requirement for drilling; b) TDR cannot determine the actual amount of movement. Relative amounts can be estimated; c) the cable must be deformed before movement can be located; simple bending of the cable, without damage, will not indicate any movement: d)

if water infiltrates a TDR cable, it will change the cable’s electrical properties and may make signatures difficult to interpret.

2.4.4.3 Microseismic monitoring

The microseismic method is routinely practiced in hard-rock opencast mining environment since 2002 for slope failure prediction and associated scenarios (Lynch and Malovichko 2006; Institute of Mine Seismology 2019). Table 2.8 provides a list of published mining sites experience where microseismic monitoring has been performed.

Table 2.8 Open-pit mine sites referred to in literature where microseismic monitoring has been performed (adapted from Sjoberg 2006, Lynch et al. 2005, Wesseloo et al. 2009)

Mine	Country	Reference
Kimbley	USA	Wisecarver et al. (1969)
Liberty and Tripp-Vetern	USA	Stateham and Merrill (1979)
Chuquicamata, Kennedy failure	Chile	Voight and Kennedy (1979) Kennedy and Niermeyer (1970)
Cerro de Pasco	Peru	Deza and Jaén (1979)
Fimiston (Super Pit)	Australia	Hudyma et al. (2003)
Navachab	Namibia	Lynch et al. (2005)
Sandsloot	South Africa	Lynch et al. (2005)
Sunrise Dam	Australia	Lynch and Malovichko (2006)
Crosscourse Pit Union Reefs	Australia	Lynch et al. (2005)
Mt Keith	Australia	Sweby et al. (2006)
Chuquicamata	Chile	Sjoberg (2006); Trifu et al. (2008)

Microseismic monitoring techniques are used to assist in characterizing the rock structure disturbance behind the slope before movements on the surface can be visualized or detected (Hustrulid and Boisen 1992). This information can be used for slope assessment and potentially warning of impending collapse (Lynch et al. 2005, Lynch and Malovichko 2006, Mendecki et al. 2010).

Seismic monitoring involves the use of seismic sensors installed in drill holes in the unstable areas of the slope. The sensor detects the microseismic activities within the slope and transmits the microseismic information to a central computer via a data logger at the top of the slope (Osasan, 2012, Vinoth and Kumar 2016) (Figure 2.31). Seismic signals from the geophones are continuously recorded, time-synchronized and transferred via cables and USBs for collection and processing. Both strong and weak microseismic events are measured and assessed to determine their source location, energy and potential impact on slope movement. Then the events are processed for identification of zone of weakness, the stress conditions and deformation mechanics and their rate within rock mass. In addition, such data can lead to a better understanding the possible excavation damage zone, the initiation of new fractures or reactivation of existing discontinuities within the monitoring zone. Correct analysis of the data helps to perform satisfactory control of the working in terms of safety in complex geological and excavation conditions (Xu et al. 2012, Vinoh and Kumar 2016)

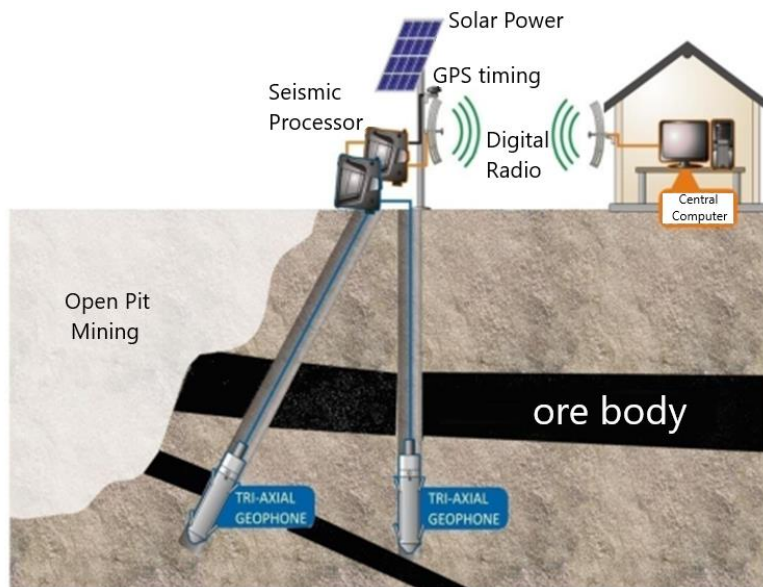


Figure 2.31 Microseismic monitoring in opencast mine (modified from Institute of Mine Seismology 2015)

According to Li et al. (2016) the hardware of this system is mainly divided into three parts, namely, sensors, data acquisition (NetADC) and data communication (NetSP) (see Figure 2.31 and Figure 2.32). The sensor is used to convert the ground motion (ground speed or acceleration) into a measurable electronic signal. Analog signals from the sensor are converted into digital signals by data acquisition. The data can be collected by continuous recording, or use the trigger mode through a special algorithm to determine whether the MS event data is recorded or not. MS data is transmitted to a central computer or local disk storing or processing. The system can use a variety of data communication to meet the needs of different system environments.

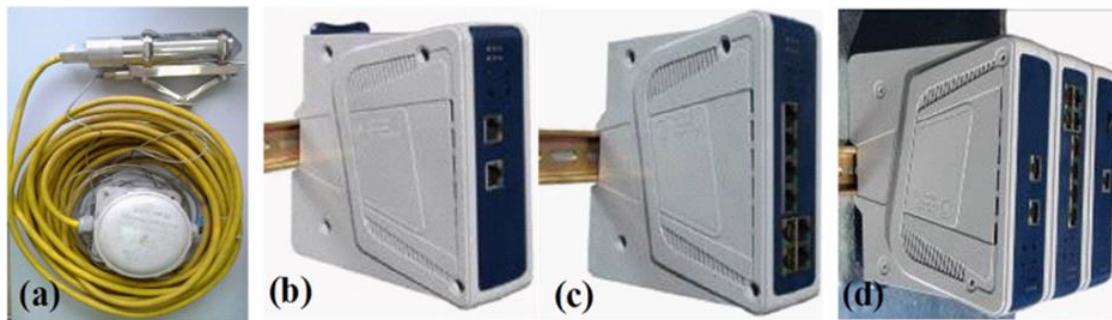


Figure 2.32 Main parts of the microseismic monitoring system. (a) microseismic sensor, (b) NetADC, (c) NetSP, (d) microseismic data collecting and processing system (reprinted after Li et al. 2016)

The method has various advantages over other slope monitoring methods regarding its high accuracy level (0.001m), providing the deformation information in real-time on a day-night continuous routine. At the same time, experience has shown that microseismic monitoring has some flaws. Sjoberg (2006) states that there is still a problem filtering out the noise from mining equipment and mining operations (e.g., blasting and boring). Correcting arrival times for the actual length of travel distance of the wave (around the pit bottom rather than across the open pit void) is also a big issue. Thus, microseismic monitoring cannot yet be regarded as a very reliable one despite the existing equipment. Microseismic monitoring still has its niche in open-pit mines

located in seismically active areas where it is used to detect seismically active zones. These zones can cause rock bursts and earthquakes, which in turn might trigger slope failure (Sjoberg 2006, Lynch and Malovichko 2006). The research results (Cao et al. 2009, Xu et al. 2012, Vinoth and Kumar 2016) show that the combination of numerical simulation, microseismic monitoring, conventional surveying, and in situ observation approaches leads to a better understanding of excavation behavior of the open pit slopes and more satisfactory control of the working in terms of safety in complex geological and excavation conditions.

2.4.5 Summary of various slope monitoring techniques

Nowadays, slope monitoring is the most reliable method for detecting slope instability and predicting slope failure (Osasan 2012). Monitoring slope displacements is an invaluable tool for optimizing open-pit mining (Coates 1977, Sjoberg 1996). There are many cases in which slope monitoring has enabled more optimized mining (Call et al. 1993, Martin and Mehr 1993, Day and Seery 2007, Zhou et al. 2008, Ward 2015). These cases are evidence of how production interruptions due to failures have been minimized through careful monitoring. In these cases, relatively large displacements were recorded before unstable failure and the warning time was relatively long.

The type of monitoring equipment affects the accurate measurement and interpretation for real-time detection and prediction of instability. The principal difference in application of the monitoring methods revolves around the type of failure mode that can be anticipated (Martin and Stacey 2018). Apart from visual inspection, conventional monitoring equipment, such as survey system theodolite and total station with reflecting prism, extensometers, inclinometers, piezometers provide information only for a single site, or at most, a small number of locations on the mine slope, therefore are limited in the area of coverage (Vaziri et al. 2010, Osasan 2012). In

addition to these limitations, conventional monitoring tools may not be easy to install at many open pits because the steep high walls and lack of benches limit access to the unstable areas above the working floor (McHugh et al. 2006). Relocating monitoring equipment from one location to another is costly, time-consuming, demanding, and unsafe for personnel on unstable slopes. Furthermore, vegetation on the rock face reduces the accuracy of the displacement measurements while trucks and other mining vehicles send wrong signals, which can cause step changes in the displacement measurements (Osasan 2012).

The advantages of the LiDAR and SSR techniques over other methods are their ability to monitor large areas on a slope surface both day and night and in almost any weather without being affected by atmospheric dust or haze (McHugh et al. 2006, Osasan 2012). Radar monitoring technique can track the failure development, and therefore based on the automated analysis if the slope movement exceeds the alarm thresholds can send an alarm signal to the mine.

In some cases, the movement cannot be detected by surface measurements, so the subsurface measurements may be required if it is necessary to locate the sliding surface or examine the propagation of subsurface movement. In addition, a subsurface monitoring system is less expensive than surface systems and gives additional, more reliable, and detailed information on the shear zone. But geotechnical sensors, such as inclinometers or extensometers, can provide only one-dimensional type of measurements. It is therefore hard to extract true three-dimensional motions with this type of equipment resulting in difficulties in detecting certain models of motion that have not been previously identified (Tsakiri and Stewart 2000).

Table 2.9 summarizes the various monitoring methods with its strength and limitations as they apply to open-pit mining slopes. The acceptable level of accuracy needed for adequate slope monitoring should have movement and deformation monitored to mm. Instrumentation should also

be moved easily and not delay or obstruct mining operations to keep production on schedule. Slope monitoring instruments are designed to aid in achieving the best possible production by knowing how and when to mine certain benches and not prevent equipment from accessing areas planned for mining. Data interpretation and analysis should be relatively simple for operators to use and produce an accurate risk assessment. (Kumar and Rathee 2017).

Through analysis of different monitoring methods, it was found that the highest success rate is obtained when a mine site uses multiple monitoring tools to evaluate the movements of slopes (Sjoberg 1999, Martin and Stacey 2018, Mohammed 2021).

Table 2.9 Different types of the monitoring systems: strength and limitations (reprinted from Osasan 2012)

Slope monitoring system	Type	Advantages	Disadvantages	Range	Slope wall coverage	Resolution
Conventional monitoring	Visual monitoring	Production personnel can be involved. No technology is required. Inexpensive	Labor intensive. Limited to safe slope areas.	Limited (20-50m)	Small area	Not applicable
Surface monitoring	Tension Crack Mapping	Economical and simple to use	Dangerous to install in unstable areas. Measures displacement of discrete points. Errors can be caused by long wire length due to sag or thermal expansion. Alarm can be triggered by falling rocks or animals	Not applicable	Discrete points	± 0.2% F.S.
	Survey Network	Automatic operation is available Valuable for identifying long term displacement trends.	Suitable only for monitoring discrete points. Prism installation is time consuming and dangerous on unstable slopes. Damaged prisms are difficult to replace on steep slope with no access. Displacement data is affected by atmospheric variation in temperature and pressure. Displacement data is affected by human error.	1500m	Discrete points	± 5.0mm
	Global Positioning System (GPS)	Easy automation High accuracy Less labor intensive.	High cost of placing a permanent GPS receiver at each monitoring points Satellite signals can be obstructed by tall vegetation Usage for slope monitoring is still relatively new and expensive. Slope surface can create signal multipath error.	4,000 - 20,000m	Discrete points	±10mm

Slope monitoring system	Type	Advantages	Disadvantages	Range	Slope wall coverage	Resolution
	LiDAR	Prisms not required for slope monitoring. Portable and can be moved around easily. Continuous and automatic operation Large area monitoring Valuable for identifying long term displacement trend	Not commonly used for slope monitoring compared to radar monitoring. Lower accuracy compared to radar monitoring. Scan processing time is too great for effectiveness. Accuracy impaired by differences in the reflectivity of the rock, the angle of the rock face, weather, vegetation Cannot provide early warning of failure.	2500m	Large area	50mm
	SSR	Continuous and automatic operation. Operates in all-weather condition. Geo-referencing is possible. Sub-millimeter displacement measurement`. Large area and point monitoring.	Expensive to procure and maintain. Uncontrollable down-time.	1000m – 4000m	Large area	± 0.2mm
Subsurface monitoring	Piezometers	Simple to install Function well in shallow and deep holes	Careful handling is required for proper installation. Requires periodic replacement of batteries. The electronic units are susceptible to damage by lightning. Borehole drilling for installation can be expensive. Requires conversion of frequency reading to pore pressure.	500m	Discrete points	0.5mm

Slope monitoring system	Type	Advantages	Disadvantages	Range	Slope wall coverage	Resolution
	Inclinometers	Subsurface displacement measurement of both shallow and deep-seated failure planes. Economical and simple to use	Manual reading is time consuming and labor intensive. If not properly installed, erroneous displacement readings may be recorded.	100m	Discrete points	$\pm 2.0\text{mm}$
	Seismic Monitoring	Provides early warning of the development of deformation. Detects displacement that cannot be identified by surface measurement.	Expensive to set-up.	2,000m	Discrete points	0.001mm
	Time Domain Reflectometry (TDR)	Rapid and remote monitoring is possible. Slope displacement can be determined immediately. Lower cost of installation. Readings take minutes. Can be installed at great depth	Cable must be destroyed before displacement can be located. Cannot measure deformation below the water surface because of changes in electrical properties of cable from water infiltration. Cannot determine the magnitude and direction of slope movement.	100m	Discrete points	$\pm 0.5\text{mm}$

3. ANALYSIS OF CASE HISTORIES OF OPEN PIT MINING SLOPE FAILURES INCLUDING RISK ^{1,2}

3.1 Existing slope failure databases

Case studies are an invaluable source of information, because they reflect the actual conditions at the site. Failures demand attention and always hold lessons about what to do to prevent it and what not to do again. Learning from failures provides the most reliable basis for anticipating what might go wrong in other cases. A final aim of the case histories study is to obtain an opportunity for transferring this information into design guidelines for slopes in similar geological, geotechnical, and geomechanical conditions. The problem often lies in how to describe (quantitatively) the prevailing conditions at a particular site so that the information becomes useful in forward designs (Sah et al. 1994, Zare Naghadehi et al. 2013, Duncan et al. 2014, Whittall 2017).

Prior documentation and the emphasis of their research are summarized in Table 3.1. The work presented in this chapter is the result of a comprehensive literature review focused primarily on open pit slope failures.

¹ Part of the data reported in this chapter and Appendix A is reprinted with permission from “Runout analysis and mobility observations for large open pit slope failures” by Whittall J.R., Eberhardt E. and McDougall S. (2017). Canadian Geotechnical Journal, Volume 54, Number 3, 373-391, Copyright 2021 by Canadian Science Publishing.

² Part of the data reported in this chapter is reprinted with permission from “Tolerable risk chart” by Timchenko A., Shidlovskaya A. and Briaud J.-L., In Proceedings of the 20th International Conference on Soil Mechanics and Geotechnical Engineering (20 ICSMGE), Sidney, Australia, 1-5 May 2022. The Australian Geomechanics Society. Copyright 2021 by 20 ICSMGE Organizing Committee.

Table 3.1 Summary of the existing slope failure datasets

Who	What was collected	Source	Number of cases	Collected parameters	What was proposed
USGS 2021	Landslides	Natural landslides happened in the US	>3000	Map of the deposit, trigger factors, runout distance, slope geometry	The US landside inventory data for improving the understanding of the causes of failure and suggesting mitigation strategies
Finlay et al. 1999	Small (less than 50 m ³) and shallow landslides	Man-made failures (civil engineering) happened in China	1100	Landslide height, slope angle landslide volume, maximum landslide depth, landslide width depth of debris at the toe of the slope, travel distance, and apparent friction coefficient	Runout distance estimation
Hunter and Fell 2004	Extremely rapid (>5m/s) landslides	Natural landslides and man-made failures (civil engineering)	350	The type of slope, the slide volume, the geometry of the slope, the degree of confinement of the travel path of the landslide	Runout distance estimation
Yost 2009	Slope failures	Open pit mining case histories happened at Boron Open Pit Mine (California, USA)	13	Geometry of the slope, runout distance, angle of repose, mass of the failure	Runout distance estimation
McQuillan et al. 2018	Failed and stable cases	Open pit mining case histories happened in Australian coal mining industry	119	The geotechnical parameters and slope geometry before and after the failure	A new risk assessment methodology for coal mine excavated slopes was developed
Sah et al. 1994	Failed and stable cases	Natural and man-made conditions (including open pit mining) from	60	The geotechnical parameters and slope geometry with corresponding FS	Proposed the method of slope safety factor estimation based on the collected parameters

Who	What was collected	Source	Number of cases	Collected parameters	What was proposed
Sjoberg 1996	Large scale slope failures	Open pit mining case histories	20	Governing factors of the large scale slope failures, failure models, triggering factors, and the geotechnical parameters of the initial slope and failed material.	Pointed out advantages and disadvantages of current design methods of the studies cases
Whittall et al. 2017	Extremely rapid (>5m/s) slope failures	Open pit mining case histories	105	The volume of the failed mass, critical slope angle, material fall height and runout distance, triggering factors	Runout distance estimation
Martin and Stacey 2018	Large scale slope failures in weak rock material	Open pit mining case histories	33	Governing factors of the slope failures, failure models, triggering factors, and the geotechnical parameters of the initial slope and failed material.	Proposed the design issues for pit slopes in materials generally classed as weak rocks

Historically datasets have solely focused on natural landslide hazards. The USGS website provides profound information about the US landside inventory data. The data are continuously collected by USGS as a part of the Landslide Hazards Program (LHP) that has operated since the mid-1970s in gathering information, conducting research, responding to emergencies and disasters, and producing scientific reports and other products. A lot of existing databases have not been validated for open pit slope failures (Finlay et al. 1999, Hunter and Fell 2004, Shea and van Wyk de Vries 2008). The majority of open slope failures data is focused on the collection of the failures that occurred either at the location of one open pit mine (Yost 2009; Bui et al. 2020) or in one particular region or country (Jhanwar and Thote 2010, McQuillan et al. 2018). Starting in the late 1990's there can be found several research reports focusing on the collection and analyses of large scale open pit failures that occurred worldwide (Sah et al. 1994, Sjoberg 1996, Mercer 2006, Whittall et al. 2017, Martin and Stacey 2018).

Sah et al. (1994) collected 60 (37 failed and 23 stable) case studies that occurred in natural and in man-made conditions. The geotechnical parameters and slope geometry with the corresponding FS were reported. Based on the collected data, authors proposed the method of slope safety factor estimation using the direct equation which requires the average values of the geotechnical parameters (γ , c , ϕ), height of the slope and slope angle.

Based on the comprehensive literature review J. Sjoberg (1996) collected 20 case histories mainly with large scale stability of pit slopes, i.e. cases where failure involves large portions of a slope or entire slopes of several hundreds of meters in height. Bench scale failures were not covered in detail in the report. The review done by J. Sjoberg in 1996 was focused on analysis of governing factors of the large scale slope failures, failure models, triggering factors, and evaluating

the geotechnical parameters of the initial slope and failed material. As a result of the study, the author pointed out advantages and disadvantages of current design methods of the studies cases.

Mercer (2006) collected a database of 30 literature case studies which documented relatively large or significant failures that have occurred in a mining environment. The principal objective of the work was to obtain actual deformation data of failures that have occurred and to review the data in the context of the models of instability and failures that were reported. The intention was for the information on the time-dependent deformation data and associated geological and structural data associated with the failures to supplement data obtained from the detailed studies in order to form a more comprehensive overall picture of deformation behavior.

A dataset of 105 extremely rapid ($>5\text{m/s}$) open pit slope failures have been compiled and analyzed by Whittall et al. (2017). The volume of the failed mass, critical slope angle, material fall height, runout distance, and triggering factors were collected in the dataset. The main purpose of the analysis was to find a reasonable runout distance estimation. The developed empirical solution for runout estimation was compared against established empirical runout relationship for natural landslides. It is also showed that open pit landslides appear to deposit predictably shaped debris aprons that either hang below the source in a 37° talus cone or flow into a continuous pile, thinning away from the source. Compared with natural landslides, they form thicker, more predictably shaped deposits with less lateral spread.

“The Guidelines for open pit slope design in weak rocks” (Martin and Stacey 2018) is based on a study of 33 open pit mining case histories. The guidelines focused on the design issues for pit slopes in materials generally classified as weak rocks (cemented transported sediments, saprolites, leached rocks/soft iron ores, mudrocks, and hydrothermally altered rocks). Using the collected case histories, the authors tried “...to link innovative geomechanics research with best

practice.... The fundamental objective is to provide the slope design practitioner with the tools to help meet the mine owner's requirements that the slope should be stable, but if they do fail, the predicted returns on the investment are achieved without loss of life, injury, equipment damage, or sustained losses of production.”

The limitations of the previous collections can be summarized in the following statements:

- Many data are collected for natural landslides or civil engineering failures, but not for mining failures;
- Existing databases are focused on one region or one particular mine.
- Existing datasets are quite limited in terms of the number of cases and presented data.

That is why there is a need to organize the open pit slope failure database containing the information that is typically missing in existing databases.

The idea of the database is to collect open pit failures from various locations in the world (Figure 3.1). The slope geometry in the form of maximum open pit slope height and unstable slope height (for slopes that have failed), as well as inter-ramp and overall slope angle, the travel distance of the debris and setback distance have to be compiled.



Country	Number of cases	Country	Number of cases	Country	Number of cases	Country	Number of cases
Algeria	1	Greece	1	Namibia	2	Spain	1
Armenia	1	Guinea	1	New Zealand	3	Tanzania	1
Australia	22	India	11	Papua New Guinea	1	Turkey	7
Botswana	1	Indonesia	4	Philippines	1	USA	45
Brazil	1	Iran	1	Peru	1	Zambia	2
Canada	22	Italy	2	Russia	2	Unknown	8
Chile	1	Japan	1	South Africa	1		
China	6	Kyrgyzstan	2			TOTAL	134

Figure 3.1 Case histories map

Usually the amount of data available for each case varies significantly. For some of the mines, good descriptions of the geotechnical environment is available, as well as there are descriptions of slope failures and monitoring systems. But for the majority of the slope failures which are going to be presented in the database, existing data is limited and only includes slope failure height and slope failure angle as well as a rough geological description. The reason for limited data is that the world mining industry has an aversion to publishing case histories describing their pit slope failures. The reference slope failure reports or case history papers are often qualitative, subjective and include only events that were recalled during accident

investigations. It should be remembered that during such investigations not all of the geotechnical phenomena are reported. It can be assumed that many events were not recorded as their geotechnical value to the investigations was not realized.

Thus, a significant and time-consuming contribution of the dissertation is the literature review collecting and cataloging the pit slope failures.

The analysis of the available data shows that in the 1970s or earlier the mining industry was building its knowledge base and searching for common stability issues and mitigation strategies so the industry shared the information about the slope failures. At that time were started a number of North-American and international conferences on open pit mining slope stability (*e.g.* The International Conference on Slope Stability in Open pit Mining, The ISRM International Symposium). There are a lot of Proceedings and publications available for that time period. In the 1980s and 1990s, this practice appears to have fallen out of favor particularly because of the legal and public disclosure concerns, but also because mining slope stability conferences became less common.

Recently, the past two decades have seen the mining geotechnical community returning to the practice of sharing case histories, primarily through the proceedings from the International Symposium on Open Pit Mining and Civil Engineering, which has been held approximately every two years since its relaunch in 2006. It should be admitted that the existing sources of the open pit mining failures are mostly written as conference papers, where the details provided are not as thorough as would be typically found in a pre-reviewed journal paper. This often required that more than one source be consulted to obtain the necessary data.

3.2 Development and Organization of the TAMU-MineSlope Spreadsheet

The presented database is the extended one started by John Whittall (Whittall et al. 2017). In his work, J. Whittall (2015, 2017) presented a result of a comprehensive public-domain literature search that returned ninety-six open pit slope failures that included a runout component involving over fifty mines: anonymous sources provided another nine case histories in his database. The database presented earlier (Whittall et al. 2017) contained the cases with high velocity ($>5\text{m/s}$) and significant volume ($>40,000\text{ m}^3$).

A detailed investigation of 134 different actual open pit mining slope failure cases that occurred between 1969 and 2020 with different failure modes available in the literature was made. In addition, geotechnical parameters, setback distance and runout length are presented in the database. Whenever possible, geometric estimates are taken from satellite imagery, particularly, Google Earth Pro. The data reflect relatively recent conditions; however, since some of the data were collected from 1969 to 2020, slope geometries of open pits may have changed since then. The specific incidents were selected based on satisfying any one of the following criteria:

- any slope failure with volume greater than $10,000\text{ m}^3$;
- any incident resulting in a fatality or injury;
- any incident resulting in equipment damage or loss;
- a representative selection of incidents with a volume lower than $10,000\text{ m}^3$, where the geometry and geotechnical data were available.

A global open pit slope failure case histories collection named TAMU-MineSlope was organized using Excel spreadsheet form. All the collected case histories are described in the same manner. The entries of each undermentioned part are described in this section. It is important to note that some cells are remained empty because of the lack of information for some case histories.

Figure 3.3 shows a general view of the TAMU-MineSlope Spreadsheet, including its six parts. As discussed earlier, the database includes 134 case histories that are 134 rows. Each row in the database consists of 40 columns. The entries for the database columns are listed in Table 3.2. Parameters are used in the database presented in Figure 3.2. The entire TAMU-MineSlope Spreadsheet in .xslm format is available by request.

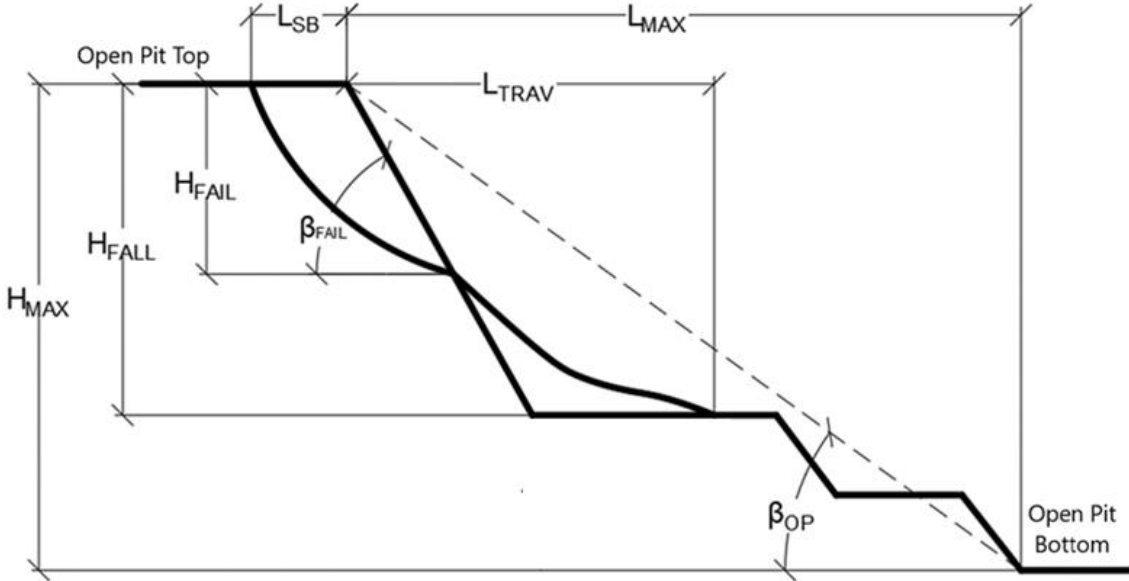


Figure 3.2 Parameters of the slope

Table 3.2 List of entries in the TAMU-MineSlope Spreadsheet

Part1: Record information	Part 4: Slope Failure Parameters
<ol style="list-style-type: none"> 1. Label 2. Mine 3. Pit 4. Wall 5. ID 6. Country 7. Date 8. Material group 9. Commodity 	<ol style="list-style-type: none"> 24. Failure Mechanism 25. Trigger 26. Volume (Mm³) 27. Mass (tons) 28. Slope Angle, $\beta_{\text{FAIL}}(^{\circ})$ 29. Fall Height, H_{FALL} (m) 30. Travel distance, L_{TRAV} (m) 31. Average Width W_{FAIL} (m) 32. Setback distance, L_{SB} (m) 33. Height of the failure, H_{FAIL} (m)
Part 2: Open Pit Parameters	Part 5: Slope Failure Plan and Scheme
<ol style="list-style-type: none"> 10. Shape of the Mine 11. Max Depth of the Mine, H_{MAX} (m) 12. Area of the Pit, (km²) 13. Shoreline (m) 14. Length of the Mine (m) 15. Width of the Mine (m) 16. Overall Slope Angle of the Mine, $\beta_{\text{OP}} (^{\circ})$ 17. Height of Benches (m) 	
Part 3: Geological and Geotechnical Characteristics	Part 6: General Information
<ol style="list-style-type: none"> 18. Lithology 19. Strength grade 20. RMR (1976) 21. Unit Weight, γ (kN/m³) 22. Cohesion c (kPa) 23. Friction angle ϕ ($^{\circ}$) 	<ol style="list-style-type: none"> 34. General View of the Failure 36. Plan View of the Failure 37. Cross-Section of the Failure <ol style="list-style-type: none"> 38. Software 39. Monitoring system 40. Reference

3.2.1 Part 1: Record information

1. Label: the row number associated with the one case history in the database.
2. Mine: the name of the company the open pit belongs to.
3. Pit: the name associated with the open pit where the slope failure occurred.
4. Wall: the name of the wall where the slope failure localized.
5. ID: Identification number of the failure according to the mine documentation.
6. Country: name of the country where the mine locates.

7. Date: date of the slope failure.
8. Material group: all the slope forming materials are divided into 9 groups: Igneous, Altered Igneous, Fault material, Metamorphic, Weathered rock, Volcano-Sedimentary, Sedimentary, Soil, Saprolite.
9. Commodity: a main raw product gaining as a result of open pit mining operations.

3.2.2 Part 2: Open Pit Parameters

1. Shape of the Mine: the overall plan view shape of the open pit.
2. Max Depth of the Mine, H_{MAX} (m) – maximum depth of the open pit at the moment when the discussed slope failure occurred.
3. Area of the Pit, (km²) – area of the open pit measured at the shoreline at the moment when the failure occurred.
4. Shoreline (m) – the average length of the open pit shoreline at the moment when the failure occurred.
5. Length of the Mine (m) – the average length of the open pit at the moment when the failure occurred.
6. Width of the Mine (m) – the average width of the open pit at the moment when the failure occurred.
7. Overall Slope Angle of the Mine, β_{OP} (°) – the angle measured between the line connecting the crest and the toe of the open pit and the horizontal line.
8. Height of Benches (m) – the average height of the open pit benches.



Record Information								Open Pit Parameters						Geological and Geotechnical Characteristics					Slope Failure Parameters								Slope Failure Plan and Scheme			General Information								
Label	Mine	Pit	Wall	ID	Country	Date	Material Group	Commodity	Shape of the Mine	Max Depth of the Mine, H _{max} (m)	Area of the Pit, (km ²)	Shoreline (m)	Length of the Mine (m)	Width of the Mine (m)	Overall Slope Angle of the Mine, β _{op} (°)	Height of Benches (m)	Lithology	Strength Grade	RMR (1976)	Unit Weight, γ (kN/m ³)	C' (kPa)	φ (°)	Failure Mechanism	Trigger factor	Volume (Mm ³)	Mass (tons)	Slope Angle, β _{fail} (°)	Fall Height, H _{fall} (m)	Travel distance, L _{trav} (m)	Average width, W _{fail} (m)	Setback distance, L _{sb} (m)	Height of the failure, H _{fail} (m)	General View of the Failure	Plan View of the Failure	Cross-Section of the Failure	Software	Monitoring system	Reference
1	Afsin-Elbistan	Kisilakoy	Northwest	-	Turkey	July 1, 1984	Sedimentary	Lignite	Rectangle	145	7.25	10765	2140	2450	18	30	Lignite	R1	Poor	17.00	15.49	9	Soil planar slide	Daylighted structure	1.60	-	20	50.0	141.0	250.0	34	50						Aydan et al. (1996)
2	Afsin-Elbistan	Kisilakoy	Southwest	-	Turkey	October 23, 2006	Sedimentary	Lignite	Rectangle	145	7.25	10765	2140	2450	14	30	Lignite	R1	Poor	16.2	8.00	9	Soil planar slide	Fault zone	10.50	-	14	117.0	481.0	300.0	39	117				Slide, FLAC3D		Oge (2008); Tutluoglu et al. (2011)
3	Afsin-Elbistan	Çöllöler	Southwest	Landslide B	Turkey	Feb. 6, 2011	Sedimentary	Lignite	Rectangle	180	2.2	6000	2100	1100	16	30	Lignite	R1	Poor	17.00	6.00	26	Rock planar slide	Daylighted structure	7.90	-	40	150.0	585.0	-	100	150				FLAC3D; Plaxis		Farina et al. (2013); UNOSAT (2011); Tutluoglu et al. (2010); Ozbay and Cabalar (2015)
4	Afsin-Elbistan	Çöllöler	Northeast	Landslide A	Turkey	Feb. 10, 2011	Sedimentary	Lignite	Rectangle	180	2.2	6000	2100	1100	16	30	Lignite	R1	Poor	17.00	6.00	26	Rock compound slide	Not reported	42.00	-	21	150.0	950.0	800.0	350	150				FLAC3D; Plaxis		Farina et al. (2013); UNOSAT (2011); Tutluoglu et al. (2010); Ozbay and Cabalar (2015)
5	Afton	-	Southeast	-	Canada	1986	Igneous	Gold, Copper, Silver	Circle	500	0.63	2903	1000	2500	36	45	Diorite	R4	Poor	29.00	65.00	52	Rock topple	Mined too steep	0.10	300000	45	198.0	250.0	80.0	25	40						Reid and Stewart (1986); Martin (1990); Mercer (2006)
6	Afton	-	Northwest	-	Canada	1984	Igneous	Gold, Copper, Silver	Circle	500	0.63	2903	1000	2500	36	45	Diorite	R4	Poor	29.00	65.00	52	Rock topple	Fault zone	-	200000	40	73.0	97.0	-	15	62						Martin (1990); Sjoberg (1996); Mercer (2006)

Note: TAMU-MineSlope Database is presented in Appendix A, and the Bibliography for TAMU-MineSlope is in Appendix B.

Figure 3.3 General view of the TAMU-MineSlope Spreadsheet

3.2.3 Part 3: Geological and Geotechnical Characteristics

1. Lithology.

Source materials include various lithologies from unique ore deposition environments and various degrees of alteration and weathering. In addition, lithological strata where the slope failure occurred are indicated for each case history.

2. Strength Grade.

ISRM (1978) classifications for weathered rock mass was used to characterize the rock mass into different grades (Table 3.3). All case histories are divided into groups according to the ISRM (1978) strength grade classification (Figure 3.4).

Table 3.3 Strength grade classification (reprinted from ISRM 1978)

Strength Grade	Description	Field Identification	Approximate Range of Uniaxial Compressive Strength (MPa)
R0	Extremely weak rock; Soil*	Intendent by thumbnail	0.25-1.0 (<0.025) - (>0.5)
R1	Very weak rock	Crumbles under firm blows with point of geological hammer, can be peeled by a pocket knife	1.0-5.0
R2	Weak rock	Can be peeled by a pocket knife with difficulty, shallow indentations made by firm blow with point of geological hummer	5.0-25
R3	Medium strong rock	Cannot be scraped or peeled by a pocket knife, specimen can be fractured with single firm blow of geological hammer	25-50
R4	Strong rock	Specimen requires more than one blow of geological hammer to fracture it	50-100
R5	Very strong rock	Specimen requires many blows of geological hammer to fracture it	100-250
R6	Extremely strong rock	Specimen can only be chipped with geological hammer	>250

*) Soil strength methods may better describe some cases in the database but for comparison purposes these are reported as R0 here.

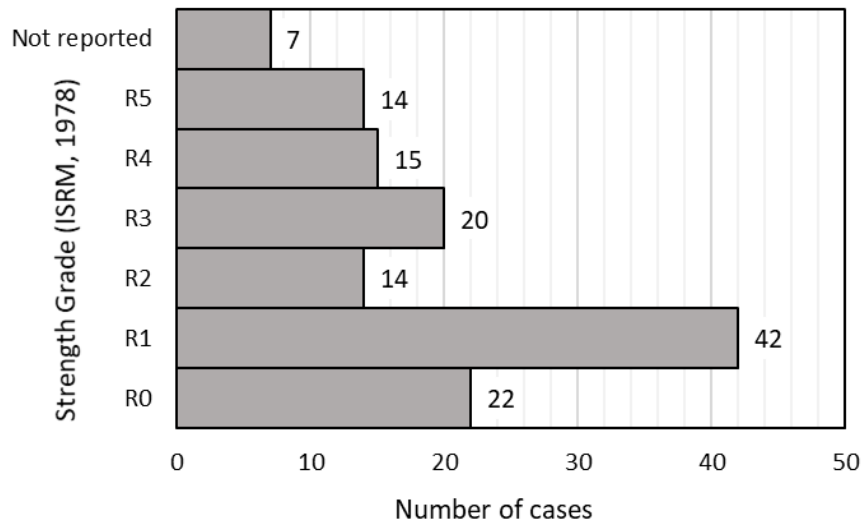


Figure 3.4 Strength grade distribution (total number of cases = 134)

3. Rock mass rating, RMR (1976)

Rock mass rating scheme is based on the subjective rating of specific attributes of the rock mass to identify the most significant parameters (e.g., intact strength, degree of fracturing, the condition of the discontinuities separation intact blocks, groundwater) influencing the behavior of rock mass (Bieniawski 1976). The value of RMR determines the geotechnical quality of the rock mass on a scale that ranges from zero to 100 and considers the 5 classes presented in Table 3.4. Figure 3.5 represents the groupings corresponding to Bieniawski's 1976 version of RMR.

Table 3.4 RMR calibrated against rock mass quality (reprinted from Read and Stacey 2009)

Description	RMR rating (1979)
Very poor	<21
Poor	40-21
Fair	41-60
Good	61-80
Very good	81-100

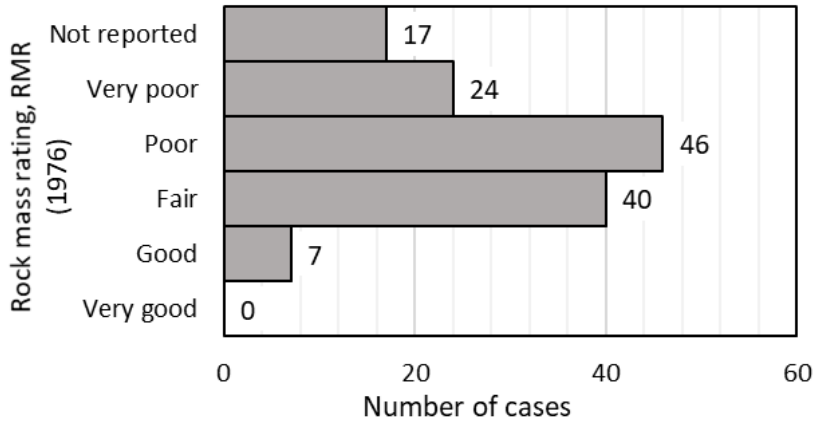


Figure 3.5 Distribution of rock mass rating (total number of cases = 134)

4. Unit Weight, γ (kN/m³): the average unit weight of the slope forming material. In some cases, the critical slip surface cut the several layers the unit weight was normalized by the length of the slip surface L (m) (Eq. 3.1):

$$\gamma = \frac{\sum \gamma_i L_i}{L} \quad \text{Eq. 3.1}$$

where γ_i =unit weight of the i-layer (kN/m³), and

L_i =length of the critical slip surface within the i-layer (m)

5. Cohesion c (kPa): the average cohesion of the slope forming material. Back-calculated values of cohesion and friction angle present the majority of the parameters in the reference sources of information. In some cases, the critical slip surface cut the several layers the cohesion was normalized by the length of the slip surface L (m) (Eq. 3.2):

$$c = \frac{\sum c_i L_i}{L} \quad \text{Eq. 3.2}$$

where c_i =cohesion of the i-layer (kN/m³)

6. Friction angle ϕ (°): the average friction angle of the slope forming material. In some cases, the critical slip surface cut the several layers the tangent of the friction angle was normalized by the length of the slip surface L (m) (Eq. 3.3):

$$\tan \varphi = \frac{\sum \tan \varphi_i L_i}{L} \quad \text{Eq. 3.3}$$

where $\tan \varphi_i$ =tangent of the friction angle of the i-layer (kN/m³)

Figure 3.6 shows the probability histogram and a log-normal parametric distribution with the arithmetic mean $E[\varphi]$ and standard deviation $\sigma[\varphi]$ plotted on the same graph.

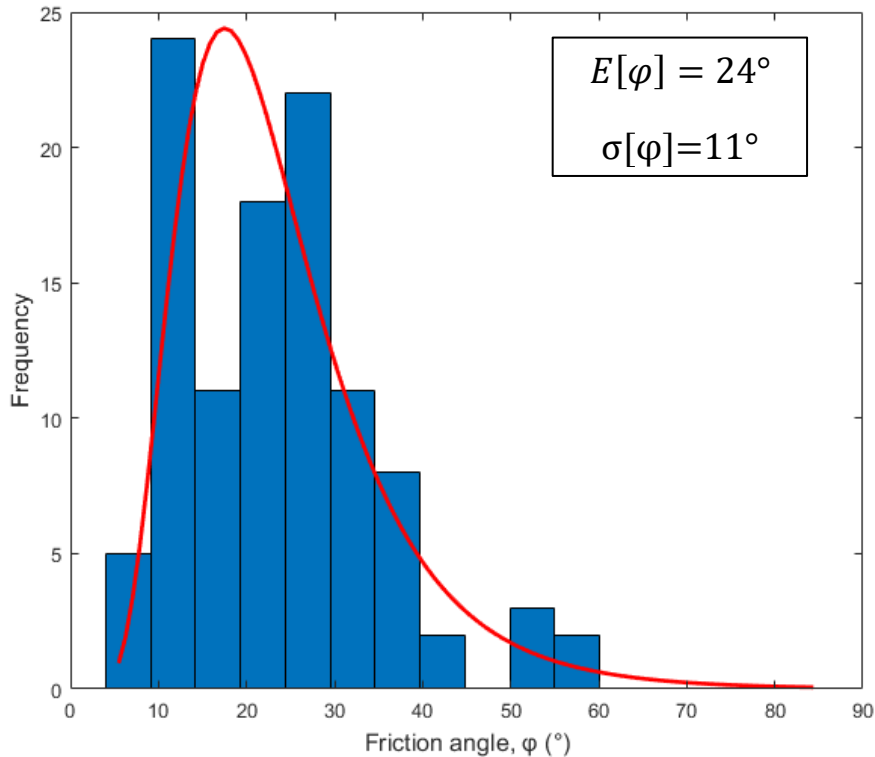


Figure 3.6 Distribution of the friction angle φ (°) (total number of cases = 106)

3.2.4 Part 4: Slope Failure Parameters

1. Failure Mechanism

There are debris slides, rock topples, rock compound slides, rock irregular slides, rock planar slides, rock rotational slides: rock wedge slides, soil planar slides, and soil rotational slide examples in the slope failure collection. Figure 3.7 presents the distribution of the cases with

different failure mechanisms. According to the bar chart, 45% of the cases represent rock planar slide and rock wedge slide.

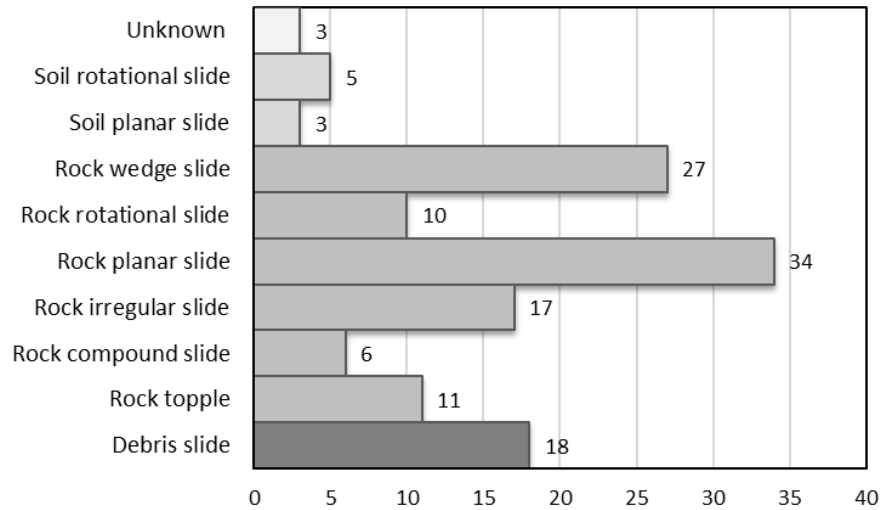


Figure 3.7 Distribution of the cases with different failure mechanisms (total number of cases = 134)

2. Trigger factor

A trigger is a factor that initiates the slope failure. Figure 3.8 illustrates the triggers reported in the literature or inferred from the open pit slope failure description. The cases are divided into seven different groups according to the trigger factor: blasting, daylighted structure, fault zone, freeze-thaw cycle, long-term weakening, mined too steep, precipitation event, and not reported. “Long-term weakening” refers to cases where the trigger event occurred long before the failure but initiated the sequence of events (Whittall 2015).

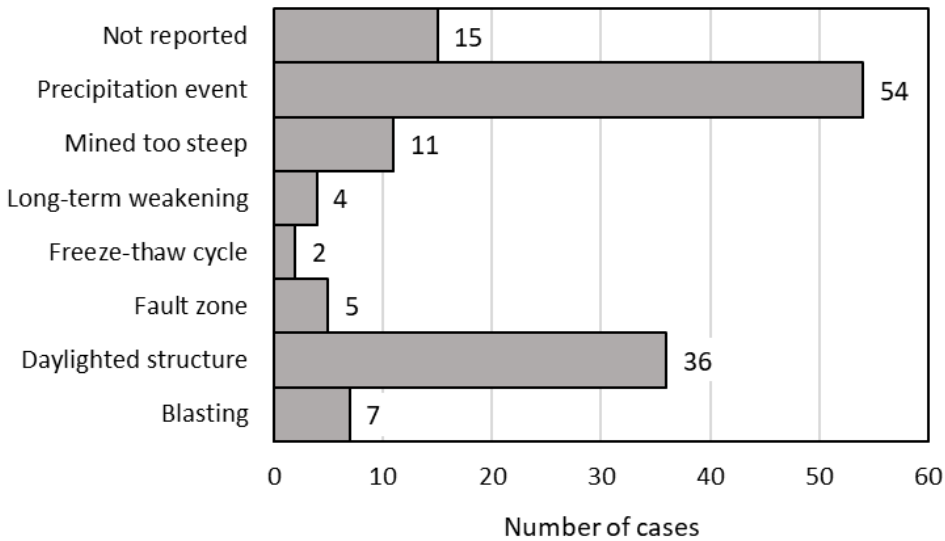


Figure 3.8 Distribution of reported triggering events (total number of cases = 134)

3. Volume (Mm³) – The volume of the failed material.

The volume of the failed material is usually reported in the public sources of information. The majority of slope failure presented in the database is in between 100,000 m³ and 5,000,000 m³. Figure 3.9 also shows that the open pit mining context requires a special perspective (Whittall 2015) compare to the natural landslides where the large amount of debris material is more often to be reported (Hsü 1975; Jacob and Hungr 2005, Davidson 2011).

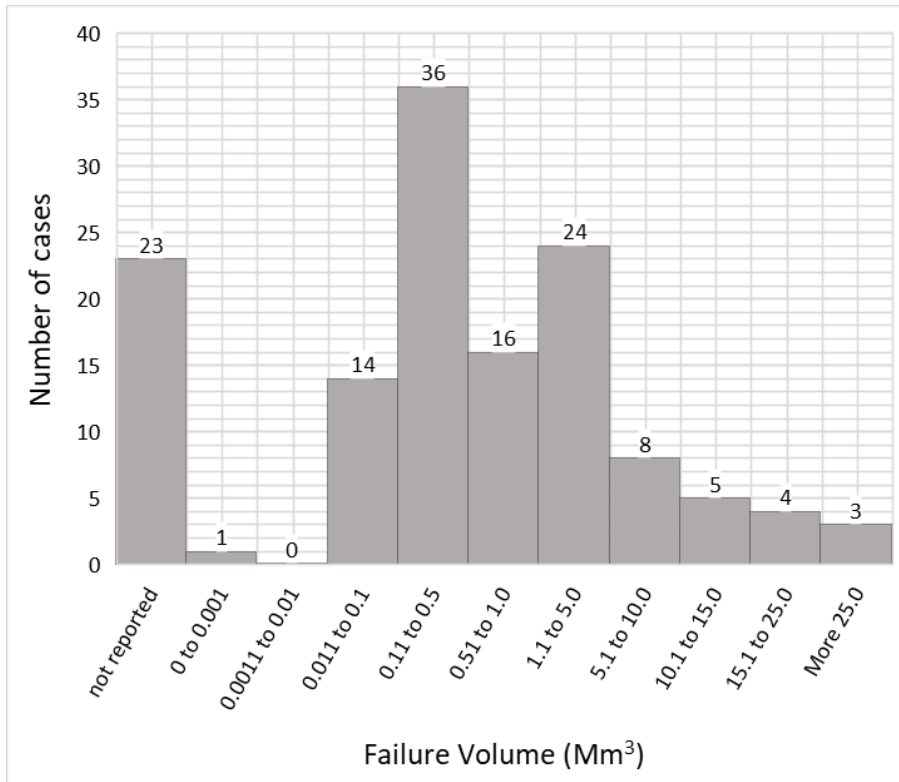


Figure 3.9 Distribution of the slope failure volume (total number of cases = 134)

Figure 3.9 shows the low frequency of events $>10,000,000 \text{ m}^3$, and no events occur above the $100,000,000 \text{ m}^3$ which can be the reason that the open pits are rarely can be deep enough to produce such a large failure.

4. Mass (tons)

The mass of the failed material is also reported in the public sources of information. The 56% cases have the reference to failure mass. The average value of the failed mass is 8,500,000 ton (based on the 75 cases) (Figure 3.10).

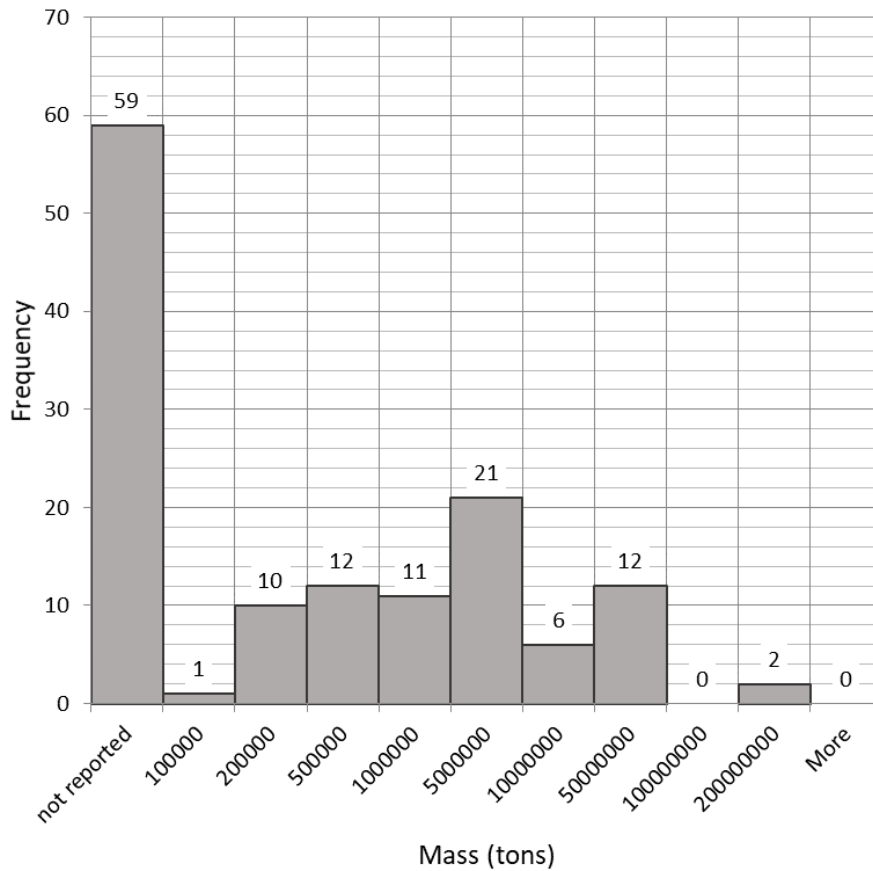


Figure 3.10 Distribution of the slope failure mass (total number of cases = 134)

5. Slope Angle, $\beta_{\text{FAIL}}(^{\circ})$

Slope angle, $\beta_{\text{FAIL}} (^{\circ})$ is the angle between the horizontal line and the line connecting the toe and the crest of a slope failure (see Figure 3.2). Figure 3.11 shows the probability histogram a normal parametric distribution with the arithmetic mean $E[\beta_{\text{FAIL}}]$ and standard deviation $\sigma[\beta_{\text{FAIL}}]$ plotted on the same graph.

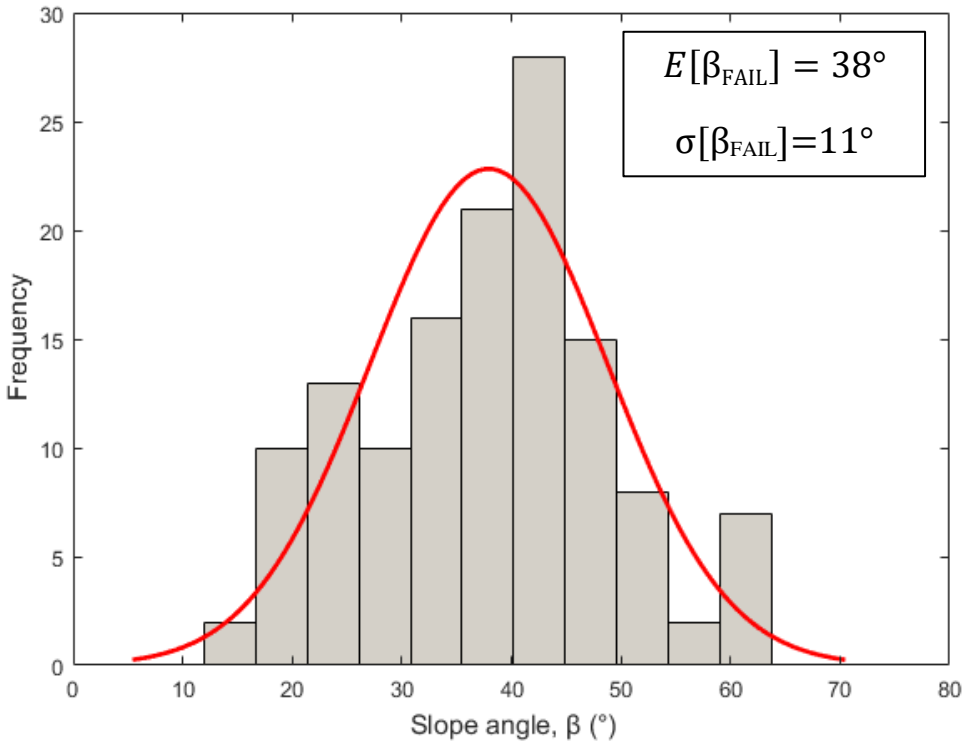


Figure 3.11 Distribution of the slope angle $\beta_{\text{FAIL}} (^{\circ})$ (total number of cases = 134)

6. Fall Height, H_{FALL} (m).

Fall height is the vertical distance from the crest of the failure to the end of the debris flow tongue (see Figure 3.2). Figure 3.12 shows the probability histogram and a log-normal parametric distribution with the arithmetic mean $E[H_{\text{FALL}}]$ and standard deviation $\sigma[H_{\text{FALL}}]$ plotted on the same graph. Arithmetic mean of the fall height for the 134 case histories is 164 m.

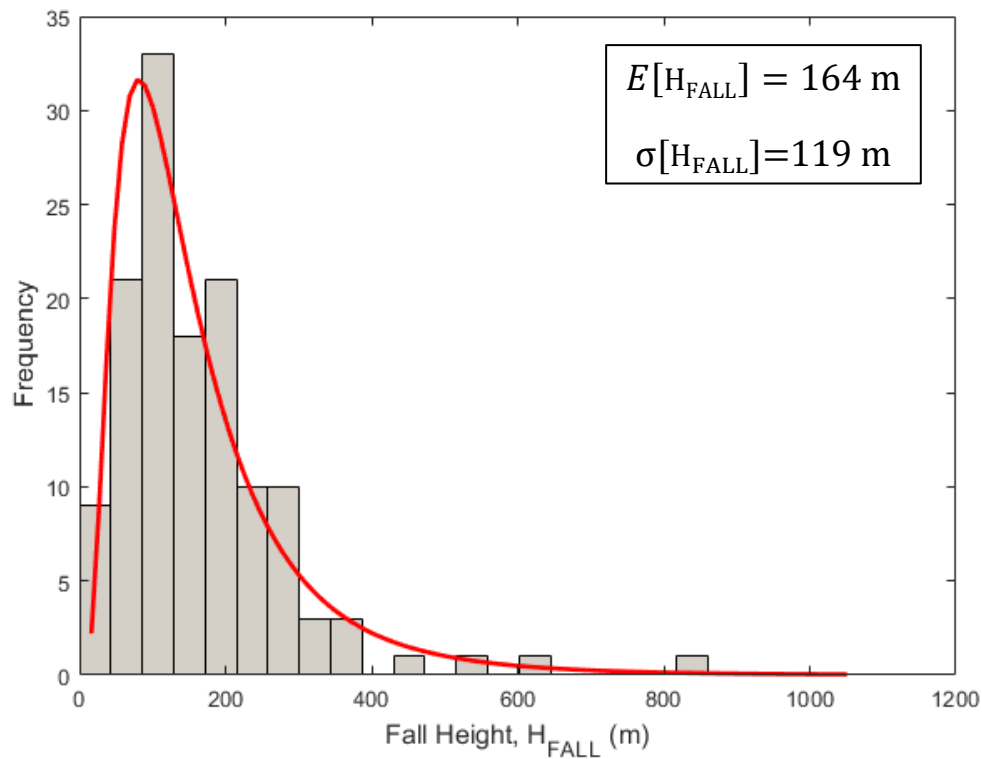


Figure 3.12 Distribution of the fall height H_{FALL} (m) (total number of cases = 134)

7. Travel distance, L_{TRAV} (m).

Travel distance is the horizontal distance from the crest of the failure to the end of the debris flow tongue (see Figure 3.2). Figure 3.12 shows the probability histogram and a log-normal parametric distribution with the arithmetic mean $E[L_{TRAV}]$ and standard deviation $\sigma[L_{TRAV}]$ plotted on the same graph. Travel distance arithmetic mean based on the 134 case history analysis is 374 m.

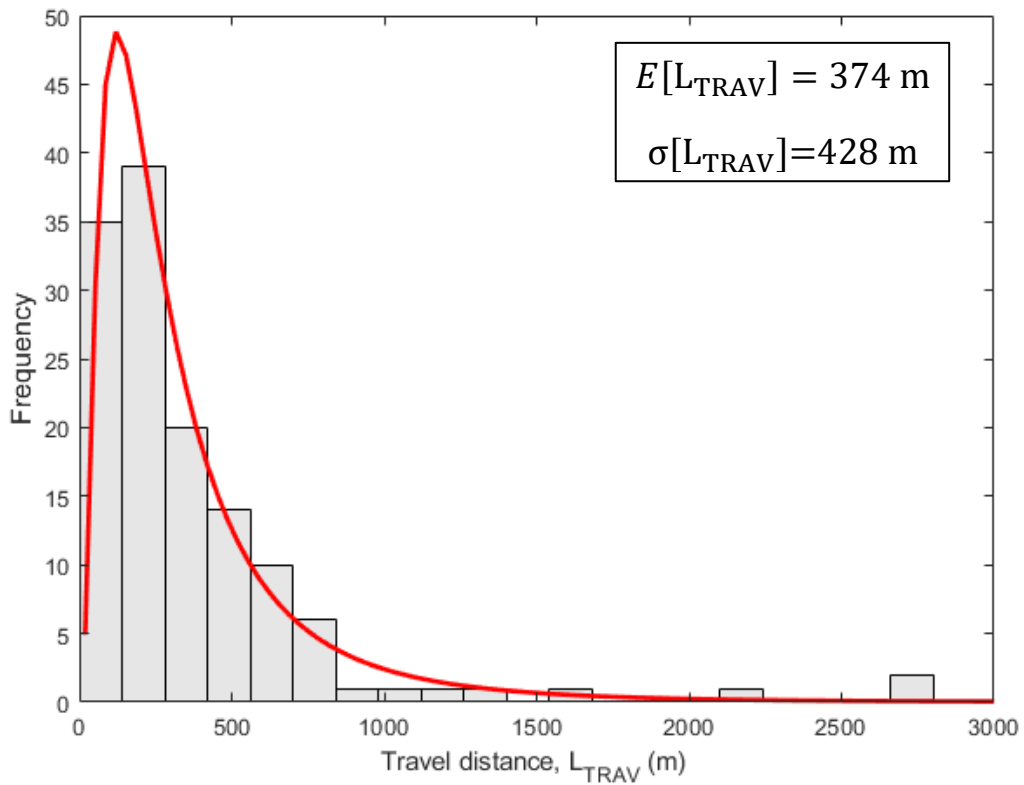


Figure 3.13 Distribution of the travel distance L_{TRAV} (m) (total number of cases = 134)

8. Average Width, W_{FAIL} (m): average width of the failure

Log-normal distribution of the average width, W_{FAIL} (m) is presented in Figure 3.14. The arithmetic mean of an average width based on the 104 case histories is 248 m.

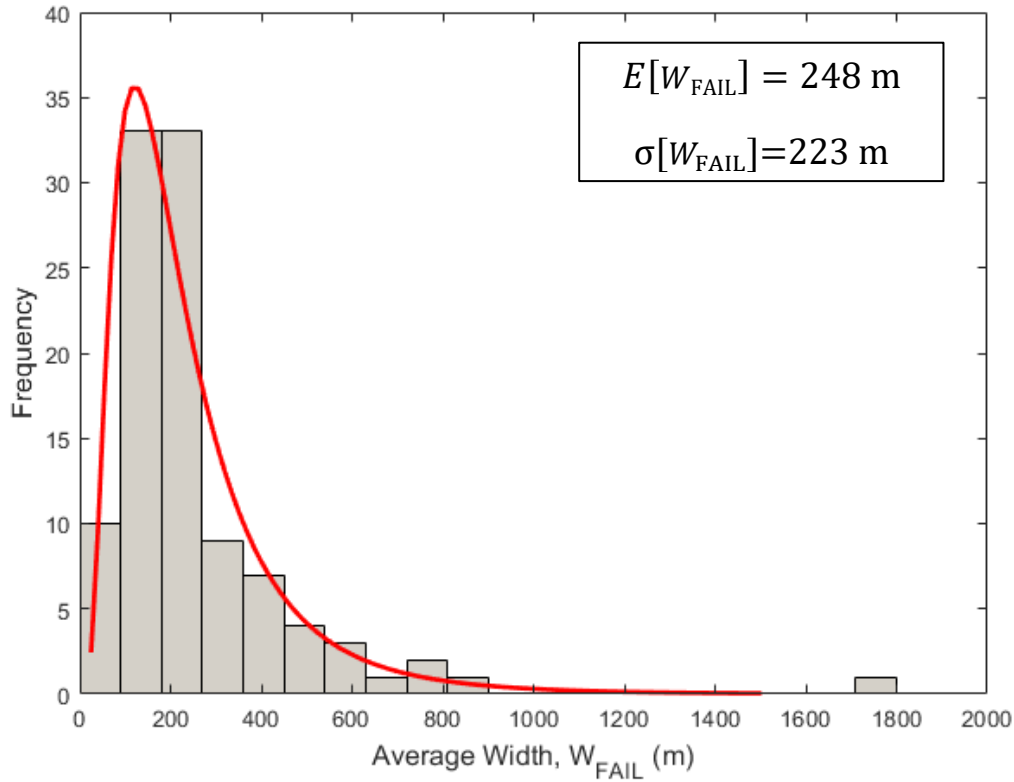


Figure 3.14 Distribution of the average width, W_{FAIL} (m) (total number of cases = 104)

9. Setback distance, L_{SB} (m)

Setback distance is the minimum safe distance from the edge of the pit wall at all stages of pit development which provides a safe buffer zone for personnel and equipment away from the slope crest (Figure 3.2). Setback distance is log-normally distributed, as can be seen in Figure 3.15. The arithmetic mean of the setback distance based on the analysis of a 112 case histories is 29 m.

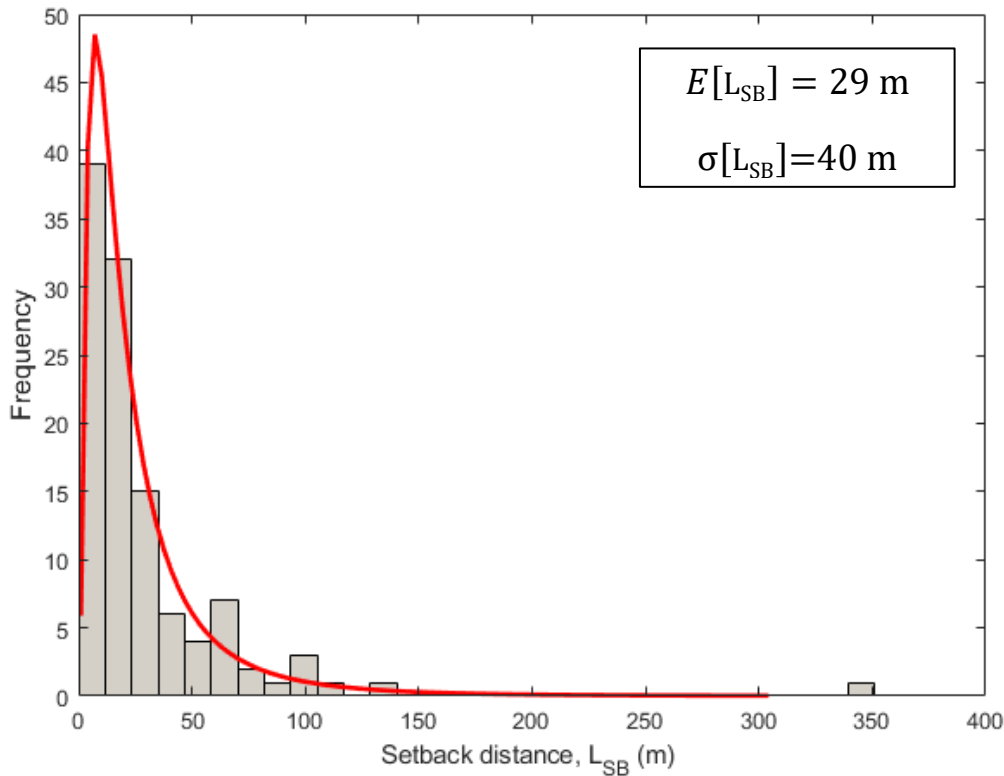


Figure 3.15 Distribution of the setback distance, L_{SB} (m) (total number of cases = 112)

10. Height of the failure, H_{FAIL} (m).

Height of the failure is the vertical distance from the crest of the failure to the toe of the slip surface (see Figure 3.2). Figure 3.16 is the log-normal distribution of the height of the failure based on the open pit failure case histories database analysis (total number of analyzed cases is

116). The arithmetic mean and the standard deviation of the failure height are presented in the figure.

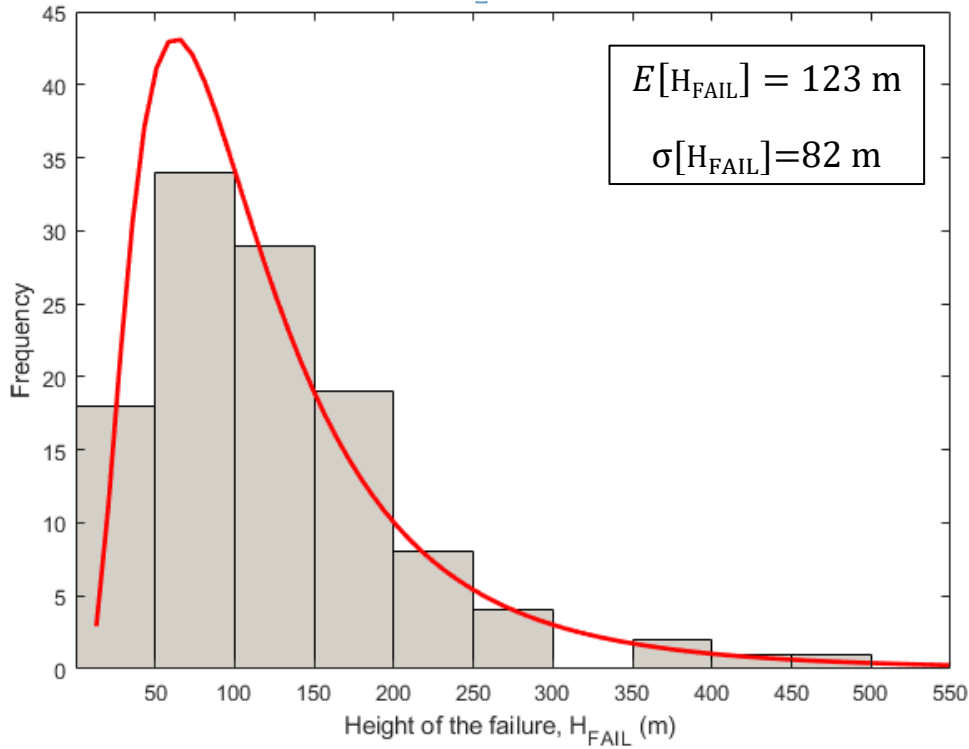


Figure 3.16 Distribution of the height of the failure, H_{FAIL} (m) (total number of cases =116)

3.2.5 Part 5: Slope Failure Plan and Scheme

Part 5 of the database contains (a) general view, (b) plan view, and (c) cross-section of the failure. It should be noted that the slope failure plane or scheme is presented in the database for 76% of the cases.

3.2.6 Part 6: General Information

General information of the case history contains a source of information, software that was used to perform the slope stability analysis, and the type of the monitoring system set up in the open pit mine.

In the public-domain, it is more likely to find information about large, mobile, interesting failures mitigated by effective slope management rather than about the small failure. Building a dataset with greater diversity is desirable but likely only possible with access to mine failure reports. No preference was given to particular regions or operations, however, authors at certain mines publish more frequently than others. The data are from over 60 open-pit mines across the world. Almost one third (29.8%) of the data comes from the US (Figure 3.17).

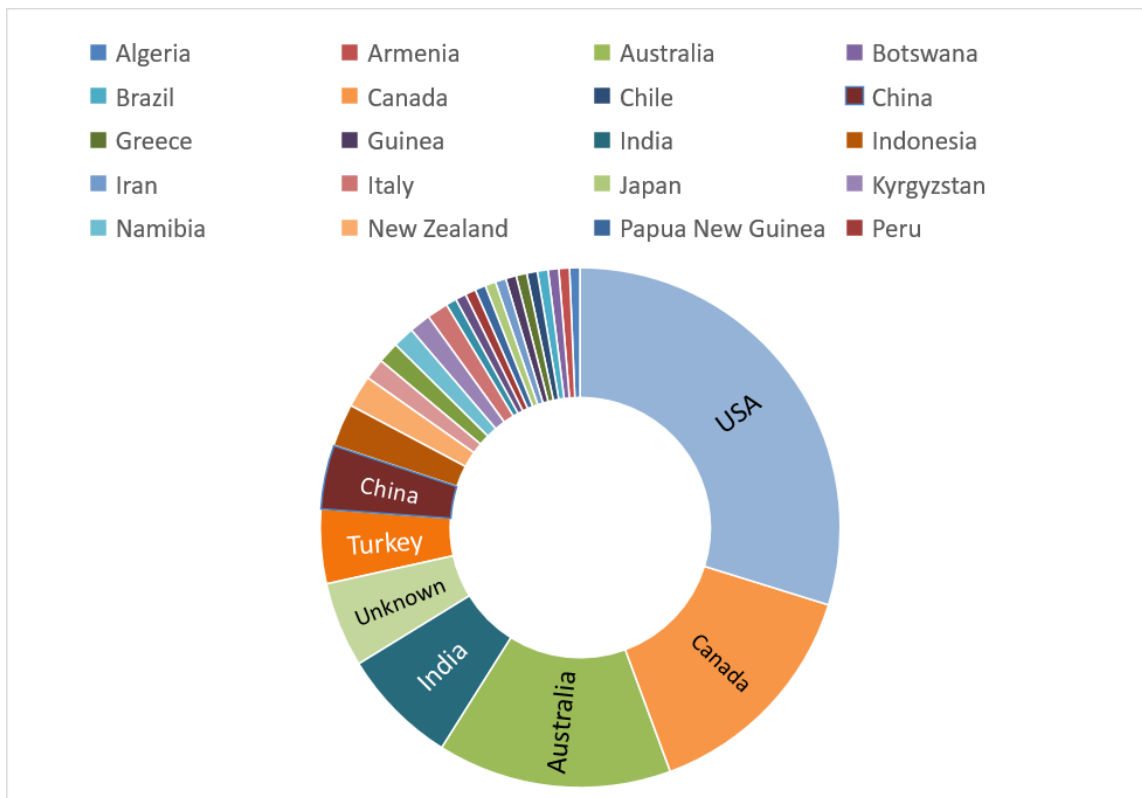


Figure 3.17 Sunburst with hierarchical data corresponding to the countries where the data were obtained

3.3 Analysis of the data

3.3.1 Travel distance prediction

3.3.1.1 Background information

Slope failures in open pit mining may result in loss of life, destruction of mining facilities, damage to the expensive equipment, and lost production. The volume and the velocity of the slide mass can be such that people in the travel path do not have time to evacuate and the kinetic energy is such that even small slope failure can severely damage mining equipment and mining facilities.

According to McDougall (2016) travel distance analysis methods can be grouped into two broad categories (Figure 3.18):

- 1) empirical-statistical methods that rely on statistical geometric correlations, and
- 2) analytical methods that rely on process-based modelling. Numerical models, including both continuum and discontinuum models, fall into the second category. Within this sub-category, hybrid ‘semi-empirical’ numerical models that rely on some form of parameter calibration are more common than pure mechanistic models that rely on independent material property estimates.

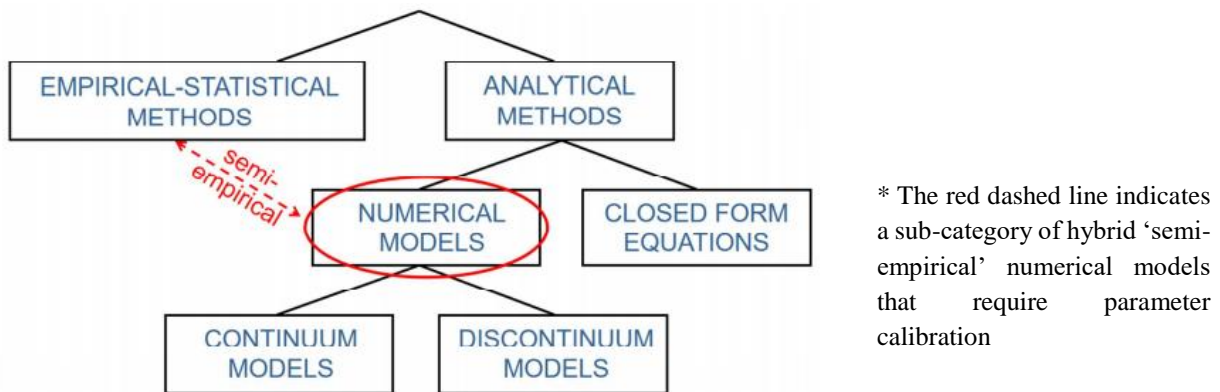


Figure 3.18 Available material travel distance analysis methods (reprinted from McDougall, 2016)

A summary of the literature on empirical methods for predicting the landslide travel distance was made by G. Hunter and R.Fell (2003); and Whittall et al. (2017).

The travel distance of slopes has been studied by many researchers, but most of them focused on natural landslides (Heim 1932; Scheidegger 1973; Hsü 1975; Sassa 1988; Van Gassen and Cruden 1989; Hungr 1995; Ayotte and Hungr 1998; Locat and Leroueil 1997; Finlay et al. 1999; Hunter and Fell 2003; Davidson 2011). Some researchers focused on the travel distance for open pit mining (Whittall 2015; Whittall et al. 2017; Mc.Quillan et al. 2018; Whittall et al. 2020).

The earliest empirical methods showed that the travel distance decreases with increasing slide volume (Heim 1932; Scheidegger 1973; Hsü 1975; Hutchinson 1988; Golder Associates Limited 1995; Corominas 1996; Finlay et al. 1999; Davidson 2011). Further differentiation was made according to the material and slope type (cut, fill, or natural slope) (e.g., Hutchinson; Golder Associates Limited; Finlay et al.), the degree of confinement of the travel path (e.g., Golder Associates Limited; Corominas), the slide classification such as rockfall or debris flow (e.g., Corominas; Hutchinson); and obstructions to the slide mass (e.g., Corominas). Scheidegger (1973); Li (1983); Nicoletti and Sorriso-Valvo (1991); Corominas (1996); Davidson (2011) analyzed the volume-based mobility and the Fahrböschung angle (the angle of the line connecting the crest of the slope left after failure and the toe of the deposit after it comes to rest) relationships. The runout length was studied by Legros (2002), and excessive travel distance vs. volume of the failed mass were studied by Hsü (1975) (see Figure 3.19). Nicoletti and Sorriso-Valvo (1991) provided an equation based on the normalization of excessive travel distance to the total runout length. The relationship between the travel distance and the inundation area was studied by Li (1983), Abele (1997) and Iverson et al. (2012).

The input parameters required for travel distance calculation include (Figure 3.19):

1. H is the fall height;
2. H_f is the failure height: vertical height from failure crest to failure toe, this may be equal or less than H ;
3. L_{SB} is setback distance: horizontal distance from pre-failure crest to failure back-scarp;
4. L is travel distance: the horizontal length from failed crest to distal toe of failed material;
5. V is volume of failed material;

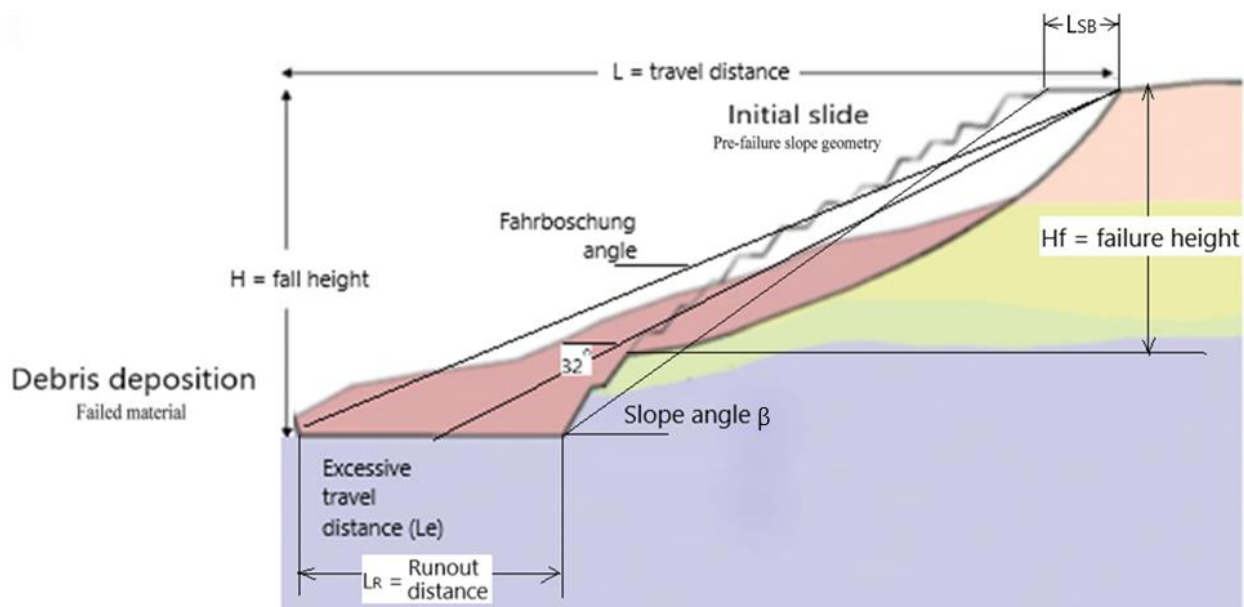


Figure 3.19 Schematic definition of the travel distance (adapted from Whittall 2017 and Crouse and Wright 2015).

6. L_R is runout distance: horizontal distance from pre-failure slope toe to distal toe of failed material, excluding isolated boulders, this may be equal or less than. Runout of the sliding material can be defined as the flow behavior of materials after a certain event (Pirulli and Pastor 2012). In the context of this research, slope failure runout can be defined as the total movement of the material debris that ejected from the top to bottom (Jakob and Hungr 2005, McQuillan et al. 2018).

7. Fahrböschung angle can be defined as the apparent friction coefficient as shown in Figure 3.20.

The difference between the Fahrböschung angle and the friction angle is the measurement of height and length (McDougall and Hungr 2004). The Fahrböschung angle is defined as the inclination of the line joining the far end of the debris deposition to the crest of the landslide scarp. Thus, the apparent friction angle (or Fahrböschung angle) can be defined as:

$$\varphi_a = \tan^{-1} \frac{H}{L} \quad \text{Eq.3.4}$$

and the real friction angle is defined as:

$$\varphi = \tan^{-1} \frac{H_g}{L_g} \quad \text{Eq.3.5}$$

where H and L are the height and length using the uppermost point of the collapse scar and the distant tip of the deposit, whereas H_g and L_g relate to the original and final gravity centers of the involved rock mass.

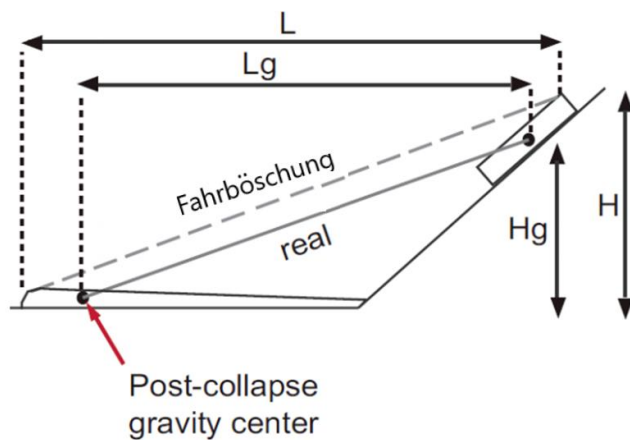


Figure 3.20 Comparison of apparent friction coefficient (Fahrböschung) with real friction coefficient (reprinted from Shea and Vries 2008)

The travel distance, L, slope angle, β , and failure height, H, defined in Figure 3.19, and are used to describe the overall longitudinal geometry of the sliding mass from the crest of the source

area to the distal toe of the travel. The actual parameters of the open pit failure can be demonstrated by the case history that occurred at the Cowal gold mine, Australia (Figure 3.21 and Figure 3.22). The Cowal gold mine experienced two large failures in 2007 (Crouse and Wright 2015; Martin and Stacey 2018). The east wall of the pit had been mined at 31-32 degrees instead of the design angle of 25 degrees, the lacustrine clays and saprolites were fully-saturated and the regional stress direction was essentially east-west. All three of these factors contributed to the failures (Crouse and Wright 2015; Martin and Stacey 2018).

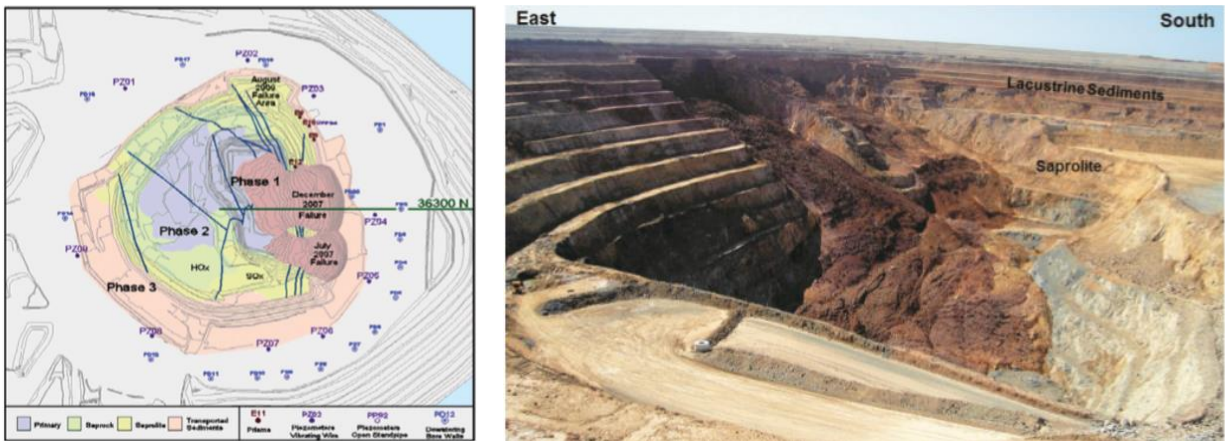


Figure 3.21 East wall failures at Cowal gold mine, Australia (reprinted from Crouse and Wright 2015)

The structural genesis of slide avalanches was studied by Shear and Vrise (2008). A number of laboratory scaled rockslide-avalanche experiments were performed by using sand. A summary diagram of the different types of rockslide avalanches is presented in Figure 3.23. The X-axis represents the transport time line, from initiation to stoppage, and the Y-axis separates distinct structure types. The bar represents the limit between the acceleration plane and the depositional plane.

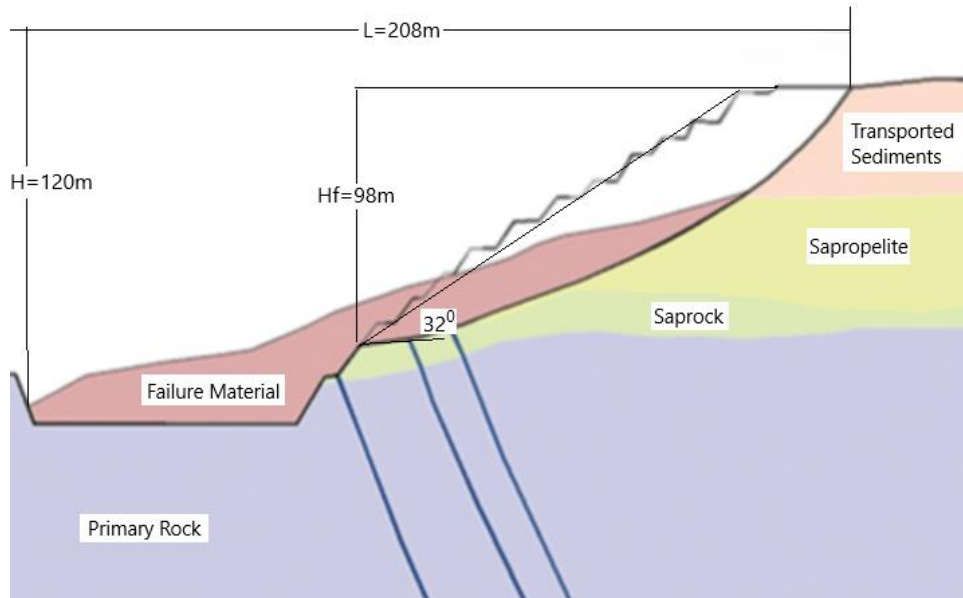


Figure 3.22 Cross section of the east wall failures at Cowal gold mine, Australia (adapted from Crouse and Wright 2015)

As shown in Figure 3.23, the slide process starts with hummocks appearing at the initiation of the accelerated mass. The mass structures form as the material is released and the slide is initiated. Normal troughs or faults are developed first as the slide propagates. Differential movements initiate strike-slip faults that remain active until the slide halts. Final deposit surfaces can be grouped into two textural types, hummocky or ridged. The hummocky textures are produced by differences in the cohesion of the initial layering. Ridged textures are produced when the initial material is homogeneous. The mass structures in the final deposits can also be grouped into two kinematic types, compressional or extensional. The limit between the two is controlled by the topographic profile of the slide. If it goes from steep to flat, then the regime is compressional; if the profile is more regular, then extension dominates.

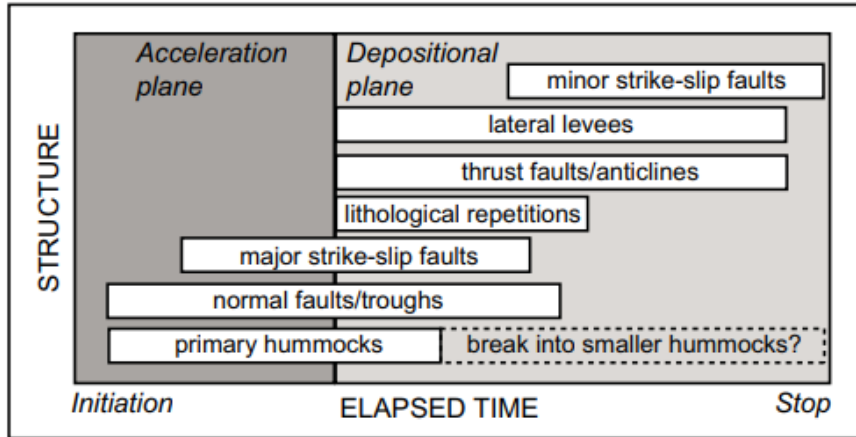


Figure 3.23 Diagram of stricture genesis in laboratory scale rockslide avalanches during flow (reprinted from Shear and Vrise 2008)

The work of Shear and Vrise (2008) showed that natural compressional rockslide avalanches have lower runout and cover a smaller area than their extensional equivalent for similar volumes. Open pit slopes have the advantage of removing the influence of morphological features, vegetation, and liquefiable substrates while controlling the travel path angle and roughness. Thus in such a controlled environment, landslide mobility has very much influenced by the slope angle, the material properties, and the fall height, while it is not very sensitive to the slide volume (Whittall et al. 2017).

Other authors studying long runout natural landslides considered landslide motion as an energy balance problem (i.e., the distance a landslide will travel is proportional to the potential energy available). Potential energy-based relationships that were analyzed included Fahrböschung angle (Howard 1973), runout length (McSaveney 1975; McDougall 2016), and inundation area (Dade and Huppert 1998). Table 3.5 presents a summary of the available mobility relationships based on different input parameters: volume of the failure mass, geometry of the failed slope and value of potential energy.

Table 3.5 Summary of the available mobility relationships (modified from Whittall et al. 2017)

Input	Mobility relationship	Best-fit equation	R ²	Source
Volume	H/L	$\frac{H}{L}=0.463V^{-0.148}$		Heim (1932)
Volume	H/L (for volume range $1.2 \cdot 10^{10} \text{m}^3$)	$\frac{H}{L}=1.03V^{-0.10}$	0.82	Corominas (1996)
Volume	H/L (for fresh strong rock)	$\frac{H}{L}=0.559V^{-0.150}$		Whittall (2015)
Volume	H/L (for weathered weak rock)	$\frac{H}{L}=0.408V^{-0.146}$		Whittall (2015)
Volume	H/L (extraterrestrial)	$\frac{H}{L}=0.25V^{-0.13}$	0.36	Shear and Vries (2008)
Volume	H/L (terrestrial)	$\frac{H}{L}=0.14V^{-0.16}$	0.63	Shear and Vries (2008)
Volume	Le	$Le=108.3 \ln(V) + 84.4$		Hsü (1975)
Volume	Le/L	$\frac{Le}{L}=0.114 \ln(V) + 0.206$		Nicoletti and Sorriso-Valvo (1991)
Volume	L	$L=321.3V^{0.383}$		Legros (2002)
Volume	Area	$A=6V^{2/3}$		Iverson et al. (1998)
Height	L _R (for planar and wedge)	$L_R=-0.459H-0.773$	0.69	McDougall (2016)
Height	L _R (for toppling)	$L_R=-0.459H-0.773$	0.84	McDougall (2016)
Slope angle	H/L	$\frac{H}{L}=0.488 \tan(\beta) + 0.117$		Hunter and Fell (2003)
Potential energy	Area	$A=0.13E_p^{0.0908}$		Dade and Huppert (1998)
Potential energy	L	$L=0.0208E_p^{0.335}$		McSaveney (1975)
Potential energy	L/H	$\frac{L}{H}=0.218 \ln(E_p) - 3.959$		Howard (1973)

A – planimetric inundation area; E_p – potential energy; V – source volume; β – original wall angle; H – fall height; L – travel distance; Le – excessive travel distance; L_R – runout distance (see Figure 3.2)

Over the years, several empirical models have been developed for regionally and type-specific natural landslides and man-made slopes which are based on databases (Corominas, 1996, Finaly et al. 1999, Fannin and Wise 2001, Hunter and Fell 2003, Whittall et al. 2015, McQuillan et al. 2018, Whittall et al. 2020). The methods cover a very large range of landslide volume, from several cubic meters to tens of billions of cubic meters. Based on the work that has been done on estimating the travel distance, it can be concluded that there is large uncertainty in the estimates of travel distance, particularly for small volume slides in man-made and natural soil slopes. However, all the estimates presented in Table 3.5 are challenging to use for the travel distance prediction from the industry point of view because they are based on parameters that are difficult to obtain in advance. Thus, slope failure case histories for open pit mines should be collected and studied more precisely. Three basic parameters have to be taken into account for the travel distance prediction: the failure height, the fall height and the slope angle (Figure 3.24).

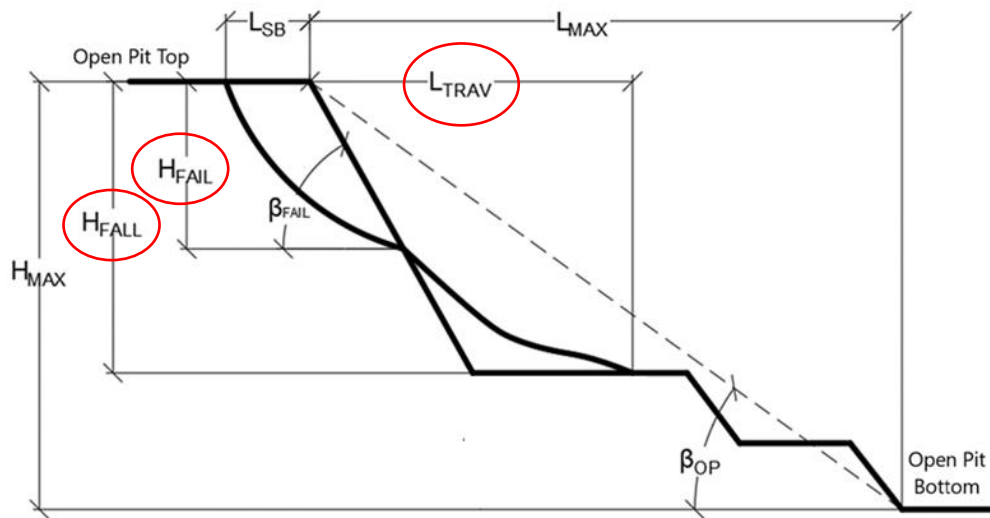


Figure 3.24 Basic geometrical parameters used for the travel distance prediction

3.3.1.2 Travel distance prediction based on the TAMU-MineSlope Spreadsheet

The following results present the analysis of 134 open pit mining slope failures between 1969 and 2020 that occurred worldwide.

First prediction that was made is that the travel distance as a function of failure height. Figure 3.25 presents the plot with the travel distance (L_{TRAV}) in the vertical axis and the failure height (H_{FAIL}) in the horizontal axis. Green line shows the best fit regression line, and equation in green box is the best equation that could be found for L_{TRAV} vs. H_{FAIL} .

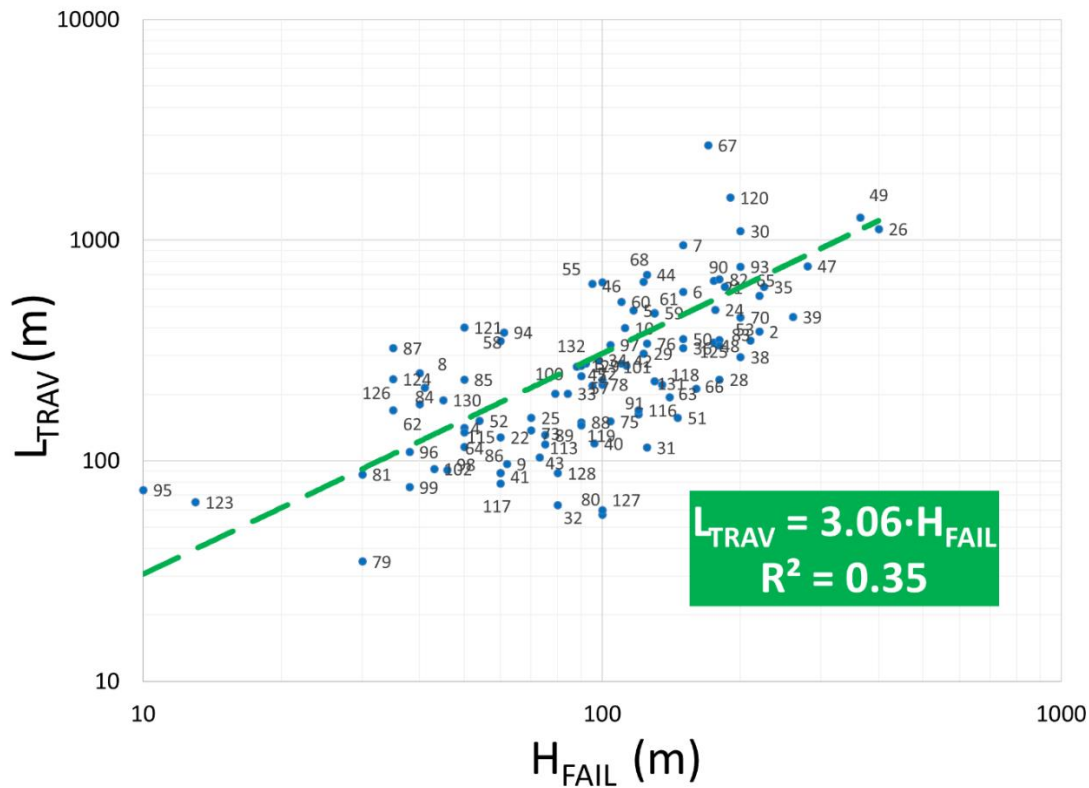


Figure 3.25 Relationship between Failure Height and Travel Distance of the failure mass based on the TAMU-MineSlope Spreadsheet

The equation listed in the green box (Figure 3.25) was obtained through a deterministic statistical analysis, meaning that it reflects the predicted value as a single number, with no quantification of the possible error associated with predicting failure event.

Another idea of the presented research is to provide the travel distance estimation equation using a reliability-based approach that assesses whenever the predicted value is conservative enough for engineering design. This approach is called the probability of over-predicting (POO) approach. It is important to know the probability that the predicted value A is greater than the actual value A_c to be on the safe side in the design problem. Eq. 3.6 shows the probabilistic model, which consists of the selected deterministic predicted parameter A_{det} and a correction factor $\alpha(\text{PoE})$:

$$A_{new} = \alpha(\text{PoE}) \cdot A_{det} \quad \text{Eq.3.6}$$

where A_{new} is the new value of the parameter, A_{det} is the deterministically predicted parameter, and $\alpha(\text{PoE})$ is the correction factor; $\alpha(\text{PoE})$ can also be defined as the ratio of A_{new} and A_{det} .

The open pit mining case histories database was used to narrow down the wide range of correlations and provide a measure of the probability that the predicted value of the travel distance would be larger than the actual travel distance.

Different correlations between the travel distance and the fall height have been proposed. All of the correlations are of the form (Eq. 3.7):

$$L_{TRAV} = \alpha(\text{PoE}) \cdot (3.06 \cdot H_{FAIL}) \quad \text{Eq.3.7}$$

where L_{TRAV} is the travel distance in meters, $\alpha(\text{PoE})$ is the correlation factor, and H_{FAIL} is the failure height in meters. Another words the equation listed in the green box (Figure 3.25) can be used in the design with the correction factor $\alpha(\text{PoE})$ because the regression line has to be in a position where the error is minimized, because the designer has to target a certain percent probability that the predicted value is greater than the observed value.

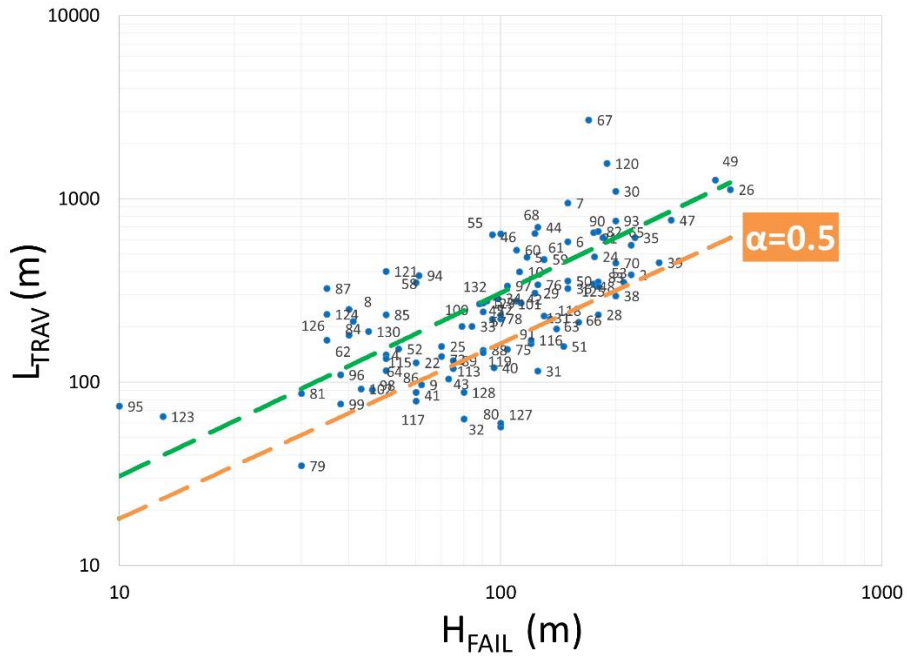
Scatter plots of predicted vs. measured parameter for various values of $\alpha(\text{PoE})$ are shown in Figure 3.26a-f. There are a total of 99 data points in the scatter plots. Figure 3.26a shows the

predicted value of the travel distance using correlation factor $\alpha(\text{PoE})=0.5$. This plot indicates that when the value of $\alpha(\text{PoE})=0.5$ is used in Equation 3.6, 10 out of the 99 predicted travel distances are larger than the measured travel distances. Therefore, in this case, there is a $10/99 = 10.1\%$ probability that the predicted travel distance will be larger than the measured one. This gives one point on the probability plot of Figure 3.27 (10.0% and 0.5).

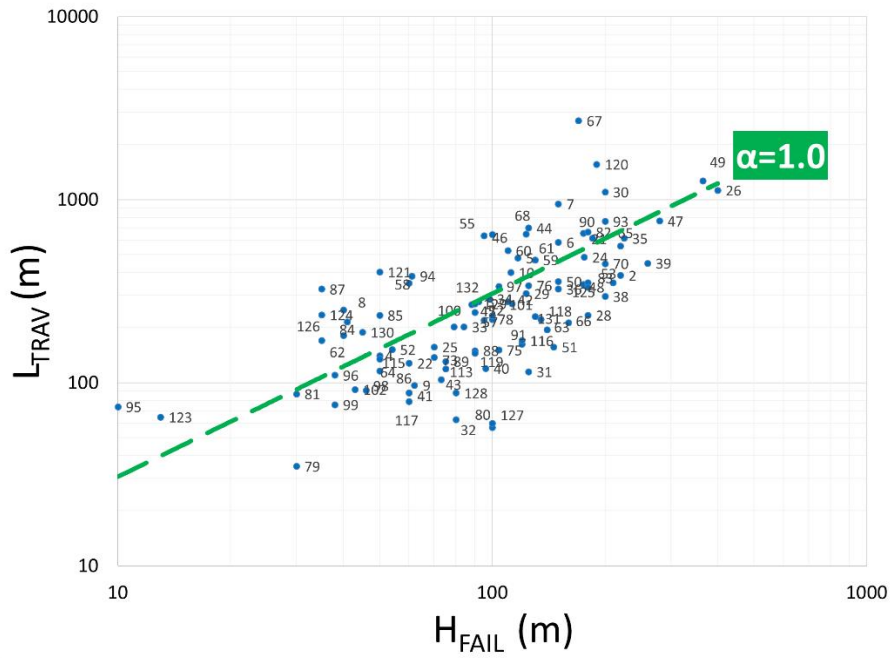
Table 3.6 Correction factor $\alpha(\text{PoE})$ and corresponding PoE (%) to predict travel distance based on the failure height

$\alpha(\text{PoE})$	0.5	1	1.5	2.0	2.1	2.5	3.0	4.0
Number of cases exceeding the predicted value	18.00	63.00	79.00	88.00	90.00	95.00	97	98
Probability of accident, PoE, %	18.18	63.64	79.80	88.89	90.91	95.96	97.98	98.99

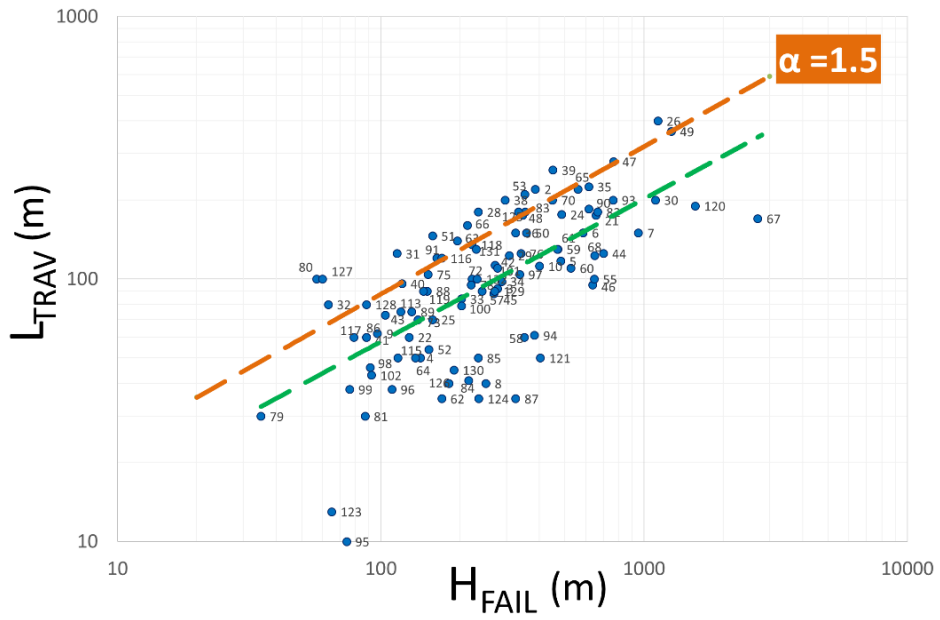
Figure 3.26b shows the predicted travel distance using a correction factor $\alpha(\text{PoF})$ equal to 1.0 in Eq.3.6. In this case, 63 out of the 99 predicted values are larger than the measured travel distances. Therefore, a $63/99= 63.64\%$ probability that the predicted travel distance will be larger than the measured one. This gives a second point on the probability plot (1.0 and 63.64%). This process was repeated for different correlation factor $\alpha(\text{PoF})$ (Figure 3.26 c-f and Table 3.6) and the results are plotted in Figure 3.27. The vertical axis in Figure 3.27 represents the probability (%) that the predicted value is greater than the observed value, or the predicted value is conservative enough for engineering design. On the horizontal axis is the correction factor $\alpha(\text{PoE}) = 0.5; 1; 1.5; 2.0; 2.5, 3.0, 4.0$.



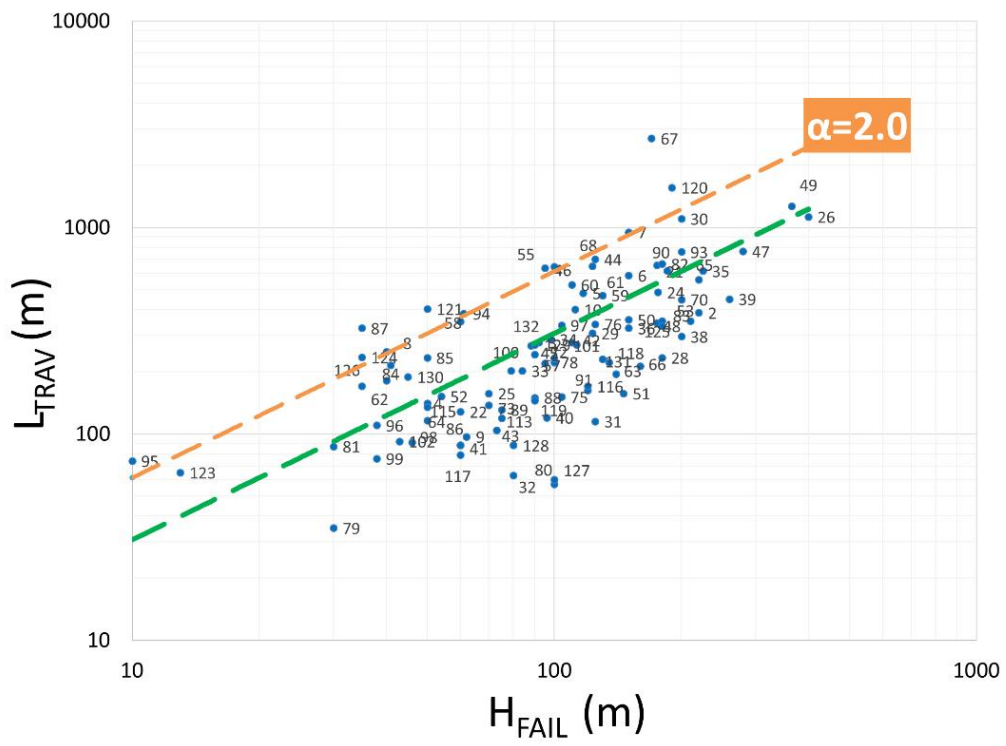
a)



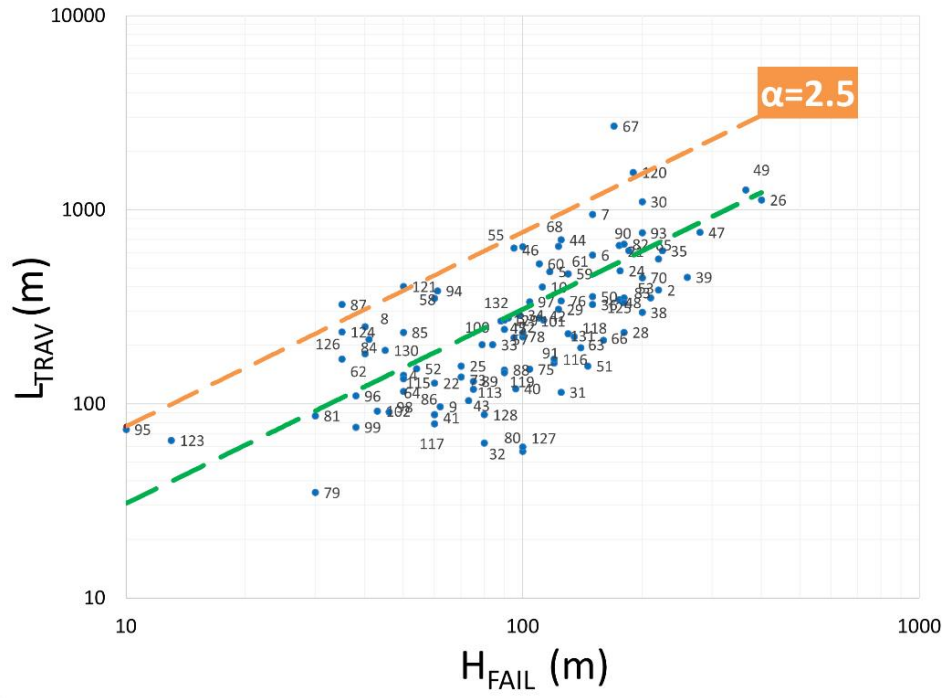
b)



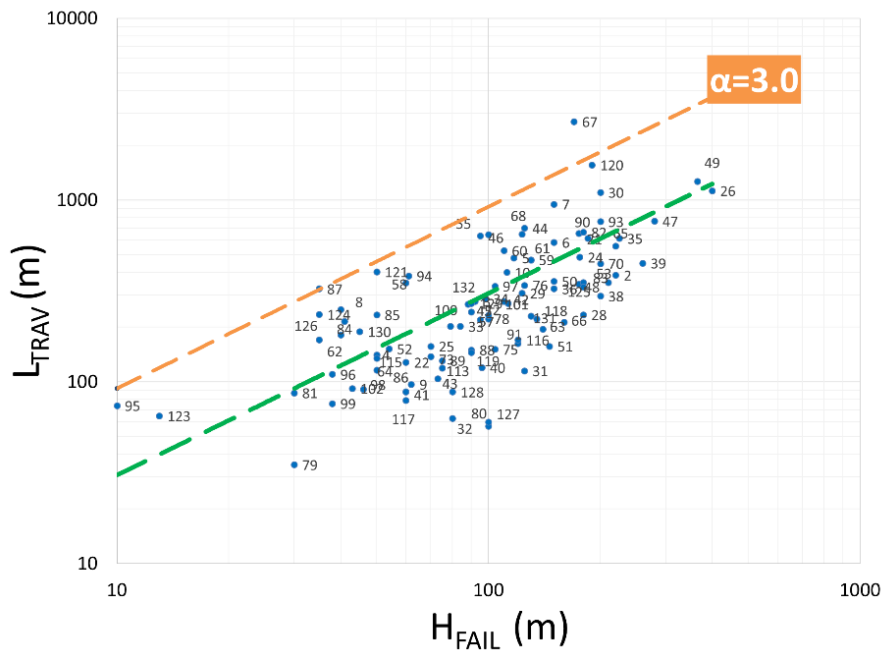
c)



d)



e)



f)

Figure 3.26 Predicted vs. measured travel distance records based on TAMU-MineSlope

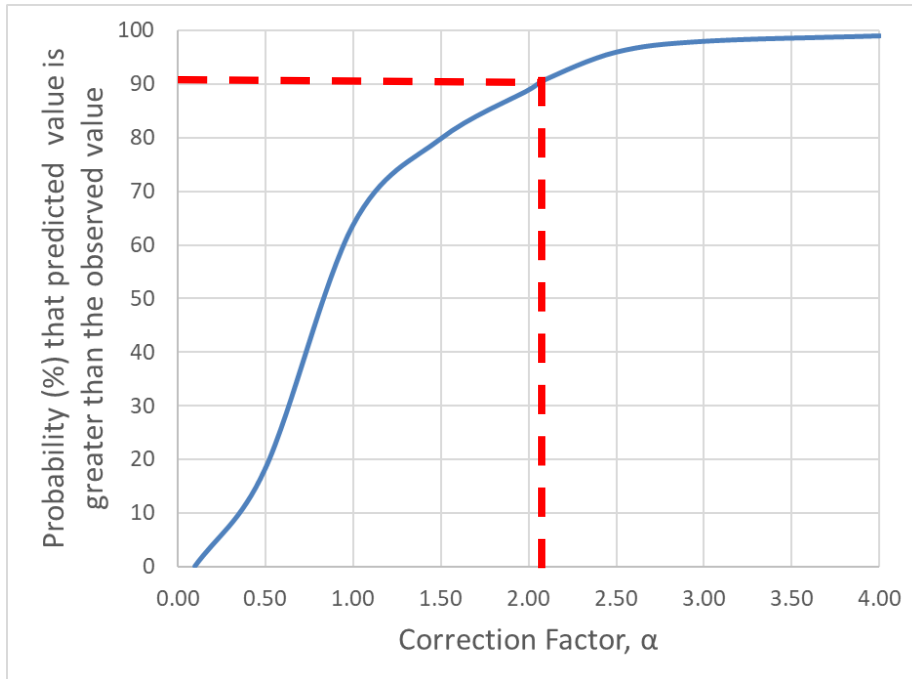


Figure 3.27 Probability of higher than predicted travel distance occurrence for all data in TAMU-MineSlope (referred equation is $L_{TRAV}=3.06 \cdot H_{FAIL}$)

The predicting value of the travel distance should be chosen based on a probability that the predicted travel distance is larger than the measured value and the corresponding correlation factor has to be used. For example, to reach a 90% probability that the predicted travel distance will be larger than the measured value a correction factor α (PoF) of 2.10 is necessary:

$$L_{TRAV} = 2.1 \cdot 3.06 \cdot H_{FAIL} \quad \text{Eq.3.8}$$

The red regression line in Figure 3.28 represents the 90% probability that the predicted travel distance is greater than the observed travel distance. For the design purposes, the best-predicted equation for the travel distance based on the knowing parameter of the failure height is:

$$L_{TRAV} = 6.43 \cdot H_{FAIL} \quad \text{Eq.3.9}$$

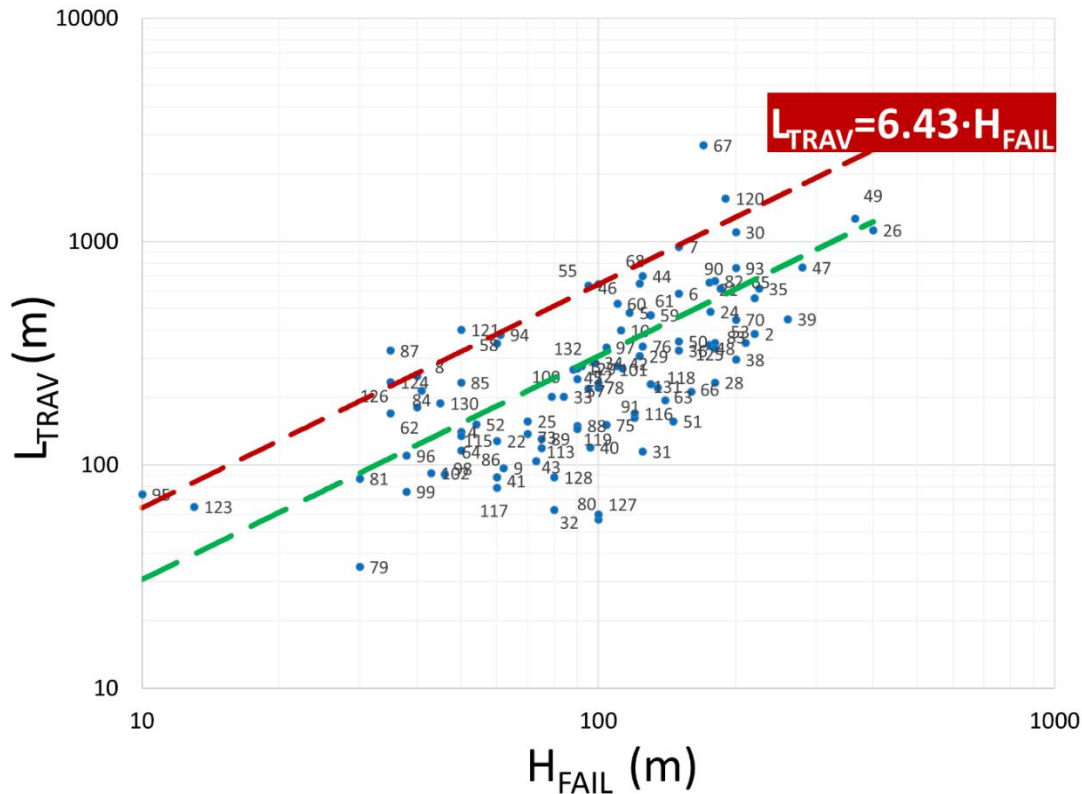


Figure 3.28 Predicted versus measured travel distance records for TAMU-MineSlope (red line represents regression line with a 90% probability to be safe, failure height is the reference value).

The accuracy of the prediction based on the developed model relies on assessing the model parameter uncertainty. A probabilistic approach using the prediction intervals provides a procedure in which uncertainty and experience can be integrated into the analysis. Prediction interval is the interval within which the unknown statistical parameter of the population, say the mean, is contained with a certain level of confidence, say 80% probability. The width of that interval depends on sample size, the parameter being estimated and correlations among observations. For a specific confidence level, the width of the confidence interval decreases as the number of observations increases. In other words, the uncertainty on the estimated statistical parameter (e.g.,

the mean) is higher for small samples. Statistical techniques for quantifying the uncertainty due to sample size, known as statistical error (El-Ramely 2001).

The equation of the prediction interval utilizes the following parameters (Eq. 3.10):

- The average of all independent variables for the points in the regression data, \bar{X}
- The independent variable for which the interval is being computed, x
- The indicator of the scatter in the data, SE. SE is an average of how much an actual y-value differs from the predicted y-value. r
- Number of points, n
- t-statistic for the input confidence level and the number of points in the regression data, t_a

$$x = y \pm t_a \cdot SE \cdot \sqrt{1 + \frac{1}{n} + \frac{(x - \bar{X})^2}{\sum_{i=0}^n (x_i - \bar{X})^2}} \quad \text{Eq.3.10}$$

To develop the prediction interval for the L_{TRAV} (m) vs. H_{FAIL} (m) model the natural logarithm of the two variables were calculated. Variation of the $\ln(L_{\text{TRAV}})$ with respect to $\ln(H_{\text{FAIL}})$ presents in Figure 3.29.

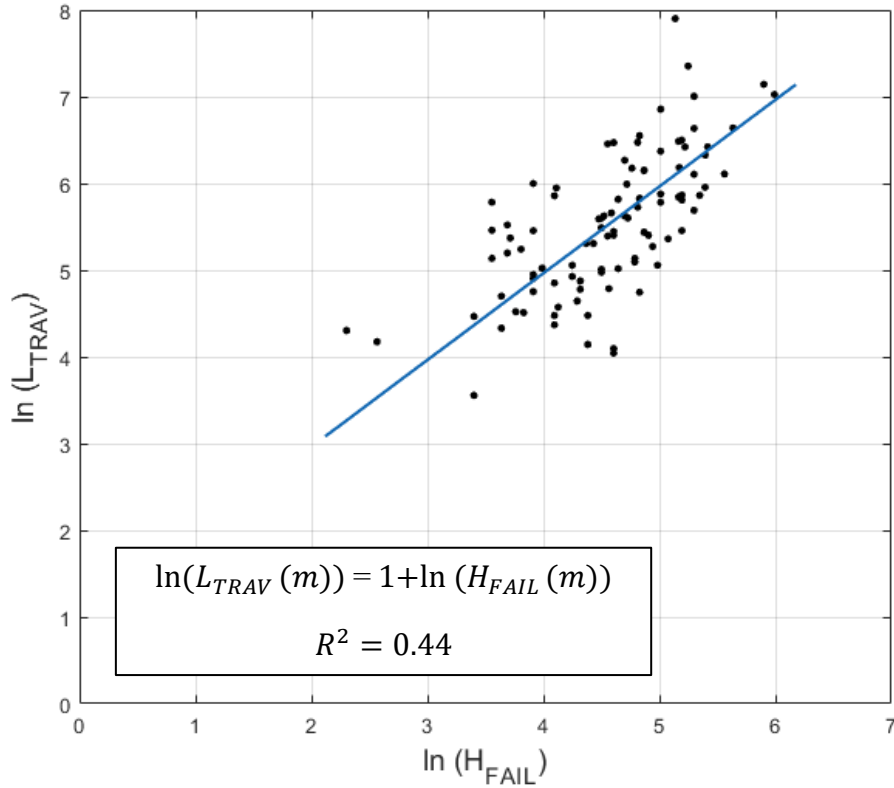


Figure 3.29 Variation of the $\ln(L_{TRAV})$ with respect to $\ln(H_{FAIL})$

A prediction interval approach gives an interval within which the expected value of L_{TRAV} lies with a specified probability. For example, assuming that the L_{TRAV} errors are normally distributed, and 80% prediction interval means that the travel distance of the failed material will be within two bounds (upper and lower bounds correspond to 90% and 10% exceedance limits consequently) in 80% of the cases (Figure 3.30).

The best fit regression line and its equation is presented in the figure above. The equation presented in Figure 3.29 can be rewritten as the exponent raised by the quantity inside the natural logarithm. Therefore the mean model can be described by the following equation:

$$L_{TRAV}(m) = 2.72 \cdot H_{FAIL}(m) \quad \text{Eq.3.11}$$

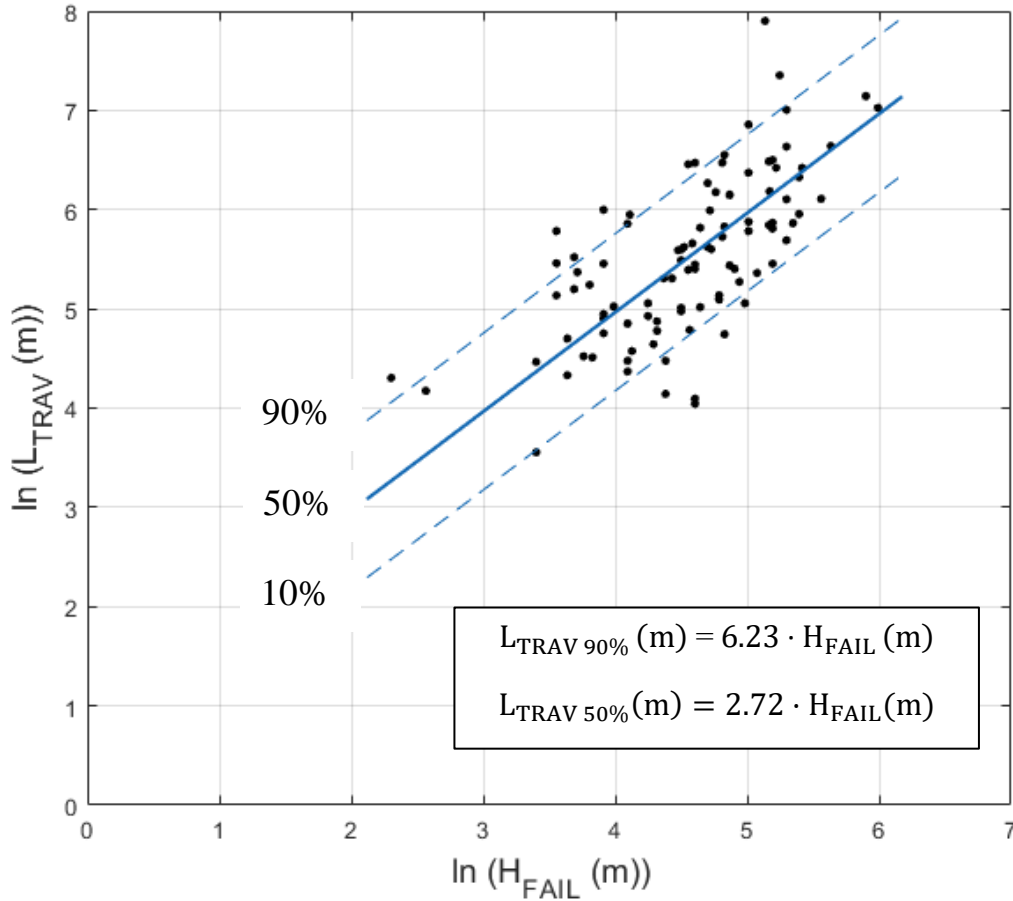


Figure 3.30 Design chart for $\ln(L_{\text{TRAV}})$ vs. $\ln(H_{\text{FAIL}})$ with 80% prediction interval plotted on the same graph. The upper level corresponds to a 90% exceedance probability, the lower level - to a 10% exceedance probability.

Figure 3.30 is the recommended relationships fitted with 80% prediction intervals analogous to the open-pit mine design risk tolerance. These are a probability of exceedance assuming a cumulative standard normal distribution based on error distribution. Prediction intervals are a relatively easy way to model the uncertainty in travel distance for the failed material. The geotechnical engineer can choose their risk tolerance and use a high and low volume estimate to bracket the expected travel distance. For example, a prediction using a 10% exceedance probability has a PoF = 0.1, or a 10% chance the travel distance of the failed material will exceed the observed values.

The comparison of the probability approach and prediction interval approach was made in the present research. Figure 3.31 shows the cloud of data points, best-fit regression line, probability line with the correction factor $\alpha=2.1$, and upper bound of the prediction interval with an 80% confidence level. As it was shown in the figure, both of the approaches give the same result.

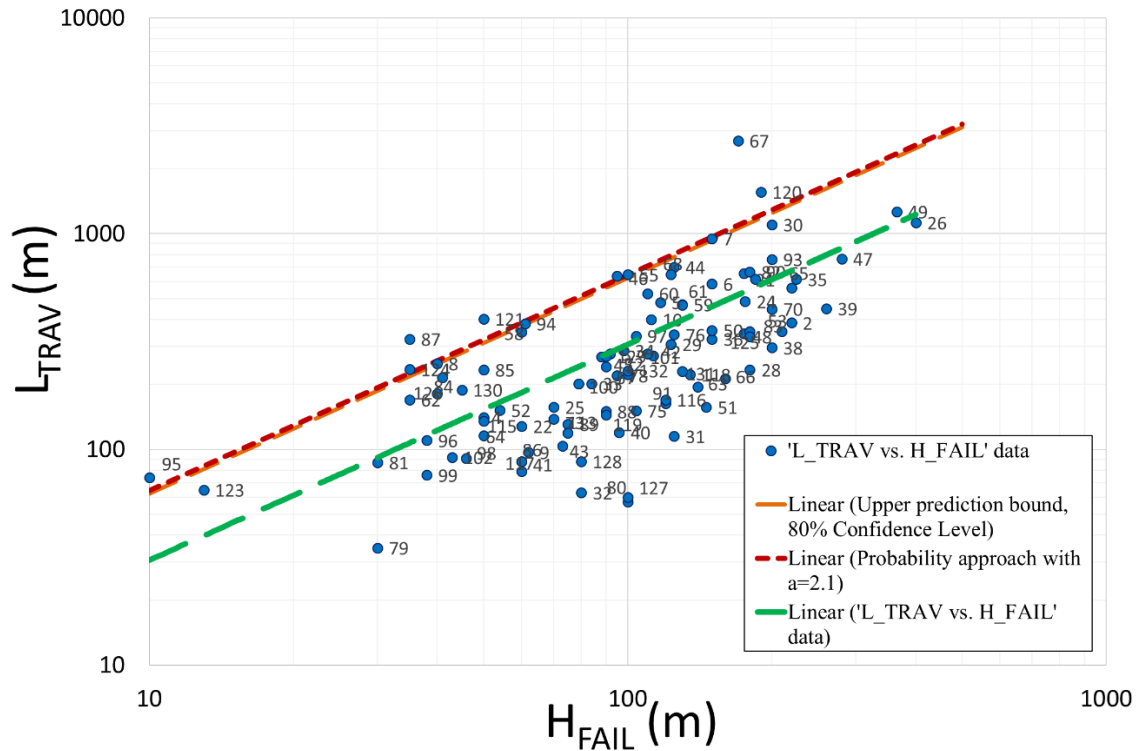


Figure 3.31 Comparison of the probability approach and prediction interval approach

Based on the actual observations of the failed mass behavior, the material may not be stopped at the toe of the slip surface and can continue to move even up to the bottom of the open pit. Therefore the correlation between travel distance and fall height was also considered in the research (Figure 3.32). The green dashed line in Figure 3.32 presents the regression line of the correlation, and the best fit equation is:

$$L_{TRAV}(m) = 2.42 \cdot H_{FALL}(m) \quad \text{Eq.3.12}$$

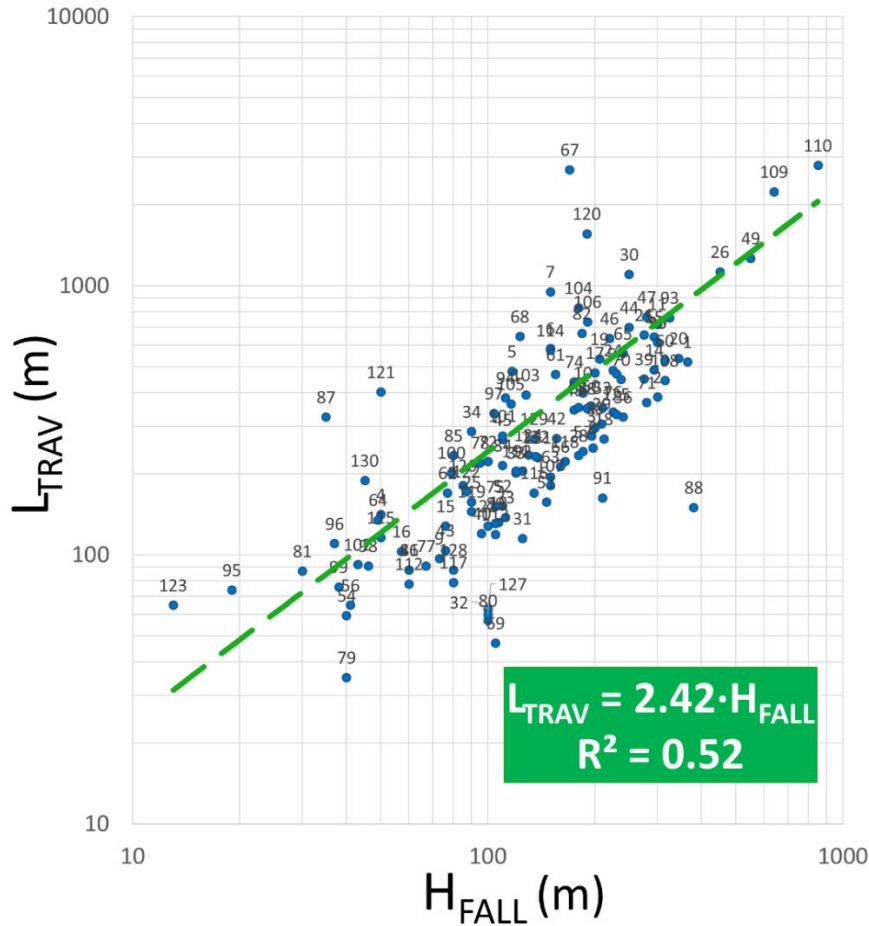


Figure 3.32 Relationship between Fall Height and Travel Distance of the failure mass (total number of points = 125)

The probability plot was built based on the procedure discussed earlier in this chapter (Figure 3.33). For the 90% probability that the predicted value of the travel distance, the correction factor $\alpha(\text{PoF})$ of 1.65 should be used, and Equation 3.12 became:

$$L_{TRAV}(m) = 4.0 \cdot H_{FALL}(m) \quad \text{Eq.3.13}$$

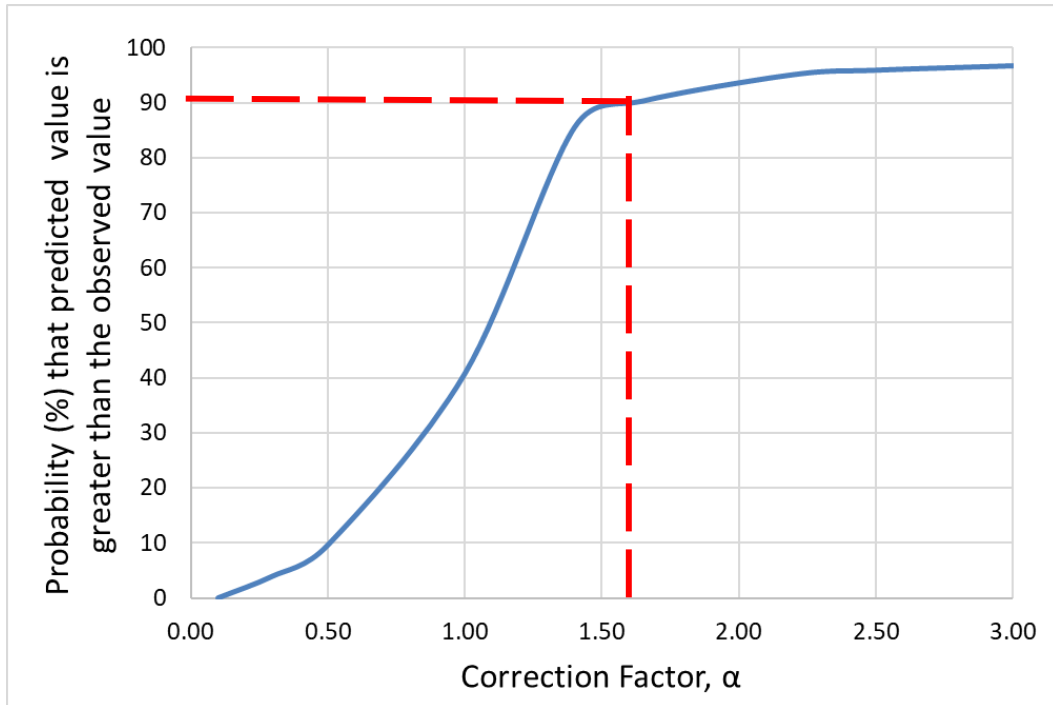


Figure 3.33 Probability of higher than predicted travel distance occurrence for all data in the TAMU-MineSlope Spreadsheet (the referred equation is $L_{TRAV}=2.42 \cdot H_{FALL}$)

The relationship where the travel distance is 4.0 times greater than the fall height is proposed to be used in the open pit design (Figure 3.34).

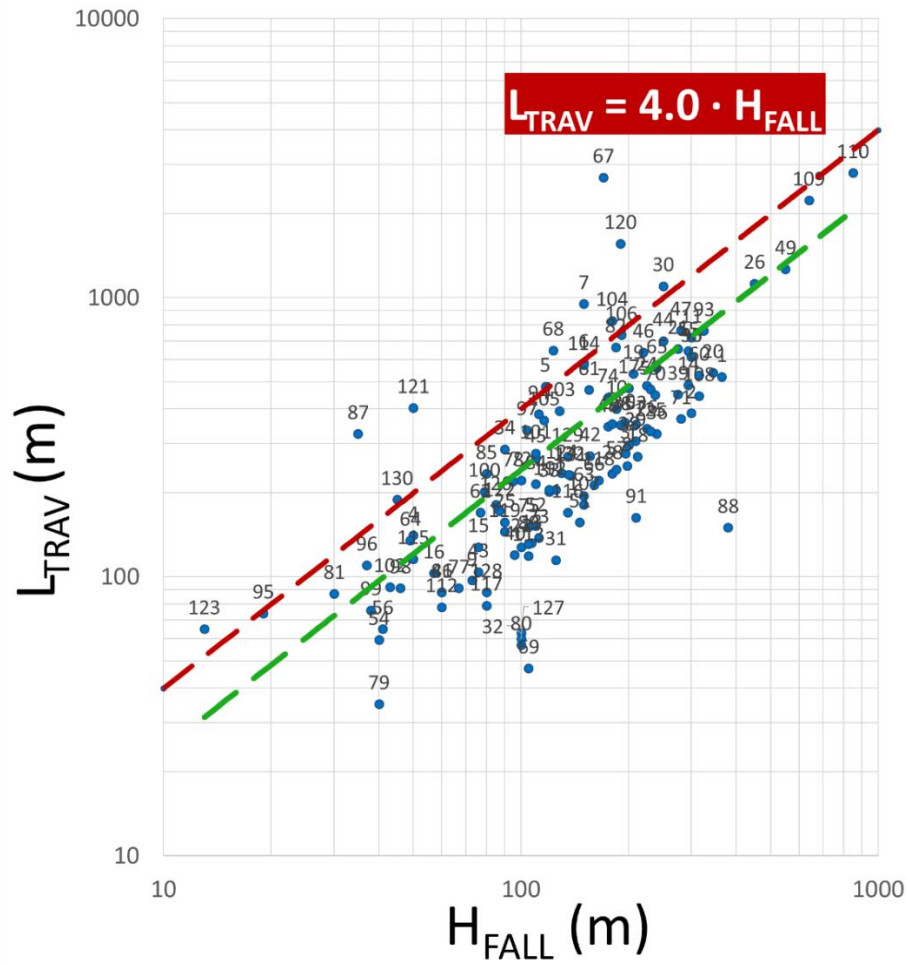


Figure 3.34 Predicted versus measured travel distance records for open pit failure database (red line represents regression line with a 90% probability to be safe; fall height is the reference value).

Design chart with an 80% prediction interval presented in Figure 3.35. The upper level corresponds to a 90% exceedance probability; the lower level corresponds to a 10% exceedance probability.

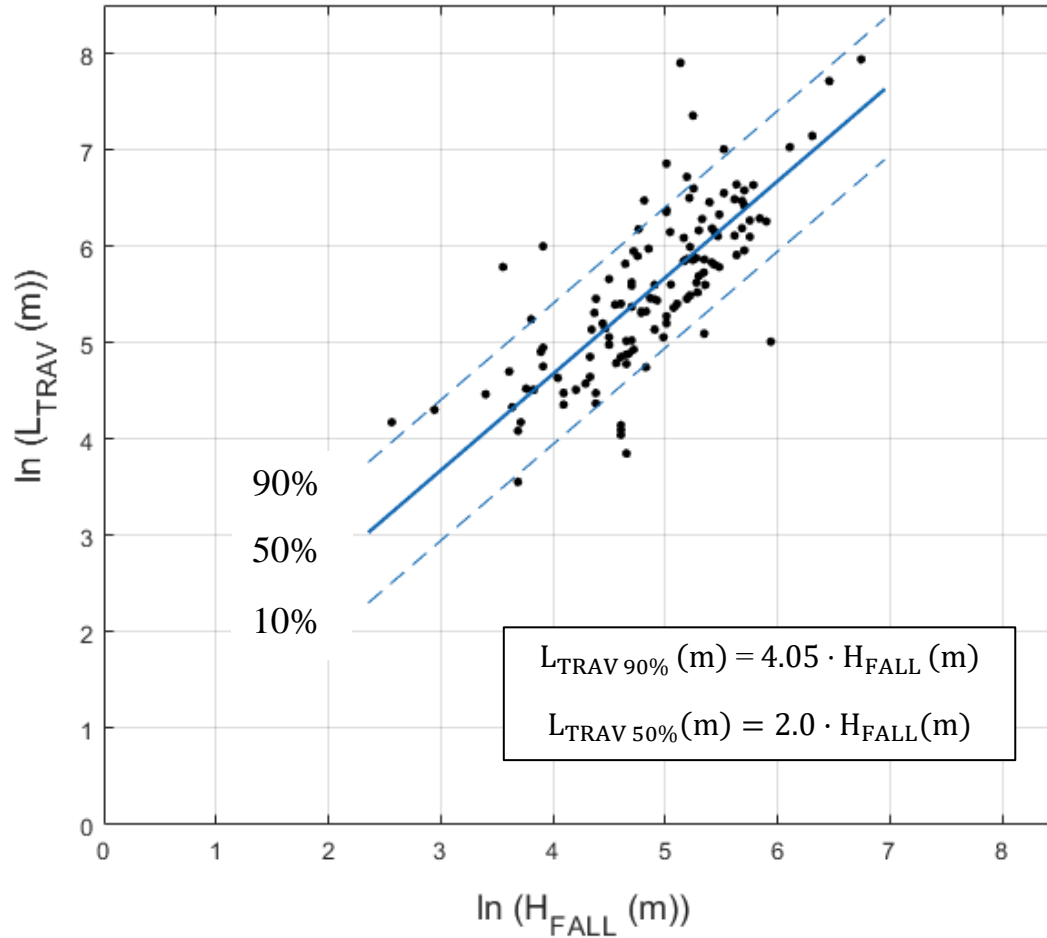


Figure 3.35 Design chart for $\ln(L_{TRAV})$ vs. $\ln(H_{FALL})$ with an 80% prediction interval plotted on the same graph. The upper level corresponds to a 90% exceedance probability: the lower level corresponds to a 10% exceedance probability.

Merging the theory and experiment always leads to a stronger and more reliable solution. Therefore the behavior of the failing material was also predicted using the energy principles. The failing mass is represented schematically by a block sliding from A to C with the intermediate position B (Figure 3.36). Assume that the travel distance consists of two parts: the inclined distance X_1 and the horizontal distance X_2 . Consider a block of mass ‘m’ on a rough inclined plane. The coefficient of friction is $\mu = \tan\varphi$. Let β be the angle of the inclination.

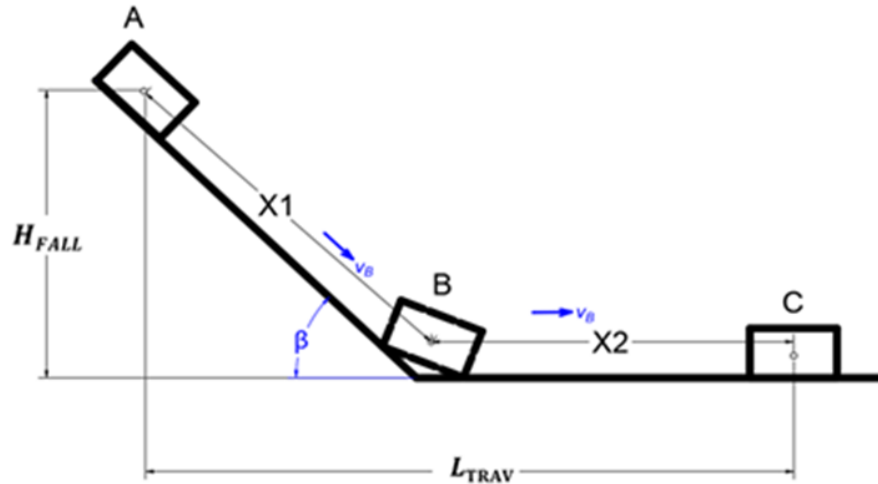


Figure 3.36 Cut slope failure geometry

The weight of the mass is 'mg' acts vertically downwards, and can be decomposed into two rectangular components (Figure 3.37a):

1. ' $mg \cdot \cos\beta$ ' acts perpendicular to the inclined plane and
2. ' $mg \cdot \sin\beta$ ' acts parallel to the inclined plane in downwards.

The component ' $mg \cdot \cos\beta$ ' is balanced by the normal reaction 'N' and the component ' $mg \cdot \sin\beta$ ' provides the driving force (F_g) when the slope fails. When the block is on the rough inclined plane, the friction force (F_f) acts opposite to the motion of the body. Therefore we can write:

$$N = mg \cdot \cos\beta \quad \text{Eq.3.14}$$

$$F_g = mg \cdot \sin\beta \quad \text{Eq.3.15}$$

$$F_f = \tan \varphi \cdot N \quad \text{Eq.3.16}$$

The mass begins to slide down the inclined plane starting from rest, thus the initial velocity of the mass is zero. The mass at the position A has only potential energy which is ' $mg \cdot H_{FALL}$ '.

At position B this potential energy will have been used in the work done by the friction force and to create kinetic energy for the mass:

$$\frac{m \cdot v_B^2}{2} + \tan \varphi \cdot mg \cdot \cos \beta \cdot X1 \quad \text{Eq.3.17}$$

So we can write the conservation of energy equation for the block traveling from A to B on an incline rough surface (Figure 3.37a):

$$mg \cdot H_{FALL} = \frac{m \cdot v_B^2}{2} + \tan \varphi \cdot mg \cdot \cos \beta \cdot X1 \quad \text{Eq.3.18}$$

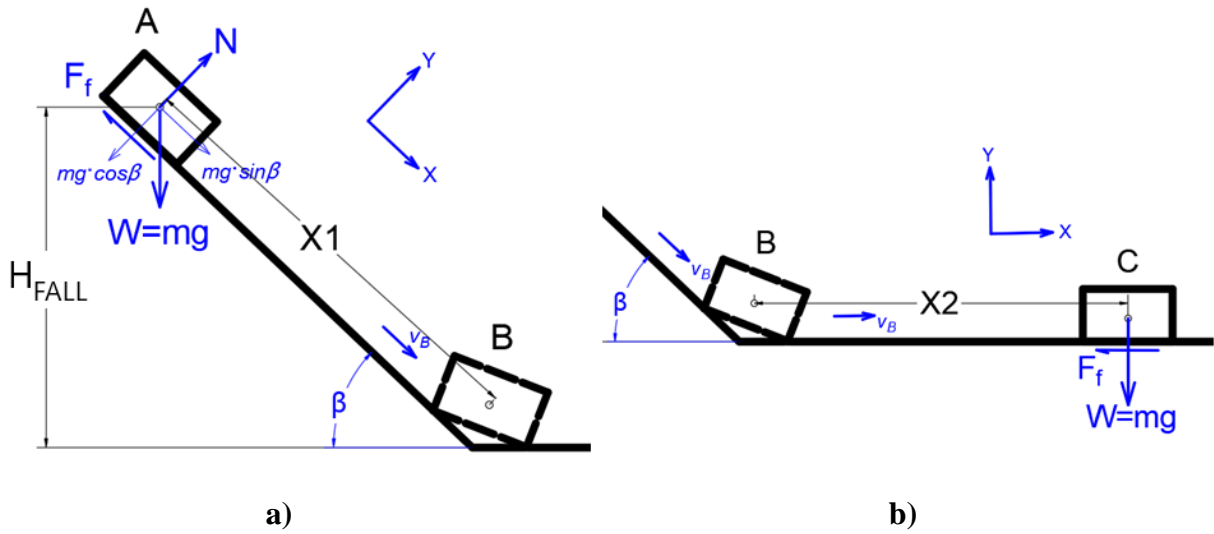


Figure 3.37 Free body diagram

$$X1 = \frac{H_{FALL}}{\sin \beta} \quad \text{Eq.3.19}$$

$$mg \cdot H_{FALL} = \frac{m \cdot v_B^2}{2} + \tan \varphi \cdot mg \cdot \cos \beta \cdot \frac{H_{FALL}}{\sin \beta} \quad \text{Eq.3.20}$$

$$v_B^2 = \left(mg \cdot H_{FALL} + \tan \varphi \cdot mg \cdot \frac{H_{FALL}}{\tan \beta} \right) \cdot \frac{2}{m} \quad \text{Eq.3.21}$$

$$v_B^2 = 2 \cdot g \cdot H_{FALL} \left(1 - \frac{\tan \varphi}{\tan \beta} \right) \quad \text{Eq.3.22}$$

At position C the mass stops (Figure 3.37b), therefore the velocity at position C $v_C = 0$ and so is the kinetic energy. The kinetic energy available to the mass at B is used in friction from B to C where the mass stops. The conservation of energy equation for the failing mass travelling from position B to position C along a rough horizontal plane is the following:

$$\frac{m \cdot v_B^2}{2} = F_f \cdot X_2 \quad \text{Eq.3.23}$$

$$\frac{m \cdot v_B^2}{2} = \tan \varphi \cdot mg \cdot X_2 \quad \text{Eq.3.24}$$

$$v_B^2 = 2 \cdot g \cdot \tan \varphi \cdot X_2 \quad \text{Eq.3.25}$$

$$2 \cdot g \cdot H_{\text{FALL}} \left(1 - \frac{\tan \varphi}{\tan \beta}\right) = 2 \cdot g \cdot \tan \varphi \cdot X_2 \quad \text{Eq.3.26}$$

The horizontal part of the travel distance can be expressed as:

$$X_2 = \frac{H_{\text{FALL}}}{\tan \varphi} \left(1 - \frac{\tan \varphi}{\tan \beta}\right) = H_{\text{FALL}} \left(\frac{1}{\tan \varphi} - \frac{1}{\tan \beta}\right) \quad \text{Eq.3.27}$$

The horizontal travel distance L is the sum of the projection of X_1 at the horizontal plane, and X_2 . Therefore:

$$L_{\text{TRAV}} = X_1 \cdot \cos \beta + X_2 \quad \text{Eq.3.28}$$

$$L_{\text{TRAV}} = \frac{H_{\text{FALL}}}{\sin \beta} \cdot \cos \beta + H_{\text{FALL}} \left(\frac{1}{\tan \varphi} - \frac{1}{\tan \beta}\right) \quad \text{Eq.3.29}$$

$$L_{\text{TRAV}} = \frac{H_{\text{FALL}}}{\tan \beta} + H_{\text{FALL}} \left(\frac{1}{\tan \varphi} - \frac{1}{\tan \beta}\right) \quad \text{Eq.3.30}$$

$$L_{\text{TRAV}} = \frac{H_{\text{FALL}}}{\tan \varphi} \quad \text{Eq.3.31}$$

This equation shows that the travel distance is proportional to the slope height and inversely proportional to the friction angle of the base material. This equation is compared to historical events of open pit slope failures.

Figure 3.38 shows the relationship between $(H_{\text{FALL}}/\tan \varphi)$ and L_{TRAV} of the failure mass based on the 134 case histories collected from the open pit mining industry. A green regression line shows that we do have 1 to 1 relationship between L_{TRAV} and $(H_{\text{FALL}}/\tan \varphi)$. This indicates that the equation $L_{\text{TRAV}} = H_{\text{FALL}}/\tan \varphi$ seems reasonable and can be used for preliminary travel distance estimates.

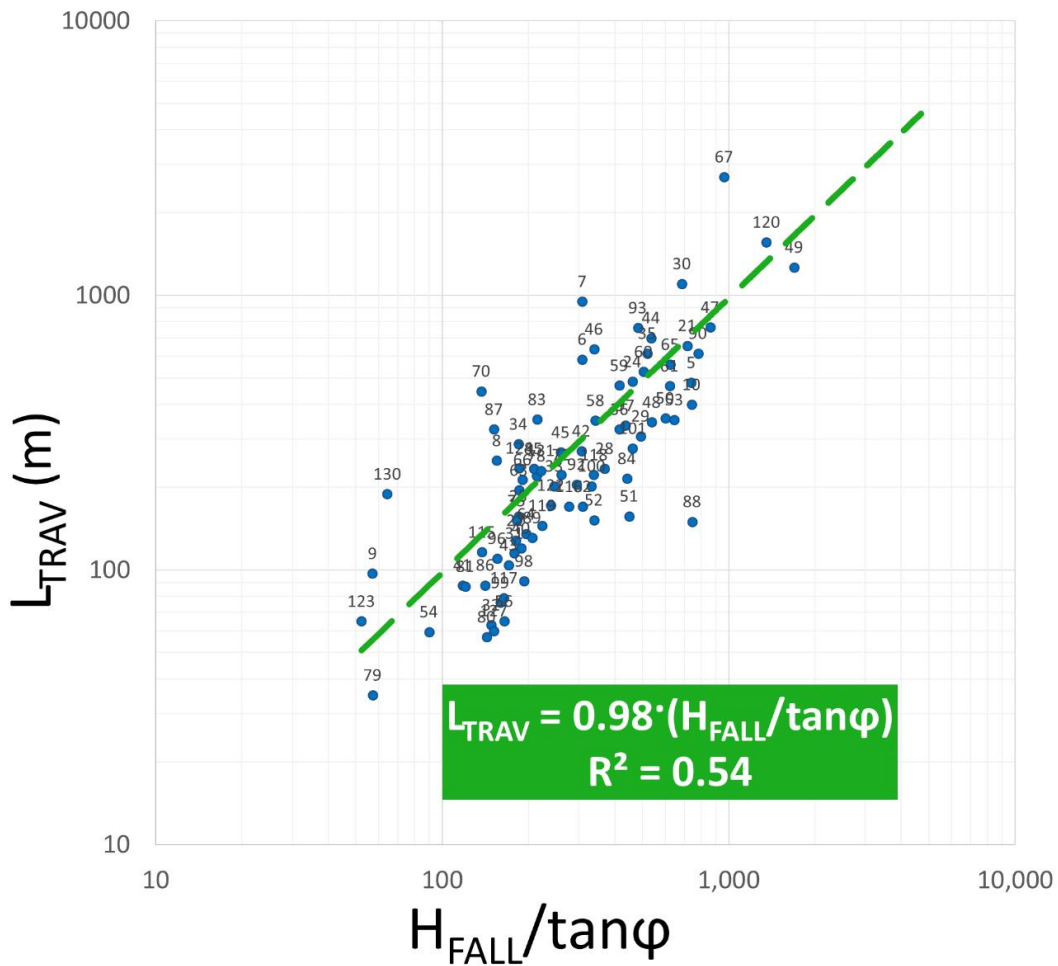


Figure 3.38 Relationship between travel distance and fall height normalized by $\tan \varphi$ (total number of points =80)

The best correlation equation that can estimate the travel distance is presented in green in Figure 3.38. It shows that there is 1 to 1 relationship between the travel distance and the fall height normalized by $\tan \varphi$, which is consistent with the energy-based approach results. The probability

plot that gave the correction factor α (PoF) of 1.8 is presented in Figure 3.39. The relationship where the travel distance is 1.8 times greater than the fall height over $\tan \phi$ is the best prediction that can be recommended for the open pit design (Figure 3.40).

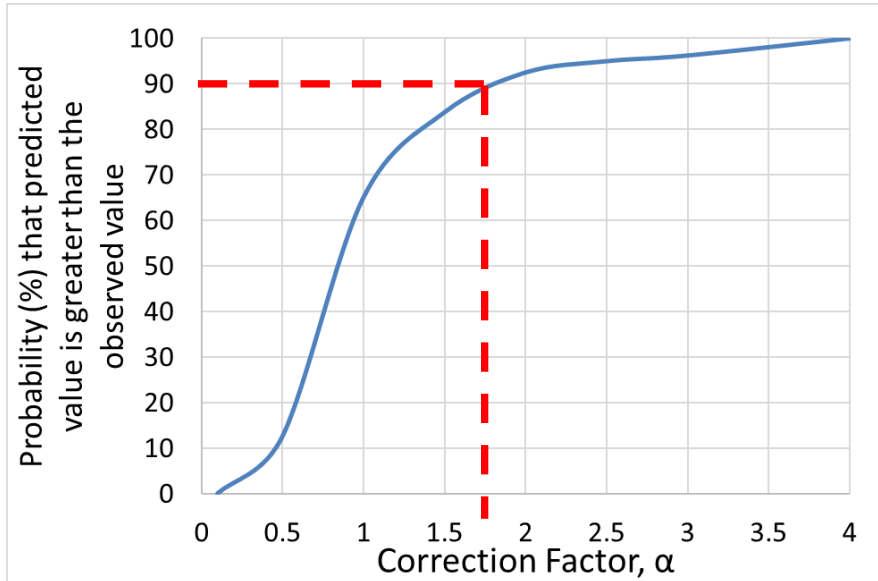


Figure 3.39 Probability of higher than predicted travel distance occurrence for all data in the TAMU-MineSlope Spreadsheet (referred equation is $L_{TRAV}=0.98 \cdot (H_{FALL}/\tan\phi)$)

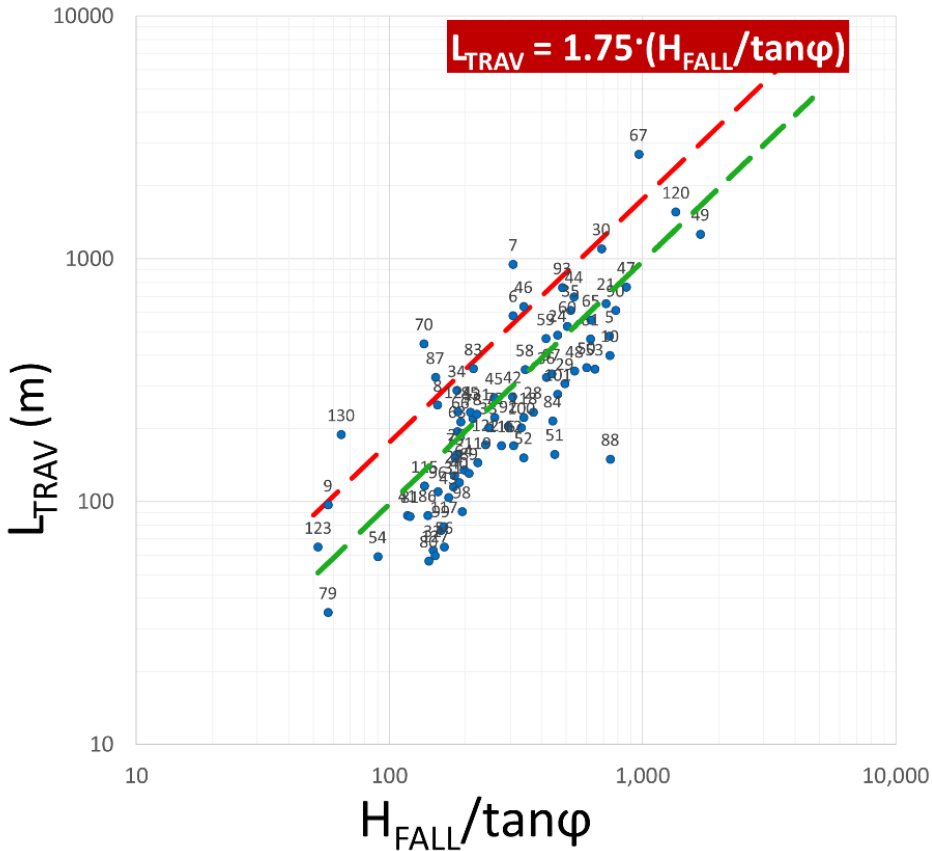


Figure 3.40 Predicted versus measured travel distance records for TAMU-MineSlope (red line represents regression line with the 90% to be safe; ($H_{FALL}/\tan\phi$) is the reference value).

Design chart with an 80% prediction interval presented in Figure 3.41. The upper level corresponds to a 90% exceedance probability: the lower level corresponds to a 10% exceedance probability.

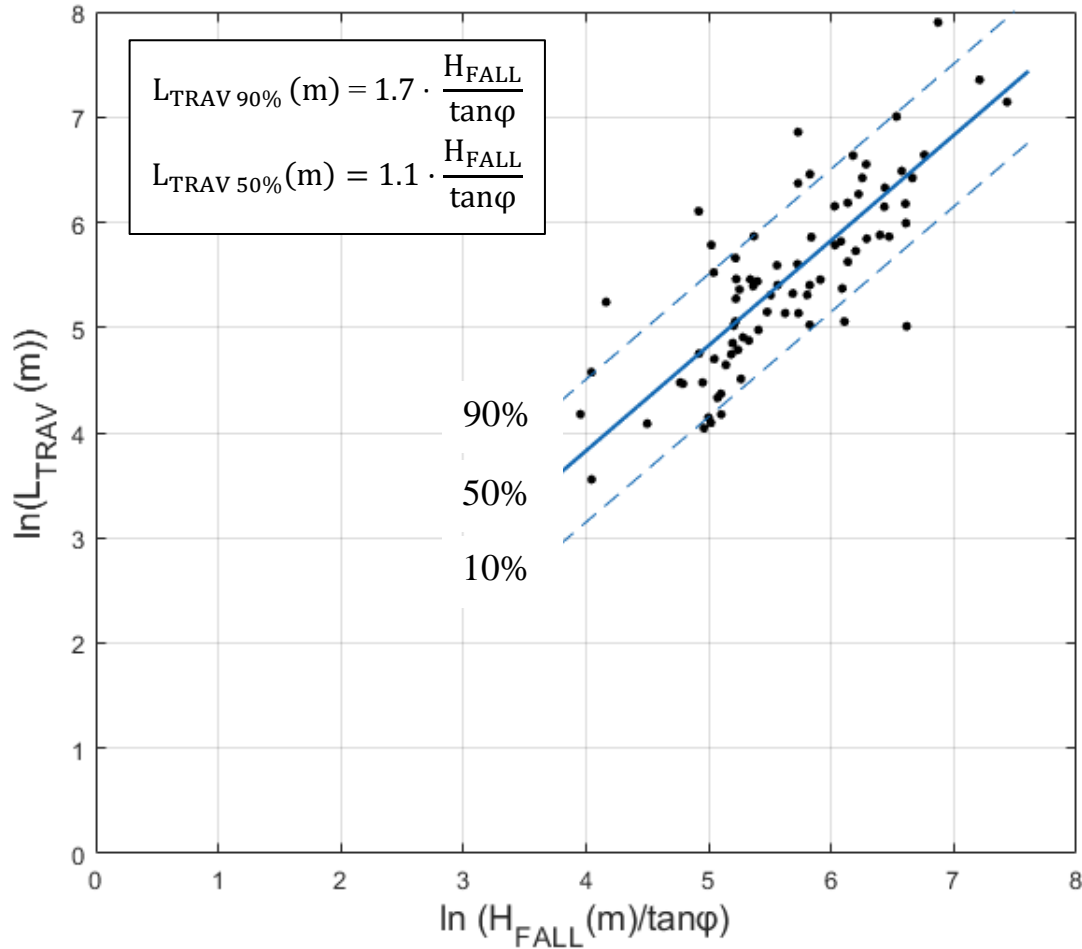


Figure 3.41 Design chart for $\ln(L_{TRAV})$ vs. $\ln(H_{FALL}/\tan\phi)$ with an 80% prediction interval plotted on the same graph. The upper level corresponds to a 90% exceedance probability: the lower level corresponds to a 10% exceedance probability.

The travel distance of a failing slope an important parameter in open pit mining because it can affect the mining operations and can also be used to design haul road width and mitigation structures, including debris barriers and berms (Mancarella and Hungr 2010, Ashwood 2014).

Figure 3.38 shows the level of uncertainty associated with the proposed equation ($R^2 = 0.54$).

$$L_{TRAV} = 1.75 \cdot \frac{H_{FALL}}{\tan \phi} \quad \text{Eq.3.32}$$

Factors not considered in the model, such as dissipation of the internal energy of the falling mass, the failure mechanism, the groundwater level, and the general geology, most likely contribute to the scatter (Shear and Vrise 2008). The precision with which the material friction is known is also a contribution to the scatter. The uncertainty should be considered in mining design. Nevertheless, the proposed equation Eq. 3.32 estimates the travel distance as a valuable input in open pit design. Probability approach that was used in the travel distance prediction helped to estimate the probability that a given element at risk (person, mining facility, equipment, and vehicle) can be affected by the failed material.

3.3.2 Setback distance prediction

3.3.2.1 Background information

A setback distance calls a minimum safe distance from the edge of the pit wall at all stages of pit development which provides a buffer zone between personnel and equipment working in the open pit (Figure 3.42). Establishing safe setback distances to define the limits for personnel and equipment access is the preferred approach to minimize public access areas that may be susceptible to slope collapse. These zones are typically delineated by bunds and signage, sometimes in conjunction with high fences. This buffer zone is maintained during the open pit construction as well as after the mining closure for safety reasons.

Careful consideration is required, to balance the objectives of minimizing the restricted land area by minimizing the setback distance and exclusion zone, and the requirement to ensure that the safety imperatives and other stability commitments are achieved. Understanding and predicting the reasonable setback distance is an important part of the open pit design and its maintenance.

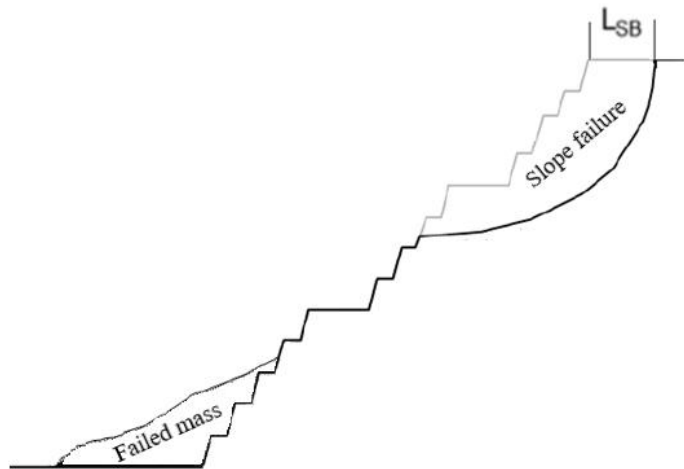
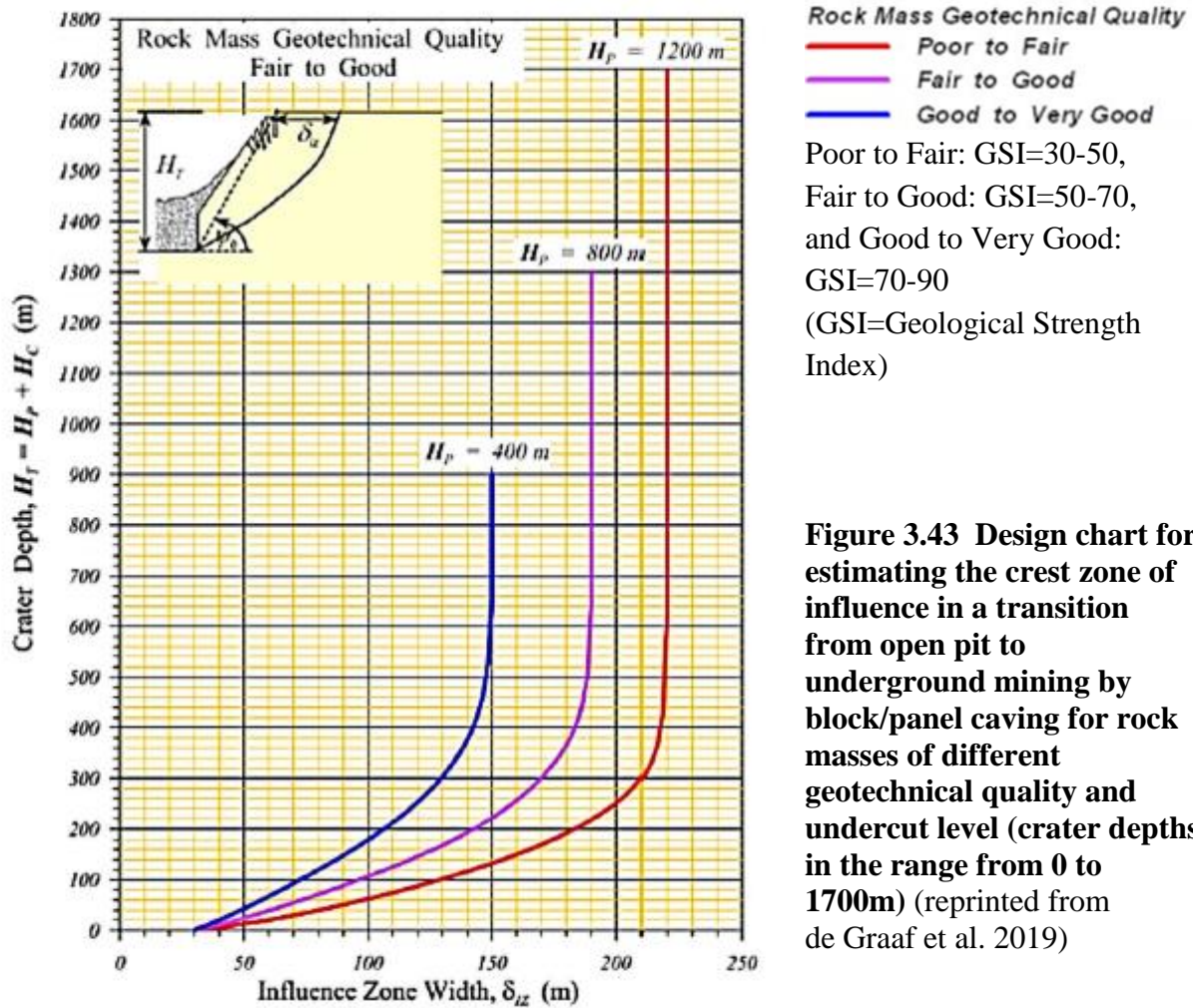


Figure 3.42 Setback distance in open pit mining

A lot of research has been conducted on the setback distance evaluation, but mostly for the prediction of the subsidence area during the transition from open pit to underground mining and for the case of the open pit closure (Hoek and Bray 1981; Carter 1992; Laubscher 2000, Flores and Karzulovic 2004; Carter 2014, de Graaf et al, 2019).

The modelling study by Flores and Karzulovic (2004) provides general guidance for subsidence analysis. Their work involved conceptualized FLAC/FLAC3D modelling of surface subsidence associated with block caving, including the varying of rock mass properties and consideration of the effects of an open pit with varying pit and undercut level depths. Based on their modelling results, complemented by limit equilibrium analysis, a series of design charts were developed correlating angle of break and zone of influence of caving with undercut level depth and crater depth for varying rock mass quality. Figure 3.43 shows one example of the design charts they developed. The validity of these charts though, has yet to be confirmed through mining experience.



Ontario Mines Regulation (2000) and the Western Australian Department of industry and Resource (1997) guideline state that the zone of potential instability is defined by a wedge of material extending from the toe of the pit wall at 45°. The Australian guideline also takes into consideration weathered rock conditions where the design angle should be further reduced to 25°. The Western Australia guidance note recommends that where the overall angle of a pit wall is less than these design criteria, the bund wall is to be positioned at least 10 m away from the final pit wall crest (Figure 3.44).

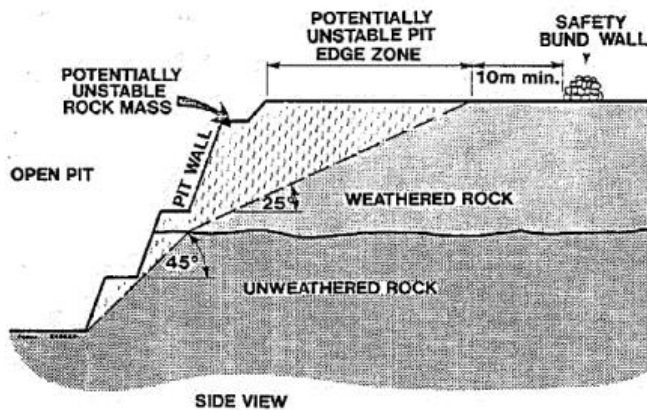


Figure 3.44 Evaluation of a zone of potential instability (reprinted from Department of Industry and Resources 1997, Safety Bund Walls Around Abandoned Open Pit Mines Guideline, Government of Western Australia)

Another method of setback distance prediction was described by de Graff et al. (2019). An ultimate setback distance was evaluated based on the monitoring data of several slope failures that have been tracked over many years at Victor Mine (North Ontario, Canada). The angles of debris repose are ranging from 13° to 20°, and the most conservative value (13°) was used to determine the ultimate long-term setback distance of the open pit of 67 m.

Hoek and Bray (1974) studied the location of the tension cracks behind the slope crest (Figure 3.45) and developed a chart for the critical tension crack location for a dry slope (Figure 3.46). The equation for the corresponding position of the tension crack in a rock mass based on the geometry of the slope is given by:

$$L_{SB} = H_{MAX}(\sqrt{\cot \beta_f \cdot \cot \beta_{OP}} - \cot \beta_f) \quad \text{Eq.3.33}$$

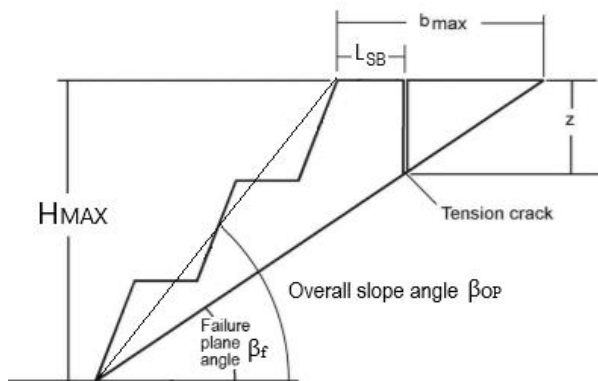


Figure 3.45 Location of the tension crack behind the slope crest (modified from Hoek and Bray 1974)

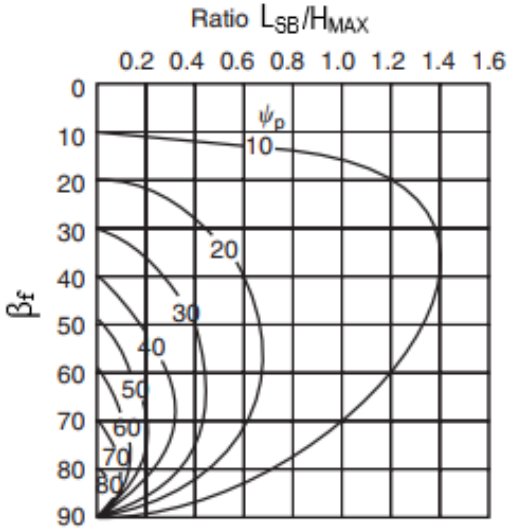


Figure 3.46 Critical tension crack location for a dry slope (reprinted from Hoek and Bray, 1974)

Later Hoek and Bray (1981) developed another set of charts for the critical tension crack location prediction for dry and wet slopes formed in rocks and have a limit equilibrium state (FS=1). One of the evaluation parameters is the distance of tension crack behind the open pit crest (Figure 3.47). It was noted by the authors, that the analysis is a two-dimensional and these dimensions refer to a 1-meter-thick slice through the slope.

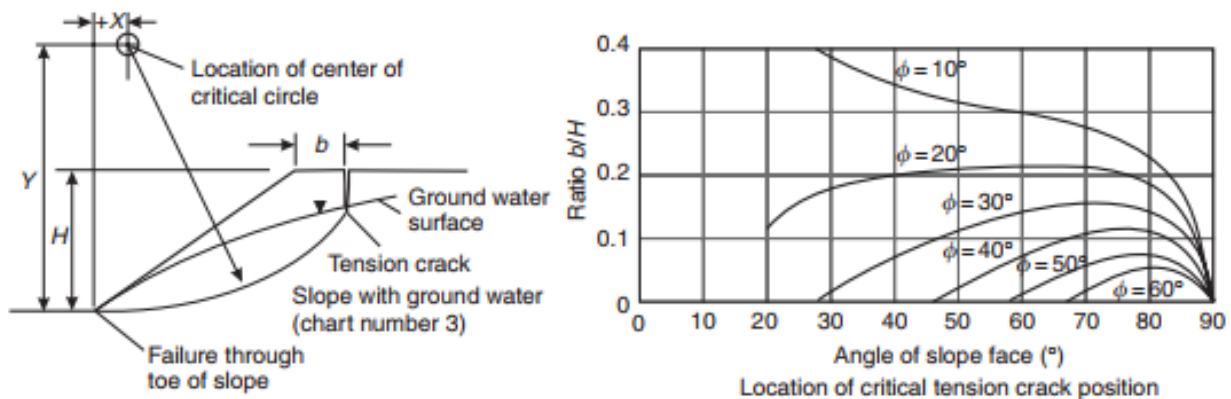


Figure 3.47 Location of critical sliding surface and critical tension crack for slopes with ground water present (reprinted from Hoek and Bray 1981; Wyllie and Mah 2005)

For an earth dam construction, Huang (1982) proposed that in case of a material with small effective cohesion and the hard layer is close to the bottom of the dam (less than 0.1H), the most

critical failure surface would intersect the top at a distance of $0.1SH$ from the edge, where H – height of the dam, and $S:1$ – slope of the dam (Figure 3.48).

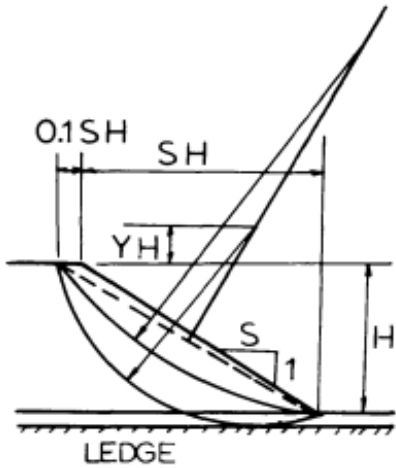


Figure 3.48 Method for a setback distance evaluation proposed by Huang (1982)

A setback distance for homogeneous slopes is also mentioned in Russian codes (VNIMI 1972). Equation 3.33 is proposed by VNIMI for the setback distance estimation. The slope parameters utilized by the equation are presented in Figure 3.49.

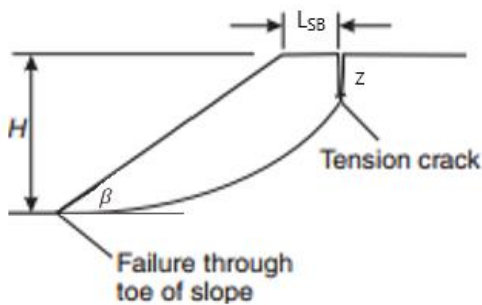


Figure 3.49 Slope parameters used in the VNIMI's equation

$$L_{SB} = \frac{2H(1 - \frac{1}{\tan \beta} \cdot \tan \frac{\beta + \varphi}{2}) - 2z}{\frac{1}{\tan(45^\circ - \frac{\varphi}{2})} + \tan \frac{\beta + \varphi}{2}} \quad \text{Eq. 3.34}$$

where L_{SB} = distance from the crest to the critical slip surface; H = height of the slope; β = slope angle; φ = friction angle; z = depth of the tension crack. The equation is valid for the homogeneous slopes in limit equilibrium states with $\varphi > 13^\circ$ and $\beta > (45^\circ - \varphi/2)$.

Establishing the requirements for the minimum available setback distance for open pits is a very important safety feature for equipment and people in the design of open pit mines. The best approach is to develop the recommendations based on the case history study. The existing knowledge proves that there is not much information about the requirements for an open pit setback distance. A few of the US mining guidelines and reports (e.g. Norman et al. 1997; MN96-1MLR 1996) have recommendations for the minimum allowable setback zone for the period of reclamation, but not for the open pit development. Thus, more study should be done on the setback distance prediction in open-pit mining.

3.3.2.2 Setback distance prediction based on TAMU-MineSlope

The following results present the analysis of 134 open pit mining slope failures between 1969 and 2020 that occurred worldwide. 90 out of 134 case histories have data on the setback distance. Using the TAMU-MineSlope Spreadsheet, the possible correlations between the setback distance and the parameters of the slope failure were determined.

Figure 3.50 presents the plot with the setback distance (L_{SB}) in the vertical axis and the failure height (H_{FAIL}) in the horizontal axis. The green line shows the best-fit regression line, and the equation in the green box is the best equation that could be found to show the relationship between the setback distance (L_{SB}) and the failure height (H_{FAIL}) based on the 90 slope failure case histories collected from the open pit mining industry (Eq. 3.35):

$$L_{SB}(m) = 0.41 \cdot H_{FAIL}^{0.82} \quad \text{Eq. 3.35}$$

The probability chart that gave the correction factor $\alpha(\text{PoF})$ of 2.5 for 90% probability that the observed value is greater than the predicted value is presented in Figure 3.51.

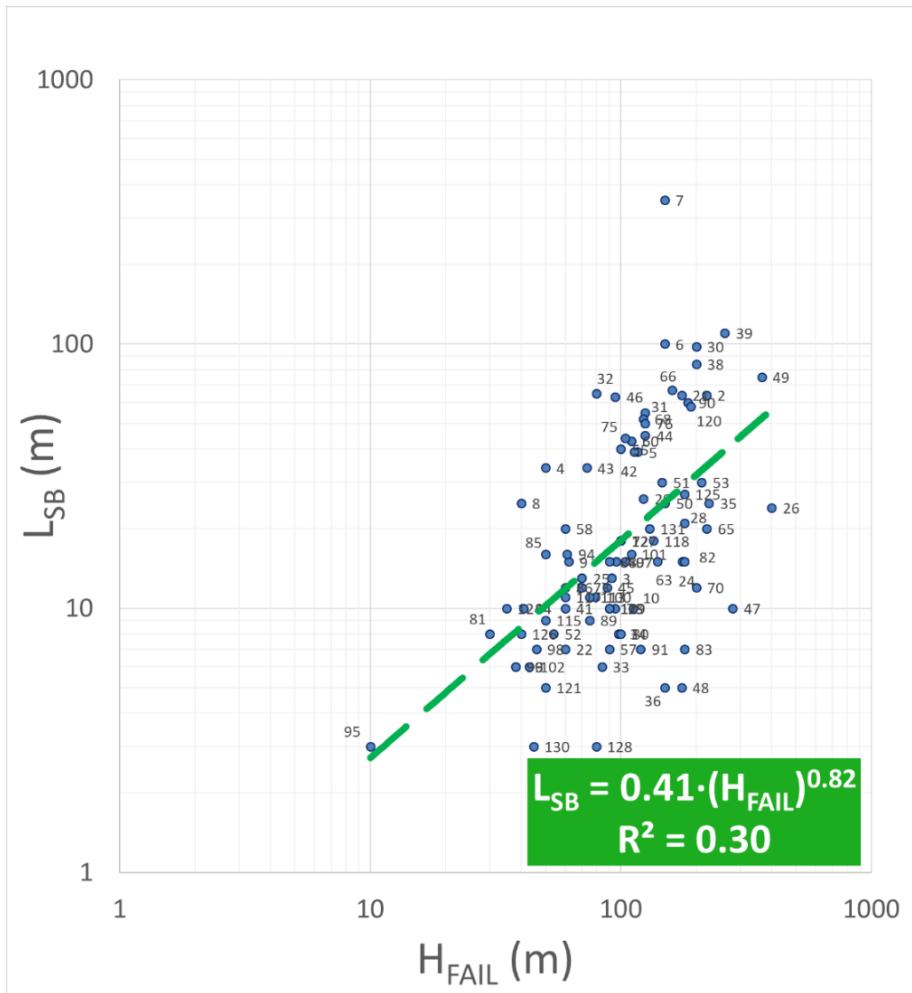


Figure 3.50 Relationship between setback distance L_{SB} and failure height H_{FAIL}

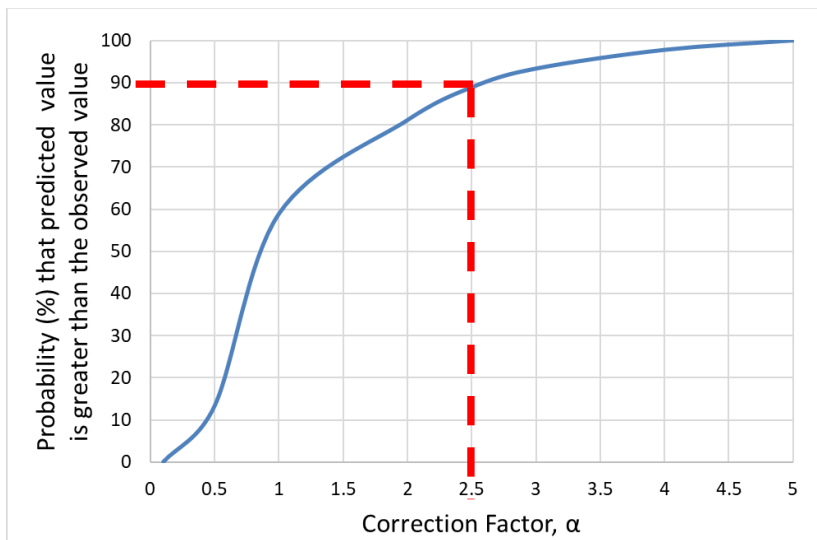


Figure 3.51 Probability of higher than predicted setback distance occurrence for all data in TAMU-MineSlope (referred equation is $L_{SB}=0.42 \cdot (H_{FAIL})^{0.82}$)

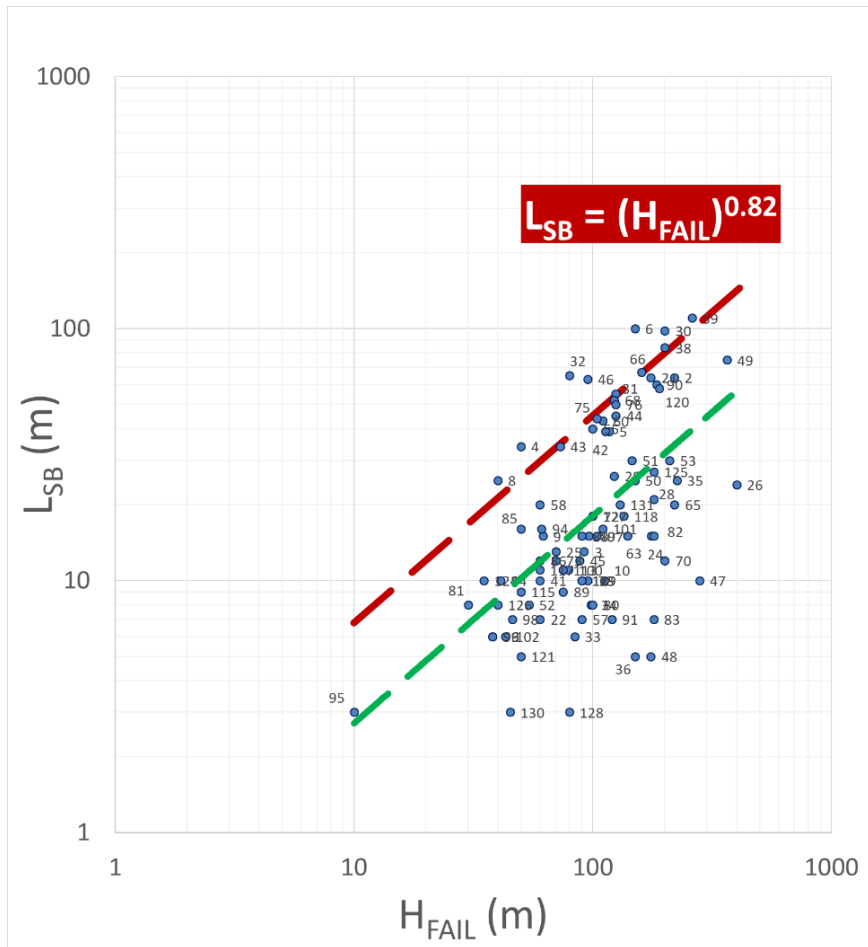


Figure 3.52 Predicted versus measured setback distance records for open pit failure database (red line represents regression line with the 90% to be safe; H_{FAIL} is the reference value).

Design chart with an 80% prediction interval presented in Figure 3.53. The upper level corresponds to a 90% exceedance probability: the lower level corresponds to a 10% exceedance probability.

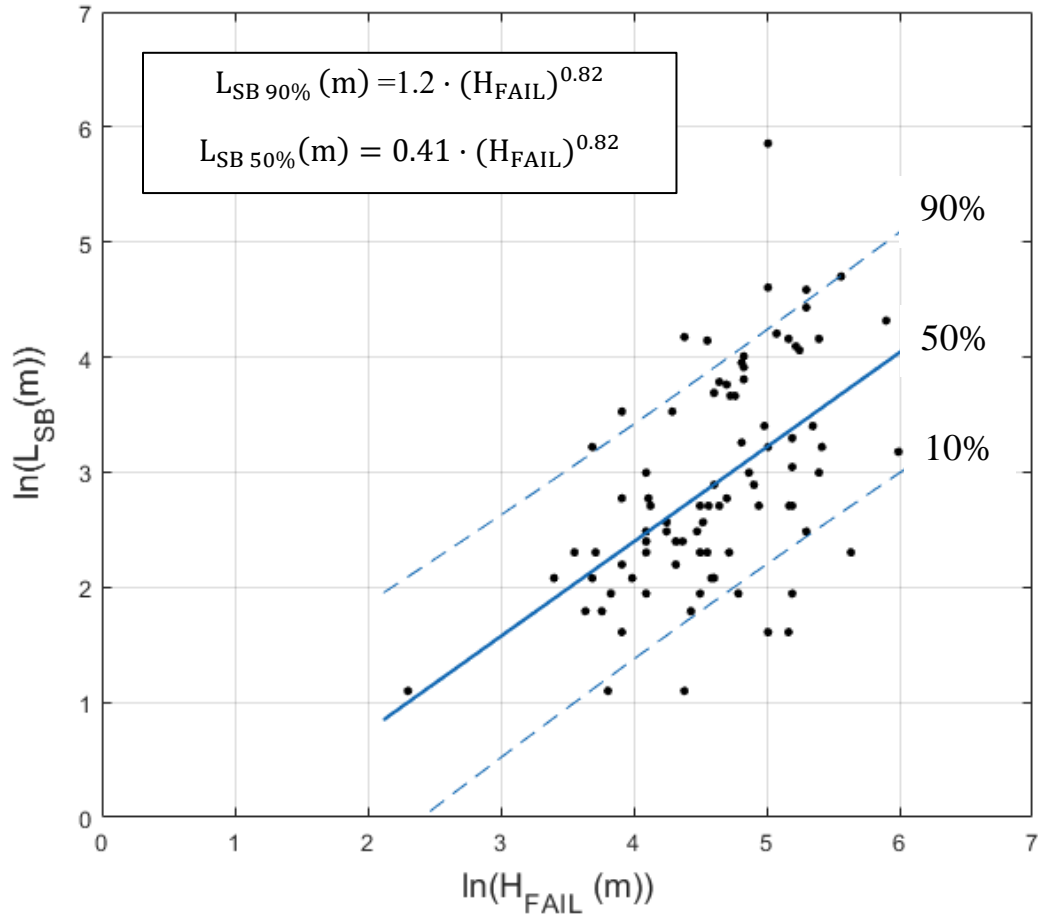


Figure 3.53 Design chart for $\ln(L_{SB})$ vs. $\ln(H_{FAIL})$ with an 80% prediction interval plotted on the same graph. The upper level corresponds to a 90% exceedance probability: the lower level corresponds to a 10% exceedance probability.

The setback distance is an important parameter in mining operations, which tells the designer how far from the slope crest the equipment and mining facility can actually be placed. The aim of the current research was to propose a reasonable prediction based on theory and the case histories. The relationship where the setback distance is equal to failure height to the power of 0.82 the best prediction that can be recommended for the open pit design (Figure 3.52).

$$L_{SB}(m) = H_{FAIL}^{0.82}(m) \quad \text{Eq. 3.36}$$

3.3.2.3 Critical distance from the slope crest to the equipment

At the design, care must be taken to select a combination of the distance from the crest to the equipment, b (m), and slope angle, β ($^\circ$) such that the stability of the mining equipment (e.g., mining truck) is not jeopardized. Thus, the loading of the slope crest by the equipment was studied in the present research. In addition, the study aimed to obtain the critical safe distance from the crest to a mining truck. Therefore, the range for the distance of a mining truck from the crest of a slope was selected such that a truck is located within one-half of the slope heights from the crest ($H/2$). Calculations were made with several assumptions and conditions:

1. A fully loaded mining truck CAT 793F (Figure 3.54) moving along the slope crest.
2. Rated gross machine weight is 386 tons.
3. Infinitely long distributed load applied as pressure on top of the slope.
4. Peripheral area of the truck is represented by the surface area of the volume occupied by the truck.
5. The pressure is calculated as the truck's weight divided by the peripheral area of the truck (Eq. 3.37):

$$P = \frac{3,860,000 \text{ (kN)}}{7.6 \text{ (m)} \cdot 5.9 \text{ (m)}} = 85 \left(\frac{\text{kN}}{\text{m}^2} \right) \quad \text{Eq. 3.37}$$

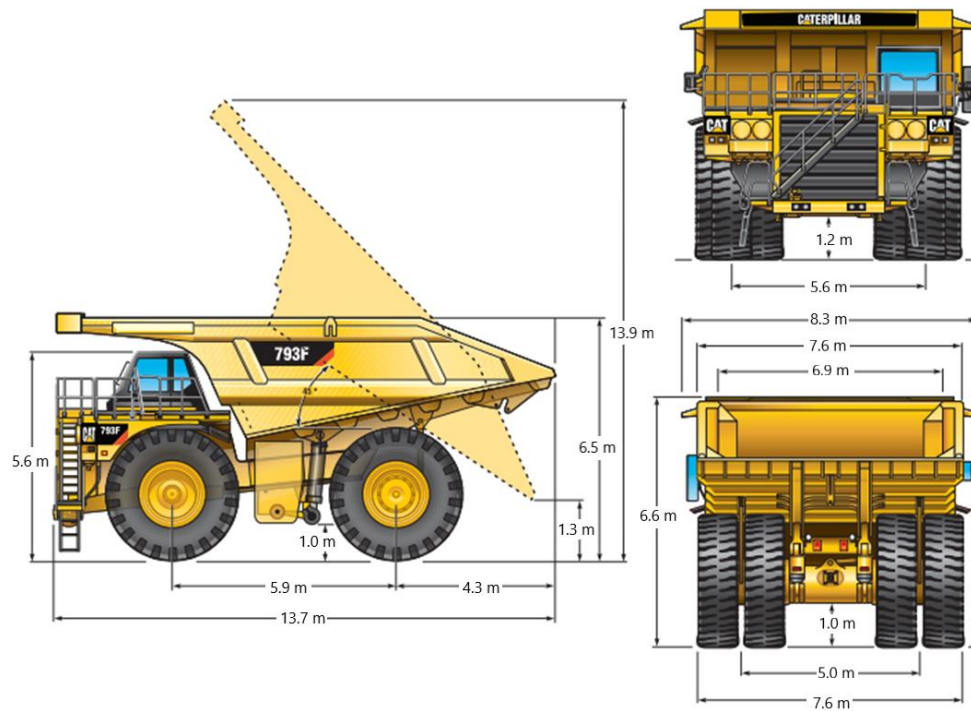


Figure 3.54 Parameters of CAT 793F (reprinted from <https://www.cat.com/>)

Parameters from Table 3.7 were used to generate slope stability models incorporating the equipment (mining truck CAT 793F) and its load positioned on the crest of a slope. The parameters of slope geometry (H , β) were selected such that to represent common slopes found in civil and mining engineering projects. The range of soil properties (γ , c , and ϕ) for the homogeneous slope was selected such that the unloaded slope is at the equilibrium ($FS=1$).

The truck was moved away from the slope crest at the distance, L (m), and for each location of the truck, the slope stability simulation was performed. Slide2 from Rocscience Inc. (Rocscience, 2021c) was used to create the models and carry out slope stability analysis. In the 2-D LEM software, the Spencer method was used; the failure surface was subdivided into 50 slices and the number of iterations for FS convergence was limited to 75. As an outcome of the stability analysis, the minimum FS, along with the location (x , y , R) of the critical circular failure surface were recorded.

Table 3.7 Parameters of the models used in calculation of the loaded slope

Model #	Height of the slope, H (m)	Slope angle, β ($^{\circ}$)	Unit weight, γ (kN/m ³)	Cohesion, c (kPa)	Friction angle, ϕ ($^{\circ}$)	FS for unloaded slope, FS
1	15	25	20	6.8	18	1.0
2	15	35	20	9	24	1.0
3	15	45	20	10	30	1.0
4	15	55	20	11	36	1.0

Figure 3.55 shows a typical slope loaded with a pressure distribution from a mining truck. Figure 3.55 also shows a critical failure surface for this model along with the corresponding (FS=1.045), distance from the crest to the equipment (b=4.3 m), and value of setback distance ($L_{SB}=5.8$ m).

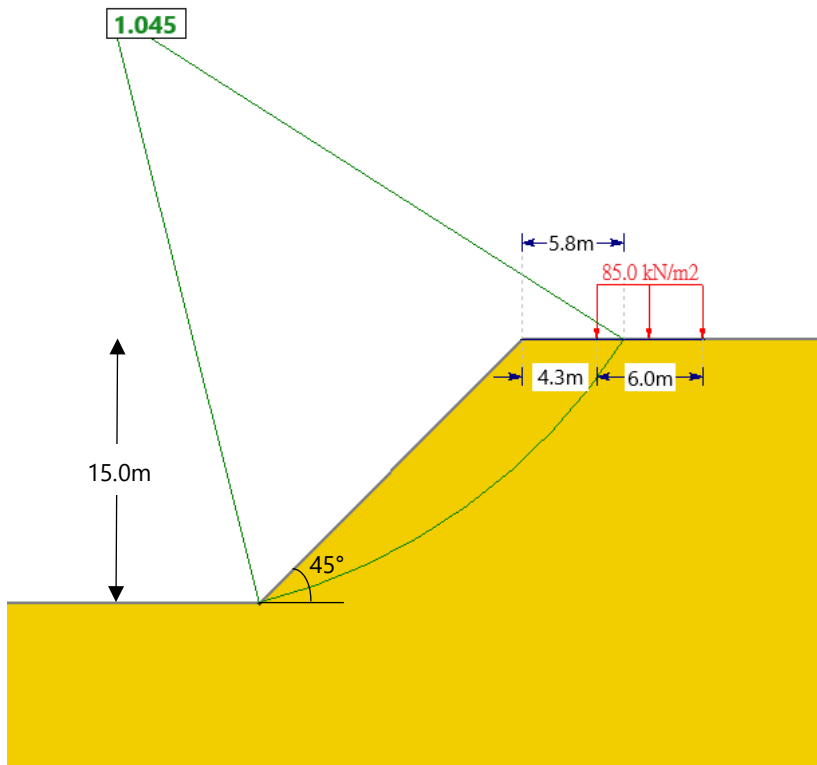


Figure 3.55 A typical slope stability model as analyzed by Slide2 (Rocscience Inc.), showing the critical failure surface and the corresponding FS

The results of simulation presented in Figure 3.56. On the horizontal axis is the distance from the crest to the equipment, b (m), and on the vertical axis is the Distance Ratio (SDR) which is given by:

$$\text{SDR} = \frac{b \text{ (m)}}{L_{\text{SB}} \text{ (m)}} \quad \text{Eq. 3.38}$$

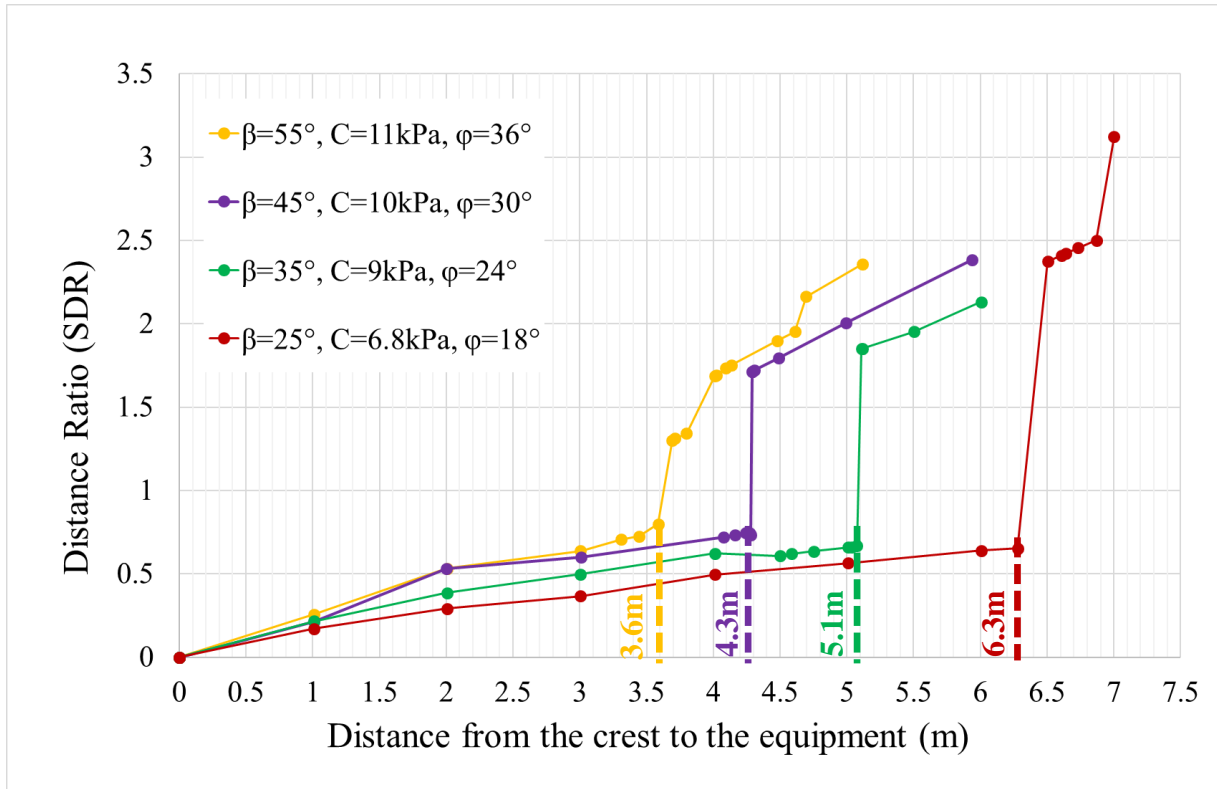


Figure 3.56 Distance ratio (SDR) vs. Distance from the crest to the mining truck (m) for different slope inclinations. Note that the parameters of the slope were picked such that the analyzed slope without loading is at failure (FS=1)

A simple numerical experiment confirmed that mining truck CAT 793F carrying a maximum load located beyond the distance presented in Figure 3.56 did not change the FS of a slope as compared to the same unloaded slope. The value of the critical distance from the crest to the equipment obtained for different models (Table 3.7) was plotted versus the parameter

$(c+\gamma H \tan \varphi)$. The equation for the critical distance determination (Eq.3.39) based on the models' parameters and the coefficient of determination R^2 are presented in Figure 3.57.

$$b(m) = \frac{165 \text{ (kPa}^{0.7} \cdot \text{m)}}{(c+\gamma H \tan \varphi)^{0.7} \text{ (kPa}^{0.7})} \quad \text{Eq. 3.39}$$

It can be concluded that the critical distance from the crest to the equipment for the data presented herein is inversely proportional to the height of the slope and strength parameters of the slope material.

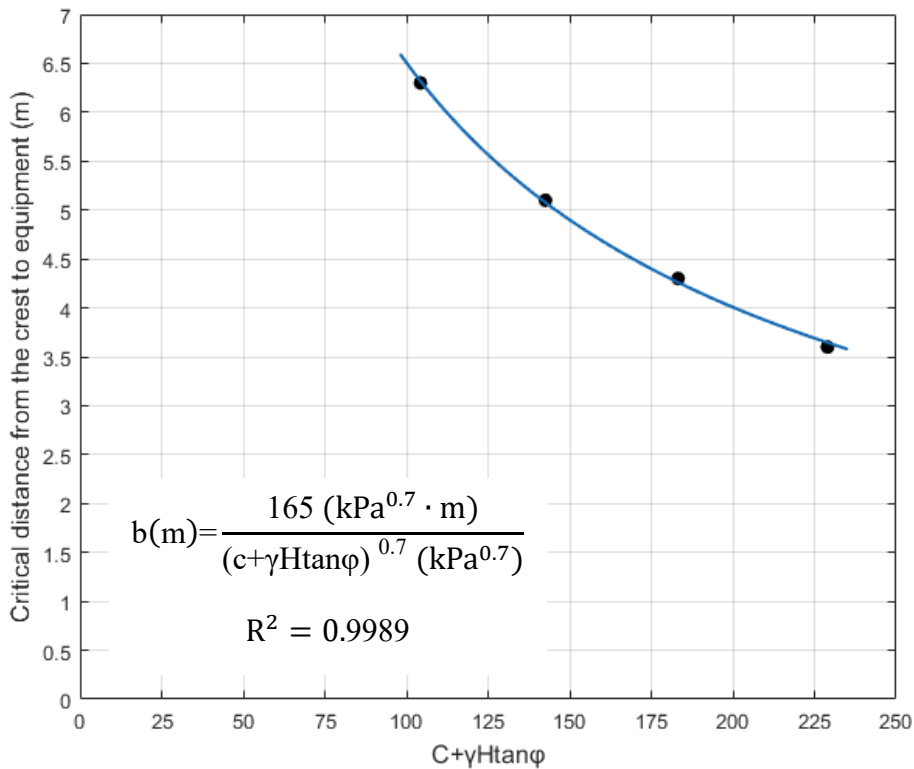


Figure 3.57 Variation of the critical distance from the crest of the slope to mining truck (m) with respect to the value of $(c+\gamma H \tan \varphi)$

3.4 Stability Charts Evaluation

3.4.1 Background information

Although different software is now available for the stability analysis of slopes, traditional stability charts are still routinely used in engineering practices as convenient and efficient tools for estimating slope safety. Stability charts can be used as a guide for preliminary designs or as a rough check for the computer solution. Another use for slope stability charts is to back-calculate strength values for failed slopes to aid in planning remedial measures.

Several studies have been made to construct stability charts that require no iterations to evaluate the FS. A large body of literature exists on the stability of slopes, and a comprehensive description of it was presented by Hunter and Schuster (1971), Huang (1982), Abramson et al. (1996), Duncan (1996), Briaud (2013) among others.

The first slope stability charts were published by Taylor (1948) who proposed simple design charts to evaluate the safety factor of homogeneous soil slopes (cohesion and friction angle are constant with depth). This chart (Figure 3.58) applies to the case in which the soil is uniform, has a unit weight γ , has no water, and can be represented by an effective stress cohesion c' and an effective stress friction angle φ' . Thus, for this chart, two factors of safety are defined by:

$$FS_{c'} = \frac{c'}{c'_d} \quad \text{Eq. 3.40}$$

$$FS_{\varphi'} = \frac{\tan \varphi'}{\tan \varphi'_d}, \quad \text{Eq. 3.41}$$

where c'_d and φ'_d are the fraction of c' and φ' required to maintain the slope in equilibrium.

To present the results in a dimensionless manner Taylor introduced a stability number defined as:

$$N = \frac{c_d}{\gamma H} = \frac{c}{\gamma H \cdot FS} \quad \text{Eq. 3.42}$$

where γ is unit weight of soil and H is slope height. For $FS=1$, the stability number N represents the combination of c , γ and H , which guarantees the slope to be at the verge of failure (limit equilibrium) for given slope inclination angle β and internal friction angle of the soil ϕ .

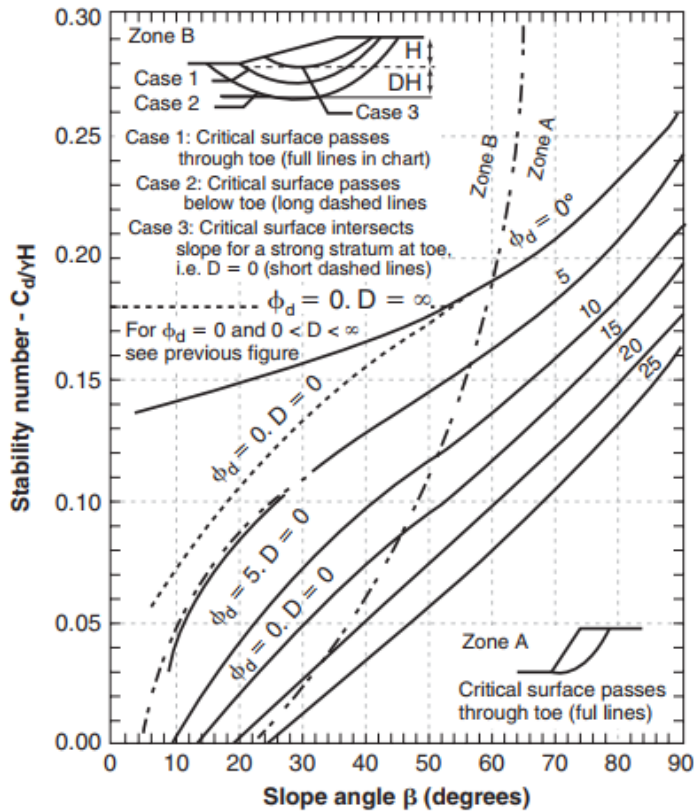


Figure 3.58 Taylor chart for $\phi' > 0$, $c' > 0$, no water in soils (reprinted from Briaud, 2013)

According to Baker (2003) and Steward et al. (2011) the disadvantage of Taylor's chart is that it does not define the location of the slip circle and also the effect of pore pressure is not considered. Another limitations of the chart are that it is not applicable to cohesionless soils, tension cracks are ignored, and the analysis does not apply to stiff, fissured materials (Hunter and Schuster 1971).

Spencer (1967) developed charts for the case where the groundwater surface is within the slope circle (Figure 3.59). The soil strength is described by the effective stress parameters c' and ϕ' . The failure surface is considered to be circular and to go through the toe of the slope. The presence of the water in the slope is quantified by using the water stress ratio:

$$r_u = \frac{u_w}{\sigma_{ov}} \quad \text{Eq.3.43}$$

where u_w is the water stress at the chosen point and σ_{ov} is the vertical total stress in the soil at the same point. Figure 3.59 shows the example of stability charts for determining the required slope angle when the FS is given. If the angle of slope is given, the FS can be determined by trial and error.

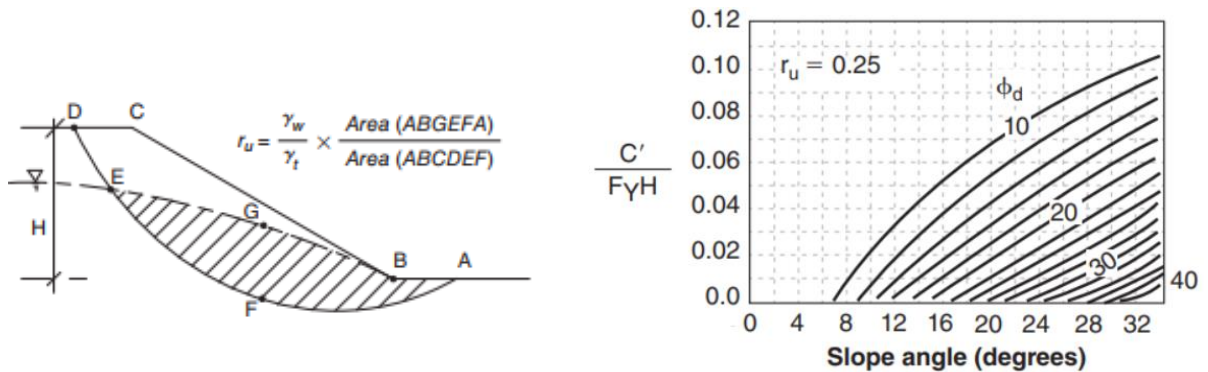


Figure 3.59 Spencer chart for $\phi' > 0$, $c' > 0$, and $r_u = 0.25$ (reprinted from Briaud 2013)

Hoek and Bray (1981) proposed a set of five circular failure charts for a jointed rock homogeneous slope with uniform shear strength properties along the slide surface which passes through the toe of the slope. The charts are numbered from 1 to 5 to correspond with the ground water conditions defined as: 1) fully drained slope; 2) surface water 8 x slope height behind toe of slope; 3) surface water 4 x slope height behind toe of slope; 4) surface water 2 x slope height behind toe of slope; 5) saturated slope subjected to heavy surface recharge.

The charts were produced by running a search routine to find the most critical combination of slide surface and tension crack for each of wide range of slope geometries and ground water conditions. Circular failure charts are optimized for a rock mass density of 18.9 kN/m³. The example of chart presented in Figure 3.60. These charts differ from those published by Taylor in that they include the influence of a critical tension crack and of ground water.

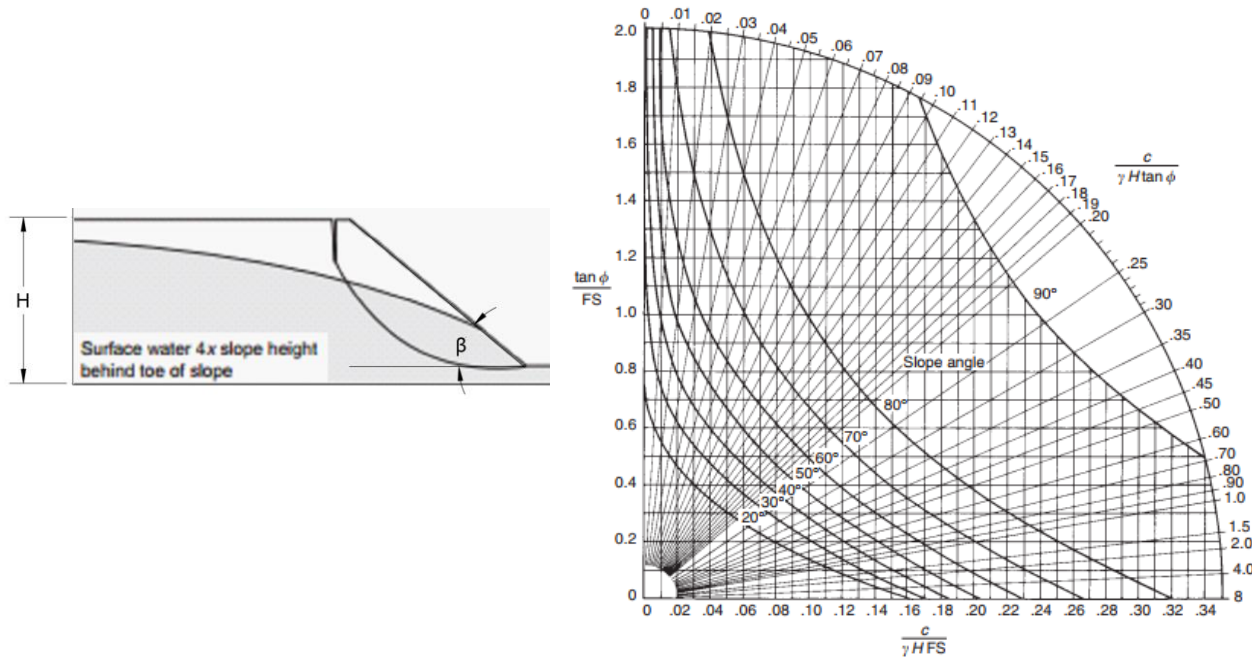


Figure 3.60 Circular failure chart with the ground water flow model #3 (reprinted from Hoek and Bray 1981)

Morgenstern (1963) developed charts for the case of a rapid drawdown in a dam (Figure 3.61). The charts are for a uniform soil slope, effective stress parameters C' and ϕ' , soil total unit weight γ , a slope with a height H , and the water level being drawn down an amount H from the top of the slope to a lower level. It is further assumed that the water stress in the soil does not have time to dissipate during the drawdown period. Example of the Morgenstern charts for rapid drawdown is shown in Figure 3.61.

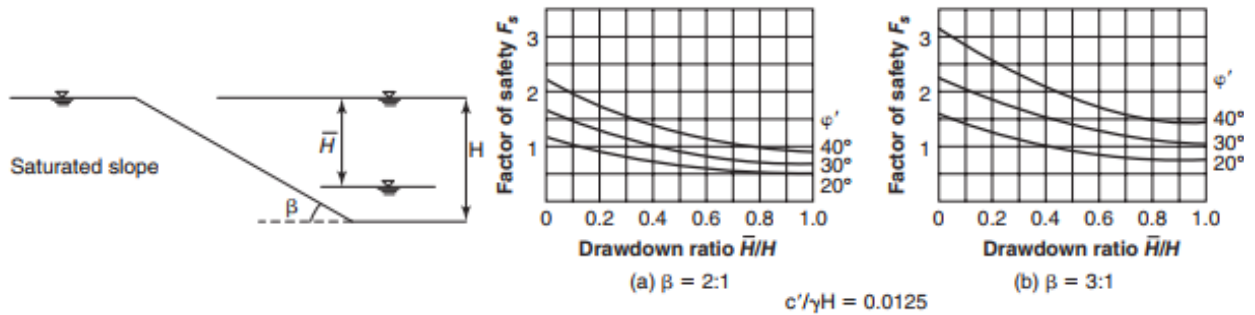


Figure 3.61 Morgenstern charts for rapid drawdown for stability number $c'/\gamma H=0.0125$ and slope angles $\beta=27^\circ$ and $\beta=18^\circ$ (reprinted from Briaud 2013)

The limitations of the charts are that they can be used only when the ledge or stiff stratum is at the toe with $D = 0$, and only when the weight of soil is assumed to be about 20 kN/m^3 .

Michalowski (2002) proposed a set of design charts based on the kinematic approach of limit equilibrium analysis utilizing the modified stability number, N^* (Eq. 3.44). Hence estimation of the safety factor from charts presented as functions of N^* will not require any iterative procedures. The limitation of the charts is that they cannot be used for slopes with zero internal friction angle (Figure 3.62).

$$N^* = \frac{C_d}{\gamma H \tan \varphi_d} = \frac{C}{\gamma H \tan \varphi} \quad \text{Eq. 3.44}$$

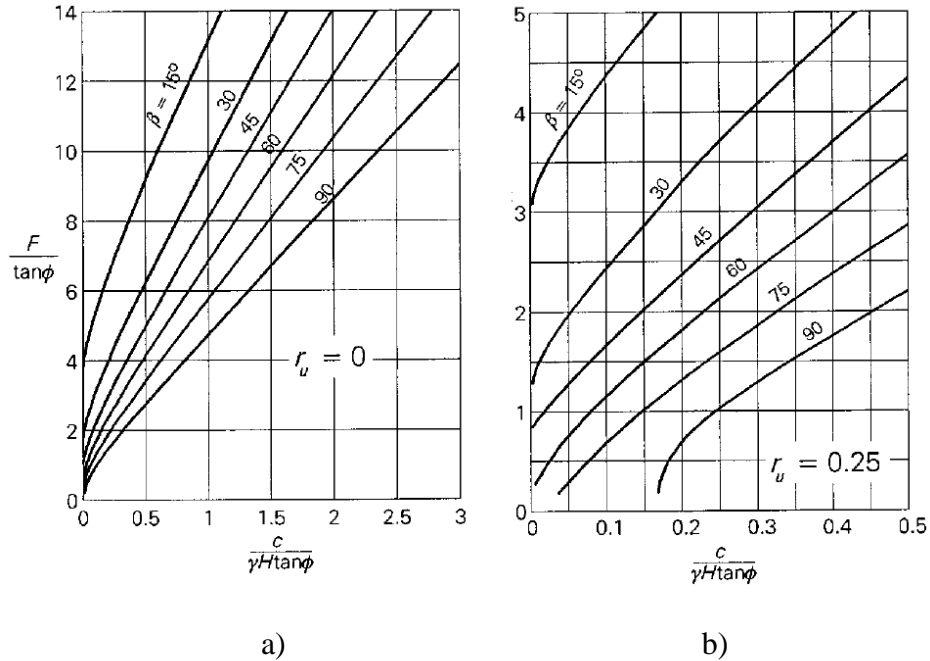


Figure 3.62 Michalowski stability charts for uniform slopes: a) for $N^* \leq 3$, $F/\tan\phi \leq 14$ and $r_u = 0$ and b) for $N^* \leq 0.5$, $F/\tan\phi \leq 5$, and $r_u = 0.25$ (reprinted from Michalowski 2002)

Analyses of stability of slopes with irregular inclination or with heterogeneous soils require the application of now computerized methods. However, charts for homogeneous slopes with a well-defined inclination are often used in practice as a quick reference, and they are a convenient tool for the first estimate of the slope safety. All the charts presented above involve a homogeneous slope with a given cohesion and angle of internal friction. Some charts assume that a ledge or stiff stratum is located at a great depth while others assume at a given depth ratio, D , ranging from 0 to 0.5. Some charts have been developed by running many thousands of circular analyses from which a number of dimensionless parameters were derived that relate the FS to the material unit weight, friction angle and cohesion, and the slope height and face angle.

In Civil Engineering it has been found that these charts give a reliable estimate for the FS, provided that the conditions in the slope meet the assumptions used in developing the charts. The accuracy in calculating the FS from the charts for open pit slope stability calculations should be

checked using the shear strength parameters obtained during the open pit slope failure case histories study. If discrepancies are found, it may be necessary to propose a new chart that matches the case histories better.

3.4.2 Taylor chart evaluation

Taylor's stability chart is one of the main tools used for preliminary analysis of homogenous slope stability problems (Figure 3.58). The charts was developed to determine FS of the critical slip surfaces in homogeneous undrained clays and soils with cohesion and friction angle.

On Taylor's chart on a vertical axis is the stability number, N (Eq.3.45), and on the horizontal axis is the slope angle, β ($^{\circ}$). The lines on the chart present $\tan\varphi_d$. As it was mentioned earlier to present the results in a dimensionless manner Taylor used a stability number defined as:

$$N = \frac{c_d}{\gamma H} = \frac{c}{\gamma H \cdot FS} \quad \text{Eq. 3.45}$$

where γ is unit weight of soil; H is slope height, and FS is the FS of the slope.

$$\tan\varphi_d = \frac{\tan\varphi}{FS} \quad \text{Eq.3.46}$$

where φ is the friction angle of the slope material.

In this chapter, the verification of Taylor's chart with the collected case histories is presented. In the case of the open pit slope failures collection FS of each case is equal to one. Therefore the stability number N represents the combination of c , γ , and H , which guarantees the slope to be at failure for given slope inclination angle β and internal friction angle of the soil φ .

A hundred and twenty cases from the open pit slope failure case histories collection were analyzed and a 120 points were placed directly on Taylor's chart. Each point presents one case history. All the points were divided into the sets according to the value of the friction angle

intervals. Then the 'safe' and 'unsafe' points were defined. Figure 3.63 shows the example of point evaluation. In the figure, all the points on the chart present the cases with the friction angle between 10 and 15°. For the point #1 according to Taylor's chart the material would fail at the slope angle of 75°, but in fact it failed at 25°. This point is called 'unsafe'. And, for example, for the point #2 Taylor's chart tells us that it would fail at 15° but according to the case history the material failed at 50°. This point is 'safe'. The point calls 'unsafe' if it is located above the referred domain, and 'safe' if the location of the point is between or below the referred domain.

Figure 3.64 (a-g) presents the results of Taylor's chart evaluation. Note that the lines on the figures are the original lines proposed by Taylor. Due to a large number of data points, the figures are sorted according to different ranges of friction angle values ($0^\circ \leq \varphi \leq 5^\circ$, $5^\circ < \varphi \leq 10^\circ$, $10^\circ < \varphi \leq 15^\circ$, $15^\circ < \varphi \leq 20^\circ$, $20^\circ < \varphi \leq 25^\circ$, $25^\circ < \varphi \leq 30^\circ$, and $30^\circ < \varphi \leq 35^\circ$). We followed this procedure for all of the domains at Taylor's chart. The results of Taylor's chart evaluation showed that 57% of the time, the points were on the safe side, and 43% of the time, the points were unsafe.

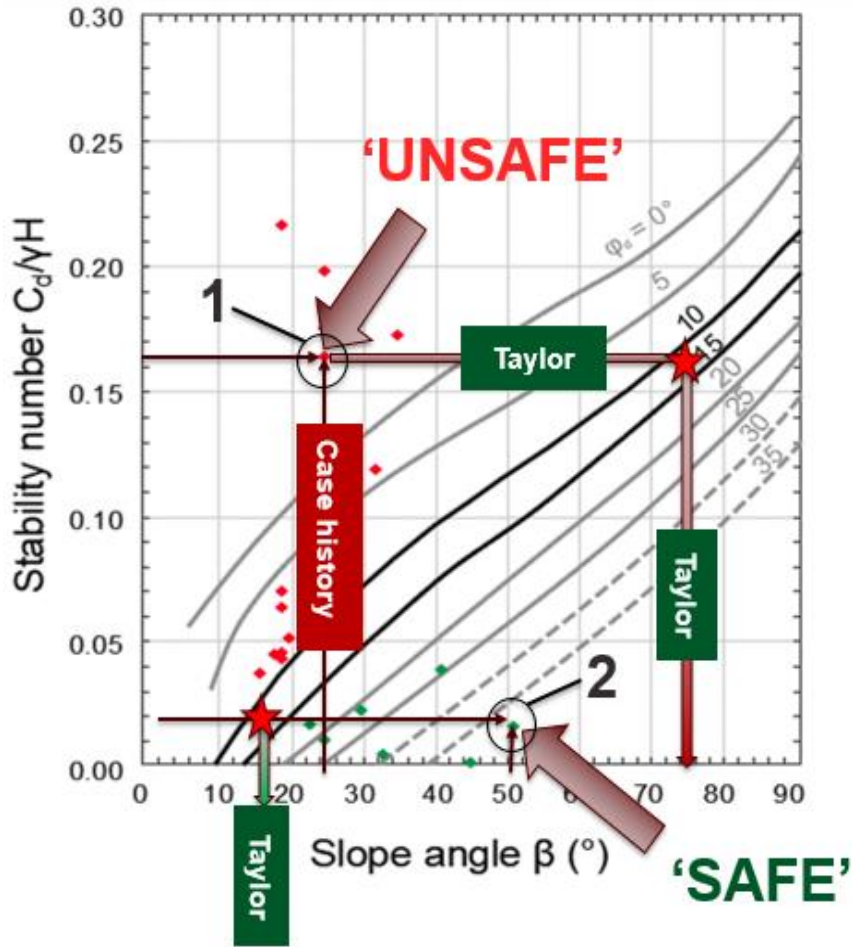
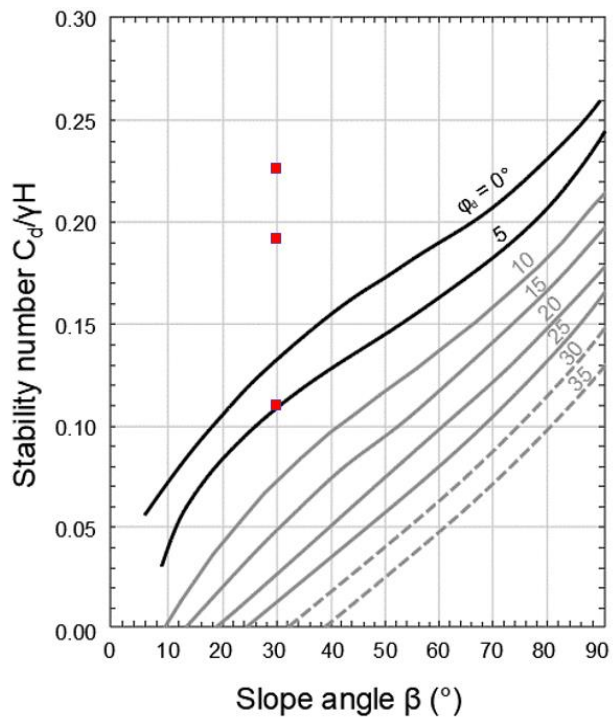
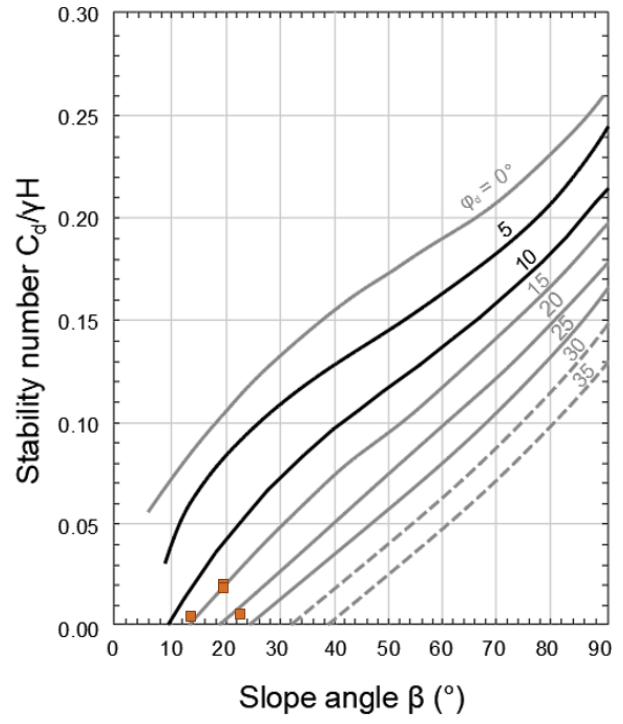


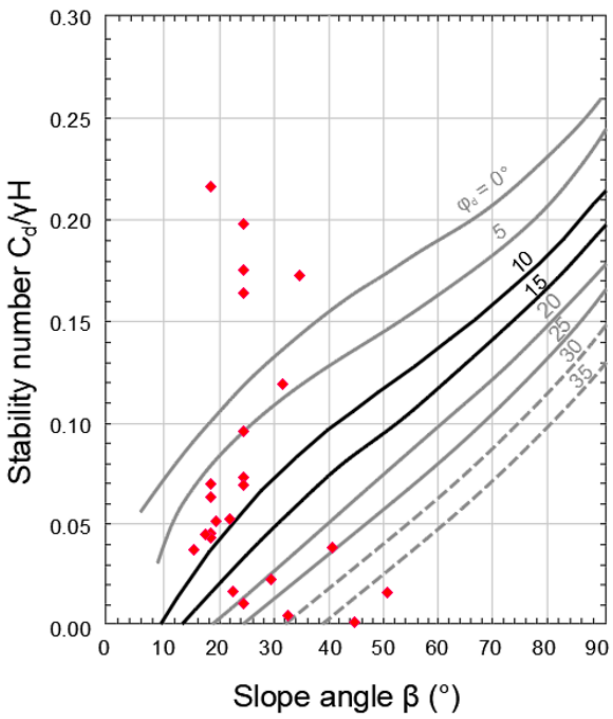
Figure 3.63 Verification of Taylor's chart with the open pit slope failure case histories (1 – 'unsafe' point, 2 – 'safe' point)



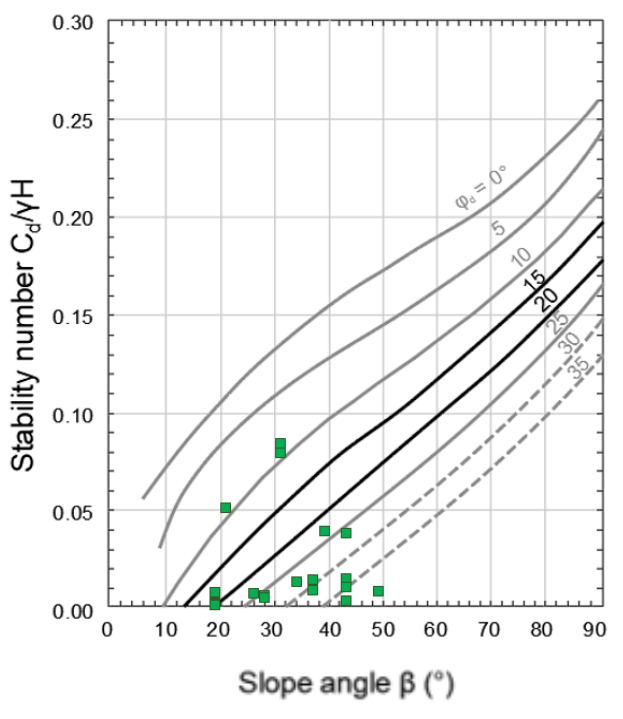
a)



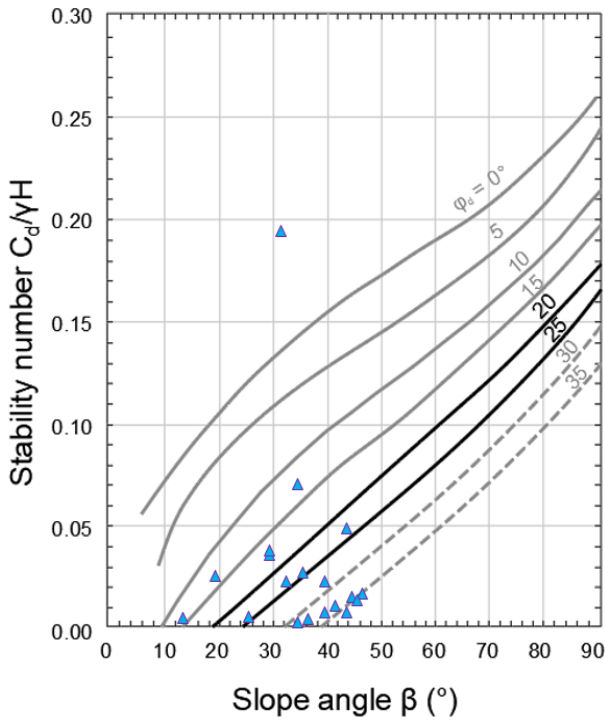
b)



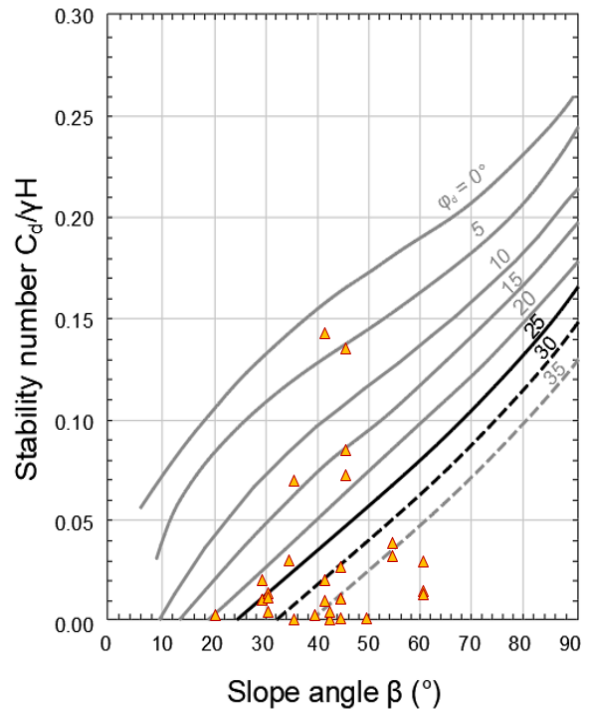
c)



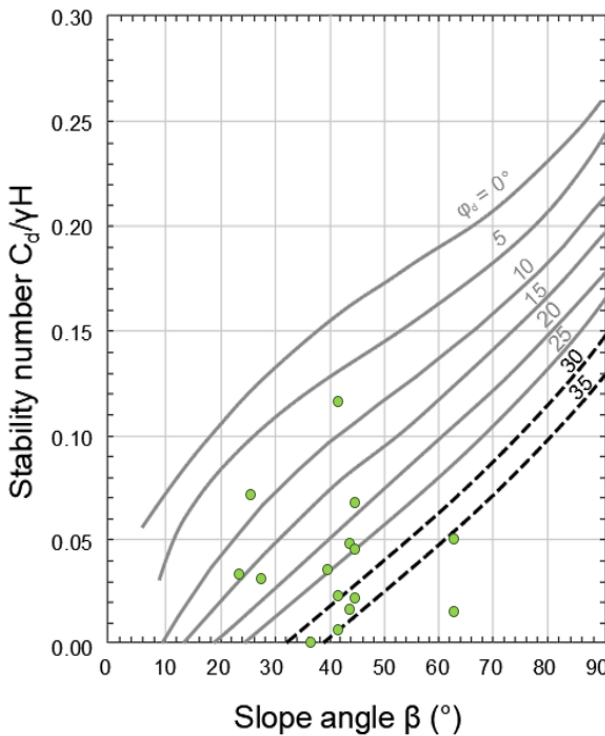
d)



e)



f)



g)

Figure 3.64 Comparison between slope angle (β , $^\circ$) from the case history database and Taylor's chart for the domain: a) $0^\circ \leq \phi \leq 5^\circ$, b) $5^\circ \leq \phi \leq 10^\circ$, c) $10^\circ \leq \phi \leq 15^\circ$, d) $15^\circ \leq \phi \leq 20^\circ$, e) $20^\circ \leq \phi \leq 25^\circ$, f) $25^\circ \leq \phi \leq 30^\circ$, and g) $30^\circ \leq \phi \leq 35^\circ$.

3.4.3 Hoek & Bray's chart evaluation

Another chart was used for the evaluation was Hoek & Bray's stability chart. On Hoek & Bray's chart, $\frac{\tan \phi}{FS}$ is on the vertical axis and stability number $\frac{C}{\gamma H \cdot FS}$ is on the horizontal axis. As it was mentioned before FS (FS) for all the case histories in the database is equal to 1. Curved lines in the plot present a slope angle.

The same case histories that were selected to analyze Taylor's chart were picked to evaluate Hoek & Bray's chart. 120 points were placed directly on Hoek & Bray's stability chart. Each point presents one case history. All the case histories were divided according to the slope angle intervals. Then the 'safe' and 'unsafe' points were defined. Figure 3.65 shows the example of point evaluation. In the figure, all the points on the chart present the cases with the slope angle between 40° and 50°.

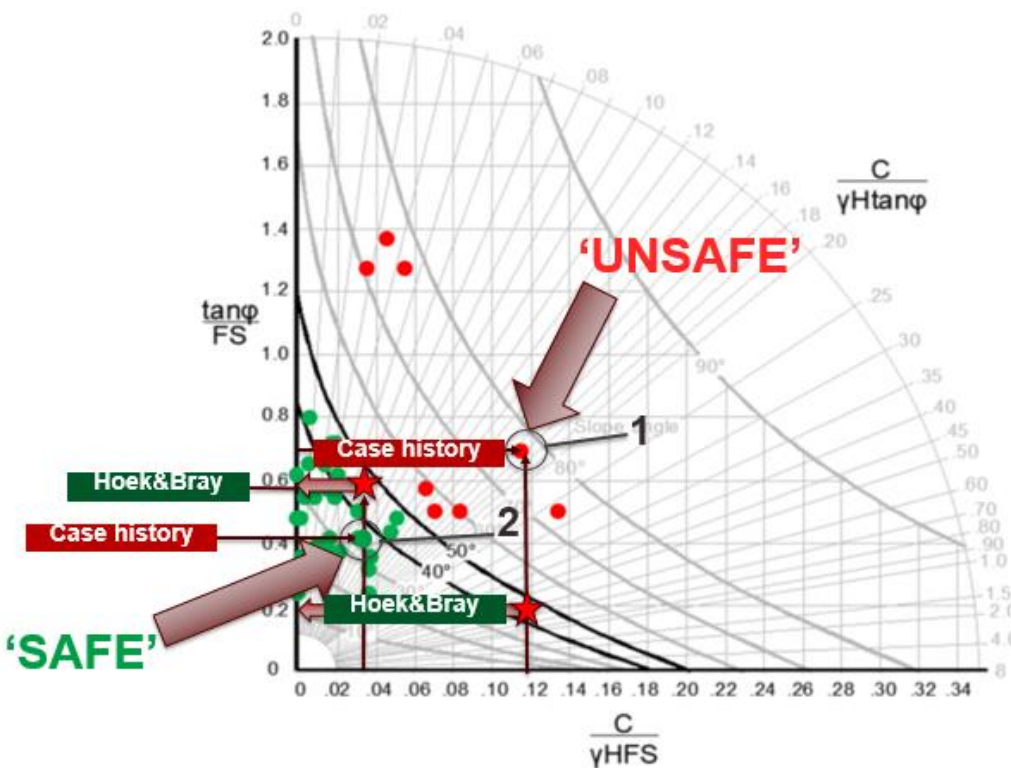


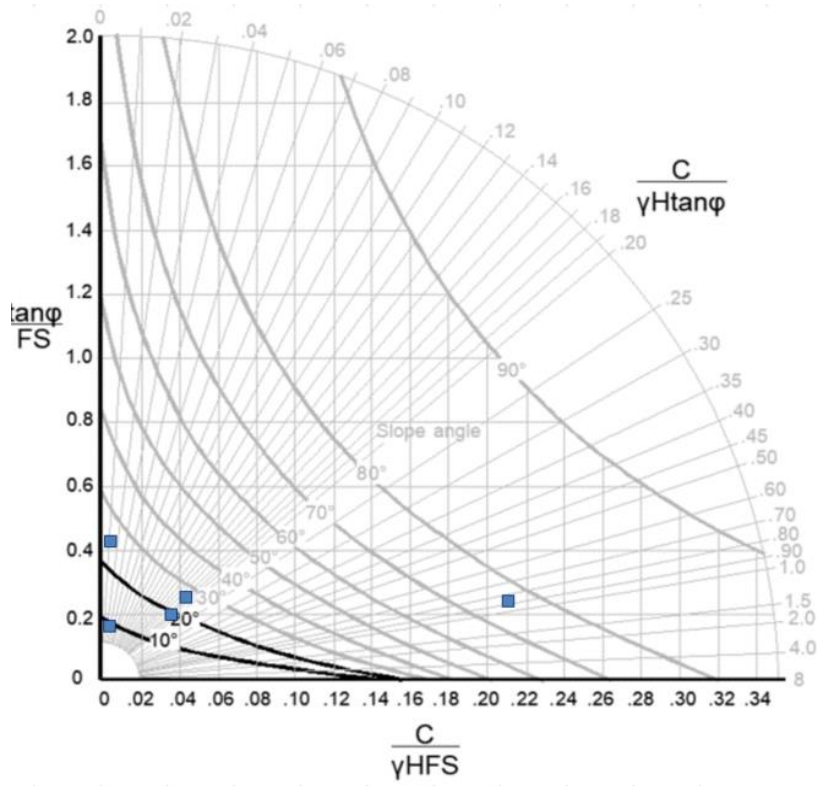
Figure 3.65 Verification of Hoek & Bray's chart with the open pit slope failure case histories (1 – 'unsafe' point, 2 – 'safe' point)

For example, for point #1 (Figure 3.65), Hoek & Bray's chart tells us that the failed material would be characterized with the friction angle $\phi=11^\circ$, but according to the case history, the failed material had the friction angle of 34° . So this point is 'unsafe.' And for example, for point #2, according to Hoek & Bray's chart, the material that would fail characterized with the friction angle of 30° , but in fact, the failed material had $\phi=14^\circ$, which is a lower value compared to the proposed by Hoek and Bray friction angle. So this point is called 'safe.' The point calls 'unsafe' if it is located above the referred domain and 'safe' if the location of the point is between or below the referred domain.

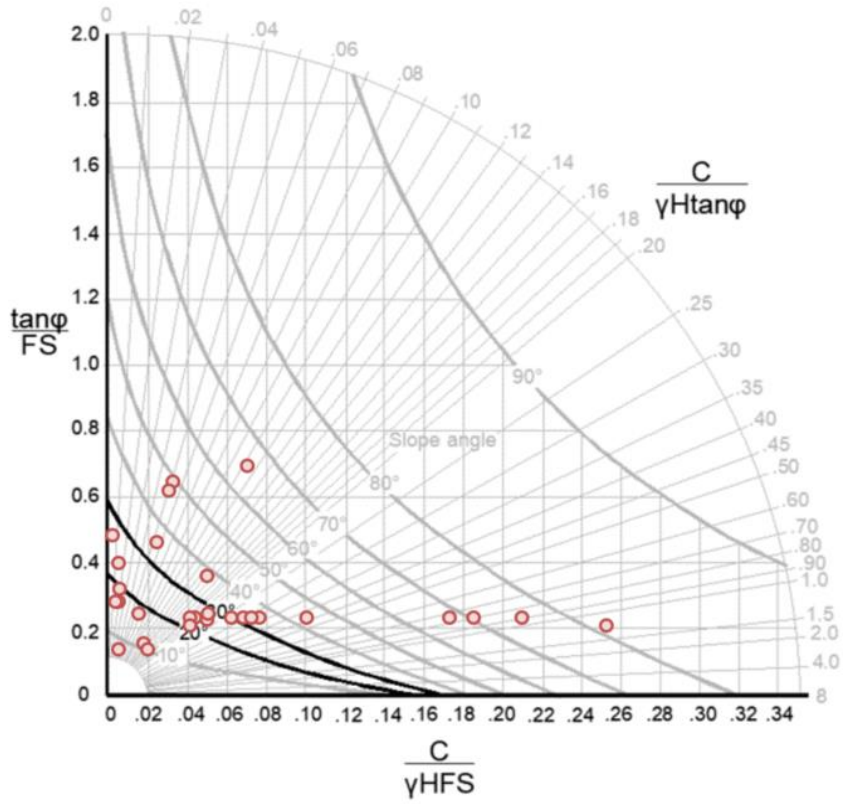
Figure 3.66 present the results of Hoek & Bray's chart evaluation. Note that the lines on the figures are the original lines proposed by Hoek and Bray. Due to a large number of data points, the figures are sorted according to different ranges of slope angle values ($10^\circ \leq \beta \leq 20^\circ$, $20^\circ \leq \beta \leq 30^\circ$, $30^\circ \leq \beta \leq 40^\circ$, $40^\circ \leq \beta \leq 50^\circ$, $50^\circ \leq \beta \leq 60^\circ$, and $60^\circ \leq \beta \leq 70^\circ$). The 'safe' and 'unsafe' points were determined for all of the domains at Hoek & Bray's chart, and for Hoek & Bray's chart the percentages were 65% of safe points and 35% of unsafe points.

Hoek & Bray's chart gives a slightly better result compared to Taylor's stability chart, but to match the open pit slope failure case histories better we decided to propose a new chart.

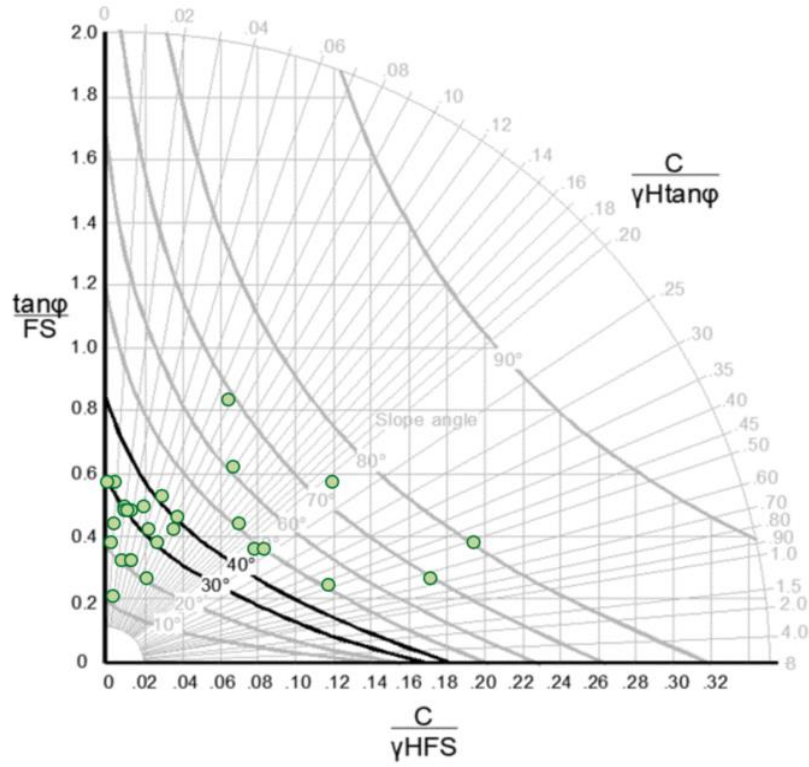
a)



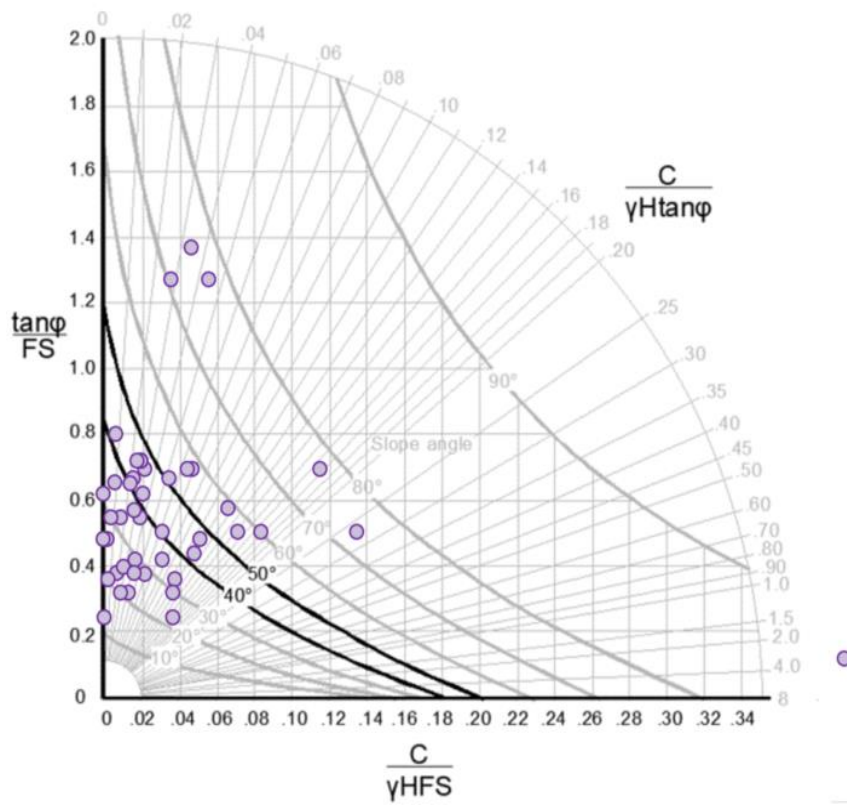
b)



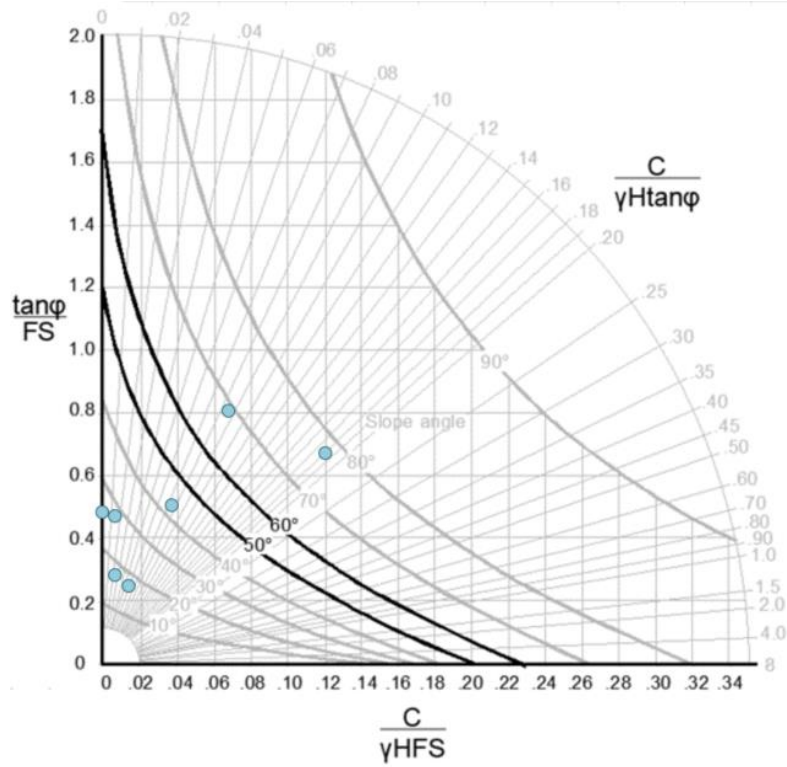
c)



d)



e)



f)

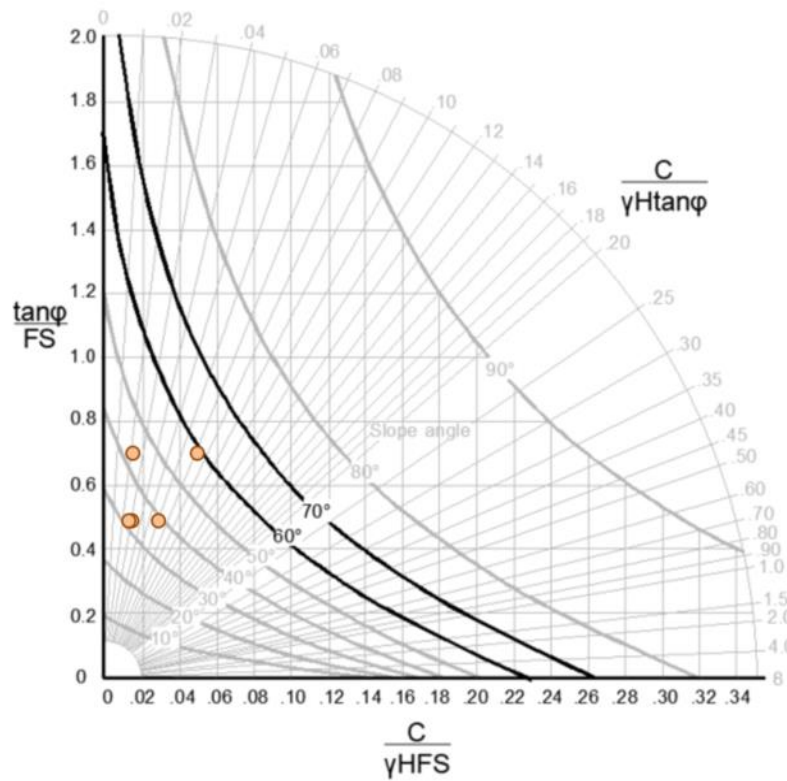


Figure 3.66 Comparison between friction angle (ϕ , °) from the case history database and Hoek and Bray's chart for the domain a) $10^\circ \leq \beta \leq 20^\circ$, b) $20^\circ \leq \beta \leq 30^\circ$, c) $30^\circ \leq \beta \leq 40^\circ$, d) $40^\circ \leq \beta \leq 50^\circ$, e) $50^\circ \leq \beta \leq 60^\circ$, and f) $60^\circ \leq \beta \leq 70^\circ$

3.4.4 A new stability chart development

The main idea of the new chart development is to provide a rapid means for determining the degree to which a slope is safe against failure in terms of a FS. As it was mentioned before there are many slope stability charts used in geotechnical engineering design practice, and in particular, all of them are based on the limit equilibrium methods. The most notable ones include those published by Taylor (1948), Bishop and Morgenstern (1960), Morgenstern (1963), Spencer (1967), and Hoek and Bray (1972).

A new stability chart for preliminary estimating the slope angle based on the collected open pit slope failure case histories is proposed. The slope development chart is based on the TAMU-MineSlope Spreadsheet. The slope geometry: failure height H_{FAIL} (m) and slope angle, β ($^{\circ}$), the effective shear strength parameters values (cohesion, c (kPa) and friction angle, ϕ ($^{\circ}$) of the slope material), and the values for the unit weight, γ (kN/m^3) of the slope materials were used in developing the slope stability chart. It should be noted that the referred the TAMU-MineSlope Spreadsheet utilized the average values of unit weight, cohesion, and friction angles for cases where slip surfaces intersected different geological strata. The procedure of parameters determination is presented in chapter 3.2.3.

On the vertical axis is the stability number ($c/\gamma H_{\text{FAIL}}$) and on the horizontal axis is the friction angle of the slope material ϕ ($^{\circ}$). The lines in the chart present the different slope angles β ($^{\circ}$). All the data points were split based on the slope angle ($\beta=15^{\circ}, 20^{\circ}, 25^{\circ}, 30^{\circ}, 35^{\circ}, 40^{\circ}, 45^{\circ}, 50^{\circ},$ and 60°). An exponential regression line was plotted for each set of data points; all the regression lines were set to intersect the origin of coordinates (Figure 3.67).

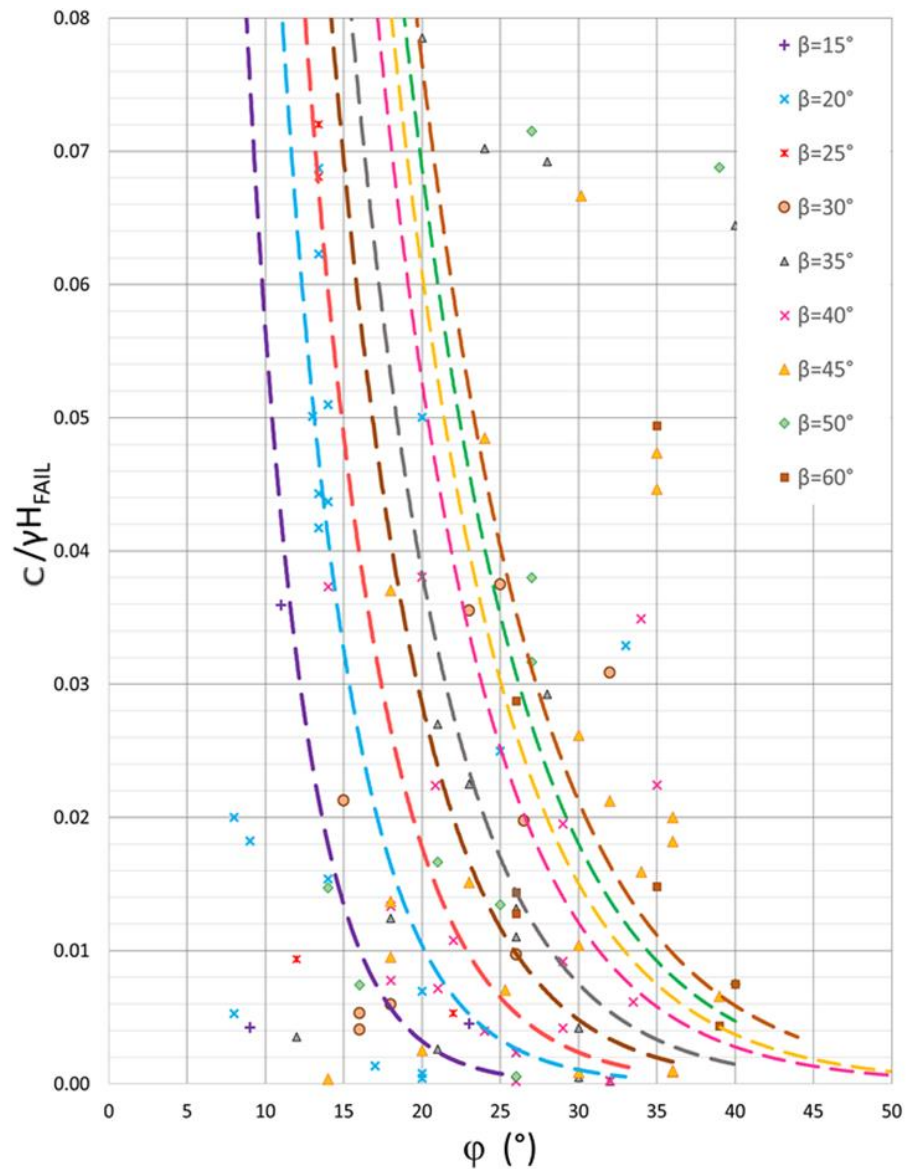


Figure 3.67 Stability chart development based on the collected open pit slope failure case histories (FS=1)

The probability charts per each set of points aiming 80% probability that the predicted value is greater than the observed value were constructed to determine the location of the regression lines associated with the different domains of the slope angle. The procedure of the probability plots development can be referred to the chapter 3.3.1 of the dissertation. Based on the

probability plots, the correction factor α_i needed to meet a given probability that the prediction will be greater than the observed value per each set of points was determined (Figure 3.68).

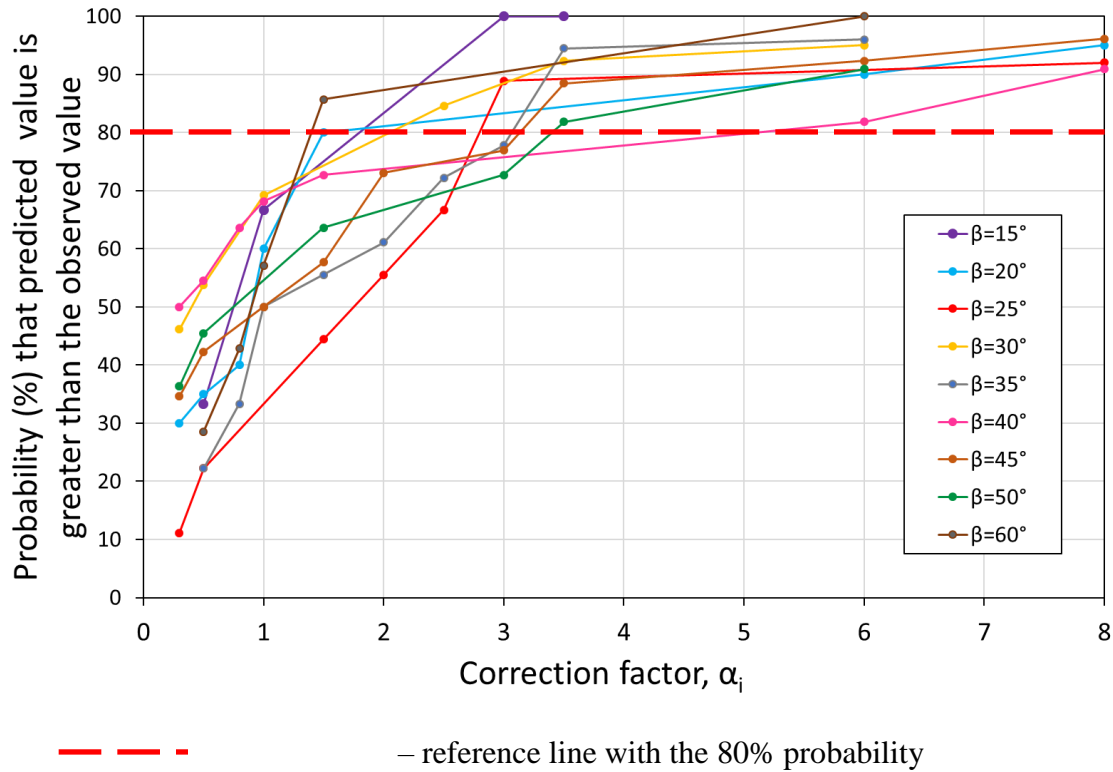


Figure 3.68 Correction factor needed to meet a given probability that the prediction will be greater than the observed value

The regression lines presented on the stability chart (Figure 3.69) were plotted based on the open pit slope failure case histories collection (134 cases) with the probability approach. Figure 3.69 presents the stability chart for open-pit mining slopes. This chart applies to the case in which the slope is simple and the material condition is uniform. The slope material has a unit weight γ (kN/m³), has no water, and can be represented by a cohesion, c (kPa) and a friction angle, ϕ (°).

Although the chart assumes a simple slope at failure and uniform soil conditions, it can be used to obtain a reasonably accurate answer for complex problems if irregular slopes are approximated by simple slopes and average values of unit weight, cohesion, and friction angles

are used. To approximate the real slope with equivalent simple and homogenous slope, it can be recommended to develop a cross-section of the slope drawn to scale. On the cross-section, using judgment, the engineer draws a geometrically simple slope that approximates the real slope as closely as possible (Duncan 1996). The shear stress parameters should be averaged too by using a weighting factor (e.g., the thickness of the stratum, length of the critical slip surface within the stratum). Finally, the weighted average strength parameters should be used to determine the FS from the chart.

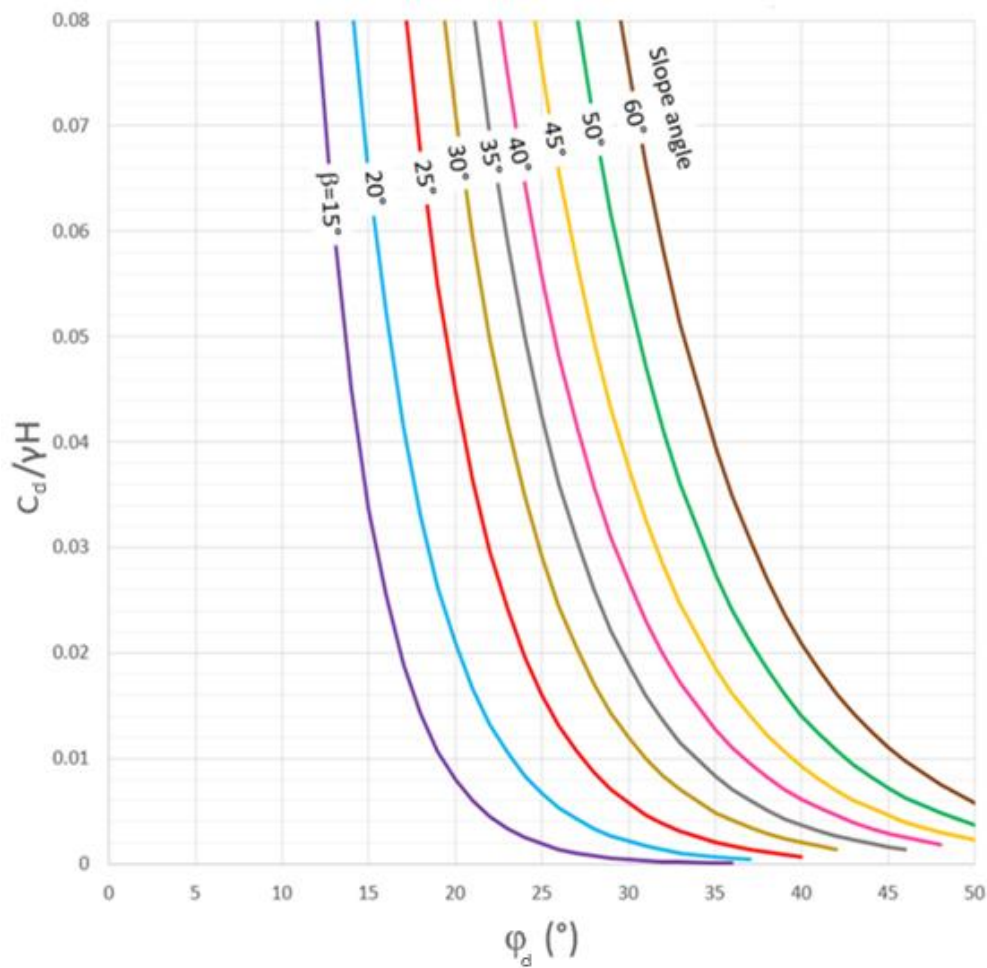


Figure 3.69 Proposed stability chart based on the 134 open pit slope failure case histories, H is the designed height of the slope in meters

The chart presented in the dissertation is developed with the engineering properties of the 134 open pit mining slope failures that occurred in 29 countries in 1968-2020. However, the chart is general and can be used for any open pit slope where the slope material properties and geometric parameters fall within the range of values used in the chart. For values of slope parameters different from ones used in the preparation of the chart, the stability condition can be inferred by interpolation.

There are two ways of using the chart: “design approach” and “analysis approach”. The procedure for using the chart for the design purposes is as follows:

1. Choose the design depth of the open pit H (m).
2. Find the slope material parameters: a unit weight γ (kN/m³), a cohesion c (kPa), and a friction angle ϕ (°). Although the chart assumes a simple slope at failure and uniform soil conditions, it can be used to obtain a reasonably accurate answer for complex problems if irregular slopes are approximated by simple slopes and average values of unit weight, cohesion, and friction angles are used. Thus, if the slope consists of several strata (Figure 3.70) determine the average γ , c and ϕ parameters using the Eqs. 3.47, 3.48 and 3.49.

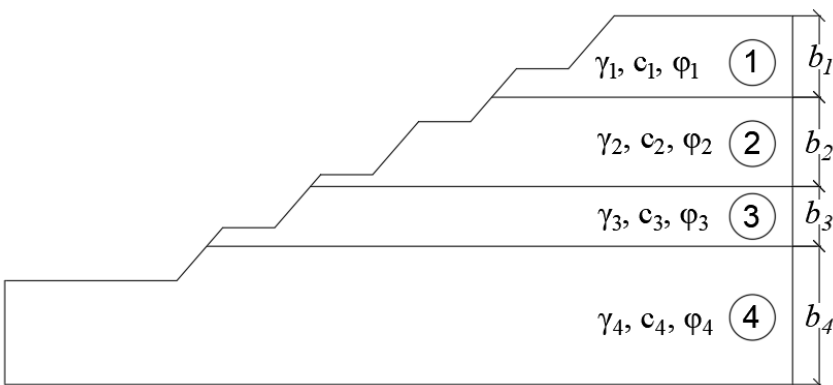


Figure 3.70 An example of an open pit slope consists of several strata

$$\gamma_{avg} = \frac{\gamma_1 \cdot b_1 + \gamma_2 \cdot b_2 + \gamma_3 \cdot b_3 + \gamma_4 \cdot b_4}{b_1 + b_2 + b_3 + b_4} = \frac{\sum \gamma_i \cdot b_i}{\sum b_i} \quad \left(\frac{\text{kN}}{\text{m}^3}\right) \quad \text{Eq.3.47}$$

$$c_{avg} = \frac{c_1 \cdot b_1 + c_2 \cdot b_2 + c_3 \cdot b_3 + c_4 \cdot b_4}{b_1 + b_2 + b_3 + b_4} = \frac{\sum c_i \cdot b_i}{\sum b_i} \quad (\text{kPa}) \quad \text{Eq.3.48}$$

$$\tan \varphi_{avg} = \frac{\tan \varphi_1 \cdot b_1 + \tan \varphi_2 \cdot b_2 + \tan \varphi_3 \cdot b_3 + \tan \varphi_4 \cdot b_4}{b_1 + b_2 + b_3 + b_4} = \frac{\sum \tan \varphi_i \cdot b_i}{\sum b_i} \quad \text{Eq.3.49}$$

where γ_{avg} , c_{avg} and φ_{avg} are averaged slope material parameters, γ_i , c_i and φ_i are unit weight, cohesion and friction angle for the i-stratum, and b_i is thickness of i-stratum. It should be noted that the parameters should be averaged only to the depth of the toe of the open pit or to the bottom of the critical slip surface.

3. Choose a design value of FS. A value of 1.3 is common in mining slope stability.
4. Using Eqs. 3.50 and 3.51, calculate the values of c_d and φ_d as:

$$c_d = \frac{c}{FS_c} \quad \text{Eq. 3.50}$$

$$\tan \varphi_d = \frac{\tan \varphi}{FS_\varphi} \quad \text{Eq. 3.51}$$

where c_d and φ_d are the fraction of initial shear strength parameters of the slope material c and φ required to maintain the slope in equilibrium.

5. Calculate the value of the dimensionless ratio $(c_d/\gamma H)$, and find this value at the vertical axis of the chart.
6. Knowing the dimensionless ratio $(c_d/\gamma H)$ and φ_d , find the corresponding slope angle β from the chart (Figure 3.69).

Consider a following example. An open pit is designed with the FS=1.3. The design depth of the pit is 70 m. The slope is designed to be excavated in overburden material with a unit weight $\gamma=18 \text{ kN/m}^3$, a cohesive strength of 38 kPa and a friction angle of 30° .

The value of $c_d=38/1.3=29.2$ (kPa); the value of $\tan \varphi_d=0.577/1.3=0.444$, therefore $\varphi_d=24^\circ$. The value of $c_d/(\gamma \cdot H) = \frac{29.2}{18 \cdot 70} = 0.023$, and the value of the friction angle is $\varphi_d=24^\circ$.

Thus for the required $FS_c=1.3$, the slope should be designed with a face angle of 28° .

In order to use the chart to back-calculate the factor of safety of the particular slope (“analysis approach”) the steps outlined below should be followed.

1. Choose the depth of the open pit H (m).
2. Choose the initial value of FS_c . A value of 1.3 is common for open pit mining.
3. Using Eq. 3.50, calculate the value of c_d .
4. Calculate the dimensionless ratio ($c_d/\gamma H$)
5. Knowing the dimensionless ratio and the slope angle β find φ_d from the chart (Figure 3.69).
6. Calculate the FS_φ and compare to FS_c .
7. If FS_φ and FS_c are not equal or within the target tolerance, go back to step 1 and try a new value of FS_c until FS_φ and FS_c are within that tolerance. Using a mean of FS_c and FS_φ is the next guess for FS_c is reasonable.

Consider a following example:

The 100 m high slope with a face angle of 40° is to be excavated in overburden material with a unit weight $\gamma=21$ kN/m³, a cohesive strength of 60 kPa and a friction angle of 35° .

Consider $FS_c=1.3$. The value of $c_d=60/1.3=46.2$ (kPa). The value of the dimensionless ratio ($c_d/\gamma H$) = $\frac{46.2}{21 \cdot 100} = 0.022$ and the corresponding value of the value of φ_d , for a 40° slope, is 31.5° . Therefore $FS_\varphi=1.14$.

Consider $FS_c=1.25$. The value of $c_d=60/1.25=48$ (kPa). The value of the dimensionless ratio $(c_d/\gamma H) = \frac{48}{21 \cdot 100} = 0.023$ and the corresponding value of the value of φ_d , for a 40° slope, is 31° . Therefore $FS_\varphi=1.17$.

Consider $FS_c=1.2$. The value of $c_d=60/1.20=50$ (kPa). The value of the dimensionless ratio $(c_d/\gamma H) = \frac{48}{21 \cdot 100} = 0.024$ and the corresponding value of the value of φ_d , for a 40° slope, is 30.5° . Therefore $FS_\varphi=1.19$.

The FS for the considered slope is $FS=1.2$.

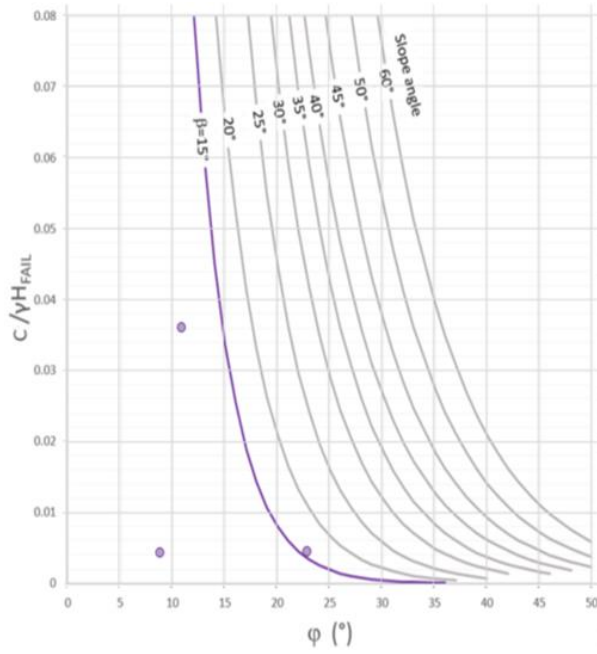
The same examples were used to obtain the design parameters from Taylor's chart and Hoek&Bray's stability chart. The comparative study results are presented in Table 3.8. It can be seen that the proposed stability chart is more conservative than Taylor's and Hoek&Bray's charts. The reason for that can be a lot of scatter in TAMU-MineSlope.

Table 3.8 Comparative study of the results obtained using Taylor's chart, Hoek&Bray's chart and proposed stability chart

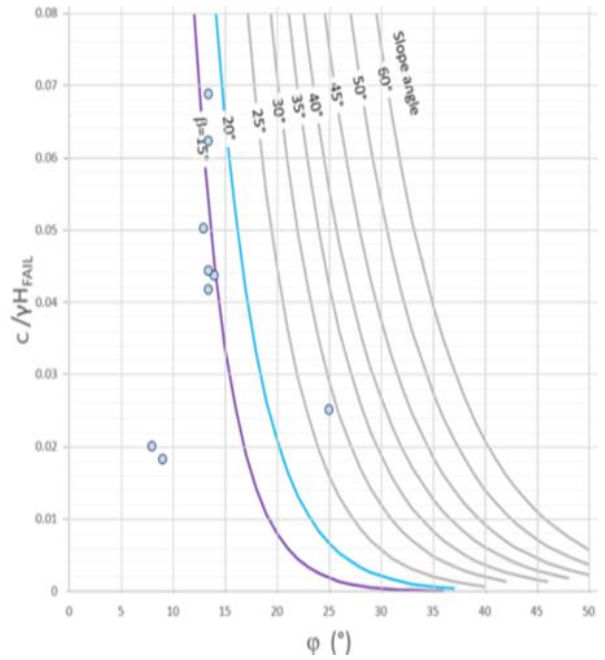
Example	Input parameters	Obtained results		
		Taylor chart	Hoek & Bray chart	Proposed stability chart
1	$FS=1.3$ $H=70$ m $\gamma=18$ kN/m ³ $c=38$ kPa $\varphi=30^\circ$	$\beta=32^\circ$	$\beta=35^\circ$	$\beta=28^\circ$
2	$H=100$ m $\beta=40^\circ$ $\gamma=21$ kN/m ³ $c=60$ kPa $\varphi=35^\circ$	$FS=1.25$	$FS=1.2$	$FS=1.2$

As it was done for Taylor's and Hoek&Bray's charts, the new stability chart was evaluated using the open pit slope stability failure case histories collection (Figure 3.71). As a result, we

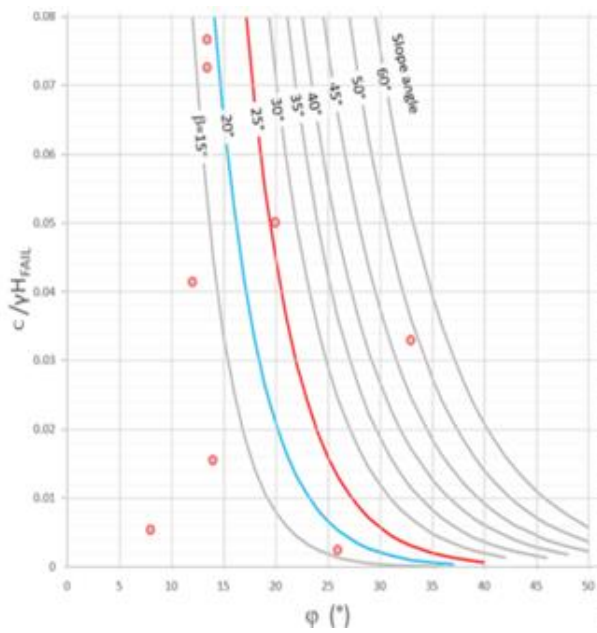
found out that the proposed stability chart gives 78% of points to be on the safe side and 22% of points on the unsafe side. That means that based on the actual data from TAMU-MineSlope, the new chart results are 40% higher than Taylor's chart and 20% higher than Hoek&Bray's chart.



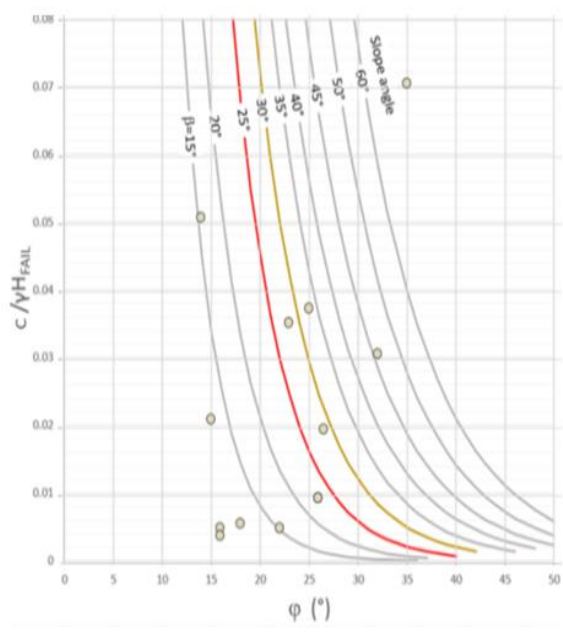
a)



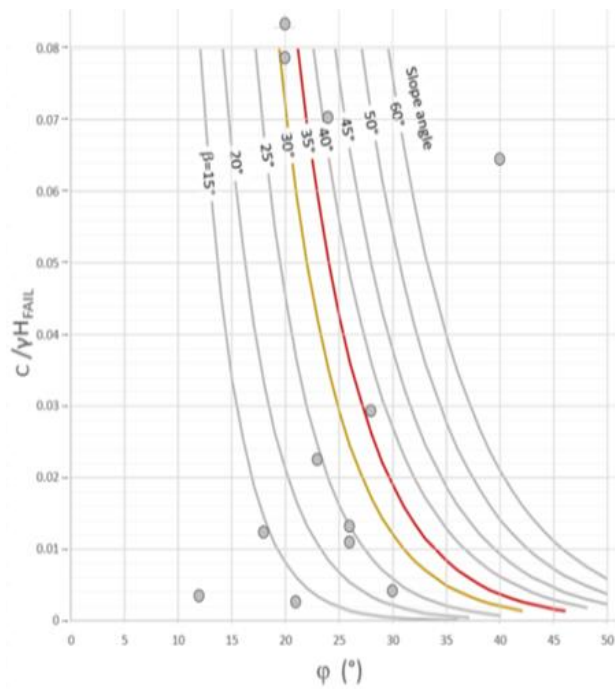
b)



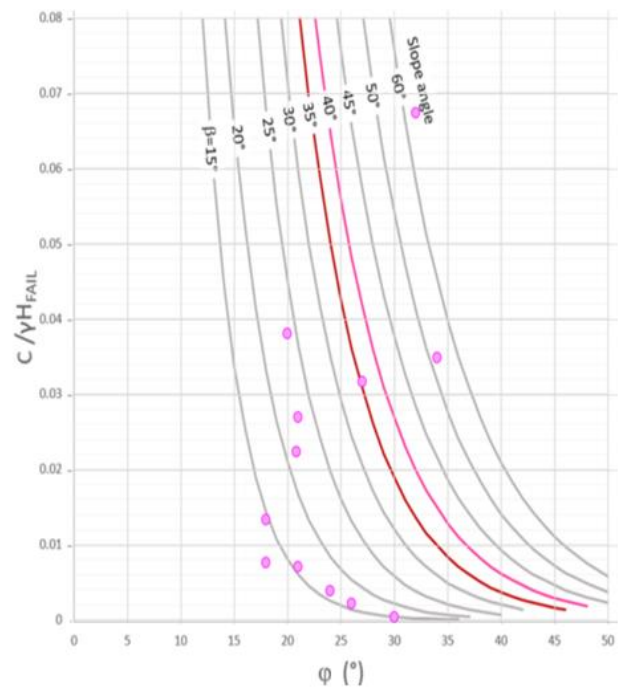
c)



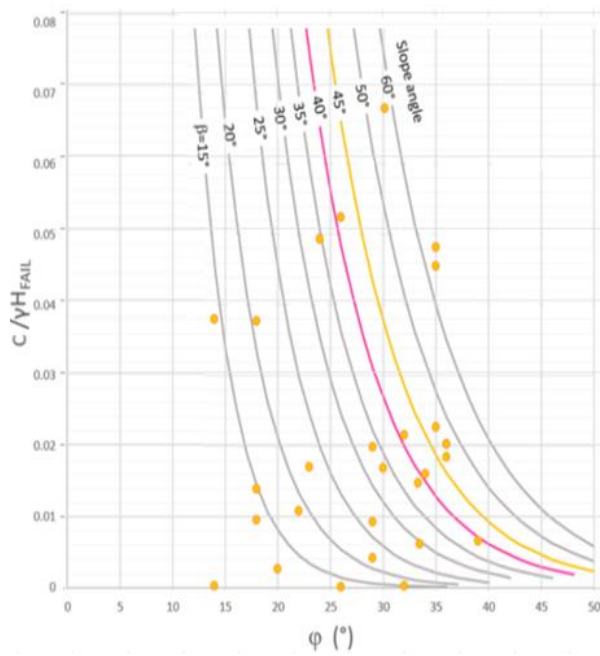
d)



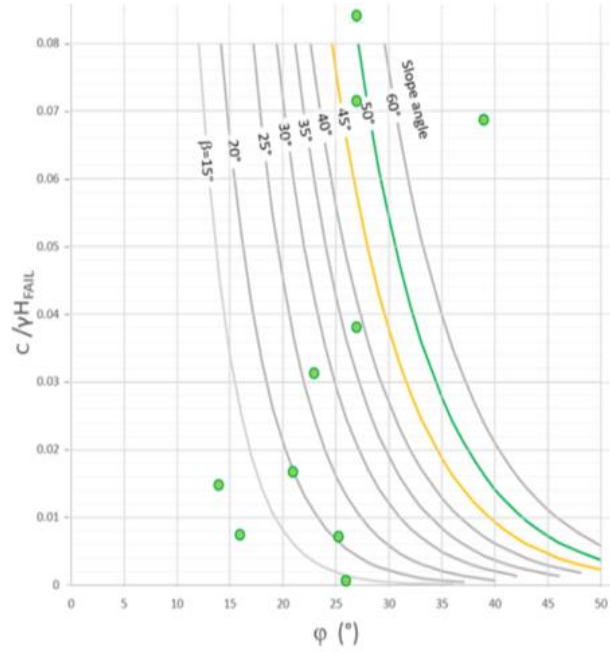
e)



f)



g)



h)

Figure 3.71 Comparison between friction angle (ϕ , $^\circ$) from the case history database and new developed stability chart for the domain a) $\beta \leq 15^\circ$, b) $15^\circ \leq \beta \leq 20^\circ$, c) $20^\circ \leq \beta \leq 25^\circ$, d) $25^\circ \leq \beta \leq 30^\circ$, e) $30^\circ \leq \beta \leq 35^\circ$, f) $35^\circ \leq \beta \leq 40^\circ$, g) $40^\circ \leq \beta \leq 45^\circ$, and h) $45^\circ \leq \beta \leq 50^\circ$

The following conclusions are drawn based on the comparative study results:

(a) the proposed stability chart is more conservative than Taylor's and Hoek&Bray's charts (Table 3.8);

(b) the developed stability chart is proposed for the preliminary estimation of the FS for the open pit slopes, and it can be used for preliminary slope design and planning;

(c) the proposed chart is based on the open pit slope failure case histories;

(d) there is a lot of scatter in the collected case histories;

(e) the choice of the curves on the chart was aiming 80% probability that the design would be safer than the observed behavior.

3.5 Risk associated with open pit mining slopes

The stability of slopes in open-pit mines is a great concern because of the significant detrimental consequences of instabilities. To ensure these mines' safe and continuous economic operation, it is necessary to assess and manage slope stability risk systematically. Risk-Informed Decisions can be used to identify, analyze, assess, and manage the risks associated with open-pit mining slopes.

Owners, agencies, and regulators have been using risk concepts and principles for quite some time to inform decisions within various industries across the world. In particular, the United States (US), the United Kingdom (UK), the Netherlands, and Hong Kong have integrated risk principles into safety decisions in various ways since the 1960s (Baecher et al. 2015). For example, in the UK, the Health and Safety Executive (HSE) was one of the first agencies over 40 years ago to broadly address individual and societal risk concerns through worker safety regulation. Although not specifically developed for dams, the HSE risk framework provided the basis for much of today's international dam safety risk guidelines.

3.5.1 Existing knowledge on ‘bubble chart’ development

In civil engineering practice, the risk R associated with a project, is defined as the product of the PoF of that project times the value of the consequence C of the failure (Eq. 3.52).

$$R = \text{PoF} \cdot C \quad \text{Eq. 3.52}$$

The PoF can be represented as the product of the probability of occurrence of an event that might cause the failure (e.g.: flood, earthquake, overload), $P(E)$, by the PoF if that event occurs $P(F/E)$ also called vulnerability or fragility (Eq. 3.53).

$$\text{PoF} = P(E) \cdot P(F/E) \quad \text{Eq. 3.53}$$

As an example, if the annual probability that the failure will occur is 0.002 and if the value of the consequence is 5 fatalities and a cost of US\$1,000,000, the risk is $5 \cdot 0.002 = 0.005$ fatalities/yr and $1,000,000 \cdot 0.002 = \$2,000/\text{yr}$. So, the units of Risk will be in fatalities per year and US dollars per year.

Eq. 3.52 can be modified by taking the decimal logarithm of the parameters (Eq. 3.54). Therefore, for a constant risk the graph of the annual PoF P_a versus the value of the consequence C on log scales will be a straight line with a slope of -1.

$$\log P_f = \log R - \log C \quad \text{Eq. 3.54}$$

Risk can be graphically presented as the risk chart first proposed by Whitman (1984) (see Figure 3.72), then updated by Baecher and Christian (2003) (Figure 3.73), Steffen et al. (2008) (Figure 3.74), Gilbert (2017), Briaud et al. (2014) (Figure 3.75) among others.

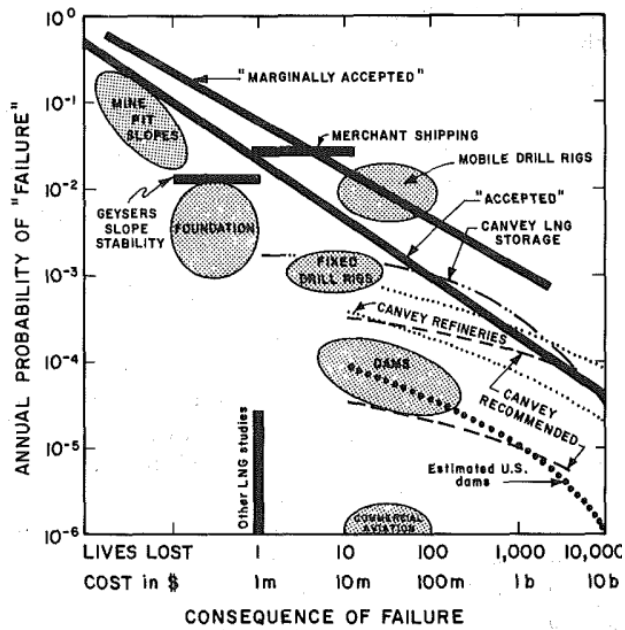


Figure 3.72 Risks for selected engineering projects (reprinted from Whitman 1984)

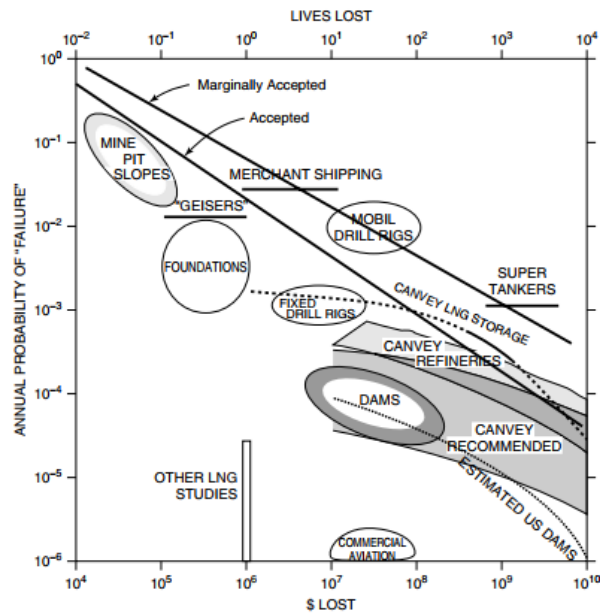


Figure 3.73 F-N chart showing average annual risks posed by a variety of traditional civil facilities and other large structures or projects (reprinted from Baecher and Christian 2003)

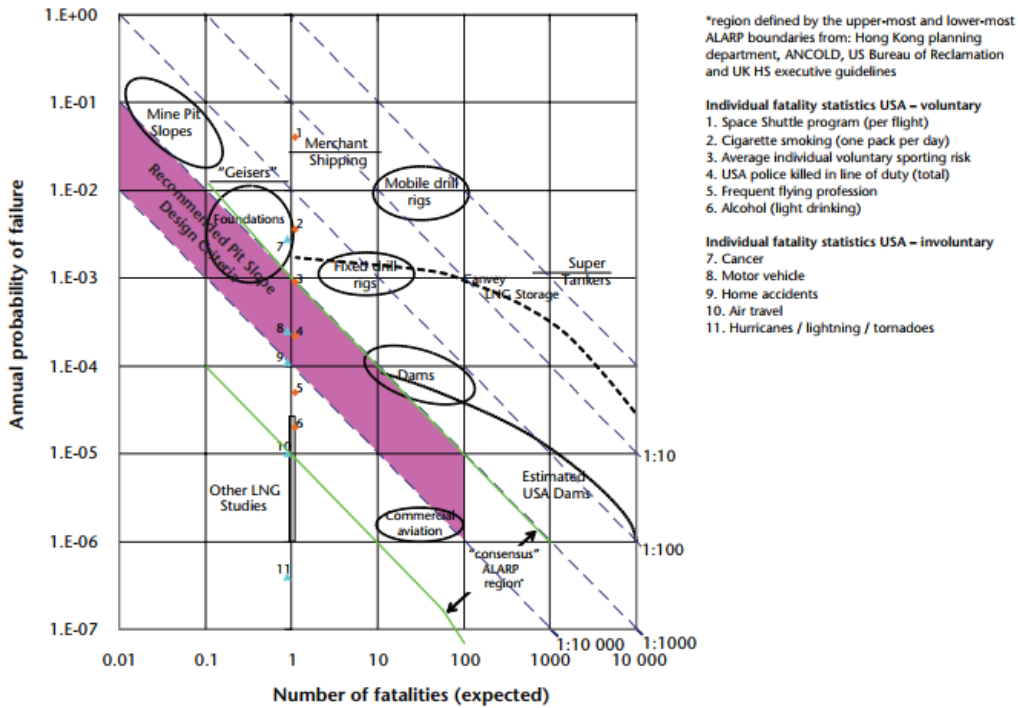


Figure 3.74 Comparison of risk acceptable criteria with statistics (reprinted from Steffen et al. 2008)

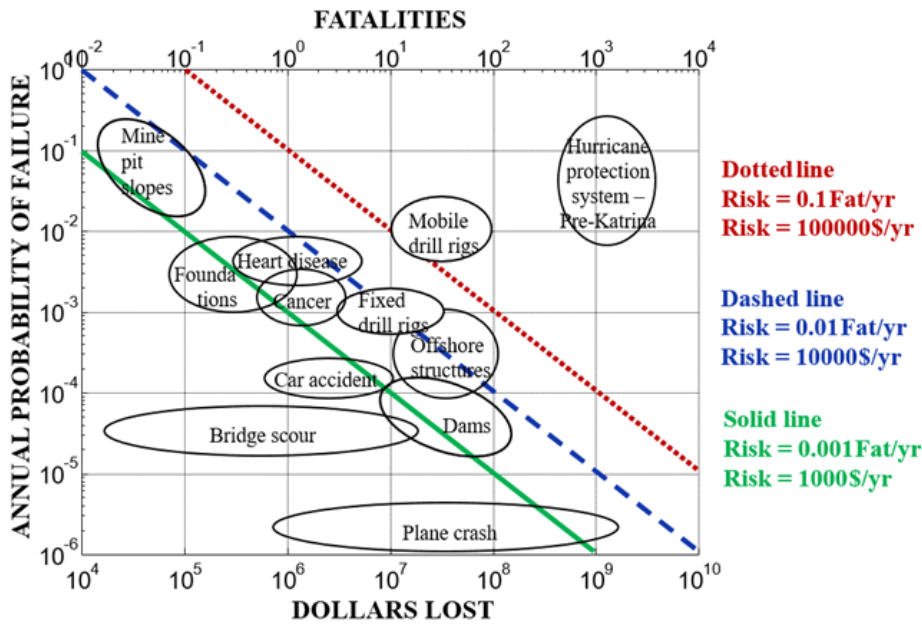


Figure 3.75 Risk f-N chart for human activities (reprinted from Briaud et al. 2012)

Briaud et al. (2014) proposed the criteria for low, medium, and high-risk levels. The solid, dashed, and dotted lines on the risk chart represent lines of equal risk. The low-risk level presented by the solid green line corresponds to an annual risk of \$1,000 per year and 0.001 fatalities per year. The medium risk level presented by the dashed blue line corresponds to an annual risk of \$10,000 per year and 0.01 fatalities per year. The dotted red line presents the high-risk level which is associated with an annual risk of \$100,000 per year and 0.1 fatalities per year.

If we look at the presented risk charts (Figure 3.72-3.74), the several bubbles' location was not changed since the first publication. At the same time, according to the NIOSH (2020), for example, the number of fatalities associated with open pit mining dropped down significantly starting from 1983 (Figure 3.76).

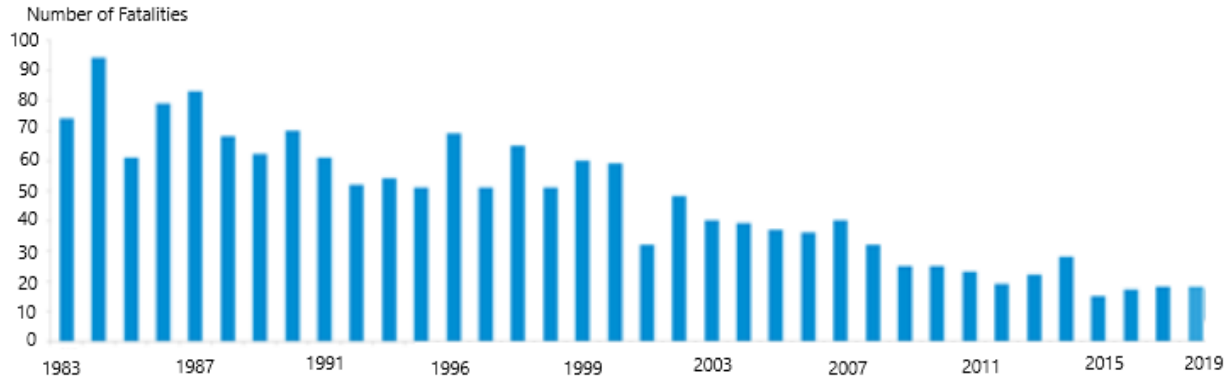


Figure 3.76 Number of fatalities in open pit mining industry by year, 1983 – 2019
(reprinted from NIOSH 2020)

The same trend can be observed for the number of fatalities due to slope instability in the US surface mining industry. Starting from 1983, the number of fatalities dropped from 13 to 0, and there were no fatalities due to the slope failures in 2019 and 2020 (NIOSH 2020). This is because mining (both surface and underground) safety in the US has improved dramatically over the last century. In 1931, the earliest year the Mine Safety and Health Administration (MSHA) recorded figures for both numbers of miners and workplace deaths, a total of 1,688 employees died from a working population of 748,712. The ratio of worker fatalities to the total number of miners was 0.00225, it is a figure that remains orders of magnitude greater than the 0.0001 ratio recorded in 2020 when 29 miners died from a workforce of 295,427 (Casey 2019; MSHA 2021).

Because of how critically important that chart is, an updated version of that chart needs to be created. The new chart has to be done based on the recent statistics with precise explanations of where the data came from and how the chart's points were obtained.

3.5.2 Procedure

A number of activities were selected to show their location on the risk chart. These activities were:

- Car accidents
- Cancer
- Heart disease and stroke
- General aviation
- Commercial aviation
- Nuclear power plants
- Bridge scour
- Open pit mine slopes

There are many different ways to evaluate the statistics associated with fatalities, cost, and probability of failure. Many factors can come into play. For this research, the approach and calculations were precisely documented because the applicability of the results can be limited by the available data. The general step-by-step procedure for obtaining the risk location of a given activity on the chart was as follows:

1. Define the failure phenomenon (for example, earth dam failure)
2. Collect information to determine the total number of failures F_t over n years (for example, 30 years).
3. Obtain the average annual number of failures F_a given by Eq.3.55

$$F_a = F_t/n \qquad \text{Eq.3.55}$$

4. Collect information to determine the total number S of structures or people involved with the activity in the inventory (for example, total number of dams in the US or total number of people in the US)
5. Calculate the average annual PoF, P_a (Eq. 3.56) and the range of P_a values for the study period.

$$P_a = F_a/S \qquad \text{Eq.3.56}$$

6. Collect the number of people that died for each documented failure for the period of n years. Add those up to obtain the total number of fatalities D over the period of n years and for F_t failures.
7. Obtain the average number of fatalities X corresponding to one failure as D/F_t and the range of X values for the study period. Note that, because of the log scale, the ellipse created for each activity was bound by 0.01 fatalities if the lower bound was 0.
8. Collect the consequence cost associated with each failure for the period of n years. Convert these values into US 2020 dollars by correcting for inflation. Add those up to obtain the total cost c of those failures over n years and for F_t failures.
9. Obtain the average cost C associated with each failure as c/F_t and the range of C values over the study period.
10. The location of the activity has coordinates of P_a and X on the fatality risk chart and P_a and C on the cost risk chart.

3.5.3 Application to various activities

The authors analyzed the risk associated with different public and civil engineering activities. They are Car accidents, Cancer, Heart disease and stroke, General aviation, Commercial aviation, Nuclear power plants, Bridge scour, Open pit mine slopes and Earth dams. Table 3.10 summarizes the results obtained.

3.5.3.1 Car accident

According to the statistics published by the National Highway Traffic Safety Administration (NHTSA) there were 36,096 lives loss on US roads in 2019 (NHTSA 2020). Since there are approximately 2.8 million deaths every year in the US car accidents account for approximately 1.3% of total deaths in the US.

First, let's define the failure as a 'car accident fatality'. The statistical data for the period of 1994-2018 (n=25 years) were analyzed. During that period the total number of failures is $F_t=973,698$, therefore the annual number of deaths due to car accidents averaged $F_a=973,698/25=38,948$ (NHTSA 2020). The average number of people in the United States from 1994 to 2018 was $S=297$ million (U.S. Census Bureau 2020). Therefore, the annual probability of a person dying in a car accident in the US is $P_a=38,948/(2.97 \cdot 10^8)=1.31 \cdot 10^{-4}$, the fatality consequence X is 1 and the economic loss C is taken as 1 million dollars, because that is a reasonable average for the life insurance carried by many people (Briaud 2013).

If we defined failure as 'a car accident with fatality' then the annual probability of a fatal car crash can be calculated as follows. During the period of 25 years the total number of failures was $F_t=880,656$, thus the annual number of fatal car accidents in the US was $F_a=880,656/25=35,226$ (NHTSA, 2020). The average annual number of registered vehicles in the US is $S=243.5$ million (Statista, 2020). According to the National Household Travel Survey (FHWA, 2020), the average light vehicle occupancy is 1.67 for the past 25 years. The economic loss of traffic crashes for the same period was US2020\$ $c=319.2$ billion (NHTSA, 2020). Therefore, the annual probability of a fatal car crash is $P_a=35,226/243,500,000=1.45 \cdot 10^{-4}$, the corresponding number of fatalities X is 1.67 and the economic loss C is 9.1 million dollars ($\$319,200,000,000/35,226$). Figure 3.78 and 3.79 show the data associated with car accidents.

3.5.3.2 Cancer

Malignant neoplasms (cancer) is the second leading cause of fatalities in the US accounting for 21.3% of all deaths (CDC, 2020). The failure is defined as 'a person dying of cancer'. The probability to die of cancer was estimated based on the statistical data from 1996-2018 (n=24 years). According to the American Cancer Society (2019), each year an average of $F_a=570,034$

people die of cancer in the US. There were $S = 301$ million people on average in the US over that period of 24 years (U.S. Census Bureau, 2020). Therefore, the annual PoF associated with cancer is $P_a = 570,034/301,000,000 = 1.89 \cdot 10^{-3}$, and the fatality consequence is $X = 1$. Also according to the American Cancer Society (2019) report, the total cost of cancer over the last 20 years is US2020\$ $c = 135.2$ billion. Thus, for an individual, the annual economic loss is calculated to be US2020 \$237,179 ($\$135,200,000,000/570,034$). The data associated with cancer is located in Figure 3.78 and 3.79.

3.5.3.3 Heart Disease and Stroke

Heart disease is the number one cause of death in the US and accounts for 23% of all deaths (NVSS 2019, CDC 2020). The failure phenomenon is defined as ‘a person dying of a heart disease’. During the period 2006-2018 ($n=13$ years) there were $F_t = 8,054,019$ fatalities, corresponding to an average fatality per year of $F_a = 619,540$ ($8,054,019/13$). The annual probability of death due to heart disease is $P_a = 619,540/313,000,000 = 1.98 \cdot 10^{-3}$, because $S = 313$ million is the average number of people in the US for the period 2006-2018. The life lost is $X = 1$.

Stroke is one of the five leading causes of death in the United States. The failure is ‘a person dying of a stroke’. Based on the statistical data for the period of 1999-2018 the total number of deaths was $F_t = 2,874,333$, and the annual number of deaths due to stroke is $F_a = 143,717$. The average US population for the same period is $S = 304$ million. Therefore, the annual probability to die due to a stroke is $P_a = 143,717/304,000,000 = 4.73 \cdot 10^{-4}$, and the life lost is $X = 1$. Figure 3.78 shows the data associated with heart disease and stroke separately.

The probability to die due to a stroke or heart disease is obtained by combining the statistics for both diseases. The annual number of death due to stroke or heart disease for the last 13 years is $F_a = 755,059$, therefore $P_a = 2.41 \cdot 10^{-3}$. The total direct and indirect cost of heart disease and stroke

in the United States for the studied period is estimated at US2020 c=\$368 billion (AHA, 2018). The annual economic loss corresponding to one fatality is therefore US2020 C=\$4.95·10⁵ (368,000,000,000/755,059). The combined data associated with the cost of heart disease and stroke is presented in Figure 3.79.

3.5.3.4 General aviation

General aviation accounts for approximately 77% of all aircraft operations in the United States. Approximately 95% of the 220,000 civil aircraft registered in the US are general aviation aircraft (Sobieralski, 2013, Mazareanu, 2020a). General aviation is defined as all flying aircraft excluding military and scheduled airline operations and includes flight training, search and rescue, aerial surveys, crop dusting, and personal/recreational use. Sobieralski (2013) states that general aviation accident and fatality rates are approximately 50 times greater than commercial aviation rates. According to The National Transportation Safety Board (NTSB, 2014) general aviation includes private aviation and operations that employ a wide range of aircraft such as airplanes, rotorcraft, gliders, balloons, and blimps, and registered experimental or amateur-built aircrafts. The vast majority of general aviation accidents involve personal or recreational flights. The Federal Aviation Administration (FAA, 2018) identified the following top three leading causes of fatal general aviation accidents from 2001 to 2016: (a) Loss of Control in flight; (b) Controlled Flight Into Terrain; (c) System Component Failure – Powerplant.

The failure in this case is defined as ‘a fatal general aviation accident’. According to the data published by the Bureau of Transportation Statistics (2018) the total number of general aviation fatal accidents in the US for the period 2002-2018 (n=17 years) is $F_t=4,642$. On average there were $F_a=273$ fatal general aviation plane accidents per year for total number of flights per year of $S=10,187,656$. Therefore, the probability of a fatal general aviation plane crash for any

given flight is $P_a=273/10,187,656=2.68 \cdot 10^{-5}$. The total number of fatalities associated with general aviation plane crashes for the same period of time is $D=8157$, and the average annual number of fatalities per failure is $X=8157/4642=1.76$.

The cost of general aviation crashes has been studied by a few researchers (Scuffham et al. 2002 and Sobieralski 2013). According to Sobieralski (2013) the total annual cost of general aviation accidents in the United States is $c=4.99$ billion dollar; therefore the average cost of one fatal accident is $C=18.3$ million dollar ($\$4,990,000,000/273$). The general aviation location on the risk chart is shown in Figure 3.78 and 3.79.

3.5.3.5 Commercial aviation

Commercial aviation is defined as scheduled airline operations involving aircraft with more than 10 seats. In the US, a commercial operator is one that has been certified by the Federal Aviation Administration (FAA) under the Code of Federal Regulation (CFR) part 121 (airlines) or CFR Part 135 (commuters) to provide air transport of passengers or cargo.

The failure is defined as ‘a plane crash’. According to the statistics published by the Bureau of Transportation Statistics (USDOT, 2019) there were $F_t=61$ fatal plane crashes for the period of 1990-2018 ($n=29$ years) and the number of departures per year was $S=9,694,928$ in the U.S. The annual number of plane crashes is therefore $F_a=60/29=2.10$. The probability of a plane crash can be determined as $P_a=2.10/9,694,928=2.17 \cdot 10^{-7}$.

According to published data (USDOT, 2019) the total number of fatalities for the period 1990-2018 is $D=1730$, and the annual number of fatalities associated with a commercial plane crash is $X=1730/61=28.36$. Figure 3.78 presents the commercial aviation data in terms of number of fatalities.

The cost of airline accidents can be associated with coverage for hull, passenger legal liability, third party liability, and products liability. The annual airline insurance cost in commercial aviation between 2000 and 2018 varies between 2.34 and 59.39 billion US\$2020 with a mean of 7.73 billion dollars (Makinen, 2002; Mazareanu, 2020b). Therefore, the cost of one commercial aviation failure is US2020 $C = \$3.68$ billion ($\$7,730,000,000/2.10$). Figure 3.79 presents the data connected to a plane crash failure.

3.5.3.6 Nuclear Power Plant

According to the World Nuclear Association (2020) the US is the world's largest producer of nuclear power, accounting for more than 30% of worldwide nuclear generation of electricity. At the end of December 2019, the US had 96 operating commercial nuclear reactors at 58 nuclear power plant sites in 29 states (Office of Nuclear Energy, 2020)

Sovacool (2009) states that sixty-three accidents have occurred since the Chernobyl disaster in 1986, and 71% of all nuclear accidents (45 out of 63) occurred in the US. Such accidents have involved meltdowns, explosions, fires and losses of coolant. They have occurred during both normal operation and extreme, emergency conditions (such as droughts and earthquakes).

The failure is defined as 'major nuclear reactor failure'. The total number of accidents in the US for the 61-year-period is 67 (Sovacool, 2009), however only four of those can be classified as major nuclear reactor failures ($F_t=4$): Sodium Reactor Experiment (Los Angeles, California, USA, 1959); SL-1 (Idaho Falls, Idaho, USA, 1961), Enrico Fermi Unit 1 (Frenchtown Charter Township, Michigan, USA, 1966), Three Mile Island (Middletown, Pennsylvania, USA, 1978). The annual number of major failures in the U.S. nuclear industry starting in 1959 is $F_a=4/61=0.066$. The annual number of working reactors for the period of 1959-2019 ($n=61$ years) is $S=76$ (EIA, 2020).

The PoF associated with the U.S. nuclear power plants is $P_a=0.066/76=8.68 \cdot 10^{-4}$. The total number of fatalities associated with major nuclear reactor failures for the studied period is $D=3$, therefore the number of fatalities associated with one failure is $X=3/4=0.75$ (Figure 3.78).

Because nuclear power plants are so large and complex, accidents onsite tend to be very expensive. The economic loss of one nuclear reactor failure varies from 21.5 million to 3.1 billion US\$2020 (Sovacool, 2009). Therefore, the average cost of one failure in the US is US2020 $C=\$618.3$ million (Figure 3.79).

3.5.3.7 Bridge scour

Bridge scour is the most common cause of bridge collapse during storms and floods in the US. Bridge scour is the loss of soil by erosion due to water flowing around bridge supports. According to statistics collected by NYSDOT between 1970 and 2005 ($n=36$ years) (Sullivan 2005; Briaud et.al 2014), 1377 bridges collapsed during those 36 years for an average rate of one bridge collapsing every 10 days; 60% of the time the collapse is due to bridge scour.

The failure is defined as ‘bridge scour failure’. The annual PoF is the average number of bridge failures per year over a given period divided by the total number of bridges that exist during that same period. According to the NYDOT database, $F_t=765$ failures due to scour (hydraulic reason) occurred between 1970 and 2005. According to the US National Bridge Inventory (NBI), about $S=500,000$ bridges over water existed during that 36-year period (Briaud et. al. 2012). Therefore, the annual probability of bridge failure due to scour is $P_a = 4.25 \cdot 10^{-5}$. The number of fatalities due to bridge scour failures from 1970 to 2005 is $D = 28$. This gives an average number of fatalities per bridge failure of $X=0.04$ ($28/765$). The total cost of the failure C of an average size bridge was estimated by Briaud et al. (2012) and varies from US2020 \$1.45 million to \$18 million for bridge scour failures. This cost includes the bridge repair or replacement cost,

the detour cost and the cost of time lost. The estimated risk of 0.04 fatalities/yr, and economic loss for bridge scour failures are used to locate the bridge scour ellipse on Figure 3.78 and 3.79.

3.5.3.8 Open pit slope stability

Open pit mining is an industry where taking a calculated risk is important to improve returns. There were 12,448 surface mining operations in the US in 2019 (NOISH 2020). The US surface mining is divided by NIOSH into 5 general groups: coal, metal, nonmetal (which includes the mining of clay, trona, barite, phosphate rock, gypsum, talc, gemstones, and pumice), stone, and sand and gravel operations. Active surface mining operations are distributed among the coal (n=849; 6.8%), metal and nonmetal (n=1,082; 8.7%), and stone, sand and gravel (n=10,517; 84.5%) industry sectors (NIOSH, 2019). According to the data collected by the National Institute for Occupational Safety and Health's (NIOSH) for the past 31 years (1982-2019), slope stability accidents are one of the leading causes of fatalities for U.S. surface mining operations with D=145 miners losing their lives as a result of slope failures.

The failure phenomenon is defined as 'an open pit slope failure in one open pit mine'. Highwall accident statistics from the MSHA database were analyzed for the ten-year period (1990-1999) including incident frequency, degree of injury, nature of injury, equipment involved, coal and non-metal breakdown, worker activity at the time of accident, and other relevant parameters (Bhatt and Mark, 2000). The annual number of slope failures in active open pit mines during those 10 years is $F_a = 43$. The annual number of active surface mines during the same period was $S=13,234$, therefore the probability of open pit slope failure is $P_a=43/13,234=3.25 \cdot 10^{-3}$. The total number of fatalities for the period 1982 to 2019 is $D=145$, therefore the life loss per failure is 0.11 ($X=145/(31 \cdot 43)=0.11$).

The average cost of one slope failure was estimated based on the published open pit mine economic loss for Kennecott' Nevada Mine Division (the failure occurred in 1979), Smoky Canyon Phosphate Mine (the failure occurred in 1992), Boron (the failure occurred in 1998), and Bingham Canyon Copper Mine (the failure occurred in 2013). The cost of the failure includes losses due to having to close the mine, due to fatalities, due to loss of the equipment, and due to recovering operations. The failure cost varied between 10^5 and $6 \cdot 10^8$ (US\$2020) and averaged $C=1.59 \cdot 10^8$.

The locations on the risk charts for failures due to slope instability in open pit mining are presented in Figure 3.78 and 3.79.

3.5.4 Fatalities and cost risk charts

The general view of the risk chart is presented in Figure 3.77. The annual P_a is plotted on the vertical axis, and the value of the consequences C is plotted on the horizontal axis. The value of the consequences can be defined as fatalities or economic loss in dollars. Straight incline lines with a slope of -1 present the constant low, medium, and high risk. Those lines depend on the chosen value of the annual risk R. A failure phenomenon on the chart is shown as an ellipse. The ellipse's width represents the range of the consequence values, while the point near the center represents the mean value.



Figure 3.77 Example of the risk chart; the location of the activity has coordinates of P_a and C .

Two risk charts for the United States were constructed based on the data presented in Table 3.9: the annual PoF vs. fatalities risk chart (Figure 3.78) and the annual PoF vs. dollars loss risk chart (Figure 3.79). They will be called the fatality risk chart and the cost risk chart respectively. For each activity, the annual PoF and the number of fatalities or dollars lost should a failure occur were used as coordinates on the chart. Ellipses were used when there was a range of values associated with the probability of failure, the number of fatalities or cost. The length of the horizontal and vertical axis of the ellipses indicate the range of the data. Several factors affect the location of the activity in the charts. They include:

- 1) The period of time over which the data is collected including the fact that the fatality period did not always match the cost period.
- 2) The country for which the data is collected. These charts are for the United States.

According to the ASCE Geo-Institute guidance document “Risk informed decisions in geotechnical engineering”, acceptable and tolerable risks are defined as follows:

Acceptable risk is a state of risk which stakeholders are willing to accept. Action to further reduce such state of risk is usually not required unless reasonable measures are available at low cost in terms of money and time.

Tolerable risk is a state of risk within a range that society can live with so as to secure certain net benefits. It is a range for a state of risk regarded as ‘non-negligible’, ‘needing to be kept under review’ and which ‘must be reduced further if possible’.

Most modern codes have been written with an accepted PoF of about 1 chance in 1000 (structural engineering); it may be estimated that geotechnical engineering operates at a somewhat higher risk than that (Briaud 2013). In any case, the choice of an acceptable/tolerable risk is difficult because so many factors enter into the decision. On one hand no fatality is acceptable, on the other hand zero risk is not possible. The choice of an acceptable/tolerable risk involves other disciplines beyond geotechnical engineering, including philosophy, politics, public awareness, and social sciences. Judging from the location of the many activities on the fatalities risk chart it appears that the public tolerates a risk of 0.001 fatalities per year and 10,000 US dollars per year. The green, orange and red lines in the two charts correspond to low, medium and high risk levels (Table 3.9).

Table 3.9 Risk Levels for the United States

Risk Level	Risk (\$/yr)	Risk (fatalities/yr)
Low	10,000	0.001
Medium	100,000	0.01
High	1,000,000	0.1

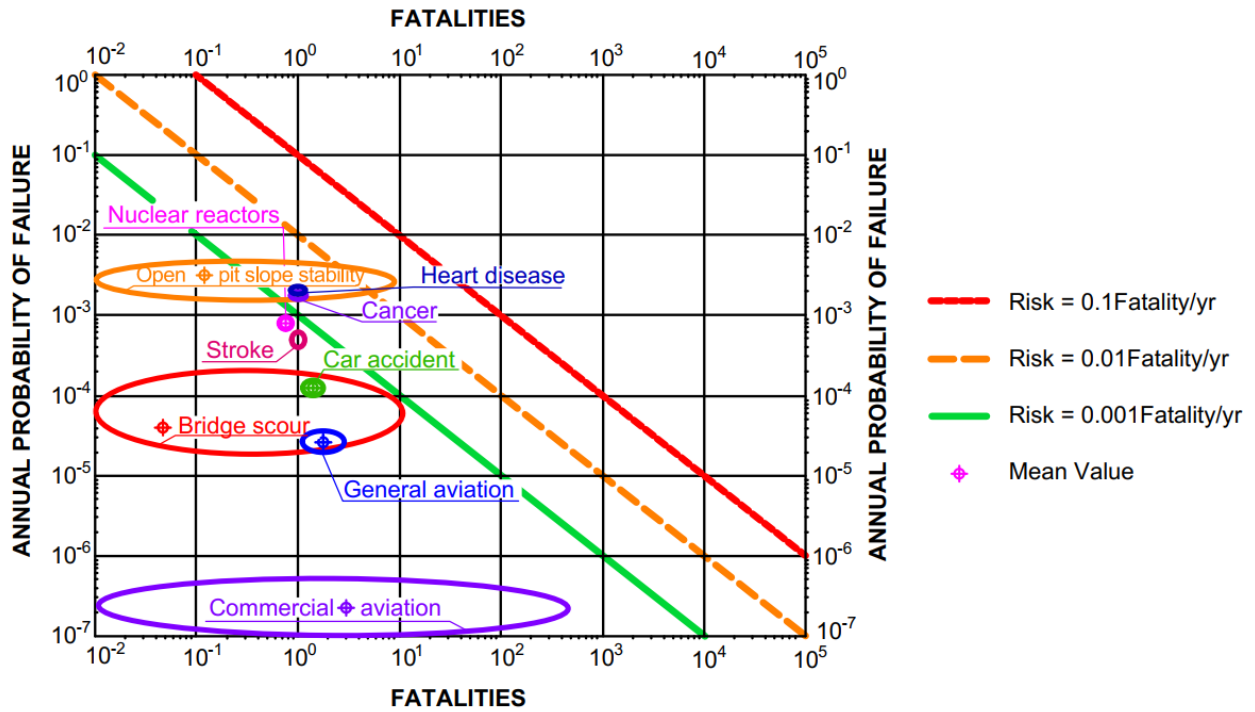


Figure 3.78 Annual PoF vs. annual number of fatalities due to the failure

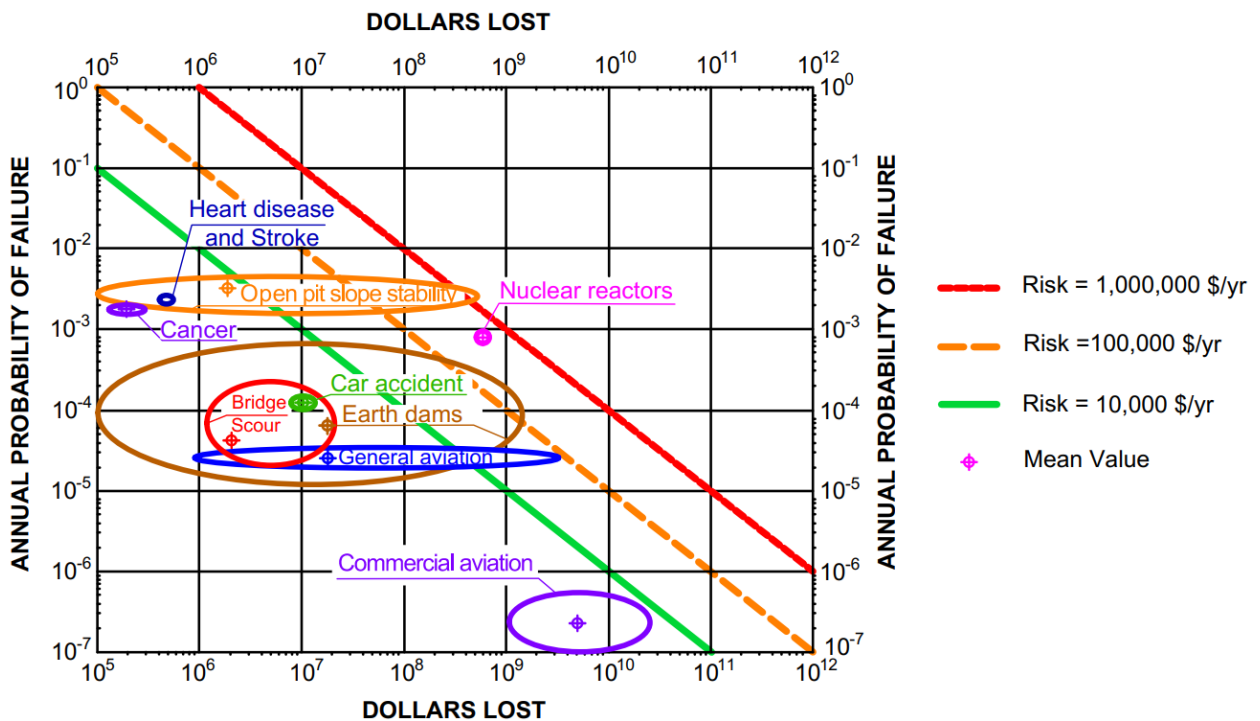


Figure 3.79 Annual PoF vs. annual economic loss corresponding to the failure

Risk is defined here as the PoF times the value of the consequences. Data associated with a set of activities is analyzed and presented in a fatality risk chart and in a cost risk chart. Risk values are \$10,000/yr and 0.001 fatalities/yr seem to correspond to low risk and possibly tolerable risk. Engineers and other decision makers can estimate the location of their project on both risk charts and plan accordingly.

The updated location of the mining slopes ellipse is presented in Figure 3.80. Whitman's chart (Whitman, 1984) is used as the reference. According to the statistics, the PoF for open pit slope stability decreased from $6 \cdot 10^{-2}$ (1982) to $3.25 \cdot 10^{-3}$ (2021), but the value of the consequences in terms of dollar lost and fatalities is increased compared to the initial data.

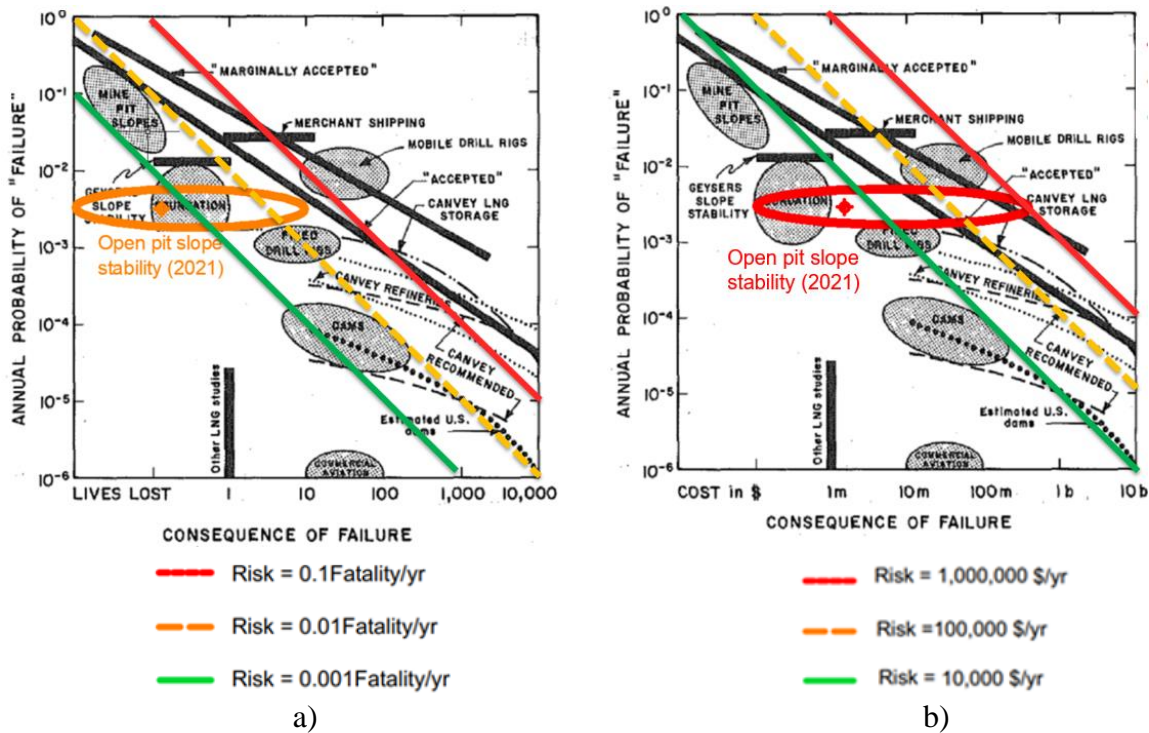


Figure 3.80 Comparison of the open pit slope risk ellipse's location (a) in term of fatalities, and (b) in terms of dollars lost (adapted from Whitman 1984)

Table 3.10 Summary of the calculations for the risks associated with the different public and civil engineering activities

Failure phenomenon	Time period	Years n	Total # of Failures F_t	Average annual # of failures F_a	Total # of structures or people, S	Average annual probability of failure, P_a with minimum and maximum	# of fatalities corresponding to one failure X with minimum and maximum values	Average cost associated with each failure C with minimum and maximum values (US\$2020)
Car accident fatality	1994-2018	25	973,698	38,948	$2.97 \cdot 10^8$	Average $1.31 \cdot 10^{-4}$ min $1.03 \cdot 10^{-4}$ max $1.57 \cdot 10^{-4}$	1	10^6
Fatal car accident	1994-2018	25	880,656	35,226	$2.43 \cdot 10^8$	Average $1.45 \cdot 10^{-4}$ min $1.09 \cdot 10^{-4}$ max $1.89 \cdot 10^{-4}$	1.67	Average $9.06 \cdot 10^6$ min $7.02 \cdot 10^6$ max $1.17 \cdot 10^7$
Cancer	1996-2019	24	13,680,806	$5.70 \cdot 10^5$	$3.02 \cdot 10^8$	Average $1.89 \cdot 10^{-3}$ min $1.84 \cdot 10^{-3}$ max $2.00 \cdot 10^{-3}$	1	Average $2.37 \cdot 10^5$ min $1.48 \cdot 10^5$ max $3.16 \cdot 10^5$
Heart Disease	2006-2018	13	8,054,019	$6.20 \cdot 10^5$	$3.13 \cdot 10^8$	Average $1.98 \cdot 10^{-3}$ min $1.91 \cdot 10^{-3}$ max $2.11 \cdot 10^{-3}$	1	-
Stroke	1999-2018	20	2,874,333	$1.44 \cdot 10^5$	$3.04 \cdot 10^8$	Average $4.73 \cdot 10^{-4}$ min $4.08 \cdot 10^{-4}$ max $6.00 \cdot 10^{-4}$	1	-

Failure phenomenon	Time period	Years n	Total # of Failures F_t	Average annual # of failures F_a	Total # of structures or people, S	Average annual probability of failure, P_a with minimum and maximum	# of fatalities corresponding to one failure X with minimum and maximum values	Average cost associated with each failure C with minimum and maximum values (US\$2020)
Heart Disease and Stroke	2006-2018	13	9,815,773	$7.55 \cdot 10^5$	$3.13 \cdot 10^8$	Average $2.41 \cdot 10^{-3}$ min $2.32 \cdot 10^{-3}$ max $2.58 \cdot 10^{-3}$	1	Average $4.95 \cdot 10^5$ min $4.33 \cdot 10^5$ max $5.20 \cdot 10^5$
General Aviation	2002-2018	17	4,642	273	$1.02 \cdot 10^7$	Average $2.68 \cdot 10^{-5}$ min $2.08 \cdot 10^{-5}$ max $3.79 \cdot 10^{-5}$	Average 1.76 min 1.21 max 2.59	Average $1.83 \cdot 10^7$ min $1.55 \cdot 10^7$ max $2.02 \cdot 10^7$
Commercial Aviation	1990-2018	29	61	2.10	$9.70 \cdot 10^6$	Average $2.17 \cdot 10^{-7}$ min 0 max $5.48 \cdot 10^{-7}$	Average 28.34 min 0 max 531	Average $3.68 \cdot 10^9$ min $1.11 \cdot 10^9$ max $2.83 \cdot 10^{10}$
Nuclear Power Plants	1960-2019	61	4	0.066	76	Average $8.68 \cdot 10^{-4}$ min 0 max $1.32 \cdot 10^{-2}$	Average 0.75 min 0 max 3	Average $6.18 \cdot 10^8$ min $2.15 \cdot 10^7$ max $3.10 \cdot 10^9$
Bridge Scour	1970-2005	36	765	21.25	$5 \cdot 10^5$	Average $4.25 \cdot 10^{-5}$ min $2 \cdot 10^{-5}$ max $1.56 \cdot 10^{-4}$	Average 0.04 min 0 max 10	Average $1.45 \cdot 10^6$ min $1.20 \cdot 10^6$ max $1.80 \cdot 10^7$
Open Pit Slope Stability	1989-2019	31	1327	43	13,234	Average $3.25 \cdot 10^{-3}$ min $1.56 \cdot 10^{-3}$ max $4.73 \cdot 10^{-3}$	Average 0.11 min 0 max 9	Average $1.91 \cdot 10^6$ min 10^5 max $5.72 \cdot 10^8$

In general, open pit slope failure consequences drive the evaluation of overall slope design, with the importance of equipment, personnel in the high-risk areas, related structures, loss of ore, and production having a direct effect on the risk evaluation. Therefore, to achieve optimum slope angles, a robust system using multidimensional risk concepts is required. By considering the governing factors, trade-off models such as cost-benefit analyses are developed to assess the shortcomings of FS and PoF analyses (Tapia et al. 2007; Read and Stacey 2009). Furthermore, risk models can assist stakeholders in making the important decisions required for optimum slope design.

Risk management is not a one-stop solution for all accidents, it does not avoid all slope failures, but it is an efficient tool that helps control and diminish them and minimize consequences if they occur. Risk management is a sufficient tool for better slope engineering and design, which helps perform wall design and understand project benefits and risks.

4. COMPARISON OF SLOPE FACTOR OF SAFETY BY VARIOUS METHODS

4.1 Definition of the FS

From the standpoint of soil mechanics, the stability of a slope is the ratio of the strength of the material to the stresses in the slope. If the strength exceeds the stress, the slope is stable, and in reverse, if the stress exceeds the strength, the slope is unstable. This ratio is termed the factor of safety (FS) and uses as the basis for stability analysis in civil and mining engineering. For example, at a safety factor of 1.00, resistive forces and disruptive forces are exactly in balance (Hoek and Bray 1981).

Because of the variability of soil and rock properties, uncertainty in obtaining the physical and geotechnical parameters, the influence of quasi-random events, such as earthquakes and rainfalls, the stresses and strengths used in stability analysis are estimates of populations with significant distributions rather than a single value. For this reason, FS greater than one has been used for slope design.

In mining slope design, the FS is greater than 1.3 is traditionally used because it takes into account the error in determining the average value of the volumetric weight, the error of calculation methods, a decrease in the calculated physical and mechanical characteristics over time under the influence of weathering processes, dynamic loads of different genesis (including from massive explosions and earthquakes), a method of taking into account hydrogeological factors, an error in determining the position of the most stressed sliding surface, and other factors (VNIMI 1972, Tapia et al. 2007, Steffen et al. 2008).

The FS is the factor by which the shear strength of the material would have to be divided to carry the slope into a state of barely stable equilibrium (Figure 4.1):

$$FS = \frac{\text{Shear stress required for equilibrium}}{\text{Shear strength of material}} = \frac{\tau_{af}}{\tau_{am}} \quad \text{Eq. 4.1}$$

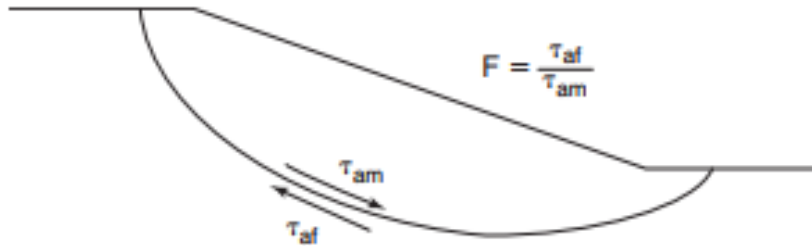


Figure 4.1 FS for the circular failure surface (reprinted from Briaud, 2013)

Hoek and Bray (1981) define the FS as the ratio of the total force available to resist failure to the total force tending to induce failure. The FS can also be defined as the ratio of the maximum resisting moment over the driving moment around the center of the circle with radius R (Figure 4.2).

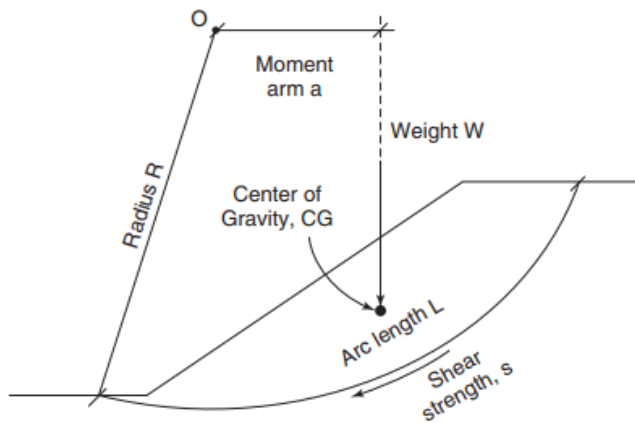


Figure 4.2 Example of the simple slope stability problem (reprinted from Briaud 2013)

$$FS = \frac{sRL}{Wa} \quad \text{Eq. 4.2}$$

where s is the constant shear strength along the length L of the failure plane, which is assumed to be an arc of a circle with a radius R and a center O ; the weight of the failing soil mass is W , with a center of gravity generating a moment arm a around the center O .

The FS is defined as a deterministic safety factor when mean value material properties are used in the design. When the material properties are entered into analyses as statistical populations with mean value and standard deviation, a probabilistic safety factor may be computed, and an estimate of the probability of slope failure may be done (Read and Stacey 2009).

4.2 2-D slope stability by the limit equilibrium method

Limit equilibrium methods (LEM) are the most commonly used approaches in slope stability analysis (Hoek and Bray 1981; Duncan and Wright 1980; Duncan et al. 2014; Briaud 2013). The fundamental assumption in these methods is that failure occurs through sliding of a mass along a slip surface. All limit equilibrium methods are based on the approach where the failing soil mass divides into slices and the forces act between the slices whereas different assumptions are made with respect to these forces in different LEM methods.

Two-dimensional slope stability methods using the limit equilibrium technique can be divided into the method of slices, circular methods, and noncircular methods. To effectively use limit equilibrium types of analyses, it is important to understand these methods, their capabilities, and limitations. Some common features and limits for equilibrium methods in slope stability analysis are summarized in Table 4.1. All methods shown in Table 4.1 use the same definition of the FS, which is the factor by which the shear strength of the soil would have to be divided to carry the slope into a state of equilibrium.

Table 4.1 Methods and Limitations for Limit Equilibrium Method (adapted from Duncan and Wright 1980, Briaud 2013)

Method	Reference	Features and Limitation
Slope Stability Charts	Taylor, 1948 Morgenstern, 1963 Spencer, 1967 Janbu, 1968 Duncan et al. 1987	<ul style="list-style-type: none"> - Accurate enough for many purposes. - Faster than detailed computer analysis. - Uniform soil. - Only for circular slip surfaces. - Simple problem
Ordinary Method of Slices	Fellenius, 1927	<ul style="list-style-type: none"> - Resultant of Z force on each slice is equal to zero. - Only for circular slip surfaces. - Satisfies moment equilibrium. - Does not satisfy horizontal or vertical force equilibrium.
Bishop's Modified Method	Bishop, 1955	<ul style="list-style-type: none"> - Shear forces on the slide of all slices are zero (i.e., Z forces are horizontal). - Only for circular slip surfaces. - Satisfies moment equilibrium. - Satisfies vertical force equilibrium. - Does not satisfy horizontal force equilibrium.
Janbu Simplified Method	Janbu, 1954	<ul style="list-style-type: none"> - Z forces are horizontal - Does not satisfy all equilibrium equations
Corps of Engineers Method	U.S. Army Corps of Engineers, 1970	<ul style="list-style-type: none"> - Z forces inclined parallel to the ground surface or parallel to the line joining the beginning and the end of the failure circle. - Any shape of slip surfaces. - Does not satisfy moment equilibrium. - Satisfies both vertical and horizontal force equilibrium.
Janbu Generalized Method	Janbu, 1968	<ul style="list-style-type: none"> - Location of point of application of the Z force on an assumed thrust line - Any shape of slip surfaces. - Satisfies all conditions of equilibrium. - Permit side force locations to be varied. - More frequent numerical problems than some other methods.
Morgenstern and Price's Method	Morgenstern and Price, 1965	<ul style="list-style-type: none"> - Inclination of Z forces given by a function of the horizontal distance multiplied by a scalar. - Any shape of slip surfaces. - Satisfies all conditions of equilibrium. - Permit side force orientations to be varied.

Method	Reference	Features and Limitation
Spencer's Method	Spencer, 1967	<ul style="list-style-type: none"> - Z forces have a constant but unknown inclination. - Any shape of slip surfaces. - Satisfies all conditions of equilibrium. - Side forces are assumed to be parallel.
Sarma method	Sarma, 1973	<ul style="list-style-type: none"> - Any shape of slip surfaces. - Inclination of Z forces given by a function of the horizontal distance multiplied by a scalar. - Makes use of horizontal seismic coefficient. - Satisfies all equilibrium equations

Many researchers compared the different 2-D LE methods. For example, Fredlund and Krahn (1976) compared six LE models commonly used for slope stability in terms of consistent procedures for deriving the FS equations. All equations were extended to the case of a composite failure surface and also consider partial submergence, line loadings, and earthquake loadings. The authors compared the factors of safety obtained by each of the methods. The FS with respect to moment equilibrium is relatively insensitive to the interslice force assumption. Therefore, the factors of safety obtained by the Spencer and Morgenstern-Price methods are in good agreement with the simplified Bishop results, whereas the simplified and rigorous Janbu factors of safety values appeared to be slightly lower. In contrast, the FS determined by the satisfying force equilibrium was very sensitive to the side force assumption. Aryal (2006) came to similar conclusion during the comparative study of the application of LE methods presented in the doctoral dissertation.

Jiang and Magnan (1997) state that although the 2-D LE methods have been known as a robust technique in slope stability, the following should be worth noting when they are used.

- a. As pointed out by different researchers (Nash 1987, Stark and Eid 1998), none of the 2-D LE methods yield the correct value of the FS because of the assumptions involved about the forces.

- b. 2-D LEM techniques do not provide the failure mechanism and do not account the slope material behavior.
- c. The assumption of circular slip interfaces in the Fellenius and the Bishop methods is not suitable for structures constituted of materials of strong heterogeneity. The Morgenstern and Price method can be more useful for such problems.
- d. It is assumed in methods of slices that soil masses in the ultimate limit state fail in shear and the linear Mohr-Coulomb criterion can be used. However, for soils modeled by more complex criterion functions of non-linear form or curved yield surfaces such as the one described by Lade (1977) for cohesionless soil, methods of slices would not be efficient for the stability analysis of soil structures.
- e. The complex cases cannot be studied with precision using 2-D LEM slope stability calculations (Cala et al. 2004).

4.3 3-D slope stability by the limit equilibrium method

Over the last two decades, the limit equilibrium approaches were extended and developed significantly. Stead et.al. (2005) summarized the development in conventional limit equilibrium techniques:

- increased availability of probabilistic techniques, including the use of geostatistics;
- introduction of 3-D methods, some with capabilities for including support;
- improved searching routines for critical failure surfaces;
- integrated groundwater–stress-limit equilibrium analysis;
- incorporation of unsaturated soil mechanics;
- incorporation of surface hydrology influences;
- integration with GIS and risk assessment

Limit equilibrium slope stability analyses can now be undertaken using 3-D commercial software for both wedge (e.g., SWEDGE - Rocscience 2021e) and circular/multiplanar failure mechanisms (Slide3 – Rocscience 2021d; Plaxis2D – Brinkgreve et al 2016; CLARA-W – Hungr, 2001).

3-D LE slope stability analysis is simple in concept, and directly analogous to 2-D methods (Kalatehjari et al. 2014, Rocscience 2021d). In 3-D analysis a sliding mass is discretized into vertical columns with a square cross-section. The 2-D methods of slices (Bishop, Janbu, Spencer and Morgenstern-Price (GLE)) which are based on satisfying force and/or moment equilibrium, can be extended to a 3-D method of columns, where forces and moments are solved in two orthogonal directions. Vertical forces determine the normal and shear force on the base of each column (Rocscience 2021d). According to Huang et al. (2002); Cheng and Yip (2007), and Rocscience (2021d) the assumptions required in the present 3-D formulation are:

1. Mohr-Coulomb failure criterion is valid;
2. For Morgenstern-Price's method, the FS is determined based on the sliding direction α' where factors of safety with respect to force and moment are equal;
3. Sliding direction is the same for all soil columns; and
4. Weight of soil and vertical load are assumed to act at the center of each column for simplicity. This assumption is not exactly true but is good enough if the width of each column is small enough, and the resulting equations will be highly simplified and should be sufficient for practical purposes.

4.4 2-D and 3-D slope stability by the finite element method

The majority of slope stability analyses performed in practice still use traditional limit equilibrium approaches involving methods of slices that have remained essentially unchanged for

decades (Fredlund et al. 1981; Duncan 1996, Duncan et al. 2014). The finite element method represents a powerful alternative approach for slope stability analysis used to be accurate, versatile, and requires fewer a priori assumptions, especially regarding the failure mechanism. Slope failure in the finite element model occurs ‘naturally’ through the zones in which the shear strength of the slope material is insufficient to resist the shear stresses. Elasto-plastic analysis of geotechnical problems using the finite element method (FEM) has been widely accepted in research for many years; however, its routine use in geotechnical practice for slope stability analysis still remains limited (Kainthola et al. 2011). At the same time, it is argued that the FEM of slope stability analysis is a more powerful alternative to traditional limit equilibrium methods, and its widespread use should be standard in geotechnical practice (Griffiths and Lane 1999, Kainthola et al. 2011).

Numerical models are used for slope stability studies for a variety reasons, including the following:

- Empirical methods cannot confidently be extrapolated outside their databases.
- Other methods (e.g., analytical, limit equilibrium) are not available or tend to oversimplify the problem, possibly leading to overly conservative solutions.
- Key geologic features, groundwater, etc. can be incorporated into numerical models, providing more realistic approximations of real slope behavior.
- Observed physical behavior can be explained
- Multiple possibilities (e.g., hypotheses, design options) can be evaluated.

The software utilizing the FEM technique quantifies the stability of a slope using the shear strength reduction method. The shear strength reduction method is discussed by several authors and is widely used in slope stability analysis (Dawson et al. 1999, Hammah et al. 2005, Read and Stacey 2009, Wei et al. 2009). With this approach, the shear strength of the simulated material

mass is incrementally reduced until instability occurs. The factor by which the strengths must be reduced to cause the instability, called the critical strength reduction factor (critical SRF), is analogous to a FS calculated by LEM methods (Kabuya et al. 2020).

The “strength reduction technique” is typically applied in factor-of-safety calculations by progressively reducing the shear strength of the material to bring the slope to a state of limiting equilibrium. The method is commonly applied with the Mohr-Coulomb failure criterion (e.g., see applications by Zienkiewicz et al. 1975; Naylor 1981; Giam and Donald 1988; Matsui and San 1992; Ugai and Leshchinsky 1995). In this case, the safety factor FS is defined according to the equations:

$$c'_f = \frac{c'}{FS} \quad \text{Eq. 4.3}$$

$$\varphi'_f = \arctan\left(\frac{\tan\varphi'}{FS}\right) \quad \text{Eq. 4.4}$$

where c' and ϕ' are the effective stress cohesion and friction angle of the slope material respectively, and c'_f and φ'_f are the factored shear strength parameters of the slope material respectively (Griffiths and Lane 1999, Briaud 2013).

The model to be studied using FEM technique should be large enough that the boundaries have only a small and tolerable influence on the stability calculations. If the height of the slope is H, the mesh should be at least (3·H) high. If the horizontal distance between the toe and the crest of the slope is L, the mesh should be at least (5·L) long (Griffiths and Lane 1999; Briaud 2013).

FEM includes the use of mesh generation techniques for dividing a slope into small elements (Figure 4.3). The results from FEM with strength reduction technique are sensitive to the design of the mesh (Zettler al 1999, Shukha and Baker 2003, Nian et al. 2012). The fine mesh gives more accurate results than the coarse mesh, therefore the optimal grid size determination is

always necessary if numerical models based on a grid-like finite element code are used (Dawson et al. 1996, Zettler et al. 1999, Hammah et al. 2005).

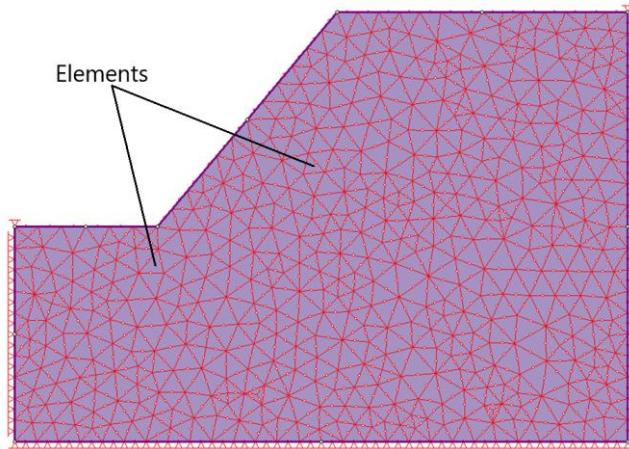


Figure 4.3 2-D finite element model of a slope

4.4.1 Advantages of Finite Element Method

Many researches pointed out the advantages of a FE approach to slope stability analysis over the LE methods (Jiang and Magnan 1997, Griffiths and Lane 1999, Zettler and Poisel 1999, Griffiths and Marquez 2007, Steffen et al. 2009, Soren et al. 2014, Vinod et al. 2017, Memon 2018). They are the following:

- a. No assumption needs to be made in advance about the shape or location of the failure surface. Failure occurs ‘naturally’ through the zones within the soil mass in which the soil shear strength is unable to sustain the applied shear stresses.
- b. Since there is no concept of slices in the FE approach, there is no need for assumptions about slice side forces. The FE method preserves global equilibrium until ‘failure’ is reached.
- c. If realistic soil compressibility data are available, the FE solutions will give information about deformations at working stress levels.

- d. The FE method is able to monitor progressive failure up to and including overall shear failure.
- e. The FE techniques are suitable for indication of the stress and strain distribution within critically instable failure zones, element displacement vectors and the plastic state of slopes.

4.4.2 Limitations of Finite Element Method

The limitations of the FEM slope stability technique was summarized by different researchers (Duncan 1996, Griffiths and Marquez 2007, Kainthola et al. 2011) and can be presented by the following statements:

- a. Require large amounts of effort and involve expensive geotechnical methods to obtain input parameters for the modelling.
- b. The software utilizing FEM technique is more expensive compare to the software based on the traditional limit equilibrium approach.
- c. Finite element analysis does not give a direct indication of the margin of safety; that is, a quantitative measure of how close the system may be to collapse.
- d. Comparisons of the results of finite element analysis with field measurements have shown a tendency for calculated deformations to be greater than measured deformations (Duncan 1996). The reasons for this difference include all the drawbacks of laboratory testing which parameters are usually used as input data for modelling.
- e. The finite element equations are in essence equations of equilibrium, and when loads are applied that push the system past the point of limiting equilibrium, it is not possible to obtain a solution to the finite element equations (Kainthola et al. 2011).

- f. The results from FEM with strength reduction technique are sensitive to the design of the mesh. The finer mesh gives more accurate result and therefore requires longer calculation time (Griffiths and Marquez 2007).

4.5 Comparison between analysis methods

Several studies have previously compared the results of slope stability analyses using the LEM and FEM techniques (Griffith and Lane 1999, Dawson 1999, Cala and Flisiak 2001, Hammah et al 2004, Cheng et al. 2006, Khabbaz et al. 2012). Many researchers have concluded that the FEM was a powerful alternative to traditional LEM technique because it can model the stress-strain behavior of slope material (Krahn 2003). Despite of these limitations, the LE methods are still common because of their simplicity and the reasonably accurate FS obtained.

Homogenous and nonhomogeneous 2-D simplified slopes were studied in order to compare LE and FE methods results. The studies concluded that the results are generally in good agreement for 2-D homogenous slopes, and the difference between LEM and FEM calculations is evident when a 2-D heterogeneous slope is analyzed (Dawson 1999, Cheng et al. 2006, Khabbaz et al. 2012, Memon 2018).

In slope stability analysis, two-dimensional (2-D) plane strain analysis techniques are commonly used for simplicity and wide applicability. However, all slope failures are, 3-D in nature, especially in the cases of complex geometric slopes or overloaded slopes (Nian et al. 2012). A number of studies were performed on the comparison between 2-D and 3-D approaches. Nian et al. (2012) prove that according to previous studies (Chen and Chameau 1985, Leshchinsky and Baker 1986, Cavounidis 1987, Hungr 1987, Duncan 1996, Chugh 2003, Griffiths and Marquez 2007), the FS for a 2-D slope is generally less than that for a 3-D slope. Usually geological features such as faults are not perfectly parallel to pit slope designs or perfectly perpendicular to selected

cross-sections, where a true orientation or dip of the structure can be modelled in two-dimensions. As such, 2-D LE analysis methods cannot adequately model, or predict, the likelihood and consequence of such failure mechanisms in most cases. In addition, the traditional 2-D approach requires an experienced geotechnical engineer to select representative (or most critical) cross-sections for anisotropic limit equilibrium analysis (Bar and McQuillan 2018). In particular, when the most pessimistic section in the 3-D problem is selected for 2-D analysis, the result obtained is very conservative (Duncan 1996a, Griffiths and Marquez 2007). On the whole, the results for 2-D analysis are more conservative from the viewpoint of engineering safety. Moreover, the actual stability and geometry cannot be appropriately considered without the third dimension.

Currently, the 3-D limit equilibrium method (LEM) and the finite-element method (FEM) or finite-difference method (FDM) with a strength-reduction technique are quite popular for analyzing the stability of a 3-D slope, even though these approaches are more time-consuming than others. The major limitation in 3-D LEM is the lack of a suitable method for locating the critical general 3-D slip surface (Cheng et al. 2005, Wei et al. 2009). However, 3-D FEM with a strength-reduction technique can simultaneously provide the safety factor and the critical slip surface (shape and location), together with the stress, deformation, and progressive shear failure of the slope. 3-D analysis can also accurately reflect the slope dimensions, boundary conditions, and a realistically complex geometric configuration in three x - y - z directions. (Nian et al. 2012).

The main inputs, advantages and limitations of the conventional and numerical methods are summarized in Table 4.2.

Table 4.2 Comparison of slope stability analysis methods (adapted Coggan et al. 1998; Stead et al. 2005)

Method	Input parameters	Advantages	Limitations
Kinematic analysis	Critical orientation of slope discontinuity, friction angle	Simple to use and shows structurally-controlled failure potential	<ul style="list-style-type: none"> – Suitable only for preliminary assessments. – Identification of critical discontinuities requires engineering judgment. – Ignore slope geometry, cohesion, groundwater and external loading conditions. No FS is calculated.
LEM	Slope geometry, shear strength of material/ discontinuity/ rock mass, groundwater and external loading conditions.	Easy to use. Software available for different failure modes with multiple materials. Mostly deterministic, but be used for probabilistic analysis. Calculates FS is short time and suitable for sensitivity analysis.	<ul style="list-style-type: none"> – In-situ stress, strains and intact material failure not considered. – Predefined slip surface needed. – Probabilistic analysis requires well defined input data.
Continuum modelling (e.g. FEM, FDM)	Slope geometry, constitutive criteria, groundwater conditions, shear strength, in-situ stress state.	Without statical assumptions, can model complex behavior and mechanism and slip surfaces of any shape in 2-D and 3-D with coupled modeling of groundwater. Incorporate creep deformation and dynamic analysis.	<ul style="list-style-type: none"> – Not easy to use and require well-trained and experienced users. – Some inputs are not routinely measured. – Software requires long run times when compared to LEM.
Discontinuum modelling (e.g. DEM, DDA)	Geometry of slope and discontinuity, intact constitutive criteria, discontinuity stiffness and strength, groundwater and stress	Allow for block deformation and movement of blocks relative to each other and model complex behavior and mechanisms. Assess effects of parameter variation on instability	<ul style="list-style-type: none"> – Not easy to use and require well-trained and experienced users. – Limited data on discontinuity properties available and need to simulate representative discontinuity geometry

A parametric study was performed to investigate the influence of the width of the 3-D model on slope stability. Consider a slope with different slope angles ($\beta = 15^\circ, 25^\circ, 35^\circ$ and 45°).

The height of the slope is 15 m and the width of the slope varies from 7.5 m to 150 m (Figure 4.4 and 4.5), while the cohesive strength, friction angle, dilation angle and unit weight of the soil are 10 kPa, 30°, 0°, and 20 kN/m² respectively. For finite element method calculations, the Young's modulus and Poisson's ratio are 30 MPa and 0.28 respectively. Each model had the same boundary conditions: bottom surface is restrained in all x-, y-, and z-directions, the left and right side surfaces are allowed to move freely in the x- and z-directions, but not in the y-direction; both front and back sides are restrained in all directions. The FS for slopes was calculated based on Mohr-Coulomb model.

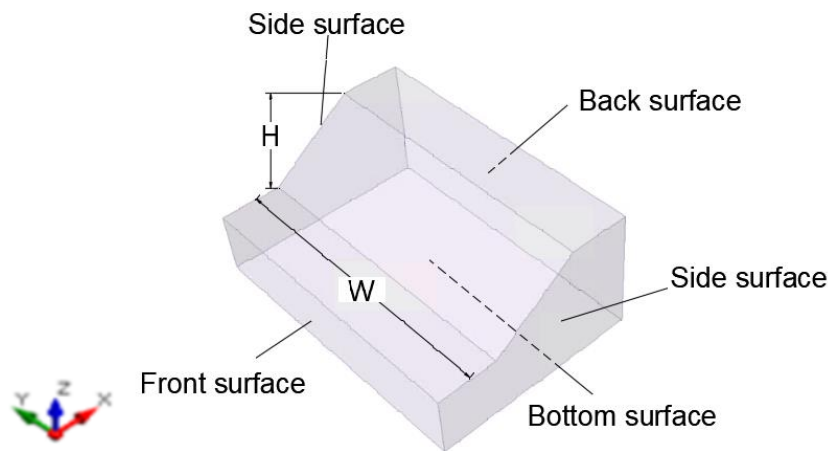


Figure 4.4 The geometry and boundary conditions of the three-dimensional slope

The calculations were done using the 3-D LE approach and the 3-D FE approach. The obtained FS was normalized by the corresponded $FS_{2D\ LEM}$. The LE and for FE final models are presented in Figure 4.6 and Figure 4.7 respectively. On the horizontal axis is the ratio of the model's width over the height of the slope (W/H), and on the vertical axis is the 3-D FS normalized by the $FS_{2D\ LEM}$.

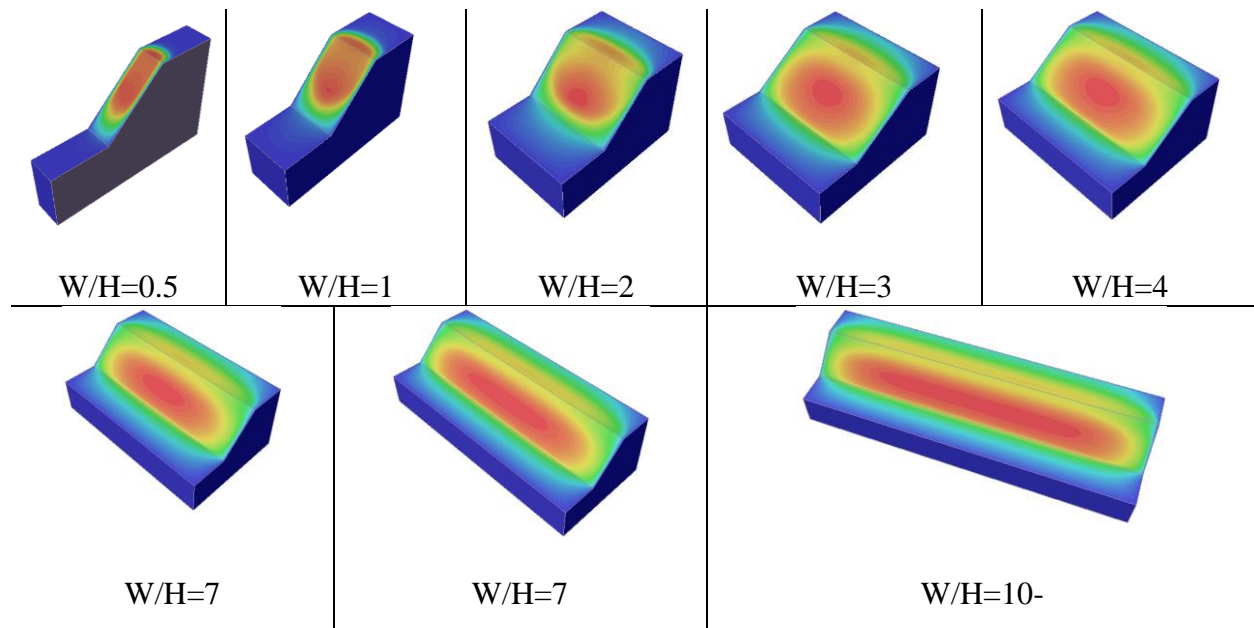


Figure 4.5 Geometry of the three-dimensional slope with $W/H=0.5, 1, 2, 3, 4, 5, 7$ and 10

The FS_{3D} was greater than the FS_{2D} for all of the W/H combinations used in the parametric study. It can be seen from Figure 4.6 and 4.7 that the FS_{3D}/FS_{2D} ratio increases with decreasing W/H ratios for a given slope inclination. The present result is consistent with the results obtained in previous studies (Chen and Chameau 1983, Leshchinsky et al. 1985, Stark 2003, Griffiths and Marquez 2007). Figure 4.6 and 4.7 show that the slope angle does not affect the value of the FS ratio when W/H is more than 4. The FS for the slopes with $W/H > 4$ is close to the FS for the plane strain slope. If $W/H < 4$, there is a need for three-dimensional analysis of the slope since the difference between the 2-D and 3-D can reach 50%.

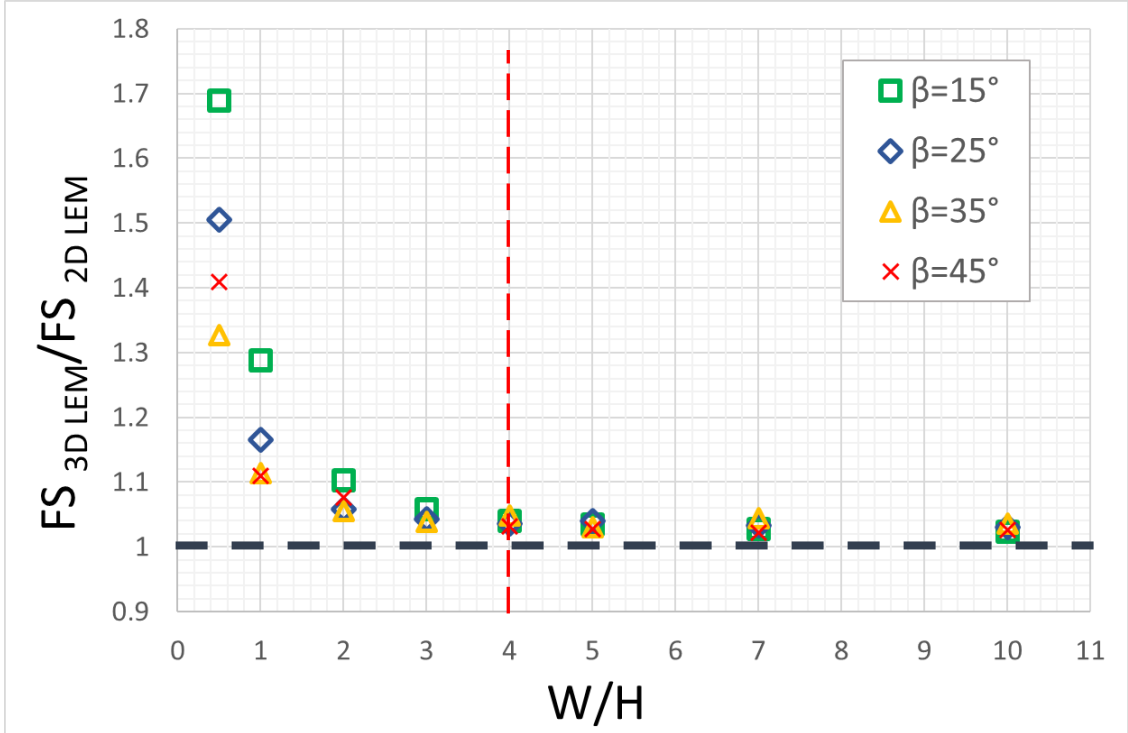


Figure 4.6 $FS_{3D LEM} / FS_{2D LEM}$ versus W/H

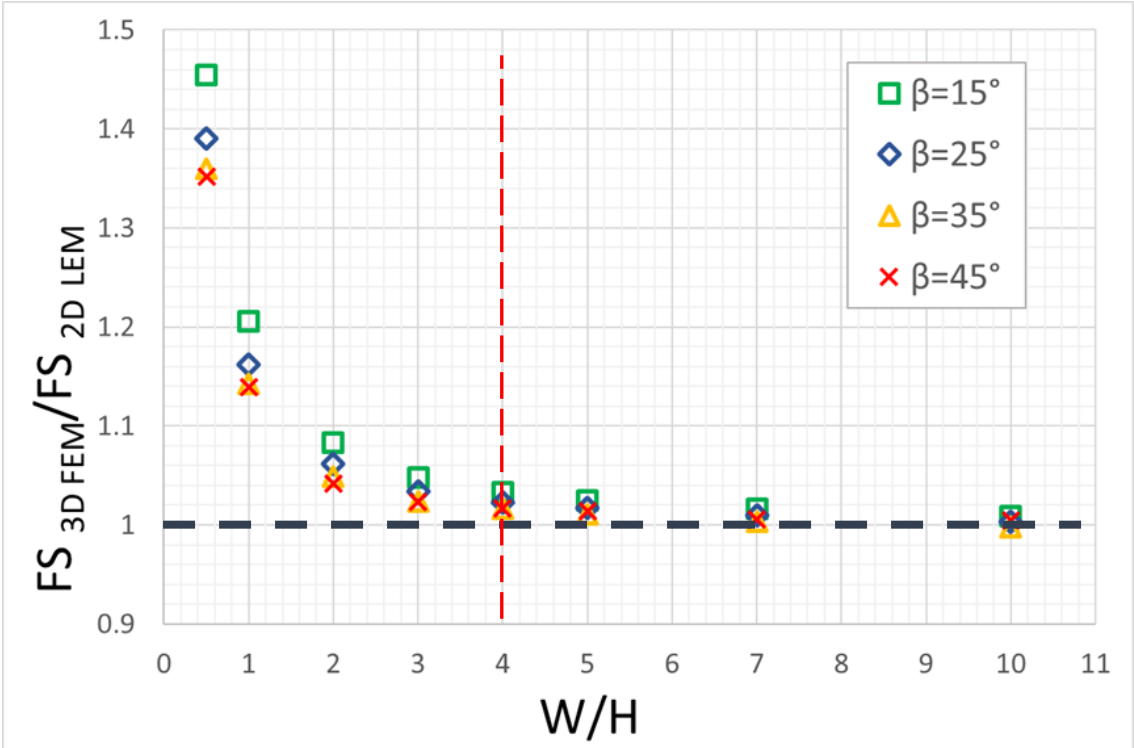


Figure 4.7 $FS_{3D FEM} / FS_{2D LEM}$ versus W/H

The W/H ratio was obtained for all cases collected in TAMU-MineSlope (see Chapter 3). Figure 4.8 presents the bar chart with the frequency of occurrence on the vertical axis and W/H on the horizontal axis. Most of the cases from the TAMU-MineSlope Spreadsheet have W/H less than 4. Based on the analysis of the open pit case histories from the database, most of the slope failures in open-pit mining have to be studied using 3-D methods because 87% of slope failures have $W/H < 4$. The mean value is around 1.5. Therefore, for $W/H = 1.5$, the FS error is of the order of 15% (Figure 4.7). So doing a two-dimensional slope stability analysis for the slopes with $W/H < 4$, the FS for those slopes is underestimated.

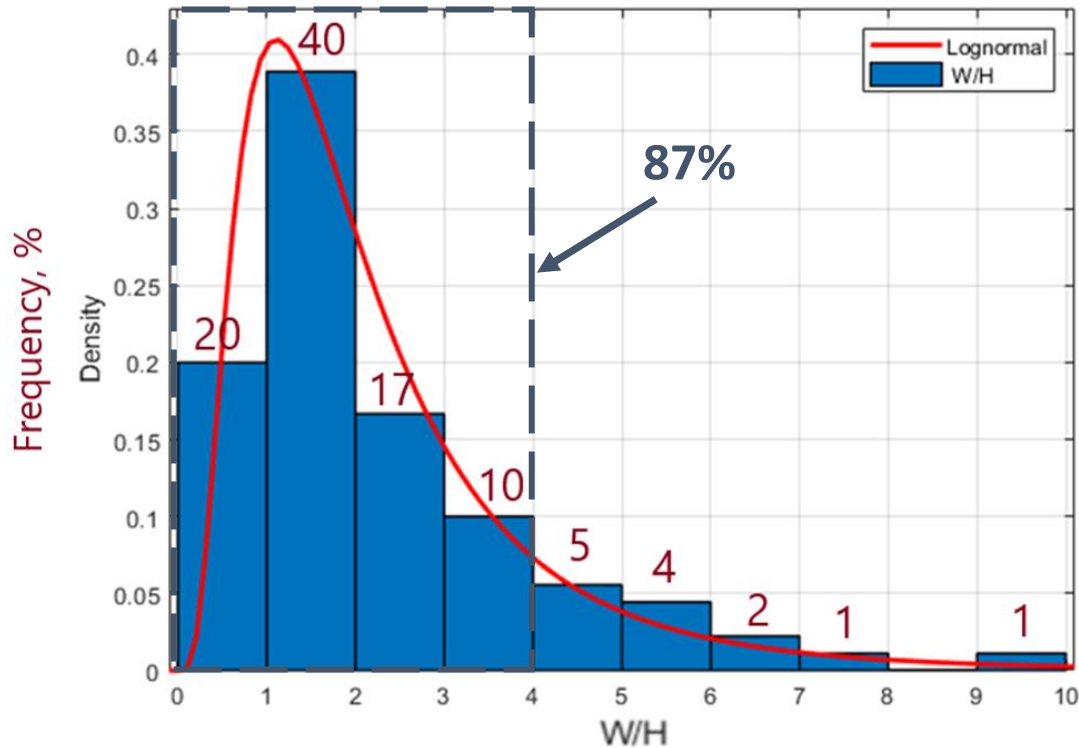


Figure 4.8 The bar chart for W/H ratio based on the open pit slope failure case history collection

The correlation between the 3-D FEM total displacement normalized by the 2-D FEM value and the corresponding FS normalized by the $FS_{2D\ FEM}$ is presented in Figure 4.9. The figure

shows that the limit of $W/H \approx 4$ also applies to the correspondence between the total displacement and the FS. For $W/H > 4$, there is a direct correlation, while for $W/H < 4$, the correlation breaks down and shows the need for three-dimensional analysis.

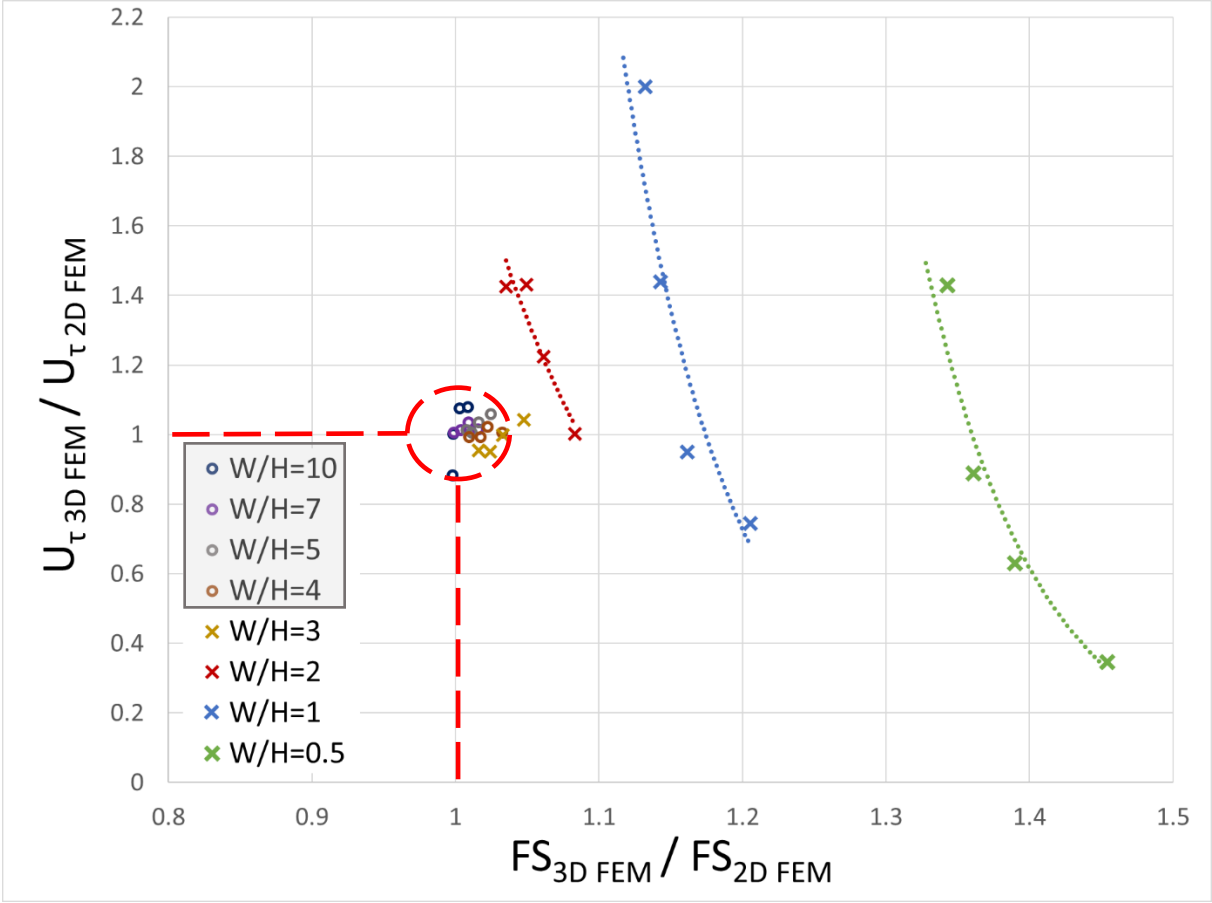


Figure 4.9 Variation of normalized total displacement with respect to the normalized FS_{3D FEM} (W/H=0.5, 1, 2, 3, 4, 5, 7 and 10)

To compare 2D and 3D slope stability methods, it was decided to analyze fictitious but realistic cases. Table 4.3 presents a reference set of average soil and model parameters selected. The FS for slopes was calculated based on Mohr-Coulomb model. Spencer method was used to obtain limit equilibrium results. In case of the finite element simulations the identical boundary conditions were used for all models: bottom side is restrained in all x-, y-, and z-directions, both

front and back sides are restrained in all directions, the left and right are allowed to move freely in the x- and z-directions, but not in the perpendicular direction to the plane, the top surface is free (Figure 4.4).

One parameter in the set was fluctuated from the average value. This led to a total of 74 FS predictions by 4 different methods (2-D LEM, 3-D LEM, 2-D FEM and 3-D FEM). The prediction by each method in each case was compared to the 2-D LEM case.

A series of graphs was developed based on the obtained results (Figure 4.10- 4.13), with A-value on the vertical axis, and the fluctuating parameter on the horizontal axis. Parameter A is the FS's value obtained by performing 2-D FEM, 3-D FEM, and 3-D LEM calculations normalized by the 2-D LEM case.

Both, 2-D LEM and 2-D FEM results in pretty much the same FS. However, the presented results showed that the 3-D FEM gives 12 to 30% higher values than the 2-D LEM. Thus, the present study results are consistent with the previous research. For example, Duncan (1992) found that the FS calculated by using 3-D analyzes will always be higher than or equal to the FS calculated by using 2-D analyzes.

According to the obtained research results, the most significant influence on the FS gives slope geometry and cohesion rather than the friction angle. To summarize, the calculations prove that the critical W/H ratio value is 4, which means that there is a need for 3-D simulations if the W/H ratio is less than 4. If the width of the model is much higher than the slope height, the 3-D model can be represented by the 2-D model.

Table 4.3 A reference set of average soil and model parameters

γ , (kN/m ³)	C, (kN/m ²)	ϕ , (°)	tan ϕ	E (kPa)	ν	Slope height, H, (m)	Slope width, W, (m)	W/H	Slope angle β , (°)	tan β	FS				Parameter A			
											2D LEM	3D LEM	2D FEM	3D FEM	<u>3D LEM</u> <u>2D LEM</u>	<u>2D FEM</u> <u>2D LEM</u>	<u>3D FEM</u> <u>2D LEM</u>	<u>3D FEM</u> <u>2D FEM</u>
20	10	30	0.577	10,000	0.35	15	7.5	0.5	40	0.839	1.174	1.740	1.193	1,661	1.415	1.016	1.482	1.392
20	10	30	0.577	10,000	0.35	15	15	1	40	0.839	1.174	1.270	1.193	1.372	1.169	1.016	1.082	1.150
20	10	30	0.577	10,000	0.35	15	30	2	40	0.839	1.174	1.242	1.193	1.253	1.067	1.016	1.058	1.050
20	10	30	0.577	10,000	0.35	15	60	4	40	0.839	1.174	1.228	1.193	1.203	1.025	1.016	1.046	1.008
20	10	30	0.577	10,000	0.35	15	120	8	40	0.839	1.174	1.206	1.193	1.185	1.009	1.016	1.027	0.993
20	10	30	0.577	10,000	0.35	15	240	16	40	0.839	1.174	1.188	1.193	1.181	1.006	1.016	1.012	0.990
20	10	30	0.577	10,000	0.35	15	100	7	30	0.577	0.992	1.057	1.000	1.069	1.078	1.008	1.066	1.069
20	10	30	0.577	10,000	0.35	15	100	7	35	0.700	1.175	1.266	1.190	1.300	1.106	1.013	1.077	1.092
20	10	30	0.577	10,000	0.35	15	100	7	40	0.839	1.331	1.454	1.360	1.472	1.106	1.022	1.092	1.082
20	10	30	0.577	10,000	0.35	15	100	7	45	1.000	1.477	1.625	1.510	1.621	1.097	1.022	1.100	1.074
20	10	30	0.577	10,000	0.35	15	100	7	50	1.192	1.037	1.109	1.030	1.077	1.039	0.993	1.069	1.046
20	10	20	0.364	10,000	0.35	15	100	7	40	0.839	1.532	1.634	1.550	1.645	1.074	1.012	1.067	1.061
20	10	25	0.466	10,000	0.35	15	100	7	40	0.839	1.336	1.429	1.360	1.452	1.087	1.018	1.070	1.068
20	10	30	0.577	10,000	0.35	15	100	7	40	0.839	1.175	1.266	1.190	1.300	1.106	1.013	1.077	1.092
20	10	35	0.700	10,000	0.35	15	100	7	40	0.839	1.040	1.127	1.070	1.166	1.121	1.029	1.084	1.090
20	10	40	0.839	10,000	0.35	15	100	7	40	0.839	0.941	1.026	0.960	1.103	1.172	1.020	1.090	1.149

γ , (kN/m ³)	C, (kN/m ²)	ϕ , (°)	tan ϕ	E (kPa)	ν	Slope height, H, (m)	Slope width, W, (m)	W/H	Slope angle β , (°)	tan β	FS				Parameter A			
											2D LEM	3D LEM	2D FEM	3D FEM	<u>3D LEM</u> 2D LEM	<u>2D FEM</u> 2D LEM	<u>3D FEM</u> 2D LEM	<u>3D FEM</u> 2D FEM
20	2	30	0.577	10,000	0.35	15	100	7	40	0.839	0.856	0.937	0.870	0.946	1.105	1.016	1.095	1.087
20	5	30	0.577	10,000	0.35	15	100	7	40	0.839	1.009	1.097	1.030	1.125	1.115	1.021	1.087	1.092
20	10	30	0.577	10,000	0.35	15	100	7	40	0.839	1.175	1.266	1.190	1.300	1.106	1.013	1.077	1.092
20	15	30	0.577	10,000	0.35	15	100	7	40	0.839	1.354	1.452	1.368	1.500	1.108	1.010	1.072	1.096
20	20	30	0.577	10,000	0.35	15	100	7	40	0.839	1.552	1.656	1.560	1.710	1.102	1.005	1.067	1.096

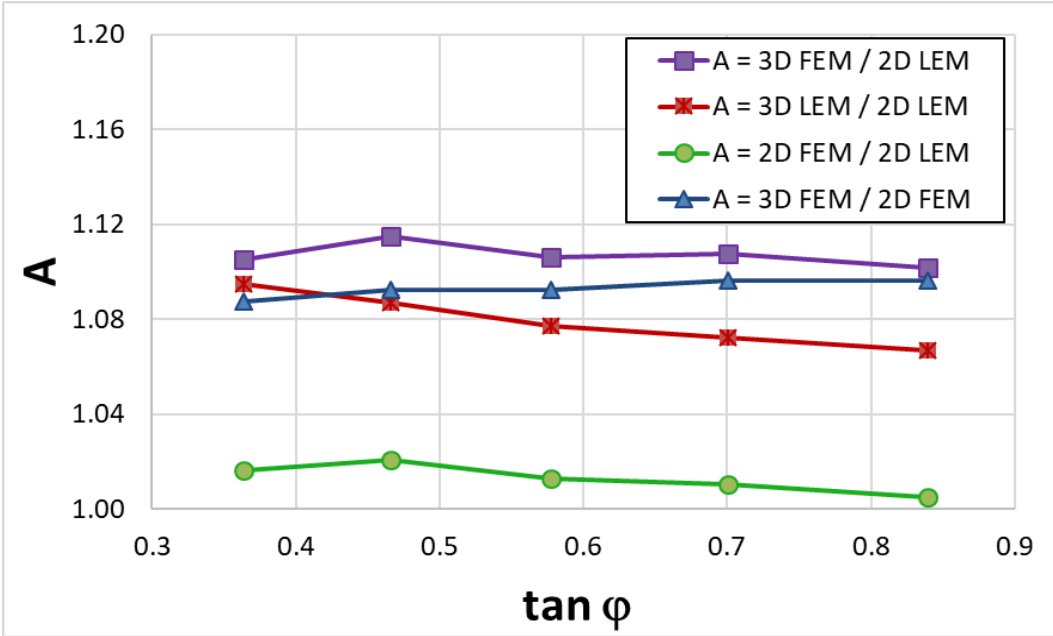


Figure 4.10 Variation of the normalized FS with respect to $\tan \phi$

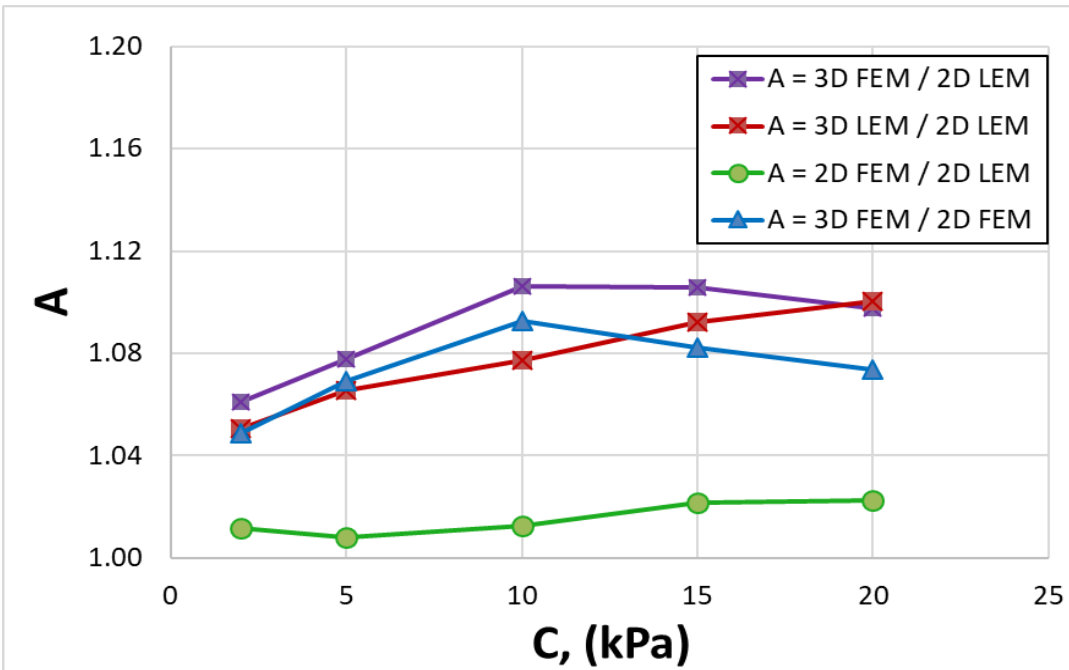


Figure 4.11 Variation of the normalized FS with respect to C, (kPa)

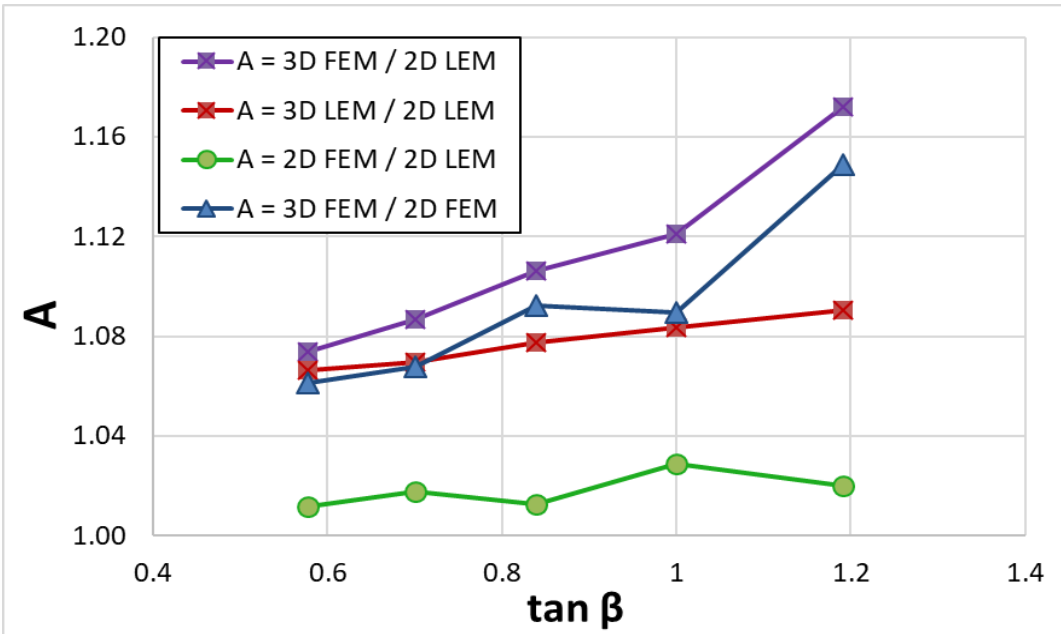


Figure 4.12 Variation of the normalized FS with respect to $\tan \beta$

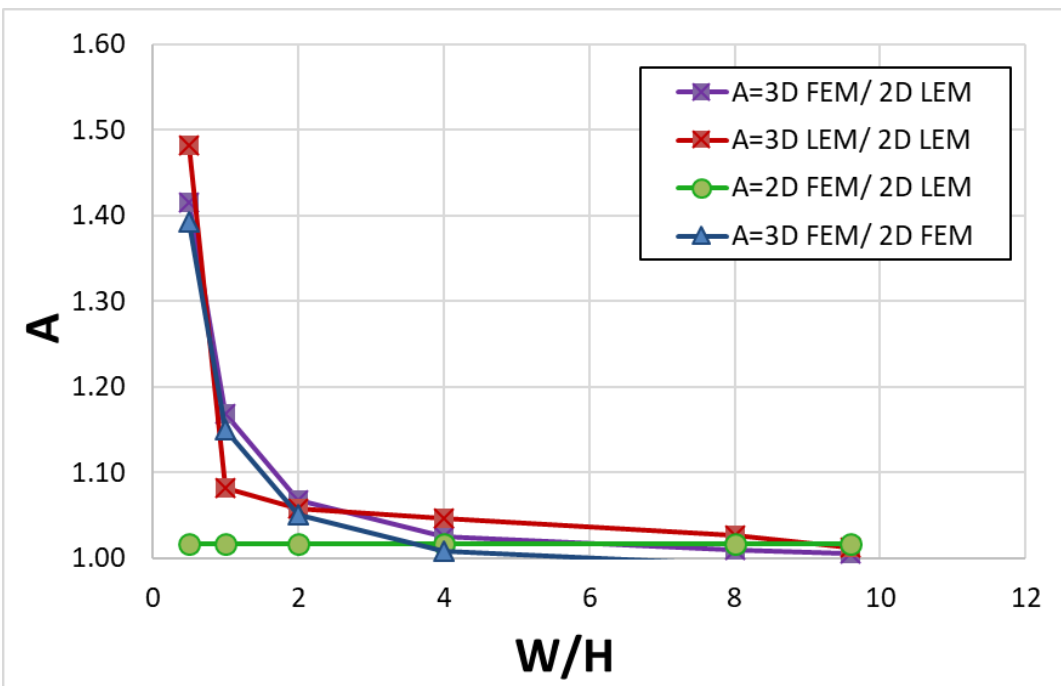


Figure 4.13 Variation of the normalized FS with respect to W/H

Nowadays, LE and FE methods are common methods for slope stability analysis. However, both LEM and FEM techniques have their advantages and limitations, and both methods are used to estimate the FS and the most critical slip surface location. While similar studies have highlighted the robust nature of FE analyses to carry out more complex problems, the LE methods provide reasonable and reliable slope stability results with limited required input (Jiang and Magnan 1997, Krahn 2003, Adams 2015, Memon 2018). This fact gives LE analyses a slight edge over the FEM technique, which involves much more input parameters. On the other hand, it is difficult in LE analysis to evaluate the interslice forces, which depend on many factors, including the stress-strain and deformation characteristics of the materials in the slope (Chowdhury 1978, Stark and Eid 1998). Therefore, the three-dimensional analysis seems to be more realistic and leads to improved accuracy and better understanding of the nature of slope failure mechanisms (Griffiths and Marquez 2007). Considering the advantages and limitations of the LE and FE methods, the geotechnical engineer is recommended to choose the method that best fits the nature and intent of slope analysis in question (Memon 2018). In some cases, it is useful to perform slope stability analysis using both LEM and FEM techniques.

4.6 Probabilistic analysis

The slope stability methods discussed so far are deterministic meaning they give one precise answer for one problem. Considering the fact that uncertainty exists in every step taken in arriving at a solution, it makes sense to calculate the uncertainty associated with the solution or predicted value (Briaud 2013). Therefore, the probabilistic method was introduced as an alternative solution to the FS approach to slope design. Probabilistic slope design has been in practice for some time (at least 30 years or so), having been pioneered by Whitman (1983), Lacasse (1994), Duncan 2000, Christian et al. 1994, Baecher and Christian (2003) and others.

As mentioned earlier, one of the most significant factors on the FS are shear strength parameters of the slope mass. At the same time, one of the most challenging aspects of conducting a slope stability analysis is the uncertainty associated with the geotechnical model. Furthermore, the probabilistic analysis differs from the deterministic methods, mainly because it considers the variability of the parameters. Therefore, most of the input data in a slope stability analysis are not known with precision.

At the same time, the reluctance of specialists to apply probabilistic methods still exists. First, engineers' training in statistics and probability theory is often limited to basic information during their early years of education. Hence, they are less comfortable dealing with probabilities than they are with deterministic factors of safety. Second, few published studies illustrate the implementation and benefits of probabilistic analyses. Lastly, acceptable probabilities of unsatisfactory performance (or probability of failure) are poorly defined, and the link between a probabilistic assessment and a conventional deterministic assessment is unclear and not precise. These create difficulties in comprehending and utilizing the results of probabilistic analysis (El-Ramly et al. 2002). On the other hand, probabilistic approaches help quantify uncertainty and estimate the likelihood of occurrence of different outcomes. Therefore it can help engineers to develop more robust and economic designs and solutions.

The main aspects and comparisons between the deterministic and probabilistic approaches are shown on Table 4.4.

Table 4.4 Comparison between deterministic and probabilistic approaches (reprinted from Assis 2020)

Engineering approach	Deterministic	Probabilistic
Input parameters of the engineering formulations (x, independent variables)	Values of input parameter are assumed constant	Some input parameters are assumed as variables
Performance indicator (y, dependent variable y)	Result is a unique or a range of values for parametric or sensitivity analyses	Result is probabilistic function or a mean value and its standard deviation
Failure criterion	Comparison between the calculated and critical values of the performance indicator y and check with the prescribed safety margin	The reliability index and failure probability of the performance indicator y are calculated and used in risk analyses

The three main parameters used to characterize the data variability are the mean, μ , standard deviation, σ , and coefficient of variation, *CoV*. The total number of data points entered is n .

The mean μ of a set of values ($x_1, x_2, x_3, \dots, x_n$) is defined as follows and also can be called as the expected value $E(X)$ of X (Eq. 4.5):

$$\mu = \frac{x_1 + x_2 + x_3 + \dots + x_n}{n} = \frac{\sum_{i=1}^n x_i}{n} = E(X) \quad \text{Eq. 4.5}$$

The standard deviation σ is a measure of the deviation of the values with respect to the mean. It is defined as:

$$\sigma = \sqrt{\frac{(x_1 - \mu)^2 + (x_2 - \mu)^2 + \dots + (x_n - \mu)^2}{n - 1}} = \sqrt{\frac{\sum_{i=1}^n (x_i - \mu)^2}{n - 1}} \quad \text{Eq.4.6}$$

Using $n-1$ as denominator instead of n is called 'Bessel's correction' and it is used to reduce bias in the estimation of variance and standard deviation of the population.

The standard deviation squared, σ^2 , is the variance *var* and the ratio of the standard deviation of a random variable, σ , to its mean, μ , is the coefficient of variation *CoV* (Eq. 4.7):

$$CoV = \frac{\sigma}{\mu} \quad \text{Eq.4.7}$$

The *CoV* gives an indication of the scatter in the data.

4.6.1 Coefficient of variation

A number of studies have been published on the variability of the properties of soils and rocks (e.g., Briaud and Tucker 1984; Phoon and Kulhawy 1999a, 1999b; Duncan 2000; Haldar and Mahadevan 2000, Nadim et al. 2005, Uzielli et al. (2006), and Kadar and Nagy 2017).

The coefficient of variation is commonly used in geotechnical variability analyses. Its dimensionless provides a great advantage, and more physically meaningful measure of dispersion relative to the mean (Uzielli et al. 2006, Hammah et al. 2009). Another advantage is that CoVs are thought to be independent of the geological age of the material. Therefore it allows the use of reference values with some confidence even at sites for which little or no data may be available (Phoon and Kulhawy 1999a).

The coefficient of variation of soil properties measured in the field can reach 100%, although values of 20-50% are more common (Baecher and Christian 2003). The typical coefficient of variation reported from soil engineering property testing ranges between 20 and 30% (Phoon and Kulhawy 1996, Christian and Baecher 2011, Briaud 2013). Harr (1987) developed a rule by which coefficients of variation below 10% are considered to be “low”, between 15% and 30% “moderate”, and greater than 30% is “high.”

Table 4.5 presents typical CoV values for different geotechnical properties suggested in the literature. Several studies (Griffiths and Fenton 2010, Allahverdzadeh et al. 2017) showed that by increasing the coefficient of variation, the PoF of the slope increases.

Table 4.5 Typical values of CoV for some geotechnical properties used in slope stability analysis

Geotechnical properties	Range of CoV	References
Unit weight (γ)	0.03-0.1	Briaud and Tucker (1983), Duncan (2000), Uzielli et al. (2007), Javankhoshdel et al. (2018)
Cohesion (c)	0.2-0.8	Baecher and Christian (2003), Javankhoshdel et al. (2018)
Undrained strength (S_u)	0.13-0.4	Lacasse & Nadim (1997); Phoon and Kulhawy (1999b); Duncan (2000); Uzielli et al. (2007)
Friction angle (ϕ)	0.02-0.2	Duncan (2000); Baecher and Christian (2003); Uzielli et al. (2007) Javankhoshdel et al. (2018)

4.6.2 Spatial variability and correlation length

The spatial variability of a soil property indicates the variation (or distribution) of the scatter of the soil property values within a certain region (Kim and Salgado 2009). The influence of spatial variability of soil properties in slope stability analyses has been the subject of investigation by a number of researchers (Griffiths and Fenton 2004; Cho 2007; Low et al. 2007; Srivastava and Sivakumar Babu 2009; Cho 2010; Srivastava et al. 2010; Griffiths et al. 2011; Wu and Wang 2011; Ji et al. 2012, Zhu and Zhang 2013; Javankhoshdela et al. 2017). Several researchers (Griffiths and Fenton 2004, Javankhoshdel and Bathurst 2014, Kasama and Whittle 2016) investigated the influence of spatial variability of undrained cohesive soil strength on the PoF of slopes. The influence of spatial variability and its parameters have been shown to have a significant influence on the probability of slope failure.

The correlation length θ is a measure of the variability of a random field. θ is the distance within which points are significantly correlated. Conversely, two points separated by a distance more than θ will be largely uncorrelated. θ is also called as an isotropic scale of fluctuation.

Mathematically in 1D space, θ is defined as the area under the correlation function (Rackwitz, 2000, Fenton and Griffiths 2008):

$$\theta = \int_{-\infty}^{+\infty} \rho(\tau) d\tau \quad \text{Eq.4.8}$$

where τ is the absolute distance between any two points in the random field or separation distance, and $\rho(\tau)$ is the correlation function between properties assigned to two points in the random field separated by τ . The expression for correlation function that commonly used for an isotropic random field generation is presented by:

$$\rho(\tau) = \exp\left(-\frac{2\tau}{\theta}\right) \quad \text{Eq. 4.9}$$

The correlation length θ is the parameter in the correlation coefficient function that controls the degree of reduction in the correlation coefficient between any two points that are τ apart when τ increases (Kim and Salgado 2009). Figure 4.14 shows how the exponential correlation coefficient function varies with separation distance τ (in one direction) for different isotropic scales of fluctuation ($\theta = 1, 3, 5,$ and 10 m).

In practice it is preferable to use the nondimensionalized parameter instead of correction length (Griffiths and Fenton 2004, Kasama and Whittle 2015, Allahverdzadeh et al. 2017). Therefore the correlation length, θ , usually normalized by the slope height H . θ/H , governs the degree of spatial variability.

The smaller the value of θ/H is, the less correlation exists between two nearby values of a variable. If the θ/H is an infinite value, all the values of a random variable in a random field are perfectly correlated; therefore, the values are the same over the whole random field, and the layer is uniform. On the other hand, when θ/H is equal to zero, the values of the random variable at all locations are independent of each other (Kim and Salgado 2009).

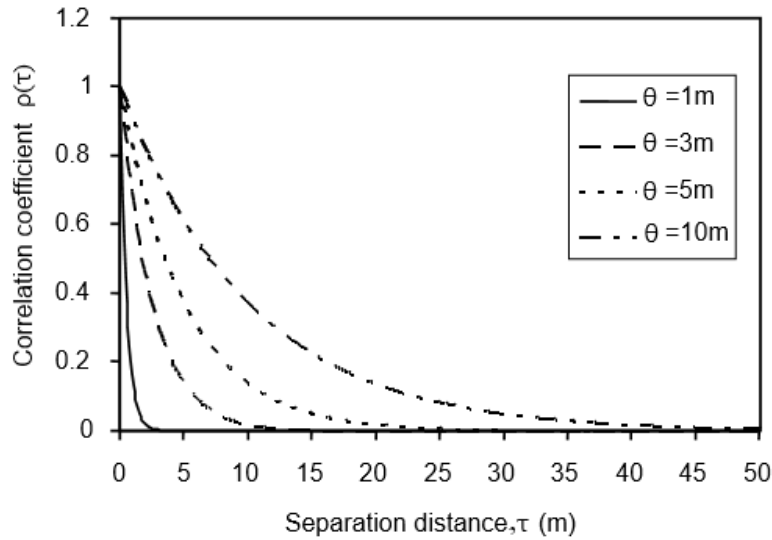


Figure 4.14 Exponential correlation coefficient functions for different isotropic separation distance τ (θ is the scale of fluctuation) (modified from Kim and Salgado 2009)

A large scale of fluctuation has two implications: first, the soil properties estimated by sampling the field at a single location will be more representative of the overall soil mass; and, second, the reduced spatial variability means that the soil will behave more like that predicted by traditional deterministic theory. Thus, for larger correlation lengths, the closer PoF would be to the value of PoF determined for the slope without spatial variability approach (Griffiths and Fenton 2004, Allahverdizadeh et al. 2017).

4.6.3 Number of layers of the slope and Probability of failure

The researcher studied the variation of the PoF due to the number of layers considered in the homogeneous and isotropic slope. This effect was studied with the help of a series of 2-D limit equilibrium analyses using 6500 circular slip surfaces. In addition, a total of 1000 simulations using the Latin-Hypercube sampling method were carried out for the lowest FS slip surface to calculate the PoF.

A studied 2D model has a height of 15 m and a slope of 1H:1V. The studied slope is formed of the cohesive material with the Mohr-Coulomb failure criterion. There are three variables involved in the calculations: Unit weight, γ (kN/m³), Cohesion, c (kPa), and Friction angle, ϕ (°). These three properties are considered to be spatially random and are characterized by their means, their coefficient of variations, and their correlation lengths (which are measures of the degree of spatial correlation). The soil properties were picked arbitrary and the mean values of the geotechnical parameters are presented in Table 4.6. The uncertainty was quantified associated with each variable engaged in the solution. A combination of the CoV of soil properties was selected, i.e. CoV_γ , CoV_ϕ , and CoV_c were set to the typical maximum values of 0.1, 0.2, and 0.3 respectively (Kim and Salgado 2009, Javankhoshdel et al. 2018). Note that all input parameters are treated as independent variables.

The unit weight and cohesion are assumed to have a log-normal distribution, primarily because it is non-negative. The friction angle, is generally bounded, which means that its distribution is a complicated function with at least four parameters. However, $\tan\phi$ varies between 0 and infinity as ϕ varies between 0° and 90° (Fenton et al. 2005). Thus a possible distribution for $\tan\phi$ is also the log-normal.

Table 4.6 Statistical input parameters

Parameter	Unit weight, γ (kN/m³)	Cohesion, c (kPa)	Friction angle, ϕ (°)
Mean value (μ)	20	10	30
Coefficient of variation (CoV)	0.1	0.3	0.2
Distribution	log-normal	log-normal	log-normal

The studied homogeneous slope was divided into a different number of layers to force the software to create multiple samples of the same materials within the simulation run. The deterministic and probabilistic slope stability calculations were performed using the commercial slope stability analysis package Slide2 (Rocscience, 2021c). Slide2 offers the ability to input statistic information for each variable. In modeling the PoF, the number of runs providing results of FS less than one is divided by the total number of runs to find the probability of occurrence.

Table 4.7 presents some results for the homogeneous slope divided into n-layers. Each layer is assigned with identical statistical input parameters from Table 4.6. In Figure 4.15a, the homogenous slope consisted of one layer. The critical slip surface had FS=1.049, and the PoF was 42.867%. In Figure 4.1b, the slope is divided into layers, each with a height (h) of 2 m. Each layer is assigned with the Mohr-Coulomb failure criterion input parameters from Table 4.6. The lowest FS was 1.049, and the same critical slip surface to Figure 4.16a was observed. The PoF dropped to 16.5%. The critical slip surface intersects eight layers with a fewer likelihood of all sampling at extremely low or high values. Figure 4.1c represents the slope divided into layers with h=1.0 m. Each layer is assigned with the same geotechnical parameters (Table 4.7). The lowest FS was 1.049, but the PoF dropped to 19.374%, and the critical slip surface intersects 15 individual layers. In Figure 4.15d the height of the layers is reduced to h=0.5 m. As in previous cases each individual layer is assigned with identical parameters from Table 4.6. The lowest FS remains as 1.049 and the same critical slip surface to Figure 4.15a-c is identified. However, the PoF is significantly dropped to 11.717%. In this case the critical slip surface intersects 30 individual layers.

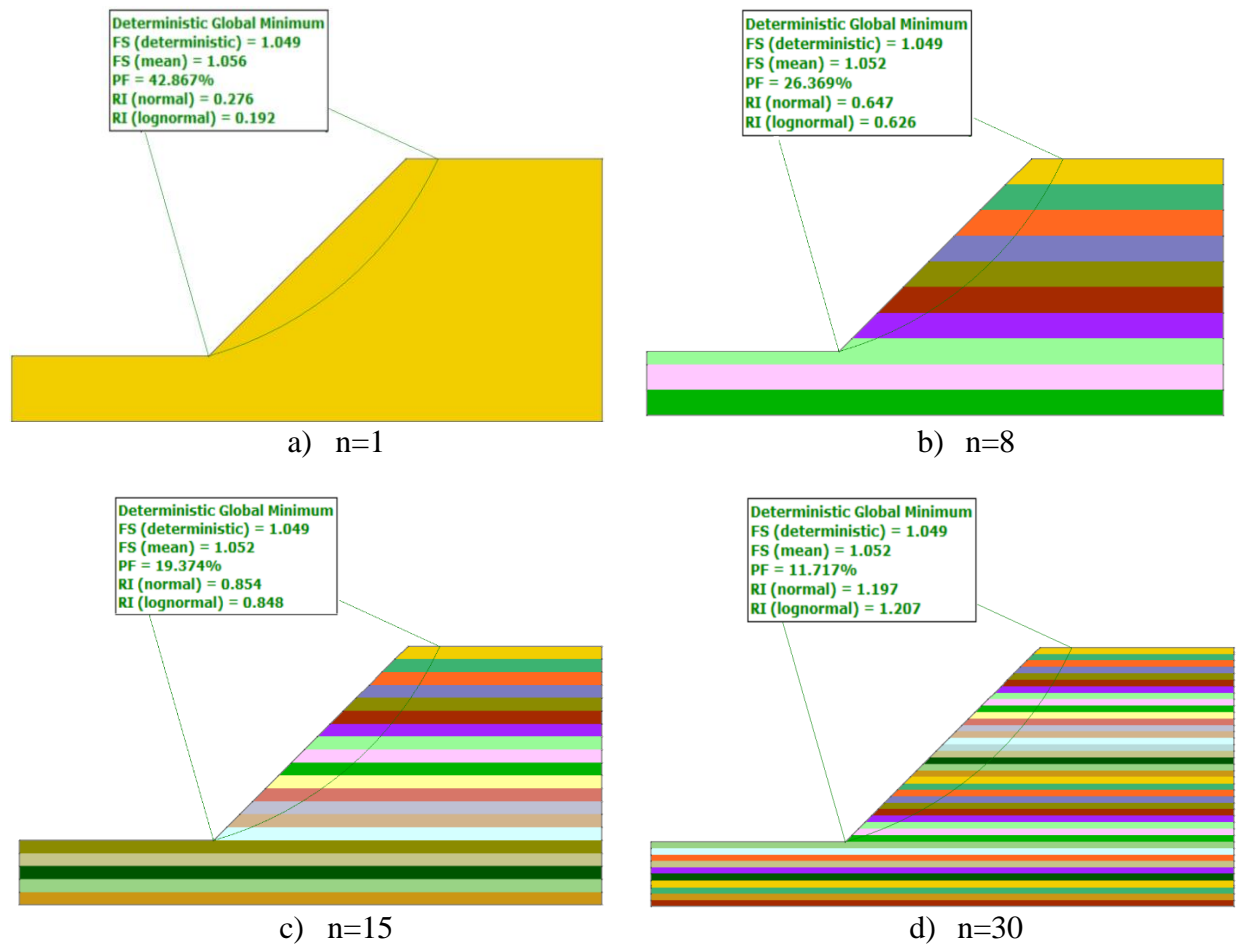


Figure 4.15 Results of the simulations for homogeneous slope divided into n -layers (n = number of layers with identical material properties intersected by the critical slip surface). Note: results are presenter for case with coefficient of correlation $\theta=0$.

Each time modeling software carries out 1000 times simulations using Latin-Hypercube sampling method to determine PoF, each material's input parameters varied based on their statistical input parameters. If we use more and more identical materials (layers) in a model, the likelihood of each individual layer having very low or very high input parameters through the entire model or slip surface decreases proportionally with the number of identical materials, as shown in Table 4.7.

Table 4.7 Limit equilibrium results for lowest FS and automatically calculated probability of failures of the layered homogenous slope

Number of identical layers intersected by the critical slip surface (n)	Deterministic FS	Mean FS	PoF (%)
1	1.049	1.056	43.0
2	1.049	1.053	41.1
3	1.049	1.053	37.2
5	1.049	1.052	32.4
8	1.049	1.052	26.4
15	1.049	1.052	19.4
30	1.049	1.052	11.7

The presented results are consistent with the ones that were obtained by Barr and Heweston (2018). They studied the effect of multiple sampling by dividing the 2-D model into different number of square elements. Results of the LE analysis were based on 5,000 non-circular slip surfaces for the lowest FS and automatically calculated PoF using Monte-Carlo simulations on heterogeneous slopes. It was concluded that having more materials could reduce the perceived PoF in a model.

Figure 4.16 shows the PoF associated with the different number of layers intersected by the critical slip surface. The figure demonstrates that the number of layers affects the probability of failure; the more layers in the slope, the lower the probability of failure. Therefore, it can be concluded that by increasing the number of identical layers, the error may cancel out, and there is less chance of having extremely low values of input parameters along the most critical slip surface.

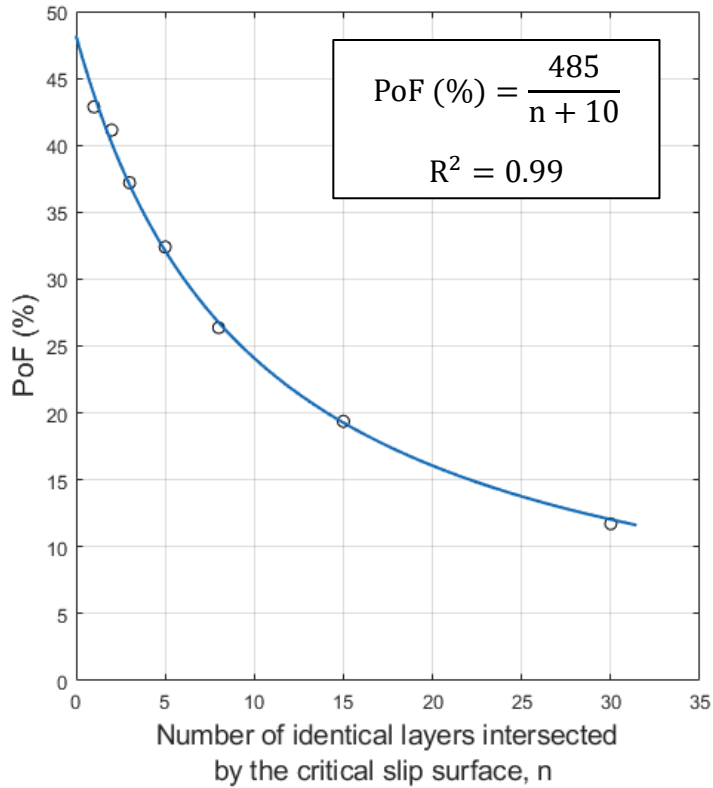


Figure 4.16 PoF vs. number of layers with identical material properties intersected by the critical slip surface (n)

Along with the set of simulations, two slope problem examples of PoF estimation were considered: 1) a slope consists of one layer, and 2) a slope consists of two layers of identical material.

Example 1 considered a slope problem involving soft material or crushed waste. In such materials, failure occurs along a surface which approaches a circular shape with radius R and length along arc L. The parameters of the model presented in Figure 4.17.

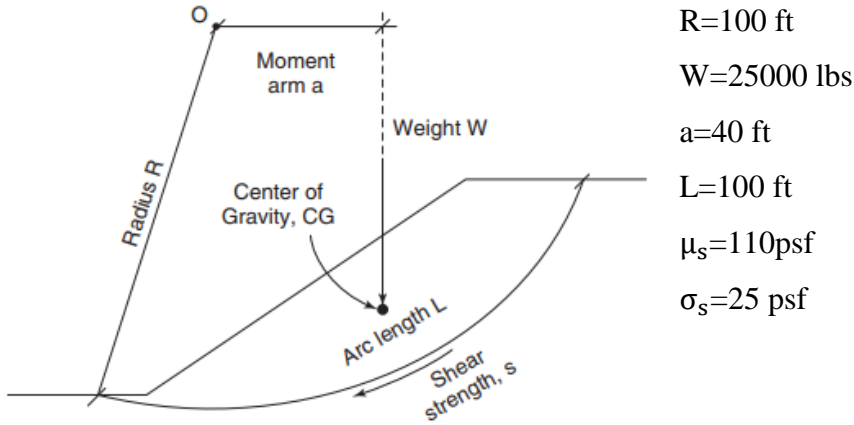


Figure 4.17 A slope formed with no layered homogeneous material (modified from Briaud 2013)

The FS is defined as the ratio of the maximum resisting moment over the driving moment around the center of the circle (Figure 4.17) (Briaud 2013).

$$FS = \frac{sRL}{Wa} \quad \text{Eq. 4.10}$$

Let $y_1=FS$, and expected value $E(y_1)$, variance $\text{var}(y_1)$, and standard deviation $\sigma(y_1)$ will be:

$$E(y_1) = \frac{\mu_s RL}{Wa} = \frac{110 \cdot 100 \cdot 100}{25000 \cdot 40} = 1.1 \quad \text{Eq.4.11}$$

$$\text{var}(y_1) = \sigma_s^2 \left(\frac{RL}{Wa} \right)^2 = 25^2 \cdot \left(\frac{100 \cdot 100}{25000 \cdot 40} \right)^2 = 0.0625 \quad \text{Eq.4.12}$$

$$\sigma(y_1) = \sqrt{\sigma_s^2 \left(\frac{RL}{Wa} \right)^2} = \sqrt{25^2 \cdot \left(\frac{100 \cdot 100}{25000 \cdot 40} \right)^2} = 0.25 \quad \text{Eq.4.13}$$

Slope fails if $y_1 < 1.0$, therefore:

$$\frac{y_1 - E(y_1)}{\sigma(y_1)} < \frac{1 - E(y_1)}{\sigma(y_1)} \quad \text{Eq.4.14}$$

$$\frac{y - 1.1}{0.25} < \frac{1 - 1.1}{0.25} = -0.4 \quad \text{Eq.4.15}$$

but $\frac{y-E(y_1)}{\sigma(y_1)}$ is standardized normal variable. If y is a normally distributed variable, the slope will fail if $u < -0.4$. The chance that $u < -0.4$ is equal to chance that $u > 0.4$. Using the table, it can be found that a chance that $u < 0.4$ is 0.6554 (Briaud 2013, Table 11.3). Thus $1-0.6554=0.3446$ is chance $u < -0.4$.

Based on the presented calculations it can be concluded that if s is normally distributed with mean $\mu_s = 110$ psf and standard deviation $\sigma_s = 25$ psf, slope has **34.46%** chance of failing.

Example 2 Now the slope from the example 1 consists of two layers A and B with the same geotechnical parameters: $s_A = N(110,25)$ and $s_B = N(110,25)$ (Figure 4.18).

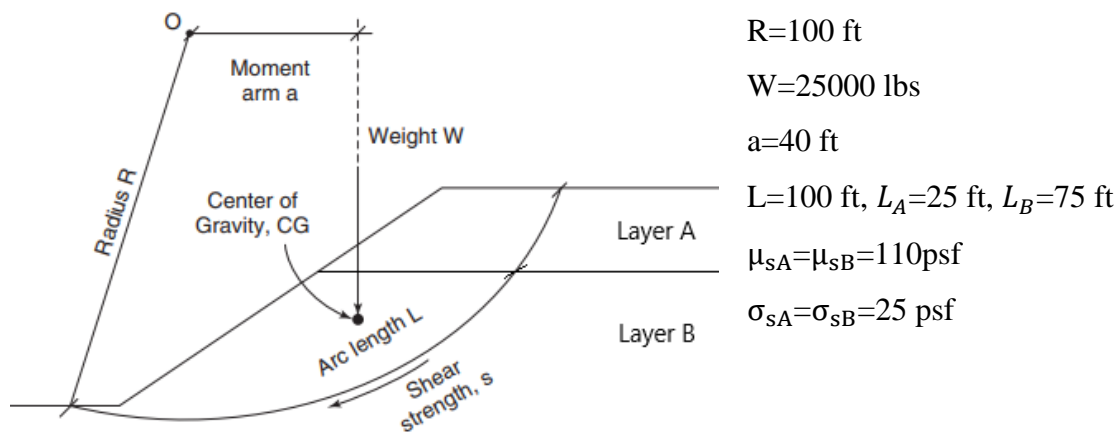


Figure 4.18 A slope formed of two layers A and B (modified from Briaud 2013)

Let M_R is the resisting moment and normally distributed variable:

$$M_R = (s_A \cdot L_A + s_B \cdot L_B)R \quad \text{Eq. 4.16}$$

$$E(M_R) = (E(s_A) \cdot L_A + E(s_B) \cdot L_B)R \quad \text{Eq. 4.17}$$

$$E(M_R) = (110 \cdot 25 + 110 \cdot 75) \cdot 100 = 1.1 \cdot 10^6 \text{ (ft} \cdot \text{lbs)} \quad \text{Eq. 4.18}$$

and expected value of the FS $E(y_2)=E(\text{FS})$ is defined as:

$$E(y_2) = \frac{(s_A \cdot L_A + s_B \cdot L_B)R}{Wa} = \frac{1.1 \cdot 10^6}{25000 \cdot 40} = 1.1 \quad \text{Eq. 4.19}$$

Let $y_2=FS$, and expected value $E(y_2)$, variance $var(y_2)$, and standard deviation $\sigma(y_2)$ will be:

$$E(y_2) = \frac{(s_A \cdot L_A + s_B \cdot L_B)R}{Wa} = \frac{1.1 \cdot 10^6}{25000 \cdot 40} = 1.1 \quad \text{Eq.4.20}$$

$$var(y_2) = \frac{R^2(\sigma_{sA}^2 \cdot L_A^2 + \sigma_{sB}^2 \cdot L_B^2)}{(Wa)^2} = \frac{3.90 \cdot 10^{10}}{10^{12}} = 0.039 \quad \text{Eq.4.21}$$

$$\sigma(y_2) = \sqrt{\frac{R^2(\sigma_{sA}^2 \cdot L_A^2 + \sigma_{sB}^2 \cdot L_B^2)}{(Wa)^2}} = \sqrt{0.039} = 0.1975 \quad \text{Eq.4.22}$$

Slope is unstable if $y_2 < 1.0$, therefore:

$$\frac{y_2 - E(y_2)}{\sigma(y_2)} < \frac{1 - E(y_2)}{\sigma(y_2)} \quad \text{Eq.4.23}$$

$$\frac{y_2 - 1.1}{0.1975} < \frac{1 - 1.1}{0.1975} = -0.51 \quad \text{Eq.4.24}$$

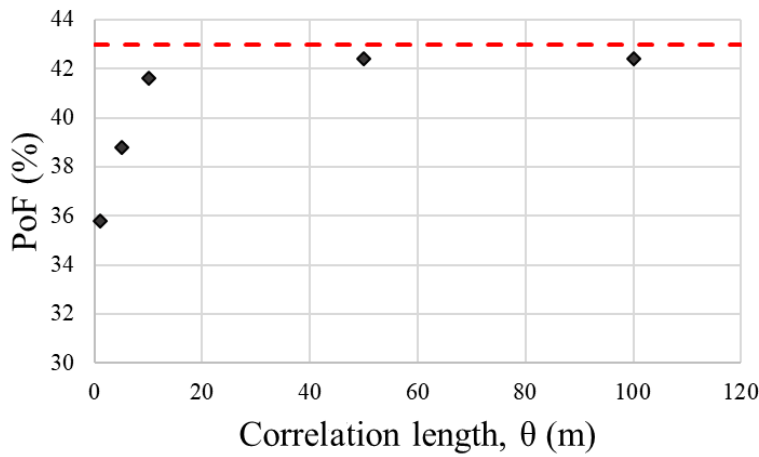
The slope will fail if $u < -0.51$. The chance that $u < -0.51$ is equal to chance that $u > 0.51$. Using Table 11.3 from Briaud (2013), it can be found that a chance that $u < 0.51$ is 0.6950. Thus $1 - 0.6950 = 0.305$ is chance $u < -0.51$

Based on the presented calculations it can be concluded that if s is normally distributed with mean $\mu_{sA} = \mu_{sB} = 110$ psf and standard deviation $\sigma_{sA} = \sigma_{sB} = 25$ psf, slope has **30.5%** chance of failing which is 4% less compare to the case in Example 1.

Results obtained using the 2-D LEM software, and the simplified calculations of the PoF presented in the two examples are consistent and prove that the PoF decreases with increasing the number of layers with identical geotechnical parameters. It has been illustrated that the PoF can be reduced for the model with a number of materials within a single isotropic material type.

In addition, a set of 2-D LE simulations utilizing a spatial variability approach was performed. The same slope geometry and material type as in the case of the layered slope calculations were used. PoF of the studied slope is 43.0%. Different correlation lengths $\theta = 1$ m,

5 m, 10 m, 50 m, and 100 m were used in the calculations. Figure 4.19 shows the effect of spatial correlation length (isotropic spatial variability) on the PoF. Our results show that the correlation length affects the value of the probability of failure. The greater the correlation length, the higher the PoF and the closer it is to the value of PoF determined for the slope without spatial variability approach (PoF = 43%).



— — — — — corresponds to the PoF determined for the slope without spatial variability approach

Figure 4.19 Variation of PoF (%) with correlation length θ (m) for the homogeneous slope

Another set of calculations was performed using the spatial variability approach for the layered slope. Variation of the PoF with different spatial correlation lengths ($\theta = 10$ m, 50 m, and 100 m) is presented in Figure 4.20. Our results show that increasing the correlation length gives the PoF close to the PoF determined for the slope without spatial variability. Figure 4.20 shows that the bigger is the number of layers and the higher is the spatial variability of soil, the closer is the PoF to the one obtained for the slope without spatial variability.

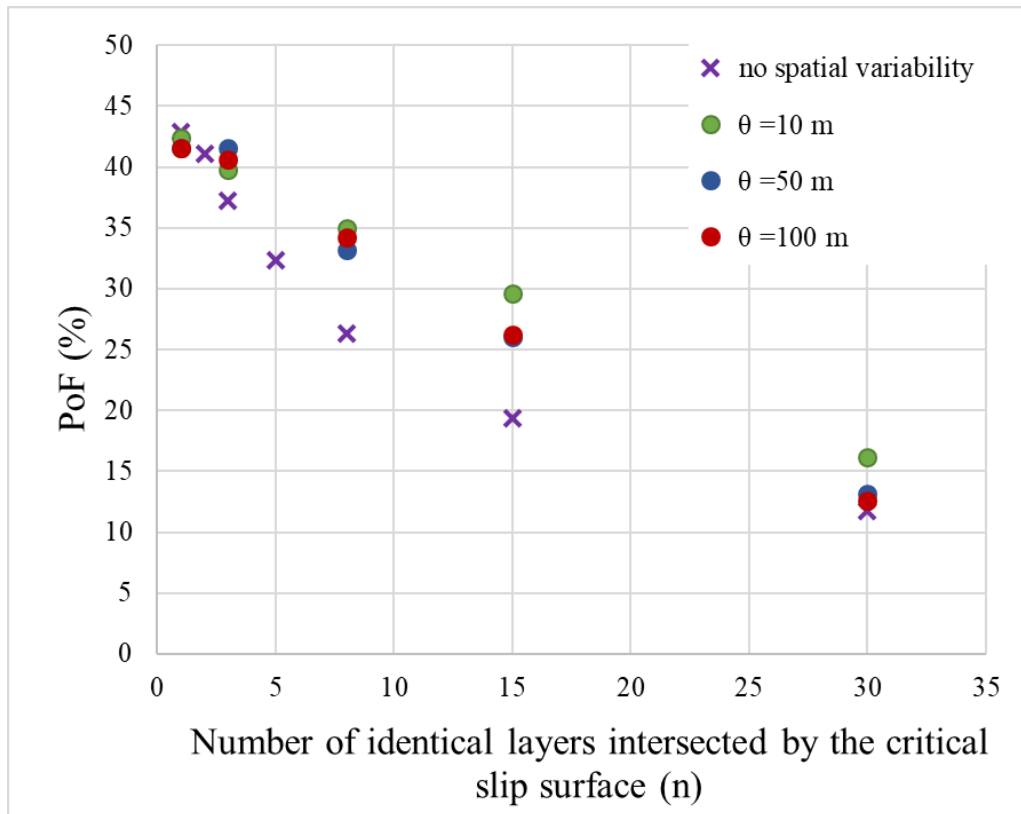


Figure 4.20 The influence of the number of identical layers intersected by the critical slip surface (n) on the PoF (%) for different spatial variability of soil and slope with no spatial variability

It has been shown that slope models with spatial variability of material properties (e.g., shear strength and unit weight) result in a lower PoF than for the same slope model without spatial variability. Presented examples (Figure 4.19 and 4.20) also illustrate that the variability of average shear strength along the length of the critical failure surface decreases as the correlation length θ , (m) decreases. The correlation distance is reduced when breaking the profile into thinner layers (the strength in each layer is the same across the layer and independent of the adjacent layers). The variability in the average strength along the slip surface is reduced too. Since there is less variability in the strength, the PoF decreases with thinner layers.

The presented results also demonstrate that the more geologically different (or uncorrelated) layers are involved in the slope stability analysis, the more likely the resultant PoF will be lower than the PoF obtained for the same slope formed of homogenous material.

The phenomenon of decreasing the PoF due to the increase in the number of identical layers in the slope clearly shows the correlation between the higher number of samples studied during the site investigation phase, the more precise the PoF would be determined. The more samples you take, the lower the PoF. The effect of sampling frequency and the type of sample average, best suited to represent the soil property, are two areas that must be investigated further for better design performance.

4.7 Target FS and PoF

4.7.1 Target FS in open pit mining slope stability

The geotechnical properties of the materials in civil engineering are well understood and variability is relatively small and remains comparatively constant from project to project, and even from country to country (Bar and Heweston 2018).

One of the main differences in slope design for open-pit mines compared to civil engineering projects such as excavations, road cuts, and earth-fill dams is that the design does not completely depend on geotechnical factors. Limitations such as the operation requirement and economics of the operation affect the mining plan. These differences result in conflicts in concepts, goals, and required conventional slope design techniques derived from civil and geotechnical engineering (Golestanifar et al., 2018). Another difference is that in such projects, geotechnical properties of open-pit slope materials are highly variable and never well understood since site investigations comprising drilling, mapping, and testing only sample a small portion of the

material, and large extrapolations are often made to characterize the studied area (Bar and Heweston 2018).

According to several researchers, a FS is only an index of slope stability, i.e., it informs us about the relative stability of a design (Hoek and Bray 1981; Mostyn and Li, 1993, Sullivan 2006). It is generally believed that a slope design with a high FS should be more stable than a design with a lower FS. The value of FS obtained as a result of slope stability calculations depends on the selected parameters and the method of analysis adopted for the particular case.

Read and Stacey (2009) summarized the acceptable design FS values recommended in the literature for civil engineering applications. The variations in design FS for civil engineering applications are quite different from those for open-pit mines, as shown in

Figure 4.21. For normal operating conditions and long-term stability, the FS may vary from 1.25 to 2, depending on the author, while for short-term slopes the recommended values vary between 1.3 and 1.5. According to the applicability of the FSs used for civil engineering slopes to open pit mine slopes can be debated due to the different operating environments. However, the values most frequently used in both disciplines are very similar, ranging from 1.2 for non-critical slopes to 1.5 for slopes containing critical access ramps or infrastructure such as in-pit crushers (Table 4.8).

	FS					
	1	1.2	1.4	1.6	1.8	2
Soil earthworks						
Retaining structures						
Civil Slopes						
Dams						
Mine Slopes						

Figure 4.21 Examples of acceptable FS values for different civil engineering projects and open pit mining (modified from Read and Stacey 2009)

Traditionally open-pit slopes are constructed to lower level of stability, considering the shorter operating lifetime involved and the high level of monitoring, both in terms of accuracy and frequency, that is typically available in the mining site. Table 4.8 summarizes the acceptable FS for open pit slope design (VNIMI 1972; Hoek and Bray 1981; Kirsten 1983; Priest and Brown 1983; McMachon 1985; Swan and Sepulveda 2000; Sullivan 2006; Read and Stacey 2009; Adams 2015). All of the stipulations presented in the table are based on the assumptions that the most critical failures surface is used in the slope stability analysis, the strength parameters are reasonably representative of the actual case, and sufficient construction control is ensured.

Table 4.8 Acceptable FS values in slope mining engineering

Slope type	Description of slope conditions		FS accepted in practice (in the numerator – range, in the denominator – preferred minimum value)
Bench	Exploration		$\frac{1.10 \text{ to } 1.25}{1.20}$
	Final wall	Cohesive soils and rocks	$\frac{1.50 \text{ to } 2.0}{1.50}$
		Cohesionless soils	$\frac{1.15 \text{ to } 1.30}{1.20}$
Inter-ramp	Exploration		$\frac{1.2 \text{ to } 1.45}{1.30}$
	Final wall		$\frac{1.20 \text{ to } 1.50}{1.5}$
General slope	Exploration		$\frac{1.20 \text{ to } 1.30}{1.20}$
	Final wall		$\frac{1.20-1.60}{1.30}$

The FS approach is routinely used for slope stability assessment. Still, the potential failure geometry with the lowest FS does not always indicate the highest risk condition, as FS does not provide a direct measure of consequences of failure (Fergusson et al. 2001). Therefore, risk criteria

incorporating the PoF with immediate consequences should be incorporated in the open pit slope design as an efficient tool for immediate and consistent comparisons between different mining designs.

4.7.2 FS and PoF acceptance criteria for open-pit slopes design

The selection of prudent safety factors and PoF often is not a simple task in mining slope stability design. In current mining engineering practice, the FS and PoF are commonly used to find a compromise between the risk of open-pit mine slope failure and economic return (Adams 2015). Acceptable FS and PoF criteria for open-pit mine slope design are typically selected by the geotechnical engineer based on the explicit consideration of uncertainties in the slope design, the consequences of slope failure, and the intended slope design life (Fergusson et al. 2001; Read and Stacey 2009; Adams 2015). The specific probability magnitudes for judging safety and risk have not been established. Nevertheless, it is desired to have a low PoF and a high FS.

Table 4.9 summarizes a typical design acceptance criteria for open-pit mining slopes. The acceptable values of FS and PoF for mining slope stability design are presented depending on the size of the slope and generic consequences.

Table 4.9 Typical FS and PoF acceptance criteria for open-pit mining slope design
(modified from Read and Stacey 2009)

Scale of the slope	Consequence of failure		
	Low	Medium	High
Bench	FoS \geq 1.1 PoF \leq 25-50%		
Inter-ramp	FoS \geq 1.15-1.2 PoF \leq 25%	FoS \geq 1.2 PoF \leq 20%	FoS \geq 1.2-1.3 PoF \leq 10%
Overall	FoS \geq 1.2-1.3 PoF \leq 15-20%	FoS \geq 1.3 PoF \leq 5-10%	FoS \geq 1.3-1.5 PoF \leq 5%

Another approach to determine the acceptance criteria for FS and PoF was presented by Schellman et al. (2006). Table 4.10 presents the acceptable FS and PoF based on the volume of material involved in the failure using at Mantoverde copper mine (Chile).

Table 4.10 Typical FS and PoF acceptance criteria for open-pit mining slopes based on the failure's tonnage (modified from Schellman et al. 2006)

Mass involved in the failure (ton/m)	FS	PoF
<15,000	>1.20	<12%
15,000-30,000	>1.25	<10%
>30,000	>1.30	<8%

The lifetime of the mine slope was taken as one of the basic parameters for the FS and PoF acceptance criteria for the development of Table 4.11. The table was developed by Swan and Sepulveda (2000) for the design of open-pit slopes at the Ujina open pit, Chile. The values of FS and PoF presented in Table 4.11 may be considered relatively high, but Read and Stacey (2009) state that all numbers are specific to the Ujina mine, but the approach can be utilized at any open-pit mine.

Table 4.11 Typical FS and PoF acceptance criteria for open-pit mining slope design based on its lifetime and volume of the failed material (reprinted from Swan and Sepulveda 2000)

Slope type	Case	Characteristic of instability		Acceptability Criterion		Comments
		Loss of Ramp Berm (%)	Material affected (ktons/m)	FS	PoF (%)	
Bench	Expansion, not adjacent to a ramp	<25	<0.5/<1.0			Berms should have a nominal width to contain unraveling wedges whose probability of occurrence is >30%; controlled blasting will be used to minimize induced damage and presplitting for final wall slopes
		25-50	<1.0/<2.0	<45		
		>50	>1.0/>2.0	<35		
	Expansion, adjacent to a ramp	<25	<0.5/<1.0			
		25-50	<1.0/<2.0	<40		
		>50	>1.0/>2.0	<30		
Final Wall, not adjacent to a ramp	<25	<0.5/<1.0				
	25-50	<1.0/<2.0	<35			
	>50	>1.0/>2.0	<25			
Final Wall, adjacent to a ramp	<25	<0.5/<1.0				
	25-50	<1.0/<2.0	<30			
	>50	>1.0/>2.0	<20			
Interramp	Expansion	<25	<5	>1.20	<30	Stability analysis must include explicit effect of rock mass structures: two independent access ramps will be made to pit bottom; measures will be implemented for slope drainage
			>5	>1.25	<25	
		25-50	<5	>1.25	<25	
			5-10	>1.30	<22	
			>10	>1.35	<20	
		>50	<10	>1.30	<22	
	10-20		>1.35	<20		
	>20		>1.45	<18		
	Final Wall	<25	<5	>1.20	<25	
			>5	>1.25	<20	
		25-50	<5	>1.30	<22	
			5-10	>1.35	<20	
>10			>1.40	<18		
>50		<10	>1.35	<20		
	10-20	>1.40	<18			
	>20	>1.50	<15			
Global	Expansion	<25	>1.30	<15	Stability analysis must include rock mass structures; all infrastructure lie outside pit perimeter limits	
		25-50	>1.40	<12		
		>50	>1.50	<10		
	Final Wall	<25	>1.30	<12		
		25-50	>1.45	<10		
		>50	>1.60	<8		

Table 4.9, 4.11, and 4.12 include scale of slope, its lifetime and failure size in the FS and PoF accepted for open-pit mining design. When the failure size increases or a large portion of the pit is involved in a potential failure, the critical FS must be increased, and the PoF is reduced (Gibson 2011). The same dependency is valid for the lifetime of mine slopes: for permanent slopes, the FS may be increased up to 1.5-2.0, and acceptable PoF should be less than 5-8%, and for temporary slopes, the acceptable PoF can be increased up to 50%.

Depending on the magnitude and variability of the input geotechnical parameters, the PoF and FS can vary widely. For example, it is entirely possible to have an FS of 1.3 and a PoF of 25% with certain input data. However, using input data specifying slightly lower strength magnitudes, but with much less variability in the data, the safety factor could decrease to 1.20, and the PoF could drop to 5%. Thus, a high FS indicates a low PoF, and a low FS indicates a higher PoF.

Terbrugge et al. (2006) and Steffen et al. (2008) suggested that the pit design criteria should be based on risk rather than the FS or PoF because the risk analysis approach tries to solve the main drawback of the other methodologies (based on the FS or PoF) with regard to the selection of the appropriate acceptability criteria. The risk is calculated considering the PoF and the consequence of the failure. Although the acceptance criteria outlined in Table 4.9, 4.11, and 4.12 can be used for open pit slope design, they do not necessarily help to quantify the risk of slope failure (Read and Stacey 2009; Adams 2015). The risk associated with the open pit slope failure is usually quantified for different data confidence and slope configurations and provides the economic value. Risk acceptance criteria are varied from site to site and differ from company to company because the failure consequences for each case are different (Read and Stacey 2009; Terbrugge et al. 2006; Chiwaye and Stacey 2010, Gibson 2011). Therefore each mine has to develop its own guidance for slope failure risk evaluation.

4.7.3 Target PoF in open pit mining slope stability

The PoF often appears alongside the FS in design acceptance criteria for open pit mining slope design. However, the design acceptance criteria generally provide no guidance in relation to how PoF should be calculated for homogenous and heterogeneous slopes or what qualifies a “reasonable” PoF assessment for a given slope design (Bar and Heweston 2018).

In slope design, limit equilibrium state is achieved when FS is equal to one. Therefore, PoF can be expressed as:

$$\text{PoF} = P[\text{FS} \leq 1] \quad \text{Eq. 4.25}$$

There is no general guidance for the open-pit mining acceptable PoF determination. Several researchers brought up some failure probabilities which can be acceptable for open pit slopes. There are complicating criteria for the PoF in probabilistic design methods, which vary in the range from 0.3% to 30% (Priest and Brown 1983; Sjoberg 1999; Swan and Sepulveda 2000; Read and Stacey 2009; Steffen et al. 2008). The summary of open pit slopes acceptance criteria for PoF is presented in the Table 4.12.

Table 4.12 Acceptable PoF in slope mining engineering

Category	Consequence of failure	Height of slope	Example of the failure level	Acceptable PoF $P[FS \leq 1]$
3 – non serious	Non critical or temporary slopes where failure has no impact on continues operations and where minimal safety hazards to personnel and equipment exist	<50 m	Bench slope failure	10-30%
2 – moderately serious	Slopes of a permanent or semi-permanent nature where failure have a significant impact on costs and safety	50-100 m	Inter-ramp slope failure	1-15%
1 – very serious	Critical slopes of a permanent or semi-permanent nature where failure may affect continuous operation and open pit safety.	>100 m	Overall slope failure	0.3-5%

Although the acceptable PoF is still disputable, for benches, PoF of <30% seems acceptable, whereas, for an overall slope, a failure probability of less than 5% would be more suitable. As it can be seen from Table 4.12, the acceptable values recommended by different researchers for mining slopes are still much higher than the commonly employed in civil engineering (PoF=0.001) (Fenton and Griffiths 2008). However, these values are not unreasonable considering that an open pit slope, in general, has a shorter life, and fewer people are at risk of mining slope collapse compared to the collapse of any civil engineering structure. On the other hand, Sjoberg (1999) pointed out that the actual criteria to be used in a specific mine cannot be determined from general guidelines like presented in Table 4.12 but should be subject to a more thorough analysis of the consequences of failure.

4.7.4 Observation on FS obtained by strength reduction and load increase techniques

Traditionally, the assessment of the level of safety of the structure is made on the basis of FS which were developed from previous experience with similar structure in similar environments or under similar conditions. Thus, the values of the FS selected for design reflect past experience and the consequences of failure (Becker 1996). According to the current state of practice the target FS for the long-term stability of slopes is 1.5, whereas most geotechnical engineers use FS = 2.5 to 3.0 for bearing capacity design, and the same range of values for safety against erosion and piping (Becker 1996, Duncan 2000, Griffiths 2015).

The difference in the factors of safety for slopes and bearing capacity problems was discussed in several papers (Duncan 2000; Duncan et al. 2014; Griffiths 2015). Griffiths (2015) states that the FS used in slopes is a type of resistance factor, i.e., the factor by which the shear strength must be reduced to reach failure, whereas that for bearing capacity is a load factor, i.e., the factor by which the load must be increased to reach failure. Therefore factors of safety that are applied to load for bearing capacity are not comparable with the factors of safety applied to shear strength, as used for slope stability analyses (Duncan et al. 2014, Griffiths 2015).

The difference between the two definitions of the FS was presented by Griffiths (2015) based on the strip footing example (Figure 4.22). The Terzaghi ultimate bearing capacity equation (Eq. 4.12) was used to illustrate the comparison of the two approaches to FS calculations:

$$q_{ult} = c'N_c + qN_q + \frac{1}{2}\gamma BN_\gamma \quad \text{Eq. 4.26}$$

where q_{ult} is the ultimate bearing capacity of the soil; c' is the effective stress cohesion intercept; N_c , N_γ , and N_q are bearing capacity factors function of the effective stress friction angle ϕ' ; γ is the effective unit weight; q is a surface surcharge, and B is the width of the foundation.

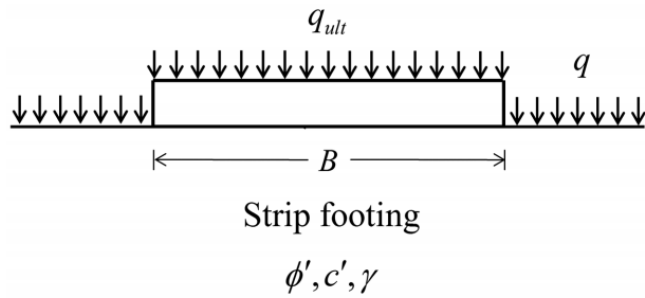


Figure 4.22 Footing problem used to illustrate differences between factors of safety applied to load and to soil shear strength ($\phi'=30^\circ$, $c'=16$ kPa, $\gamma=18$ kN/m³, $B=4$ m, and $q=18$ kPa)

The bearing capacity analysis is based on the allowable design pressure that the footing can safely support. As it was mentioned before the target FS against bearing failure of about $FS_{load} \sim 3.0$ therefore:

$$q_{ult} = \frac{q_{all}}{FS_q} = \frac{q_{all}}{3.0} \quad \text{Eq. 4.27}$$

For comparison purposes, the FS against bearing failure based on strength reduction is now considered. In this case, the strength reduction FS given by $FS_{strength}$, is the factor by which c' and $\tan\phi'$ must be reduced in Eq.4.50 to cause bearing failure, i.e., $q_{ult} = q_{all}$. For the sake of the comparison the following expressions for the bearing capacity factors was used by Griffiths (2015):

$$N_c = (K_p e^{\pi \tan\phi'} - 1) \frac{1}{\tan\phi'} \quad \text{Eq. 4.27}$$

$$N_q = K_p e^{\pi \tan\phi'} \quad \text{Eq. 4.28}$$

$$N_\gamma = 1.5(K_p e^{\pi \tan\phi'} - 1) \tan\phi' \quad \text{Eq. 4.29}$$

Eqs. 4.30-4.32 all include the passive earth pressure coefficient K_p which can be commonly expressed in several different ways, e.g.:

$$K_p = \tan^2 \left(45 + \frac{\varphi'}{2} \right) = \frac{1 + \sin\varphi'}{1 - \sin\varphi'} = (\tan\varphi' + \sqrt{1 + \tan^2\varphi'})^2 \quad \text{Eq 4.30}$$

Firstly, the q_{ult} as a function of c' and $\tan\varphi'$ was obtained:

$$\begin{aligned} q_{ult} = & c' \left((\tan\varphi' + \sqrt{1 + \tan^2\varphi'})^2 \cdot e^{\pi \tan\varphi'} - 1 \right) \cdot \frac{1}{\tan\varphi'} + \\ & + q \cdot (\tan\varphi' + \sqrt{1 + \tan^2\varphi'})^2 \cdot e^{\pi \tan\varphi'} N_q + \\ & + \frac{3}{4} \gamma B \cdot \left((\tan\varphi' + \sqrt{1 + \tan^2\varphi'})^2 \cdot e^{\pi \tan\varphi'} - 1 \right) \tan\varphi' \end{aligned} \quad \text{Eq. 4.31}$$

Secondly, the allowable pressure, q_{all} based on strength reduction approach was determined:

$$\begin{aligned} q_{all} = & \frac{c'}{FS_{strength}} \left(\left(\frac{\tan\varphi'}{FS_{strength}} + \sqrt{1 + \frac{\tan^2\varphi'}{FS_{strength}^2}} \right)^2 \cdot e^{\frac{\pi \cdot \tan\varphi'}{FS_{strength}}} - 1 \right) \cdot \frac{FS_{strength}}{\tan\varphi'} + \\ & + q \cdot \left(\frac{\tan\varphi'}{FS_{strength}} + \sqrt{1 + \frac{\tan^2\varphi'}{FS_{strength}^2}} \right)^2 \cdot e^{\frac{\pi \cdot \tan\varphi'}{FS_{strength}}} + \\ & + \frac{3}{4} \gamma B \cdot \left(\left(\frac{\tan\varphi'}{FS_{strength}} + \sqrt{1 + \frac{\tan^2\varphi'}{FS_{strength}^2}} \right)^2 \cdot e^{\frac{\pi \cdot \tan\varphi'}{FS_{strength}}} - 1 \right) \frac{\tan\varphi'}{FS_{strength}} \end{aligned} \quad \text{Eq 4.32}$$

Thirdly, consider the example presented in Figure 4.22, determine q_{ult} . The value of the bearing capacity factors for $\varphi' = 30^\circ$ is obtained using Eq.4.51-4.53: $N_c = 30.1$, $N_q = 18.4$, and $N_\gamma = 15.1$ (Griffiths 2015). Therefore q_{ult} is given:

$$q_{ult} = 16 \cdot 30.1 + 18 \cdot 18.4 + \frac{1}{2} \cdot 18 \cdot 4 \cdot 15.1 = 1356 \text{ (kPa)} \quad \text{Eq.4.33}$$

Fourthly, based on a typical load-based FS against bearing failure ($FS_q = 3$), the allowable bearing pressure is given by:

$$q_{all} = \frac{1356}{3} = 452 \text{ (kPa)} \quad \text{Eq.4.34}$$

Fifthly, according to Griffiths (2015) from a strength reduction perspective, the value of $FS_{c',\tan\phi'}$, that would be needed to reduce the bearing capacity given in Eq. 4.36 from $q_{ult} = 1356$ kPa to $q_{ult} = q_{all} = 452$ (kPa) is given by:

$$\begin{aligned}
452 = & \frac{16}{FS_{strength}} \left(\left(\frac{\tan 30^\circ}{FS_{strength}} + \sqrt{1 + \frac{\tan^2 30^\circ}{FS_{strength}^2}} \right)^2 \cdot e^{\frac{\pi \cdot \tan 30^\circ}{FS_{strength}}} - 1 \right) \cdot \frac{FS_{strength}}{\tan 30^\circ} + \\
& + 18 \cdot \left(\frac{\tan 30^\circ}{FS_{strength}} + \sqrt{1 + \frac{\tan^2 30^\circ}{FS_{strength}^2}} \right)^2 \cdot e^{\frac{\pi \cdot \tan 30^\circ}{FS_{strength}}} + \\
& + \frac{3}{4} \cdot 18 \cdot 4 \cdot \left(\left(\frac{\tan 30^\circ}{FS_{strength}} + \sqrt{1 + \frac{\tan^2 30^\circ}{FS_{strength}^2}} \right)^2 \cdot e^{\frac{\pi \cdot \tan 30^\circ}{FS_{strength}}} - 1 \right) \frac{\tan 30^\circ}{FS_{strength}}
\end{aligned} \tag{Eq.4.35}$$

which after the solution gives:

$$FS_{strength} = 1.544 \tag{Eq.4.36}$$

This example gives $FS_{load} \approx 2 \cdot FS_{strength}$, which might be expected for bearing capacity on soil with $\phi' = 30^\circ$. The difference between two FSs would be greater with a higher friction angle and vice versa. In case of the $\phi' = 0^\circ$ the $FS_{load} = FS_{strength}$ (Duncan et al. 2014, Griffiths 2015).

As it was mentioned before, Griffiths (2015) presented an example based on Terzaghi's ultimate bearing capacity equation. It should be pointed out that the assumptions made in deriving Terzaghi's equation are that the soil has no water, that it has a constant friction angle ϕ , and cohesion, c , and that it has a constant unit weight, γ . As such, it corresponds to a soil strength profile that increases linearly with depth (Briaud, 2013). However, several researchers (Briaud and Gibbens 1999, Briaud 2007) showed that the spread footing load tests do not always follow the trend of linear increase with depth. Thus, Terzaghi's equation does not work when the strength

profile is different from a linear increase with depth. Moreover, such linear strength increase with depth is rarely encountered in the field. Therefore, the following conclusions were made:

- (a) In case of undrained shear strength (s_u) $FS_{load} = FS_{strength}$.
- (b) For $c-\phi$ soils for a shallow foundation assuming Terzaghi's equation is applied, FS_{load} different from $FS_{strength}$.
- (c) Terzaghi's bearing capacity equation does not work when the strength profile is different from a linear increase with depth. In addition, such linear strength increase with depth is rarely encountered in the field. Thus, (b) above is rarely the case.
- (d) If Terzaghi's equation does not apply and the direct strength equations do apply, $p_u = ks + \gamma D$, where p_u is the ultimate bearing pressure, k is bearing capacity factor, s is a soil strength measurement (CPT_{qc}, PMT_{pL}, SPT_N, undrained shear strength s_u), then $FS_{load} = FS_{strength}$.
- (e) For a friction pile $FS_{load} = FS_{strength}$ for any soil types.
- (f) For end bearing piles FS_{load} different from $FS_{strength}$ if (b) is accepted.
- (g) All these points cast doubt on the validity of the FS for load (FS_{load}) different from the FS for soil strength ($FS_{strength}$).

The variation in the PoF with respect to the FS is shown in Figure 4.23. The plot that was presented by Briaud and Gardoni (2009) refers to the case when $FS_{load} = FS_{strength}$. It can be seen that it is a highly nonlinear process because a little bit of decrease in the FS leads to a significant increase in the PoF. In that case and for a reasonable CoV, the PoF associated with the current state of practice for foundation design generally lies in the range of 10^{-3} to 10^{-4} , whereas the PoF for the slope stability design is at 10^{-1} (Figure 4.23).

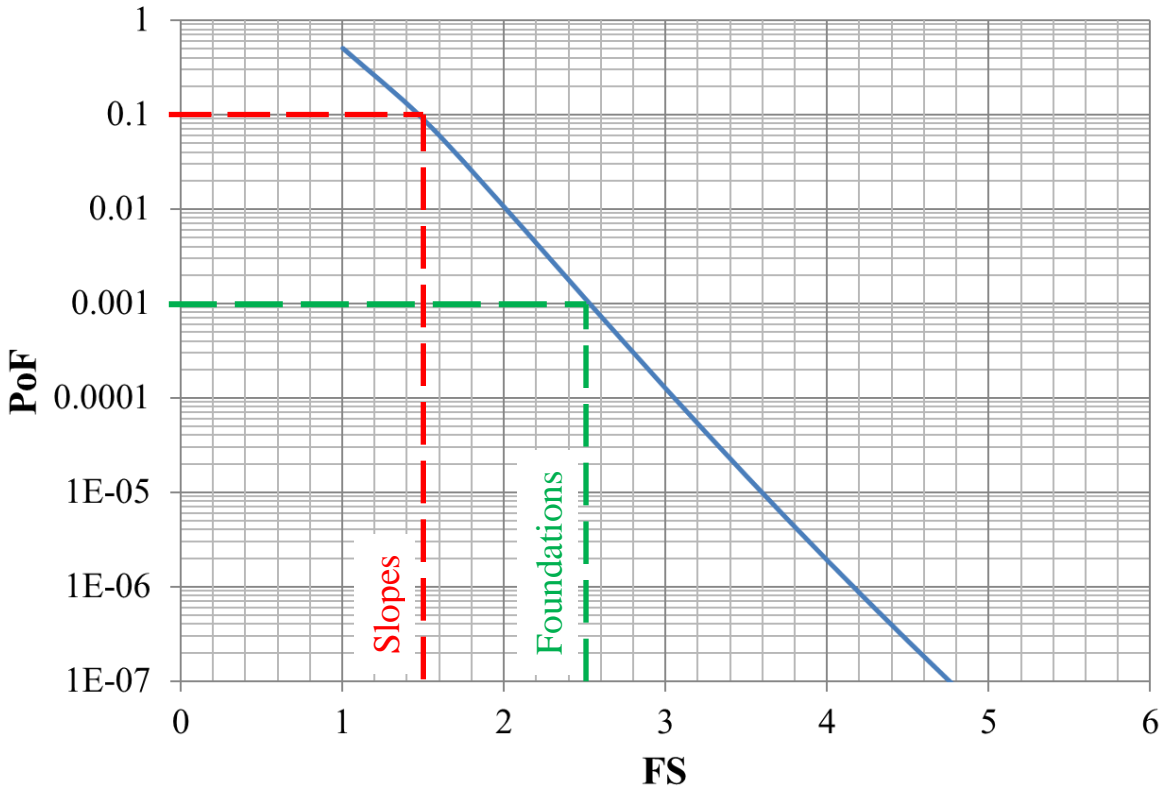


Figure 4.23 Variation of the PoF with respect to the FS, assuming a log normal distribution of FS, CoV of shear strength = 0.3, and CoV of shear stress = 0 (modified from Briaud and Gardoni 2009)

It can be concluded that for the slope design if we aim for lower PoF than 10%, we should aim for a higher FS than the traditional FS=1.5.

5. STABILITY OF SLOPE CORNERS AND OTHER UNUSUAL SLOPE CASES

5.1 Corner slopes

5.1.1 Existing knowledge on slope corner stability

In the framework of slope stability analysis, the vast majority of calculations are performed in 2-D under the assumption of plane strain conditions (Griffiths and Marquez 2007, Nian et al. 2012, Zhang et al. 2013). The plane strain condition is valid if one of dimension is very large compared to the other two. It also require that no curvature or corner exists in the geometry of the slope and no curvature exists in the shape of the failure surface in the direction perpendicular to the plane of interest, which means that the failure surface is the same in any cross section. However, the majority of slopes, both natural and man-made, exhibit a complex configuration and 3-D state (Figure 5.1).

The cases where 3-D effects may have a significant impact on the FS include (Akhtar 2011):

1. slopes that are curved in plan view,
2. slopes that form corners,
3. slopes that have asymmetric geometries (geosynthetic liner system, drainage blankets, faults or rock joints),
4. slopes that have shear strength or piezometric conditions that vary in the direction perpendicular to direction of slide movement, and
5. slopes that are surcharged by localized loads or cut by excavation.

Existing 3-D slope stability analysis mainly emphasizes 3-D effect and boundary conditions or influence of the mesh size (Zettler et al. 1999; Chugh 2003; Shukha and Baker 2003; Griffiths and Marquez 2007; Wei et al. 2009; Akhar and Stark 2017; Lin et al. 2020), whereas the

effect of complex geometries on 3-D slope stability is rarely studied. Yet such geometries are relatively common in the open pit mining industry and decision on slope angles have major economic and safety impact. In the paper the terms of concave and convex corners will be used; they are illustrated in Figure 5.1.



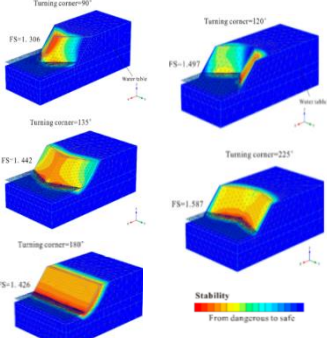
Figure 5.1 Convex shape of the pit wall. This “nose” shape is less stable than plane strain wall (reprinted from McQuillan et al. 2018)

The stability of slope corners has been studied from two points of view: open pit mining case history studies and numerical simulations. Piteau and Jennings (1970) studied five large diamond mines in South Africa with respect to the influence of plan view curvature. They found that the slope angle can be increased when the plan view radius of curvature decreases. Hoek and Bray (1981) summarized the slope design experience around the world and came to the conclusion that when the radius of curvature of a concave slope is less than the height of the slope, the slope angle can be 10° steeper compared with the angle obtained by conventional stability methods. For convex slopes with a plane curvature radius smaller than the slope height, the slope should be 10° flatter than the angle predicted by stability analysis. They also found that for radii of curvature in excess of twice the slope height, the slope angle given by a conventional stability analysis should be used for the open pit design.

In the past few decades, several researchers have studied the problem of slope corners using numerical simulations including 3D Finite Element Method (FEM) and Finite Difference Method (FDM). Table 5.1 summarizes the results and conclusions of some important studies undertaken in the area.

Table 5.1 Summary of significant studies on the FS for homogeneous slopes with turning corners

Who	Software	Type of corner	Illustration	What was found
Zettler et al. (1999)	Flack3D (3-D FDM)	3-D convex and concave corners with a 90° plan view angle and a relative curvature radius of the slope R/H=0.5		Showed that the FS for the concave structure is 30% higher than for the straight slope, but the convex slope is 3% less stable compare to the plane strain case
Wei et al. (2009)	Flack3D (3-D FDM)	3-D vertical cut slope with a 90°convex-turning		The slip surface is found to be composed of two 2-D failure modes for the convex corner
Nian et al. (2012)	Abaqus (3-D FEM)	3-D vertical convex and concave corners		Reported that the maximum horizontal displacement of a vertical 3-D slope is always located at the intersection of the turning corner line and the slope crest
Zhang et al. (2013)	Flac3D (3-D FDM)	3-D slopes with various geometries in terms of slope curvature, slope angle, and boundary conditions		It was found that for convex and concave corners the FS is maximum for 90° plan view angle and decreases approaching the 180° (3-D plane strain)
Sun et al. (2017)	Abaqus (3-D FEM)	3-D slopes with various geometries in terms of the relative curvature radius of the slope (R/H) and slope angle β		Proposed a set of charts for the estimation of FS of 3-D convex and concave homogeneous slopes in plan-view for a range of slope angles (β), relative curvatures of slope (R/H), and dimensionless strength parameters ($c/\gamma H \tan \phi$).

Zhou et al. (2020)	Plaxis3D (3-D FEM)	3-D slopes with various geometries in terms of slope curvature, slope angle, and boundary conditions		Proved that a concave slope can provide beneficial constraints, with each part divided by the axis of symmetry which is contributes to the higher stability of slopes with corner angles. It was also found that for concave and convex plan view angles the failure mass was divided into two parts by the axis of symmetry
--------------------	--------------------	--	--	--

Zettler et al. (1999), used the Flack3D software and, investigated a 2:1 slope with the height of 25 m and 90°convex- and concave-turning corners. He showed that the FS for the concave structure is 30% higher than for the straight slope, but the convex slope is 3% less stable compare to the plane strain case. It should be noted that the author compared the results obtained for a different radius of curvature (R) of concave (R=12 m) and convex (R=55.5m) corners.

Cheng and Yip (2007), Wei et al. (2009) and Nian et al. (2012) studied a vertical cut slope with a 90°convex-turning corner in their papers regarding the comparative analysis of different 3-D slope stability analysis methods utilizing 3-D limit equilibrium and shear strength reduction techniques. Wei et al. (2009) reported that for the vertical cut with two unconstrained vertical planes intersecting at 90°, the slip surface is found to be composed of two 2-D failure modes (Figure 5.2). The authors mentioned that it is difficult to determine a precise FS according to the classical concept of SRF for the slopes with complicated geometry and the new convergent criterion needs to be suggested.

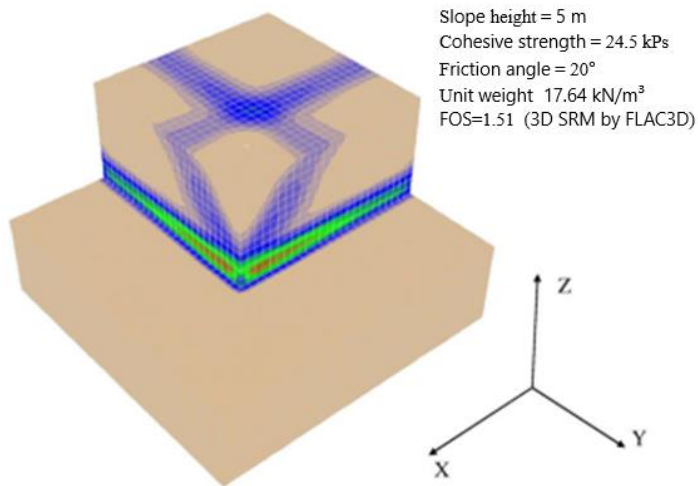


Figure 5.2 Slip surface of a vertical cut with two unconstrained vertical planes. The slip surface is found to be composed of two 2D failure modes (reprinted from Wei et al. 2009)

Nian et al. (2012) used the Abaqus software and found that the FS for the vertical convex and concave corner is 5% less and 8.5% greater compare to the FS for the 3-D plane strain slope respectively. They stated (Nian et al. 2012) that in the case of the convex corner the maximum horizontal displacement of a vertical 3-D slope is always located at the intersection of the turning corner line and the slope crest, which is the most dangerous zone and can be defined according to the maximum horizontal displacement and equivalent plastic strain contours. The authors concluded that a potential landslide can readily occur around this intersection region, therefore should be studied more closely. Based on their results, Nian et al. (2012) suggested using a straight vertical slope instead of a concave-shaped vertical slope with a 90° corner angle for computation of the safety factor the minimizing computational time and cost.

Using the strength-reduction method, Zhang et al. (2013) and Zhou et al. (2020) conducted a comprehensive study on 3-D slopes with various geometries in terms of slope curvature, gradient, and boundary conditions using Flac3D and Plaxis3D software consequently.

Zhang et al. (2013) found that for convex and concave corners the FS is maximum for 90° plan view angle and decreases approaching the 180° (3-D plane strain) which is not consistent with the results obtained by Zhou et al. (2020) (see Figure 5.3 and Figure 5.4). Zhang et al. (2013) also states that convex-turning slopes turning arc has insignificant influence on the FS (less than 2%) and the minor difference was obtained for concave-turning slopes (3-12%) compare to the FS of 3-D plane strain slope.

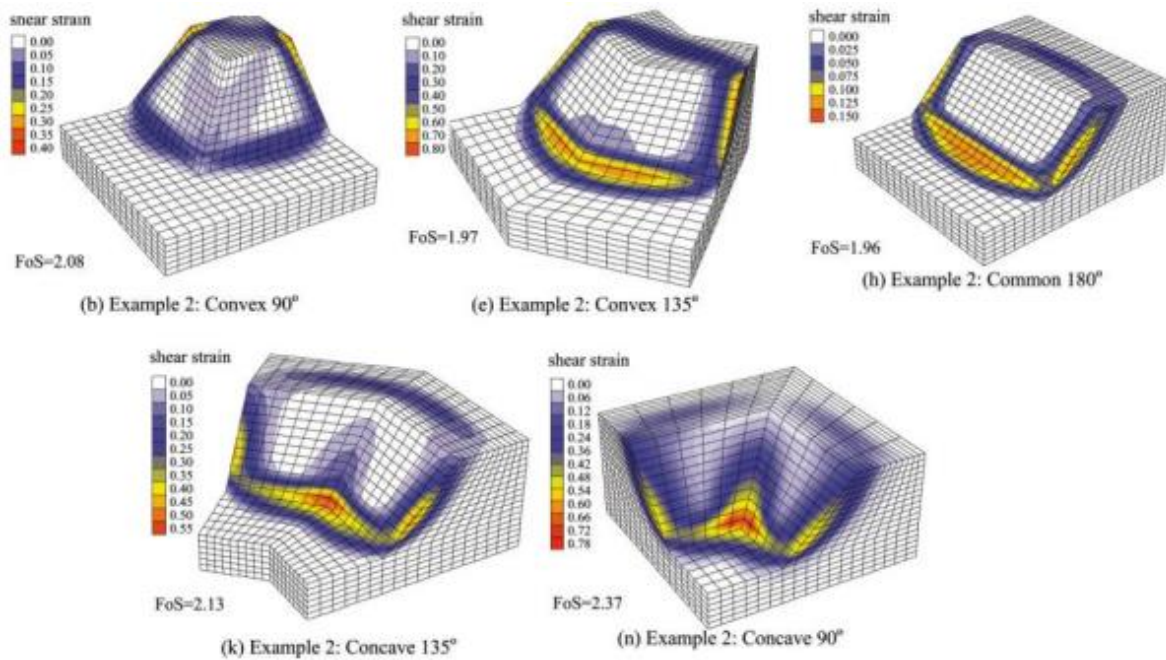


Figure 5.3 Shear strain contours of different turning corners with FS (reprinted from Zhang et al. 2013)

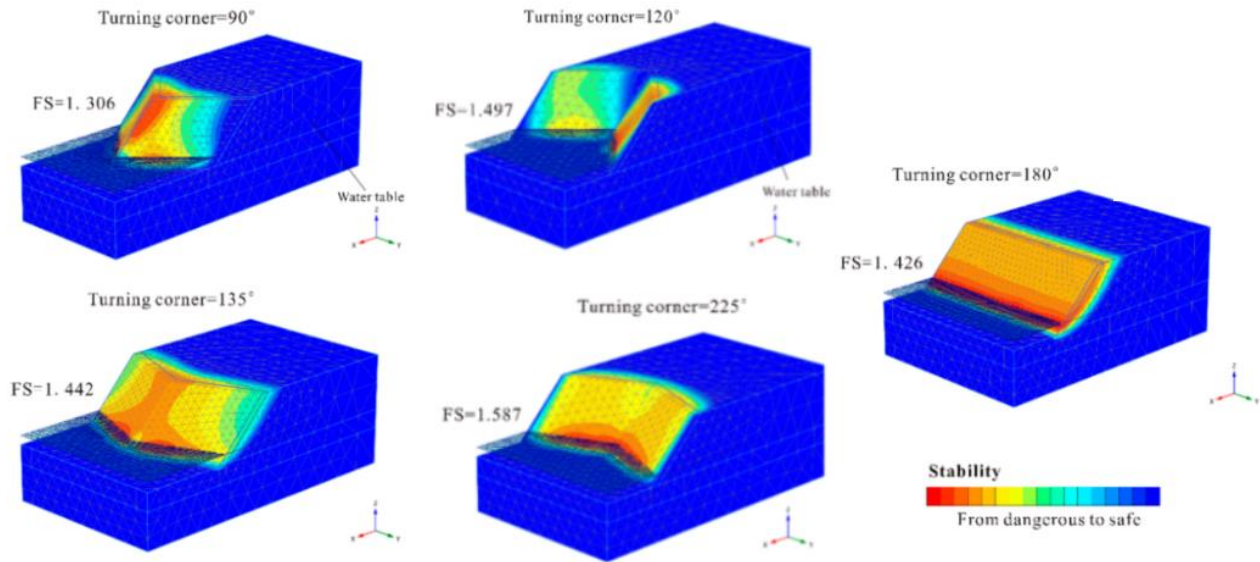


Figure 5.4 The failure mechanism of convex- and concave-shaped slopes with different corner angles and FS (reprinted from Zhou et al. 2020)

Zhou et al. (2020) showed that a concave slope can provide beneficial constraints, with each part divided by the axis of symmetry which contributes to the higher stability of slopes with corner angles. It was also found that for concave – and convex plan view angles the failure mass was divided into two parts by the axis of symmetry. Zhou et al. (2020) also compared the potential failure mechanism of the three slopes with 90° corner angles: H2:V1, H1:V1, H1:V2, and made a conclusion that the slip surface became deeper and wider as the slope angle increased.

Sun et al. (2017) proposed a set of charts for the estimation of FS of 3-D convex-shaped and concave-shaped homogeneous slopes in plan-view for a range of slope angles (α), relative curvatures of slope (R/H), and dimensionless strength parameters ($C/\gamma H \tan \phi$). A 3-D effect for convex and concave corners was studied using the finite-element (FE) software Abaqus 6.10

In engineering practice, concave-shaped slopes always show better stability than convex-shaped slopes. In the mining industry, convex slopes with small turning corners tend to be avoided since they are prone to deformations and slope failures (Figure 5.5). Meanwhile, the slope has to

be maintained to balance between safety and economy to determine the location and the slope angle at the preliminary design stage of the project. The effect of complex geometries on 3-D slope stability is still not very clear, but it is important in slope engineering, especially in the safe and economical design of open pit infrastructure. In the paper the terms of concave and convex corners will be used; they are illustrated in Figure 5.5 and 5.6.



Kalgoorlie gold mine (Australia)
(reprinted from Basov, 2020)



Boron mine (USA)
photo from a public source Valley Press Staff, 2019)



Savage River mine (Australia)
(reprinted from Hutchison and Widehki, 2007)



Highland Valley Copper Mine (USA)
(reprinted from Brouwer, 2016)



Sandsloot mine (South Africa)
(reprinted from Bye and Bell, 2001)

Figure 5.5 Examples of concave and convex shapes in open pit mining

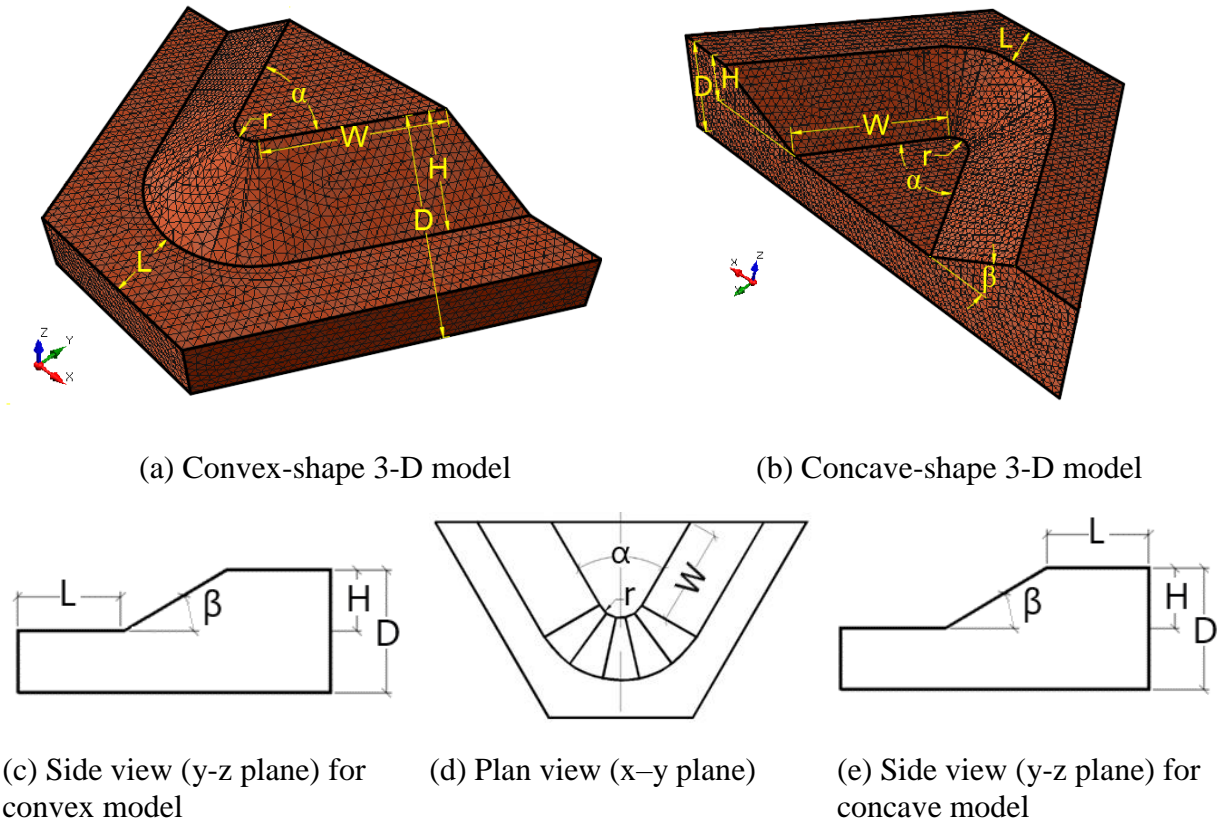


Figure 5.6 Typical shapes and parameters of convex and concave 3-D models

5.1.2 Parameters for various corner configurations

The effects of complex geometries on 3-D slope stability using an elastoplastic FE method with a strength reduction technique are analyzed in the present work. A series of special 3-D slope models with various geometric configurations (Figure 5.6), including turning concave and convex corners with different plan view radii of curvature of the slope crest, are presented in terms of FS, the value of the displacement, and the shear slip surface.

The first step was to define optimum parameters for the model geometry. The following parameters were picked arbitrary: height of the slope, H (m), the height of the model, D (m), slope angle, β ($^\circ$), plan view angle, α ($^\circ$), and radius of curvature, r (m) (Table 5.2).

Table 5.2 Studied cases

Convex																				
	α (°)	30				60				90				120				150		
β (°)	15	25	35	45	15	25	35	45	15	25	35	45	15	25	35	45	15	25	35	45
r (m)	1	1	1	1	1	1	1	1	1	1	1	1	1	1	1	1	1	1	1	1
	5	5	5	5	5	5	5	5	5	5	5	5	5	5	5	5	5	5	5	5
	10	10	10	10	10	10	10	10	10	10	10	10	10	10	10	10	10	10	10	10
	15	15	15	15	15	15	15	15	15	15	15	15	15	15	15	15	15	15	15	15
H (m)	15				15				15				15				15			
W (m)	40				40				40				40				40			
D (m)	30				30				30				30				30			
L (m)	15				15				15				15				15			
α (°)	210				240				270				300				330			
Concave																				

The researcher considered six 3-D plane strain models with a slope high of $H=15$ m and a slope angle of $\beta=45^\circ$ for the shoulder width W (m) evaluation. The parameter W was increased until the FS for the model gave the same factor of safety as the 2-D plane strain FS, Figure 5.7 shows the factor of safety for the 3-D FEM case, $FS_{3D\ FEM}$, normalized with respect to the 2-D factor of safety, $FS_{2D\ FEM}$, as a function of the ratio W/H . The figure indicates that when $W/H \geq 2.65$, $FS_{3D\ FEM}$ approaches $FS_{2D\ FEM}$ and thus that W is large enough. For all other FEM simulations, the width W of the shoulder was taken as $W = 40$ m or greater.

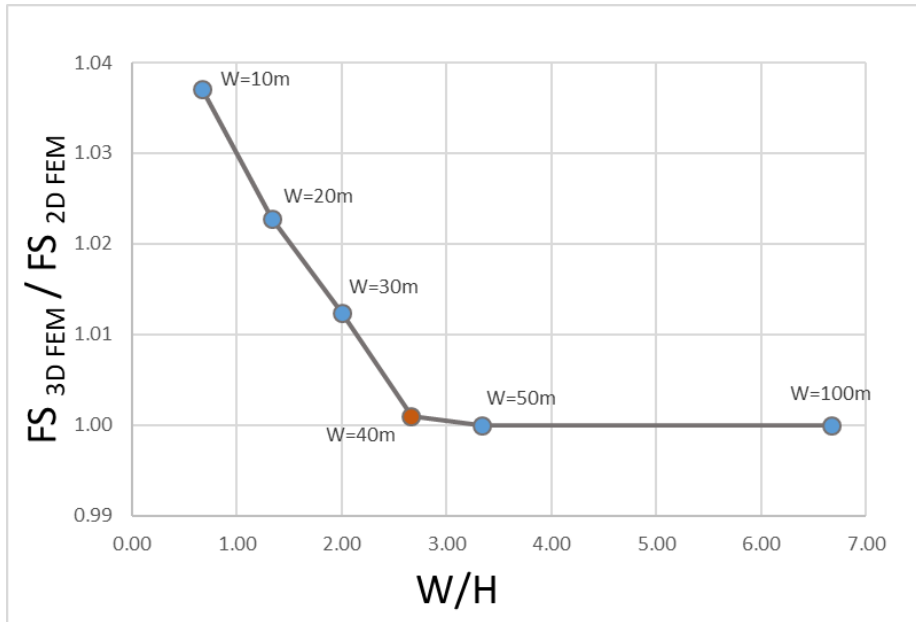


Figure 5.7 Variation of the normalized 3-D FS with respect to W/H ratio. Homogenous slope, $\gamma=20 \text{ kN/m}^3$, $c=10 \text{ (kPa)}$, $\phi=30^\circ$, $\psi=0^\circ$, $E=30 \text{ MPa}$, $\nu=0.28$

The parameter L, distance from the crest to the model's backside L (m) was varied next and its influence on the FS was studied. Figure 5.8 shows that even for values as small as 7.5 m, the value of L does not affect the FS. The value of L was chosen arbitrarily as 15 m.

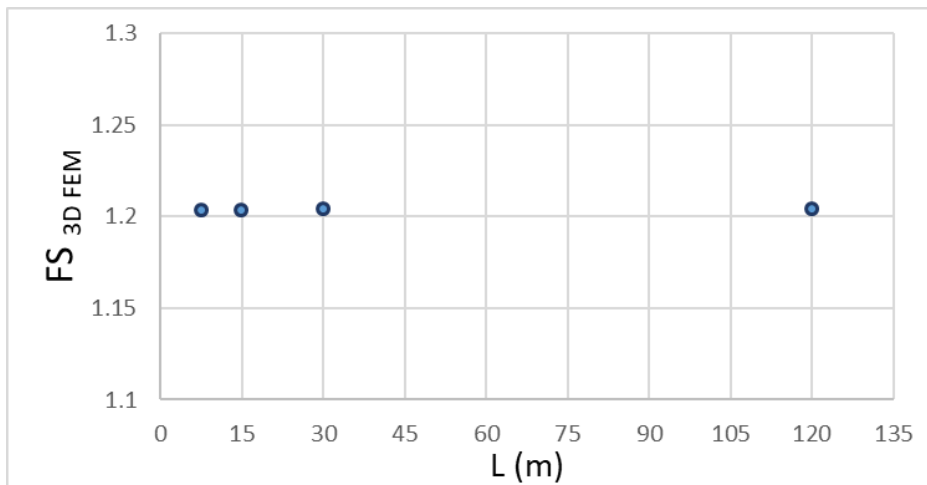


Figure 5.8 Variation of the FS with respect to distance from crest to the back side of the model, L (m). Homogenous slope, $\gamma=20 \text{ kN/m}^3$, $c=10 \text{ (kPa)}$, $\phi=30^\circ$, $\psi=0^\circ$, $\nu=0.28$.

During the presented research, more than 170 3-D FEM simulations were performed. All of the 3-D models with various geometry presented in Table 5.2 were calculated, and the results are discussed in detail.

5.1.3 Mesh and boundary conditions

The mesh size and the number of elements in the model affect the result's accuracy and computational time (Griffiths and Marquez 2007; Nian et al. 2012; Zhang et al. 2013; Camargo et al. 2016; Zhou et al. 2020). For example, FE models with a fine mesh (small element size) lead to highly accurate results but may take a longer computing time. On the contrary, those FE models with coarse mesh (large element size) may lead to less accurate results but save more computing time.

Due to its importance in generating FE models, the foremost problem is to choose the appropriate element size so that the created models will yield accurate FE analysis results while saving as much computing time as possible.

The 3-D plane strain model was used to reveal the effects of the element size on the finite element simulation results' accuracy. A nonlinear relationship between the number of elements and the FS is plotted in Figure 5.9. As can be seen, the influence is not very significant (about 7.5% for the range of 6500 to 900,000 elements) and with 200,000 elements the difference is down to about 0.5%. This is consistent with what others have found (Zettler et al. 1999, Zhang et al. 2013, Camargo et al. 2016).

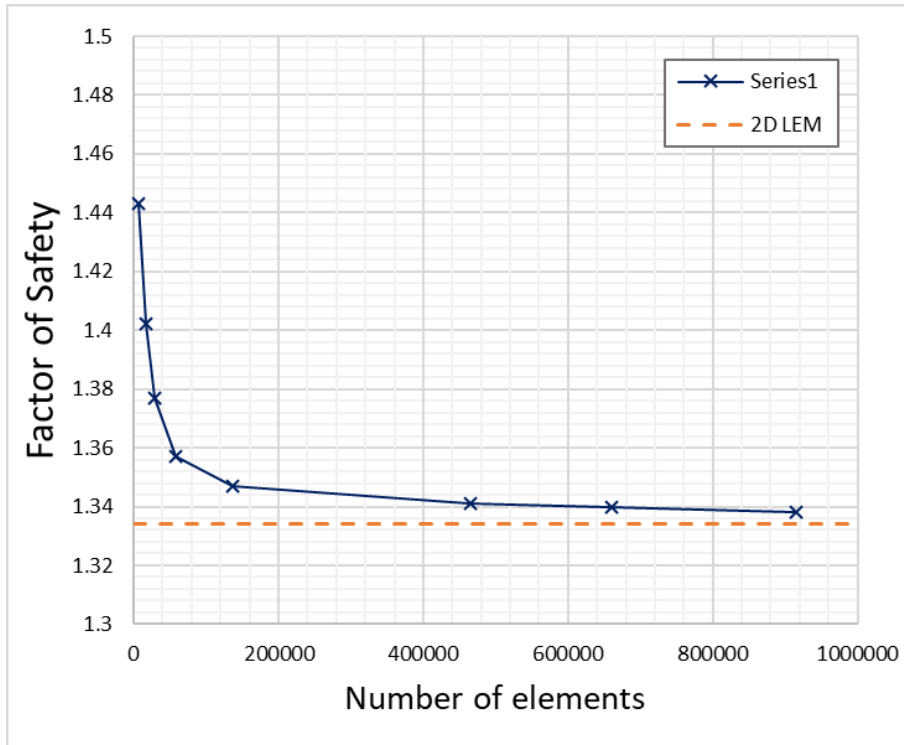


Figure 5.9 Influence of mesh size on FS

The element size also affects the accuracy of the critical slip surface prediction (Ching and Phoon 2013, Cheng et al. 2018). The smaller is the element size, the smoother is the obtained slip surface and the closer to the real value is the obtained failed mass (Figure 5.10).

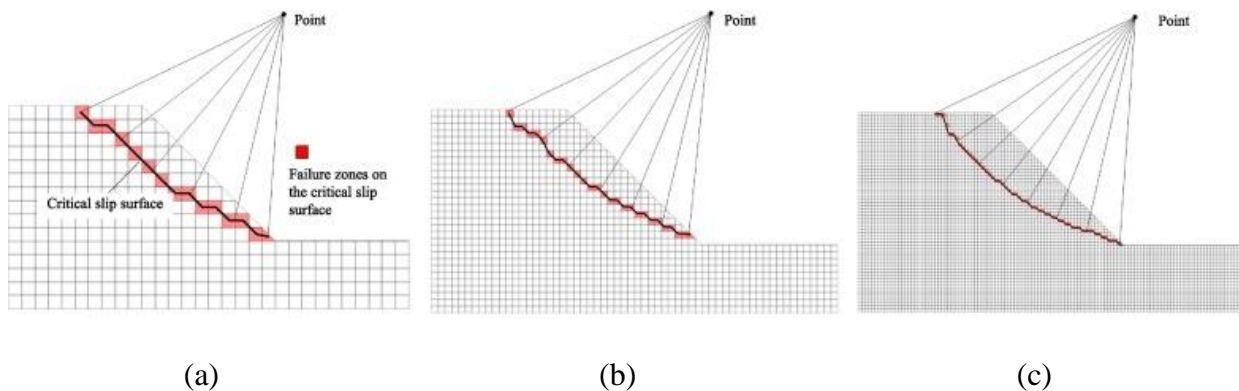


Figure 5.10 Effect of element size on the critical slip surface: a) element size – 1.0m, b) element size – 0.5m , c) element size – 0.25 m (reprinted from Cheng et al. 2018)

The influence of the refinement of the mesh on the location and shape of the failure surface was also investigated. Figure 5.11 shows the evolution of that shape as the number of element is increased. As can be seen, the shape does not changed markedly beyond 60,000 elements.

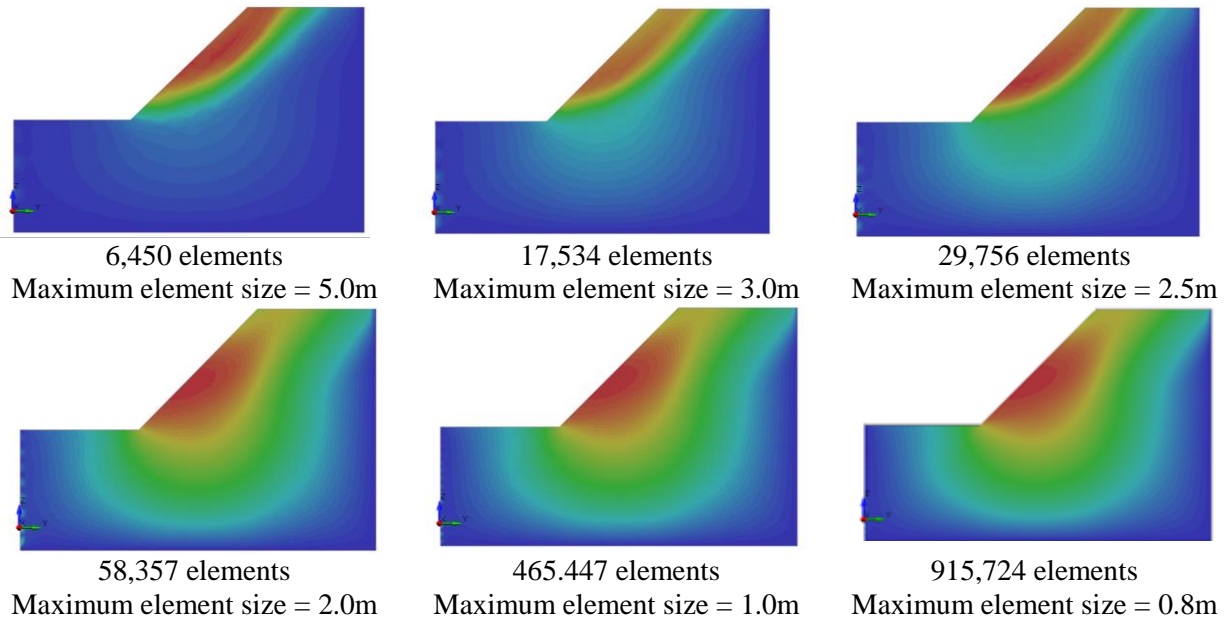


Figure 5.11 The failure shape variation due to the size of the mesh element

The decrease in the element size initiates the increase in the computational effort. Therefore, the element size should be refined to obtain higher computational accuracy within an acceptable computational effort. Considering the result in Figure 5.9 and Figure 5.11, a total of 200,000 elements was selected, which led to the biggest element being a 1.5 m size tetrahedron element (m). Despite the maximum size of the element was set to 1.5m, but because of the graded mesh type, the nasal shape of the models was automatically discretized by the elements with a size up to 0.2 m (Figure 5.6a and 5.6b).

Boundary conditions also affect the stresses computations in finite element analyses. For a 3-D slope with any complex shape, boundary surfaces can be generally one of the following four types: (1) bottom surface, (2) front surface, (3) back surface, and (4) side surface (Figure 5.12a).

For all plane strain 3-D analyses presented below, infinite boundaries were modeled by constraining displacement normal to the boundary while allowing free movement parallel to the boundary, i.e., ‘roller’ constraints (Figure 5.12b).

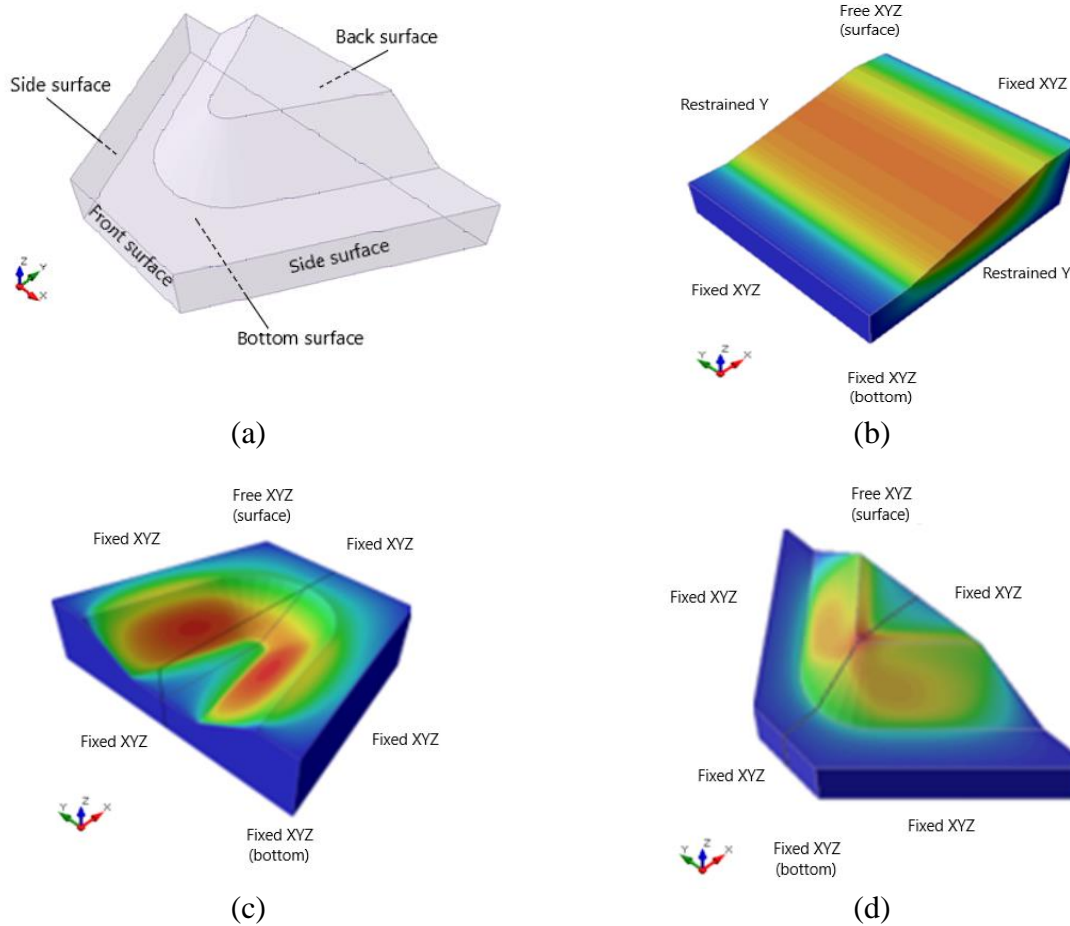


Figure 5.12 Boundary conditions: (a) general model, (b) plane strain case, (c) concave-shaped corner, (d) convex-shaped corner

Usually, all movements are restrained in the bottom plane of a model (i.e., $u_x, y, z = 0$, where u is the displacement); front-surface and back-surface types are restrained in the normal direction but are free to move in the dip and strike directions. Thus, different side surface conditions embody different boundary conditions. As in most literature about 3-D FEM or FDM slope stability analysis (Zettler et al. 1999; Chugh 2003; Griffiths and Marquez 2007; Nian et al.

2012, Zhang et al. 2013), the side-surface boundary conditions can be generally classified into three types:

a) All side surfaces are restrained in the normal direction but a free to move in the dip and strike directions

b) Half of the side surfaces are restrained in the normal direction but are free to move in the dip and strike directions; the other half of the side surfaces are restrained in all three directions: normal, dip, and strike.

c) All side surfaces are restrained in all three directions: normal, dip, and strike.

Combining the practices in the studied models to reduce calculation time and determine the actual slope failure mechanism at the turning corner, the front, back, bottom, and side surfaces were restrained in all directions for convex- and concave-shaped models

5.1.4 Role of convergence criteria and parameters

The choice of convergence criteria also needs to be considered in the calculations using the FE method. It is important to establish a combination of convergence method, tolerance value, and a number of iterations that provided ‘accurate’ and ‘reliable’ results. According to Rocscience (2021) the convergence of a finite element solution is characterized by three attributes:

a) the type of stopping criterion

b) the tolerance value of the stopping criterion, and

c) the number interactions allowed before a solutions is assesses to have not converged.

The definition of convergence and the finite element solution process can be explained with the simple case of a single force applied to a non-linear spring (Rocscience 2021a). For static finite element analysis, the equation representing equilibrium can be written in the following matrix form:

$$K \cdot \Delta u = P - F \quad \text{Eq. 5.1}$$

where P is the vector of applied loads; F is the vector of internal forces; Δu is the vector of current nodal displacements, and K is a non-linear stiffness.

FE analysis involves solving the equation for Δu , and for the n -th load step, the equation is often solved through iterations ($i=0, 1, 2, 3, \dots$) of the form:

$$K \cdot \Delta u_{(i-1)} = P_{(n)} - F_{(i)} \quad \text{Eq.5.2}$$

To calculate the current displacement increment $\Delta U_{(1)}$ and update the solution:

$$K_{(0)} \cdot \Delta u_{(1)} = P_{(n+1)} - F_{(0)} \quad \text{Eq.5.3}$$

$$\Delta u_{(1)} = \frac{P_{(n+1)} - F_{(0)}}{K_{(0)}} \quad \text{Eq.5.4}$$

$$u_{(n+1)} = U_{(n)} + \Delta u \quad \text{Eq.5.5}$$

The finite element solution process and the definition of convergence are best explained with the simple case of a single force applied to a non-linear spring (Figure 5.13).

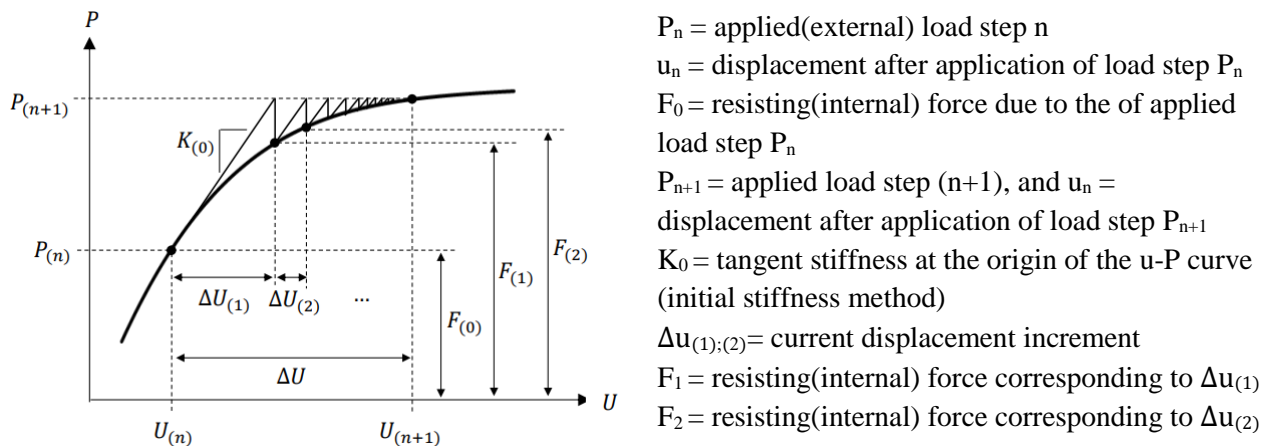


Figure 5.13 The iterative finite element procedure for determining the spring's behavior under applied loads (reprinted from Rocscience 2021a).

From the current displacement state $u_{(n+1)}$ the internal force $F_{(1)}$ can be calculated, and the load imbalance $(P_{(n+1)} - F_{(1)})$ is estimated. There is an equilibrium state if the external load

$P_{(n+1)}$ is equal to the internal force $F_{(i)}$. The key aim of the iterations is to reduce the load imbalance to zero ($P_{(n+1)} - F_{(i)} \rightarrow 0$) to reach the equilibrium. Therefore the aim of the FE calculations is the displacement increments goes to zero ($\Delta u_{(i)} \rightarrow 0$).

The role of convergence parameters was studied by Hammah et al. (2005). Three different stopping criteria – displacement, residual force, and energy were compared using 2-D FE software. In finite element analysis the displacement convergence criterion is met for a current iteration when increments in displacement are negligible. Residual force convergence is satisfied when residual force change is negligible for a current configuration. The energy convergence stopping rule is a measure of energy balance in the system being solved, and is satisfied when the imbalance falls below a specified value (Hammah et al. 2005; Rocscience 2021a).

After several tests involving numerous different models (Hammah et al. 2005), the energy norm criterion proved to be the most robust stopping rule due to the fact that it has the least sensitivity to model attributes. It was also established that a tolerance of 0.001 combined with >300 iterations produced consistently good results in an acceptable time.

For this study, the energy balance criterion was selected along with a tolerance of 0.001 for stresses and 0.001 for the SRF, and 500 iterations.

5.1.5 Soil model

As it was mentioned before, numerical models divide the studied mass into elements. Each element is assigned a material model and properties. To model the material mass using the FE software, the program utilized the six main parameters presented below:

- Unit weight, γ (kN/m³)
- Friction angle, ϕ' (°)
- Cohesion, c' (kPa)

- Dilation angle, ψ ($^{\circ}$)
- Young's modulus, E (kPa)
- Poisson's ratio, ν

All simulations assumed dry conditions, no external load at the top of the slope, and no seismicity loading to minimize the complexity of the problem.

In the current research, the material models are idealized stress/strain relations is a linear elastic plastic soil model, which uses the elastic properties (Young's modulus and Poisson's ratio), as well as the three key parameters of the material: the total unit weight γ and the shear strength parameters ϕ' and c' (or $\phi_u = 0$ and c_u in undrained analysis). Because the elastic parameters (Young's modulus and Poisson's ratio) have little influence on the FS (Griffiths 2001; Hammah et al. 2005), they were assigned reasonable values of $(3 \cdot 10^4)$ kN/m² and 0.28 respectively for all the performed simulations.

Two basic parameters can be obtained by performing the finite-element calculation: factor of safety and displacement (m). The resultant total displacement u_t (m) is defined as:

$$u_t(m) = \sqrt{u_x^2 + u_y^2 + u_z^2} \quad \text{Eq.5.6}$$

where u_x – displacement in x-direction, u_y – displacement in y-direction, and u_z -displacement in z-direction.

The reference point where the values of the total displacement for convex and concave corner was collected is presented in Figure 5.14.

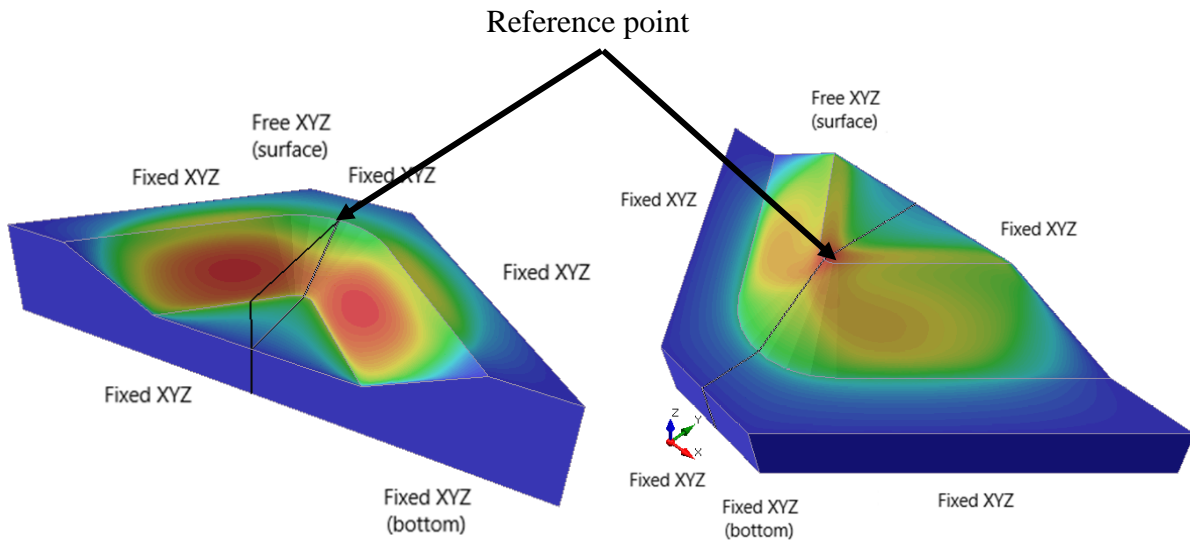


Figure 5.14 Location of the reference point for data collection

The impact of dilation angle was tested on case of homogeneous slope with $E=(3 \cdot 10^4)$ kPa and Poisson's ratio $\nu=0.28$. Five different dilation angles were considered $\psi=0^\circ, 5^\circ, 10^\circ, 12^\circ,$ and 15° . The results are presented in terms of normalized FS ($FS_{(\psi=i)}/FS_{(\psi=0)}$) (Figure 5.15) and in terms of the normalized total displacement at the tip of the slope crest ($u_t(\psi=i)/u_t(\psi=0)$) (Figure 5.16).

Figure 5.15 presents the normalized FS versus the dilation angle, ψ ($^\circ$). On the vertical axis, the FS is normalized by the value of the FS for the case with $\psi=0^\circ$. Factors of safety ranged from 1.344 to 1.421. These minimum and maximum values were less than 7% away from the limit-equilibrium benchmark value of 1.329.

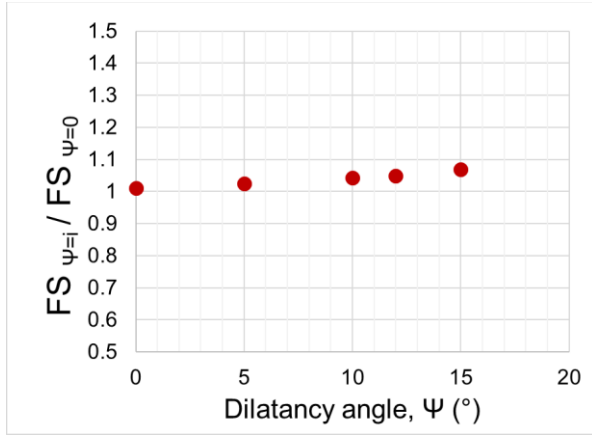


Figure 5.15 The impact of the dilation angle on the slope stability result for a homogeneous slope with $E=30$ MPa and $\nu=0.28$. Normalized FS vs. Dilation angle.

Variation of the normalized total displacement with respect to the dilation angle is presented in Figure 5.16. The total displacement value is varied within 2% from the reference value of the total displacement for the plane strain case. This finding confirms that, as indicated by other researchers (Griffith and Lane 1999, Griffiths 2001, Hammah et al. 2005), the dilation angle does not significantly impact slope problems due to the generally low confinement environment. Therefore, the dilation angle has been set to zero in this study, suggesting no volume change during output.

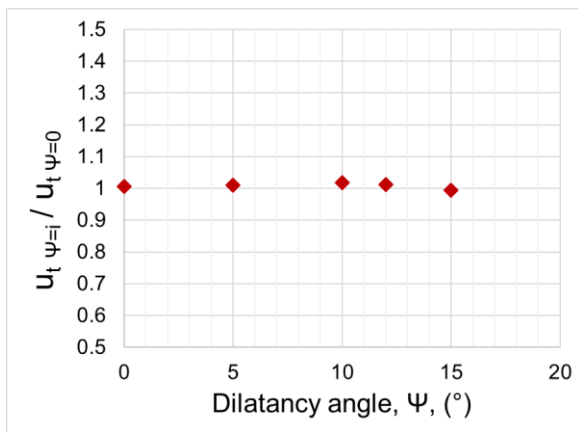


Figure 5.16 The impact of the dilation angle on the slope stability result for a homogeneous slope with $E=30$ MPa and $\nu=0.28$. Normalized total displacement vs. Dilation angle (°).

The FEM code was used to carry out the computation. The three-dimensional analysis of elastic, perfectly plastic soils with a Mohr–Coulomb yield criterion (Figure 5.17) combined with the non-associative flow rule (dilation angle $\psi=0^\circ$, and the residual strength parameters are equal to the peak parameters) was performed in the present work.

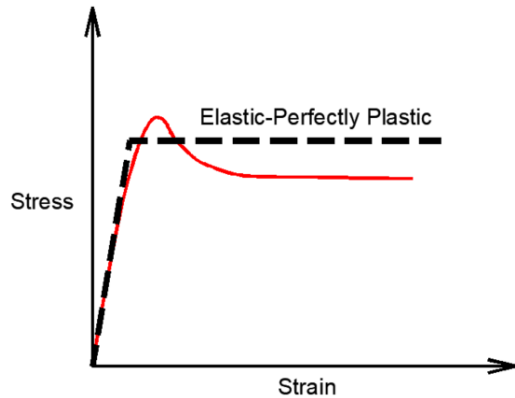


Figure 5.17 Elastic-perfectly plastic assumption for Mohr-Coulomb model

The Mohr-Coulomb failure criterion is the most common failure criterion encountered in geotechnical engineering (Hoek and Bray 1984; Read and Stacey 2009) The Mohr-Coulomb criterion describes a linear relationship between normal and shear stresses (or maximum and minimum principal stresses), in which the peak shear strength is given by Eq. 5.7:

$$\tau = c' + (\sigma - u_w) \tan \varphi' \quad \text{Eq. 5.7}$$

where τ is the peak shear strength, c' is the effective stress cohesion, σ is the total normal stress, u_w is the water pressure, and φ' is the effective stress friction angle. In slope stability analysis using the Finite Element Method with Shear Strength Reduction, the factored shear strength can be calculated by applying the Strength Reduction Factor the shear strength defined in equation (Eq. 5.8).

$$\frac{\tau}{SRF} = \frac{c' + (\sigma - u_w) \tan \phi'}{SRF} \quad \text{Eq. 5.8}$$

The factored Mohr Coulomb properties after the application of SRF can be defined as:

$$c'_r = \frac{c'}{SRF} \quad \text{Eq. 5.9}$$

$$\tan \phi'_r = \frac{\tan \phi'}{SRF} \quad \text{Eq. 5.10}$$

Figure 5.18 presents a graphical interpretation of a Mohr-Coulomb criterion drawn in shear-normal stress space, and the resulting curve when the envelope is reduced by a shear strength reduction factor.

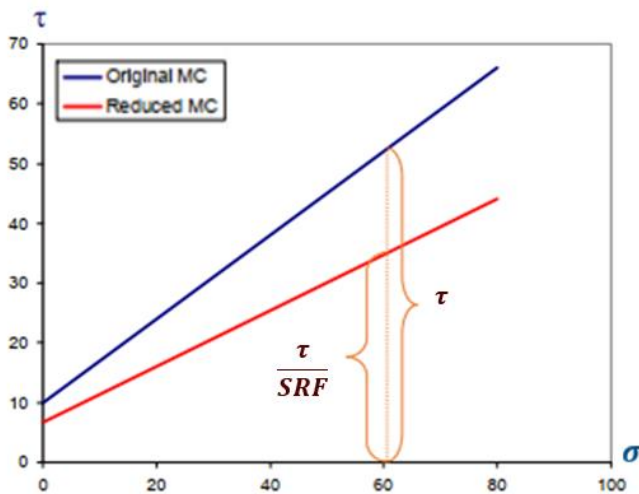


Figure 5.18 A Mohr-Coulomb criterion drawn in shear-normal stress space, and the resulting curve when the envelope is reduced by a shear strength reduction factor (reprinted from Yacoub 2016)

An example of the shear stress reduction solution using the FE method (RS3, Rocscience Inc.) is presented in Figure 5.19. Maximum total displacement u_t (m) is plotted on the horizontal axis and the value of the SRF on the vertical axis. As the SRF is increased, the strength properties are decreased. With the decrease in strength, the maximum displacement increases. At some point, the slope will fail, deformations will increase rapidly (e.g., four red points on the graph), and the

finite-element analysis will not converge. It is this point of non-convergence that defines the critical SRF. The critical SRF for the current example is 1.346, as is shown in Figure 5.19.

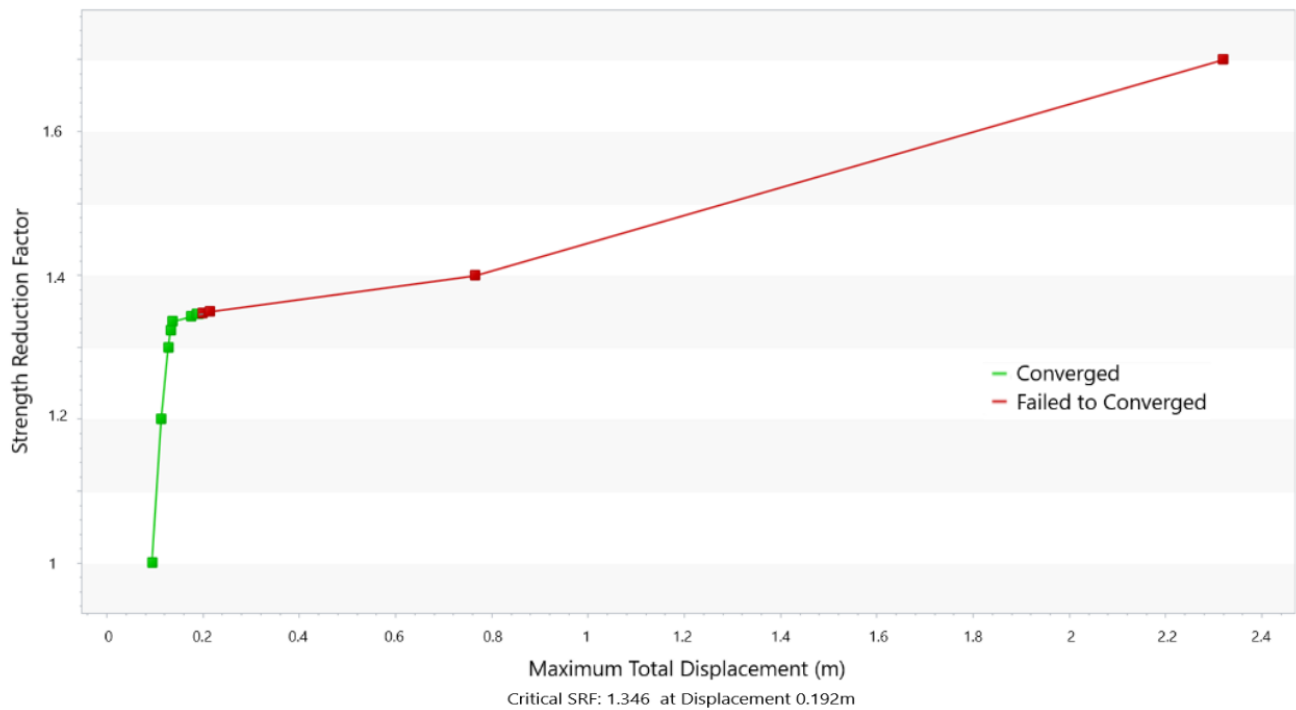


Figure 5.19 The shear stress reduction solution using FE method (Software: RS3) (reprinted from Rocscience 2021b)

5.1.6 Displacement based approach to corner stability

The two main parameters which were obtained from the finite-element calculations were the FS and the total displacement u_t , (m) at the corner of the crest of the slope (Figure 5.14). The first step of the presented research was to run all the convex- and concave-shaped corners using the 3-D FEM software (RS3, Rocscience Inc.) and collect the FS and u_t , (m).

The normalized total displacement was defined as the ratio of the normalized total displacement was defined as the ratio of 3-D total displacement at the crest of the corner over the 2-D total displacement $\left(\frac{u_t(3D\ FEM\ corner)}{u_t(2D\ FEM)}\right)$. The normalized FS was defined as the ratio of 3-D FS over

2-D FS $\left(\frac{FS_{(3D\ FEM\ corner)}}{FS_{(2D\ FEM)}} \right)$. A plot of normalized total displacement vs. normalized FS is presented in

Figure 5.20 for many different convex and concave corners. As can be seen for the 3D analysis of corners, the FS changes very little (~1%) while the displacement changes a lot. The possible reason the FS does not change is that the FEM technique is unable to identify the local zone at the corner of the two slopes. Instead, the SSR method seems to concentrate on the global failure zone associated with the plane strain case on either side of the corner. This appears to be a limitation of the FEM/SSR method. For this reason, the decision was made to evaluate the slope corners' behavior by using a displacement-based approach rather than an FS approach.

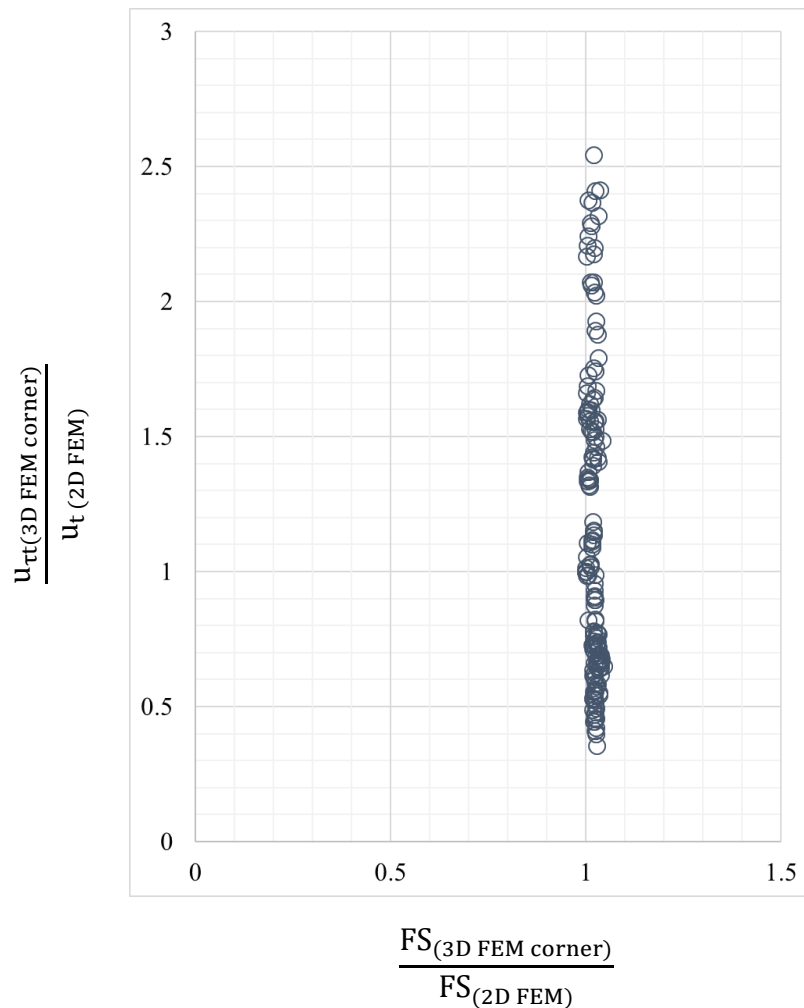


Figure 5.20 Normalized total displacement vs. normalized FS for the performed corner stability simulation

The first and simplest case was to consider a 15 m high homogeneous slope with different slope angles $\beta = 15^\circ, 25^\circ, 35^\circ, 45^\circ, 50^\circ$ and 60° . The purpose was to determine the variation of the total displacement for the different FS. A general 3-D slope model (Figure 5.21a) was constructed by extending the 2-D model presented in Figure 5.21b. The analysis made use of three different sets of strength parameters shown as model-1, model-2, and model-3 in Table 5.3.

As can be seen in the table, the unit weight, cohesion, friction angle, dilation angle, and Poisson's ratio had the same values in all three models while the Young's modulus varied. Each model had the same boundary conditions: bottom side and both front and back sides are restrained in all x-, y-, and z-directions, the left and right are allowed to move freely in the x- and z-directions, but not in the y-direction, the upper side is free. The FS for slopes was calculated based on the Mohr-Coulomb failure criterion.

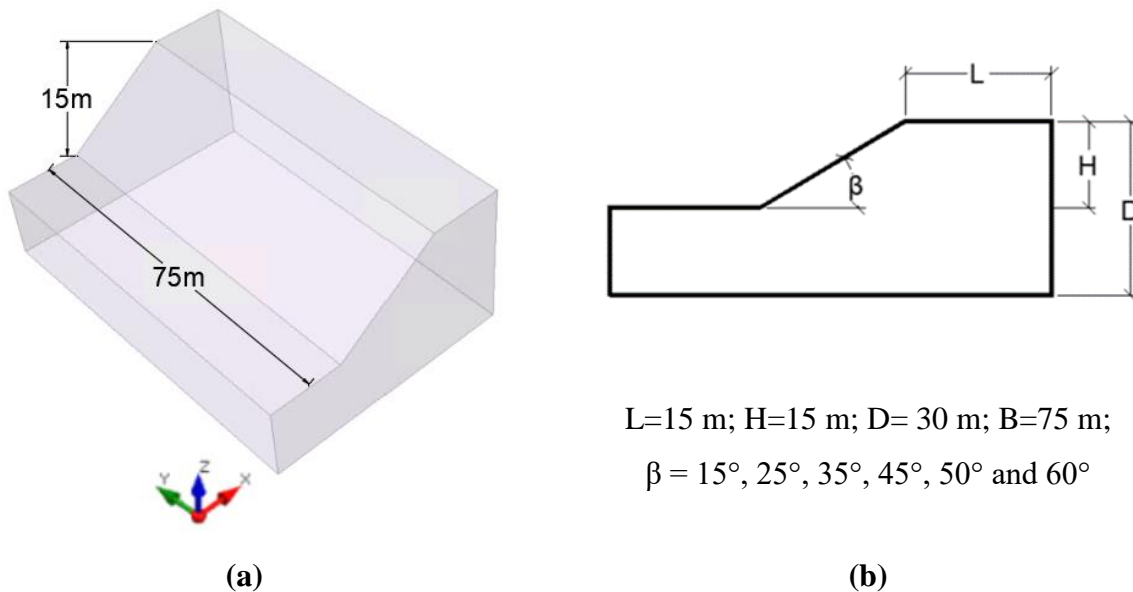


Figure 5.21 3D slope conceptual model: (a) 3D slope sketch; (b) side view (x-z plane)

Table 5.3 Material properties

Material properties	Model 1	Model 2	Model 3
Unit weight, γ (kN/m ³)	20	20	20
Cohesion, C (kPa)	10	10	10
Friction angle, ϕ (°)	30	30	30
Dilation angle, ψ (°)	0	0	0
Young's modulus, E (kPa)	50000	30000	10000
Poisson's ratio, ν	0.28	0.28	0.28

The sixteen RS3 models were run using the different strength parameters given in Table 5.3. Variation of the total displacement with respect to the FS for material model-1, -2 and -3 is presented in Figure 5.22, Figure 5.23, and Figure 5.24 respectively. The figures show that the total displacement is inversely proportional to the FS.

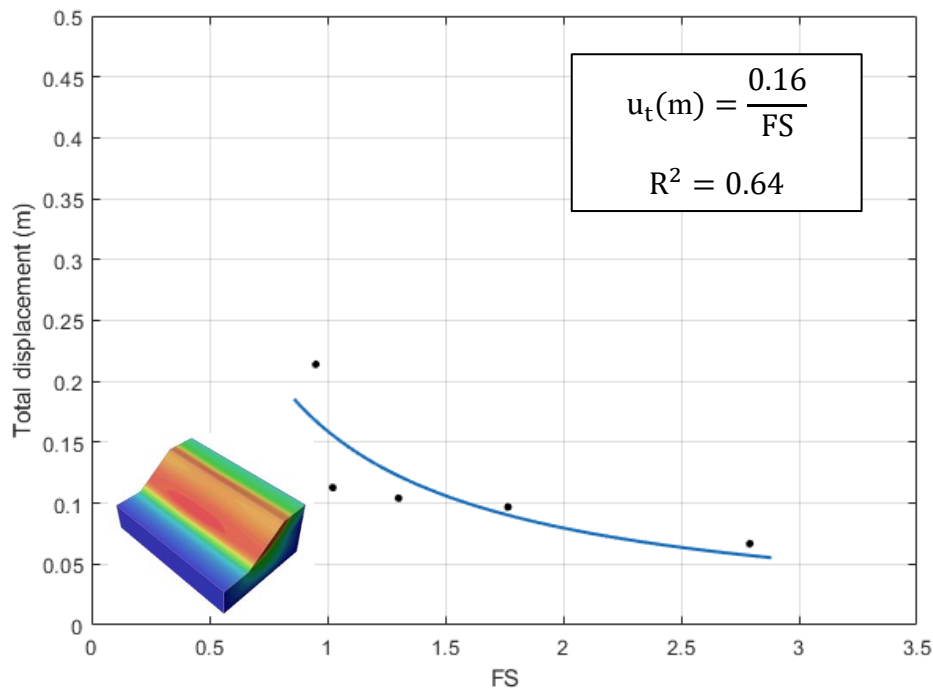


Figure 5.22 Variation of the total displacement with respect to the FS (E=50,000 kPa)

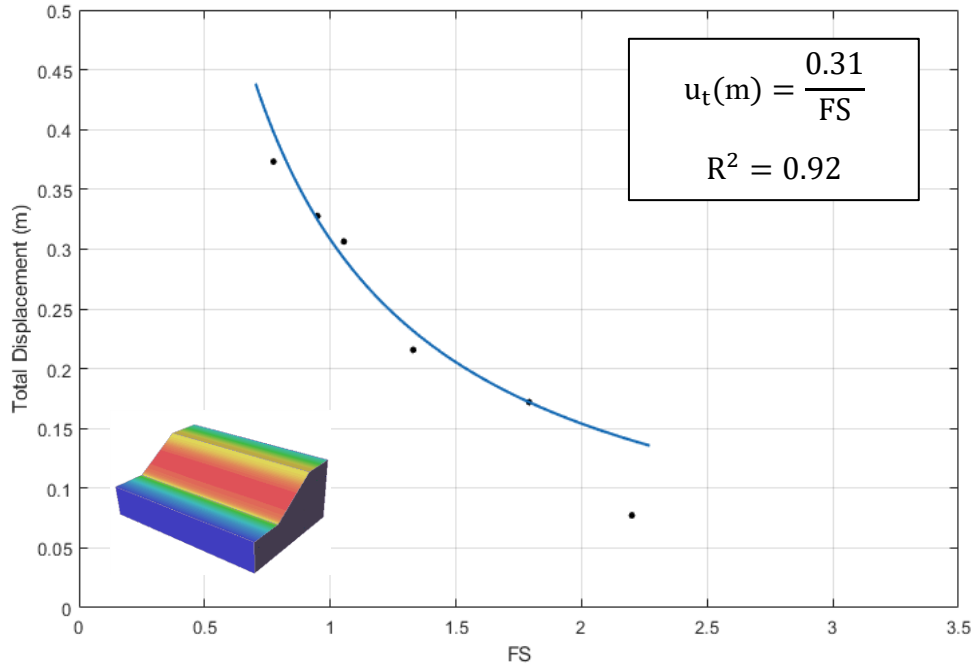


Figure 5.23 Variation of the total displacement with respect to the FS (E=30,000 kPa)

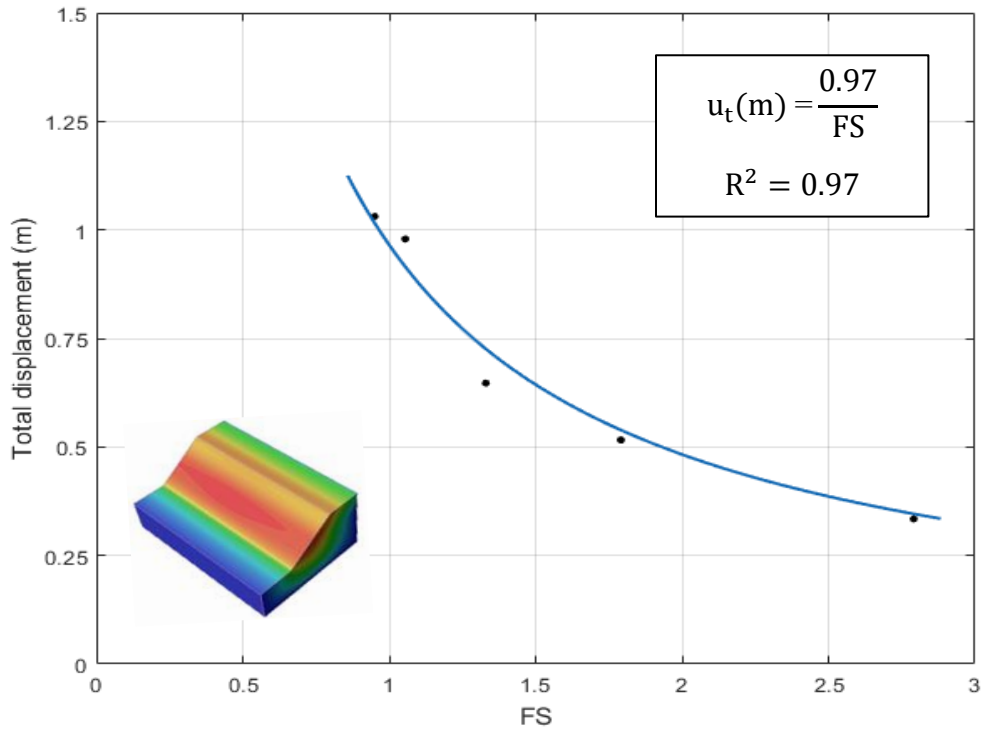
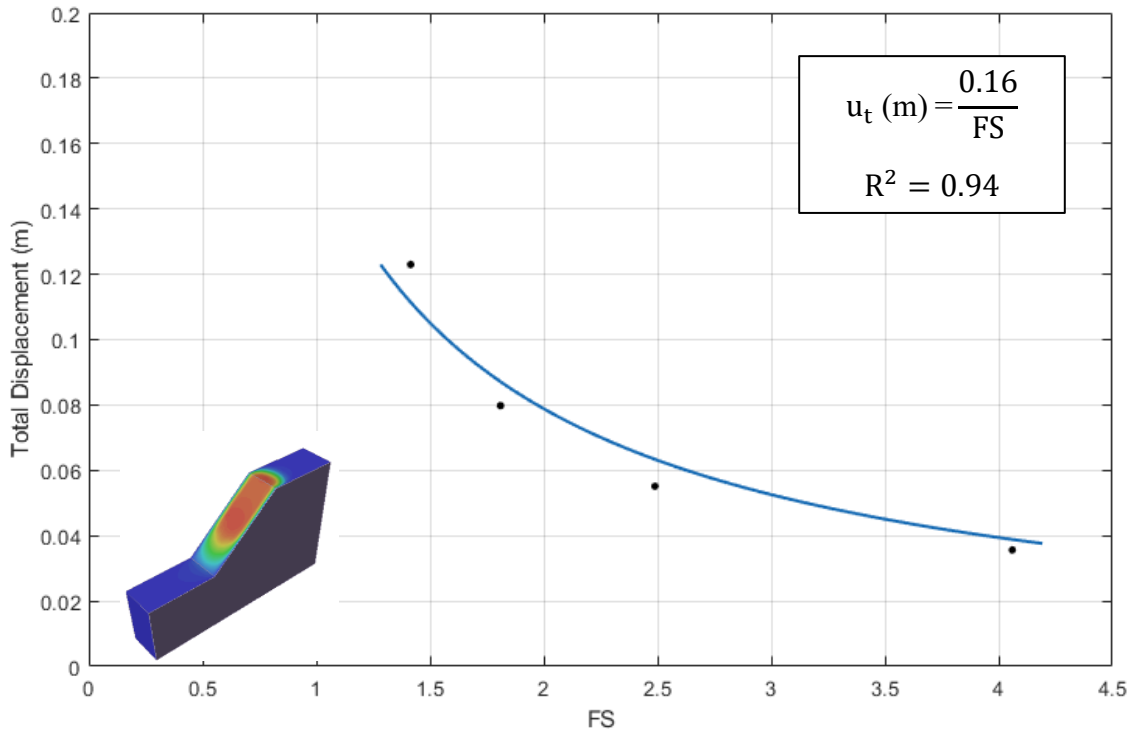


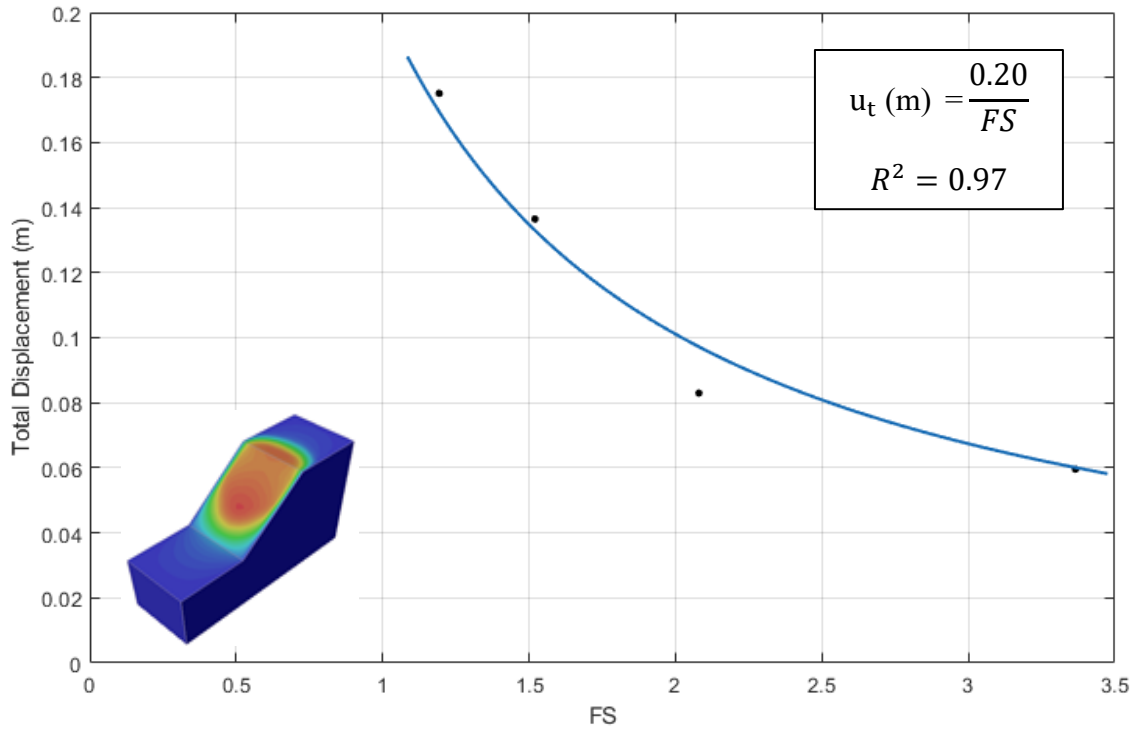
Figure 5.24 Variation of the total displacement with respect to the FS (E=10,000 kPa)

The previous results were obtained for a W/H ratio of 5. The variation of the total displacement with respect to the FS was also determined for smaller W/H ratios (W/H = 0.5, 1, 2, and 3). The slope geometry and soil parameters were kept the same: 15 m slope height and slope angles $\beta = 15^\circ, 25^\circ, 35^\circ$ and 45° . The input parameters are presented in Table 5.3. All models are characterized with the same boundary conditions: front, back, bottom, left, and right sides are restrained in all x-, y-, and z-directions, the surface side is restrained free. The FS for slopes was calculated based on the Mohr-Coulomb model.

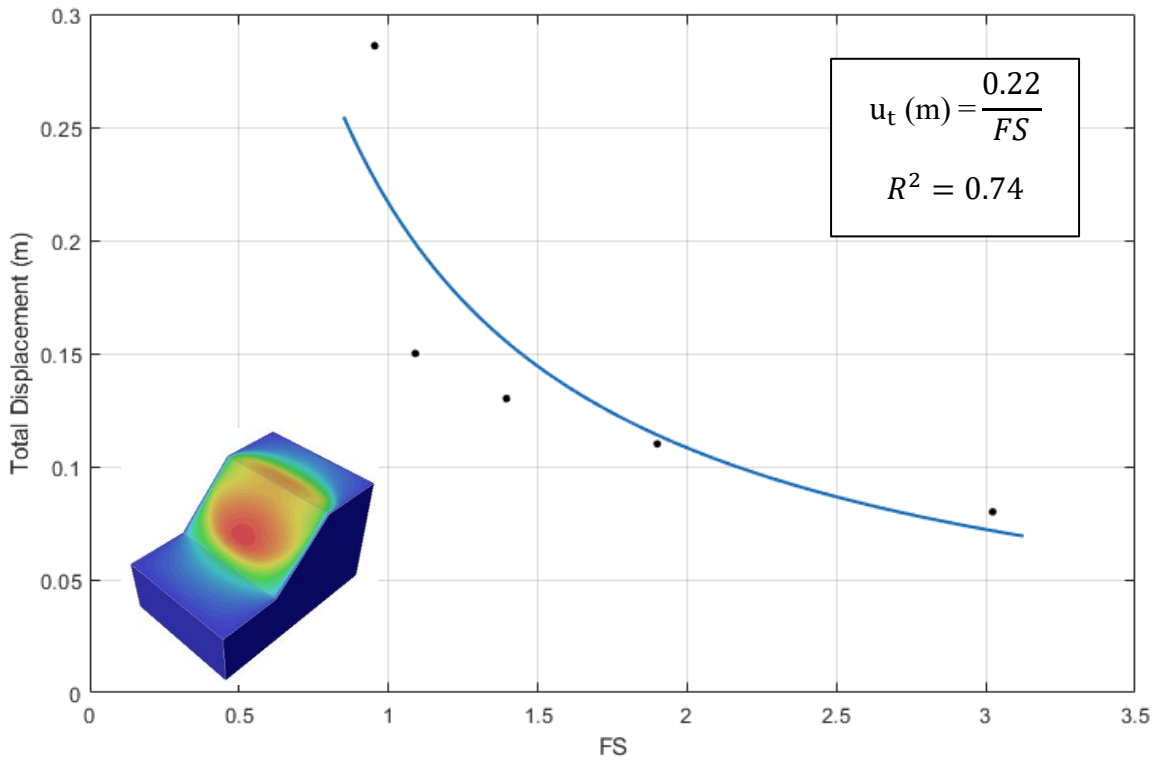
Four plots were generated (Figure 5.25 a-d) with the total displacement u_t (m) on the vertical axis and FS on the horizontal axis. The obtained results are consistent with the results presented in Figure 5.23, 2.24 and 2.25, and show the same trend for ‘ u_t (m) – FS’ relationship.



(a) W/H=0.5



(a) W/H=1



(b) W/H=2

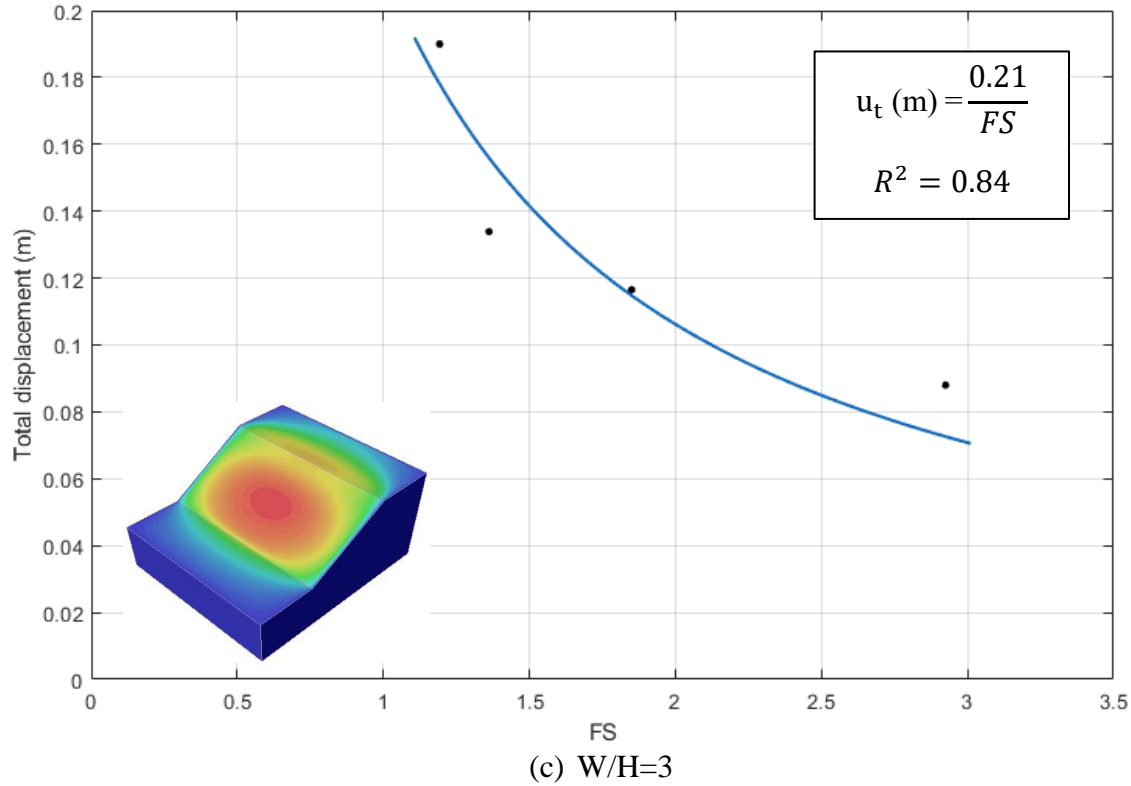


Figure 5.25 Variation of the total displacement with respect to the FS: (a) W/H=0.5; (b) W/H=1; (c) W/H=2; (d) W/H= 3.

Based on the performed calculations for the 3-D plane strain slopes with different W/H ratio and slope angle β , it was shown that for material types presented in Table 5.3 that the displacement is inversely proportional to the FS:

$$u_t (m) = \frac{K}{FS} \quad \text{Eq.5.11}$$

in which $u_t (m)$ is the total displacement in meters, FS is the factor of safety, and K is a constant. If we assume that ‘ $u_t (m) - FS$ ’ relationship (Eq. 5.11) holds for the general case, we can use that to lead to further calculations.

K-value seems to be mostly dependent on Young’s modulus. Figure 5.26 presents a variation of the K-value with respect to Young’s modulus, E (kPa). The figure indicates that the K-value is inversely proportional to the Young’s modulus.

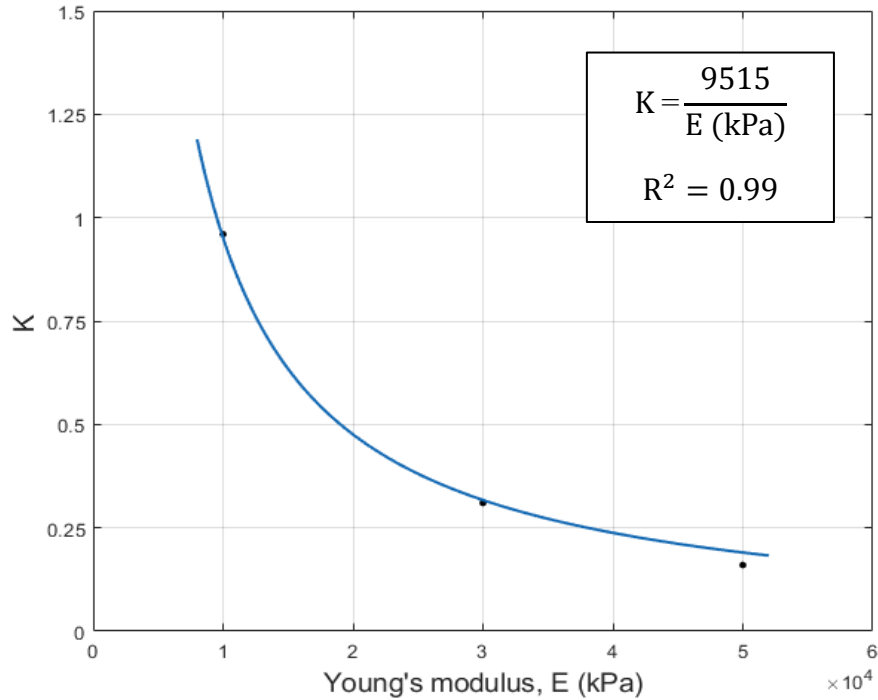
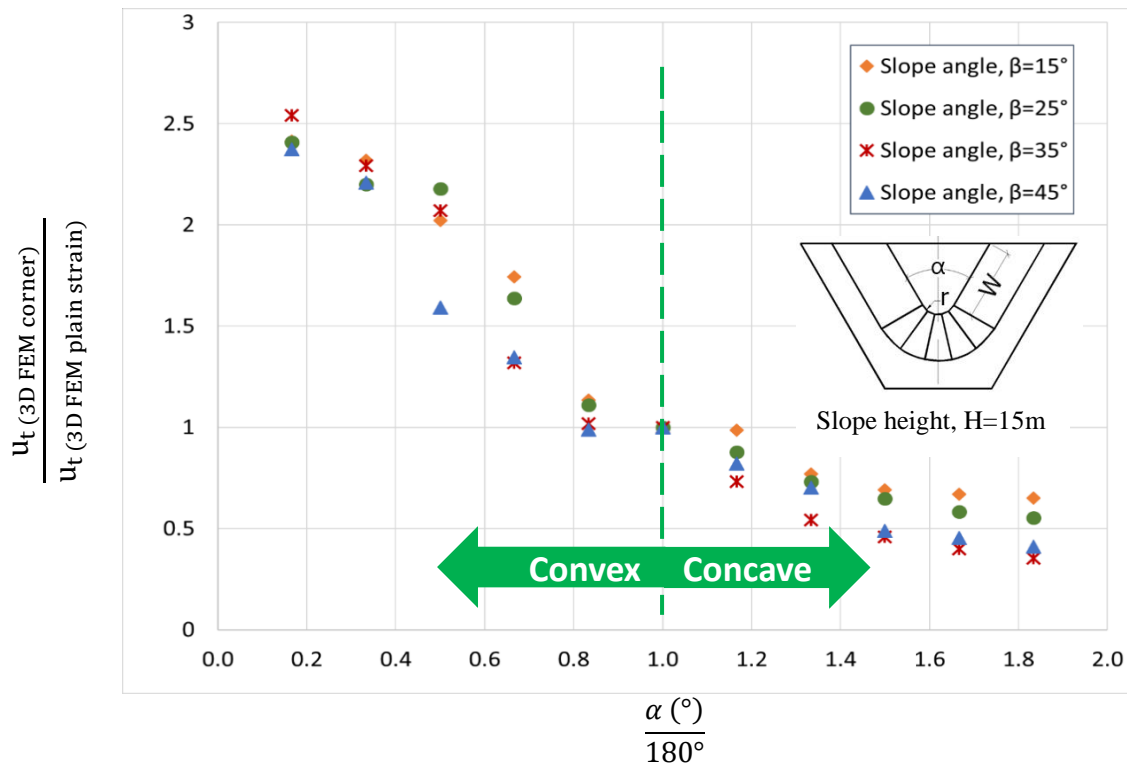


Figure 5.26 Variation of the K-value with respect to Young's modulus, E (kPa). Homogenous slope, $\gamma=20$ kN/m³, $c=10$ (kPa), $\phi=30^\circ$, $\psi=0^\circ$, $\nu=0.28$

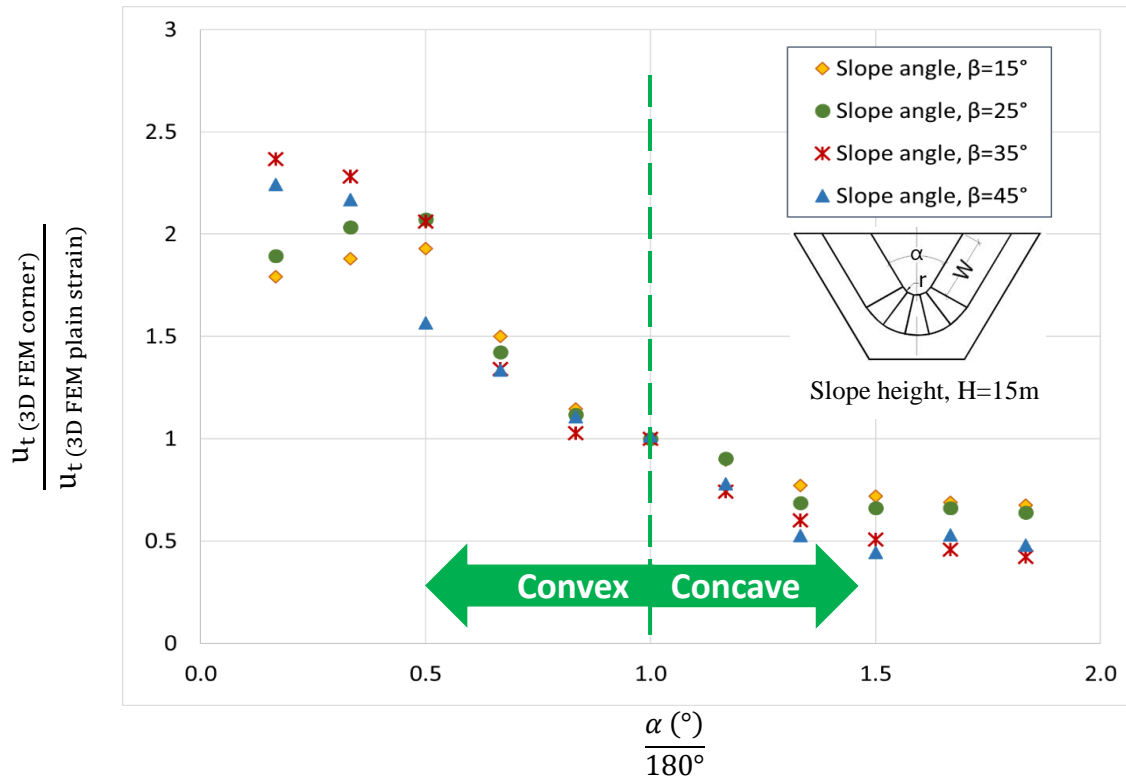
5.1.7 Effect of 3-D complex geometry for corner stability

A total of 164 different conditions were analyzed. They included ten different corner plan view angles (30° , 60° , 90° , 120° and 150° with convex shapes, 210° , 240° , 270° , 300° and 330° with concave shapes, along with 180° for comparison), and four different radii of curvature at the corner (1 m, 5 m, 10 m and 15 m), and four different slope angles (15° , 25° , 35° and 45°) (see and Table 5.2). The results of calculations are presented in Figure 5.27 (a, b, c, and d). On the vertical axis is the normalized total 3-D FEM displacement collected at the tip of the slope (see Figure 5.14), and on the horizontal axis are different plan view angles normalized by 180° . Each figure corresponds to a value of the ratio of the radius of curvature r over the height of the slope H ($r/H = 0.07$, 0.33 , 0.67 , and 1 in Figure 5.27 a, b, c, and d respectively).

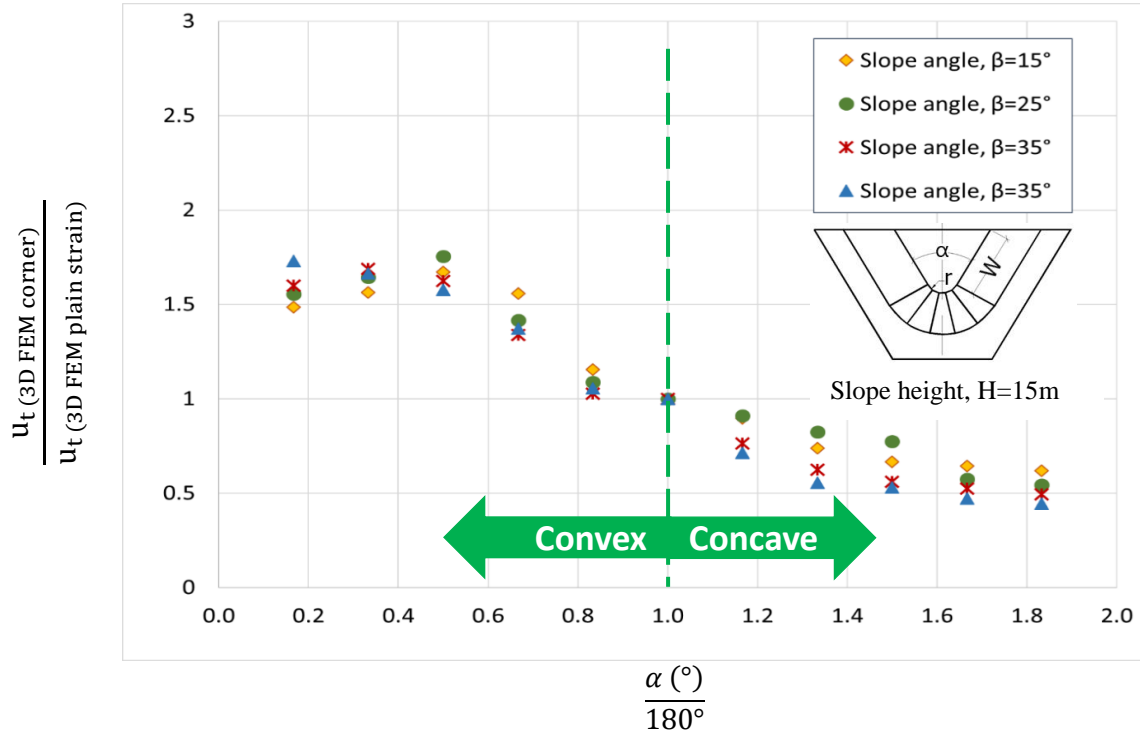
In the case of the very sharp concave angle, the total displacement is only about half that of the plane strain case). In the case of the very sharp convex angle, the total displacement is about 2.5 times larger than the plane strain case. For convex-shaped corner slopes, the total displacement decreases as the plan view angle of the corner increases from 30° to 150°. For concave-shaped corners, this displacement increases as the plan view angle of the corner decreases from 330° to 210°. The near-flat corner angles (150° and 210°) are characterized by a total displacement close to the plane strain case. The slope angle does not much influence on the value of the normalized displacement. However the plan view radius of curvature of the corner has more influence; indeed, as the radius of curvature r is increase from $(0.07 \cdot H)$ to (H) , the value of the normalized total displacement at the crest-tip of the corner crest is decreasing from 2.5 to 1.5 for the convex corners and from 0.75 to 0.3 for concave corners.



(a) $r/H=0.07$



(b) $r/H=0.33$



(c) $r/H=0.67$

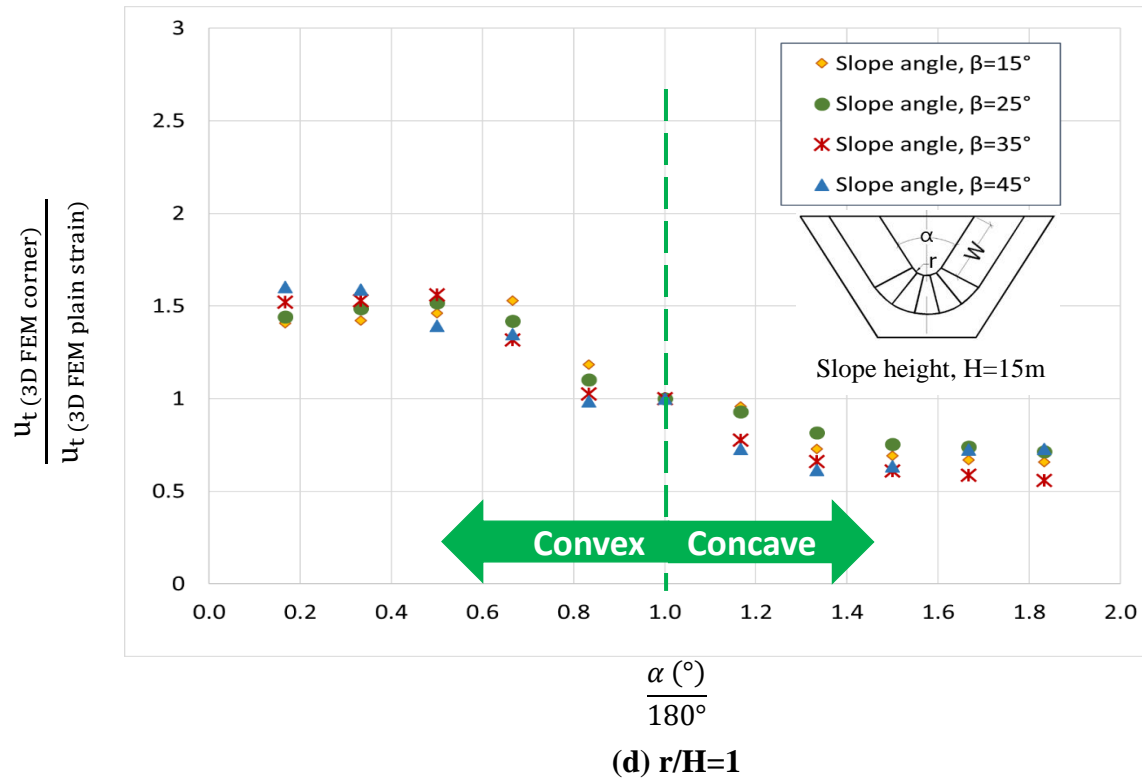


Figure 5.27 The difference in the normalized total displacement with respect to the normalized plane view angle for different slope angles: (a) $r/H=0.07$, (b) $r/H=0.33$, (c) $r/H=0.67$, and (d) $r/H=1$

Sigmoid equations fit the data quite well with high R^2 values (see Figure 5.28 to 5.31). The obtained values of the coefficient of determination ($R^2 > 0.94$) listed in Figure 5.28-5.31 indicate that the model describes the analyzed system with high statistical reliability. Moreover, the high predicted value of R^2 (>0.94) suggests that the predictive power of the proposed models is extremely high, indicating its great practical reliability.

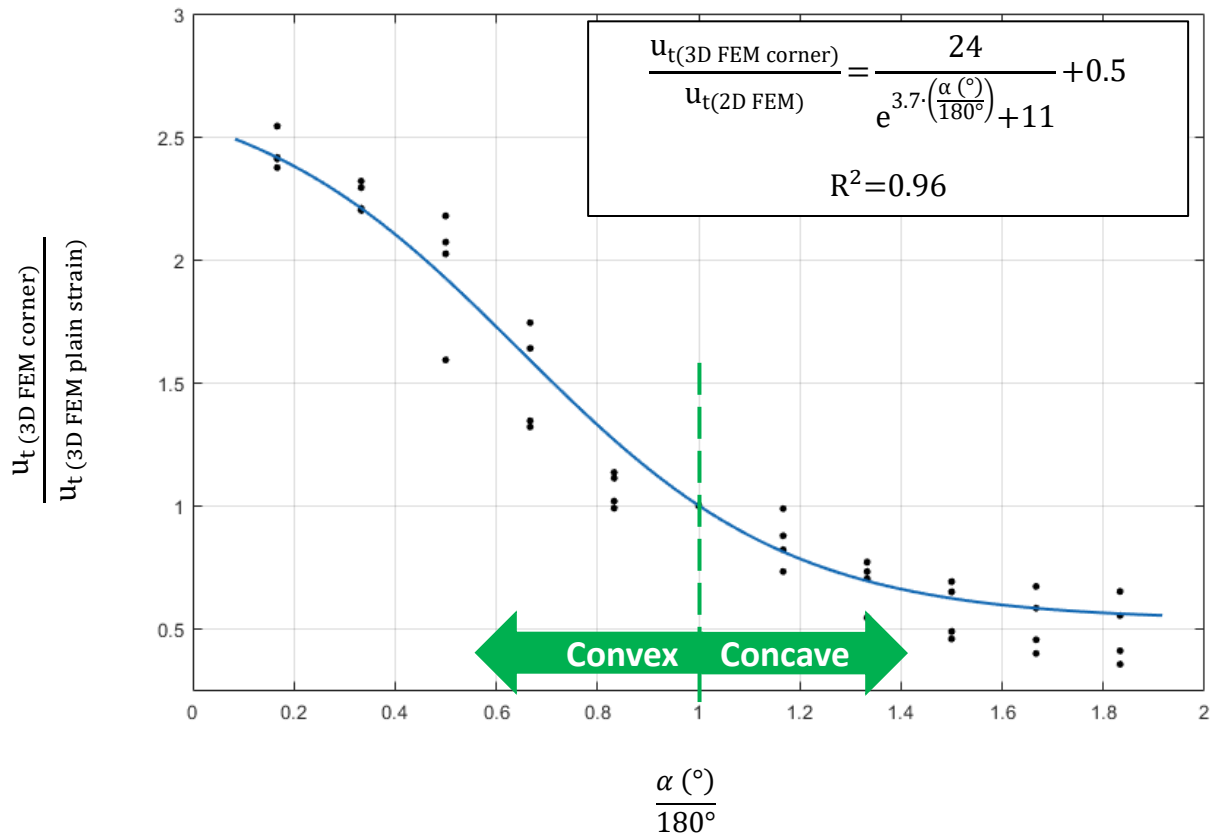


Figure 5.28 Variation of the normalized total displacement with respect to the normalized plane view angle (for $r/H=0.07$)

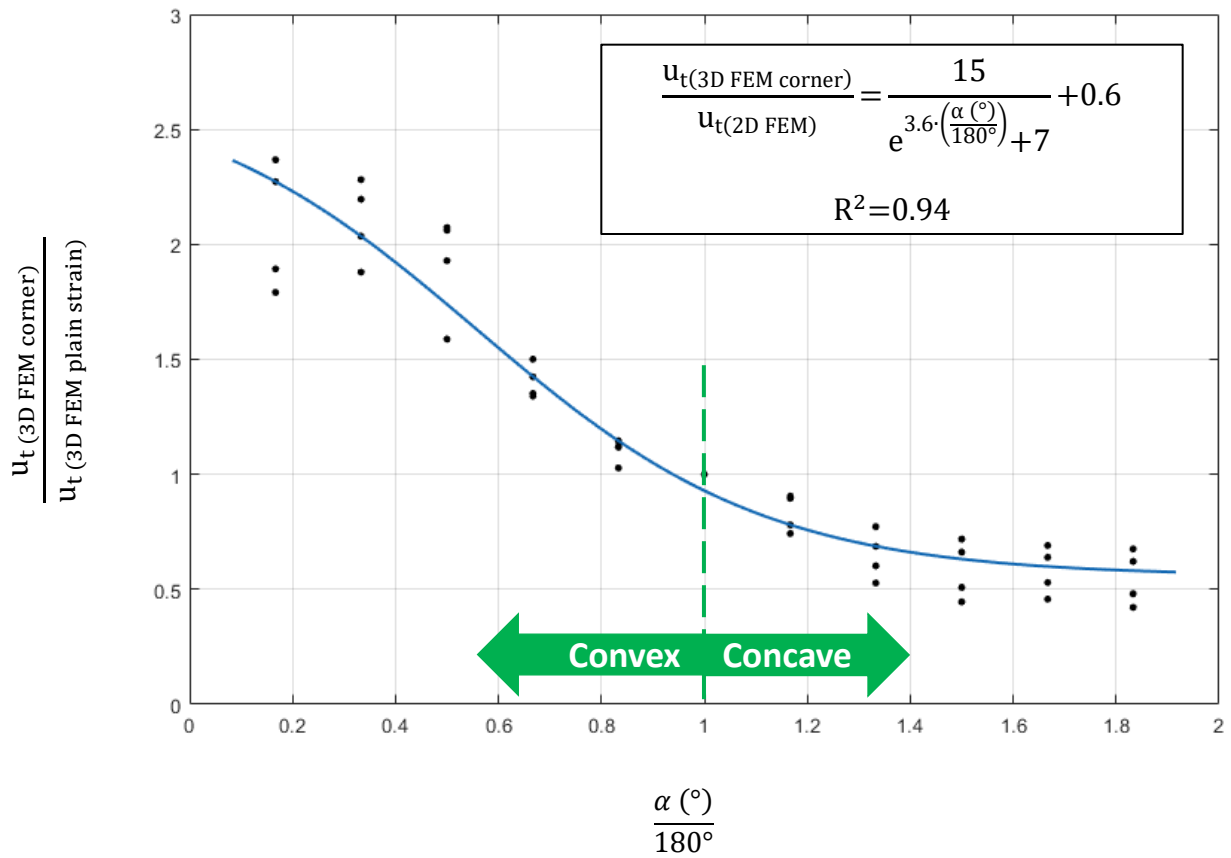


Figure 5.29 Variation of the normalized total displacement with respect to the normalized plane view angle (for $r/H=0.33$)

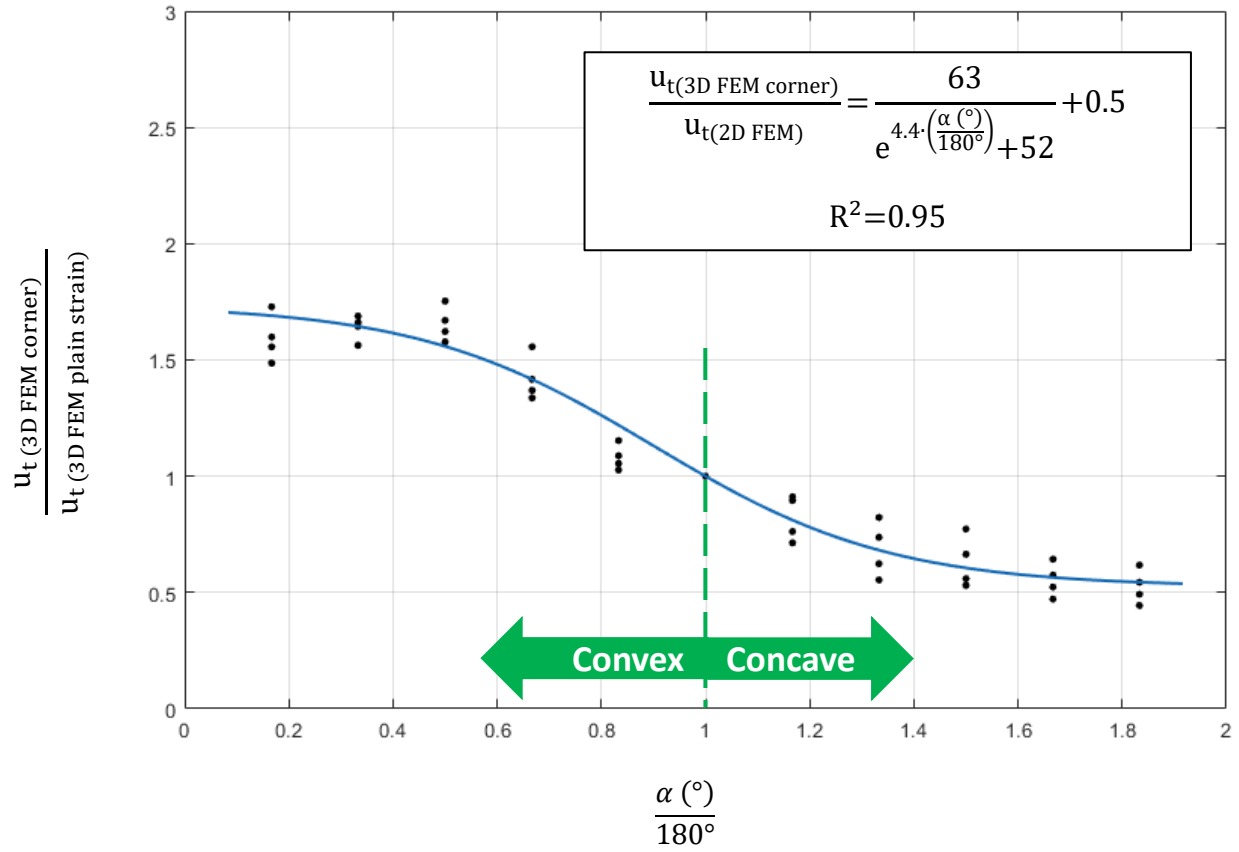


Figure 5.30 Variation of the normalized total displacement with respect to the normalized plane view angle (for $r/H=0.67$)

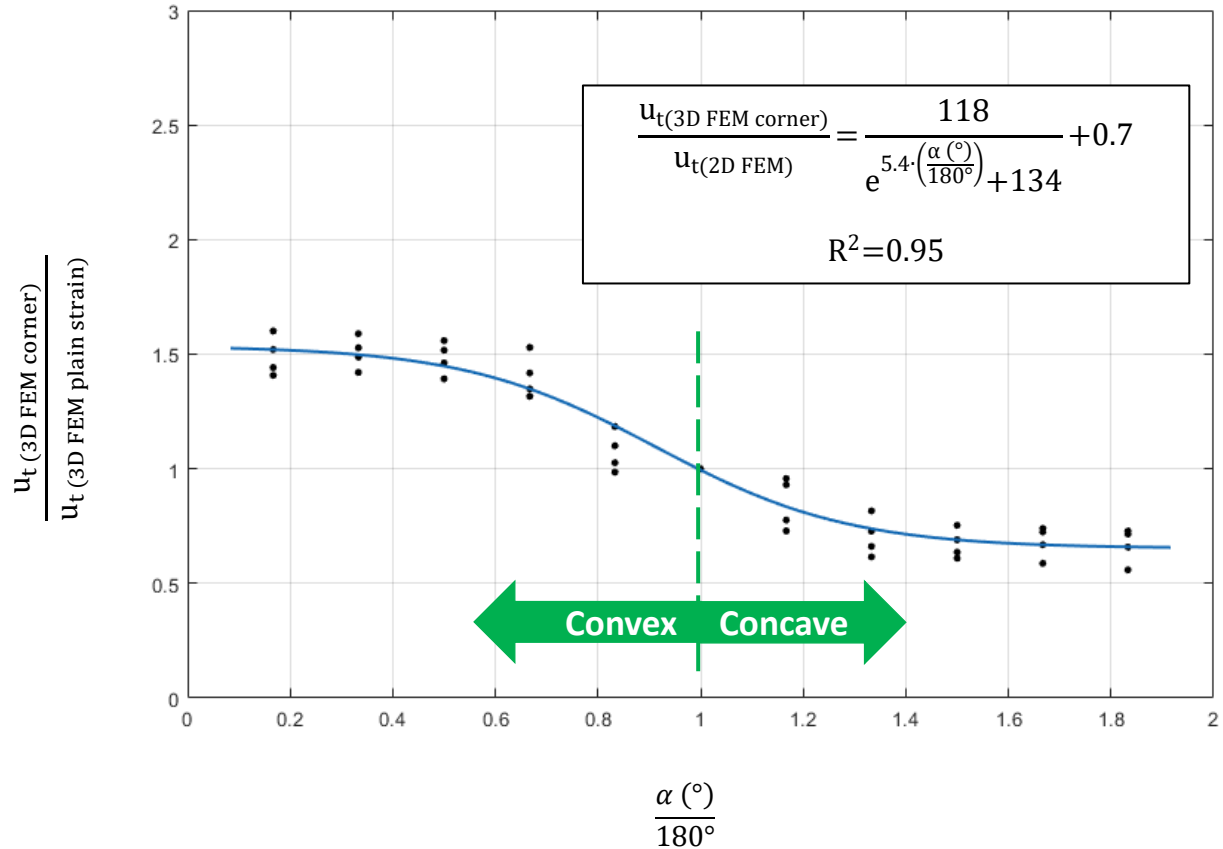


Figure 5.31 Variation of the normalized total displacement with respect to the normalized plane view angle (for $r/H=1$)

As it was discussed earlier the 3-D FEM stability analysis of the corners did not allow to obtain a direct estimate of the corner FS. Instead, the strength reduction finite element method seems to focus on the plane strain zone of the model which is always larger than the corner zone. This is why the total displacement approach was utilized instead of the conventional FS approach.

As it was proved earlier (see Eq. 5.11) the total displacement (m) is inversely proportional to the FS. Therefore, the normalized total displacement (m) is inversely proportional to the normalized FS:

$$\frac{u_t(3D FEM plane strain)}{u_t(2D FEM)} = \frac{FS_{(2D FEM)}}{FS_{(3D FEM plane strain)}} \quad \text{Eq. 5.12}$$

The FS obtained using 2-D limit equilibrium and 2-D finite element methods is assumed to be the same values (see Figure 4.10 –Figure 4.13), thus Eq.5.13 can be replaced by:

$$\frac{u_t(3D \text{ FEM plane strain})}{u_t(2D \text{ FEM})} = \frac{FS_{(2D \text{ LEM})}}{FS_{(3D \text{ FEM plane strain})}} \quad \text{Eq. 5.13}$$

Assume that Eq.5.12 can be extended to the corner situation, and if the total displacement ratios on Figure 5.22– 5.24 are used as one over the FS ratio, then:

$$\frac{u_t(3D \text{ FEM corner})}{u_t(2D \text{ FEM})} = \frac{FS_{(2D \text{ LEM})}}{FS_{(3D \text{ FEM corner})}} \quad \text{Eq. 5.14}$$

Based on the regression line analysis presented in Figure 5.28, a sharp convex corner ($\alpha < 30^\circ$) may have a FS as low as 40% of the plane strain FS (Eq. 5.15) and that the sharp concave corner ($\alpha > 150^\circ$) may have a FS 3.33 times larger than the plane strain FS (Eq. 5.16):

$$FS_{\text{Sharp Convex } (r/H=0.07)} = 0.4 \cdot FS_{2D \text{ LEM}} \quad \text{Eq. 5.15}$$

$$FS_{\text{Sharp Concave } (r/H=0.07)} = 3.33 \cdot FS_{2D \text{ LEM}} \quad \text{Eq. 5.16}$$

With the radius of curvature increase, the difference between sharp corner stability and the plane strain case decreases. For the case when the radius of curvature is equal to the height of the slope ($r/H=1$):

$$FS_{\text{Sharp Convex } (r/H=1)} = 0.67 \cdot FS_{2D \text{ LEM}} \quad \text{Eq.5.17}$$

$$FS_{\text{Sharp Concave } (r/H=1)} = 1.54 \cdot FS_{2D \text{ LEM}} \quad \text{Eq.5.18}$$

For $r/H=0.33$ the FS for sharp convex and concave corners can be obtained using Eq. 5.19 and 5.20:

$$FS_{\text{Sharp Convex } (r/H=0.33)} = 0.45 \cdot FS_{2D \text{ LEM}} \quad \text{Eq.5.19}$$

$$FS_{\text{Sharp Concave } (r/H=0.33)} = 2.5 \cdot FS_{2D \text{ LEM}} \quad \text{Eq.5.20}$$

For the sharp corners with $r/H=0.67$:

$$FS_{\text{Sharp Convex } (r/H=0.67)} = 0.59 \cdot FS_{2D \text{ LEM}} \quad \text{Eq.5.21}$$

$$FS_{\text{Sharp Concave (r/H=0.67)}} = 2 \cdot FS_{2D LEM} \quad \text{Eq.5.22}$$

Eqs. 5.23-5.27 are offered to preliminary estimate the concave and convex FS based on the FS for the plane strain case. The sigmoid equations can be used for the more precise calculations of the corner FS based on the FS obtained for the plane strain case. For example, consider an equation presented in Figure 5.28. This equation represents the case for convex and concave corners with $r/H=0.07$:

$$\frac{u_t (3D FEM \text{ corner})}{u_t (2D FEM)} = \frac{24}{e^{3.7 \cdot \left(\frac{\alpha (^\circ)}{180^\circ}\right)} + 11} + 0.5 \quad \text{Eq.5.23}$$

Considering Eq.5.12 and the equation presented in Figure 5.28, the FS for the 3-D FEM corner with $r/H=0.07$ can be characterized as follows:

$$FS_{3D FEM \text{ corner (r/H=0.07)}} = \frac{2 \cdot FS_{(2D LEM)} \cdot \left(11 + e^{3.7 \cdot \left(\frac{\alpha (^\circ)}{180^\circ}\right)}\right)}{\left(59 + e^{3.7 \cdot \left(\frac{\alpha (^\circ)}{180^\circ}\right)}\right)} \quad \text{Eq.5.24}$$

The same approach was used to determine the FS for corners with $r/H=0.33$, 0.67 and 1 (Eqs. 5.25, 5.26 and 5.27 consequently):

$$FS_{3D FEM \text{ corner (r/H=0.33)}} = \frac{1.7 \cdot FS_{(2D LEM)} \cdot \left(7 + e^{3.6 \cdot \left(\frac{\alpha (^\circ)}{180^\circ}\right)}\right)}{\left(32 + e^{3.6 \cdot \left(\frac{\alpha (^\circ)}{180^\circ}\right)}\right)} \quad \text{Eq. 5.25}$$

$$FS_{3D FEM \text{ corner (r/H=0.67)}} = \frac{2 \cdot FS_{(2D LEM)} \cdot \left(52 + e^{4.4 \cdot \left(\frac{\alpha (^\circ)}{180^\circ}\right)}\right)}{\left(178 + e^{4.4 \cdot \left(\frac{\alpha (^\circ)}{180^\circ}\right)}\right)} \quad \text{Eq.5.26}$$

$$FS_{3D FEM \text{ corner (r/H=0.1)}} = \frac{1.4 \cdot FS_{(2D LEM)} \cdot \left(134 + e^{5.4 \cdot \left(\frac{\alpha (^\circ)}{180^\circ}\right)}\right)}{303 + e^{5.4 \cdot \left(\frac{\alpha (^\circ)}{180^\circ}\right)}} \quad \text{Eq.5.27}$$

Eqs. 5.24, 5.25, 5.26, and 5.27 are suggested to use to determine the FS for different concave- and convex-shaped corners based on the FS for the 2-D plane strain case.

The result of a series of 3-D slope stability calculations performed for various convex and concave corner configurations is presented in the chapter. A displacement-based approach was used because of the limitation of the FEM FS-approach for corner stability. The total displacement of the crest of the slope at the tip of the corner is significantly impacted by the plan view angle of the corner. For sharp corners the ratio between the displacement of the corner and that of the plane strain can reach 3 for convex corners and 0.4 for concave corners. The crest displacement was shown to be inversely proportional to the FS for plane strain cases. If that relationship is extended to corner configuration, the factor of safety of a sharp convex corner would be 3 times less than the plane strain case, and the FS of a concave corner would be 2.5 times higher. It is also shown that the impact on the displacement and FS decreases as the plan view radius of curvature of the corner increases.

5.2 Stability of benched slopes

5.2.1 Bench configuration

All open pit slopes are consist of a series of benches, which geometry controls the overall slope design. Three parameters: a bench slope angle, bench height, and berm width (Figure 5.32), are required to define the geometry of a bench. Once this design element is complete, it is usual then to evaluate both inter-ramp and overall slopes.

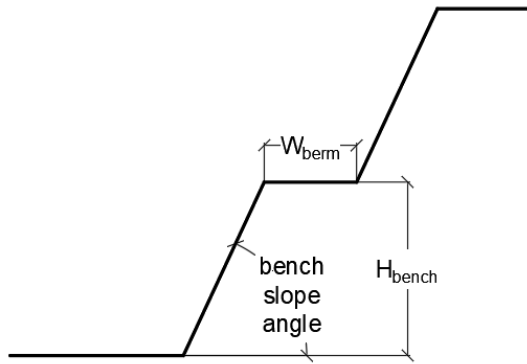


Figure 5.32 Components of bench geometry

Based on the current mining engineering practice (Ryan and Pryor 2001), most large mining operations drill and blast 12-to 15 intervals, with 15 m intervals being the most common. The collected case histories discussed in Chapter 3 prove that fact. According to statistics, 44% of all case histories from TAMU-MineSlope have 15 m height of the benches. Determination of the bench height depends on the type of mining equipment used in mining operations, and therefore bench height is usually fixed based on equipment specifications.

Stable bench slope angles are usually controlled by many factors, including (Ryan and Pryor 2001; Read and Stacey 2009):

- the excavation technique (drilling, blasting, excavation sequence and equipment type);
- the structural fabric (orientation, spacing, continuity of discontinuities);
- the condition of the discontinuities (shear strength, planarity);
- the competency of the rock mass;
- environmental factors (freeze–thaw, precipitation);
- service life of the bench and the overall slope.

Based on the traditional mining practice a bench angle is always steeper than an overall open pit slope angle, therefore the FS for the bench would be less compared to the overall slope FS.

Berm width design is based on a variety of criteria, including (Read and Stacey 2009):

- competency of the rock mass;
- height of the bench;
- volume of potential bench scale failures;
- rockfall catchment criteria;
- performance and condition of overlying benches;
- service life of the bench and the overall slope;
- inter-ramp slope angle and height;
- access requirements;
- general risk tolerance.

Bench height is one of the most important parameter controls design parameter of the bench width, so an empirical relationship between the preferred bench widths was developed (Call 1992; Ryan and Pryor 2001; Bar et al. 2016) and can be presented the following equation:

$$W_{\text{berm}}(\text{m}) = 0.2 \cdot H_{\text{bench}} + 4.5 \text{ m} \quad \text{Eq.5.28}$$

where $W_{\text{bench}}(m)$ is the bench width in meters; H_{bench} is the height of the bench (Figure 5.32). For the typical bench height $H_{\text{bench}}=15\text{m}$, the preferred width of the berm is of the order of 7.5-8 m.

5.2.2 Influence of benching on the open pit slope stability

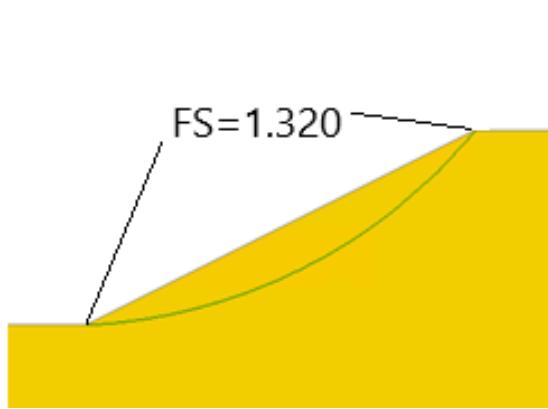
In order to study the influence of benching on the slope FS, the five sets of 2-D models were established. Basic parameters adopted in the models are: overall slope height 120 m, overall slope angle 27° (2 to 1 slope), bench slope 45° , height and width of the benches were varied depending on the number of benches in the slope. In addition, each set of models has geotechnical parameters, as given in Table 5.4. For all cases, the friction angle and unit weight of the slope material remained the same, but the cohesion was varied from 0 to 20 kPa.

The FS was obtained for simple slope and slopes with 2, 4, 8, and 16 benches, and a comparative study was conducted. Through analysis, the FS is inversely proportional to the number of benches; thus, the bigger the number of benches, the closer the FS to the one obtained for the simple slope. In the case with the few benches (6 or less), the FS is increased compared to the simple slope because the lower benches are loading the bottom of the slope, and the top of the slope is lightening (Table 5.4 and Figure 5.33).

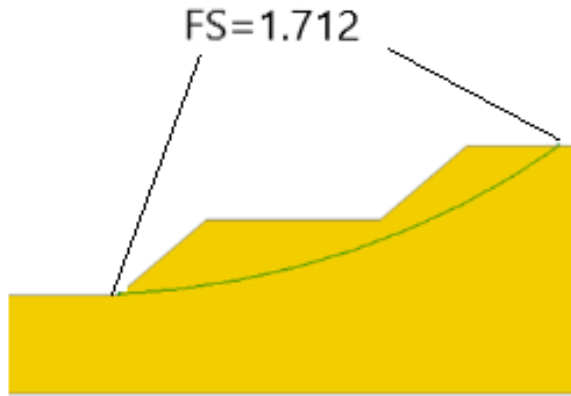
The results of the performed calculations are presented in Figure 5.34-5.37. Figure 5.34 and Figure 5.35 present the bench stability. On the vertical axis, the bench FS is normalized by the FS of the simple slope; on the horizontal axis is the number of benches or the bench's width normalized by the bench's height. Figure 5.36 and Figure 5.37 present the overall slope stability. Again, on the vertical axis, the benched slope FS is normalized by the FS of the simple slope; on the horizontal axis is the number of benches or the bench width normalized by the bench height.

Table 5.4 A number of studied cases and results illustrating the influence of benching in open pit mining

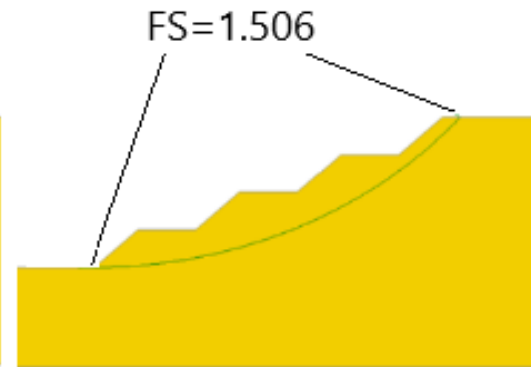
Height (m)	slope	C (kPa)	ϕ (°)	γ (kN/m ³)	Bench				FS _{benched slope}	$\frac{FS_{benched\ slope}}{FS_{simple\ slope}}$	FS _{bench}	$\frac{FS_{bench}}{FS_{simple\ slope}}$	$\frac{W_{bench}}{H_{bench}}$
					# of benches	height (m)	width (m)	face angle β (°)					
120	2H:1V	0	30	20	1	120	360	45	1.256	1.000	0.757	0.603	3.000
120	2H:1V	0	30	20	2	60	120	45	1.658	1.320	0.747	0.595	2.000
120	2H:1V	0	30	20	4	30	40	45	1.442	1.148	0.717	0.571	1.333
120	2H:1V	0	30	20	8	15	17.14	45	1.35	1.075	0.7	0.557	1.143
120	2H:1V	0	30	20	16	7.5	8	45	1.292	1.029	0.679	0.541	1.067
120	2H:1V	5	30	20	1	120	360	45	1.288	1.000	0.783	0.608	3.000
120	2H:1V	5	30	20	2	60	120	45	1.684	1.307	0.792	0.615	2.000
120	2H:1V	5	30	20	4	30	40	45	1.476	1.146	0.844	0.655	1.333
120	2H:1V	5	30	20	8	15	17.14	45	1.38	1.071	0.873	0.678	1.143
120	2H:1V	5	30	20	16	7.5	8	45	1.325	1.029	1.046	0.812	1.067
120	2H:1V	10	30	20	1	120	360	45	1.32	1.000	0.807	0.611	3.000
120	2H:1V	10	30	20	2	60	120	45	1.712	1.297	0.83	0.629	2.000
120	2H:1V	10	30	20	4	30	40	45	1.506	1.141	0.873	0.661	1.333
120	2H:1V	10	30	20	8	15	17.14	45	1.41	1.068	1.046	0.792	1.143
120	2H:1V	10	30	20	16	7.5	8	45	1.358	1.029	1.339	1.014	1.067
120	2H:1V	15	30	20	1	120	360	45	1.352	1.000	0.81	0.599	3.000
120	2H:1V	15	30	20	2	60	120	45	1.738	1.286	0.82	0.607	2.000
120	2H:1V	15	30	20	4	30	40	45	1.536	1.136	0.966	0.714	1.333
120	2H:1V	15	30	20	8	15	17.14	45	1.438	1.064	1.201	0.888	1.143
120	2H:1V	15	30	20	16	7.5	8	45	1.39	1.028	1.592	1.178	1.067
120	2H:1V	20	30	20	1	120	360	45	1.386	1.000	0.827	0.597	3.000
120	2H:1V	20	30	20	2	60	120	45	1.763	1.272	0.873	0.630	2.000
120	2H:1V	20	30	20	4	30	40	45	1.563	1.128	1.046	0.755	1.333
120	2H:1V	20	30	20	8	15	17.14	45	1.467	1.058	1.338	0.965	1.143
120	2H:1V	20	30	20	16	7.5	8	45	1.421	1.025	1.833	1.323	1.067



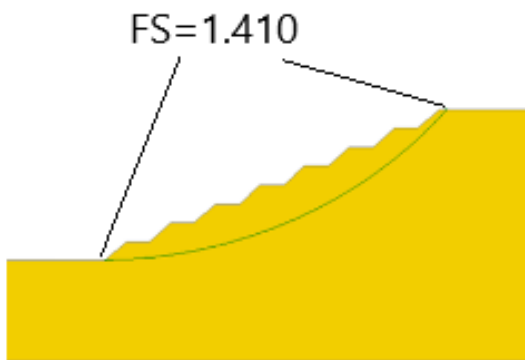
(a) no benches



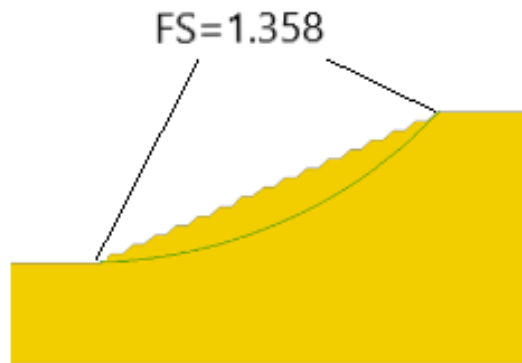
(b) two benches



(c) four benches



(d) eight benches



(e) sixteen benches

Figure 5.33 Example of the FS calculation results (for the slope formed by material with $c=10\text{kPa}$, $\phi=30^\circ$ and $\gamma=20\text{kN/m}^3$): a) no benches, b) two benches, c) four benches, d) eight benches, and e) sixteen benches

It can be seen from Figure 5.34 and Figure 5.37 that the cohesion and height of the slope affect the stability of the bench and the overall slope. If the cohesion of the material increases, the influence of benching is increasing as well. For materials with low cohesion, the role of benching is less favorable and vice versa. For the cohesive materials, the bench FS depends on the height of the bench: for a lower height of the bench, the FS increases dramatically (Figure 5.34 and Figure 5.35).

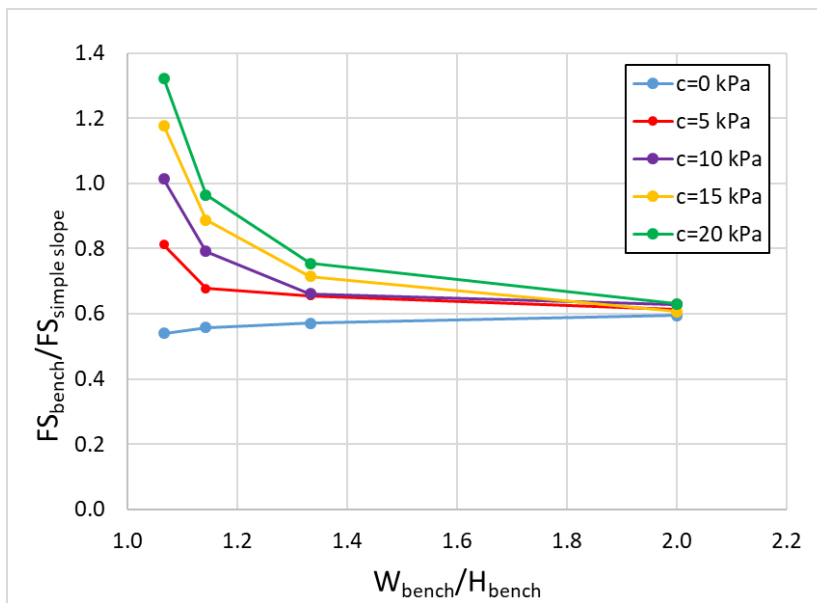


Figure 5.34 Relationship between normalized bench FS and $W_{\text{bench}}/H_{\text{bench}}$

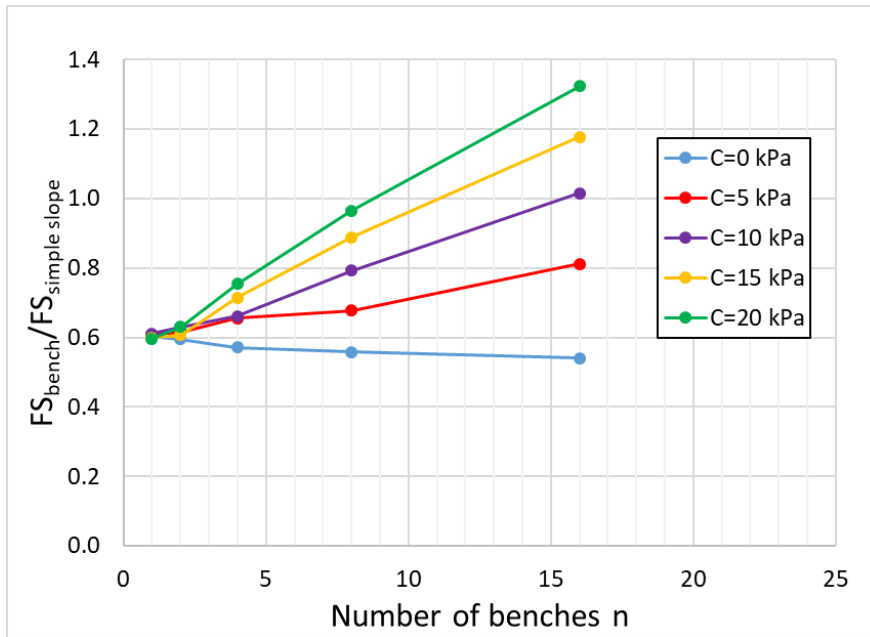


Figure 5.35 Relationship between normalized bench FS and the number of benches forming the slope

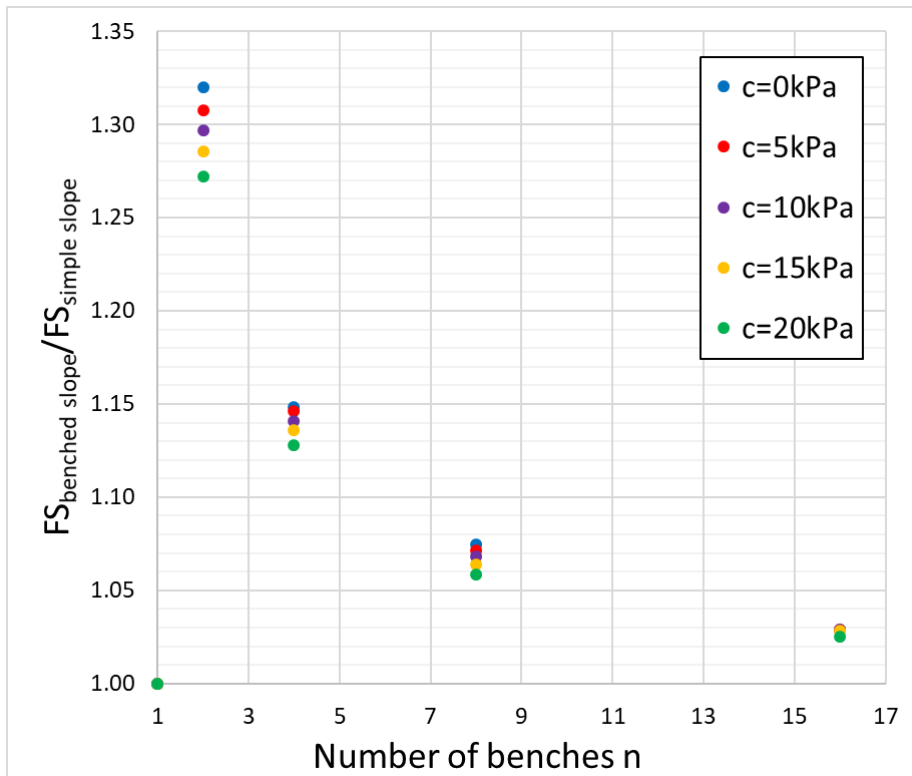


Figure 5.36 Relationship between normalized benched slope FS and the number of benches forming the slope

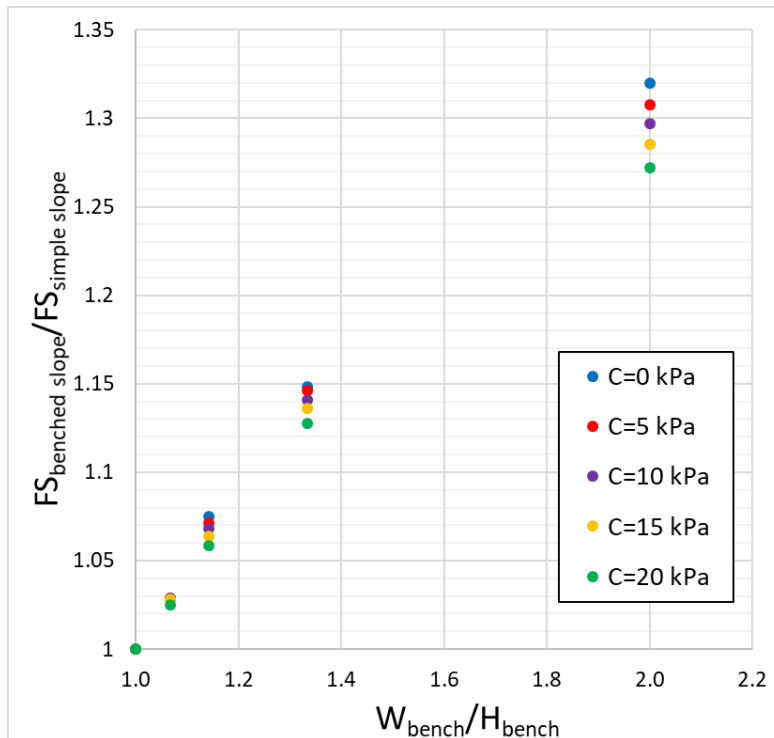


Figure 5.37 Relationship between normalized benched slope FS and $W_{\text{bench}}/H_{\text{bench}}$

5.2.3 A risk-based approach to the stability of benches

The optimum design of the open pit requires the determination of the most economic pit limits, which normally results in steep slope angles. The steepening slope of the walls leads to reducing the stripping ratio and the improvement of mining economics (Read and Stacey 2009). However, these benefits are counteracted by an increased risk to the operation. Thus, the determination of the acceptable slope angle is a key aspect of the mining business (Contreras 2015).

As mentioned before, a bench angle is always steeper than an overall open pit wall slope angle; therefore, the FS for the bench would be less compared to the overall slope FS. In mining engineering, the cost of a "no failures" approach is generally not able to be carried by the project. Thus designers accept (either knowingly or unknowingly) some risk of failure. In mining

engineering practice, bench-scale slope failures, for example, are generally expected and can be acceptable when adequately managed by catch berms. At the same time, the overall slope failure is not acceptable because it may have a huge impact on the economy and the safety of the recovery process (Sjoberg 1999; Read and Stacey 2009; Gibson 2011; Contreras 2015). Therefore the existing recommendations for acceptable PoF for slope design (Kristen 1983; Priest and Brown 1983; Swan and Sepulveda 2000; Sullivan 2006; Read and Stacey 2009) are utilized the constant risk approach. In slope design the risk (R) associated with slope failure are defined as:

$$R = PoF \cdot C \quad \text{Eq.5.29}$$

where R= risk associated with slope failure, PoF = probability of slope failure, C = value of the consequences of slope failure. Read and Stacey (2009) categorized the consequences of slope failure into six groups:

1. Fatalities or injuries to personnel, including the costs of industrial and legal action.
2. Damage to equipment and infrastructure, including the costs of replacing equipment and infrastructure.
3. Economic impacts on production, including the costs of:
 - removing failed rock material to the extent that mining can safely continue;
 - slope remediation – the slope may have to be cut back to prevent secondary failures due to steeper upper slopes, or slope support systems may be required;
 - haul road repair and re-access – the haul road and ramp may be damaged and re-access to the mine may need to be considered;
 - equipment re-deployment – the cost of equipment being isolated by the failure and the cost of moving equipment to other parts of the mine unaffected by the failure where it can be used productively should be considered;

– unrecoverable ore – the loss of a ramp or part of an inter-ramp slope may lead to sterilizing sections of the orebody, at least on a temporary basis.

4. Force majeure (a major economic impact), which should normally equate to failure of an overall slope or loss of medium- to long-term access to ore such that contracts cannot be fulfilled.

5. Industrial action, i.e. loss of worker confidence.

6. Public relations, such as stakeholder resistance due to social views and/or environmental impacts arising from the failure. Increased regulatory supervision.

The concept of the constant risk in open pit slopes stability can be presented by the following example. Consider three different categories for pit slope failures, presented in Table 5.5. The possible impact in terms of dollar loss for each slope failure category assumed based on the data presented by Steffen et al. (2008).

For the equipment loss which in our case corresponds to the bench failure Steffen et al. (2008) reported that the economic implications could imply an additional cost in the range of US\$10M to US\$30M in any one year. Economic impact is firstly the cost of repair or replacement of equipment and secondly the loss of production that may result. In the example the average number of US\$20M was used (Table 5.5 and Figure 5.38).

An interramp and global pit failure would affect continuous operations and open pit safety and, as a result, significant loss of profit. According to Steffen et al. (2008), the loss of profit would typically range from US\$40M to US\$200M. So the lower bound was taken to illustrate the consequences in terms of dollar loss for interramp slope failure and the average number of US\$120M for the global failure (Table 5.5).

Table 5.5 Constant risk design approach for the different categories of the open-pit slope failures

Category of the open-pit slope failure	Value of the consequences	Acceptable PoF (%)*	Impact (US\$)**	Risk (Eq. 5.28)
Overall slope level	Failure may affect continuous operations and open pit safety, and as a result – loss of profit	<5	120M	0.05*120M= US\$6M/yr***
Interramp slope level	Failure may affect the safety and cost of operations	<15	40M	0.15*40M= US\$6M/yr
Bench level	Failure has minimal safety hazard, but may cause loss of equipment	<30	20M	0.30*20M= US\$6M/yr

*) Read and Stacey (2009)

**) Steffen et al. (2008)

***) For other projects acceptable risk is US\$0.01M/yr (see Figure 3.79)

Figure 5.38 presents the acceptable risk levels for the different activities, including civil engineering projects, open-pit slope failures, and mining slope design. From the risk point of view, the chart shows that mining slope design is at a much higher risk than what is typically acceptable in other industries. The red dotted line indicates the constant risk associated with the open pit slope design, plotted based on the data presented in Table 5.5. Note that there is a discrepancy between the actual events presented by the orange ellipse in the chart and the published targets due to an underestimation of the soil shear strength, including unsaturated soil behavior.

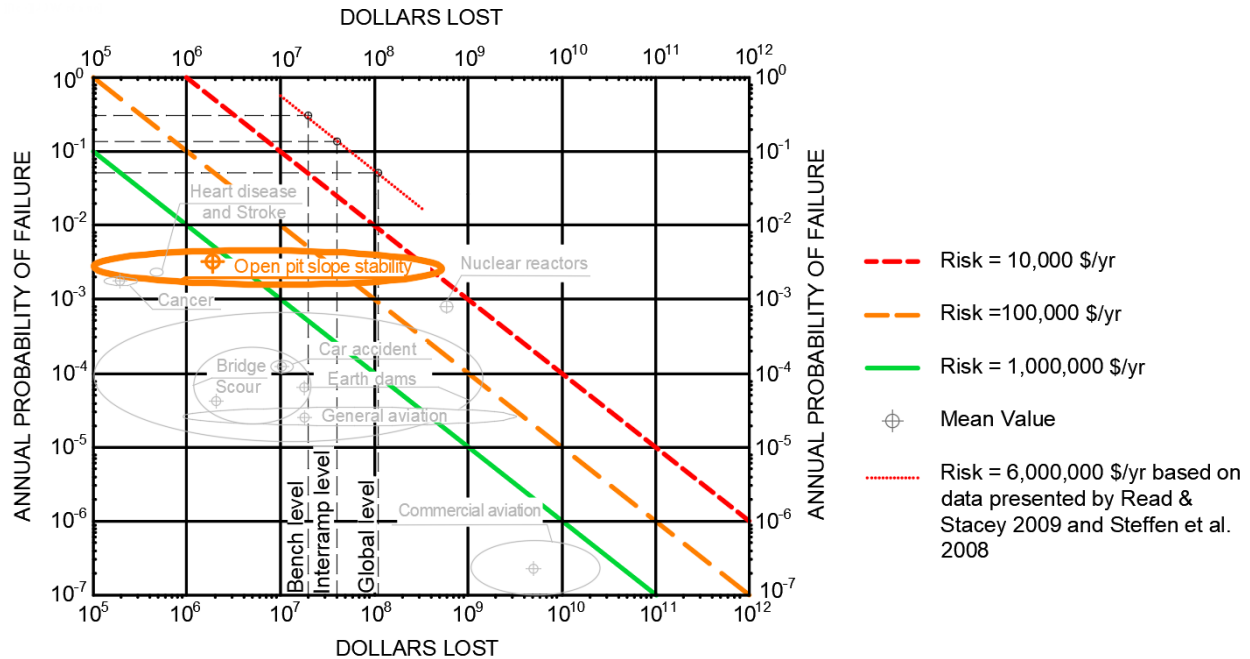


Figure 5.38 Constant risk approach in terms of dollars loss (dotted red line indicates risk based on Read and Stacey 2009 and Steffen et al. 2008)

Another example of the constant risk approach can be presented in terms of actual failure volume (m^3). Fergusson et al. (2001) introduced this approach based on the study of Rotowaro open pit slope conditions. An assessment of the tolerable risk criteria was developed, setting an upper bound on acceptable risk levels as shown in Figure 5.39. The lower tolerable risk volume of the failure was chosen for the highwalls of the open pit (Eq. 5.30). The risk-volume criteria make an allowance for small but high probability failures to be acceptable within the design. However, larger-scale failures require high levels of stability (low probabilities of failure) to achieve the design criteria (Fergusson et al. 2001)

$$PoF \cdot \text{Failure Volume} = \text{Constant} \qquad \text{Eq.5.30}$$

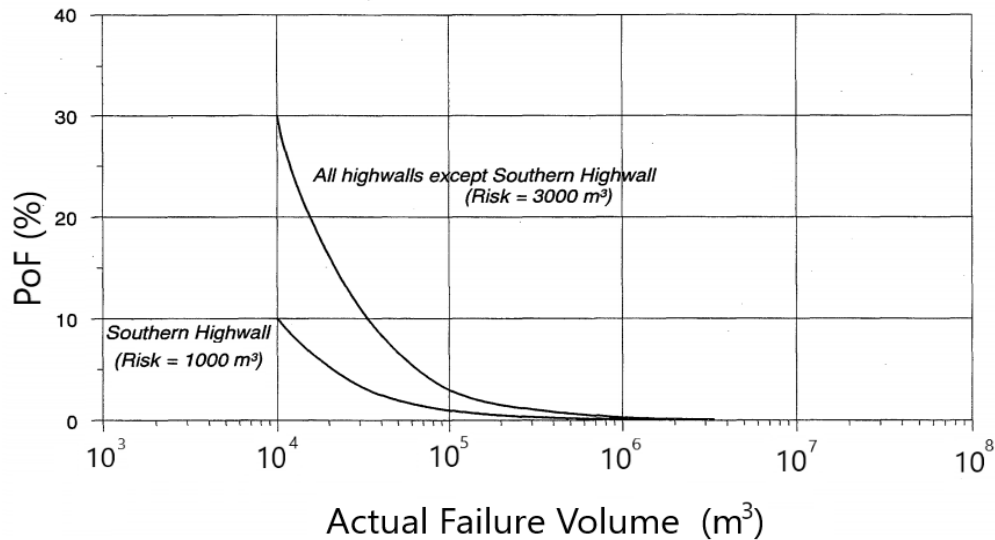


Figure 5.39 Constant risk approach in term of volume of the failure (m³) (reprinted from Fergusson et al. 2001)

For example, Figure 5.39 shows that a risk volume criteria of 1,000 m³ would equate to a 10,000 m³ failure having a 10% probability. While small failures of this size represent an inconvenience to the mining operation, possibly adding to operational cost, they do not result in a major loss, disruption, or cessation of mining. Conversely, a large failure, say 400,000 m³ in volume, would have a major adverse consequence. To meet a risk volume criterion of 1,000 m³, the PoF would need to be 0.25% or lower (Fergusson et al. 2001).

These two examples show the advantages of the constant risk design approach based on a set of geotechnical criteria (e.g., slope failure level, the failure volume) that can reflect the economic and operational risks of the open pit development.

Mining is considered to be a high risk business in terms of both safety and economics (Sullivan 2006; Terbrugge et al. 2006; Steffen et al. 2008; Contreras 2015; Rendu 2017). There is always the possibility that an excavated slope may not perform as predicted and could fail with significant and even catastrophic results. Therefore risks associated with slope failures are a key aspect in the open-pit mining production. The determination of the acceptable slope angle for open

pits is a key aspect of the mineral business, as it implies seeking the optimum balance between the additional economic benefits gained from having steeper slopes, and the additional risks resulting from the consequent reduced stability of the pit slopes. The decision on the acceptability of risk level is up to the owner of a given project while satisfying the safety regulations of various government organizations. Once the risk criteria are defined by management, the risk tolerance and the tolerable probability of failure are set up.

5.3 Impact of the water-level variations on slope stability

The three governing factors for slope stability are slope geometries, stress conditions, geological conditions, and material properties. Changes in pore pressure, external water loading, and hydrodynamic impact from water flow influence material properties. The water-level variations have been reviewed as a part of the present study. Figure 5.40 presents the basic models of water level change in slopes: (A) water-level drawdown, (B) water-level rise, and (C) water-level fluctuations.

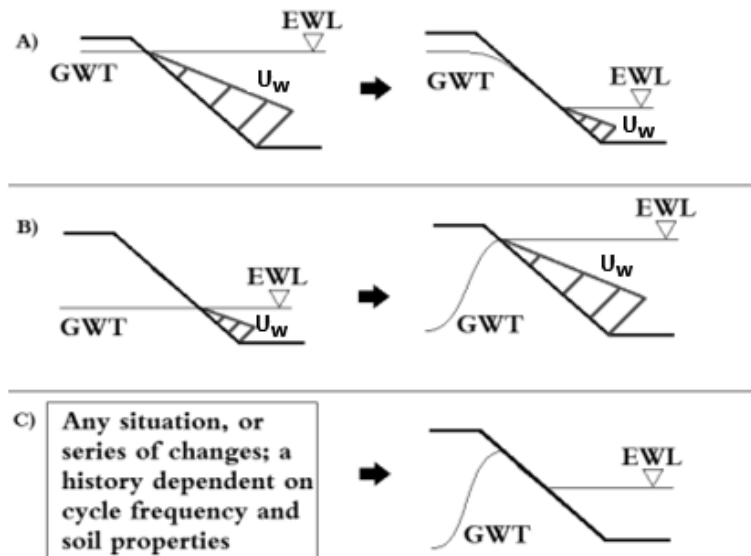


Figure 5.40 Basic modes of water level change; water level drawdown (A), raised water level (B), and fluctuating water level (C). Water loads (U_w), positions of the ground-water table (GWT), and the external water level (EWL), are shown (reprinted from Johansson 2014)

The factors of safety on simple geometry slopes with low, intermediate, and steep slope angles are investigated using selected shear strength parameters ($c=10$ kPa and $\phi=30^\circ$), unit weight $\gamma=20$ kN/m³, and various groundwater conditions. The typical geometry of the slope is presented in Figure 5.41.

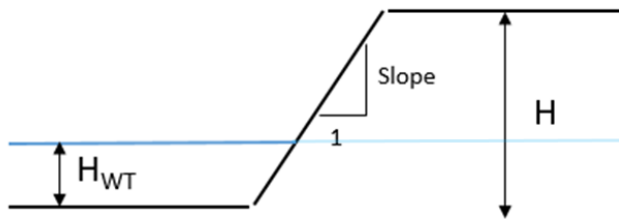


Figure 5.41 Typical scheme of the slope

The effect of free water level on slope stability was studied using 2-D LEM simulations, indicating that the water level rises from the bottom of the slope to the top of the slope. Different levels of groundwater table are considered: a shallow groundwater table which represents the situation where the water level locates at the slope toe, an intermediate groundwater table where the slope is half saturated, and high groundwater table where the slope is completely submerged. The pore-water pressure conditions in the slope are assumed to be hydrostatic both above and below the piezometric line. Therefore, the problem could be interpreted as a “slow” water rise problem. A reservoir, initially dry, is gradually filling up with water, which is raised to the crest with the water level within the slope maintaining the same level. Thus, a constant total unit weight of 20kN/m³ has been assigned to the entire slope above and below the water level. The reference geometry of the model used in calculations is the height of the slope $H=50$ m, the height of the water table H_{WT} varies from 0 m to 50 m, and slope inclination 1H:1V, 2H:1V, and 3H:1V.

The results shown in Figure 5.42 indicate that the FS first decreases and then increases as the water gets closer to the top of the slope. The minimum FS for all three models (Table 5.6) is

obtained for the case when $H_{WT}/H=0.35-0.45$. It turned out that the minimum FS is observed for the cases with the height of the water table (H_{WT}) equal to 35%-45% of the slope height (H).

Table 5.6 Summary of the simulation results for the water level rise

H	H_{WT}	H_{WT}/H	Slope 1H:1V		Slope 2H:1V		Slope 3H:1V	
			FS	$FS_{WT}/FS_{no\ WT}$	FS	$FS_{WT}/FS_{no\ WT}$	FS	$FS_{WT}/FS_{no\ WT}$
50	0	0	0.711	1.000	1.304	1.000	1.939	1.000
50	10	0.2	0.698	0.982	1.249	0.958	1.768	0.912
50	12	0.24	0.696	0.979	1.237	0.949	1.749	0.902
50	15	0.3	0.695	0.977	1.217	0.933	1.729	0.892
50	18	0.36	0.692	0.973	1.213	0.930	1.722	0.888
50	19	0.38	0.694	0.976	1.212	0.929	1.725	0.890
50	20	0.4	0.694	0.976	1.21	0.928	1.726	0.890
50	21	0.42	0.694	0.976	1.21	0.928	1.728	0.891
50	22	0.44	0.695	0.977	1.21	0.928	1.731	0.893
50	23	0.46	0.696	0.979	1.211	0.929	1.734	0.894
50	25	0.5	0.697	0.980	1.215	0.932	1.74	0.897
50	30	0.6	0.706	0.993	1.237	0.949	1.763	0.909
50	40	0.8	0.741	1.042	1.313	1.007	1.866	0.962
50	50	1	0.791	1.113	1.397	1.071	2.047	1.056

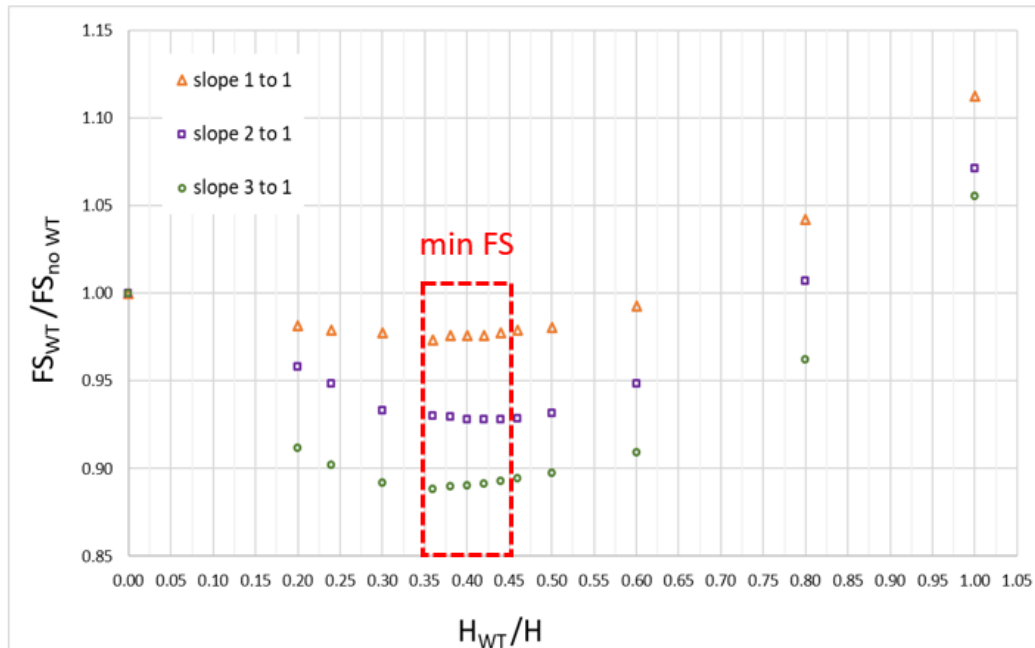


Figure 5.42 Normalized FS vs. the normalized height of the water table

An explanation of the observed minimum of H_{WT}/H is due to the cohesive strength of the slope (which is unaffected by buoyancy) and the balance between soil weight and soil shear strength as the water rise level is varied (Griffiths 2001). This phenomenon is explained graphically in Figure 5.43-5.45.

Figure 5.43 presents the case with the no water slope which gives a FS FS_1 .

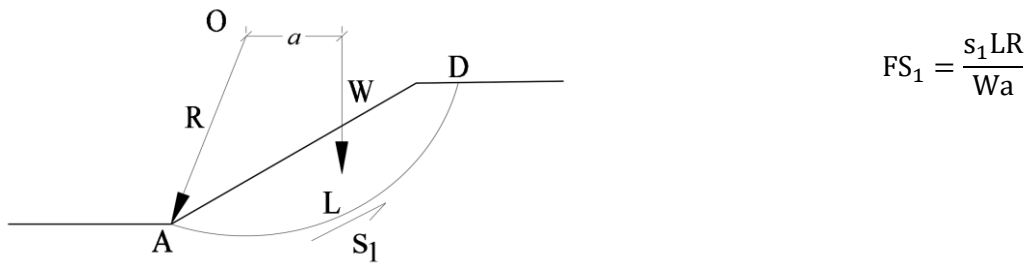


Figure 5.43 Case with the no water slope

With the water rise, the buoyancy on the soil grains decreases the friction in the slope. Figure 5.44 presents the slope with a little bit of water at the bottom. The water at the toe has two effects: it weakens the soil strength along the failure surface within the saturated zone (Points A to B), but the water also provides support by pushing against the slope surface. In Case #2, the influence of the weakening of the soil along the failure surface (A to B on the sketch) prevails over the help provided by the water support against the slope surface. Therefore, the increased weight of the slope has a proportionately greater destabilizing effect than the increased frictional strength and the FS falls.

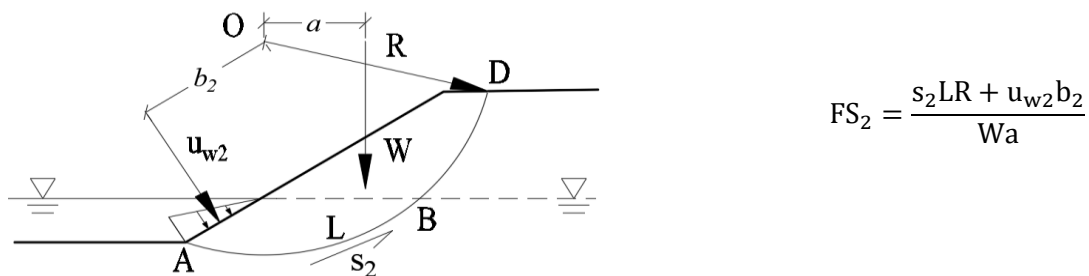


Figure 5.44 Case with the a little bit of water at the bottom

In Figure 5.45 where the water level is much higher, the contrary is true and the water push against the slope surface prevails over the weakening of the shear strength along the failure surface. Therefore the increased frictional strength starts to have a greater influence than the increased weight, and the FS rises.

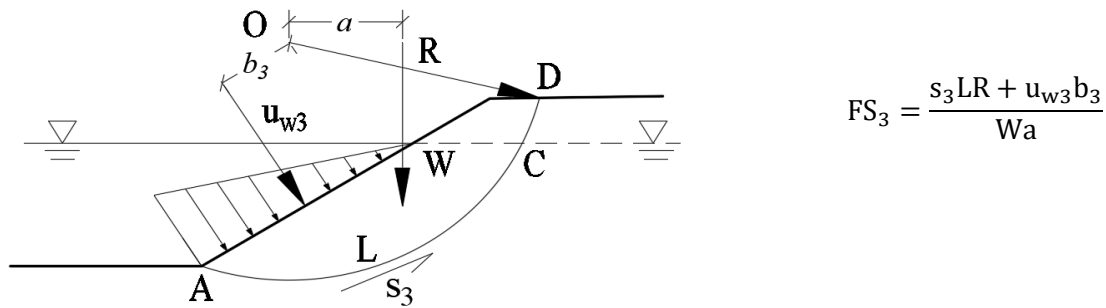


Figure 5.45 Case with the a water level at 2/3 of the height of the slope

Griffiths (2001) studied the phenomenon of a “slow” drawdown problem using an example of the slope with height H and a horizontal free surface at a depth L below the crest. The FS of the slope has been computed for several different values of the drawdown ratio (L/H) which has been varied from -0.2 (slope completely submerged with water level $0.2H$ above the crest), to 1.0 (water level at the base of the slope).

The results shown in Figure 5.46 indicate that the FS reaches a minimum of $FS=1.3$ when L/H varies in between 0.6 and 0.8 (which corresponds to the ration $H_{WT}/H=0.4$ and 0.2 consequently). The figure is also proves that the fully submerged slope ($L/H \leq 0$) is more stable than the “dry” slope ($L/H \geq 1$) as an indicated by a higher FS.

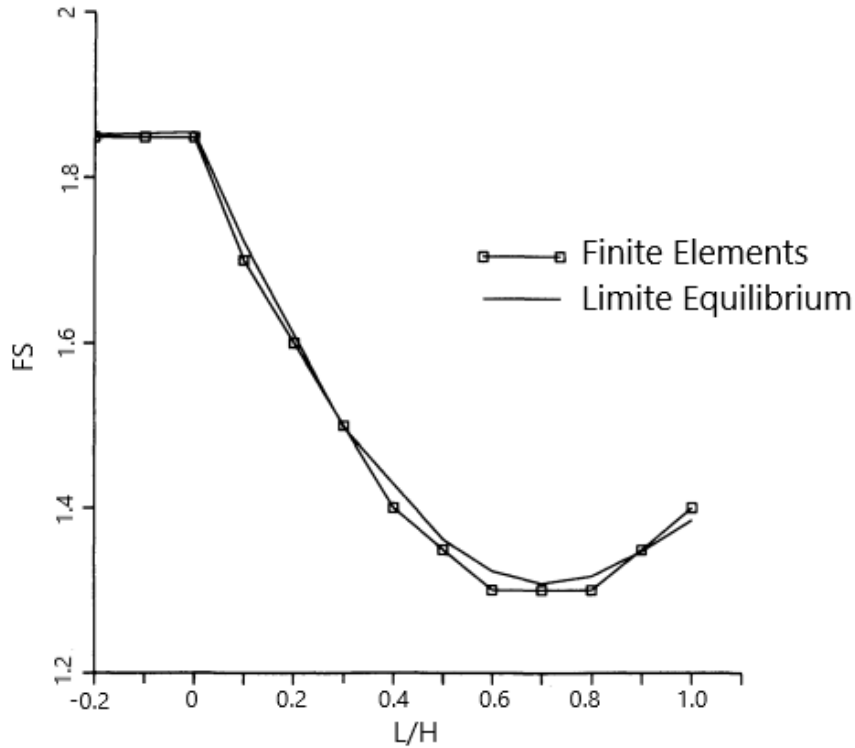


Figure 5.46 FS in a “slow” drawdown problem for different values of the drawdown ratio L/H . Homogeneous slope 2H:1V with a horizontal free surface, $\phi'=20^\circ$, $c'/\gamma H=0.05$ (adapted from Griffiths 2001)

The results obtained by Griffiths (2001) are consistent with the data presented in the current research. The stable “dry” or fully submerged slope ($FS > 1$) became unstable ($FS < 1$) when the water level is at 40% of the slope height.

6. CONCLUSIONS AND RECOMMENDATIONS

6.1 Summary

There are three primary objectives of the study. The first objective is to develop solutions to predict the debris travel distance for improved management and repairs, the setback distance for equipment at the top of the slope, and a stability chart for preliminary selection of the slope angle. The second objective is to compare the 2-D and 3-D slope stability methods to obtain the FS. The third objective is to compare the slope behavior at corners and in plane strain.

6.2 Conclusions and recommendations

Bellow the main results of this dissertation were summarized. They are presented in the order of the chapters in this work.

6.2.1 Chapter 1 – Introduction

In the first chapter the introduction to the research topic, the research objectives, and a step-by-step plan to tackle these research objectives are presented.

6.2.2 Chapter 2 – Overview of open-pit mining

Chapter 2 provides an overview of existing knowledge on slope stability and open-pit mining with the description of the basic open-pit mining geometry and terminology. Several definitions of the slope failures, their types in open-pit mining industry and common failure trigger factors are explained and described.

The three principal levels of slope failures in open-pit mines are emphasized: (a) bench level, (b) inter-ramp level, (c) and overall (global) level. All these three levels of the slope failures (Figure 6.1) are directly related to the volume of the failed material and, therefore, related to the value of the consequences of these failures.

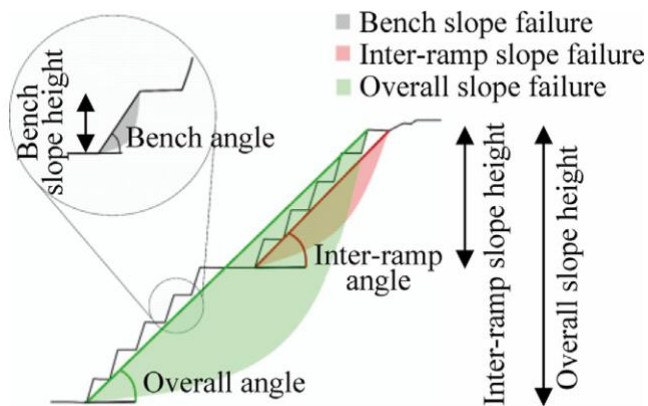


Figure 6.1 (REPEATED) Three principal levels of slope failures in open-pit mining

Chapter 2 offered an extensive literature review on the different types of monitoring techniques utilized by the surface mining industry. Monitoring slope movement has proved to be the most reliable method for detecting slope instability. It was shown that the more accurate measurements were linked to earlier detection of a developing problem. It was discussed that analysis of documented case studies of large-scale rock masses indicates that collapse doesn't happen without warning. Prior to a major movement, measurable deformation and other observable phenomena occur from hours to years before major displacements. Therefore, the main recommendations for the slope monitoring techniques are the following: 1) to verify the open pit design; 2) to maintain safe operational practice; 3) to serve as a warning system as to which areas of the pit are unstable; 4) to identify the location and geometry of the moving mass with precision; 5) to determine the groundwater level and others.

The advantages and drawbacks of different monitoring techniques are discussed. It was found that the best practice for the mine site is to use multiple monitoring tools to evaluate the slope movements.

6.2.3 Chapter 3 – Analysis of case histories of open pit mining slope failures including risk

- Chapter 3 presents the comprehensive literature review on the existing slope failure databases with discussion of their advantages and drawbacks. The limitations of the previous slope failure datasets are summarized in the following statements: (a) many data are collected for natural landslides or civil engineering failures, but not for mining failures; (b) existing databases are focused on one country/region or one particular mine; and (c) existing datasets are quite limited in terms of the number of cases and presented data. Thus, there is a need to organize the open pit slope failure database containing up to date the information that is typically missing in existing databases.

- A 134 open pit slope failure case histories from various mining locations worldwide (29 countries, and over 60 open-pit mines) were organized in the TAMU-MineSlope Spreadsheet. The presented database represents the extended version of the database first started by John Whittall (Whittall 2017). All the collected case histories are described in the database in the same manner. The record information, open pit parameters, geological and geotechnical characteristics, slope failure parameters (including travel distance, fall height and setback distance), its plan and scheme, and literature source are collected for each case. It is important to note that some cells in TAMU-MineSlope are remained empty because of the lack of information for some case histories.

- There are several empirical models for the travel distance prediction for regionally and type-specific natural landslides and man-made slopes. However, from the industry point of view all the existing estimates for the travel distance prediction are challenging to use because they are based on parameters that are difficult to obtain in advance. The best way to develop design equation for the travel distance prediction is to study open pit slope failure database.

- Several approaches were used for travel distance prediction: prediction based on energy principals, a probabilistic approach and prediction interval approach.
- If we assume that the failing mass can be represented by the block sliding down the slope with the height of H_{FALL} and slope angle β , the slope material coefficient of friction is $\tan\phi$, and the travel distance consists of two parts: the inclined distance $X1$ and the horizontal distance $X2$ (Figure 6.2), then the travel distance is proportional to the slope height and inversely proportional to the friction angle of the base material (Eq. 6.1).

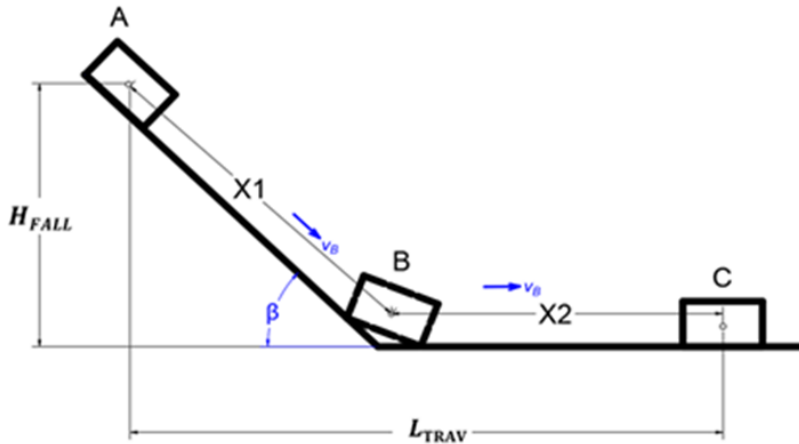


Figure 6.2 (REPEATED) Cut slope failure geometry

$$L_{TRAV}(m) = \frac{H_{FALL}(m)}{\tan \phi} \quad \text{Eq. 6.1}$$

- The same relationship was obtained from the TAMU-MineSlope Spreadsheet, and aiming for the 90% probability when the design value would be greater than observed one, the proposed equation for the preliminary travel distance estimation is shown in Eq. 6.2:

$$L_{TRAV}(m) = 1.8 \cdot \frac{H_{FALL}(m)}{\tan \phi} \quad \text{Eq. 6.2}$$

- For the calculations it is important to know the setback distance for the open pit design because it will help estimate a minimum safe distance from the edge of the pit wall at all

stages of pit development which would provide a buffer zone between personnel and equipment working in the open pit.

- A lot of research has been conducted on the setback distance evaluation, but it mostly addressed the prediction of the subsidence area during the transition from open pit to underground mining and for the case of the open pit closure. A few of the US mining guidelines and reports (e.g. Norman et al. 1997; MN96-1MLR 1996) have recommendations for the minimum allowable setback zone for the period of reclamation, but not for the open pit development. Thus, more study should be done on the setback distance in open-pit mining.

- From our point of view, the best approach for the setback distance estimation is to develop the recommendations based on the open pit slope failure case histories study. Therefore, in this work the relationship between L_{SB} (m) and H_{FAIL} (m) was studied. The proposed equation for the preliminary estimation of the setback distance aiming for 90% probability that the designed L_{SB} would be greater than the observed value is given by the following equation:

$$L_{SB}(m) = H_{FAIL}^{0.82}(m) \quad \text{Eq. 6.3}$$

- The critical distance from the slope crest to the equipment (b, m) was also studied in the presented dissertation. Over 50 slope stability simulations are performed using the 2-D LEM approach (software Slide2, Rocscience Inc.). The crest of the slope was loaded with the mining truck CAT 793F. The truck was moved away from the slope crest at a distance, L (m), and for each location of the truck, the slope stability simulation was performed (Figure 6.4).

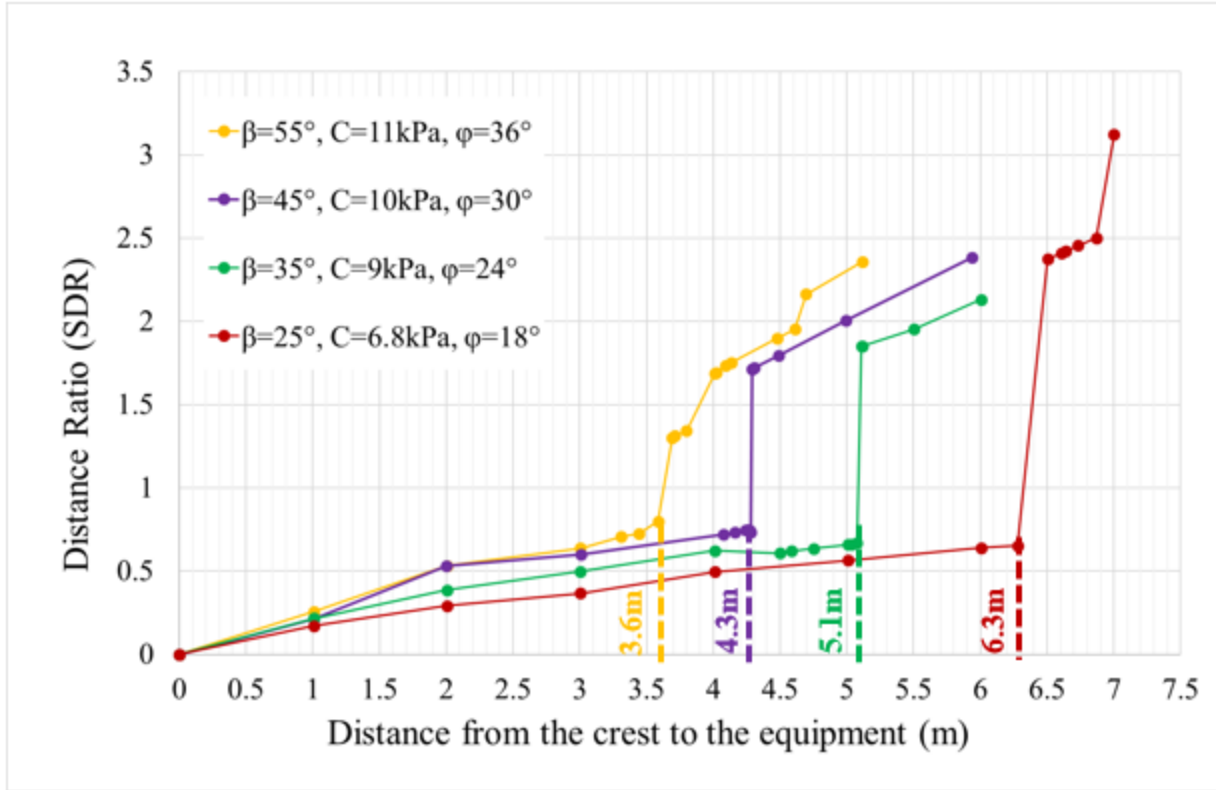


Figure 6.3 (REPEATED) Distance ratio (SDR) vs. Distance from the crest to the mining truck (m) for different slope inclinations. Note that the parameters of the slope were picked such that the analyzed slope without loading is at failure (FS=1)

The obtained results, presented in Figure 6.4, are based on the 2-D model with the slope that has a height of 15 m and various slope angles. The critical distance from the slope crest to equipment is inversely proportional to the height of the slope and geotechnical parameters of the soil.

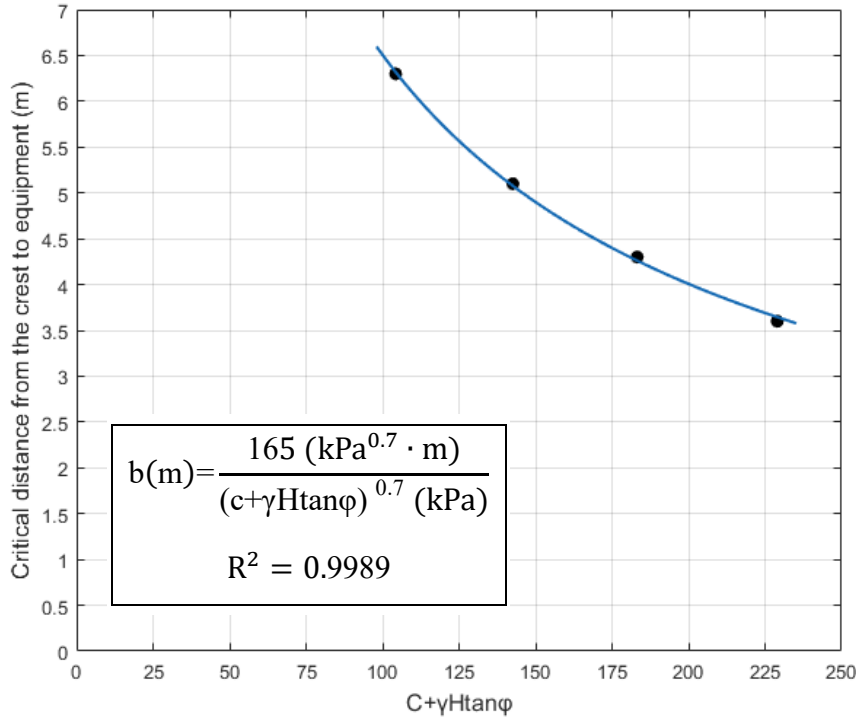


Figure 6.4 (REPEATED) Variation of the critical distance from the crest of the slope to mining truck, b (m), with respect to the value of $(c+\gamma H \tan \phi)$

- Taylor's and Hoek&Bray's stability charts were evaluated using the case histories from the TAMU-MineSlope Spreadsheet. A hundred and twenty cases from the open pit slope failure case histories collection were analyzed, and 120 points were placed directly on Taylor's chart and Hoek&Bray's chart. All points were divided into sets according to the value of the friction angle or slope angle intervals according to the value for Taylor's and Hoek&Bray's chart. Then the 'safe' and 'unsafe' points were defined. The results of Taylor's chart evaluation showed that 57% of the time, the points were on the safe side, and 43% of the time, the points were unsafe, and for Hoek & Bray's chart, the percentages were 62% of safe points and 48% of unsafe points. Hoek & Bray's chart gives a slightly better result than Taylor's stability chart, but to match the open pit slope failure case histories better we decided to propose a new chart.

- A new proposed stability chart for preliminary estimating the slope angle is based on the collected open pit slope failure case histories (Figure 6.5). On the vertical axis is the stability number ($c/\gamma H$) and on the horizontal axis is the friction angle of the slope material ϕ ($^\circ$). The lines in the chart present the different slope angles ($\beta=15^\circ, 20^\circ, 25^\circ, 30^\circ, 35^\circ, 40^\circ, 45^\circ, 50^\circ, \text{ and } 60^\circ$).

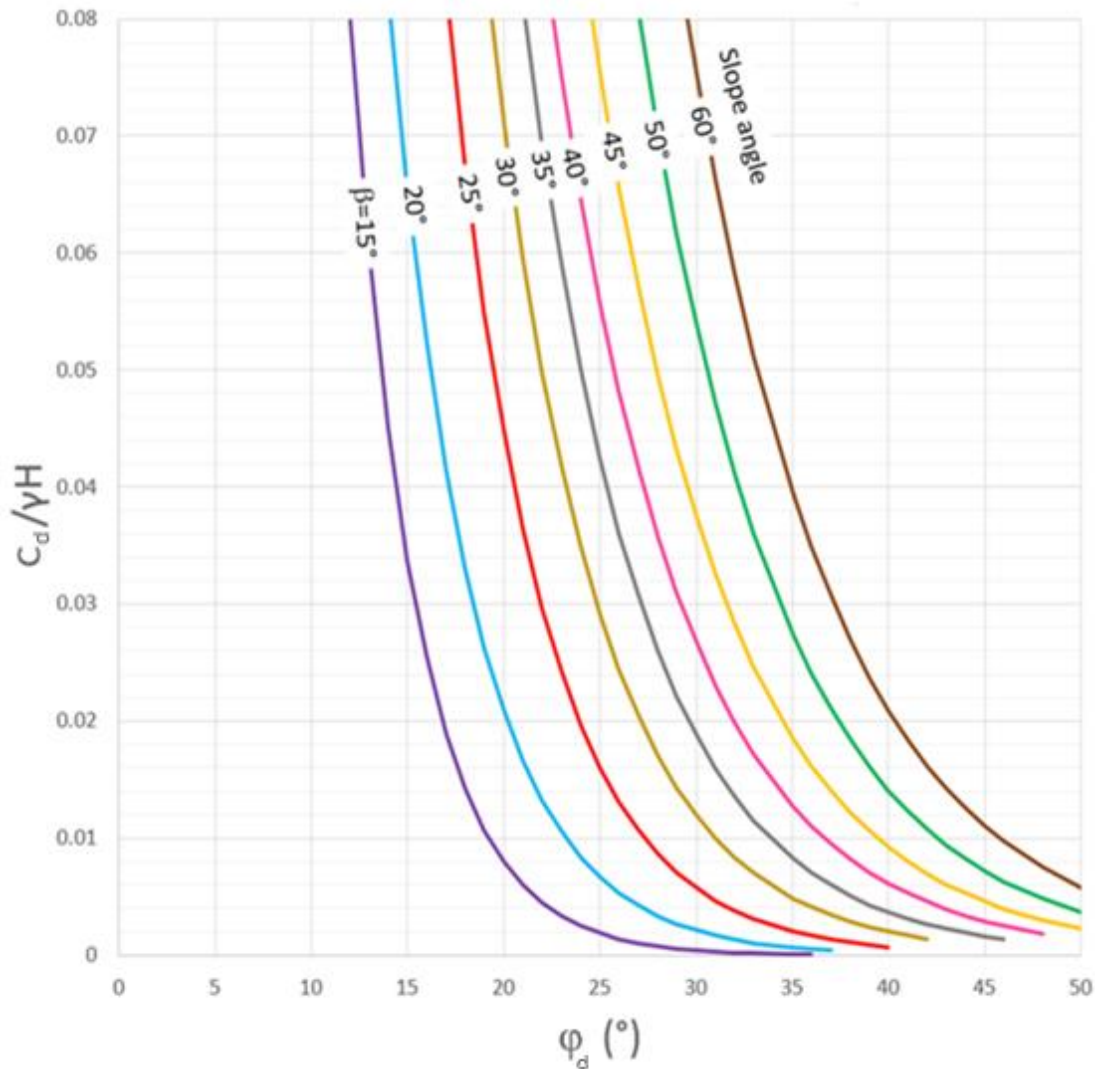


Figure 6.5 (REPEATED) Proposed stability chart based on the 134 open pit slope failure case histories, H is the designed height of the slope in meters

- The dissertation presents the comparative study of the results obtained using Taylor's chart, Hoek&Bray's chart, and the proposed stability chart. The following conclusions

are drawn based on that study results: (a) the proposed stability chart is more conservative than Taylor's and Hoek&Bray's charts (Table 6.1); (b) the developed stability chart is proposed for the preliminary estimation of the FS for the open pit slopes, and it can be used for preliminary slope design and planning; (c) the proposed chart is based on the open pit slope failure case histories; (d) there is a lot of scatter in the collected case histories; (e) the choice of the curves on the chart was aiming for 80% probability that the design would be safer than the observed behavior; (f) based on the actual data from the TAMU-MineSlope Spreadsheet, the proposed stability chart gives 78% of points to be on the safe 'side' and 22% of points on the 'unsafe' side, which is 40% better than Taylor's chart result and 20% higher than Hoek&Bray's chart evaluation result.

Table 6.1 (REPEAED) Comparative study of the results obtained using Taylor's chart, Hoek&Bray's chart and proposed stability chart

Example	Input parameters	Obtained results		
		Taylor's chart	Hoek & Bray's chart	Proposed stability chart
1	FS=1.3 H=70 m $\gamma=18 \text{ kN/m}^3$ c=38 kPa $\phi=30^\circ$	$\beta=34^\circ$	$\beta=30^\circ$	$\beta=26^\circ$
2	H=100 m $\beta=40^\circ$ $\gamma=21 \text{ kN/m}^3$ c=60 kPa $\phi=35^\circ$	FS=1.25	FS=1.2	FS=1.2

- In civil engineering practice, the risk R associated with a project, is defined as the product of the annual probability of failure PoF of that project times the value of the consequence C of the failure. Two risk charts for the United States were constructed based on the analysis of

the data associated with a number of civil and mining engineering activities: the annual PoF versus fatalities risk chart (Figure 6.6) and the annual PoF versus dollars loss risk chart (Figure 6.7).

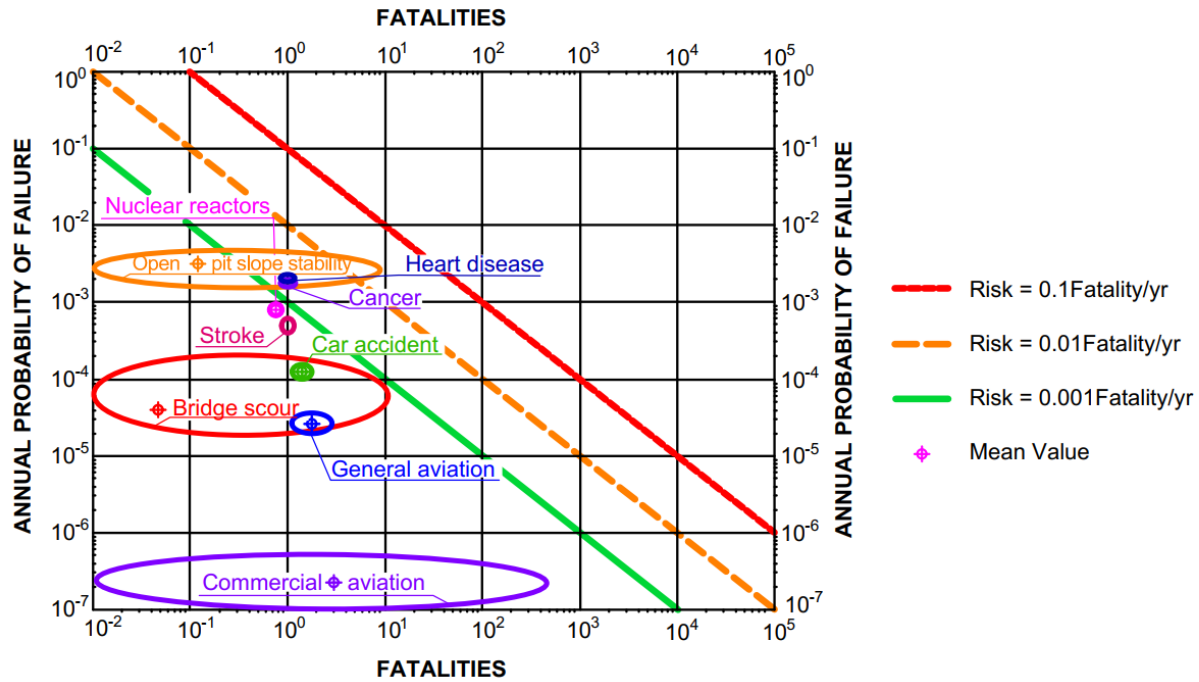


Figure 6.6 (REPEATED) Annual PoF vs. annual number of fatalities due to the failure

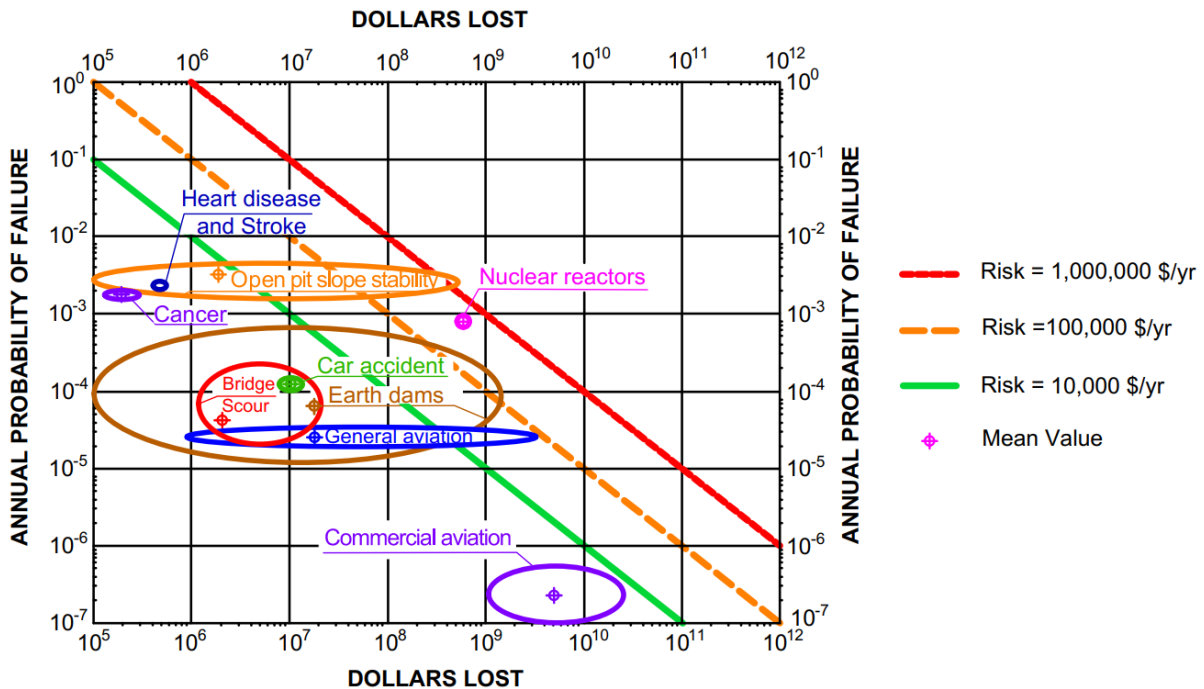


Figure 6.7 (REPEATED) Annual PoF vs. annual economic loss corresponding to the failure

- It should be noted, that there are many different ways to evaluate the statistics associated with fatalities, cost and probability of failure. Many factors can come into play. We chose to precisely document our approach and our calculations considering that the available data limits the applicability of the results. Therefore Chapter 3.5.2 of the dissertation provides a step by step procedure for obtaining the risk location of a given activity on the charts (Figure 6.6 and 6.7)
- The choice of acceptable/tolerable risk is difficult because so many factors beyond geotechnical engineering enter into the decision, including philosophy, politics, public awareness, and social sciences. Judging from the location of the ellipses on the two risk charts, it appears that the public tolerates a risk of 0.001 fatalities per year and 10,000 US dollars per year based on the United States data. The green, orange, and red lines in the two charts (Figure 6.6 and 6.7) correspond to low, medium, and high-risk levels.

Table 6.2 (REPEATED) Risk Levels for the United States

Risk Level	Risk (\$/yr)	Risk (fatalities/yr)
Low (green line)	10,000	0.001
Medium (orange line)	100,000	0.01
High (red line)	1,000,000	0.1

- The mean value for open-pit mining slopes risk drawn based on the actual events is within acceptable limits compared to other risks. But when it comes to the open pit slope design, the target risk is traditionally at a much higher risk than what is typically acceptable in other industries.

6.2.4 Chapter 4 – Comparison of FS by various methods

The comparison of the FS obtained by various methods (2-D LEM, 3-D LEM, 2-D FEM, and 3-D FEM) are presented in this study.

- Extensive literature review analysis shows that slope stability analyses mostly rely on conservative limit equilibrium procedures rather than finite element procedures in mining practice. But on the other hand, many researchers have concluded that the FEM is a powerful alternative to the traditional LEM technique because it can model the stress-strain behavior of slope material.

- In open-pit mining slope stability analysis, two-dimensional (2-D) plane strain analysis techniques are commonly used for simplicity and wide applicability. However, all slope failures are, 3-D in nature, especially in the cases of complex geometric slopes.

- The influence of the model width on the FS is investigated in the presented research. Obtained results show that the slope angle does not affect the value of the FS ratio when W/H is greater than 4. The FS for the slopes with $W/H > 4$ is close to the FS for the plane strain slope. If $W/H < 4$, there is a need for a three-dimensional analysis of the slope since the difference between the 2-D and 3-D can reach 50%.

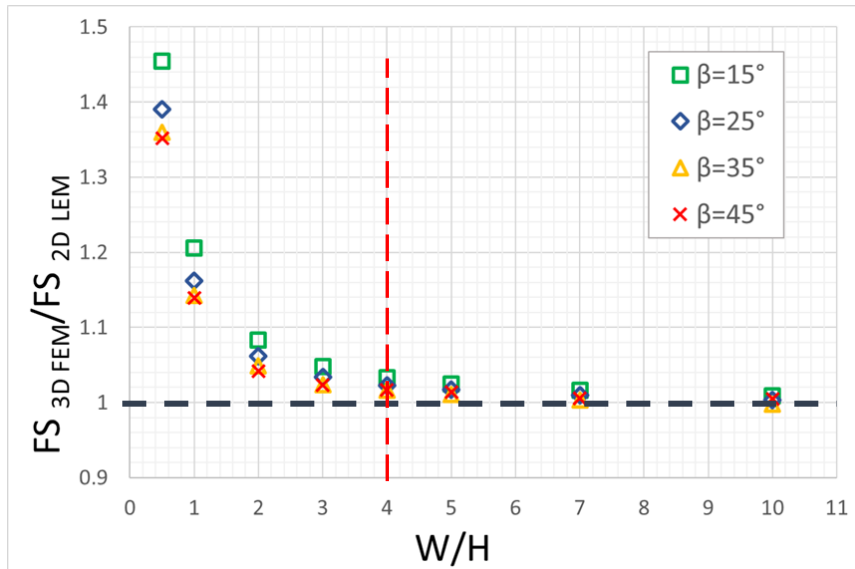


Figure 6.8 (REPEATED) $FS_{3D FEM}/FS_{2-D LEM}$ versus W/H

- Based on the TAMU-MineSlope data, we obtained the W/H ratio for the actual slope failures. Results presented in the dissertation show that 85% of open-pit mining failures have $W/H < 4$, thus performing a 2-D slope stability analysis for the slopes with $W/H < 4$, we will result in underestimating the FS for those slopes.

- Based on a review of existing literature and 2-D and 3-D LE and FE analyses performed in the present study, we concluded that the minimum 3-D FS is greater than the minimum 2-D FS for all conditions considered herein. It was also shown that the most significant influence on the FS gives slope geometry and cohesion rather than the friction angle.

- 3-D slope stability analyses are recommended to compare the FS obtained from 2-D analyses, which are generally considered to provide conservative results (i.e., low FS). With the expected higher FS in 3-D analyses, a cost-effective steeper slope may be designed to maintain adequate stability.

- Due to the high variability of the parameters and uncertainties associated with the geotechnical model, we recommend conducting deterministic and probabilistic analyses.

- Based on the literature review the typical values of CoV are summarized in the Table

6.3

Table 6.3 (REPEATED) Typical values of CoV for some geotechnical properties used in slope stability analysis

Geotechnical properties	Range of CoV	References
Unit weight (γ)	0.03-0.1	Briaud and Tucker (1983), Duncan (2000), Uzielli et al. (2007), Javankhoshdel et al. (2018)
Cohesion (c)	0.2-0.8	Baecher and Christian (2003), Javankhoshdel et al. 2018
Undrained strength (S_u)	0.13-0.4	Lacasse & Nadim (1997); Phoon & Kulhawy (1999); Duncan (2000); Uzielli et al. (2007)
Friction angle (ϕ)	0.02-0.2	Duncan (2000); Baecher and Christian (2003); Uzielli et al. (2007) Javankhoshdel et al. (2018)

- We studied the effect of multiple sampling by dividing the 2-D model into a different number of identical layers. Figure 6.9 shows the PoF associated with the different number of layers intersected by the critical slip surface. It also can be concluded that by increasing the number of identical layers, the error may cancel out, and there is less chance of having extremely low values of input parameters along the most critical slip surface.

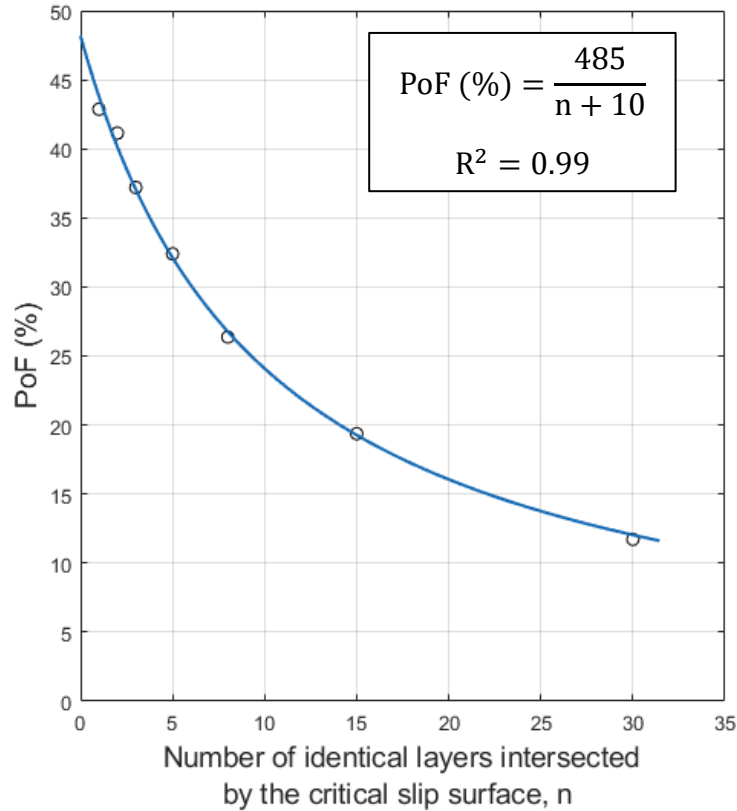


Figure 6.9 (REPEATED) PoF vs. number of layers with identical material properties intersected by the critical slip surface (n)

- The typical FS and PoF acceptance criteria for open-pit mining slope design were investigated in the dissertation (Table 6.4). The design criteria for open-pit slopes should be based on the idea that the more serious the consequence of failure or the higher the uncertainty, the higher the FS and the lower the allowable PoF.

Table 6.4 (REPEATED) Typical FS and PoF acceptance criteria for open-pit mining slopes

Scale of the slope	Consequence of failure		
	Low	Medium	High
Bench	FoS ≥ 1.1 PoF ≤ 25-50%		
Inter-ramp	FoS ≥ 1.15-1.2 PoF ≤ 25%	FoS ≥ 1.2 PoF ≤ 20%	FoS ≥ 1.2-1.3 PoF ≤ 10%
Overall	FoS ≥ 1.2-1.3 PoF ≤ 15-20%	FoS ≥ 1.3 PoF ≤ 5-10%	FoS ≥ 1.3-1.5 PoF ≤ 5%

- We were trying to answer why according to the current state of practice, the target FS for the long-term stability of slopes is 1.5 and PoF is around 0.1, whereas most geotechnical engineers use FS = 2.5 to 3.0 and PoF=0.001 for bearing capacity design. Several researchers have studied that phenomenon (Duncan et al. 2014, Griffiths 2015), and, based on the literature analysis, we made the following conclusions:

(a) In case of undrained shear strength (s_u) $FS_{load} = FS_{strength}$.

(b) For $c-\phi$ soils for a shallow foundation assuming Terzaghi's equation is applied, FS_{load} different from $FS_{strength}$.

(c) Terzaghi's bearing capacity equation does not work when the strength profile is different from a linear increase with depth. In addition, such linear strength increase with depth is rarely encountered in the field. Thus, (b) above is rarely the case.

(d) If Terzaghi's equation does not apply and the direct strength equations do apply, $p_u = ks + \gamma D$, where p_u is the ultimate bearing pressure, k is bearing capacity factor, s is a soil strength measurement (CPT_{qc} , PMT_{pL} , SPT_N , undrained shear strength s_u), then $FS_{load} = FS_{strength}$.

(e) For a friction pile $FS_{load} = FS_{strength}$ for any soil types.

(f) For end bearing piles FS_{load} different from $FS_{strength}$ if (b) is accepted.

(g) All these points cast doubt on the validity of the FS for load (FS_{load}) different from the FS for soil strength ($FS_{strength}$).

6.2.5 Chapter 5 – Stability of slope corners and other unusual slope cases

Chapter 5 provides the results of concave and convex corner stability calculations and all the results are compared with 2-D plane strain case.

- A comprehensive literature review on 3-D slope stability analysis emphasizes that the effect of complex geometries on 3-D slope stability is rarely studied. In engineering practice, concave-shaped slopes always show better stability than convex-shaped slopes. At the same time, in the mining industry, convex slopes with small turning corners tend to be avoided since they are prone to deformations and slope failures. The effect of complex geometries on 3-D slope stability is still unclear, but it is important in slope engineering, especially in the safe and economical design of open pit infrastructure.

- It was found that the FS changes very little while the displacement changes a lot: the FS varied within 1% for the different concave and convex corner simulations. The possible reason for the such small variation of FS is that the FEM technique is unable to identify the local zone at the corner of the two slopes. Instead, the SR methods seem to concentrate on the global failure zone associated with the plane strain case on either side of the corner. This appears to be a limitation of the FEM/SR method. This is why we suggest a displacement-based approach rather than an FS approach to evaluate the slope corners' behavior.

- The series of the 3-D FEM simulations allowed to prove that the displacement is inversely proportional to the FS (Eq. 6.4).

$$u_t(m) = \frac{K}{FS} \quad \text{Eq.6.4}$$

in which $u_t(m)$ is the total displacement in meters, FS is the factor of safety, and K is a constant, which mostly dependent on Young's modulus (Figure 6.10).

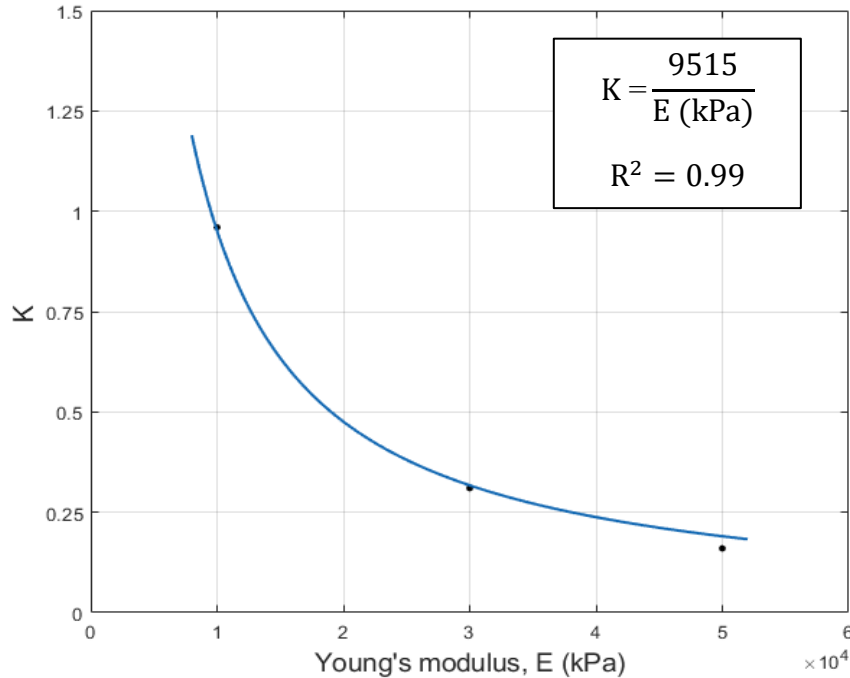


Figure 6.10 (REPEATED) Variation of the K-value with respect to Young's modulus, E (kPa). Homogenous slope, $\gamma=20$ kN/m³, $c=10$ (kPa), $\phi=30^\circ$, $\psi=0^\circ$, $\nu=0.28$

- A total 164 different conditions were analyzed using ten different corner angles (30° , 60° , 90° , 120° and 150° with convex shape, and 210° , 240° , 270° , 300° and 330° with concave shape, along with 180° for comparison), four different slope angles (15° , 25° , 35° and 45°) and four different turning corners (1 m, 5 m, 10 m and 15 m). The results of calculations are presented in Figures 6.11-6.14. On the vertical axis is the normalized total 3-D FEM displacement collected at the tip of the slope, and on the horizontal axis are different plan view angles normalized by 180° . Each set of points presents the corresponding radius of curvature to the height of the slope ratio, $R/H = 0.07, 0.33, 0.67$, and 1 (see Figures 6.11, 6.12, 6.13, and 6.14 respectively).

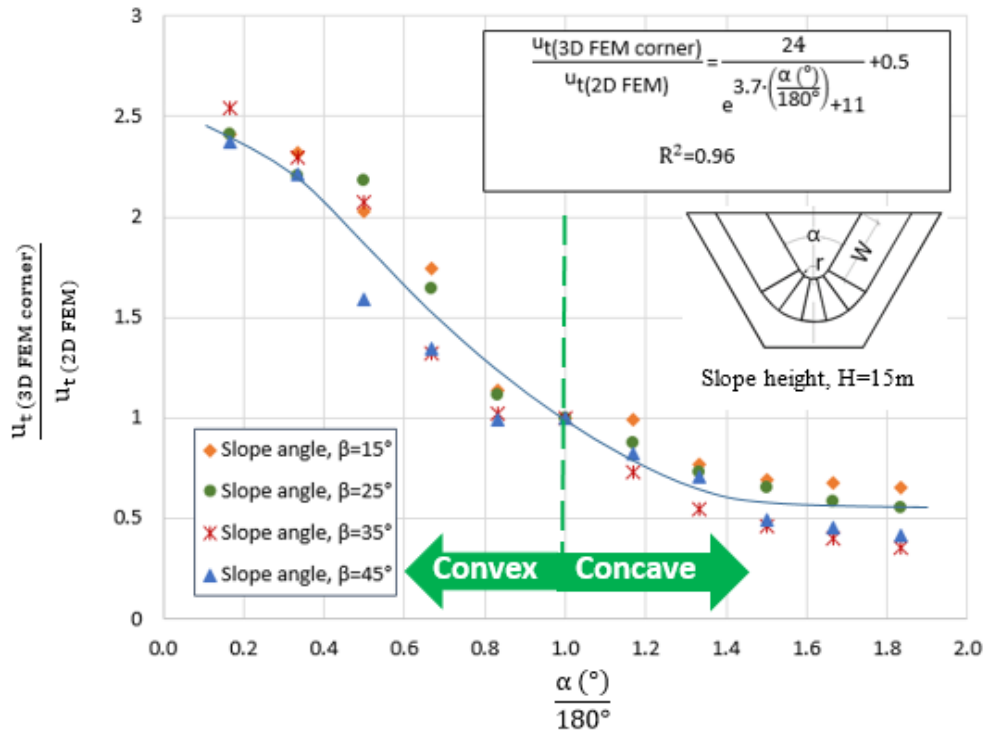


Figure 6.11 The difference in the normalized total displacement with respect to the normalized plan view angle for different slope angles (for $r/H=0.07$)

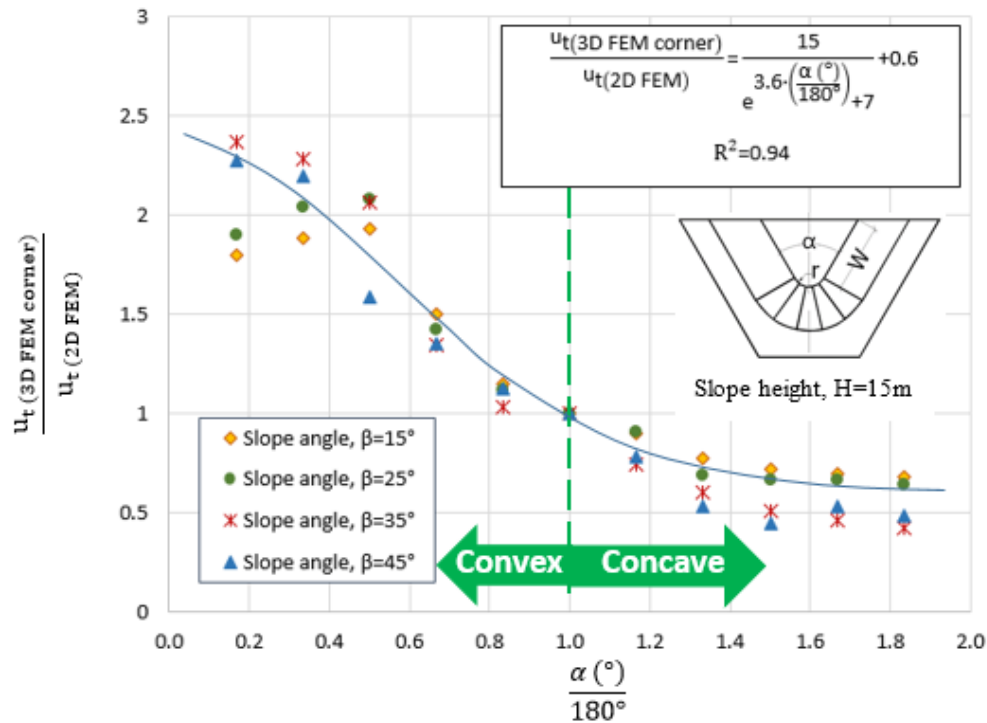


Figure 6.12 The difference in the normalized total displacement with respect to the normalized plan view angle for different slope angles (for $r/H=0.33$)

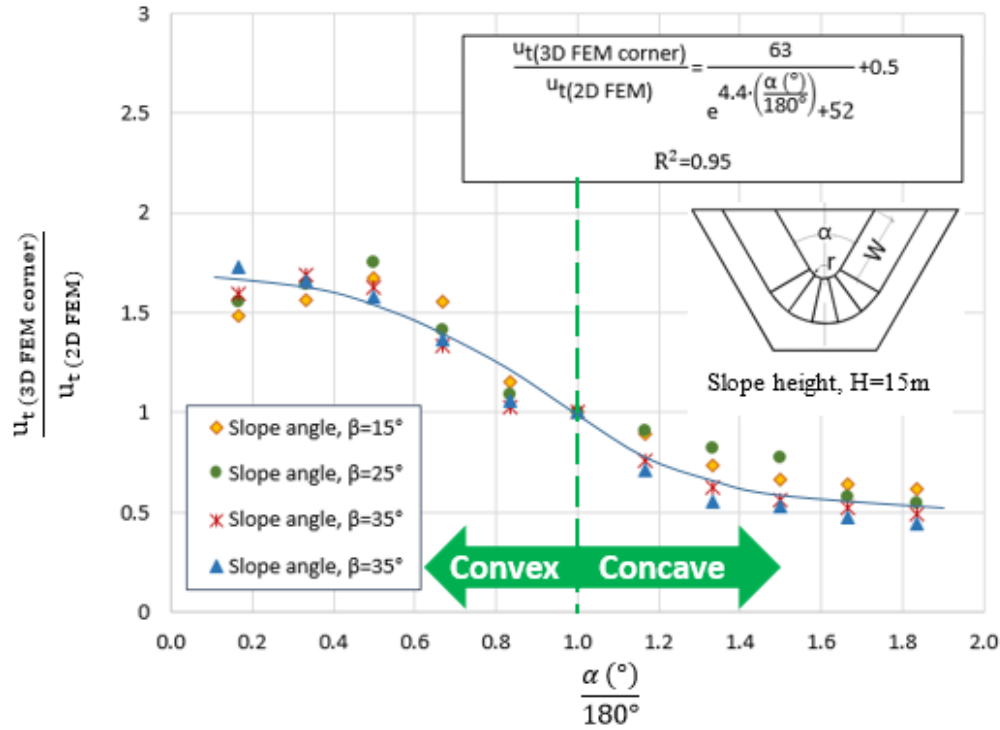


Figure 6.13 The difference in the normalized total displacement with respect to the normalized plan view angle for different slope angles (for $r/H=0.67$)

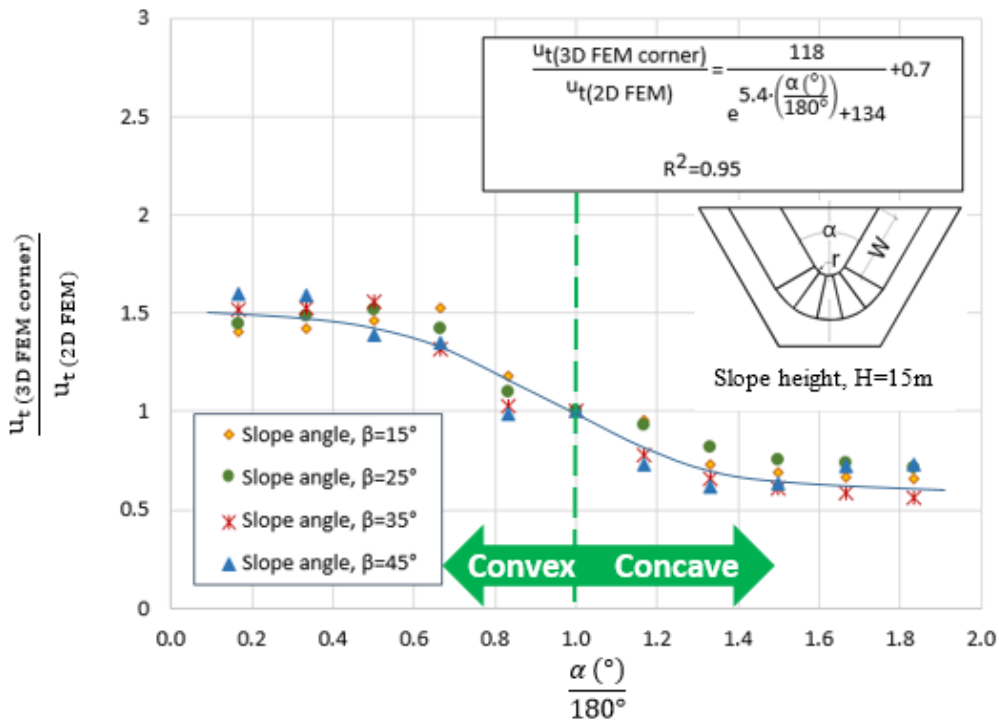


Figure 6.14 The difference in the normalized total displacement with respect to the normalized plan view angle for different slope angles (for $r/H=1$)

- In the case of the very sharp concave angle, the total displacement is a lot less (about 50% compared to the plane strain case). In the case of the very sharp convex angle, the total displacement is about 2.5 times greater compared to the plane strain case. For convex-shaped slopes, the total displacement decreased as the slope turning corner value increases from 30° to 150°, and for concave-shaped corners, it is increased as the slope turning corner value decreases from 330° to 210°. The near-flat corner angles (150° and 210°) are characterized by the value of total displacement close to the plane strain case. The slope angle does not significantly affect the value of the normalized displacement. Moreover, with the increasing of the radius of curvature, the value of normalized total displacement at the peak of the corner crest is decreasing from 2.5 to 1.5 for the convex corner and decreasing from 0.75 to 0.3 for concave corners.

- One example of the obtained results is presented herein. Based on the regression line analysis presented in Figure 6.11, the sharp convex corner ($\alpha < 30^\circ$) may have a FS can be 40% smaller than the FS of the plane strain case (Eq. 6.5) and for the sharp concave ($\alpha < 150^\circ$) corner it may have a FS 3.33 times larger than the plane strain FS (Eq. 6.6). With the radius of curvature increase, the difference between sharp corner stability and the plane strain case decreases.

$$FS_{\text{Sharp Convex}(r/H=0.07)} = 0.4 \cdot FS_{2D \text{ LEM}} \quad \text{Eq. 6.5}$$

$$FS_{\text{Sharp Concave}(r/H=0.07)} = 3.33 \cdot FS_{2D \text{ LEM}} \quad \text{Eq. 6.6}$$

- Two parameters affect the stability of the bench and the overall slope: the cohesion of the slope material and the height of the slope. If the cohesion of the material increases, the influence of benching is increasing as well. For materials with low cohesion, the role of benching is less favorable and vice versa. For the cohesive materials, the bench FS depends on the height of the bench: for a lower height of the bench, the FS increases dramatically.

- The FS first decreases and then increases as the water gets closer to the top of the slope. It turned out that the minimum FS is observed for the cases with the height of the water table (H_{WT}) equal to 35%-45% of the slope height (H). In other words, the stable “dry” or fully submerged slope ($FS > 1$) became unstable ($FS < 1$) at a critical water level $H_{WT} \approx 0.4H$ (Figure 6.15).

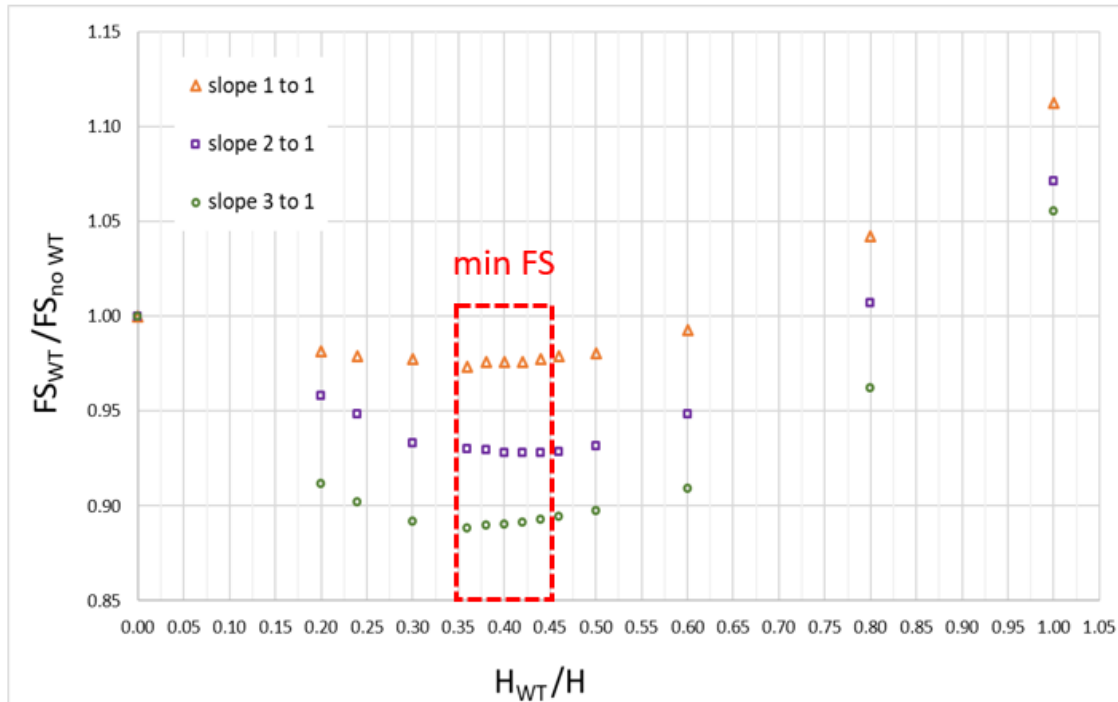


Figure 6.15 (REPEATED) Normalized FS vs. the normalized height of the water table

6.3 Summary contribution to new knowledge

- A detailed database on open mine slope failures (134 cases) named the TAMU-MineSlope Spreadsheet was developed.
- Prediction equations including probability of exceedance of debris travel distance was proposed.
- Prediction equations including probability of exceedance of equipment setback distance and safety buffer zone at the slope crest were proposed.
- Existing slope stability charts using the TAMU-MineSlope Spreadsheet (Taylor, Hoek and Bray) were evaluated.
- A new stability chart based on the TAMU-MineSlope Spreadsheet was proposed.
- Method of quantification of the risk associated with open pit mining slopes was proposed.
- The difference in FS between 2-dimensional limit equilibrium method, 3-dimensional limit equilibrium method, and 3-dimensional finite element method was evaluated and quantified.
- And, lastly, the difference in behavior between a slope corner and a plane strain slope was quantified.

6.4 Future research directions

Open-pit slope failure case histories collection has to be continuously updated with the new cases of slope failures.

There is a need to investigate effective and efficient use of software utilizing FEM techniques for back analysis of failed slopes.

3-D corner stability should be investigated for the models with different slope height and different geotechnical parameters.

Very little work has been done on 3-D seismic slope stability, therefore the 3-D concave and convex corner stability study should be performed to evaluate the influence of the seismic conditions.

More emphasis needs to be placed on 3-D slope stability for unsaturated soil conditions.

And, lastly, there is a need to study the influence of the loading at the crest of the concave and convex corner.

REFERENCES

- Abele G. (1997). Rockslide movement supported by the mobilization of groundwater-saturates valley floor sediments. *Zeitschrift für Geomorphologie*, 41: 1-20.
- Abramson L.W., Lee T.S., Sharm S., and Boyce G.M. (1996). *Slope Stability and Stabilization Methods*. John Wiley & Sons, New York.
- Abzar S. (2019). Slope stability monitoring in open pit and underground mining. Published on May 21, 2019. <https://www.linkedin.com/pulse/slope-stability-monitoring-open-pit-underground-mining-samin-abzar/> (accessed June 22, 2021).
- Adams B. (2015). Slope stability acceptance criteria for opencast mine design. In *Proceeding of the 12th Australia New Zealand Conference on Geomechanics*. Wellington, New Zealand Paper No. 120.
- Afeni T.B., and Cawood F.T. (2013). Slope monitoring using total station: What are the Challenges and How Should these be mitigated? *South African Journal of Geomatics*, 2(1), February 2013: 41-53.
- Akhtar K. (2011). Three-dimensional slope stability analyses for natural and manmade slopes. PhD Dissertation. University of Illinois at Urbana-Champaign. Urbana, Illinois.
- Akhtar K. and Stark T. (2017). Importance of Side Resistance in a 3D Stability Analysis. *Geotechnical Frontiers 2017 GSP 278*: 285-293.
- Albataineh N. (2006) Slope stability analysis using 2d and 3d methods. Master of Science thesis. The University of Akron. August 2006.
- Allahverdizadeh P., Griffiths D.V., and Fenton G.A. (2017). The random finite element method (RFEM) in probabilistic slope stability analysis with consideration of spatial variability of soil properties. In *Proceedings of the International Foundations Congress and Equipment Expo: IFCEE 2015, San Antonio, TX 17-21 March, 2015*: 1946-1955.
- American Heart Association (AHA). (2018). *Heart Disease and Stroke Statistics – 2018 Update: Summary A Report From the American Heart Association*. (Ed. E.J. Benjamin et al.). 426p.
- American Society of Civil Engineers (ASCE). (2020). 2017 Infrastructure Report Card. 2020. <<https://www.infrastructurereportcard.org/>>
- Angeli M.-G., Pasuto A, and Silvano S. (2000). A critical review of landslide monitoring experiences. *Engineering Geology*. 55 (2000): 133–47.

- Aryal K.P. (2006). Slope stability evaluations by limit equilibrium and finite element methods. PhD dissertation. Norwegian University of Science and Technology. Trondheim, Norway.
- Assis A. (2020) Risk management for geotechnical structures: consolidating theory into practice. *Soils and Rocks*, 43(3): 311-336.
- Association of State Dam Safety Officials (ASDSO). (2020a). <<https://damsafety.org/>>
- Association of State Dam Safety Officials (ASDSO). (2020b). Case Study: Teton Dam (Idaho, 1976) <https://damfailures.org/case-study/canyon-lake-dam-south-dakota-1972> (accessed December 14, 2020)
- Association of State Dam Safety Officials (ASDSO). 2020c. Lessons Learned From Dam Incidents and Failures. <<https://damfailures.org/lessons-learned/>>
- Ayotte D., and Hungr O. (1998). Runout analysis of debris flows and debris avalanches in Hong Kong, Final Report. Report to the Geotechnical Engineering Office, Hong Kong. University of British Columbia, Vancouver, B.C.
- Baecher G.B., and Christian J.T. (2003). *Reliability and Statistics in Geotechnical Engineering*. John Wiley and Sons, United Kingdom
- Baker R. (2003). A second look at Taylor's stability chart. *Journal of Geotechnical and Geoenvironmental Engineering*, 129(12): 1102–1108.
- Bar N., and Heweston A. (2018). Considerations for effectively using probability of failure as a means of slope design appraisal for homogeneous and heterogeneous rock masses. *International Scholarly and Scientific Research & Innovation*, 2018, 12(2): 66-72.
- Bar N., Kostadinovski M., Tucker M., Byng G., Rachmatullah R., Maldonado A., Pötsch M., Gaich A., McQuillan A., and Yacoub T. (2020). Rapid and robust slope failure appraisal using aerial photogrammetry and 3D slope stability models, *International Journal of Mining Science and Technology*, 30(5): 651-658.
- Bar N., Nicoll S., and Pothitos F. (2016). Rock fall trajectory field testing, model simulations and considerations for steep slope design in hard rock. APSSIM 2016, Brisbane, Australia: 457-466.
- Barreto dos Santos T., Lana S.M., Pereira T.M., and Canbulat I. (2019). Quantitative hazard assessment system (Has-Q) for open pit mine slopes. *International Journal of Mining Science and Technology* 29 (2019): 419–427.

- Becker D. E. (1996). "Eighteenth Canadian Geotechnical colloquium: Limit states design for foundations. Part 1. An overview of the foundation design process." *Canadian Geotechnical Journal*, 33(6): 956–983.
- Bhatt S.K., and Mark C. (2000). Analysis of Safety Aspects And Mining Practices For Effective Ground Control in Surface Mining. *Proceedings of the 19th International Conference on Ground Control in Mining, 2000, Morgantown, WV (2000): 395-404.*
- Bieniawski ZT. (1976). Rock mass classification in rock engineering. In *Exploration for Rock Engineering* (ed. ZT. Bieniawski), Vol. 1, Balkema, Cape Town: 97-106.
- Bishop A.W. (1955) The use of the slip circle in the stability analysis of earth slopes. *Geotechnique*. Vol.5 (1955): 7-14.
- Bishop A.W., and Morgenstern N. (1960) Stability coefficients for earth slopes. *Geotechnique*, 10 (1960): 29-150.
- Bond J., Chrzanowski A., and Wilkins R. (2005). Using GPS for Augmenting Deformation Monitoring Systems in Open Pit Mines- Problems and Solutions. *Geomatica 2005*, 59(1): 73-82.
- Bond J.; Kim D., Chrzanowski A., and Szostak-Chrzanowski A. (2007). Development of a Fully Automated, GPS Based Monitoring System for Disaster Prevention and Emergency Preparedness: PPMS^{+RT}. *Sensors 2007*, 7: 1028-1046.
- Briaud J.-L. (2007). Spread footings in sand: load settlement curve approach. *Journal of Geotechnical and Geoenvironmental Engineering*, 2007, 133(8): 905-920.
- Briaud J.-L., and Gardoni P. (2009). The concept of geotechnical risk and its implementation, presented at the 17th International Conference on Soil Mechanics and Geotechnical Engineering Alexandria, Egypt, 5–9 October 2009.
- Briaud J.-L., and Tucker L. (1984). Coefficient of variation of in situ tests in sand. *ASCE Symposium on "Probabilistic Characterization of Soil Properties: Bridge Between Theory and Practice"* Atlanta, Georgia, May 17, 1984.
- Briaud J.-L., and Gibbens R. (1999). Behavior of five large spread footings in sand. *Journal of Geotechnical and Geoenvironmental Engineering*, 1999, 125(9): 787-796.
- Briaud J.-L. (2013). *Geotechnical Engineering: unsaturated and saturated soils*, New Jersey, USA: Wiley, 998 p.
- Briaud J.-L., Gardoni P., and Yao C. (2012). Bridge Scour Risk. In *Proceedings of the 6th*

- Conference on Scour and Erosion ICSE-6 Paris - August 27-31, 2012.
- Briaud J.-L., Gardoni P., and Yao C. (2014). Statistical, Risk, and Reliability Analyses of Bridge Scour. *Journal of Geotechnical Engineering* 140(2): 04013011(10).
- Broadbent C. D. and Ko K. C. (1971). Rheologic aspects of rock slope failures. In *Proceedings of the 13th U. S. Symposium on Rock Mechanics*, University of Illinois, Urbana, Aug. 30-Sept. 1, 1971.
- Bui XN., Hoang Nguyen H., Choi H., Nguyen-Thoi T., Zhou J., and Dou J. (2020). Prediction of slope failure in open pit mines using a novel hybrid artificial intelligence model based on decision tree and evolution algorithm. *Scientific reports* 10:9939(2020).
- Bye A.R., and Bell F.G. (2001). Stability assessment and slope design at Sandsloot open pit, South Africa. *International Journal of Rock Mechanics & Mining Sciences* 38 (2001): 449–466.
- Cala M., and Flisiak J. (2001). Slope stability analysis with FLAC and limit equilibrium methods. In *Bilaux, Rachez, Detournay & Hart (eds.) FLAC and Numerical Modelling in Geomechanics*: 111-114.
- Cala M., Flisiak J., and Tajdus A. (2004). Slope stability analysis with modified shear strength reduction technique. In *Proceedings of the 9th International Symposium on Landslides*. Rio de Janeiro, Brazil, 2004.
- Call R.D. (1992). Slope Stability. In: *SME Mining Engineering Handbook*. Vol. 1. Colorado: Society for Mining, Metallurgy and Exploration, Inc. Littleton, 1992: 881-896.
- Call R.D., and Savely J.P. (1990). Open Pit Rock Mechanics. In *Surface Mining*, 2nd Edition (ed. B.A. Kennedy). Littleton: Society for Mining, Metallurgy and Exploration, Inc.: 860-882.
- Call R.D., Ryan T.M., and Barkley R.C. (1993). Geotechnical analyses for open pit mining in areas of large-scale slope instability. In: *Innovative Mine Design for the 21st Century*, Bawden & Archibald (eds): 45-56.
- Call R.D., Cicchini P.F., Ryan T.M. and Barkley R.C. (2000). Managing and Analyzing Overall Pit Slopes in Slope Stability in Surface Mining. W.A. Hustrulid. Ed., Soc. for Mining, Metallurgy, and Exploration, Inc: Littleton, Colorado: 39-46.
- Camargo J., Velloso R.Q., and Vargas Jr. E.A. (2016). Numerical limit analysis of three-dimensional slope stability problems in catchment areas. *Acta Geotechnica* (2016) 11: 1369–1383.

- Cao A.Y., Dou L.M., Yan R.L., Jiang H., Lu C.P., Du T.T. and Lu Z.Y. (2009). Classification of microseismic events in high stress zone. *Mining Science and Technology*, 19(6): 718–723.
- Carter T.G. (1992). A New Approach to Surface Crown Pillar Design. In *Proceedings of the 16th Canadian Rock Mechanics Symposium*, Canadian Rock Mechanics Association, Sudbury 1992: 75–83.
- Casey J.P. (2019). US mining industry accidents and fatalities in 2018 analyzed in *Mining Technology*, 20 June 2019 <www.mining-technology.com>
- Cavounidis S. (1987). On the ratio of factors of safety in slope stability analyses. *Geotechnique* 1987, 37 (2): 207-210.
- Cawood F.T. and Stacey T. R. (2006). Survey and Geotechnical Slope Monitoring Considerations, *Journal of the South African Institute of Mining and Metallurgy*, 106 (7): 495-501.
- Centers for Disease Control and Prevention (CDC). (2020). Deaths and Mortality, <<https://www.cdc.gov/nchs/fastats/deaths.htm>>
- Chakraborty, A. and Goswami, D. (2016). State of the art: Three Dimensional (3D) Slope-Stability Analysis, *International Journal of Geotechnical Engineering*, 10:5: 493-498.
- Chappel A.P. (1998). An engineering geological investigation into pit slope stability at Macraes Gold Mine, Macraes Flat, Otago, New Zealand. *Marter Thesis*. University of Canterbury, New Zealand.
- Chen R.H. and Chameau J.-L. (1983). Three-Dimensional Limit Equilibrium Analysis of Slopes. *Geotechnique* 1983, 32(1): 31-40.
- Cheng H., Chen J., Chen R., Chen G., and Zhong Y. (2018) Risk assessment of slope failure considering the variability in soil properties. *Computers and Geotechnics* 103 (2018): 61–72.
- Cheng Y.M., Lansivaara T., and Wei W. B. (2007). Two-dimensional slope stability analysis by limit equilibrium and strength reduction methods. *Computers and Geotechnics* 2007, 34(3): 137–150.
- Cheng Y.M., Liu H.T., Wei W.B., and Au S.K. (2005). Location of critical three-dimensional nonspherical failure surface by NURBS functions and ellipsoid with applications to highway slopes. *Computers and Geotechnics* 2005, 32(6): 387–99.

- Cheng Y.M. and Yip C.J. (2007). Three-dimensional asymmetrical slope stability analysis extension of Bishop's, Janbu's, and Morgenstern-Price's techniques. *Journal of Geotechnical and Geoenvironmental Engineering*, 2007, 133(12): 1544-1555.
- Ching J., and Phoon K.K. (2013). Effect of element sizes in random field finite element simulations of soil shear strength. *Computers and Structures*, 126 (2013): 120-134.
- Chiwye H.T. and Stacey T.R. (2010). A comparison of limit equilibrium and numerical modelling approaches to risk analysis for open pit mining. *The Journal of the Southern African Institute of Mining and Metallurgy* 2010, 110: 571-580.
- Cho S.E. (2007). Effects of spatial variability of soil properties on slope stability. *Engineering Geology* 92 (2007): 97-109.
- Cho S.E. (2010). Probabilistic assessment of slope stability that considers the spatial variability of soil properties. *Journal of Geotechnical and Geoenvironmental Engineering* 2010, 136 (7): 975-984.
- Chowdhury R.N. (1978). Slope analysis. *Developments in geotechnical engineering*, Vol 22. Amsterdam, Oxford, New York: Elsevier: 423 p.
- Christian J. and Baecher G. (2011). Unresolved Problems in Geotechnical Risk and Reliability. In *Proceedings of the conference "Georisk 2011" June 26-28, 2011. Atlanta, Georgia. ASCE* 2011: 50-63.
- Christian J.T, Ladd C.C., and Baecher G.B. (1994). Reliability applied to slope stability analysis. *Journal of Geotechnical Engineering, ASCE*, 120(12): 2180-2207.
- Chugh A.K. (2003). On the boundary conditions in slope stability analysis. *International Journal for Numerical and Analytical Methods in Geomechanics*. 2003; 27: 905-926.
- Coates B.J., Slinger S.J. Summers J.D. and Bayley H.S. (1977). Metabolizable energy values and chemical and physical characteristics of wheat and barley. *Canadian Journal of Animal Science*, 57: 195-207..
- Coggan J.S., Stead D. and Eyre J.M. (1998). Evaluation of techniques for quarry slope stability assessment. *T.I.M.M. -Section B 107: B139-B147*.
- Collier P.A. (1993). Deformation monitoring using the Global Positioning System. In *Geotechnical Instrumentation and Monitoring in Open Pit and Underground Mining*, Szwedzicki T. (ed.)

- Contreras L.F. (2015). An economic risk evaluation approach for pit slope optimization. *The Journal of the Southern African Institute of Mining and Metallurgy*, Volume 115, July 2015: 607-622.
- Corominas J. (1996). The angle of reach as a mobility index for small and large landslides. *Canadian Geotechnical Journal*, 33: 260–271.
- Corominas J., Moya J., Lloret A., J. Gili A., Angeli M.G., Pasuto A., and Silvano S. (2000). Measurement of landslide displacements using a wire extensometer. *Engineering Geology* 55 (2000): 149–166.
- Crescenzo G.D. and Santo A. (2007). High-resolution mapping of rock fall instability through the integration of photogrammetric, geomorphological and engineering–geological surveys, *Quaternary International*, Vol. 171–172: 118–130.
- Crouse R. and Wright S. (2015). Cowal gold mine; Success in mining through saprolites - a case history. *Mining Engineering*, September 2015: 3-16.
- Cruden D.M. and Varnes D.J. (1996). *Landslide Types and Processes*, Transportation Research Board, U.S. National Academy of Sciences, Special Report, 247: 36-75.
- Dade W.B., and Huppert H.E. (1998). Long-runout rockfalls. *Geology*, 26 (1998): 803–806.
- Davidson C. (2011). Rock avalanches. M.Eng. thesis (unpublished), Department of Geological Engineering, The University of British Columbia, Vancouver, B.C.
- Dawson E. M., Roth W. H. and Drescher A. (1999). Slope stability analysis by strength reduction. *Geotechnique* 1999, 49(6): 835-840.
- Day A.P., and Seety J.M. (2007). Monitoring of a large wall failure at tom price iron ore mine. In *Proceedings of the International Symposium on rock slope stability in open pit mining and civil engineering*, 2007, Perth, 2007: 333-340.
- Dick G.J., Eberhardt E., Cabrejo-Liévano A.G., Stead D., and Rose N.D. (2015). Development of an early-warning time-of-failure analysis methodology for open-pit mine slopes utilizing ground-based slope stability radar monitoring data. *Canadian Geotechnical Journal*. 52: 515–529.
- Duncan J. M., Wright S. G., and Brandon T.L. (2014). *Soil strength and slope stability*. Second edition, Wiley, Hoboken.
- Duncan J.M. (1992). State of the Art: Static Stability and Deformation Analysis. *ASCE Geotechnical Special Publication* 1992, 1(31): 222-266.

- Duncan J. M. (1996). Soil slope stability analysis. In *Landslides: Investigation and mitigation* Turner and Schuster (Eds.), Transportation Research Board Special Report 247, National Research Council, National Academy of Sciences, Washington, D.C. (1996): 337-371.
- Duncan J. M. (2000). Factors of Safety and Reliability in Geotechnical Engineering. *Journal of Geotechnical and Geoenvironmental Engineering* 2000, 126(4): 307-316.
- Dunncliff J., Marr W.A., and Standing J. (2012). *Principals of Geotechnical Monitoring*. ICE Manual of Geotechnical Engineering, Volume 2 - Geotechnical Design, Construction and Verification. Eds. Burland, J.B., Chapman, T., Skinner, H., Brown, M. 2012. ICE Publishing.
- Eaton T. (2000). Operation and Monitoring Considerations from a British Columbia Mountain Terrain Perspective. In *Slope Stability at Surface Mining*. (eds. Hustrulid W.A., McCarter M.K., and Van Zyl D.J.A.), SMA: 311-321.
- El-Ramly H., Morgenstern N.R., Cruden D.M. (2002). Probabilistic slope stability analysis for practice. *Canadian Geotechnical Journal*, 39 (2002): 665–683.
- El-Ramly H. (2001). Probabilistic analyses of landslide hazards and risks: Bridging theory and practice. Ph.D. thesis, University of Alberta, Edmonton, Alta.
- Evolutionary and Revolutionary Technologies for Mining. (2002) Washington, DC: The National Academies Press.
- Fannin R.J., and Wise M.P. (2001). An empirical–statistical model for debris flow travel distance. *Canadian Geotechnical Journal*, 38: 982–994.
- Federal Aviation Administration (FAA). (2018). Fact Sheet – General Aviation Safety <https://www.faa.gov/news/fact_sheets/news_story.cfm?newsId=21274> (accessed December 09, 2020).
- Federal Aviation Administration (FAA). (2020). <<https://www.faa.gov/>> (accessed December 12, 2020).
- Federal Highway Administration (FHWA) (2020). National Household Travel Survey 2018 <<https://nhts.ornl.gov/>> (accessed December 09, 2020)
- Fenton G.A. and Griffiths D.V. (2008). *Risk Assessment in Geotechnical Engineering*. John Wiley & Sons, Inc., Hoboken, New Jersey. 463 p.
- Fenton G.A., Griffiths D.V. and Williams M.B. (2005). Reliability of traditional retaining wall design. *Geotechnique* 2005, 55(1): 55–62.

- Fergusson D., Paris M., Anderson C.K., McMorrان T., and Johnson D. (2001). Opencast Hightwall Slope Design, Rotowaro Coalfield. In Proceedings of the New Zealand Geotechnical Society Symposium “Engineering and Development in Hazardous Terrain”. Christchurch, August 2001: 35-51.
- Finlay P.J., Mostyn, G.R., and Fell R. (1999). Landslide risk assessment: prediction of travel distance, Canadian Geotechnical Journal 1999, 36(3): 556–562.
- Firpo G, Salvini R, Francioni M and Ranjith P.G. (2011). Use of Digital Terrestrial Photogrammetry in rocky slope stability analysis by Distinct Elements Numerical Methods, International Journal of Rock Mechanics & Mining Sciences 2011, 48: 1045–1054.
- Flores G. and Karzulovic A. (2002). Geotechnical Guidelines for a Transition from Open Pit to Underground Mining, Benchmarking Report for ICSII, Task 4.
- Forward T. Stewart M. Penna N. and Tsakiri M. (2001). Steep Wall Monitoring Using Switched Antenna Arrays and Permanent GPS Networks, Proceedings of the tenth FIG International Symposium on Deformation Measurements: 33-41.
- Fredlund D.G. and Krahn J. (1976). Comparison of slope stability methods of analysis. In Proceedings of the 29th Canadian Geotechnical Conference, Vancouver, B.C., October 13-15, 1976: 429-439.
- Galperin A.M. (2003). Geomechanics in surface mining. Moscow, Publishing House of Moscow State Mining University: 473 p.
- Gayer R., Hathaway T., and Davis J. (1995). Structural geological factors in open pit coal mine design, with special reference to thrusting: case study from the Ffyndaff sites in the South Wales Coalfield. In: Whateley, M. K. G. and Spears, D. A. (eds), 1995, European Coal Geology, Geological Society Special Publication No. 82: 233-249.
- Gibson W. (2011). Probabilistic methods for slope analysis and design. Australian Geomechanics 46(3) (2011): 29-39.
- Gilbert R.B. (2017). Beyond protecting the public from risk. The Bridge. 47(1): 30-35.
- Ginting A., Stawski M., and Widiadi R. (2011). Geotechnical Risk Management and Mitigation at Grasberg Open Pit, PT Freeport Indonesia. In Proceedings of the International Symposium on Rock Slope Stability in Open Pit Mining and Civil Engineering. 18-21 September 2011 Vancouver, Canada.

- Girard J.M. (2001). Assessing and monitoring open pit mine highwalls. NIOSH paper: 1-13.
- Golder Associates Limited. (1995). Mined rock and overburden piles: runout characteristics of debris from dump failures in mountainous terrain. Stage 2: analysis, modelling and prediction. Interim Report, Report No. 932-1493. Prepared in association with O. Hungr Geotechnical Research Ltd. British Columbia Mine Waste Rock Pile Research Committee and CANMET. Contract No. 23440-0-9198-X86.
- Golestanifar M., Ahangari K., Goshtasbi K., Akbari Dehkharghani A, and Terbrugge P. (2018). Governing risk elements through open pit slope optimization. *The Journal of the Southern African Institute of Mining and Metallurgy*. Vol. 118, January 2018: 47-55.
- Griffiths D.V. (2001). Stability analysis of highly variable soils by elasto-plastic finite elements. In: Griffiths V.D., Gioda G. (eds) *Advanced Numerical Applications and Plasticity in Geomechanics. International Centre for Mechanical Sciences (Courses and Lectures)*. Vol. 426. Springer, Vienna.
- Griffiths D.V. and Fenton G.A. (2004). Probabilistic slope stability analysis by finite elements. *Journal of Geotechnical and Geoenvironmental Engineering*, 130(5) (2004): 507–518.
- Griffiths D.V. and Lane, P.A. (1999). Slope stability analysis by finite elements. *Geotechnique* 1999, 49(3): 387-403.
- Griffiths D.V. and Marquez R.M. (2007). Three-dimensional slope stability analysis by elasto-plastic finite elements. *Geotechnique* 2007, 57(6): 537-546.
- Griffiths D.V., Huang J., Fenton G.A. (2011). Probabilistic infinite slope analysis. *Computers and Geotechnics*, 38 (2011): 577–584.
- Griffiths D.V. (2015). Observations on load and strength factors in bearing capacity analysis. *J Geotechnical and Geoenvironmental Engineering*, 141(7): 06015004/1-4.
- GroundProbe Pty Ltd. (2012). *SSRViewer 5.4 user manual*. Brisbane, Australia.
- Haldar A., and Mahadevan S. (2000). *Probability, reliability and statistical methods in engineering design*, John Wiley & Sons, New York. 2000. 328 p.
- Hammah R. E., Yacoub T. E., Corkum B. and Curran J. H. (2005). A comparison of finite element slope stability analysis with conventional limit-equilibrium investigation. *Proc. 58th Canadian Geotechnical and 6th Joint IAHCNC and CGS Groundwater Specialty Conferences – GeoSask 2005*, Saskatoon: 480-487.

- Hammah R.; Yacoub T. and Curran J. (2009). The influence of correlation and distribution truncation on slope stability analysis results. Rocscience (www.roscience.com), 6 p.
- Haneberg W.C. (2008). Using close range terrestrial digital photogrammetry for 3-D rock slope modeling and discontinuity mapping in the United States, *Bulletin of Engineering Geology and the Environment*, 6 (2008): 457–469.
- Harr M. (1987). *Reliability-based design in civil engineering*. McGraw-Hill Book Company. 68 p.
- Harraz H.Z. (2016). *Mining Methods-Part I-Surface mining*. Power Point presentation. <https://www.slideshare.net/hzharraz/atud-gold-mine-egypt-9998734>. (Accessed 26 July 2021)
- Harries N., Noon, D., and Rowley, K. (2006). Case studies of slope stability radar used in open cut mines. *In Proceedings of Stability of Rock Slopes in Open Pit Mining and Civil Engineering Situations*, Johannesburg, South Africa. SAIMM: 335–342.
- Hawley, M., Marisett S., Beale G. and Stacey P. (2009). Performance assessment and monitoring. *In Guidelines for Open Pit Slope Design*. (eds. Read, J. and Stacey, P.), CSIRO Publishing, Collingwood: 327-379.
- Heim A. (1932). *Landslides and human lives (Bergstruz and Menchen leben)*. Translated by N. Skermer. BiTech Publishers, Vancouver, B.C.: 195 p.
- Hill C.D. and Sippel K.D. (2002). *Modern Deformation Monitoring: A Multi Sensor Approach*. In *Proceedings of the FIG XXII International Congress Washington, D.C. USA, April 19-26 2002*: 1-12.
- Høeg K. (2013). Slope Stability. In: Bobrowsky P.T. (eds) *Encyclopedia of Natural Hazards*. *Encyclopedia of Earth Sciences Series*. Springer, Dordrecht.
- Hoek E. (1972). *Recent Rock Slope Stability Research at the Royal School of Mines, London*, *Geotechnical practice for stability in open pit mining*. Eds. C.O. Brawner and V. Milligin. The American Institute of Mining, Metallurgical, and Petroleum Engineers, Inc., New York, 1972: 23-46.
- Hoek E. and Bray J.W. (1981). *Rock slope engineering*. 3rd edn., Institute of Mining and Metallurgy, London.

- Hoek E., Marinos P., and Marinos V. (2005). Characterization and engineering properties of tectonically undisturbed but lithologically varied sedimentary rock masses. *International Journal of Rock Mechanics and Mining Sciences* 2005;42(2): 277-285.
- Hoek E., Rippere K.H., Stacey P.F. (2000). Large-scale slope designs – a review of the state of the art. *Slope stability in surface mining* / edited by Hustrulid W. et al. SME. 2000: 3-10.
- Hoek E. and Bray J. (1977). *Rock Slope Engineering*, 1st edn, Institute of Mining and Metallurgy, London.
- Howard K. (1973). Avalanche mode of motion: Implications from lunar examples: *Science*, 180(1973): 1052–1055.
- Hsü K.J. (1975). Catastrophic debris streams (sturzstroms) generated by rockfalls. *Geological Society of America Bulletin*, 86(1) (1975): 129–140.
- Hungr O. (1987). An extension of Bishop’s simplified method of slope stability analysis to three dimensions. *Geotechnique*, 37(1): 113-117.
- Hungr O. (1995). A model for the runout analysis of rapid flow slides, debris flows, and avalanches. *Canadian Geotechnical Journal*, 32 (1995): 610–623.
- Hungr O., Evans S.G., Bovis M. J., and Hitchinson I.N. (2001). A review of the classification of landslides of the flow type. *Environmental and Engineering Geoscience* 2001; 7 (3): 221–238.
- Hungr O., Leroueil S., and Picarelli L. (2014). The Varnes classification of landslide types, an update. *Landslides*, 11(2): 167-194.
- Hunter G. and Fell R. (2004). Travel distance angle for “rapid” landslides in constructed and natural soil slopes. *Canadian Geotechnical Journal*, 40 (2003): 1123–1141.
- Hunter J. H. and Schuster R.L. (1971). Chart solutions for analysis of earth slopes. *Highway Research Record*, No. 345: 77-89.
- Hustrulid W., Kuchta M., and Martin R. (2013). *Open pit planning and design. Volume 1 – Fundamentals*. CRC Press, Balkema. 1027p.
- Hustrulid W., McCarter M., Dirk J., Van Zyl (2001). *Slope Stability in Surface Mining*. Edition 1. Society for Mining, Metallurgy, and Exploration. 442 p.
- Hustrulid W.A., and Boisen B.P. (1992). Geomechanics instrumentation. In *SME Mining Engineering Handbook*. 2nd edition. Volume 1, (senior ed. H.L. Hartman), SME, Littleton, Colorado, 1992. 1269: 848-880.

- Hutchinson J.N. (1988). General report: morphological and geotechnical parameters of landslides in relation to geology and hydrogeology. In Proceedings of the 5th International Symposium on Landslides, Lausanne, Switzerland. Vol. 1. Edited by C. Bonnard. A.A. Balkema, Rotterdam, the Netherlands: 3–35.
- Institute of Mine Seismology. (2019). <http://www.imseismology.org/mining/> (accessed December 20, 2020)
- ISRM (1978) Suggested methods for the quantitative description of discontinuities in rock mass. *International Journal of Rock Mechanics and Mining Science*, Pergamon, 15(6): 319-368.
- Iverson R.M. (2012). Elementary theory of bed-sediment entrainment by debris flows and avalanches. *Journal of Geophysical Research: Earth Surface* (2003–2012), 117(F3).
- Jaboyedoff M., Oppikofer T., Abellan A., Derron M.-H. Loye A., Metzger R., and Pedrazzini A. (2012). Use of LIDAR in landslide investigations: a review. *Nat Hazards* (2012) 61: 5-28.
- Jacob M. and Hungr O. (2005). *Debris-flow Hazards and Related Phenomena*. Springer, Berlin, Heidelberg: 795p.
- Janbu N. (1954). *Stability Analysis for Slopes with Dimensionless Parameters* (Harvard University Soil Mechanics Series No. 46). Doctor of Sciences thesis in the Field of Civil Engineering.
- Janbu N. (1968). *Slope Stability Computations* (Soil Mechanics and Foundation Engineering Report). Trondheim, Norway: Technical University of Norway.
- Javankhoshdel S., Cami B., Mafi R., Yacoub T, and Bathurst R. (2018). Optimization techniques in non-circular probabilistic slope stability analysis considering spatial variability. *GeoEdmonton 2018*, Edmonton, AB, Canada, September 2018.
- Javankhoshdel S., Luo N., and Bathurst R. (2017). Probabilistic analysis of simple slopes with cohesive soil strength using RLEM and RFEM. *Georisk 2017: Assessment and Management of Risk for Engineered Systems and Geohazards*, 11(3): 231–246.
- Javankhoshdel, S., and Bathurst R. J. (2014). Simplified probabilistic slope stability design charts for cohesive and $c-\phi$ soils. *Canadian Geotechnical Journal*, 51(9): 1033–1045.
- Jhanwar J.C., and Thote N. R. (2011). Slope failures in the opencast coal mines of Wardha Valley Coalfield in central India: a study. *Rock mechanics and rock engineering*, 44(5): 635-640.
- Ji J., and Low B.K. (2012). Stratified response surfaces for system probabilistic evaluation of slopes. *Journal of Geotechnical and Geoenvironmental Engineering*, 138(11)(2012): 1398–406.

- Jiang G.-L., and Magmam J.-P. (1997). Stability analysis of embankments: comparison of limit analysis with methods of slices. *Geotechnique*, 47(4): 857–872.
- Johansson J. (2014). *Impact of Water-Level Variations on Slope Stability*. Licentiate thesis. Lulea University of Technology. 136 p.
- Kaab A., Paul F., Maisch M., Hoelzle M., and Haeberli W. (2002). The new remote-sensing-derived Swiss glacier inventory: II. First results, *Annual Glaciology*, 34(2002): 362 – 366.
- Kadar I. and Nagy L. (2017). The examination of different soil parameters' coefficient of variation values and types of distributions. In *Proceedings of the 6th International Young Geotechnical Engineers' Conference (iYGEC6)*.
- Kane, W. F and Beck, T. J. (1998) Instrumentation Practice for Slope Monitoring, *Journal of Engineering Geology Practice in Northern California*, Available at: <http://www.civil.northwestern.edu/> (Accessed 27 June 2021)
- Kasama K., and Whittle A. (2016). Effect of spatial variability on the slope stability using Random Field Numerical Limit Analyses. *Georisk 2016: Assessment and Management of Risk for Engineered Systems and Geohazards*, 10(1): 42-54.
- Kayesa G. (2006). Prediction of slope failure at Letlhakane Mine with the Geomos sope monitoring system. In *Proceedings of the International Symposium on Stability of Rock Slopes in Open Pit Mining and Civil Engineering Situations*. S44: 606-622.
- Khabbaz H., Fatahi B., and Nucifora C. (2012). Finite element methods against limit equilibrium approaches for slope stability analysis. In *Proceedings of the 11th Australia - New Zealand Conference on Geomechanics (Melbourne, 2012)*: 1293-1298.
- Kim D. and Salgado R. (2009). Limit states and load and resistance design of slopes and retaining structures (FHWA/IN/JTRP-2008/5). Final Report. Purdue University West Lafayette, Indiana.
- Kirsten H. (1983). Significance of the probability of failure in slope engineering. *The civil engineering in South Africa*, January 2013: 17-27.
- Krahn J. (2003). The 2001 R.M. Hardy Lecture: The limits of limit equilibrium analyses. *Canadian Geotechnical Journal* 40(2003): 643–660.
- Kuhlmann H. and Glaser A. (2002). "Investigation of New Measurement Techniques for Bridge Monitoring." 2nd Symposium on Geodesy for Geotechnical and Structural Engineering, Berlin, Germany: 1-10.

- Kumar A. and Villuri V. (2015). Role of mining radar in mine slope stability monitoring at open cast mines. *Procedia Earth and Planetary Science*, 11 (2015): 76-83.
- Kumar A., and Rathee R. (2017). Monitoring and evaluating of slope stability for setting out of critical limit at slope stability radar. *Geo-Engineering* (2017) 8:18: 3-16.
- Lacasse S. (1994). Reliability and probabilistic methods. In *Proceedings of the 13th International Conference for Soil Mechanics and Foundation Engineering*, New Delhi, India: 225-227.
- Lacasse S., and Nadim F. (2009). Landslide risk assessment and mitigation strategy. In: Sassa K., Canuti P. (eds) *Landslides – Disaster Risk Reduction*. Springer, Berlin, Heidelberg: 31-61.
- Lade, P. V. (1977). Elasto-plastic stress–strain theory for cohesionless soil with curved yield surfaces. *International Journal of Solid Structures*, 13: 1019–1035.
- Laubscher D.H. (2000). *Block Caving Manual*, Prepared for International Caving Study, JKMRC and Itasca Consulting Group, Brisbane.
- Legros F., (2002). The mobility of long-runout landslides: *Engineering Geology*, 63 (2002): 301–331.
- Lelono H.D., Basson FRP., Lupo J., and Adriansyah Y. (2016). Pit slope evaluation based on the historical failure database at Batu Hijau mine. In the *Proceedings of the APSSIM 2016*, Brisbane, Australia.
- Leshchinsky D. and Baker R. (1986). Three-dimensional slope stability: end effects. *Soils and Foundations*, 26 (4): 98-110.
- Leshchinsky D., Baker R., and Silver M. L. (1985). Three Dimensional Analysis of Slope Stability. *International Journal for Numerical and Analytical Methods in Geomechanics*, 9(2): 199-223.
- Levy M.E. and Visca P.J. (2009). Statistical characterization of rock structure using LiDAR. In *Proceedings of the 43rd US Rock Mechanics Symposium and 4th U.S.-Canada Rock Mechanics Symposium*, Asheville, NC June 28th –July 1st, 2009. ARMA 09-155: 1-7.
- Li T. (1983). A mathematical model for predicting the extent of a major rockfall. *Zeitschrift für Geomorphologie*, 27, (1983): 473-482.
- Li. Y., Yang T., Liu H., Wang H., Hou X., Zhang P., and Wang P. (2016). Real-time microseismic monitoring and its characteristic analysis in working face with high-intensity mining. *Journal of Applied Geophysics* 132 (2016): 152–163.

- Liang Z. Xu N. Ma K. Tang S. and Tang C. (2013). Microseismic monitoring and numerical simulation of rock slope failure. *International Journal of Distributed Sensor Networks*, 2013.
- Lichti D.D., Gordon S.J. and Stewart M.P. (2002). Ground-based laser scanners: operation, systems and applications. *Geomatica* 56(1): 21–33.
- Lin H.D., Wang W.C., Li A.J. (2020). Investigation of dilatancy angle effects on slope stability using the 3D finite element method strength reduction technique. *Computers and Geotechnics* 118 (2020) 103295: 1-13.
- Little M.J. (2006) The Benefit to Open Pit Rock Slope Design of Geotechnical Databases, *International Symposium on Stability of Rock Slopes in Open Pit Mining and Civil Engineering*, The South African Institute of Mining and Metallurgy, Symposium Series 44: 97-116.
- Locat J., and Leroueil S. (1997). Landslide stages and risk assessment issues in sensitive clays and other soft sediments. In *Proceedings of the International Workshop on Landslide Risk Assessment*, Honolulu, Hawaii, 19–21 February 1997. Balkema, Rotterdam: 261–270.
- Low B.K., and Tang W.H. (2007). Efficient spreadsheet algorithm for first-order reliability method. *Journal of Geotechnical and Geoenvironmental Engineering*, 133(12) (2007): 1378–1387.
- Lynch R.A. and Malovichko, D.A. (2006). Seismology and Slope Stability in Open Pit Mines, *International Symposium on Stability of Rock Slopes in Open Pit Mining and Civil Engineering*, South African Institute of Mining and Metallurgy: 375-390.
- Lynch, R.A.; Wuite, R.; Smith, B.S. and Cichowicz, A. (2005). Micro-seismic monitoring of open pit stopes. In *Proceedings of the 6th Symposium on Rockbursts and Seismicity in Mines*, (ed. Y. Potvin and M. Hudyma), ACG, Perth, Australia, 2005: 581-592.
- Ma E., Chen Y., Ding Z. (2001). Monitoring of Slope Stability by using Global Positioning System (GPS). *Proc. Inter. Symp. On Kinematic Systems in Geodesy, Geomatics and Navigation – KIS2001*, Alberta: 298-310.
- Makinen G. (2002). *The Economic Effects of 9/11: A Retrospective Assessment*. Report for Congress. Congressional Research Service/ The Library of Congress. 60 p.
- Martin D., and Stacey P. (2018). *Guidelines for open pit slope design in weak rocks*. CRC Press. Balkema. 398 p.

- Martin D.S., and Mehr E.F. (1993). Assessment of slope deformation and deep seated instability in the Cassiar Open Pit. Canadian Institution of Mining and Metallurgy Bulletin. July, 86(972): 58-66.
- Matsui T., and San K. (1992). Finite element slope stability analysis by shear strength reduction technique. Soils and Foundations, 32(1): 59-70.
- Mazareanu, E. (2020a). Number of aircraft in the United States 1990-2020. <www.statista.com>
- Mazareanu, E. (2020b). Plane crashes - insurance costs 2007-2018. <www.statista.com>
- McDougall S. (2016). 2014 Canadian Geotechnical Colloquium: Landslide runout analysis — current practice and challenges Canadian Geotechnical Journal, 54 (2017): 605–620.
- McHugh E.L., Long D.G. and Sabine Ch. (2003). Applications of ground-based radar to mine slope monitoring.
- McIntosh K. and Krupnik A. (2002). Integration of Laser-Derived DSMs and Matched Image Edges for Generating an Accurate Surface Model. ISPRS Journal of Photogrammetry & Remote Sensing 56: 167-176.
- McMachon B.K. (1985). Some practical considerations for the estimation of shear strength of joints and other discontinuities. In Proceedings of the International Symposium: Fundamentals of Rock Joints, Sweden 1985: 475-485.
- McQuillan A., Canbulat I., Payne D., and Oh J. (2018). New risk assessment methodology for coal mine excavated slopes. International Journal of Mining Science and Technology 28 (2018) 583–592.
- Melnikov N., Kozyrev A., Reshetnyak E., Kasparin E., Rybin V., Melik-Gaikazov I., and Svinin V. (2005). Conceptual principles of open pit wall design optimization, the Kola peninsula. In Proceedings of the 8th International Symposium on Mining in the Arctic (edited by Nickolay N. Melnikov & Serguei P. Reshetnyak) / Apatity / Murmansk Region / Russia / June 20-23, 2005: 3-14.
- Memon Y. (2018). A comparison between Limit Equilibrium and Finite Element Methods for slope stability analysis. Missouri University of Science and Technology, Rolla.
- Mendecki, A.J., Lynch, R. A. and Malovichko, D.A. (2010). Routine micro-seismic monitoring in mines. In Proceedings of Australian Earthquake Engineering Society 2010 Conference. Perth, Western Australia, November 2010: 1-33.

- Mercer K. (2006) “Investigation into the time dependent deformation behavior and failure mechanism of unsupported rock slopes on the interpretation of observed deformation behavior”. PhD thesis. University of the Witwatersland, Johannesburg. 380 p.
- Michalowski R.L. and Drescher A. (2009). Three-dimensional stability of slopes and excavations. *Geotechnique*. 59(10): 839-850.
- Mine Safety and Health Administration (MSHA). 2021. Fatality Reports <www.msha.gov>
- Mitchell J.K. (1993). *Fundamentals of soil behavior*. 2nd Edition, John Wiley & Sons, Hoboken. 456p.
- Mohammed M.M. (2021) A review on slope monitoring and application methods in open pit mining activities. *International journal of scientific & technology research*, 10(02) (2021): 181-186.
- Morgenstern N. R., and Price V. E. (1965). The Analysis of the Stability of General Slip Surfaces. *Geotechnique*. 15(1): 77–93.
- Morgenstern N.R. (1963) Stability charts for earth slopes during rapid drawdown. *Geotechnique*. 13 (1963): 121-131.
- Morrison R.G.K, and Russel P.L. (1973) Selecting a Mining Method-rock Mechanics, Other Factors. *SME Mining Engineering Handbook*, V.1: 9-2 to 9-22.
- Mostyn G.R., and Li K.S. (1993). Probabilistic slope analysis - State of play, *Proceedings of the Conference on Methodology in Geotechnical Engineering*, 10-12 February 1993, Canberra, 1993: 89-109.
- Nadim F., and Lacasse S. (2008). Strategies for mitigation of risk associated with landslides. *Landslides-Disaster Risk Reduction*.
- Nadim F., Einstein H., and Roberds W. (2005). Probabilistic stability analysis for individual slopes in soil and rock. *Landslide Risk Management – Hungr, Fell, Couture & Eberhardt (eds) 2005: 63-98*.
- Naghadehi Z.M., Jimenez R., Khalo R., Seyed-Mohammad K., and Jalali E. (2013). A new open-pit mine slope instability index defined using the improved rock engineering systems approach. *International Journal of Rock Mechanics & Mining Sciences* 61 (2013): 1–14.
- National Highway Traffic Safety Administration (NHTSA). (2020). Preview of motor vehicle traffic fatalities in 2019 (Research Note. Report No. DOT HS 813 021) <<https://www.nhtsa.gov/>>

- National Inventory of Dams (NID). (2020). U.S. Army Corps of Engineers <<https://nid-test.sec.usace.army.mil>> (accessed December 09, 2020)
- National Transportation Safety Board (NTSB). (2014). Summary of US Civil Aviation Accidents for Calendar Year 2014. <<https://www.nts.gov/investigations/data/Pages/2014-Aviation-Accidents-Methods-Used.aspx>> (accessed December 09, 2020)
- National Vital Statistics Reports (NVSS). (2019). Deaths: Final Data for 2017. Vol. 68, No. 9, by K.D., Kochanek, S.L., Murphy, J. Xu, and E., Arias. U.S. Department of Health and Human Services, CDC. 77p.
- Newcomen H.W., Shwydiuk L., and Maggs C.S. (2003). Managing pit slope displacements: Highland Valley Copper's Lornex pit southwest wall. *CIM Bulletin*; May 2003; 96(1071): 43-48.
- Nian T.-K., Huang R.-Q., Wan S.-S., and Chen G.-Q. (2012). Three-dimensional strength-reduction finite element analysis of slopes: geometric effects. *Can. Geotech. J.* 49 (2012): 574–588.
- Nicoletti P.G., and Sorriso-Valvo M. (1991). Geomorphic controls of the shape and mobility of rock avalanches. *Geological Society of America Bulletin*, 103 (1991): 1365-1373.
- NIOSH. (2019). Fatalities Cost in Mining Technical Guide <www.cdc.gov>
- Nuclear reactor accidents in the United States (2020, October 19) In Wikipedia <https://en.wikipedia.org/wiki/Nuclear_reactor_accidents_in_the_United_States#:~:text=According%20to%20a%202010%20survey,Mile%20Island%20accident%20in%201979> (accessed December 09, 2020)
- Nunoo S., Tannant D.D., and Newcomen H.W. (2016). Slope monitoring practices at open pit porphyry mines in British Columbia, Canada. *International Journal of Mining, Reclamation and Environment*, 2016, 30 (3): 245-256.
- Office of Nuclear Energy. (2020). Nuclear Power Summary, April 2019. <www.energy.gov>
- Ohnishi Y., Nishiyama S., Yano T., Matsuyama H., and Amano K. (2006). A study of the application of digital photogrammetry to slope monitoring systems. *International Journal of Rock Mechanics and Mining Sciences*, 43(5): 756-766.
- Oliphant J., and Horne R.M. (1992). A comparative review of commercially-available software for soil stability analysis. *Geotechnical and Geological Engineering*, 1992, 10: 321-344.

- Osasan K.S., and Afeni T.B. (2013). Review of surface mine slope monitoring techniques. *Journal of mining science*; 46(2): 177-186.
- Osasan, K.S. (2012). *Open-Cast Mine Slope Deformation and Failure Mechanisms Interpreted from Slope Radar Monitoring*. PhD dissertation. Johannesburg, 2012.
- Patton F.D and Deere D.U. (1970). Significant geologic factors in rock slope stability. In *Proceeding of the open pit mining symposium. Planning open pit mines*. Johannesburg, 29 August – 4 September 1970. SAIMM: 143-151.
- Peng R., Ju Y., Wang J., Xie H., Gao F., and Mao L. (2015). Energy dissipation and release during coal failure under conventional triaxial compression. *Rock Mech Rock Eng* (2015) 48: 509-526.
- Phoon K.K. and Kulhawy F.H. (1996). On quantifying inherent soil variability. *Geotechnical Special Publication* (58 I): 326-340.
- Phoon, K. K., and F. H. Kulhawy (1999a) Characterization of geotechnical variability. *Canadian Geotechnical Journal*, 35(4): 612-624.
- Phoon, K. K., and F. H. Kulhawy (1999b). Evaluation of geotechnical property variability. *Canadian Geotechnical Journal*, 35(4): 625-639.
- Phoon, K.-K. 2008. *Reliability-Based Design in Geotechnical Engineering Computations and Applications*, CRC Press, NY, USA
- Piteau D.R. and Jennings J.E. (1970). The effects of plan geometry on the stability of natural slopes in rock in the Kimberley area of South Africa. In *Proceedings of the 2nd Congress of the International Society of Rock Mechanics*. Belgrade, 3(1970), paper 7-4.
- Priest S.D. and Brown E.T. (1983). Probabilistic stability analysis of variable rock slopes. *Trans. Inst. Min. Metall. (Sect. A)* 92: 1-12.
- Rackwitz, R. (2000). Reviewing Probabilistic Soils Modelling. *Computers and Geotechnics*, 26: 199-223.
- Rapinski J., Kowalczyk K., and Smieja M. (2014). Ground water level monitoring device on marshland. In *Proceedings of the 9th International Conference “environmental Engineering” 22–23 May 2014, Vilnius, Lithuania*.
- Read J. and Stacey P. (2009). *Guidelines for Open Pit Slope Design*. CRC Press/ Balkema. 496 p.
- Rendu J.-M. (2017) *Risk management in evaluating mineral deposits*. SME. Englewoods, Colorado. 310 p.

- Rocscience (2021). Convergence Criteria RS2 Theory. Available at: <https://www.rocscience.com/help/rs2/assets/docs/convergence%20criteria.pdf> (Accessed: July 2021).
- Rocscience Inc. (2020) RS2 v11.0 – Two-Dimensional Geotechnical Finite Element Analysis. Verification Manual – Convergence criteria.
- Rocscience Inc. (2021) RS3 v4.0 – Three-Dimensional Geotechnical Finite Element Analysis. Verification Manual
- Ryan T. and Pryor P. (2001). Designing catch benches and interramp slopes. In: Stability in open pit mining, ed. W.A. Hustrulid, M.K. McCarter, and D.J.A. Van Zyl: 27-38.
- Sah N., Sheorey P., and Upadhyaya L. (1994). Maximum likelihood estimation of slope stability. International journal of rock mechanics and mining & geomechanics. 31(I): 47-53.
- Sarma, S. K. (1973). Stability Analysis of Embankments and Slopes. Geotechnique. 23(3): 423–433.
- Sassa K. (2000). Mechanism of flows in granular soils. In Proceedings of GeoEng2000, Melbourne, Australia, 19–24 November 2000. Australian Geomechanics Society, Perth: 1671–1702.
- Savvaidis P.D. (2003). Existing Landslide Monitoring Systems and Techniques. From Stars to Earth and Culture: 242-258.
- Scheidegger A.E. (1973). On the prediction of the reach and velocity of catastrophic landslides. Rock Mechanics, 5(4) (1973): 231–236.
- Schellman M., Sepulveda R., and Kazlovic A. (2006). Slope design for the east wall of Mantoverde mine, Chanaral, Chile. Proceedings International Symposium on Stability of rock slopes in open pit mining and civil engineering situations. Cape Town: 451-470.
- Scuffham P., Chalmers D., O'Hare D., and Wilson E. (2002). Direct and indirect cost of general aviation crashes. Aviation, Space, and Environmental Medicine 73(9): 851–858.
- Shankar V., Kumar D., and Rao A N. (2013). Application of ground based LiDAR for monitoring & stability analysis of dump slope in open pit coal mine: a case study. Mining Engineering Journal, April 2013, 14(9): 17-23.
- Shea T., and van Wyk de Vries B. (2008). Structural analysis and analogue modeling of the kinematics and dynamics of rockslide avalanches. Geosphere, August 2008, 4(4): 657–686.

- Shimizu N., Y. Mizuta H., Kondo and Ono H. (1996). A New GPS real-time Monitoring System for Deformation Measurements and its Application. In Proceedings of the 8th FIG International Symposium on Deformation Measurements, Hong Kong, 25-28 June: 47-54.
- Shukha R. and Baker R. (2003). Mesh geometry effects on slope stability calculation by FLAC strength reduction method – linear and non-linear failure criteria. In Proceedings of the 3rd international conference on FLAC and numerical modeling in geomechanics, Sudbury, Ontario, Canada, 2003: 109–116.
- Singh R.N. and Ghose A.K. (2006). Engineered rock structures in mining and civil construction. Taylor & Francis Group. 528 p.
- Sjoberg J. (1996). Large Scale Stability in Open Pit Mining- A Review, Technical Report, Division of Rock Mechanics, Lulea University of Technology, Lulea, Sweden: 16-17.
- Sjoberg J. (1999). Analysis of Large Scale Rock Slopes. Ph.D. thesis, Lulea University of Technology, Sweden.
- Sobieralski J.B. (2013). The cost of general aviation accidents in the United States. Transportation Research Part A 47 (2013): 19–27.
- Sovacool B.K. (2009). The Accidentsl Century – Prominent Energy Accidents in the Last 100 Year. Exploration & Production 7(2): 132-137.
- Spencer E. (1967). A method of analysis of the stability of embankments assuming parallel interslice forces. Geotechnique, 17 (1967): 11-26.
- Srivastava A., and Sivakumar Babu G.L. (2009). Effect of soil variability on the bearing capacity of clay and in slope stability problems. Engineering Geology, 14 September 2009, 108(1-2): 142-152.
- Srivastava A., Sivakumar Babu G.L., and Haldar S. (2010). Influence of spatial variability of permeability property on steady state seepage flow and slope stability analysis. Engineering Geology, 9 February 2010, 110(3-4): 93-101.
- Stacey T.R., Wesseloo J., and Lynch R. (2004). Extension' and seismicity in a hard rock open pit mine. In Proceedings of the 2nd International Seminar on Deep and High Stress Mining, South Africa, 2004, South African Institute of Mining and Metallurgy: 41–53.

- Stark T.D. (2003). Three-dimensional slope stability methods in geotechnical practice. In Proceedings of the 51st Annual geotechnical engineering conference. University of Minnesots: 1–33.
- Statista. 2020. Number of motor vehicles registered in the United States from 1990 to 2018 (Apr 21, 2020). Statista Research Department, <[https://www.statista.com/statistics/183505/number-of-vehicles-in-the-united-states-since-1990/#:~:text=How%20many%20 registered%20motor%20vehicles,at%206.3%20million%20in%202016](https://www.statista.com/statistics/183505/number-of-vehicles-in-the-united-states-since-1990/#:~:text=How%20many%20registered%20motor%20vehicles,at%206.3%20million%20in%202016)> (accessed December 09, 2020).
- Stead D. and Wolter A. (2015). A Critical Review of Landslide Failure Mechanisms. *Journal of Structural Geology* 74 (2015): 1-23. .
- Steffen O.K.H., Contreras L.F., Terbrugge P.J., Venter J. (2008). A risk evaluation approach for pit slope design. In Proceedings of the 42nd U.S. Rock Mechanics Symposium (USRMS), San Francisco, California, June 2008.
- Steffen O.K.H., Contreras L.F., Terbrugge, and Venter J. (2008). A Risk Evaluation Approach for Pit Slope Design. ARMA 08-231.
- Steward T., Sivakugan N., Shukla S.K. and Das B.M. (2011). Taylor’s Slope Stability Charts Revisited. *International journal of geomechanics /ASCE/July/August 2011*.
- Sturzenegger M and Stead D. (2009). Close-range terrestrial digital photogrammetry and terrestrial laser scanning for discontinuity on rock cuts, *Engineering Geology*, 106:163 –182.
- Sullivan M. (2005). “NYDOT national bridge failure database.” compiled by the Structures Division of the New York State Department of Transportation, USA.
- Sullivan TD (2006). Pit slope design and risk – a view of the current state of the art. Proceedings of the South African Institute of Mining and Metallurgy International Symposium on Stability of Rock Slopes in Open Pit Mining and Civil Engineering, 2006: 51-78.
- Sullivan TD. (1993). Understanding pit slope movement. In: Szwedzicki, editor. Proceedings of the Conf. on Geotechnical Instrumentation and Monitoring in Open Pit and Underground Mining. Balkema, 1993.
- Sun Ch., Chai J., Xu Z., and Qin Y. (2017). 3D stability charts for convex and concave slopes in plan view with homogeneous soil based on the strength-reduction method. *International Journal of Geomechanics*, 2017, 17(5): 06016034.


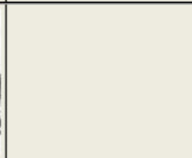
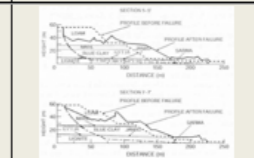
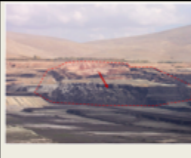

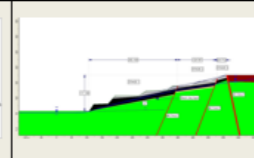


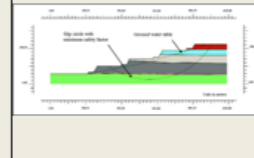


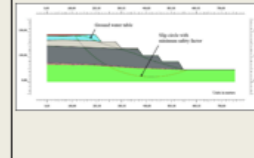

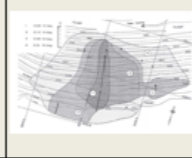
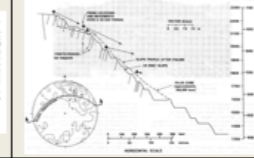
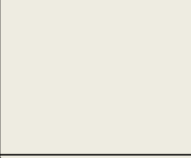
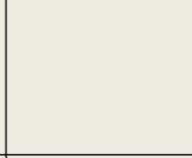
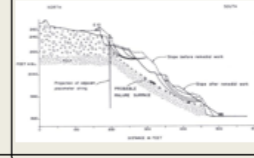

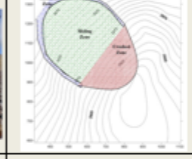
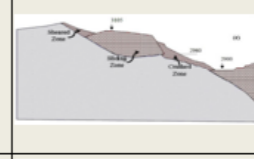
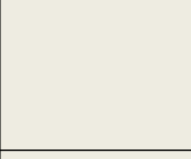
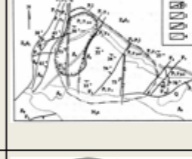
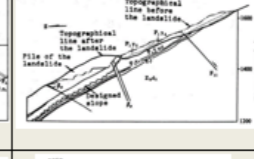

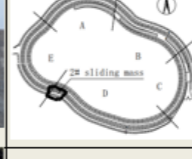
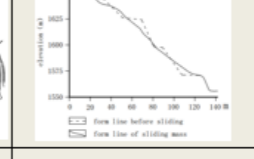

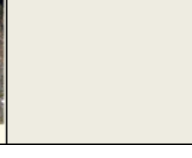
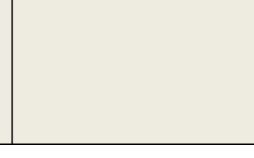
- Swan G., and Sepulveda R. (2000). Slope stability of Collahuasi. Slope Stab. Surf. Min. (1st ed.), Society for Mining, Metallurgy, and Exploration, Colorado (2000): 163-170.
- Szwedzicki T. (2001) Geotechnical precursors to large-scale ground collapse in mines. International Journal of Rock Mechanics and Mining Sciences, 38(7): 957-965.
- Tapia A., Contreras L.F., Jefferies M., and Steffen O.K.H. (2007). Risk evaluation of slope failure at the Chuquicamata Mine. Proceedings of the 2007 International Symposium on Rock Slope Stability in Open Pit Mining and Civil Engineering, Perth, Australia, 12-14 September 2007. Potvin, Y. (ed.). Australian Centre for Geomechanics.
- Taylor D. W. (1948) Fundamentals of Soil Mechanics. New York: John Wiley & Sons.
- Terbrugge P.J., Wesseloo J., Venter J., and Steffen O.K.H. (2006), A risk consequence approach to open pit slope design. The Journal of The South African Institute of Mining and Metallurgy, July 2006, 106: 503-511.
- Teskey W.F. and Radovanovic R.S. (2001). Free station method of leveling. Journal of Surveying Engineering 2001, 127(1): 25-29.
- The Code of Federal Regulations (https://www.ecfr.gov/cgi-bin/text-idx?SID=151b89ef54ca55ac6b6185857be1cbb1&mc=true&tpl=/ecfrbrowse/Title30/30cfr56_main_02.tpl)
- The Federal Mine Safety and Health Act of 1977 (Public Law 91-173, as amended by Public Law 95-164) (<https://arlweb.msha.gov/REGS/ACT/ACT2.HTM>)
- Timchenko A., Shidlovskaya A., and Briaud J.-L. Tolerable risk chart. In Proceedings of the 20th International Conference on Soil Mechanics and Geotechnical Engineering (ICSMGE 2022), Sidney, Australia, 1-5 May 2022. The Australian Geomechanics Society. (accepted for publication 15 September 2021)
- Tsakiri M. and Stewart M. (2000) Stability monitoring of open pit mines in Australia using GPS. At Mine Planning and Equipment Selection, Panagiotou & Michalakopoulos (eds). 2000 Balkema, Rotterdam.: 387-390.
- U.S. Energy Information Administration (EIA). (2020). Monthly Energy Review (MER). DOE/EIA-0035(2020/12).
- United States Census Bureau (2020). <<https://www.census.gov/>>
- USDOT (2019). National Transportation Statistics. Bureau of Transportation Statistics. 469 p.
- Uzielli M., Lacasse S., Nadim F., and Phoon K.K. (2007). Soil variability analysis for geotechnical practice. Characterization and Engineering Properties of Natural Soils 3-4: 1653-1752.

- Van Gassen W., and Cruden D.M. (1989). Momentum transfer and friction in the debris of rock avalanches. *Canadian Geotechnical Journal*, 26 (1989): 623–628.
- Vanmarcke, E.H. (1983). *Random Fields: Analysis & Synthesis*, MIT Press, Cambridge. 383 p.
- Varnes D.J. (1978). Slope movement types and processes, In *Landslides Analysis and Control*. In: R.L. Schuster & R.J. Krizek (eds), Transportation Research Board, Special Report 176, National Academy of Science, Washington, D.C.:12-33.
- Vaziri A., Moore L., and Ali H. (2010). Monitoring systems for warning impending failures in slopes and open pit mines. *Natural Hazards* (2010) 55: 501–512. (doi 10.1007/s11069-010-9542-5).
- Vinod B.R., Shivananda P., Swathivarma R., and Bhaskar M.B. (2017). Some of limit equilibrium method and finite element method based software are used in slope stability analysis, *International Journal of Application or Innovation in Engineering & Management*, 6(9): 6-10.
- Vinoth S., Kumar L.A., and Mishra A.K. (2016). Status and developments of slope monitoring techniques in opencast mines. In *Proceedings of the 6th Indian Rock Conference INDOROCK 2016*, 17-18 June 2016: 767-781.
- VNIMI (1972) *Methodological guidelines for determination of open pit slope angles, open pit and waste dump face angles for constructed and operating mines* ed. by G.L. Fisenko (in Russian) VNIMI, Leningrad, 164 p.
- Ward J.T. (2015). *Bingham Canyon Landslide: Analysis and Mitigation*. BS thesis. University of Nevada, Reno, May 2015.
- Wei W.B., Cheng Y.M., and Li L. (2009). Three-dimensional slope failure analysis by the strength reduction and limit equilibrium methods. *Computers and Geotechnics* 36 (2009): 70-80.
- Wesseloo J., Dight P., and Potvin Y. (2009). *High resolution seismic monitoring in open pit mines*. Technical report. MERIWA Project No. M366. April 2009. 106 p.
- Wessels, S. D. N. (2009). *Monitoring and management of a large open pit failure*. M.Sc.E thesis, Faculty of Engineering and the Built Environment, University of Witwatersrand, Johannesburg, South Africa. 99 p.
- Whitman R.V. (1984). Evaluationg calculated risk in geotechnical engineering. *Journal of Geotechnical engineering* 110(2): 143-188.

- Whittall J., Mitchell A., and McDougall S. (2020). Runout of open pit slope failures: an update, in PM Dight (ed.), Proceedings of the 2020 International Symposium on Slope Stability in Open Pit Mining and Civil Engineering, Australian Centre for Geomechanics, Perth: 1149-1162.
- Whittall J.R., Eberhardt E. and McDougall S. (2017). Runout analysis and mobility observations for large open pit slope failures. *Canadian Geotechnical Journal*, 54(3) (2017): 373–391.
- Whittall JR. (2015). Runout exceedance prediction for open pit slope failures. M.Sc. Thesis, the University of British Columbia, Vancouver, August 2015.
- Wu Z., and Wang W. (2011). Effects of random field modeling methods on slope stability. In Proceedings of the 2011 International Conference on Multimedia Technology: 1531-1534.
- Wyllie D.C. and Mah C.W. (2005). *Rock slope engineering civil and mining*. 4th edition. Taylor & Francis.
- Xu, N. Tang, C. Li, H. Dai, F. Ma, K. Shao, J. and Wu, J. (2012). Excavation-induced microseismicity: microseismic monitoring and numerical simulation. *Journal of Zhejiang University-Science*, 13(6): 445–460.
- Yacoub T. (2016). Using shear strength reduction method for 2D and 3D slope stability analysis. Presentation at the occasion of the Annual Kansas City Geotechnical Conference 2016.
- Yang H., Peng J., and Zhang D. (2011). Slope of large-scale open-pit mine monitoring deformations by using Ground-Based Interferometry. *Progress in Geophysics*, 27(4): 1804–1811.
- Yarmuch J.L., Brazil M., Rubinstein H., and Thomas D.A. (2020). Optimum ramp design in open pit mines, *Computers & Operations Research*, Volume 115, 2020.
- Yost R.R. (2009). The time value of risk: a case study at the Boron operations open pit mine. Ph.D. thesis, Department of Mining, Geology, and Geological Engineering, The University of Arizona, Tucson, Arizona.
- Zahariadis H. and Tsakiri M. (2006). Low cost monitoring system in the open pit lignite mines of Megalopoli, Greece. In Proceedings of the 3rd IAG / 12th FIG Symposium, Baden, May 22-24, 2006: 1-10.

- Zare Naghadehi M., Jimenez R., Khalo Kakaie R., and Esmaeil Jalali S.M. (2013). A new open-pit mine slope instability index defined using the improved rock engineering systems approach. *International Journal of Rock Mechanics & Mining Sciences*, 61 (2013): 1-14.
- Zavodni Z.M. (2000). Time-dependent movements of open-pit slopes. In *Slope Stability in Surface Mining*, Hustrulid, McCarter and Van Zyl (eds.), SME, Colorado: 81–87.
- Zettler A.H., Poisel R., Roth W., and Preh A. (1999). Slope stability analysis based on the shear reduction technique in 3D. *FLAC and Numerical Modeling in Geomechanics*. Eds. by Detournay & Hart. Balkema, Rotterdam: 11-16.
- Zhang K., Cao P., Liu Z., Hu H., and Gong D. (2011). Simulation analysis on three-dimensional slope failure under different conditions. *Transactions of Nonferrous Metals Society of China* 21(2011): 2490-2502.
- Zhang Y., Chen G., Wang B., and Li L. (2013). An analytical method to evaluate the effect of a turning corner on 3D slope stability. *Computers and Geotechnics* 53 (2013): 40-45.
- Zhou Ch., Li X., Qin S., Qui D., Wu Y., Xiao Y., and Zhou J (2008). Automatic monitoring system for high-steep slope in open-pit mine based on GPS and data analysis. In *Proceedings of the International Conference on Earth Observation Data Processing and Analysis (ICEODPA)*, edited by Deren Li, Jianya Gong, Huayi Wu, Proc. of SPIE Vol. 7285.
- Zhou Y., Qi S.-Ch., Fan G., Chen M.-L., and Xhou J.-M. (2020). Topographic effects on three-dimensional slope stability for fluctuating water conditions using numerical analysis. *Water* 2020, 12(615): 1-24.
- Zhu H., and Zhang LM. (2013). Characterizing geotechnical anisotropic spatial variations using random field theory. *Canadian Geotechnical Journal* 2013, 50(7):723–734.

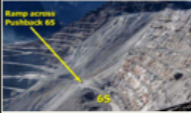



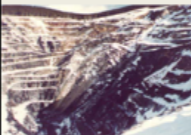

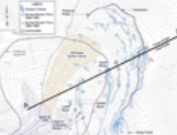

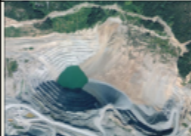
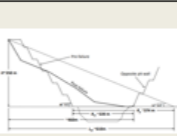


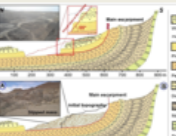
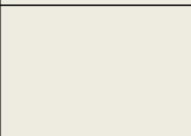

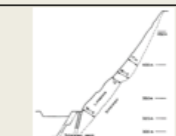
APPENDIX A. TAMU-MINESLOPE DATABASE

Record Information								Open Pit Parameters						Geological and Geotechnical Characteristics					Slope Failure Parameters								Slope Failure Plan and Scheme			General Information								
Label	Mine	Pit	Wall	ID	Country	Date	Material Group	Commodity	Shape of the Mine	Max Depth of the Mine, H _{max} (m)	Area of the Pit, (km ²)	Shoreline (m)	Length of the Mine (m)	Width of the Mine (m)	Overall Slope Angle of the Mine, β _{op} (°)	Height of Benches (m)	Lithology	Strength Grade	RMR (1976)	Unit Weight, γ (kN/m ³)	C' (kPa)	φ (°)	Failure Mechanism	Trigger factor	Volume (Mm ³)	Mass (tons)	Slope Angle, β _{fail} (°)	Fall Height, H _{fall} (m)	Travel distance, L _{travel} (m)	Average width, W _{fail} (m)	Setback distance, L _{sb} (m)	Height of the failure, H _{fail} (m)	General View of the Failure	Plan View of the Failure	Cross-Section of the Failure	Software	Monitoring system	Reference
1	Afsin-Elbistan	Kisilakoy	Northwest	-	Turkey	July 1, 1984	Sedimentary	Lignite	Rectangle	145	7.25	10765	2140	2450	18	30	Lignite	R1	Poor	17.00	15.49	9	Soil planar slide	Daylighted structure	160	-	20	50.0	141.0	250.0	34	50						Aydan et al. (1996)
2	Afsin-Elbistan	Kisilakoy	Southwest	-	Turkey	October 23, 2006	Sedimentary	Lignite	Rectangle	145	7.25	10765	2140	2450	14	30	Lignite	R1	Poor	16.2	8.00	9	Soil planar slide	Fault zone	10.50	-	14	117.0	481.0	300.0	39	117				Slide, FLAC3D		Oge (2008); Tutluoglu et al. (2011)
3	Afsin-Elbistan	Çöller	Southwest	Landslide B	Turkey	Feb. 6, 2011	Sedimentary	Lignite	Rectangle	180	2.2	6000	2100	1100	16	30	Lignite	R1	Poor	17.00	6.00	26	Rock planar slide	Daylighted structure	7.90	-	40	150.0	585.0	-	100	150				FLAC3D; Plaxis		Farina et al. (2013); UNOSAT (2011); Tutluoglu et al. (2010); Ozbay and Cabalar (2015)
4	Afsin-Elbistan	Çöller	Northwest	Landslide A	Turkey	Feb. 10, 2011	Sedimentary	Lignite	Rectangle	180	2.2	6000	2100	1100	16	30	Lignite	R1	Poor	17.00	6.00	26	Rock compound slide	Not reported	42.00	-	21	150.0	950.0	800.0	350	150				FLAC3D; Plaxis		Farina et al. (2013); UNOSAT (2011); Tutluoglu et al. (2010); Ozbay and Cabalar (2015)
5	Aiton	-	Southeast	-	Canada	1986	Igneous	Gold, Copper, Silver	Circle	500	0.63	2903	1000	2500	36	45	Diorite	R4	Poor	29.00	65.00	52	Rock topple	Mined too steep	0.10	300000	45	198.0	250.0	80.0	25	40						Reid and Stewart (1986); Martin (1990); Mercer (2006)
6	Aiton	-	Northwest	-	Canada	1984	Igneous	Gold, Copper, Silver	Circle	500	0.63	2903	1000	2500	36	45	Diorite	R4	Poor	29.00	65.00	52	Rock topple	Fault zone	-	200000	40	73.0	97.0	-	15	62						Martin (1990); Sjoberg (1996); Mercer (2006)
7	Angouran	-	Northwest	-	Iran	2008	Sedimentary	Zinc-lead ore	Circle	100	0.93	3710	110	1025	45	10	Limestone	R5	Fair	25.00	1.00	14	Rock planar slide	Freeze-thaw cycle	12.00	3500000	45	185.0	400.0	430.0	10	112						Behbahani et al. (2013); Mooreivand et al. (2012); Darbor et al. (2010); Taherkhani (2016)
8	Boguanhe	-	West	-	China	June 10, 1981	Sedimentary	Limestone	Circle	300	-	-	1200	750	30	10	Limestone	R0	-	24.00	30.00	21	Rock planar slide	Daylighted structure	4.50	11000000	40	275.0	656.0	200.0	64	175						Sheng and Lui (1995)
9	Baiyun'cbo mine	-	South-West	#2 of D Area	China	-	Sedimentary	Iron	Oval	95	1.13	3940	1360	1020	42	25	Dolomite	R3	Poor	28	7.00	29	Debris slide	Fault zone	0.68	1900000	43	100	128.0	182	7	60				FLAC3D	3D laser scanning	Zhang et al. (2015)
10	Berkeley	Berkeley	Southeast	-	USA	March 17, 1978	Altered igneous	Copper	Circle	485	2.66	6310	2135	1705	-	30	Oxidized quartz monzonite	R0	Fair	28.00	-	-	Rock rotational slide	Precipitation event	0.30	800000	43	120.0	240.0	-	-	-						Goldberg and Frizzell (1989); http://duluthreader.com/articles/2016/12/14/8500_lessons_from_the_most_toxic_open_pit_copper_mine





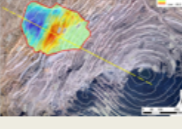
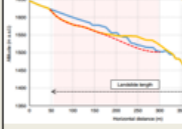

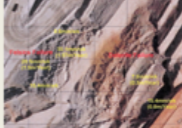





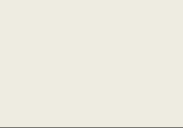


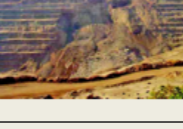

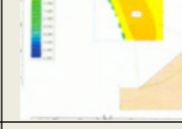

Record Information									Open Pit Parameters							Geological and Geotechnical Characteristics						Slope Failure Parameters										Slope Failure Plan and Scheme			General Information			
Label	Mine	Pit	Wall	ID	Country	Date	Material Group	Commodity	Shape of the Mine	Max Depth of the Mine, H _{max} (m)	Area of the Pit, (km ²)	Shoreline (m)	Length of the Mine (m)	Width of the Mine (m)	Overall Slope Angle of the Mine, β _{op} (°)	Height of Benches (m)	Lithology	Strength Grade	RMR (1976)	Unit Weight, γ (kN/m ³)	C' (kPa)	φ (°)	Failure Mechanism	Trigger factor	Volume (Mm ³)	Mass (tons)	Slope Angle, β _{fail} (°)	Fall Height, H _{fall} (m)	Travel distance, L _{travel} (m)	Average Width, W _{fail} (m)	Setback distance, L _{sb} (m)	Height of the failure, H _{fail} (m)	General View of the Failure	Plan View of the Failure	Cross-Section of the Failure	Software	Monitoring system	Reference
11	Brenda		West		Canada	April 14, 1990	Igneous	Copper	Circle	335	0.87	3474	914	914	45	30	Quartz diorite	R5	Fair	30.00	1.00	26	Rock planar slide	Blasting	2.00	15000000	43	225.0	485.0	150.0	15	176						Weichert et al. (1994); Sjöberg (1996)
12	Brenda		North		Canada	Spring 1978	Igneous	Copper	Circle	220	0.87	3474	914	914	45	30	Quartz diorite	R5	Fair	25.60	1.00	26	Rock topple	Blasting	-	1126400	50	90.0	157.0	45.0	13	70					An electronic theodolite with a built-in laser; automatic recording device (Goodst)	Calder and Blackwell (1980); Mercer (2007)
13	ok Mining Ltd (OTML)	Ok Tedi	West	Block 1A	Papua New Guinea	Mag 10, 2015	Sedimentary	Copper, gold	Circle	700	1.56	4700	3000	2000	40	15	Limestone and siltstone	-	-	26.4	-	-	Rock wedge slide	Precipitation event	8.00	-	42	450	1126.0	250	24	400				Slide, Flac3D, Udec	Visual monitoring, slope stability radars, automatic total stations and survey prisms and manually-	Kennedy and Casagrande (2020);
14	Cassiar		North-East		Canada	January 6, 1969	Igneous	Asbestos	Oval	370	0.29	2210	900	380	39	30	Volcanic	R4	Fair	27	250.00	26	Rock topple	Precipitation event	-	17600000	42	180.0	234.0	-	21	180				UDEC		Mercer (2006); Sjöberg (1999)
15	Chuquibambilla		Southeast		Chile	Feb. 18, 1969	Igneous	Copper, gold, silver	Oval	400	0.87	3474	3300	1000	44	24	Granodiorite	R5	Fair	26.00	100.00	23	Rock irregular slide	Fault zone	150	4100000	46	209.0	307.0	225.0	26	123				UDEC, Phase2	Distance-measuring device	Kennedy and Niermeyer (1970); Voight and Kennedy (1973)
16	Cobre Las Cruces	Las Cruces mine	North		Spain	January 23, 2019	Melano-Sedimentary	Copper, Gold, Silver	Oval	250	1.31	4250	1600	900	28	10	Marl	R1	Poor	15	250.00	20	Soil rotational slide	Precipitation event	14.0	-	32	250.0	1102.0	750.0	98	200				Flac2D, Slide2	Piezometers, Inclinometers, and Prisms	López-Vinielles et al. (2020)
17	Confidential		Southeast		Canada	July 05, 2018	Igneous	Iron								30	Quartzite	R5	Good	26	154.00	35	Rock wedge slide	Daylighted structure	-	30000000	44	125.0	115.0	200.0	55	125				Slide3, RS2	Ground Probe Radar, Photogrammetry Mapping	Zevgolis et al. (2019)
18	Copper Mountain Mine	Pit 3	East		Canada	Nov. 4, 2011	Igneous	Copper	Oval	300	0.8	3715	1380	800	41	12	Porphyry	R3	Fair	30	290.00	34	Rock planar slide	Daylighted structure	0.015	-	55	100.0	63.0	-	65	80				UDEC	Visual inspection	Nunoo (2018)
19	Cowal	Phase 1 pit	West		Australia	July, 2007	Saprolite	Gold, Silver	Circle	325	1	4200	1300	1250	37	9	Saprolite	R0	Very poor	19.00	21.00	26	Debris slide	Precipitation event	0.80	-	31	120.0	202.0	150.0	6	84				Slide2		Sharon (2011); Sharon et al. (2013); Battison et al. (2015); Crouse and Wright (2015); Martin and Stacey (2018)
20	Cowal		Southwest		Australia	Dec. 20, 2007	Saprolite	Gold, Silver	Circle	325	1	4200	1300	1250	37	9	Saprolite	R0	Very poor	19.40	21.00	26	Debris slide	Precipitation event	0.20	-	31	90.0	287.0	100.0	8	98				Slide2		Sharon (2011); Sharon et al. (2013); Crouse and Wright (2015); Martin and Stacey (2018)

Record Information									Open Pit Parameters							Geological and Geotechnical Characteristics						Slope Failure Parameters										Slope Failure Plan and Scheme			General Information							
Label	Mine	Pit	Wall	ID	Country	Date	Material Group	Commodity	Shape of the Mine	Max Depth of the Mine, H _{max} (m)	Area of the Pit, (km ²)	Shoreline (m)	Length of the Mine (m)	Width of the Mine (m)	Overall Slope Angle of the Mine, β _{ox} (°)	Height of Benches (m)	Lithology	Strength Grade	RMR (1976)	Unit Weight, γ (kN/m ³)	C' (kPa)	φ (°)	Failure Mechanism	Trigger factor	Volume (Mm ³)	Mass (tons)	Slope Angle, β _{fail} (°)	Fall Height, H _{fall} (m)	Travel distance, L _{trav} (m)	Average Width, W _{fail} (m)	Setback distance, L _{sb} (m)	Height of the failure, H _{fail} (m)	General View of the Failure	Plan View of the Failure	Cross-Section of the Failure	Software	Monitoring system	Reference				
21	Cuajone		East	D15	Peru	February, 1999	Igneous	Copper	Circle	950	4.19	7597	3000	2500	30	10	Basaltic andesite	R1	Poor	26.00	700.00	30	Rock rotational slide	Precipitation event	4.60	12000000	36	300.0	615.0	430.0	25	225				SBlock, 3DEC		Hormazabal et al. (2013); Fippere et al. (1999)				
22	Dage Iron Mine	East Pit	North	A2	China	July 13, 1996	Igneous	Iron	Triangle	444	0.92	3875	2400	1000	42	-	Diorite	R3	Fair	24.00	60.00	30	Rock wedge slide	Mined too steep	0.10	-	45	240.0	325.0	80.0	5	150					GPS Monitoring since 1998	Zhou et al. (2008)				
23	Gamsberg mine	South Pit	West		South Africa	Nov. 17, 2020	Weathered rock	Zinc-lead ore	Rectangular	-	-	-	520	330	-	-	-	-	-	-	-	-	-	-	Not reported	-	1600000	-	-	120.0	290.0	60	-	-						https://blogs.agu.org/landslideblog/2020/12/02/gamsberg-1/		
24	Geita	Nyankanga pit	Southwest		Tanzania	Feb. 3, 2007	Igneous	Gold	Circle	-	1.02	3728	1188	1025	-	-	-	R2	Fair	27.00	-	-	-	Rock wedge slide	Precipitation event	2.70	7300000	48	200.0	296.0	270.0	84	200							Dyke (2009)		
25	Gibraltar Mines Ltd.	Granite Pit	Southwest	Main Instability Zone	Canada	October 7, 2016	Sedimentary	Copper, molybdenum	Oval	400	2.8	5600	2300	1300	32	15	Tonalite	-	Fair	26	-	-	-	Rock wedge slide	Fault zone	1.10	-	40	275	450.0	200	110	260						Ground-Based Radar, and Drone Photogrammetry	Dick et al. (2020)		
26	Gold Quarry		East	Phase 2	USA	Dec. 1, 2004	Altered igneous	Gold	Oval	396	4.11	8125	2400	1600	37	30	Carlin formation	R0	Very poor	16.00	129.30	27	-	Debris slide	Precipitation event	0.20	311000	46	96.0	120.0	90.0	15	96							Survey Prisms, Extensometer, and Laser Scanner; Visual Inspection	Sheets (2011)	
27	Gold Quarry		East	Phase 2	USA	Dec. 27, 2004	Altered igneous	Gold	Oval	396	4.11	8125	2400	1600	37	30	Carlin formation	R0	Very poor	16.00	129.30	27	-	Debris slide	Precipitation event	0.30	415000	46	60.0	88.0	90.0	10	60							Survey Prisms, Extensometer, and Laser Scanner; Visual Inspection	Bates et al. (2006); Sheets (2011)	
28	Gold Quarry		East	Phase 2	USA	October 12, 2005	Altered igneous	Gold	Oval	396	4.11	8125	2400	1600	37	30	Carlin formation (laminated tuff)	R0	Very poor	16.00	129.30	27	-	Debris slide	Precipitation event	0.80	1270000	46	156.0	271.0	225.0	39	113								Survey Prisms, Extensometer, and Laser Scanner	Bates et al. (2006); Sheets (2011)
29	Gold Quarry		East	Phase 4	USA	July 19, 2007	Metamorphic	Gold	Oval	396	4.11	8125	2400	1600	37	30	Carlin formation	R1	Fair	16.00	82.00	24	-	Rock wedge slide	Precipitation event	0.40	640000	35	76.0	104.0	180.0	34	73									Sheets (2011)
30	Gold Quarry		East		USA	April 26, 2009	Altered igneous	Gold	Oval	396	4.11	8125	2400	1600	37	30	Carlin formation	R0	Very poor	16.00	75.00	25	-	Debris slide	Precipitation event	4.00	8000000	30	250.0	700.0	400.0	45	125									Sheets et al. (2014); Yang et al. (2011a)

Record Information									Open Pit Parameters							Geological and Geotechnical Characteristics						Slope Failure Parameters								Slope Failure Plan and Scheme			General Information					
Label	Mine	Pit	Wall	ID	Country	Date	Material Group	Commodity	Shape of the Mine	Max Depth of the Mine, H _{max} (m)	Area of the Pit, (km ²)	Shoreline (m)	Length of the Mine (m)	Width of the Mine (m)	Overall Slope Angle of the Mine, β _{op} (°)	Height of Benches (m)	Lithology	Strength Grade	RMR (1976)	Unit Weight, γ (kN/m ³)	C' (kPa)	φ (°)	Failure Mechanism	Trigger factor	Volume (Mm ³)	Mass (tons)	Slope Angle, β _{fail} (°)	Fall Height, H _{fall} (m)	Travel distance, L _{travel} (m)	Average Width, W _{fail} (m)	Setback distance, L _{sb} (m)	Height of the failure, H _{fail} (m)	General View of the Failure	Plan View of the Failure	Cross-Section of the Failure	Software	Monitoring system	Reference
31	Gold Quarry		East	South Ramp Slide	USA	October 14, 2009	Altered igneous	Gold	Oval	396	4.11	8125	2400	1600	37	30	Carlin formation	R0	Very poor	16.00	50.00	23	Debris slide	Precipitation event	1.10	1800000	30	110.0	268.0	230.0	12	88				FLAC2D, Phase4		Sheets (2011)
32	Gold Quarry		East	Nine Points	USA	Dec. 24, 2009	Altered igneous	Gold	Oval	396	4.11	8125	2400	1600	37	30	Carlin formation	R0	Very poor	16.00	50.00	33	Debris slide	Precipitation event	6.50	12000000	24	220.0	637.0	400.0	63	95						Sheets et al. (2014); Yang et al. (2011a)
33	Goldstrike	Betze Post	Southeast	SE-96-A	USA	March, 1997	Altered igneous	Gold	Circle	460	0.71	3120	2450	1500	30	12	Altered granodiorite (SAG)	R3	Poor	23.00	50.00	18	Rock wedge slide	Precipitation event	7.30	18000000	38	280.0	785.0	400.0	10	280				CLARA, UDEC		Rose and Sharon (2000); Sharon (2000)
34	Goldstrike	Betze Post	Southeast	S-97-B	USA	March, 1997	Altered igneous	Gold	Circle	460	0.71	3120	2450	1500	30	12	Altered granodiorite (SAG)	R3	Poor	23.00	50.00	18	Rock wedge slide	Precipitation event	2.00	5000000	35	175.0	345.0	300.0	5	175				CLARA, UDEC		Rose and Sharon (2000); Sharon (2000)
35	Goldstrike	Betze Post	Southeast	S-01-A	USA	August 23, 2001	Altered igneous	Gold	Circle	460	0.71	3120	2680	2200	30	12	Altered granodiorite (SAG)	R2	Poor	23.00	50.00	18	Rock wedge slide	Mined too steep	19.00	47000000	27	550.0	1266.0	450.0	75	365				CLARA/W	Survey Prisms	Rose (2011); http://elkorose.sohopine.com/china-springs.html
36	Goldstrike	Betze Post	Southwest	S-05-B	USA	May 22, 2005	Metamorphic	Gold	Circle	460	0.71	3120	2680	2200	30	12	Metasediments	R3	Fair	25.00	50.00	18	Rock wedge slide	Daylighted structure	2.00	5000000	38	195.0	357.0	250.0	25	150				UDEC	Survey Prisms, Extensometer	Rose (2011); Armstrong and Rose (2009)
37	Goldstrike	Betze Post	South	S-07-B	USA	Sept. 10, 2007	Metamorphic	Gold	Circle	460	0.71	3120	2680	2200	30	12	Metasediments	R3	Fair	25.00	50.00	18	Rock irregular slide	Daylighted structure	0.20	500000	44	146.0	157.0	155.0	30	146						Rose (2011); Armstrong and Rose (2009)
38	Goldstrike	Betze Post	South	S-09-B	USA	October 9, 2008	Metamorphic	Gold	Circle	460	0.71	3120	2680	2200	30	12	Metasediments	R3	Fair	25.00	50.00	18	Rock irregular slide	Daylighted structure	0.30	-	44	110.0	152.0	73.0	8	54						Armstrong (2011); Whittall (2015)
39	Goldstrike	Betze Post	South	S-09-B	USA	2009	Metamorphic	Gold	Circle	460	0.71	3120	2680	2200	30	18	Metasediments	R3	Fair	25.00	50.00	18	Rock irregular slide	Long-term weakening	1.10	2700000	44	210.0	352.0	135.0	30	210						Rose (2011); Armstrong and Rose (2009)
40	Grande Cache	No. 12S B2	North		Canada	July 7, 2006	Sedimentary	Coal	Polygon	200	1.98	5913	2000	1000	42	15	Shale and coal	R1	-	25.00	40.00	24	Rock rotational slide	Precipitation event	0.10	150000	44	40.0	53.5	100.0	4.5	33					Photogrammetry, Surveys, Survey Prisms	Tannant and LeBreton (2007)

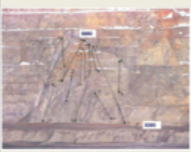
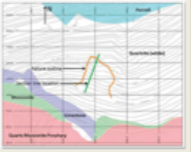
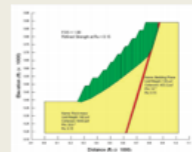

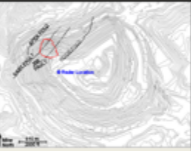
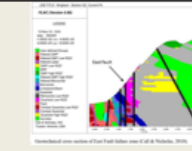
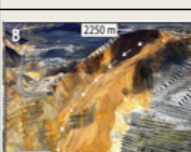

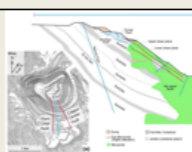
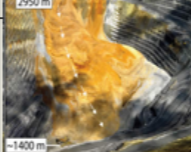
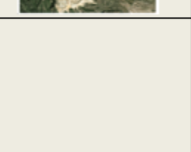
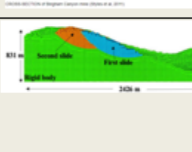
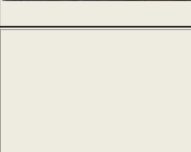

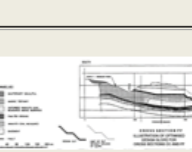
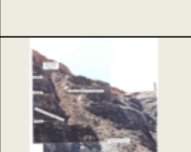




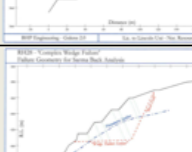
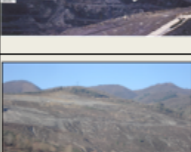
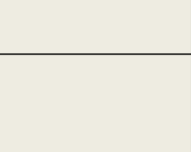
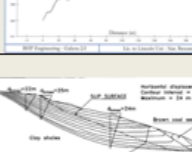
Record Information									Open Pit Parameters							Geological and Geotechnical Characteristics					Slope Failure Parameters								Slope Failure Plan and Scheme			General Information							
Label	Mine	Pit	Wall	ID	Country	Date	Material Group	Commodity	Shape of the Mine	Max Depth of the Mine, H _{max} (m)	Area of the Pit, (km ²)	Shoreline (m)	Length of the Mine (m)	Width of the Mine (m)	Overall Slope Angle of the Mine, β _{op} (°)	Height of Benches (m)	Lithology	Strength Grade	RMR (1976)	Unit Weight, γ (kN/m ³)	C' (kPa)	φ (°)	Failure Mechanism	Trigger factor	Volume (Mm ³)	Mass (tons)	Slope Angle, β _{fail} (°)	Fall Height, H _{fall} (m)	Travel distance, L _{trav} (m)	Average Width, W _{fail} (m)	Setback distance, L _{sb} (m)	Height of the failure, H _{fail} (m)	General View of the Failure	Plan View of the Failure	Cross-Section of the Failure	Software	Monitoring system	Reference	
41	Grasberg		South		Indonesia	October 9, 2003	Igneous	Copper, gold, silver	Circle	1100	5.77	9080	3270	2730	39	20	Intrusives complex	-	Poor	27.00	126.00	54	Rock irregular slide	Precipitation event	1.10	2500000	40	294.0	646.0	190.0	40	100				RS2, Phase2	GPS, Extensometers, 5 Total Stations, VWP, Inclinometers, Piezometers	Srikant et al. (2007); Ginting et al. (2011); Widjanto (2017)	
42	Hindustan Lalpeth				India	August 11, 1995	Sedimentary	Coal	Elongated oval	41	0.68	3651	1430	566	37	10	Overburden and sandstone	R2	Very poor	17.00	26.00	14	Debris slide	Precipitation event	0.11	-	45	41.0	65.0	-	-	-					Jhanwar and Thote (2011)		
43	Hogarth	Hogarth	Northwest		Canada	June 23, 1975	Igneous	Iron		350	-	-	-	-	40		Diorite	R5	-	-	-	-	Rock topple	Precipitation event	0.20	-	52	185.0	242.0	-	7	90					USTADAS; Laser Electronic Distance Measuring device (EDM), Seismograph, Extensometers	Brawner et al. (1975); Brawner and Stacey (1979)	
44	Homestake Pitch	North	East		USA	March, 1983	Igneous	Uranium	Polygon	180	0.76	3712	366	305	42	15	Sericite clay and weathered pegmatite	R1	Poor	20.40	23.90	29	Rock compound slide	Precipitation event	0.90	-	42	190.0	350.0	125.0	20	60					UDEC		Cremins (2003); Cremins et al. (2000)
45	Homestake Pitch	North	East		USA	October, 1983	Igneous	Uranium	Polygon	180	0.76	3712	366	305	42	15	Sericite clay and weathered pegmatite	R1	Poor	20.00	23.90	29	Rock compound slide	Precipitation event	1.70	-	42	230.0	469.5	125.0	25.5	130					Piezometers	Cremins (2003); Cremins et al. (2000)	
46	Huckleberry	East Zone	North		Canada	June 22, 2007	Igneous	Copper	Circle	315	0.48	2515	800	680	39	15.00	Andesite	R3	Fair	27.00	200.00	32	Rock compound slide	Daylighted structure	2.00	5400000	36	315.0	527.0	500.0	43	110					AGA Geodimeter	Nano (2016)	
47	Jebel Onk	Kert Esrinoun	North_east		Algeria	August 9, 2008	Sedimentary	Phosphate	Oval	70	0.1	1260	375	305	20	30	Limestone	R4	Good	22.5	45.00	14	Rock planar slide	Daylighted structure	0.60	-	23	155	467.5	-	8.5	130					Slide2, Plaxis		Fredj et al. (2018); Gadi et al. (2015)
48	Junad		South		India	August 13, 2006	Sedimentary	Coal		-	-	-	-	-	25	-	Overburden and sandstone	R2	Very poor	17.00	26.00	14	Rock planar slide	Precipitation event	0.20	-	18	77.0	170.0	125.0	-	35					Galena		Jhanwar and Thote (2011)
49	Kagemori		South		Japan	Sept. 20, 1973	Sedimentary	Limestone	Oval	150	0.49	3170	1280	455	43	8.00	Limestone	R5	Fair	27.00	260.00	39	Rock irregular slide	Long-term weakening	0.40	-	50	150.0	195.0	100.0	15	140						Yamaguchi and Shimotani (1986)	
50	Kawadi				India	June 24, 2000	Sedimentary	Coal	Rectangle	75	0.92	4372	1770	590	48	-	Overburden and sandstone	R2	Very poor	17.00	12.50	14	Debris slide	Precipitation event	0.30	-	51	49.0	135.0	-	-	50						Jhanwar and Thote (2011)	


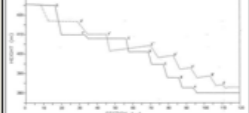


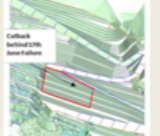


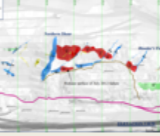



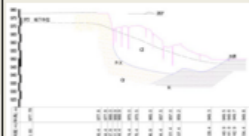
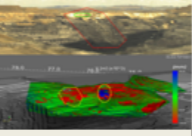
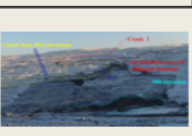
Record Information								Open Pit Parameters							Geological and Geotechnical Characteristics					Slope Failure Parameters							Slope Failure Plan and Scheme			General Information								
Label	Mine	Pit	Wall	ID	Country	Date	Material Group	Commodity	Shape of the Mine	Max Depth of the Mine, H _{max} (m)	Area of the Pit, (km ²)	Shoreline (m)	Length of the Mine (m)	Width of the Mine (m)	Overall Slope Angle of the Mine, β _{op} (°)	Height of Benches (m)	Lithology	Strength Grade	RMR (1976)	Unit Weight, γ (kN/m ³)	C' (kPa)	φ (°)	Failure Mechanism	Trigger factor	Volume (Mm ³)	Mass (tons)	Slope Angle, β _{fail} (°)	Fall Height, H _{fall} (m)	Travel distance, L _{trav} (m)	Average Width, W _{fail} (m)	Setback distance, L _{sb} (m)	Height of the failure, H _{fail} (m)	General View of the Failure	Plan View of the Failure	Cross-Section of the Failure	Software	Monitoring system	Reference
51	KBI Morgul	Cakmakkeya	East	-	Turkey	1989	Altered igneous	Copper	Circle	-	0.64	3265	900	750	-	-	Weathered dacite and tuffite	R1	Very poor	26.00	15.00	21	Rock rotational slide	Precipitation event	0.90	-	35	240.0	560.0	220.0	20	220					Monitoring Stations	Nazuf et al. (1993); Arikan et al. (2010)
52	Kemess	-	Northwest	-	Canada	May, 2004	Altered igneous	Copper-gold ore	Oval	350	1.76	5127	2000	1100	47	30.00	Clay altered lapilli tuff	R3	Poor	-	-	40	Rock planar slide	Precipitation event	0.60	1500000	47	160.0	213.0	130.0	67	160				SLOPEW, UDEC, Phase2	GroundProbe SSR, Prisms Survey, Visual Inspections	Yang et al. (2011b)
53	Kennecott Nevada Mine Division	Tripp Pit	North-East	-	USA	January 4, 1970	Metamorphic	Copper	-	-	-	-	-	-	40	-	-	-	-	60.00	10	Rock wedge slide	Mined too steep	11.7	3.3E+07	40	170	2700.0	460	-	170						Miller (1979), Miller (1982)	
54	Kirka Borax	-	Northwest	-	Turkey	1974	Sedimentary	Borate	Circle	60	0.66	2875	940	940	33	8.00	Silicified limestone and marl	R0	Very poor	23.00	10.00	12	Rock irregular slide	Precipitation event	52.00	#####	33	123.0	648.0	480.0	52	123						Türk and Koca (1993)
55	Kovdorsk GOK	Kovdor	East	-	Russia	August 28, 2015	Igneous	Iron, Apatite	Oval	500	3.18	6530	2300	1600	50	30	Phoscorites and carbonates	R5	Good	27.5	520.00	7	Rock planar slide	Daylighted structure	0.10	-	44	105.0	47.0	170.0	1	48						Melnikov et al. (2015)
56	Kumtor	Central open pit	Northeast	-	Kyrgyzstan	July 13, 2006	Igneous	Gold	Oval	342	3.95	8100	3100	1500	36	24.00	Metasomatite	R4	Fair	28.00	-	60	Rock irregular slide	Precipitation event	1.00	-	36	237.0	448.0	190.0	12	200				CPLOPE	Automated prism monitoring system (since 2002)	Oldcorn and Seago (2007), Torgoev (2014)
57	Kumtor	KS13	-	-	Kyrgyzstan	July 8, 2002	Igneous	Gold	Oval	342	3.95	8100	3100	1500	42	24.00	Metasomatite	R5	Fair	28.50	-	60	Rock irregular slide	Precipitation event	2.70	-	42	280.0	368.0	270.0	12	280				ADVENTURE, ParaView 3.2.0, CSLOPE	5 geodetic monitoring points in the collapse zone	Dolgushev et al. (2008); Melnikov et al. (2015); Torgoev (2014)
58	Leigh Creek	Upper Series	Northeast	L24	Australia	June 6, 2001	Sedimentary	Black Coal	Polygon	450	4.67	11636	4000	990	30	15.00	Mudstone	R1	Poor	18.00	350.00	21	Rock planar slide	Daylighted structure	1.10	-	32	100.0	222.0	650.0	18	100				UDEC	Piezometers	Coulthard et al. (2004), Alejano and Sánchez (2010)
59	Lethakane	DK1	West	-	Botswana	July 14, 2005	Sedimentary	Diamond	Circle	290	0.83	3260	1050	1000	29	14.00	Sandstone	R3	Good	22.00	-	-	Rock topple	Not reported	0.20	520000	52	112.0	138.0	138.0	12	70					Slope Stability Radar (SSR); visual inspections	Kajesa (2006); Mercer (2006)
60	Liberty	-	-	-	USA	May, 1966	Metamorphic	Copper	-	-	-	-	-	-	-	-	-	R2	Fair	29.00	-	-	Rock wedge slide	Precipitation event	6.00	7000000	33	175.0	440.0	350.0	-	-						Broadbent and Zavodni (1981); Brawner (1986)

Record Information									Open Pit Parameters							Geological and Geotechnical Characteristics					Slope Failure Parameters										Slope Failure Plan and Scheme			General Information				
Label	Mine	Pit	Wall	ID	Country	Date	Material Group	Commodity	Shape of the Mine	Max Depth of the Mine, H _{max} (m)	Area of the Pit, (km ²)	Shoreline (m)	Length of the Mine (m)	Width of the Mine (m)	Overall Slope Angle of the Mine, β _{op} (°)	Height of Benches (m)	Lithology	Strength Grade	RMR (1976)	Unit Weight, γ (kN/m ³)	C' (kPa)	φ (°)	Failure Mechanism	Trigger factor	Volume (Mm ³)	Mass (tons)	Slope Angle, β _{fail} (°)	Fall Height, H _{fall} (m)	Travel distance, L _{trav} (m)	Average Width, W _{fail} (m)	Setback distance, L _{sb} (m)	Height of the failure, H _{fail} (m)	General View of the Failure	Plan View of the Failure	Cross-Section of the Failure	Software	Monitoring system	Reference
61	Luscar	51-B2	North		Canada	Nov. 1979	Sedimentary	Coal	Square	227	0.81	3600	900	900	35	10.00	Interbedded sandstone and siltstone	R2	Fair	20.00	1.00	30	Rock planar slide	Precipitation event	1.10	-	36	105.0	151.0	245.0	44	104						MacRae (1985)
62	Madenköy copper mine		Northwest		Turkey	Nov. 17, 2016	Metamorphic	Copper	Circle	400	0.82	3335	1070	935	27	25	Spilite	R2	Poor	-	-	-	Rock rotational slide	Precipitation event	0.64	-	27	225.0	340.0	225.0	50	125					Ground-based radar	Carlià et al. (2017), Carlià et al. (2018)
63	Monroe County		North		USA	April 26, 2000	Metamorphic	Coal									Gneiss	R0	Fair	-	-	-	Rock irregular slide	Blasting	0.60	2000000	60	67.0	91.0	100.0	-	-						Kelly et al. (2002)
64	Mount Keith Mine	Mount Keith Mine	Southeast		Australia	Dec. 7, 2001	Saprolite	Nickel	Oval	325	3.27	7175	2785	1530	30	30.00	Saprolite	R0	Very poor	-	27.00	24	Debris slide	Precipitation event	0.40	1000000	31	95.0	220.0	100.0	10	95					3 SSR Units, Leica Prisms Monitoring	Mercer (2006)
65	Navachab		East		Namibia	Dec. 1997	Metamorphic	Gold	Oval	190	0.8	4030	1550	510	43	10.00	Schist	R5	Fair	27.00	40.00	35	Rock wedge slide	Blasting	-	120000	63	40.0	35.0	-	10	30				Slide2, FLAC2D	Seismic Monitoring (StandAlone and QS data acquisition units)	Rous et al. (2006); Mercer (2006); Lynch and Malovichko (2006)
66	Navachab		East		Namibia	March, 2001	Metamorphic	Gold	Oval	190	0.8	4030	1550	510	43	10.00	Schist	R5	Fair	27.00	40.00	35	Rock planar slide	Precipitation event	-	110000	63	100.0	57.0	107.0	8	100				Slide2, FLAC2D	Seismic Monitoring	Rous et al. (2006); Mercer (2006); Lynch and Malovichko (2006)
67	Navin Kundata				India	August 23, 2001	Soil	Coal	Triangle	42	0.63	3527	1157	638	26	-	Overburden	R1	Very poor	17.00	26.00	14	Soil rotational slide	Precipitation event	0.10	-	28	30.0	87.0	-	8	30				Galena		Jhanwar and Thote (2011)
68	Nchanga		South		Zambia	April, 1980	Sedimentary	Copper	Elongated oval	272	-	-	4000	-	30	10.00	Interbedded sandstone and quartzite	R1	Poor	25.00	-	-	Rock planar slide	Precipitation event	10.00	-	30	184.0	665.0	850.0	15	180						Terbrugge and Hanif (1981)
69	Nchanga	Pit 20	North	21E	Zambia	July 16, 2004	Sedimentary	Copper	Elongated oval	400	3.66	9200	4080	1125	32	30.00	Shale	R2	Poor	25.00	290.00	40	Rock topple	Daylighted structure	1.80	4500000	35	180.0	353.0	200.0	7	180				FLAC	SSR Ground Probe radar, Prisms Survey, Visual Inspections	Naismith and Wessels (2005); Wessels (2009); Umar et al. (2018)
70	New Majri		West		India	June 30, 2005	Soil	Coal	Rectangle	90	0.51	3850	1530	360	41	8.00	Overburden and waste rock	R0	Very poor	17.00	26.00	14	Soil rotational slide	Precipitation event	0.20	-	41	110.0	215.0	85.0	10	41				Galena		Jhanwar and Thote (2011)



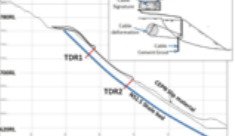
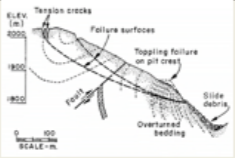
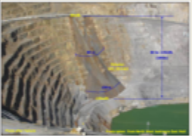
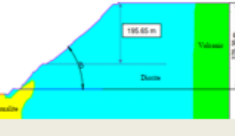
Record Information									Open Pit Parameters							Geological and Geotechnical Characteristics						Slope Failure Parameters										Slope Failure Plan and Scheme			General Information				
Label	Mine	Pit	Wall	ID	Country	Date	Material Group	Commodity	Shape of the Mine	Max Depth of the Mine, H _{max} (m)	Area of the Pit, (km ²)	Shoreline (m)	Length of the Mine (m)	Width of the Mine (m)	Overall Slope Angle of the Mine, β _{op} (°)	Height of Benches (m)	Lithology	Strength Grade	RMR (1976)	Unit Weight, γ (kN/m ³)	C' (kPa)	φ (°)	Failure Mechanism	Trigger factor	Volume (Mm ³)	Mass (tons)	Slope Angle, β _{fail} (°)	Fall Height, H _{fall} (m)	Travel distance, L _{travel} (m)	Average width, W _{fall} (m)	Setback distance, L _{sb} (m)	Height of the failure, H _{fall} (m)	General View of the Failure	Plan View of the Failure	Cross-Section of the Failure	Software	Monitoring system	Reference	
71	Newmont Boddington Gold (NBG)	South pit	Southeast	Wandoo south	Australia	2001	Saprolite	Gold, copper	Circle	100	0.83	3500	1000	870	27	20	Saprolite	R1	Very poor	20	27.00	21	Debris slide	Mined too steep	0.50	1000000	36	80.0	234.0	370.0	16	50						Martin and Stacey (2013)	
72	Newmont Boddington Gold (NBG)	North pit	West	Wandoo north	Australia	2009	Saprolite	Gold, copper	Oval	100	1.6	5000	1900	1050	27	20	Saprolite	R1	Very poor	20	27.00	23	Debris slide	Mined too steep	0.30	500000	33	60.0	88.0	-	12	60							Martin and Stacey (2013)
73	Nijjai				India	August 12, 2002	Soil	Coal	Oval	200	2.54	-	4720	1000	20	-	Overburden	R0	Very poor	17.00	29.80	13	Soil rotational slide	Precipitation event	0.30	-	20	35.0	325.0	95.0	-	35				Galena		Jhanwar and Thote (2011).	
74	P.T. Newmont Nusa Tenggara	Batu Hijau	Southwest	SS_P4_D28	Indonesia	October 12, 2007	Igneous	Copper-gold ore	Circle	700	3.62	6855	2130	2130	36	15	Tonalite	R3	-	20.00	57.00	27	Rock irregular slide	Not reported	0.50	-	40	380.0	150.0	200.0	15	90						Arif and Baker (2004), Asof et al. (2010), Aprilia and Indrawan (2014)	
75	P.T. Newmont Nusa Tenggara	Batu Hijau	West	WS_P5_064	Indonesia	August 24, 2010	Igneous	Copper-gold ore	Circle	700	3.62	6855	2130	2130	36	15	Volcanic	R3	-	20.00	57.00	27	Rock irregular slide	Daylighted structure	0.30	-	55	105.0	131.0	100.0	9	75						Almenara et al. (2011); Aprilia and Indrawan (2014); Lelono et al. (2016)	
76	Permanente	North Quarry	Northwest	Main Slide	USA	1987	Metamorphic	Limestone	Oval	620	1.07	3870	1525	790	45	15	Greenstone	R1	Poor	26.00	80.00	21	Rock irregular slide	Not reported	2.70	-	47	300.0	615.0	265.0	60	185						EnviroMine (2011), Golder Associates (2011)	
77		Olimpiada	South		Russia	May 23, 2016	Metamorphic	Gold	Circle	500	2.09	5175	1690	1600	40	30	Schist	R4	Fair	28.1	-	-	Rock planar slide	Freeze-thaw cycle	0.20	565000	49	210.0	163.0	90.0	7	120							www.eRUDA.ru
78	Public Power Cooperation (PPC)	Maropigi mine	Southeast		Greece	Not reported	Sedimentary	Lignite		120	-	-	-	12	25	Marl and Lignite	R1	Poor	17	5.00	23		Not reported	6.00	-	14	125.0	205.0	-	75	65					20 Prism Monitoring Stations, 2 Inclinometers, and 2 Piezometers		Kavvadas et al. (2013)	
79	Quadrilitero Ferrifero	Agua Citras	Northwest	Patrimônio failure	Brazil	April 23, 1992	Metamorphic	High-grade iron ore	Oval	234	0.67	3772	770	1150	44	30	Hematite and Itabirite	R0	Very poor	22.00	70.00	34	Soil planar slide	Mined too steep	0.70	2000000	44	325.0	761.0	200.0	17	200					SLIDE, PHASE2		Martin and Stacey (2013); da Franca (1997); Fisher (2009)
80	Rio Tinto Borates	Boron	North	E-17	USA	1970	Sedimentary	Borate	Circle	190	3.64	7154	3200	2800	20	15	Weakly cemented arkose	R1	Poor	21.00	53.00	12	Rock planar slide	Daylighted structure	-	5200000	25	112.0	383.0	-	16	61				FLAC, SlopeW	Prisms, Extensometers, Inclinometers, and Pin Sets		Yost (2009)


Record Information									Open Pit Parameters							Geological and Geotechnical Characteristics					Slope Failure Parameters								Slope Failure Plan and Scheme			General Information						
Label	Mine	Pit	Wall	ID	Country	Date	Material Group	Commodity	Shape of the Mine	Max Depth of the Mine, H _{max} (m)	Area of the Pit, (km ²)	Shoreline (m)	Length of the Mine (m)	Width of the Mine (m)	Overall Slope Angle of the Mine, β _{op} (°)	Height of Benches (m)	Lithology	Strength Grade	RMR (1976)	Unit Weight, γ (kN/m ³)	C' (kPa)	φ (°)	Failure Mechanism	Trigger factor	Volume (Mm ³)	Mass (tons)	Slope Angle, β _{fail} (°)	Fall Height, H _{fall} (m)	Travel distance, L _{trav} (m)	Average Width W _{fail} (m)	Setback distance, L _{sb} (m)	Height of the failure, H _{fail} (m)	General View of the Failure	Plan View of the Failure	Cross-Section of the Failure	Software	Monitoring system	Reference
81	Rio Tinto Borates	Boron	North	E-19	USA	1974	Sedimentary	Borate	Circle	190	3.64	7154	2278	1865	20	15	Weakly cemented arkose	R1	Poor	21.00	53.00	12	Rock planar slide	Daylighted structure	-	330000	25	19.0	74.0	-	3	10.0				FLAC	Prisms, Extensometers, Inclinometers, and Pin Sets	Yost (2009)
82	Rio Tinto Borates	Boron	North	22250	USA	1979	Sedimentary	Borate	Circle	190	3.64	7154	2278	1865	20	15	Weakly cemented arkose	R2	Poor	21.70	173.00	13	Rock planar slide	Daylighted structure	-	150000	19	37.0	110.0	-	6	38.0				FLAC	Prisms, Extensometers, Inclinometers, and Pin Sets	Yost (2009)
83	Rio Tinto Borates	Boron	North	23250	USA	1982	Sedimentary	Borate	Circle	250	3.64	7154	2278	1865	20	15	Weakly cemented arkose	R1	Poor	21.70	173.00	13	Rock planar slide	Daylighted structure	-	5120000	25	104.0	336.0	-	15	104.0				FLAC	Prisms, Extensometers, Inclinometers, and Pin Sets	Yost (2009)
84	Rio Tinto Borates	Boron	North	20000	USA	1984	Sedimentary	Borate	Circle	250	3.64	7154	2278	1865	20	15	Weakly cemented arkose	R1	Poor	21.70	173.00	13	Rock planar slide	Daylighted structure	-	370000	25	46.0	91.0	-	7	46.0				FLAC	Prisms, Extensometers, Inclinometers, and Pin Sets	Yost (2009)
85	Rio Tinto Borates	Boron	North	19500	USA	1984	Sedimentary	Borate	Circle	250	3.64	7154	2278	1865	20	15	Weakly cemented arkose	R1	Poor	21.70	173.00	13	Rock planar slide	Daylighted structure	-	190000	25	38.0	76.0	-	6	38.0				FLAC	Prisms, Extensometers, Inclinometers, and Pin Sets	Yost (2009)
86	Rio Tinto Borates	Boron	North	20500	USA	1986	Sedimentary	Borate	Circle	250	4.74	9575	3200	2800	20	15	Weakly cemented arkose	R1	Poor	21.70	173.00	13	Rock planar slide	Daylighted structure	-	2220000	25	79.0	202.0	-	11	79.0				FLAC	Prisms, Extensometers, Inclinometers, and Pin Sets	Yost (2009)
87	Rio Tinto Borates	Boron	North	-	USA	1992	Sedimentary	Borate	Circle	300	4.74	9575	3200	2800	20	15	Weakly cemented arkose	R1	Poor	21.70	173.00	13	Rock planar slide	Daylighted structure	-	2250000	25	110.0	277.0	-	16	110.0				FLAC	Prisms, Extensometers, Inclinometers, and Pin Sets	Yost (2009)
88	Rio Tinto Borates	Boron	North	19500	USA	1995	Sedimentary	Borate	Circle	300	4.74	9575	3200	2800	20	15	Weakly cemented arkose	R1	Poor	21.70	173.00	13	Rock planar slide	Daylighted structure	-	330000	25	43.0	92.0	-	6	43.0				FLAC	Prisms, Extensometers, Inclinometers, and Pin Sets	Yost (2009)
89	Rio Tinto Borates	Boron	North	-	USA	1996	Sedimentary	Borate	Circle	300	4.74	9575	3200	2800	20	15	Weakly cemented arkose	R1	Poor	21.70	173.00	13	Rock planar slide	Daylighted structure	-	4380000	20	128.0	393.0	-	18	128.0				FLAC	Prisms, Extensometers, Inclinometers, and Pin Sets	Yost (2009)
90	Rio Tinto Borates	Boron	Northwest	-	USA	1997	Sedimentary	Borate	Circle	300	4.74	9575	3200	2800	20	15	Weakly cemented arkose	R1	Poor	21.70	173.00	13	Rock planar slide	Daylighted structure	-	18700000	20	180.0	828.0	-	25	180.0				FLAC	Prisms, Extensometers, Inclinometers, and Pin Sets	Yost (2009)

Record Information									Open Pit Parameters							Geological and Geotechnical Characteristics					Slope Failure Parameters										Slope Failure Plan and Scheme			General Information				
Label	Mine	Pit	Wall	ID	Country	Date	Material Group	Commodity	Shape of the Mine	Max Depth of the Mine, H _{max} (m)	Area of the Pit, (km ²)	Shoreline (m)	Length of the Mine (m)	Width of the Mine (m)	Overall Slope Angle of the Mine, β _{op} (°)	Height of Benches (m)	Lithology	Strength Grade	RMR (1976)	Unit Weight, γ (kN/m ³)	C' (kPa)	φ (°)	Failure Mechanism	Trigger factor	Volume (Mm ³)	Mass (tons)	Slope Angle, β _{fail} (°)	Fall Height, H _{fall} (m)	Travel distance, L _{travel} (m)	Average width, W _{fail} (m)	Setback distance, L _{sb} (m)	Height of the failure, H _{fail} (m)	General View of the Failure	Plan View of the Failure	Cross-Section of the Failure	Software	Monitoring system	Reference
91	Rio Tinto Borates	Boron	Northwest	-	USA	1997	Sedimentary	Borate	Circle	300	4.74	9575	3200	2800	20	15	Weakly cemented arkose	R1	Poor	21.70	173.00	13	Rock planar slide	Daylighted structure	-	11000000	20	116.0	364.0	-	17	116.0				FLAC	Prisms, Extensometers, Inclinometers, and Pin Sets	Yost (2009)
92	Rio Tinto Borates	Boron	Northeast	-	USA	1998	Sedimentary	Borate	Circle	300	4.74	9575	3200	2800	20	15	Weakly cemented arkose	R1	Poor	21.70	173.00	13	Rock planar slide	Daylighted structure	-	13200000	20	191.0	735.0	-	27	191.0				FLAC	Prisms, Extensometers, Inclinometers, and Pin Sets	Yost (2009)
93	Rio Tinto Kennecott	Bingham Canyon	South	07 Opus	USA	Early 2009	Igneous	Copper, gold, molybdenum, silver	Circle	365	11.7	12643	4000	3800	44	15-30	Quartzite	R1	Poor	24.50	25.90	25	Rock rotational slide	Daylighted structure	0.45	1100000	50	150.0	181.0	152.0	29	150				Slope/W	slope stability radar (not monitored before)	Nutakor (2012)
94	Rio Tinto Kennecott	Bingham Canyon	Northeast	-	USA	August 15, 2010	Igneous	Copper, gold, molybdenum, silver	Circle	1200	11.7	12643	4000	3800	23	15-30	Quartzite	R3	Poor	24.50	50.00	16	Rock wedge slide	Daylighted structure	24.40	750000	50	315.0	445.0	160.0	15	275				FLAC	Prisms, slope stability radar, and spotter logs	Doyle and Reese (2011)
95	Rio Tinto Kennecott	Bingham Canyon	Northeast	1st event	USA	April 10, 2013	Igneous	Copper, gold, molybdenum	Circle	1200	11.7	12643	4000	3800	23	30-46	Quartz monzonite	R5	Good	24.50	50.00	16	Rock planar slide	Daylighted structure	24.40	165000000	29	640.0	2236.0	550.0	94	385				FLAC	IBIS radars and three GroundProbe slope stability radars	Pankow et al. (2014); Moharana and Lonergan (2014); Hibert et al. (2014); Fross and Sutherland (2015); Septian 2016; Zavodni and Erickson (1995)
96	Rio Tinto Kennecott	Bingham Canyon	Northeast	2nd event	USA	April 10, 2013	Igneous	Copper, gold, molybdenum	Circle	1200	11.7	12643	4000	3800	23	30-46	Quartz monzonite	R1	Good	24.50	50.00	16	Rock planar slide	Daylighted structure	24.40	-	29	850.0	2800.0	550.0	130	500				FLAC	IBIS radars and three GroundProbe slope stability radars	Pankow et al. (2014); Moharana and Lonergan (2014); Hibert et al. (2014); Fross and Sutherland (2015); Septian 2017; Zavodni and Erickson (1995)
97	Rotowaro	Waipuna	Northeast	-	New Zealand	Not reported	Sedimentary	Coal	Oval	100	0.76	3265	1080	830	-	-	Claystone	R2	-	22.00	5.00	20	Rock rotational slide	Not reported	0.50	-	44	120.0	205.0	170.0	15	86				FLAC, SLOPEW		Johnson et al. (2007); Fergusson et al. (2001)
98	Round Hill open pit mine	-	North	RH27	New Zealand	Dec. 5, 1994	Metamorphic	Gold	Circle	130	1.66	5050	800	700	41	15	Pelitic schist	R4	Fair	27	8.00	39	Rock wedge slide	Daylighted structure	0.001	2430	45	60	78.0	247	7	45						Brown et al. (2016); Chapple (1996)
99	Round Hill open pit mine	-	North	RH28	New Zealand	June, 1996	Metamorphic	Gold	Circle	130	1.66	5050	800	700	35	15	Pelitic schist	R4	Fair	27	8.00	24	Rock wedge slide	Daylighted structure	0.43	166700	37	105	119.0	110	11	75				TSLOPE	extensometer	Chapple (1996)
100	Santa Barbara	-	North	-	Italy	1983	Soil	Lignite	Polygon	200	0.18	2520	1300	400	30	15	Lacustrine overburden	R0	Very poor	23.50	75.00	15	Soil rotational slide	Precipitation event	12.00	-	30	150.0	575.0	580.0	25	150				FLAC		D'Elia et al. (1999); Coli et al. (2009)

Record Information									Open Pit Parameters							Geological and Geotechnical Characteristics						Slope Failure Parameters										Slope Failure Plan and Scheme			General Information					
Label	Mine	Pit	Wall	ID	Country	Date	Material Group	Commodity	Shape of the Mine	Max Depth of the Mine, H _{max} (m)	Area of the Pit, (km ²)	Shoreline (m)	Length of the Mine (m)	Width of the Mine (m)	Overall Slope Angle of the Mine, β _{op} (°)	Height of Benches (m)	Lithology	Strength Grade	RMR (1976)	Unit Weight, γ (kN/m ³)	C' (kPa)	φ (°)	Failure Mechanism	Trigger factor	Volume (Mm ³)	Mass (tons)	Slope Angle, β _{fail} (°)	Fall Height, H _{fall} (m)	Travel distance, L _{travel} (m)	Average width, W _{fail} (m)	Setback distance, L _{sb} (m)	Height of the failure, H _{fail} (m)	General View of the Failure	Plan View of the Failure	Cross-Section of the Failure	Software	Monitoring system	Reference		
101	Sanu Tinti	Stage 1	Footwall	-	Guinea	1998	Suprolite	Gold	Oval	100	0.22	1970	580	350	30	10	Saprolite	R0	Very poor	27.00	106.00	20	Debris slide	Precipitation event	0.30	-	32	50.0	116.0	250.0	9	50							Fourie and Haines (2007)	
102	Savage River	North	East	-	Australia	June 17, 2010	Metamorphic	Iron	Oval	330	0.36	2245	815	550	60	30	Amphibolite	R4	Fair	29.00	50.00	26	Rock wedge slide	Long-term weakening	0.10	400000	61	135.0	170.0	80.0	15	120						Reutech Monitoring and Surveying Radar (MSR)	Hutchinson et al. (2013); MacQueen et al. (2013); Hutchinson et al. (2000)	
103	Savage River	North	East	-	Australia	August 20, 2010	Metamorphic	Iron	Oval	330	0.36	2245	815	550	60	30	Amphibolite	R4	Fair	29.00	50.00	26	Rock wedge slide	Not reported	0.10	200000	61	80.0	79.0	90.0	11	60						Reutech Monitoring and Surveying Radar (MSR)	Hutchinson et al. (2013); MacQueen et al. (2013)	
104	Savage River	North	East	-	Australia	July, 2012	Metamorphic	Iron	Oval	330	0.36	2245	815	550	60	30	Amphibolite	R4	Fair	29.00	50.00	26	Rock wedge slide	Not reported	0.70	1900000	61	165.0	222.0	210.0	18	135						Reutech Monitoring and Surveying Radar (MSR)	Hutchinson et al. (2013); MacQueen et al. (2013)	
105	ShengLi	No. 1	East	D1	China	May, 2005	Sedimentary	Coal	Rectangle	100	-	-	1800	900	20	10	Mudstone	R1	-	21.00	10.00	22	Rock wedge slide	Precipitation event	0.40	-	26	90.0	145.0	250.0	10	90				FLAC	GPS points, SSR radar, and total stations	Yanbo et al. (2010); Jiang et al. (2013)		
106	ShengLi	East	Southeast	-	China	August 16, 2013	Sedimentary	Coal	Polygon	200	14.1	17625	4583	3820	20	10	Mudstone	R1	-	20.00	20.00	8	Rock wedge slide	Precipitation event	85.00	-	23	190.0	1562.0	1800.0	58	190						FLAC	GPS points, SSR radar, and total stations	Yongbo et al. (2016)
107	ShengLi	North	Northeast	-	China	August 31, 2011	Sedimentary	Coal	Square	140	5.89	9935	2550	2400	20	10	Mudstone	R1	-	20.00	20.00	8	Rock wedge slide	Precipitation event	1.10	-	20	50.0	403.0	200.0	5	50						FLAC	GPS points, SSR radar, and total stations	Yongbo et al. (2016)
108	Shirley Basin	-	Southeast	-	USA	April, 1971	Sedimentary	Uranium	Oval	120	0.63	3085	1140	655	35	8	Shale	R1	-	20.00	70.00	20	Rock rotational slide	Mined too steep	1.10	-	38	87.0	172.0	250.0	-	-							Atkins and Pasha (1973); Clough et al. (1979)	
109	Shirya	-	-	-	India	October 15, 2000	Sedimentary	Coal	-	60	-	-	-	-	32	-	Sandstone	R2	Very poor	17.00	26.00	14	Rock planar slide	Precipitation event	0.14	-	32	13.0	65.0	-	-	13						Galema		Jhanwar and Thote (2011)

Record Information									Open Pit Parameters							Geological and Geotechnical Characteristics					Slope Failure Parameters								Slope Failure Plan and Scheme			General Information						
Label	Mine	Pit	Wall	ID	Country	Date	Material Group	Commodity	Shape of the Mine	Max Depth of the Mine, H _{max} (m)	Area of the Pit, (km ²)	Shoreline (m)	Length of the Mine (m)	Width of the Mine (m)	Overall Slope Angle of the Mine, β _{op} (°)	Height of Benches (m)	Lithology	Strength Grade	RMR (1976)	Unit Weight, γ (kN/m ³)	C' (kPa)	φ (°)	Failure Mechanism	Trigger factor	Volume (Mm ³)	Mass (tons)	Slope Angle, β _{fail} (°)	Fall Height, H _{fall} (m)	Travel distance, L _{travel} (m)	Average width, W _{fail} (m)	Setback distance, L _{sb} (m)	Height of the failure, H _{fail} (m)	General View of the Failure	Plan View of the Failure	Cross-Section of the Failure	Software	Monitoring system	Reference
110	Steep Rock	Roberts	West	No. 2	Canada	October 1968	Igneous	Iron	Elongated oval	168	1.63	7600	2970	533	36	10	Faulted ashrock	R0	-	27.00	109.00	35	Rock irregular slide	Precipitation event	0.50	400000	42	130.0	235.0	240.0	10	35						Coates et al. (1979)
111	Steep Rock	Roberts	West	No. 4	Canada	Sept. 1972	Igneous	Iron	Elongated oval	168	1.63	7600	2970	533	36	10	Ashrock	R2	-	27.00	109.00	35	Rock compound slide	Precipitation event	0.80	-	42	230.0	333.0	204.0	27	180						Coates et al. (1979)
112	Sunrise Dam	Cleo	Southwest	-	Australia	Dec. 2000	Soil	Gold	Oval	190	1.74	5370	1645	1050	36	15	Transported lake clay	R0	Very poor	-	-	-	Debris slide	Precipitation event	0.20	-	38	85.0	181.0	90.0	8	40				DIPS, SLIDE and ROCKFALL		Speight (2002)
113	Teghout mine	-	West	-	Armenia	-	Igneous	Copper and molybdenum	Oval	170	0.76	3450	1225	785	42	15	Porphyry	R3	Poor	22	13.50	34	Rock wedge slide	Daylighted structure	0.05	-	42	100.0	60.0	30.0	18	100				Slide, FLAC2D		Asadzadeh and Babanouri (2018)
114	Telfer	Pit 1A	Highwall	-	Australia	October 31, 1992	Sedimentary	Gold, Copper	Polygonal	120	1.93	5845	2370	1050	60	20	Interbedded sandstone and siltstone	R2	Fair	-	-	-	Rock planar slide	Blasting	0.20	176000	60	80.0	88.0	200.0	3	80				GroundProbe SSR, Stability Radars (SSR)		Dight (2006); Swedzicki (2001), Mercer (2006)
115	Tom Price	South East Prongs	South	-	Australia	January 8, 2007	Sedimentary	Iron	Oval	250	0.7	3500	1200	700	32	30	Dale Gorge formation	R1	Poor	35.00	110.00	34	Rock rotational slide	Precipitation event	0.40	1000000	40	135.0	270.0	265.0	10	90				Slide	GroundProbe SSR, Electronic Distance Measurement (EDM) prism monitoring	Day and Seery (2007); Lucas (2013); Taylor et al. (2001)
116	Tom Price	NTD	East	NTD 2009	Australia	Sept. 28, 2009	Sedimentary	Iron	Oval	180	0.62	3585	1545	520	26	30	Shale	R1	Poor	22.00	70.00	35	Rock planar slide	Precipitation event	0.40	1000000	26	45.0	189.0	180.0	3	45				Slide	GroundProbe SSR, Electronic Distance Measurement (EDM) prism monitoring	Venter et al. (2013)
117	Twin Buttes	-	South	-	USA	Nov. 1970	Sedimentary	Copper	Circle	335	2.8	7030	2160	1950	41	15	Quartzite, conglomerate, tuff, andesite, and dacite	R5	Fair	18.84	52.00	32	Rock wedge slide	Precipitation event	1.10	3000000	45	138.0	230.0	300.0	20	130				Slide, FLAC	Piezometers	Seegmiller (1972);
118	Wallaby	-	West	Scallop	Australia	2006	Sedimentary	Gold	Oval	140	0.67	3115	1075	825	33	20	Sandy claystone	R0	Poor	-	39.00	25	Debris slide	Precipitation event	0.20	-	43	136.0	232.0	90.0	18	100				Slide, Phase2	MSR-3 radar, GPS cannot be safely installed	Jones et al. (2011)
119	Wallaby	-	Southwest	Alpha	Australia	January 1, 2005	Sedimentary	Gold	Oval	140	0.67	3115	1075	825	33	18	Sandy claystone	R0	Poor	-	39.00	25	Debris slide	Precipitation event	0.10	-	42	135.0	168.0	140.0	10	125				Slide, Phase3	MSR-3 radar	Jones (2011), Whittall (2015)

Record Information									Open Pit Parameters							Geological and Geotechnical Characteristics						Slope Failure Parameters							Slope Failure Plan and Scheme			General Information						
Label	Mine	Pit	Wall	ID	Country	Date	Material Group	Commodity	Shape of the Mine	Max Depth of the Mine, H _{max} (m)	Area of the Pit, (km ²)	Shoreline (m)	Length of the Mine (m)	Width of the Mine (m)	Overall Slope Angle of the Mine, β _{op} (°)	Height of Benches (m)	Lithology	Strength Grade	RMR (1976)	Unit Weight, γ (kN/m ³)	C' (kPa)	φ (°)	Failure Mechanism	Trigger factor	Volume (Mm ³)	Mass (tons)	Slope Angle, β _{fail} (°)	Fall Height, H _{fall} (m)	Travel distance, L _{travel} (m)	Average width, W _{fail} (m)	Setback distance, L _{sb} (m)	Height of the failure, H _{fail} (m)	General View of the Failure	Plan View of the Failure	Cross-Section of the Failure	Software	Monitoring system	Reference
120	West Angelas	Centre Pit North	North		Australia	February 3, 2010	Sedimentary	Iron	Triangle	170	3.67	9475	3600	1460	40	18	Shale	R1	Fair	30.00	100	32	Rock planar slide	Daylighted structure	0.20	600000	42	140.0	235.0	220.0	15	140				Slide, Slide 3	Survey prisms and Radar monitoring, TDR cables	Joass et al. (2013); Venter et al. (2013); Lopes and Le (2013)
121	"Case 2"					Not reported	Igneous	-									Intrusives	-	-	-	-	-	Rock topple	Not reported	1.00	-	44	365.0	521.0	-	-	-						Rose and Hungr (2006)
122	"Case 2"					Not reported	Sedimentary	Coal		310					34		Sandstone	R3	Fair	-	-	-	Rock topple	Not reported	0.60	-	50	300.0	386.0	-	64	220						Vyllie (1980)
123	"Mine X"				Indonesia	May 10, 2011	Igneous	-	Oval	275					40	18	Diorite	R4	Fair	25.50	-	-	Rock irregular slide	Mined too steep	0.10	-	40	196.0	277.0	80.0	13	92						Kramadibrata et al. (2012)
124	Anonymous		East			Not reported	Igneous	-									Rhyolite tuff	R5	Good	22.00	-	-	Rock compound slide	Not reported	6.00	-	30	300.0	720.0	300.0	-	-						Whittall (2015)
125	Anonymous		Northeast		USA	January 4, 2011	Sedimentary	-									Oxidized rock	R1	Poor	25.00	-	-	Rock topple	Not reported	0.10	-	43	90.0	115.0	60.0	-	-						Whittall (2015)
126	Anonymous		Southwest		Canada	2004	Igneous	-									Tonalite	R3	Fair	27.00	-	-	Rock topple	Not reported	0.10	400000	45	107.0	132.0	125.0	-	-						Whittall (2015)
127	Anonymous		East		Canada	March 1, 1984	Igneous	-									Weathered tonalite	R4	Fair	27.00	-	-	Rock wedge slide	Not reported	0.10	270000	38	294.0	486.0	-	-	-						Whittall (2015)
128	Anonymous		Southwest		Canada	July 25, 2014	Igneous	-									Tonalite	R4	Fair	27.00	-	-	Rock planar slide	Precipitation event	0.30	-	40	76.0	128.0	99.0	-	-						Whittall (2015)
129	Anonymous		East		Canada	April 24, 2001	Sedimentary	-									Sandstone	R1	Poor	-	-	-	Rock rotational slide	Blasting	-	-	35	57.0	103.0	65.0	-	-						Whittall (2015)

Record Information									Open Pit Parameters							Geological and Geotechnical Characteristics						Slope Failure Parameters									Slope Failure Plan and Scheme			General Information					
Label	Mine	Pit	Wall	ID	Country	Date	Material Group	Commodity	Shape of the Mine	Max Depth of the Mine, H _{max} (m)	Area of the Pit, (km ²)	Shoreline (m)	Length of the Mine (m)	Width of the Mine (m)	Overall Slope Angle of the Mine, β _{op} (°)	Height of Benches (m)	Lithology	Strength Grade	RMR (1976)	Unit Weight, γ (kN/m ³)	C' (kPa)	φ (°)	Failure Mechanism	Trigger factor	Volume (Mm ³)	Mass (tons)	Slope Angle, β _{fail} (°)	Fall Height, H _{fall} (m)	Travel distance, L _{travel} (m)	Average width, W _{fail} (m)	Setback distance, L _{sb} (m)	Height of the failure, H _{fail} (m)	General View of the Failure	Plan View of the Failure	Cross-Section of the Failure	Software	Monitoring system	Reference	
129	Anonymous		South		USA	May 17, 2014	Sedimentary										Conglomerate and waste rock	R1	Poor	22.00	-	-	Rock irregular slide	Long-term weakening	0.70	-	34	200.0	475.0	360.0	-	-						Whittall (2015)	
131	Anonymous		North		USA	December 9, 2008	Igneous										Quartz monzonite porphyry	R4	Fair	25.00	-	-	Rock wedge slide	Blasting	-	110000	44	212.0	270.0	105.0	-	-						Whittall (2015)	
132	Anonymous		South		USA	1992	Metamorphic										Schist	R3	Poor	24.00	-	-	Rock wedge slide	Mined too steep	180	-	43	206.0	535.0	150.0	-	-						Whittall (2015)	
133	Anonymous		North		Canada	October 14, 2003	Igneous										Granodiorite	R3	Fair	26.00	-	-	Rock irregular slide	Daylighted structure	0.30	600000	41	344	538.0	300.0	-	-							Whittall (2015)
134	Carmen Copper Corporation	Carmen pit	North		Philippines	Dec. 21, 2020		Copper	Oval																												https://blogs.agu.org/landslideblog/2020/12/24/carmen-copper-mine-1/		

APPENDIX B. BIBLIOGRAPHY FOR TAMU-MINESLOPE

- Alejano L.A., and Sanchez J. (2010). Stability analyses of footwall slopes in open pit mining. *Dyna*, March 2010, 77(161): 61-70.
- Almenara J.R., Poespito T.S., and Lelono H.D. (2011). Batu Hijau open pit slope design based on geotechnical models and past performance. In *Proceedings of the International Symposium on Rock Slope Stability in Open Pit Mining and Civil Engineering (Slope Stability 2011)*, Vancouver, B.C., 18-21 September 2011. Canadian Rock Mechanics Association.
- Aprilia F., and Indrawan G.B. (2014). An evaluation of rock slope stability using limit equilibrium analyses. *Journal of Applied Geology*, Jul–Dec 2014, 06(02): 79–88.
- Arif J., and Baker T. (2004). Gold paragenesis and chemistry at Batu Hijau, Indonesia: implications for gold-rich porphyry copper deposits. *Mineralium Deposita*, 39 (2004): 523–535.
- Arikan F., Yoleri F., Sezer S., and Caglan D. (2010). Geotechnical assessments of the stability of slopes at the Cakmakkaya and Damar open pit mines (Turkey): a case study. *Environmental Earth Sciences*, 61(2010).
- Armstrong J. (2011). Management of progressive slope deformation at Goldstrike – Challenges and lessons learned. Presentation at 2011 Barrick Geomechanics and Hydrogeology Conference, Kalgoorlie, Australia.
- Armstrong J., and Rose N.D. (2009). Mine operation and management of progressive slope deformation on the south wall of the Barrick Goldstrike Betze-Post Open Pit. In *Proceedings of the International Symposium on Rock Slope Stability in Open Pit Mining and Civil Engineering (Slope Stability 2009)*, Santiago, 9-11 November 2009, CSIRO publishing.
- Asadizadeh M., and Babanouri N. (2018). Back analysis of inter-ramp slope failure in the Teghout copper mine. *International Journal of Mining and Geotechnical Engineering (IJMGE)*, 52-2 (2018): 207-214.
- Asof M., Dyah Hastuti E. W., Manuhutu H. I., and Nasution Y. (2010). The study of landslide using slope stability radar within failure SS_P4_028 in PT Newmont, Nusa Tenggara Barat, Indonesia. In *Proceedings of the Twin International Conferences on Geotechnical and Geo-Environmental Engineering*, Seoul, South Korea, 24-25 June 2010: 177-186.

- Atkins J.T., and Pasha M.A. (1973). Controlling open pit slope failures at Shirley Basin Mine. In Proceedings of AIME Annual meeting, Chicago.
- Aydan O., Ulusay R., and Kumsar H. (1996). Buckling failure at an open-pit coal mine. In Proceedings Eurock '96, Barla (ed.). Balkema, Rotterdam: 641-648.
- Bates E., St Louis R., Douglas S., and Sheets R. (2006). Slope Monitoring and Failure Mitigation Techniques Applied in the Gold Quarry Open Pit. In Proceedings of Golden Rocks 2006: The 41st US Symposium on Rock Mechanics, Golden, Colorado, 17-21 June 2006. American Rock Mechanics Association: 1047-1059.
- Battison R., Esen S., Duggan R., Henley K., and Dare-Bryan P. (2015). Reducing Crest Loss at Barrick Cowal Gold Mine. In Proceedings of the 11th International symposium on rock fragmentation by blasting / Sydney, NSW, 24–26 august 2015: 1-14.
- Behbahani S.S., Moarefvand P., Ahangari K., and Goshtasbi K. (2013). Unloading scheme of Angooran mine slope by discrete element modeling. International Journal of Rock Mechanics & Mining Sciences, 64 (2013): 220–227.
- Brawner C.O. (1982). Stabilization of Rock Slopes. In Stability in Surface Mining, Vol. 3. Edited by C.O. Brawner. SME-AIME, New York: 289-310.
- Brawner C.O., and Stacey P.F. (1979). Hogarth pit slope failure, Ontario, Canada. In Rock slides and avalanches. Edited by B. Voight. Elsevier, Amsterdam: 691-707.
- Brawner C.O., Stacey P.F., and Stark R. (1975). A successful application of mining with pit wall movement. In Proceedings of Canadian Institute of Mining annual western meeting, Edmonton, Alberta, October 1975: 20 p.
- Broadbent C. D., and Zavodni Z. M. (1982). Influence of rock structure on stability. In Stability in Surface Mining, Vol. 3. Edited by C.O. Brawner. SME-AIME, New York: 7-18.
- Brown I.R., Wood P.J. and Elmouttie M.K. (2016). Estimation of in situ strength from back-analysis of pit slope failure. In Proceedings of the First Asia Pacific Slope Stability in Mining Conference (APSSIM 2016), Australian Centre for Geomechanics, Perth: 331-338.
- Calder P.N. and Blackwell G. (1980). Investigation of a complex rock slope displacement at Brenda Mines. CIM Bulletin, August, 1980: 73-82.

- Carlà T., Farina P., Intrieri E., Botsialas K., and Casagli N. (2017). On the monitoring and early-warning of brittle slope failures in hard rock masses: Examples from an open-pit mine. *Engineering Geology*, 228 (2017): 71–81.
- Carlà T., Farina P., Intrieri E., Ketizmen H., and Casagli N. (2018). Integration of ground-based radar and satellite InSAR data for the analysis of an unexpected slope failure in an open-pit mine. *Engineering Geology*, 235 (2018): 39–52.
- Chappel A.P. (1998). An engineering geological investigation into pit slope stability at Macraes Gold Mine, Macraes Flat, Otago, New Zealand. M.Sc. thesis, the University of Canterbury, Christchurch, New Zealand.
- Clough G.W., West L.J., and Murdock L.T. (1979). Pit slope performance in shale, Wyoming, USA. In *Rock Slides and Avalanches*, Vol. 2. Elsevier (ed.), Amsterdam: 667-689.
- Coates D.F., Yu Y., and Gyenge M. (1979). A case history of pit slope design. In *Proceedings of the 4th ISRM Congress*, Montreaux, Switzerland, September 1979: 591-595.
- Coli N., Berry P., Boldini D. and Bruno R. (2009). In situ large size non conventional shear tests for the mechanical characterization of a bimrock in The Santa Barbara open pit mine (Italy). In *Proceedings of the 43rd US Rock Mechanics Symposium and 4th U.S.-Canada Rock Mechanics Symposium*, held in Asheville, NC June 28th – July 1, 2009. American Rock Mechanics Association (ARMA 09-1984).
- Coulthard M. A., Lucas D. S., and Fuller P. G. (2004). Application of UDEC to a stress-related mine slope failure at Leigh Creek, South Australia. In *Proceedings of the Symposium on Numerical Modelling of Discrete Materials*, Bochum, Germany, 29 September – 1 October 2004. Balkema, Rotterdam: 289-296.
- Creameens J., Gilbride L., Cellan R., and Cox A. (2000). Numerical Simulation of Complex Slope Displacement. In *Proceedings of the 4th North American Rock Mechanics Symposium*, Seattle, Washington, 31 July – 3 August 2000. Balkema, Rotterdam: 561-567.
- Creameens J.A. (2003). Geologic controls on complex slope displacement at the Pitch reclamation project. In *Engineering Geology in Colorado: Contributions, Trends, and Case Histories*. Edited by Douglas Boyer. Association of Engineering Geologists: 14 p.
- Crouse R. and Wright S. (2015). Cowal gold mine; Success in mining through saprolites - a case history. *Mining Engineering*, September 2015: 3-16.

- D'Elia B., Esu F., Tommasi P., and Utzeri L. (1999). FLAC modeling of the deformation and failure mechanism of a high cut in clay shales. In *FLAC and Numerical Modelling in Geomechanics*, (eds.: Detoumay and Hart), Balkema, Rotterdam, 1999: 47-54.
- Da Franca P.R.B. (1997). Analysis of slope stability using limit equilibrium and numerical methods with case examples from the Aguas Claras mine, Brazil. Ph.D. thesis, Department of Mining Engineering, Queen's University, Kingston, Canada.
- Darbor M., Jalalifar H., and Moarefv P. (2010). A developed technique to predict support system for plane failure; case study: lead-zinc Angoran mine. In *Proceedings of the 6th Asian Rock Mechanics Symposium*, New Delhi, India, 23-27 October 2010. International Society for Rock Mechanics: 9 p.
- Day A.P., and Seery J.M. (2007). Monitoring of a large wall failure at Tom Price Iron Ore Mine. In *Proceedings of the International Symposium on Rock Slope Stability in Open Pit Mining and Civil Engineering (Slope Stability 2007)*, Perth, Australia, 12-14 September 2007, Australian Centre for Geomechanics, Perth: 333-340.
- Dick G., Nunoo S., Smith S., Newcomen W., Kinakin D., Stilwell I., and Danielson J. (2020). Monitoring and managing large deformation pit slope instabilities at a British Columbia copper mine. In *Proceedings of the 2020 International Symposium on Slope Stability in Open Pit Mining and Civil Engineering (Slope Stability 2020)*, Australian Centre for Geomechanics, Perth: 439-452.
- Dight P.M. (2006). Pit wall failures on 'unknown' structures. *The Journal of the South African Institute of Mining and Metallurgy*, 106 (2006): 451-458.
- Dolgushev V., Kovalenko V., and Usmanov S. (2008). Three-dimensional stress-strain numerical modeling of the Kumtor open pit walls (Kyrgyzstan). *Bulletin of People's Friendship University of Russia, Engineering researches series*, 3(2008): 49-52.
- Doyle J.B., and Reese J.D. (2011). Slope Monitoring and Back Analysis of the East Fault Failure, Bingham Canyon Mine, Utah. In *Proceedings of the International Symposium on Rock Slope Stability in Open Pit Mining and Civil Engineering (Slope Stability 2011)*, Vancouver, Canada (September 18-21, 2011).
- Dyke G. (2009). Best practice and new technology in open pit mining geotechnics: Geita gold mine, Mali -a case study. In *Proceedings of the World Gold Conference*, Gauteng, South

- Africa, 26-30 October 2009. South African Institute of Mining and Metallurgy, Johannesburg: 169-176.
- EnviroMine (2011). Reclamation Plan Amendment for Permanente Quarry. State Mine ID # 91-43-0004. Report prepared for Lehigh Southwest Cement Company, Santa Clara County, California: 109 p.
- Farina P., Coli N., Yon R., Eken G., and Ketizmen H. (2013). Efficient real time stability monitoring of mine walls: the Çöllolar mine case study. In Proceedings of the 23rd International Mining Congress and Exhibition of Turkey, 16-19 April 2013, Antalya: 111-117.
- Fergusson D., Paris M., Anderson C.K., McMorran T., and Johnson D. (2001). Opencast Hightwall Slope Design, Rotowaro Coalfield. In Proceedings of the New Zealand Geotechnical Society Symposium “Engineering and Development in Hazardous Terrain”. Christchurch, August 2001: 35-51.
- Fisher B. R. (2009). Improved characterization and analysis of bi-planar dip slope failures to limit model and parameter uncertainty in the determination of setback distances. Ph.D. thesis, Department of Geological Engineering, The University of British Columbia, Vancouver, B.C.
- Fourie A.B., and Haines A. (2007). Obtaining Appropriate Design Parameters for Slopes in Weathered Saprolites, in Proceedings of the 2007 International Symposium on Rock Slope Stability in Open Pit Mining and Civil Engineering (Slope Stability 2007), Australian Centre for Geomechanics, Perth: 105-116.
- Fredj M., Hafsaoui A., Khedri Y., Boukarm R., Nakache R., Saadoun A., and Menacer K. (2018). Study of Slope Stability (Open Pit Mining, Algeria). In Soil Testing, Soil Stability and Ground Improvement, Sustainable Civil Infrastructures, W. Frikha et al. (eds.):1-11.
- Gadri L., Hadji R., Zahri F., Benghazi Z., Boumezbeur A., Laid B.M., and Raïs K. (2015). The quarries edges stability in opencast mines: a case study of the Jebel Onk phosphate mine, NE Algeria. *Arabian Journal of Geosciences*, 8 (2015): 8987-8997.
- Ginting A., Stawski M., and Widiadi R. (2011). Geotechnical risk management and mitigation at Grasberg Open Pit, PT Freeport Indonesia. In Proceedings of the International Symposium on Rock Slope Stability in Open Pit Mining and Civil Engineering (Slope Stability 2011), Vancouver, B.C., 18-21 September 2011. Canadian Rock Mechanics Association.

- Goldberg W.C., and Frizzell E.M. (1989). A case history of pit slope monitoring and back analysis, Berkeley pit, Butte, Montana. In Proceedings of the SME Annual Meeting, Las Vegas, Nevada, 27 February – 2 March 1989. Society of Mining Engineers, Littleton, Colorado: 8 p.
- Golder Associates. (2011). Geotechnical evaluations and design recommendations (revised): Permanente quarry reclamation plan update, Santa Clara County, California. Available from <http://www.scribd.com/doc/62193085/Volume-I-07-C-Geotechnical-Report-amp-Figures>.
- Hibert C., Ekström G., and Stark C. P. (2014). Dynamics of the Bingham Canyon Mine landslides from seismic signal analysis. *Geophysical Research Letters*, 41(13): 4535-4541.
- Hormazabal E., Veramendi R., Barrios J., Zuniga G., and Gonzalez F. (2013). Slope design at Cuajone Pit, Peru. In Proceedings of the International Symposium on Slope Stability in Open Pit Mining and Civil Engineering, Brisbane, Australia, 25-27 September 2013. Australian Centre for Geomechanics, Perth: 527-540.
- Hutchison B., Dugan K., and Coulthard M. (2000). Analysis of flexural toppling at Australian bulk minerals Savage River Mine.
- Hutchison B.J., Macqueen G.K., Dolting S.L. and Morrison A.T. (2013). 'Drape mesh protection at the Savage River Mine, Tasmania. In Proceedings of the 2013 International Symposium on Slope Stability in Open Pit Mining and Civil Engineering (Slope Stability 2013), Australian Centre for Geomechanics, Perth: 1345-1358.
- Jhanwar J.C., and Thote N.R. (2011). Slope failures in the opencast coal mines of Wardha Valley Coalfield in central India: a study. *Rock mechanics and rock engineering*, 44(5): 635-640.
- Jiang S., Kong X., Ye H., and Zhou N. (2013). Groundwater dewatering optimization in the Shengli no. 1 open-pit coalmine, Inner Mongolia, China. *Environmental Earth Science* (2013) 69: 187–196.
- Joass G.G., Dixon R., Sikma T., Wessels S.D.N., Lapwood J., and de Graaf P.J.H. (2013). Risk management and remediation of the north wall slip, West Angelas Mine, Western Australia. In Proceedings of the International Symposium on Slope Stability in Open Pit Mining and Civil Supplementary Data for Engineering, Brisbane, Australia, 25-27 September 2013. Australian Centre for Geomechanics, Perth: 995-1010.

- Johnson J.D., Fergusson D., and Guy G. (2007). Risk Based Slope Design for Opencast Coal Mines at Rotowaro, Huntly, New Zealand. In Proceedings of the 2007 International Symposium on Rock Slope Stability in Open Pit Mining and Civil Engineering (Slope Stability 2007), Perth, Australia, 12-14 September 2007, Australian Centre for Geomechanics, Perth: 157-170.
- Jones E. (2011). Development of the Wallaby Pit instabilities. In Mining in Saprolites short course at Slope Stability 2011: International Symposium on Rock Slope Stability in Open Pit Mining and Civil Engineering, Vancouver, B.C., 18-21 September 2011. Canadian Rock Mechanics Association.
- Jones E., Andrews P., and Holley S. (2011). The Wallaby Mine: Maintaining pit wall stability for continued underground mining. In Proceedings of the International Symposium on Rock Slope Stability in Open Pit Mining and Civil Engineering (Slope Stability 2011), Vancouver, B.C., 18-21 September 2011. Canadian Rock Mechanics Association.
- Kavvadas M., Agioutantis Z., Schilizzi P., and Steiakakis C. (2013). Stability and movements of open-pit lignite mines in Northern Greece. In Proceedings of the 18th International Conference on Soil Mechanics and Geotechnical Engineering (ICSMGE), Paris, France: 2193-2196.
- Kayesa G. (2006). Prediction of slope failure at Letlhakane Mine with the Geomos Slope Monitoring System. In Proceedings of the International Symposium on Stability of Rock Slopes in Open Pit Mining and Civil Engineering, Cape Town, South Africa, 3-6 April 2006. South African Institute of Mining and Metallurgy, Johannesburg: 605-622.
- Kelly C., Wu K., Ward B., and Cook R. (2002). Highwall stability in an open pit stone operation. In Proceedings of the 21st International Conference on Ground Control in Mining, Morgantown, West Virginia, 6-8 August 2002. West Virginia University: 228-235.
- Kennedy B. A., Niermeyer K. E., and Fahm B. A. (1969). A major slope failure at the Chuquicamata Mine, Chile. Mining Engineering AIME, 12(12), 60.
- Kennedy G. and Casagrande D. (2020). Evolution and management of large-scale instability: a case study from Ok Tedi. In Proceedings of the 2020 International Symposium on Slope Stability in Open Pit Mining and Civil Engineering (Slope Stability 2020), Australian Centre for Geomechanics, Perth: 265-280.

- Kramadibrata S., Wattimena R. K., Sidi I. D., Azizi M. A., and Adriansyah Y. (2012). Open Pit Mine Slope Stability and Uncertainty. In Proceedings of the 7th Asian Rock Mechanics Symposium, Seoul, South Korea, 15-19 October 2012. International Society for Rock Mechanics: 1233-1240.
- Lelono H.D., Basson F.R.P., Lupo J. and Adriansyah Y. (2016). Pit slope evaluation based on the historical failure database at Batu Hijau mine. In Proceedings of the First Asia Pacific Slope Stability in Mining Conference (APSSIM 2016), Australian Centre for Geomechanics, Perth: 213-224.
- Lopes P.J.G., and Le T.T. (2013). Rockfall stabilisation of a steep and high slope at West Angelas Mine using pre-tensioned anchored mesh. In Proceedings of the 2013 International Symposium on Slope Stability in Open Pit Mining and Civil Engineering (Slope Stability 2013), Australian Centre for Geomechanics, Perth: 1261-1272.
- López-Vinielles J., Ezquerro P., Fernández-Merodo J.A. et al. (2020). Remote analysis of an open-pit slope failure: Las Cruces case study, Spain. *Landslides*, 17 (2020): 2173–2188.
- Lucas D.S., and de Graaf P.J.H. (2013). Iterative geotechnical pit slope design in a structurally complex setting: a case study from Tom Price, Western Australia. In proceedings of the 2013 International Symposium on Slope Stability in Open Pit Mining and Civil Engineering, Australian Centre for Geomechanics (Slope Stability 2013), Perth: 513-526.
- Lynch R. A., and Malovichko D. A. (2006). Seismology and slope stability in open pit mines. In Proceedings of the International Symposium on Rock Slope Stability in Open Pit Mining and Civil Engineering (Slope Stability 2006), Cape Town, South Africa, 3-6 April 2006, South African Institute for Mining and Metallurgy, Johannesburg: 375-390.
- Macqueen G.K., Salas E.I., and Hutchison B.J. (2013). Application of radar monitoring at Savage River Mine, Tasmania. In Proceedings of the 2013 International Symposium on Slope Stability in Open Pit Mining and Civil Engineering (Slope Stability 2013), Australian Centre for Geomechanics, Perth: 1011-1020.
- MacRae A. M. (1985). Case History of an Open Pit Coal Mine Slope Failure at Luscar Alberta. M.Eng. thesis, Department of civil engineering, The University of Alberta, Edmonton, Alberta.
- Martin D. and Stacey P. (2018). Guidelines for open pit slope design in weak rocks. CRC Press. Balkema. 398 p.

- Martin D.C. (1990). Deformation of open pit mine slopes by deep seated toppling. *International Journal of Surface Mining, Reclamation and Environment*, 4(1990): 153-164.
- Melnikov N. and Kozirev A. (2015). Changes in the geodynamic behavior of the geological environment at large-scale deep open-pit mining. *Mining Informational and analytical bulletin (scientific and technical journal)*, 56(2015): 7-23. (in Russian)
- Mercer K. (2006) Investigation into the time dependent deformation behavior and failure mechanism of unsupported rock slopes on the interpretation of observed deformation behavior. Ph.D. thesis. Faculty of Engineering and the Built Environment, the University of Witwatersrand, Johannesburg, South Africa. 380 p.
- Miller V.J. (1979). The Northwest Tripp slide at Kennecott's Nevada Mines division. In *Proceedings of the 20th U.S. Symposium on Rock Mechanics*, Austin, Texas, June4-6, 1979: 327-335.
- Miller V.J. (1982). The Northeast Tripp Slide – A 11.7 million cubic meter wedge failure at Kennecott's Nevada Mine Division. In *Proceedings of the 3rd International Conference on Stability in Surface Mining*, Vancouver, B.C., 1-3 June 1981. SME-AIME, New York: 725-743.
- Moarefvand P., Ahmadi M., and Afifipour M. (2012). Unloading scheme to control sliding mass at Angouran open pit mine, Iran. *Harmonizing Rock Engineering and the Environment – Qian & Zhou (eds): 1963–1966.*
- Moharana A., and Lonergan J. (2014). Managing the medium term mine scheduling challenges at Bingham Canyon mine after the slide. In *Proceedings of the 2014 SME Annual Meeting and Exhibit (SME 2014)*, Salt Lake City, Utah, USA, 23-26 February 2014: 399-402.
- Nasuf E., Eskikaya S., Bilgin N., Copur H., and Kont R. (1993). Slope stability analysis in K.B.I Murgul Copper Mine of Turkey. In *Proceedings of the International Symposium on Assessment and Prevention of Failure Phenomena in Rock Engineering*, Istanbul, Turkey 5-7 April 1993. Balkema, Rotterdam: 549-554.
- Nunoo S. (2016). Bayesian belief network approach to slope management in British Columbia open pits. Ph.D. thesis. The College of Graduate Studies. The University of British Columbia, Okanagan. April 2016: 239 p.
- Nunoo S. (2018). Lessons learnt from open pit wall instabilities: case studies of BC Open Pit Hard Rock Mines. *Journal of Mining Science*, 54(5)(2018): 2018804-812.

- Nutakor D. (2012). Mitigation of the Cplus failure in the Q7 cut at Rio Tinto's Bingham Canyon Mine. *Mining Engineering*, June 2012, 64(6): 107-111.
- Oge I.F. (2008). Slope stability analysis and design in Elbistan-Çöllolar open cast mine. M.S. thesis. Middle East Technical University, September 2008. 162 p.
- Oldcorn R.C., and Seago R. (2007). Understanding the bigger picture: Interpretation of geological structure in open pit rock slope stability. In *Proceedings of the 2007 International Symposium on Rock Slope Stability in Open Pit Mining and Civil Engineering (Slope Stability 2007)*, Perth, Australia, 12-14 September 2007, Australian Centre for Geomechanics, Perth: 449-462.
- Ozbay A., and Cabalar A.F. (2015). FEM and LEM stability analyses of the fatal landslides at Çöllolar open-cast lignite mine in Elbistan, Turkey. *Landslides* 12 (2015): 155–163.
- Pankow K.L., Moore J., Hale M., Koper K., Kubacki T., Whidden K., and McCarter M. (2014). Massive landslide at Utah copper mine generates wealth of geophysical data. *GSA Today*, January 2014: 4-8.
- Reid G., and Stewart D. (1986). A large scale toppling failure at Afton. In *Proceedings of the International Symposium on Geotechnical Stability in Surface Mining*, Calgary, Alberta, 6-7 November 1986: 215-223.
- Rippere K., Sun Y., and Tejada L. (1999). Geotechnical monitoring and modeling at Cuajone open-pit mine. In *Proceedings of Mining Science and Technology symposium*, Beijing, China, 29-31 August 1999. CRC Press: 379-383.
- Rose N.D. (2011). Investigating the Effects of Mining-Induced Strains on Open Pit Slopes. In *Proceedings of the International Symposium on Rock Slope Stability in Open Pit Mining and Civil Engineering (Slope Stability 2011)*, Vancouver, B.C., 18-21 September 2011. Canadian Rock Mechanics Association.
- Rose N.D., and Hungr O. (2006). Forecasting potential slope failure in open pit mines – contingency planning and remediation. *International Journal of Rock Mechanics and Mining Science*, 44(2007): 308-320.
- Rose N.D., and Sharon R.P. (2000). Practical rock slope engineering designs at Barrick Goldstrike. In *Slope Stability in Surface Mining*. Edited by W.A. Hustrulid, M.K McCarter, and D.J.A. Van Zyl. Society for Mining, Metallurgy, and Exploration, Inc, Littleton, Colorado: 213-218.

- Ross B., and Sutherlin C. (2015). March 11. Lessons from Kennecott Utah Copper's Manefay slide [Webinar]. In SME Annual Meeting 2015. Available from <https://smenet.webex.com>.
- Roux R., Terbrugge P., and Badenhorst F. (2006). Slope Management at Navachab Gold Mine, Namibia. In Proceedings of the International Symposium on Rock Slope Stability in Open Pit Mining and Civil Engineering (Slope Stability 2006), Cape Town, South Africa, 3-6 April 2006, South African Institute for Mining and Metallurgy, Johannesburg: 579-594.
- Seegmiller B.L. (1972). Rock stability analysis at Twin Buttes. In Proceedings of the 13th Symposium on Rock Mechanics, Urbana, Illinois, 30 August – 1 September 1971. American Society of Civil Engineers: 511-536.
- Septian A. (2016). Influence of Geotechnical Properties on the Run-out Process at Bingham Canyon Slope Failure. Ph.D. thesis. The University of Queensland, Australia.
- Sharon R. (2000). Slope stability and operational control at Barrick Goldstrike. In Slope Stability in Surface Mining. Edited by W.A. Hustrulid, M.K McCarter, and D.J.A. Van Zyl. Society for Mining, Metallurgy, and Exploration, Inc, Littleton, Colorado: 219-226.
- Sharon R.P. (2011). Challenges of open pit mine development in weak rocks. In Mining in Saprolites short course at Slope Stability 2011: International Symposium on Rock Slope Stability in Open Pit Mining and Civil Engineering, Vancouver, B.C., 18-21 September 2011. Canadian Rock Mechanics Association.
- Sharon R.P., Bywater A., and Greenhill P. (2013). Cowal Gold Mine (CGM). In Guidelines for evaluating water in pit slope stability. Edited by G. Beale and J. Read. CSIRO publishing, Clayton, Australia: 520-525.
- Sheets R.J. (2011). Lessons learned from Carlin Formation slope instability at the Gold Quarry operation. In Proceedings of the International Symposium on Rock Slope Stability in Open Pit Mining and Civil Engineering. Mining in Saprolites short course at Slope Stability 2011, Vancouver, B.C., 18-21 September 2011. Canadian Rock Mechanics Association.
- Sheets R.J., Douglas S.J., St Louis R.M., and Bailey J.A. (2014). Remediation of large-scale slope failures and impact on mine development at the Gold Quarry Mine. Mining Engineering, 66(11): 57-64.

- Sheng Z., and Lui Z. (1995). Analysis of the landslide at a limestone open pit mine in China. Proceedings of the 8th ISRM Congress, Tokyo, Japan, 25-29 September 1995. International Society for Rock Mechanics: 437-439.
- Sjöberg J. (1996). Large scale slope stability in open pit mining-a review. Technical Report 1996:10T, Lulea University of Technology, Division of Rock Mechanics, Lulea, Sweden. 229 p.
- Sjöberg J. (1999). Analysis of large scale rock slopes. PhD Thesis, Lulea University of Tecknology. Department of Civil, Environmental and Natural Resources Engineering, Mining and Geotechnical Engineering.
- Speight H.E. (2002). Solving a slope stability problem at the Cleo open pit in Western Australia. Snowdon mining industry consultants.
- Srikant A., Brannon C., Flint D. C., and Casten T. (2007). Geotechnical characterization and design for the transition from the Grasberg open pit to the Grasberg block cave mine. In Proceedings of the 1st Canada-US Rock Mechanics Symposium, Vancouver, B.C., 27-31 May 2007. American Rock Mechanics Association: 1277-1286.
- Szwedzicki T. (2001). Geotechnical precursors to large-scale ground collapse in mines. International Journal of Rock Mechanics and Mining Sciences, 38 (2001): 957–965.
- Taherkhani H., and Doostmohammadi R. (2016). Investigation of Geotechnical Parameters Effect on Open Pit Mining Operation Cost (Case Study: Angouran Mine). Archives of Mining Sciences, 61(1) (2016): 169-182.
- Tannant D.D., and LeBreton R. (2007). Footwall slope slab failure at a mountain coal mine. In Proceedings of the 1st Canada-US Rock Mechanics Symposium, Vancouver, B.C., 27-31 May 2007. American Rock Mechanics Association: 156-164.
- Taylor D., Dalstra H.J., Harding A.E., Broadbent G.C., and Barley M.E. (2001). Genesis of High-Grade Hematite Orebodies of the Hamersley Province, Western Australia. Economic Geology, 96 (2001): 837–873.
- Terbrugge P. J., and Hanif M. (1981). Discussion of a large scale failure on the footwall of the Nchanga open pit, Zambia. In ISRM International Symposium, Tokyo, Japan, 21-24 September 1981. Balkema, Rotterdam: 1499-1501.
- Torgoev I., and Torgoev A. (2014). Rockslides in the open pit of Kumtor goldmine (Kyrgyzstan). In Proceedings of World Landslide Forum 3, 2-6 June 2014, Beijing.

- Turk N., and Koca M.Y. (1993). Influence of historic landslides in design of the Borax open pit mine. In Proceedings of the International Symposium on Assessment and Prevention of Failure Phenomena in Rock Engineering, Istanbul, Turkey 5-7 April 1993. Balkema, Rotterdam: 573-578.
- Tutluoglu L., Oge I.F., and Karpuz C. (2011). Two and three dimensional analysis of a slope failure in a lignite mine. *Computers and Geosciences*, 37 (2011): 232–240.
- Umar S.B., Krishna R., Besa B., and Ahmed A. (2018). Validation of the slope monitoring program at Nchanga open pit mine, Zambia. *International Journal of Recent Engineering Research and Development (IJRERD)*, 03(05): 142-149.
- UNOSAT (2011). Post-Landslide assessment for Çöllolar Coalfield Kahramanmaraş, Turkey. 08 March 2011 - Version 2.0 - LS-2011-000170-TUR. United Nations Institute for Training and Research.
- Venter J., Kuzmanovic A., and Wessels S.D.N. (2013). An evaluation of the CUSUM and inverse velocity methods of failure prediction based on two open pit instabilities in Pilbara. In Proceedings of the International Symposium on Slope Stability in Open Pit Mining and Civil Engineering, Brisbane, Australia, 25-27 September 2013. Australian Centre for Geomechanics, Perth. 1061-1076.
- Voight B., and Kennedy B. A. (1979). Slope failure of 1967–1969, Chuquicamata mine, Chile. *Rockslides and avalanches*, 2: 595-632.
- Weichert D., Horner R.B., and Evans S.G. (1994). Seismic Signatures of Landslides: the 1990 Brenda Mine Collapse and the 1965 Hope Rockslides. *Bulletin of the Seismological Society of America*, October 1994, 84(5): 1523-1532.
- Wessels S.D.N. (2009). Monitoring and management of a large open pit failure. M.Sc.E thesis, Faculty of Engineering and the Built Environment, University of Witwatersrand, Johannesburg, South Africa.
- Wessels S.D.N. and Naismith W.A. (2005). Management of a major slope failure at Nchanga Open Pit, Chingola, Zambia. *Journal of the South African Institute of Mining and Metallurgy*, 105(9), 619-626.
- Whittall J.R. (2015). Runout exceedance prediction for open pit slope failures. M.Sc. thesis, the University of British Columbia, Vancouver, August 2015.

- Widijanto E., Wattimena R.K., Kramadibrata S., and Rai M.A. (2017). Geometry effects on slope stability at Grasberg Mine through the transition from open pit to underground block cave mining. *Electronic Journal of Geotechnical Engineering*. 22(05) (2017): 1733-1745.
- Wyllie D.C. (1980). Toppling rock slope failures examples of analysis and stabilization. *Rock Mechanics*, 13(2): 89-98.
- Yamaguchi U., and Shimotani T. (1986). A case study of slope failure in a limestone quarry. *International Journal of Rock Mechanics and Mining Sciences* 23(1): 95-104.
- Yanbo Z., Zhanjin L., and Zhiqiang K. (2010). Analysis on landslide catastrophe mechanism and landslip forecasting for open-pit coal mine. *Rock Stress and Earthquakes*, Xie (ed.). Taylor & Francis Group, London: 401-405.
- Yang D.Y., Brouwer K.J., Sheets R.J., St Louis R.M., and Douglas S.J. (2011a). Large-Scale Slope Instability at the Gold Quarry Mine, Nevada. In *Proceedings of the International Symposium on Rock Slope Stability in Open Pit Mining and Civil Engineering (Slope Stability 2011)*, Vancouver, B.C., 18-21 September 2011. Canadian Rock Mechanics Association.
- Yang D.Y., Mercer R.A., Brouwer K.J., and Tomlinson C. (2011b). Managing pit slope stability at the Kemess South Mine - changes over time. In *Proceedings of the International Symposium on Rock Slope Stability in Open Pit Mining and Civil Engineering (Slope Stability 2011)*, Vancouver, B.C., 18-21 September 2011. Canadian Rock Mechanics Association.
- Yongbo F., Shihai L., Yang Z., Zhiyong., and Xiaoyu L. (2016). Lessons learned from the landslides in Shengli east open pit mine and north open-pit mine in Xilinhot city, Inner Mongolia province, China. *Geotechnical and Geological Engineering* (2016) 34: 425–435.
- Yost R. R. (2009). *The Time Value of Risk: A Case Study at the Boron Operations Open Pit Mine*. Ph.D. thesis, Department of Mining, Geology, and Geological Engineering, The University of Arizona, Tucson, Arizona.
- Zavodni Z.M., and Ericksent S.D. (1995). Slope design procedures at the Bingham Canyon Mine. *Environmental and Engineering Geology of the Wasatch Front Region Utah Geological Association Publication 24*, 1995 (ed.: W.R.Lund): 161-168.

- Zevgolisa I.E., Deliverisb A.V., and Koukouzas N.C. (2019) Slope failure incidents and other stability concerns in surface lignite mines in Greece. *Journal of Sustainable Mining* 18 (2019): 182–197.
- Zhang B., Ye F., Wang Y., Lin W., and Zhang Z. (2015). Slope stability analysis and prevention measures in D Area of South Part of Baiyun'ebo open –pit iron mine. In *Proceedings of the 10th Asian Regional Conference of IAEG*.
- Zhou C., Li X., Qin S., Qiu D., Wu Y., Xiao Y., and Zhou J. (2008). Automatic monitoring system for high-steep slope in open-pit mine based on GPS and data analysis. In *Proceedings of the International Conference on Earth Observation Data Processing and Analysis, Wuhan, China, 28-29 December 2008*. American Society of Civil Engineers: 4098-4103.